# TOTAL-SYSTEM PERFORMANCE ASSESSMENT (TPA) VERSION 4.0 CODE:

# MODULE DESCRIPTIONS AND USER'S GUIDE

*Prepared for*

**Nuclear Regulatory Commission**
**Contract NRC-02-97-009**

*Coordinated by*

**Sitakanta Mohanty (CNWRA)**
**Timothy J. McCartin (NRC)**
**David W. Esh (NRC)**

**Center for Nuclear Waste Regulatory Analyses**
**San Antonio, Texas**

**January 2002**

# ABSTRACT

Total system performance assessment (TSPA) is playing an increasingly critical role in regulatory decision making. Within the Nuclear Regulatory Commission (NRC) high-level waste (HLW) program, TSPA studies are performed to focus the activities of the NRC technical staff, to evaluate the implementability of anticipated changes to the NRC and U.S. Environmental Protection Agency (EPA) regulations, to evaluate the principal factors identified in the U.S. Department of Energy (DOE) Repository Safety Strategy, and to prepare for the NRC review of the DOE site recommendation consideration report (SRCR) and any eventual license application (LA) for Yucca Mountain (YM).

Conducting a TSPA for the proposed repository involves application of a total-system model that simulates the processes affecting repository performance including propagation of the uncertainties associated with model parameters, conceptual models, and future system states. The simulation process, which implements a probabilistic framework, integrates a broad spectrum of site-specific data and information and produces estimates for a set of regulatory-based performance measures. Building on the previously developed NRC assessment methodology, a new Total-system Performance Assessment (TPA) code, designated TPA Version 4.0 code, was developed by the NRC and the Center for Nuclear Waste Regulatory Analyses (CNWRA) to evaluate the relative significance of the NRC-identified integrated subissues and to assess the assumptions and models in forthcoming DOE TSPAs, such as the DOE TSPA SRCR for the YM site.

The TPA Version 4.0 code is designed to estimate total-system performance measures of annual individual dose or risk expected to be specified in the EPA standard and the NRC conforming regulations. The TPA Version 4.0 code is a combination of an executive driver, a set of consequence modules, and a library of utility modules. The executive driver controls the probabilistic sampling of input parameters, the calculational sequence and data transfers among consequence modules, and the generation of output files. The various output files are used in parameter sensitivity analyses, postprocessing of time-dependent risk curves, and synthesis of statistical distributions (e.g., cumulative distribution functions and complementary cumulative distribution functions) for appropriate performance measures. Consequence models simulate physical processes and events such as unsaturated zone infiltration, evolution of the near-field thermal-hydrologic environment, failure of the drip shield and waste packages (WP), dissolution and release of waste, transport of waste in the groundwater system, extraction of groundwater, and consumption of groundwater. In addition to considering climate change, the TPA Version 4.0 code is designed to calculate the effects of disruptive events such as faulting, seismicity, and volcanism.

This report has been prepared to facilitate use of the TPA Version 4.0 code by a variety of users at the NRC and the CNWRA. The report contains descriptions of

- Overall TSPA methodology
- Executive or main program that controls execution of the code
- Utility modules used to manipulate data and enhance computational capabilities
- Consequence modules that simulate physical processes and events that affect the release, transport, and evolution of the waste
- Content and format of the input file
- Content and format of output files
- Instructions for program installation and execution

The TPA Version 4.0 code represents an improvement to the Version 3.2 used in the review of the DOE TSPA-VA. Major modifications to the TPA code include incorporation of the EDA II repository design, improvements to the dynamic capabilities of the code, adjustments in the conservatism of model representation, and added flexibility in defining the receptor group. Specifically, modifications include

- Incorporation of the EDA II repository design
- Introduction of a drip shield
- Revision of WP temperature calculations
- Modification of the repository layout
- Addition of new thermal output and radionuclide inventory data
- Flexibility in defining the exposure scenario
  - Incorporation of GENII into the TPA code for considering the stochastic biosphere and receptor group and for providing a framework to calculate age-specific doses
- General modification by
  - Adding time-dependent mass loading parameters
  - Adding alluvium length variation
  - Improving saturated zone matrix diffusion
  - Reformulating number of WPs affected by volcanic events
  - Adding time-dependent flow rate modification factors
  - Generating seismic events in repeatable manner for long and short simulations
  - Adding log-beta and integer-uniform distribution functions to the LHS sampler
  - Making water contact model dependent on WP failure mode
  - Incorporating effects of radiolysis via $H_2O_2$
  - Building efficiency in reflux calculations
  - Updating shallow infiltration model
  - Revising unsaturated zone hydrostratigraphy
  - Improving flexibility by moving source term and thermal output information to data files

In addition to the modifications to the code, data for the basecase parameter set have undergone significant revision. The modifications to the code and data increase the confidence of the NRC staff in assessing the performance of a HLW repository.

# CONTENTS


Section Page

FIGURES ..... xv
TABLES ..... xvii
ACRONYMS ..... xix
FOREWORD ..... xxi
ACKNOWLEDGMENTS ..... xxii
QUALITY OF DATA AND CODE DEVELOPMENT ..... xxii

1 INTRODUCTION ..... 1-1
*S. Mohanty, D. Esh, T. McCartin, G. Wittmeyer, M. Lee*
1.1 TPA CODE ..... 1-2
1.2 DESCRIPTION OF THE PROPOSED REPOSITORY SITE ..... 1-4
1.3 REPORT CONTENT ..... 1-8
1.4 UPGRADING TPA VERSION 3.1.4 TO TPA VERSION 3.2 CODE ..... 1-8
1.5 UPGRADING TPA VERSION 3.2 TO TPA VERSION 4.0 CODE ..... 1-9

2 OVERVIEW OF THE TPA CONCEPTUAL MODELS ..... 2-1
*T. McCartin, S. Mohanty, R. Baca*
2.1 CONCEPTUALIZATION OF REPOSITORY AND GEOLOGIC SETTING ..... 2-1
2.2 CONCEPTUAL MODELS IMPLEMENTED IN THE TPA COMPUTER CODE ..... 2-3
2.2.1 Infiltration and Deep Percolation ..... 2-5
2.2.2 Near-Field Environment ..... 2-5
2.2.3 Radionuclide Releases from the Engineered Barrier System ..... 2-6
2.2.4 Treatment of Aqueous-Phase Transport in the Unsaturated and Saturated Zones ..... 2-9
2.2.5 Airborne Transport for Direct Releases ..... 2-9
2.2.6 Exposure Pathways and Reference Biosphere ..... 2-10

3 TPA CODE STRUCTURE AND MODULES ..... 3-1
*S. Mohanty, R. Janetzke, R. Rice, R. Codell, J. Weldy, K. Poor*
3.1 OVERVIEW OF THE TPA COMPUTER CODE ..... 3-2
3.2 EXEC MODULE OPERATION ..... 3-5
3.2.1 Realization Loop ..... 3-7
3.2.2 Subarea Loop ..... 3-7
3.2.3 Release Consequence ..... 3-10
3.3 UTILITY MODULES ..... 3-11
3.3.1 SAMPLER ..... 3-11
3.3.1.1 Parameter Sampling ..... 3-11
3.3.1.2 Modifications to the Latin Hypercube Sampling Routine ..... 3-12
3.3.1.3 Distributions ..... 3-12
3.3.1.4 User-Defined Distribution ..... 3-14

# CONTENTS (cont'd)


| Section | | | | Page |
|---|---|---|---|---|
| | | 3.3.1.5 | Specified Correlation | 3-14 |
| | | 3.3.2 | INVENT | 3-18 |
| | 3.4 | | CONSEQUENCE MODULES | 3-24 |
| 4 | | | UZFLOW MODULE DESCRIPTION | 4-1 |
| | *S. Stothoff, R. Janetzke, R. Fedors* | | | |
| | 4.1 | | INFORMATION FLOW WITHIN TPA | 4-1 |
| | | 4.1.1 | Information Supplied to UZFLOW | 4-1 |
| | | 4.1.2 | Information Provided by UZFLOW | 4-1 |
| | 4.2 | | INTERMEDIATE RESULTS | 4-1 |
| | 4.3 | | CONCEPTUAL MODEL | 4-2 |
| | | 4.3.1 | Climate Model | 4-2 |
| | | 4.3.2 | Shallow Infiltration Model | 4-8 |
| | | 4.3.3 | Deep Percolation Model | 4-9 |
| | 4.4 | | ASSUMPTIONS AND CONSERVATISM OF THE UZFLOW APPROACH | 4-9 |
| 5 | | | NFENV MODULE DESCRIPTION | 5-1 |
| | *S. Mohanty, R. Green, S. Painter, D. Esh, R. Janetzke, G. Rice, S. Stothoff, B. Leslie* | | | |
| | 5.1 | | INFORMATION FLOW WITHIN TPA | 5-1 |
| | | 5.1.1 | Information Supplied to NFENV | 5-1 |
| | | 5.1.2 | Information Provided by NFENV | 5-1 |
| | 5.2 | | INTERMEDIATE RESULTS | 5-1 |
| | 5.3 | | CONCEPTUAL MODEL | 5-2 |
| | | 5.3.1 | Heat Transfer and Temperature Calculation | 5-2 |
| | | 5.3.2 | Near-Field Chemical Composition | 5-13 |
| | | 5.3.3 | Near-Field Groundwater Infiltration | 5-16 |
| | 5.4 | | ASSUMPTIONS AND CONSERVATISM OF THE NFENV APPROACH | 5-23 |
| 6 | | | EBSFAIL MODULE DESCRIPTION | 6-1 |
| | *O. Pensado, G. Cragnolino, S. Mohanty, T. Ahn, K. Gruss* | | | |
| | 6.1 | | INFORMATION FLOW WITHIN TPA | 6-1 |
| | | 6.1.1 | Information Supplied to EBSFAIL | 6-1 |
| | | 6.1.2 | Information Provided by EBSFAIL | 6-1 |
| | 6.2 | | INTERMEDIATE RESULTS | 6-1 |
| | 6.3 | | CONCEPTUAL MODEL | 6-2 |
| | | 6.3.1 | Corrosion and Mechanical Failures | 6-2 |
| | | 6.3.2 | Dry-Air Oxidation | 6-3 |
| | | 6.3.3 | Humid-Air Corrosion | 6-4 |
| | | 6.3.4 | Aqueous Corrosion | 6-5 |
| | | 6.3.5 | Mechanical Failure | 6-8 |
| | | 6.3.6 | Drip Shield | 6-10 |

# CONTENTS (cont'd)


| Section | | | | Page |
|---|---|---|---|---|
| | | 6.3.7 | Radiolysis | 6-11 |
| | 6.4 | | ASSUMPTIONS AND CONSERVATISM OF THE EBSFAIL APPROACH | 6-12 |
| 7 | | | SEISMO MODULE DESCRIPTION | 7-1 |
| | *S. Hsiung, J. Stamatakos, S. Mohanty, A.-B. K. Ibrahim* | | | |
| | 7.1 | | INFORMATION FLOW WITHIN TPA | 7-1 |
| | | 7.1.1 | Information Supplied to SEISMO | 7-1 |
| | | 7.1.2 | Information Provided by SEISMO | 7-1 |
| | 7.2 | | INTERMEDIATE RESULTS | 7-1 |
| | 7.3 | | CONCEPTUAL MODEL | 7-1 |
| | | 7.3.1 | Impact Load and Stress Calculation | 7-2 |
| | | 7.3.1.1 | Failure Criterion | 7-5 |
| | | 7.3.2 | Joint Spacing and Rock Conditions in the TSw2 Unit | 7-5 |
| | | 7.3.2.1 | Fractional Coverage of Rock Conditions and Determination of Number of Waste Package Ruptured | 7-6 |
| | | 7.3.2.2 | Seismic Hazard Parameters | 7-7 |
| | 7.4 | | ASSUMPTIONS AND CONSERVATISM OF THE SEISMO APPROACH | 7-7 |
| 8 | | | EBSREL MODULE DESCRIPTION | 8-1 |
| | *R. Codell, S. Mohanty, T. Ahn, W. Murphy, O. Pensado* | | | |
| | 8.1 | | INFORMATION FLOW WITHIN TPA | 8-1 |
| | | 8.1.1 | Information Supplied to EBSREL | 8-1 |
| | | 8.1.2 | Information Provided by EBSREL | 8-1 |
| | 8.2 | | INTERMEDIATE RESULTS | 8-1 |
| | 8.3 | | CONCEPTUAL MODEL | 8-2 |
| | | 8.3.1 | Radionuclide Inventory and Mass Transfer | 8-2 |
| | | 8.3.2 | Advective Mass Transfer | 8-4 |
| | | 8.3.3 | Waste Package Inventory | 8-5 |
| | | 8.3.4 | Spent Fuel Dissolution Rate | 8-6 |
| | | 8.3.5 | Spent Fuel Surface Area | 8-9 |
| | | 8.3.6 | Cladding | 8-11 |
| | | 8.3.7 | Water Dripping Abstraction | 8-11 |
| | | 8.3.8 | Computational Approach | 8-13 |
| | | 8.3.9 | EBSFILT Model for Transport of Radionuclides through the Invert | 8-13 |
| | 8.4 | | ASSUMPTIONS AND CONSERVATISM OF THE EBSREL APPROACH | 8-15 |
| 9 | | | UZFT MODULE DESCRIPTION | 9-1 |
| | *T. McCartin, R. Janetzke, N. Coleman, R. Fedors* | | | |
| | 9.1 | | INFORMATION FLOW WITHIN TPA | 9-1 |
| | | 9.1.1 | Information Supplied to UZFT | 9-1 |
| | | 9.1.2 | Information Provided by UZFT | 9-1 |

# CONTENTS (cont'd)


| Section | | | Page |
|---|---|---|---|
| | 9.2 | INTERMEDIATE RESULTS | 9-1 |
| | 9.3 | CONCEPTUAL MODEL | 9-2 |
| | 9.3.1 | Unsaturated Zone Flow Model | 9-2 |
| | 9.3.2 | Unsaturated Transport | 9-5 |
| | 9.3.3 | Efficiency of Simulating Flow and Transport | 9-8 |
| | 9.4 | ASSUMPTIONS AND CONSERVATISM OF THE UZFT APPROACH | 9-8 |
| 10 | SZFT MODULE DESCRIPTION | | 10-1 |
| | *J. Winterle, G. Wittmeyer, R. Rice, R. Janetzke, T. McCartin, R. Baca, D. Turner, D. Farrell, J. Menchaca* | | |
| | 10.1 | INFORMATION FLOW WITHIN TPA | 10-1 |
| | 10.1.1 | Information Supplied to SZFT | 10-1 |
| | 10.1.2 | Information Provided by SZFT | 10-1 |
| | 10.2 | INTERMEDIATE RESULTS | 10-1 |
| | 10.3 | CONCEPTUAL MODEL | 10-3 |
| | 10.3.1 | Saturated Zone Flow Model | 10-3 |
| | 10.3.2 | Saturated Zone Transport Model | 10-5 |
| | 10.4 | ASSUMPTIONS AND CONSERVATISM OF THE SZFT APPROACH | 10-6 |
| 11 | DCAGW MODULE DESCRIPTION—FARMING RECEPTOR GROUP | | 11-1 |
| | *P. LaPlante, M. Smith, C. McKenney, M. Muller, J. Weldy, G. Wittmeyer, M. Jarzemba, S. Mohanty, R. Rice, R. Fedors, L. Deere* | | |
| | 11.1 | INFORMATION FLOW WITHIN TPA | 11-1 |
| | 11.1.1 | Information Supplied to DCAGW | 11-1 |
| | 11.1.2 | Information Provided by DCAGW | 11-2 |
| | 11.2 | INTERMEDIATE RESULTS | 11-2 |
| | 11.3 | CONCEPTUAL MODEL | 11-2 |
| | 11.3.1 | Development of Radionuclide Concentrations in Water for a Farming Receptor Group | 11-3 |
| | 11.3.2 | Development of Dose Conversion Factors | 11-4 |
| | 11.4 | ASSUMPTIONS AND CONSERVATISM OF DCAGW APPROACH | 11-5 |
| 12 | DCAGW MODULE DESCRIPTION—RESIDENTIAL RECEPTOR GROUP | | 12-1 |
| | *M. Smith, P. LaPlante, M. Muller, G. Wittmeyer, M. Jarzemba, S. Mohanty, R. Rice, R. Fedors, C. McKenney, L. Deere* | | |
| | 12.1 | INFORMATION FLOW WITHIN TPA | 12-1 |
| | 12.1.1 | Information Supplied to DCAGW | 12-1 |
| | 12.1.2 | Information Provided by DCAGW | 12-2 |
| | 12.2 | INTERMEDIATE RESULTS | 12-2 |
| | 12.3 | CONCEPTUAL MODEL | 12-2 |
| | 12.3.1 | Development of Radionuclide Concentrations in Water for a Residential Receptor Group | 12-3 |

# CONTENTS (cont'd)


| Section | | | Page |
|---|---|---|---|
| | 12.3.2 | Calculation of Dose Conversion Factors | 12-5 |
| | 12.4 | ASSUMPTIONS AND CONSERVATISM OF DCAGW APPROACH | 12-6 |
| 13 | FAULTO MODULE DESCRIPTION | | 13-1 |
| | *J. Stamatakos, A. Ghosh, S. Mohanty, A.-B. K. Ibrahim* | | |
| | 13.1 | INFORMATION FLOW WITHIN TPA | 13-1 |
| | 13.1.1 | Information Supplied to FAULTO | 13-1 |
| | 13.1.2 | Information Provided by FAULTO | 13-1 |
| | 13.2 | INTERMEDIATE RESULTS | 13-1 |
| | 13.3 | CONCEPTUAL MODEL | 13-1 |
| | 13.4 | ASSUMPTIONS AND CONSERVATISM OF THE FAULTO APPROACH | 13-3 |
| 14 | VOLCANO MODULE DESCRIPTION | | 14-1 |
| | *B. Hill, C. Connor, J. Trapp, S. Mohanty* | | |
| | 14.1 | INFORMATION FLOW WITHIN TPA | 14-1 |
| | 14.1.1 | Information Supplied to VOLCANO | 14-1 |
| | 14.1.2 | Information Provided by VOLCANO | 14-1 |
| | 14.2 | INTERMEDIATE RESULTS | 14-1 |
| | 14.3 | CONCEPTUAL MODEL | 14-1 |
| | 14.4 | ASSUMPTIONS AND CONSERVATISM OF THE VOLCANO APPROACH | 14-4 |
| 15 | ASHPLUMO MODULE DESCRIPTION | | 15-1 |
| | *B. Hill, M. Jarzemba, C. Connor* | | |
| | 15.1 | INFORMATION FLOW WITHIN TPA | 15-1 |
| | 15.1.1 | Information Supplied to ASHPLUMO | 15-1 |
| | 15.1.2 | Information Provided by ASHPLUMO | 15-1 |
| | 15.2 | INTERMEDIATE RESULTS | 15-1 |
| | 15.3 | CONCEPTUAL MODEL | 15-2 |
| | 15.4 | ASSUMPTIONS AND CONSERVATISM OF THE ASHPLUMO APPROACH | 15-6 |
| 16 | ASHRMOVO MODULE DESCRIPTION | | 16-1 |
| | *R. Codell, M. Jarzemba, R. Manteufel* | | |
| | 16.1 | INFORMATION FLOW WITHIN TPA | 16-1 |
| | 16.1.1 | Information Supplied to ASHRMOVO | 16-1 |
| | 16.1.2 | Information Provided by ASHRMOVO | 16-1 |
| | 16.2 | INTERMEDIATE RESULTS | 16-1 |
| | 16.3 | CONCEPTUAL MODEL | 16-1 |
| | 16.4 | ASSUMPTIONS AND CONSERVATISM OF THE ASHRMOVO APPROACH | 16-3 |
| 17 | DCAGS MODULE DESCRIPTION—FARMING RECEPTOR GROUP | | 17-1 |
| | *P. LaPlante, J. Weldy, D. Esh, M. Jarzemba, C. McKenney, R. Abu-Eid* | | |

# CONTENTS (cont'd)


| Section | | | Page |
|---|---|---|---|
| | 17.1 | INFORMATION FLOW WITHIN TPA | 17-1 |
| | 17.1.1 | Information Supplied to DCAGS | 17-1 |
| | 17.1.2 | Information Provided by DCAGS | 17-1 |
| | 17.2 | INTERMEDIATE RESULTS | 17-1 |
| | 17.3 | CONCEPTUAL MODEL | 17-1 |
| | 17.4 | ASSUMPTIONS AND CONSERVATISM OF THE DCAGS APPROACH | 17-5 |
| 18 | | DCAGS MODULE DESCRIPTION—RESIDENTIAL RECEPTOR GROUP | 18-1 |
| | | *P. LaPlante, D. Esh, J. Weldy, M. Jarzemba, C. McKenney, R. Abu-Eid* | |
| | 18.1 | INFORMATION FLOW WITHIN TPA | 18-1 |
| | 18.1.1 | Information Supplied to DCAGS | 18-1 |
| | 18.1.2 | Information Provided by DCAGS | 18-1 |
| | 18.2 | INTERMEDIATE RESULTS | 18-1 |
| | 18.3 | CONCEPTUAL MODEL | 18-2 |
| | 18.4 | ASSUMPTIONS AND CONSERVATISM OF THE DCAGS APPROACH | 18-3 |
| 19 | | INPUT DATA | 19-1 |
| | | *S. Mohanty, R. Rice, R. Janetzke* | |
| | 19.1 | STRUCTURE OF THE *tpa.inp* FILE | 19-1 |
| | 19.2 | DEVELOPMENT OF INPUT FILE *tpa.inp* | 19-2 |
| | 19.2.1 | Problem Definition Keywords | 19-3 |
| | 19.2.1.1 | title | 19-3 |
| | 19.2.1.2 | iflag | 19-3 |
| | 19.2.1.3 | subarea | 19-4 |
| | 19.2.1.4 | aqueousnuclides | 19-6 |
| | 19.2.1.5 | endoffile | 19-7 |
| | 19.2.2 | Distribution Definition Keywords | 19-7 |
| | 19.2.2.1 | constant | 19-7 |
| | 19.2.2.2 | iconstant | 19-10 |
| | 19.2.2.3 | uniform | 19-10 |
| | 19.2.2.4 | iuniform | 19-10 |
| | 19.2.2.5 | loguniform | 19-11 |
| | 19.2.2.6 | normal | 19-11 |
| | 19.2.2.7 | lognormal | 19-12 |
| | 19.2.2.8 | beta | 19-12 |
| | 19.2.2.9 | logbeta | 19-13 |
| | 19.2.2.10 | triangular | 19-13 |
| | 19.2.2.11 | logtriangular | 19-13 |
| | 19.2.2.12 | exponential | 19-14 |
| | 19.2.2.13 | finiteexponential | 19-14 |
| | 19.2.2.14 | hazardcurve | 19-14 |

# CONTENTS (cont'd)


| Section | | | | Page |
|---|---|---|---|---|
| | | 19.2.2.15 | userdistribution | 19-15 |
| | | 19.2.2.16 | correlateinputs | 19-15 |
| | 19.3 | AUXILIARY DATA FILES | | 19-16 |
| | 19.4 | DISCUSSION ON GLOBAL PARAMETERS | | 19-16 |
| 20 | OUTPUT FILES | | | 20-1 |
| | *T. McCartin, R. Janetzke, R. Rice, S. Mohanty* | | | |
| | 20.1 | DESCRIPTION OF PRIMARY OUTPUT FILES | | 20-1 |
| | 20.2 | DESCRIPTION OF SECONDARY OUTPUT FILES | | 20-10 |
| | 20.3 | LIST OF OTHER OUTPUT FILES | | 20-10 |
| 21 | PROGRAM INSTALLATION AND EXECUTION | | | 21-1 |
| | *R. Janetzke, S. Mohanty* | | | |
| | 21.1 | SYSTEM ADMINISTRATION | | 21-1 |
| | | 21.1.1 | Installing Source Code from an 8-mm Tape | 21-1 |
| | | 21.1.2 | Customizing the Code for a Specific Host Machine | 21-1 |
| | | 21.1.2.1 | Customizing Using Environment Variables | 21-5 |
| | | 21.1.2.2 | Customizing By Changing Path References in the Source Code | 21-5 |
| | | 21.1.3 | Program Setup | 21-6 |
| | 21.2 | PROGRAM EXECUTION | | 21-7 |
| | | 21.2.1 | Input Preparation | 21-7 |
| | | 21.2.2 | Editing Basic Files in the User Work Space | 21-8 |
| | | 21.2.3 | Execution of the TPA Version 4.0 Code | 21-8 |
| | 21.3 | PORTABILITY LIMITATION OF TPA VERSION 4.0 CODE | | 21-8 |
| | 21.4 | USER SUPPORT | | 21-9 |
| | 21.5 | SOFTWARE QUALITY ASSURANCE | | 21-9 |
| | 21.6 | TROUBLESHOOTING | | 21-10 |
| 22 | TOOLS FOR SUPPLEMENTARY ANALYSES | | | 22-1 |
| | *R. Janetzke, S. Mohanty, R. Rice* | | | |
| | 22.1 | TOTAL COMPLEMENTARY CUMULATIVE DISTRIBUTION FUNCTION CODE | | 22-1 |
| | | 22.1.1 | Complementary Cumulative Distribution Function | 22-1 |
| | | 22.1.2 | Conditional Complementary Cumulative Distribution Function | 22-2 |
| | | 22.1.3 | Total Complementary Cumulative Distribution Function | 22-3 |
| | | 22.1.4 | Total Complementary Cumulative Distribution Function Code | 22-3 |
| | | 22.1.5 | Total Complementary Cumulative Distribution Function Input Description | 22-4 |
| | 22.2 | IMPORTANCE ANALYSES | | 22-5 |

# CONTENTS (cont'd)


Section Page

23 FUTURE IMPROVEMENTS TO THE TPA CODE ..... 23-1
*D. Esh, T. McCartin*

24 REFERENCES ..... 24-1

INDEX

APPENDIX A REFERENCE DATA SET
*M. Smith, O. Pensado, M.R. Byrne, J. Weldy, S. Mohanty, D. Esh, S. Brossia, T. McCartin, R. Codell, R. Fedors, D. Farrell, D. Sims, J. Ciocco, J. Stamatakos, S. Stothoff, B. Leslie, R. Pabalan, D. Turner, G. Wittmeyer, S. Hsiung, P. LaPlante, G. Cragnolino, B.J. Davis, T. Ahn, R. Green, M. Jarzemba, C. McKenney, W. Murphy, H.L. McKague, B. Hill, C. Connor, N. Coleman, J. Winterle, J. Bradbury, R. Fedors, L. Yang, A. Ghosh*

APPENDIX B AUXILIARY INPUT DATA FILES
*R. Rice, S. Mohanty, R. Janetzke, M. Smith, R. Fedors, R. Benke, S. Mayer, S. Stothoff, J. Winterle*

APPENDIX C UTILITY MODULE DESCRIPTION
*S. Mohanty, R. Janetzke, R. Rice, R. Codell, J. Weldy*

APPENDIX D PROBABILITY DISTRIBUTION FUNCTIONS
*R. Codell, S. Mohanty, R. Rice*

APPENDIX E INTERMEDIATE DATA TRANSFER FILES
R. Janetzke, R. Rice, S. Mohanty

APPENDIX F EBSREL FLOW FACTOR DERIVATION
*R. Codell, D. Esh*

APPENDIX G DIET OF THE EXPOSED GROUP FROM LOCAL SOURCES
*P. LaPlante, M. Smith*

APPENDIX H ITYM PREPROCESSOR DESCRIPTION
*S. Stothoff, R. Fedors*

# FIGURES


| Figure | | Page |
|---|---|---|
| 1-1 | Map location of Yucca Mountain region | 1-5 |
| 2-1 | Repository system | 2-2 |
| 2-2 | Saturated zone conceptual model representation showing the 20-km receptor location and boundaries of the three saturated zone streamtubes | 2-4 |
| 3-1 | Flow Diagram for TPA Version 4.0 code | 3-3 |
| 3-2 | Examples of the three consequence module implementations used in the TPA Version 4.0 code: (a) table look-up, (b) subroutines(s), and (c) external stand-alone program | 3-6 |
| 3-3 | TPA Version 4.0 code screen output | 3-9 |
| 3-4 | Beta densities for various choices of the parameters $p$ and $q$ (Iman and Shortencarier, 1984) | 3-15 |
| 3-5 | Examples of (a) uniform, (b) loguniform, (c) normal, (d) lognormal, (e) triangular, and (f) log-triangular distributions | 3-16 |
| 3-6 | Examples of (a) exponential, (b) finite exponential, (c) beta, and (d) user-defined (e) log-beta, and (f) integer-uniform distributions | 3-17 |
| 3-7 | Example of specified correlation between two sampled parameters | 3-19 |
| 3-8 | $^{243}Cm$, $^{244}Cm$, $^{245}Cm$, and $^{246}Cm$ decay chains | 3-22 |
| 3-9 | Radionuclide inventories as a function of time (calculated by the INVENT module) | 3-23 |
| 4-1 | UZFLOW conceptual model | 4-3 |
| 4-2 | Boundary of proposed Yucca Mountain repository with only eight subareas (1–8) filled | 4-4 |
| 4-3 | Response of mean annual infiltration with changes in mean annual precipitation during a climate cycle: (a) mean climate signal only, and (b) with perturbation | 4-6 |
| 5-1 | Heat sources represented as parallel lines in the modeled repository region for the NFENV module | 5-3 |
| 5-2 | Mountain-scale heat transfer model with line sources | 5-4 |
| 5-3 | Plan view of repository showing emplacement drifts and waste packages | 5-6 |
| 5-4 | Schematic showing (a) waste package, drip shield, and backfill emplacement in a drift (2D cross-section); (b) idealization of the emplacement for performing thermal calculation | 5-7 |
| 5-5 | Internals of a large waste package | 5-11 |
| 5-6 | Time evolution of chloride concentration at the drift wall computed by the MULTIFLO code | 5-15 |
| 5-7 | Conceptualization of drift-scale thermal hydrologic model | 5-17 |
| 7-1 | (a) Waste package equivalent beam and (b) waste package vertical supports for SEISMO | 7-3 |
| 7-2 | SEISMO stress-strain relationship | 7-6 |
| 8-1 | Schematic of bathtub model with incoming and outgoing water conduits | 8-3 |
| 8-2 | Schematic drawing for advective mass transfer from the waste package to the host rock | 8-6 |

# FIGURES (cont'd)


| Figure | | Page |
|---|---|---|
| 9-1 | UZFT contaminant transport legs | 9-7 |
| 10-1 | Saturated zone streamtubes model showing three streamtubes from just upgradient of the repository footprint southward to the proposed 20-km compliance boundary | 10-2 |
| 11-1 | Farmer exposure pathways | 11-6 |
| 13-1 | Simulated faults within the repository boundary | 13-4 |
| 14-1 | Schematic of subsurface disruption associated with extrusive volcanic events | 14-3 |
| 15-1 | ASHPLUMO contaminant release and deposition | 15-3 |
| 16-1 | A plot of the areal radionuclide density as a function of time for radionuclide in the $^{245}Cm$ decay chain | 16-5 |
| 17-1 | Cases where fraction of resuspended mass that emanated from the contaminated volcanic ash layer ($f_R$): (a) is unity and (b) is less than unity | 17-4 |
| 22-1 | Example complementary cumulative distribution function | 22-2 |

# TABLES


| Table | | Page |
|---|---|---|
| 1-1 | Comparison TSPA-VA and EDA II Design | 1-7 |
| 3-1 | Current implementation for consequence modules in the TPA Version 4.0 code | 3-8 |
| 3-2 | Latin Hypercube Sampling distribution functions | 3-13 |
| 3-3 | List of 43 nuclides in the INVENT database | 3-21 |
| 5-1 | Initial fluid composition and pH corresponding to J-13 well water (adapted from Harrar et al., 1990) | 5-14 |
| 8-1 | Reactions and mass action relations | 8-9 |
| 8-2 | Parameters for the Van't Hoff equation | 8-10 |
| 9-1 | Hydrostratigraphic thicknesses (m) for each of the 10 repository subareas extending from the repository horizon to the water table | 9-3 |
| 11-1 | Categories used for age-dependent dose calculations for farming receptor group | 11-6 |
| 12-1 | Categories used for age-dependent dose calculations for residential receptor group | 12-7 |
| 16-1 | A listing of the nonradionuclide specific data used in estimating the surficial radionuclide areal density for members of the $^{245}$Cm decay chain | 16-4 |
| 16-2 | A listing of the radionuclide-specific data used in estimating the surficial radionuclide areal density for members of the $^{245}$Cm decay chain | 16-4 |
| 19-1 | List of 43 radionuclides in the TPA Version 4.0 code with associated half-lives, isotopic weights, initial waste package inventories | 19-8 |
| 19-2 | Description of auxiliary data files | 19-18 |
| 20-1 | TPA Version 4.0 code primary output files | 20-2 |
| 20-2 | Detailed data structure for the primary output files | 20-4 |
| 20-3 | Stand-alone cumulative files | 20-12 |
| 20-4 | Consequence module output files | 20-12 |
| 20-5 | Consequence module input echo files | 20-13 |
| 20-6 | Other useful output files | 20-14 |

# TABLES (cont'd)


| Table | | Page |
|---|---|---|
| 21-1 | TPA Version 4.0 code *tpa* directory files | 21-2 |
| 21-2 | TPA Version 4.0 code *tpa/data* directory files | 21-3 |
| 21-3 | Files associated with TPA Version 4.0 code *tpa/codes* directory | 21-3 |
| 21-4 | Files associated with TPA Version 4.0 code *tpa/ccdf* directory | 21-3 |
| 21-5 | Files associated with TPA Version 4.0 code *tpa/ccdf/gentpa* directory | 21-4 |
| 22-1 | Possible values for *nnn* | 22-5 |

# ACRONYMS

| | |
|---|---|
| 1D | one-dimensional |
| 2D | two-dimensional |
| 3D | three-dimensional |
| AML | areal mass loading |
| BWR | boiling water reactor |
| CCDF | complementary cumulative distribution function |
| CDF | cumulative distribution function |
| CLST | Container Life and Source Term |
| CM | consequence module |
| CNWRA | Center for Nuclear Waste Regulatory Analyses |
| CP | compliance point |
| DCF | dose conversion factor |
| DCM | dual continuum model |
| DEM | digital elevation model |
| DOE | U.S. Department of Energy |
| DVM | distributed velocity method |
| EBS | engineered barrier system |
| ECM | equivalent continuum model |
| EDA II | enhanced design alternative II |
| EPA | U.S. Environmental Protection Agency |
| ENFE | evolution of the near-field environment |
| EPRI | Electric Power Research Institute |
| ESF | Exploratory Studies Facility |
| GWd | gigawatt-day |
| GWTT | groundwater travel time |
| HLW | high-level waste |
| IA | igneous activity |
| IPA | iterative performance assessment |
| IRSR | issue resolution status report |
| ITYM | infiltration tabulator for Yucca Mountain |
| JS | joint spacing |
| KTI | key technical issue |
| LA | license application |
| LHS | Latin Hypercube Sampling |
| *MAI* | mean annual infiltration |
| *MAP* | mean annual precipitation |
| *MAT* | mean annual temperature |
| MAV | mean annual atmospheric vapor density |
| MCS | Monte Carlo Sampling |
| NIST | National Institute of Standards and Technology |
| MTU | metric tons of uranium |
| NFENV | near-field environment |
| PA | performance assessment |
| PDF | probability density function |

# ACRONYMS (cont'd)

| | |
|---|---|
| PWR | pressurized water reactor |
| QA | quality assurance |
| RH | relative humidity |
| RT | radionuclide transport |
| SF | spent fuel |
| SR | site recommendation |
| SRCR | site recommendation considerations report |
| SS | stainless steel |
| SZ | saturated zone |
| TEDE | total effective dose equivalent |
| USFIC | Unsaturated and Saturated Flow under Isothermal Conditions |
| TPA | Total-system Performance Assessment |
| TPI | time period of interest |
| TSPA | total system performance assessment |
| TSPAI | total system performance assessment and Integration |
| UDEC | Universal Distinct Element Code |
| U.S. NRC | U.S. Nuclear Regulatory Commission |
| UTM | Universal Transverse Mercator |
| UZ | unsaturated zone |
| VA | viability assessment |
| WP | waste package |
| YM | Yucca Mountain |
| YMR | Yucca Mountain region |

# FOREWORD

In accordance with the provisions of the Nuclear Waste Policy Act of 1982, the U.S. Nuclear Regulatory Commission (NRC) has the responsibility to evaluate any license application (LA) for geological repositories constructed for emplacement of high-level nuclear waste (HLW) (i.e., commercial spent fuel and vitrified HLW). This act was amended in 1987 to designate one site for detailed characterization in the unsaturated region of the tuffaceous rocks of Yucca Mountain (YM), in part located on the Nevada Test Site in southern Nevada. To execute its mandated prelicensing and licensing functions, the NRC staff will review the critical aspects of the U.S. Department of Energy (DOE) total system performance assessment for the site recommendation considerations report (TSPA-SRCR) and any potential LA. In addition to these reviews, the NRC also will develop preliminary comments on the sufficiency of the at-depth site characterization program and adequacy of the waste form. Although the DOE TSPA-SRCR is not a licensing document, the NRC staff will review the document as a basis for future reviews of DOE's draft LA to develop its sufficiency comments, which will be included as part of DOE's site recommendation. The principal approach the staff will use to evaluate these products is the evaluation of total system performance.

In support of these review activities, the NRC staff is focusing on detailed technical assessments to obtain a quantitative understanding of the isolation characteristics and capabilities of the proposed repository system at the YM site. Concurrent with these assessment studies, the NRC and its support contractor, the Center for Nuclear Waste Regulatory Analyses (CNWRA), are enhancing the Total-system Performance Assessment (TPA) computer code. The TPA code is designed to simulate the behavior of the geologic repository taking into account the essential characteristics of the natural barriers and the engineered barrier system, as well as the evolutionary changes in the definition of the geologic setting (i.e., climate, seismicity, faulting, and volcanism). This document presents the latest version of the TPA code, designated as 4.0. This version succeeds two previous versions, the first version (3.1.4) was released as a NUREG (NUREG-1668) and the second version (3.2) as a CNWRA report. Staff used these two versions to review the critical aspects of the DOE viability assessment. This interim version of the code is expected to be succeeded in the near term by an improved version prior to the review of the potential LA.

It is important to note that the TPA Version 4.0 code was developed to allow the NRC and CNWRA staffs to perform interim evaluations of the DOE total system performance assessment approaches and parameter values used to estimate the performance of the proposed HLW repository. Because investigations at the YM site are ongoing and the analyses are iterative, the TPA Version 4.0 code was developed with flexibility to analyze a variety of designs, site characteristics, and compliance demonstration factors. It is also important to note that the particular conceptual models and assignment of initial model parameter values (and distributions) in this description of the TPA code do not constitute regulatory acceptance. It is expected that at the time of licensing, different conceptual models and parameter values and distributions will be used in performance assessments. Thus, estimates of the performance using the TPA Version 4.0 code do not represent a regulatory determination of total system performance for the YM site.

# ACKNOWLEDGMENTS

This report was prepared to document work performed by the Center for Nuclear Waste Regulatory Analyses (CNWRA) for the Nuclear Regulatory Commission (NRC) under Contract No. NRC-02-97-009. The activities reported were performed on behalf of the NRC Office of Nuclear Material Safety and Safeguards, Division of Waste Management. The report is an independent product of the CNWRA and does not necessarily reflect the views or regulatory position of the NRC.

# TPA VERSION 4.0 CODE

This report is an updated version of the user's guide for the TPA code Versions 3.1.4 and 3.2. This report presents several conceptual and code design changes; the basic framework of the code and the user's guide is essentially the same as the user's guide for the TPA Version 3.2 code.

The authors wish to thank R. Benke, D. Dunn, D. Esh, D. Farrell, R. Fedors, D. Gute, B. Hill, R. Janetzke, O. Pensado, M. Smith, J. Weldy, J. Winterle, and G. Wittmeyer of the CNWRA for their thorough technical reviews and numerous helpful technical comments. The authors also thank B. Sagar for the programmatic review and valuable suggestions for improving the quality of the report. Technical support provided by R. Rice (consultant) at various stages and in almost all parts of this report is gratefully acknowledged. Thanks are also expressed to M. Muller and J. Menchaca (Southwest Research Institute) for their help in code development and testing. The authors appreciate the editorial reviews conducted by the staff of Publications Services at Southwest Research Institute—especially the efforts of C. Cudd. C. Gray, B. Long, and A. Woods. Skillful formatting help was provided by L. Selvey at the CNWRA. The authors are particularly grateful for the secretarial support of J. Gonzalez, A. Mandujano, C. Patton, and A. Ramos.

Numerous CNWRA and NRC staff members tested the TPA Version 4.0 code: R. Benke, S. Brossia, R. Codell, D. Esh, W. Illman, R. Janetzke, S. Mayer, M. Menchaca, S. Mohanty, T. McCartin, R. Rice, M. Smith, and J. Weldy. Their efforts are gratefully acknowledged. D. Sims provided help in generating ArcView plots.

In preparing this document and in developing the Total-system Performance Assessment (TPA) Version 3.2 code, numerous individuals made strong technical contributions. Insofar as was possible, those who contributed to writing the report, developing the conceptual models, and programming and testing the code have been recognized by listing their names after the appropriate chapter and section headings in the table of contents. The lead author identified in the table of contents for each chapter, section, or appendix is the designated point of contact. The effort of D. Esh in coordinating NRC technical support for modifying the TPA code from Version 3.2 to 4.0 is recognized. T. McCartin coordinated NRC technical support for the TPA Version 3.1.4 and 3.2 codes and user's guide development effort. G. Wittmeyer, the element manager for the Total System Performance Assessment and Integration (TSPA&I) key technical issue (KTI) at the CNWRA, who coordinated production of this user's guide is also recognized.

# TPA VERSION 3.2 CODE

T. McCartin and S. Mohanty coordinated NRC and CNWRA technical efforts for the development of TPA Version 3.2 code and the user's guide. The coordinators wish to thank M.P. Miklas, Jr., E.C. Pearcy, and N. Sridhar (CNWRA) for their thorough technical reviews and numerous helpful technical comments. The coordinators also thank B. Sagar, K. McConnell, and P. Mackin for programmatic reviews and valuable suggestions to improve the quality of the report. Technical support provided by R. Rice (consultant) at various stages and in almost all parts of this report is gratefully acknowledged. The authors appreciate the thorough editorial reviews conducted by the staff of Publications Services at Southwest Research Institute—especially the efforts of B. Ford, C. Gray, S. Harley, B. Long, and A. Woods. Skillful formatting help was provided by B. Caudle, L. Moreno, and J. Wike (CNWRA). The authors are particularly grateful for the secretarial support of C. Garcia, L. Selvey, and A. Brune without whose extra effort this report could not have been produced in a timely manner. Thanks are also expressed to K. Poor (Portage Environmental, Inc.), J. Bogan (consultant), and C. Scherer (Southwest Research Institute) for their assistance in reviewing the document, testing the code, and preparing quality assurance-related documentation. Several staff members tested the initial version of the code. Their contributions are acknowledged and much appreciated. The efforts of C. Lui and J. Firth, TSPA&I in coordinating the preparation of this user's guide are also recognized.

# QUALITY OF DATA AND CODE DEVELOPMENT

**DATA**: CNWRA-generated data contained in this report meet quality assurance (QA) requirements described in the CNWRA QA Manual. Data from other sources, however, are freely used. The respective sources of non-CNWRA data should be consulted for determining levels of QA.

**CODE**: The TPA Version 4.0 code has been developed following the procedures described in the CNWRA Technical Operating Procedure (TOP) 018, which implements the QA guidance contained in the CNWRA QA Manual.

# 1 INTRODUCTION

To more effectively fulfill its statutory responsibilities for the prelicensing and licensing actions for the proposed high-level waste (HLW) repository at the Yucca Mountain (YM) site, the U.S. Nuclear Regulatory Commission (NRC) has focused its repository program on resolving issues most critical to overall system performance. This has led to a major restructuring of the NRC HLW program to encompass 10 key technical issues (KTIs) (Sagar, 1997). Limiting the program scope to these KTIs was necessary to focus and streamline the regulatory decision making process. In addition, the use of the KTI framework provides a vehicle for ensuring early, clear, and sound technical feedback to the U.S. Department of Energy (DOE) regarding possible licensing vulnerabilities in the DOE safety case for the proposed YM repository.

Some of the core objectives of the restructured NRC HLW repository program are to

- Evaluate the DOE repository program [including field studies, laboratory experiments, and performance assessments (PA)] to provide early feedback to the DOE
- Evaluate the attributes of the DOE Repository Safety Strategy, Total System Performance Assessment (TSPA)—Site Recommendation (SR), and TSPA—License Application (LA)
- Provide input for the NRC management decision making on prioritization of the KTIs and related subissues
- Assist the NRC KTI teams with resolution of individual subissues
- Provide support for the NRC rulemaking for the HLW repository

The NRC Total System Performance Assessment and Integration (TSPAI) KTI, through the Total-system Performance Assessment (TPA) activity, contributes significantly towards achieving these important objectives.

One of the important prerequisites to pursuing the aforementioned program objectives is development of a generalized computer code, specifically tailored for evaluating the total system performance for the proposed repository at the YM site. Although the NRC previously developed computer codes (Codell et al., 1992; Wescott et al., 1995) to analyze repository performance, a more general and versatile TSPA code was necessary to (i) accommodate the most current DOE repository design [e.g., repository layout, waste package (WP), and emplacement design]; (ii) quantify total system performance in terms of the new compliance performance measure (i.e., annual individual dose or risk) expected in the forthcoming U.S. Environmental Protection Agency (EPA) standard and new NRC HLW regulation; and (iii) include the latest site data (e.g., tracer testing at C-well complex), knowledge base, and improved models. In addition, a versatile and user-friendly computer code was needed because the code will be used by a wide spectrum of individuals with diverse technical backgrounds.

This user's guide was prepared to facilitate the effective use of the TPA Version 4.0 computer code, which was recently developed through a joint effort between the NRC and the Center for Nuclear Waste Regulatory Analyses (CNWRA) staffs. This report contains descriptions of the conceptual and mathematical models; instructions for preparing input files, code installation, and execution; explanation of options for

generating various intermediate and summary outputs; and example input files for the basecase scenario class.

## 1.1 TPA CODE

One of the basic purposes for using the TPA Version 4.0 code to simulate performance of the proposed repository is to secure a detailed and quantitative understanding of the key factors controlling (i) the degradation of the engineered barrier system (EBS), (ii) release of the waste from the repository, (iii) subsequent transport of the waste through various environmental pathways, and (iv) possible human exposure at the location(s) of the designated receptor group. To achieve this understanding, the total repository system is modeled in a probabilistic manner (Thompson and Sagar, 1993) that considers significant physical and chemical processes, phenomenological interactions and couplings, and potentially disruptive events and processes. This probabilistic approach, although computationally intensive, yields a range of potential future evolutions of the repository system. In addition, this approach is widely favored because it avoids many of the technical shortcomings associated with completely deterministic scenario-based assessments such as inability to account for uncertainty in model parameter and site characterization data (Thompson, 1988).

To date, three TSPAs for the proposed YM repository have been conducted by the NRC and the CNWRA using the probabilistic approach. The first TSPA, referred to as Iterative Performance Assessment (IPA) Phase 1 (Codell et al., 1992), was conducted to assemble and demonstrate the NRC assessment methodology. The second TSPA, designated as IPA Phase 2 (Wescott et al., 1995), was performed using the TPA Version 2.0 code and those analyses yielded many valuable insights into the features, events, and processes influencing isolation performance of the proposed YM repository; these insights were put to use in the NRC and CNWRA reviews of early DOE TSPAs for YM. The third TSPA[1] emphasized updating and advancing the NRC TSPA capability for reviewing the DOE TSPA-viability assessment (VA) (TRW Environmental Safety Systems, Inc., 1996) and for assisting the NRC in focusing the KTI activities on technical issues of critical importance to repository performance. In the current effort, the IPA activity places emphasis on (i) updating the NRC TSPA capability in preparation for the forthcoming review of the DOE TSPA-SR (TRW Environmental Safety Systems, Inc., 1999) and (ii) resolving remaining subissues identified in the issue resolution status report (IRSR) (U.S. Nuclear Regulatory Commission, 1999a).

Consistent with the recommendations of IPA Phase 2 (Wescott et al., 1995), the TPA Version 4.0 code and its predecessor, TPA Version 3.2 code, were developed to include

- Most recent site data and knowledge base for conceptual models
- Most recent repository design specifications
- Updated abstractions for features, events, and processes (FEPs)
- Streamlined data transfers between executive and consequence modules

---

[1]Mohanty, S., R. Codell, R.W. Rice, J. Weldy, Y. Lu, M.R. Byrne, T. J. McCartin, M. Jarzemba, and G.W. Wittmeyer. *System-Level Repository Sensitivity Analyses Using TPA Version 3.2 Code.* NUREG–1721. Washington, DC: U.S. Nuclear Regulatory Commission. Accepted for publication. 2000.

- More flexible design to accommodate future code modifications
- Improved computational algorithms permitting more detailed analyses
- Improved capabilities for parameter importance analysis and ranking

Federal radiation protection standards and regulations for HLW disposal in geologic repositories are being developed by the EPA and the NRC. Site data continue to be acquired, and repository and WP designs continue to evolve. Therefore, it was deemed important to enhance the TPA Version 4.0 code by increasing its flexibility to evaluate alternative repository and design features, analyze the effect of different areal mass loadings (AML), assess the significance of various disruptive scenario classes, assess the impact of radionuclide dilution in the saturated zone (SZ), and compute the peak dose for a 10,000-yr compliance period or longer time periods that may be of interest.

The TPA Version 4.0 code is composed of an executive driver program with a set of consequence modules and a library of utility modules. The executive driver controls the sampling of stochastic input parameters, the calculational sequence and data transfers between modules, and the production of output files. Various intermediate output files are generated for later use in parameter importance analyses, postprocessing of time-dependent risk curves, and synthesis of statistical distributions [e.g., cumulative distribution functions (CDF) and complementary cumulative distribution functions (CCDFs)] for appropriate performance measures. Utility modules ensure that consistent data sets and computational algorithms are used by all consequence modules and facilitate the discretization of the repository system and surrounding geologic media.

Development of the TPA Version 4.0 code, which is an update of Version 3.2, took place over several stages. Development at various stages involved technical contributions from KTIs other than the TSPAI KTI. Noteworthy contributions include

- Unsaturated and Saturated Flow under Isothermal Conditions KTI—Improved information on climate, shallow infiltration through vegetated soil, distribution of infiltration over the repository area, focusing of flow on WPs, and information for sampling the length of the alluvium transport path
- Container Lifetime and Source Term KTI—Consideration of drip shield, new WP design, and source term models describing a range of spent fuel (SF) dissolution modes and rates
- Evolution of the Near-Field Environment KTI—Estimates of the chemical composition of the aqueous environment contacting the WP
- Radionuclide Transport KTI—Updated estimates of near-field radionuclide solubilities and far-field sorption coefficients
- Thermal Effects on Flow KTI—Improved capability to predict time-dependent temperature and relative humidity (RH) in the presence of ventilation and backfill for use in the source term module
- Structural Deformation and Seismicity KTI—Improved hydrostratigraphic model and a new faulting consequence module

- Igneous Activity KTI—Alternative conceptual model for magma intrusion, improved technical basis for (i) probability and scenario characteristics for volcanic activity and (ii) effect of ash dispersal and mass loading on resulting dose to an individual from the receptor group

- Repository Design and Thermal-Mechanical Effects KTI—Improved modeling capability for the seismic consequence module

- Activities Related To Development of the NRC HLW Regulations KTI—More realistic representation of plume dilution induced by receptor group well pumping

To focus code development, various phenomena governing the total system were broken down into a total of 14 integrated subissues (ISIs). The ISIs were used in model abstraction methodology to emphasize that a high level of integration is necessary when evaluating a complex process with many components. The ISIs required involvement of technical staff from various KTIs. The specific KTIs that were involved in the model abstraction to address ISIs were determined on the basis of KTI subissues linked to a given ISI.

In addition to contributing to the development of the new TPA Version 4.0 code and its predecessors, KTI staff members participated in the testing and documentation of the code as well as in preparation of the input data set for the reference case.

## 1.2 DESCRIPTION OF THE PROPOSED REPOSITORY SITE

The conceptual and mathematical models included in the code largely were selected to be specific to the characteristics and conditions of the YM site. For completeness, a brief description of the YM site geology, hydrology, climatology, and current repository design are presented in this section.

Located in Nye County, the YM site (see figure 1-1) is approximately 120 km (75 mi) northwest of Las Vegas in southern Nevada. The site is entirely on federal land mostly controlled by the DOE, Bureau of Land Management, and Nellis Air Force Range. Climate at the site is generally arid to semiarid, with an average precipitation of about 180 mm/yr in the form of winter snow and summer thunderstorms. The YM area exhibits sparse vegetation and has a relatively low population density.

YM is an irregularly shaped cuesta 40 km long by 6 to 10 km wide, located in the southern part of the Great Basin, the northernmost subprovince of the Basin and Range Physiographic Province. The crest of the mountain varies between altitudes of 1,500 and 1,930 m or about 650 m higher than the floor of Crater Flat to the west of the site. The mountain is dominated by a subparallel series of north-trending ridges and valleys controlled by steeply dipping faults. YM is bounded by Crater Flat on the west, by Jackass Flat-Fortymile Wash on the east and southeast, by the Amargosa Desert to the south, and by the Timber Mountain Caldera complex to the north. The stratigraphy at YM is composed of a gently dipping sequence of Micocene ash-flow tuffs, lavas, and volcanic breccias more than 1,800-m thick. The rock unit being considered for the repository facility is a densely welded ash-flow tuff of the Topopah Spring Member of the Paintbrush Tuff. There are considerable data for the hydraulic and transport properties of the unsaturated zone (UZ) in Wittwer et al. (1995), Rautman et al. (1995), Schenker et al. (1995), Flint et al. (1996), Flint (1998), and Civilian Radioactive Waste Management System, Management and Operating Contractor (1998).

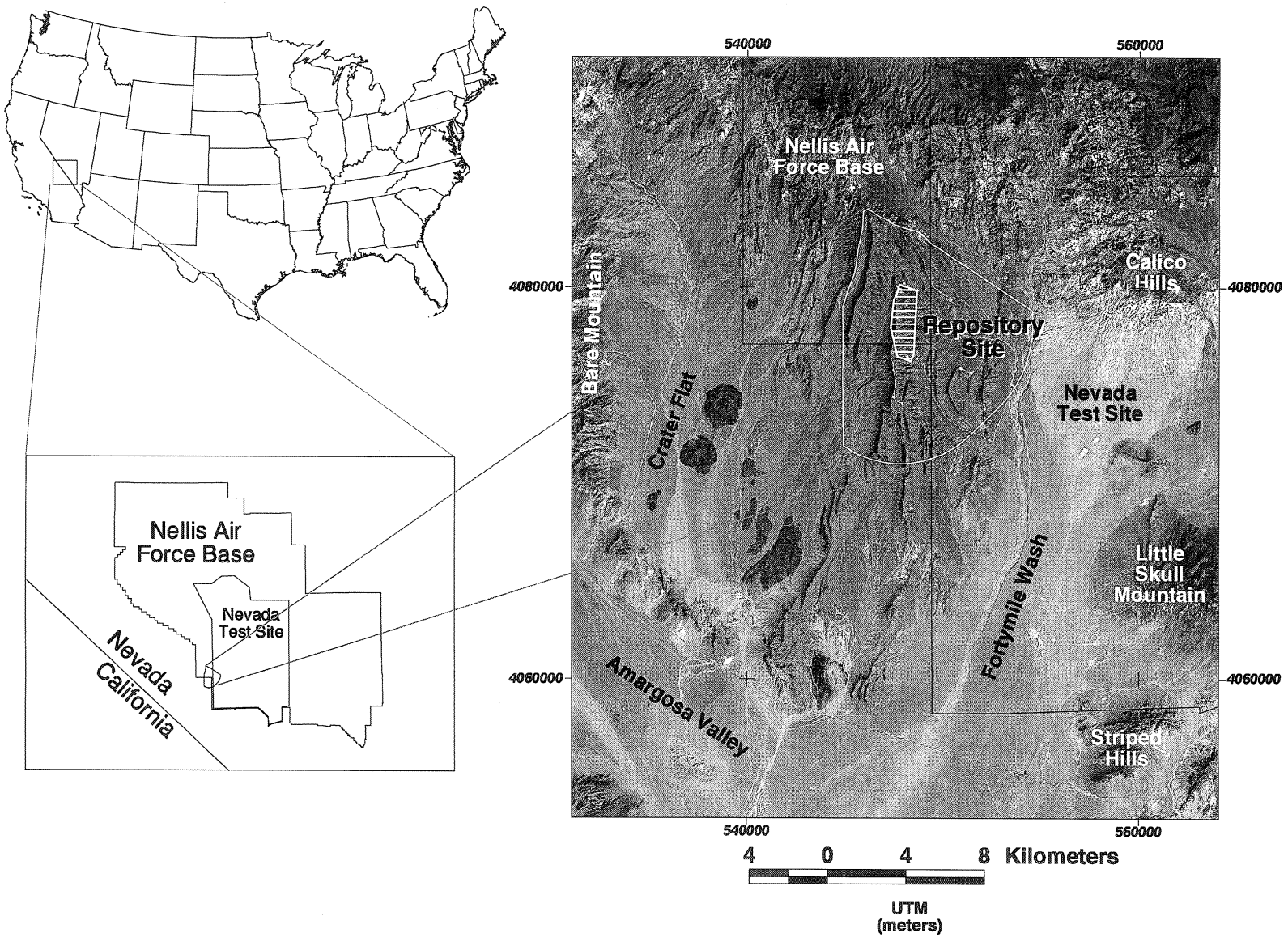


**Figure 1-1. Map location of Yucca Mountain region**

The SZ in the YM region (YMR) can be divided into two major aquifer systems, a fractured tuff aquifer below the repository location extending approximately 5–20 km downgradient and an alluvial aquifer extending southward from the terminus of the tuff aquifer to the Amargosa Desert. Patterns of groundwater flow in the tuff aquifer appear to be determined by the combined effects of hydraulic boundary conditions, dipping layers, and the presence of fault zones and laterally extensive shear fracture zones (Geldon, 1993). In contrast, groundwater flow in the alluvial aquifer is likely controlled by the interrelationship of recharge and discharge areas, interbasin transfers, and water well pumping in the Amargosa Desert area. Modeling studies of regional groundwater flow have been published by the U.S. Geological Survey (e.g., Czarnecki and Waddell, 1984; D'Agnese et al., 1997).

Depth to groundwater varies from over 350 m directly below the repository block at YM to less than 10 m along a short reach of the Amargosa River in the south central portion of the Amargosa Desert. Water quality throughout the YM and Amargosa Desert regions is generally adequate to drink, to water stock, and to irrigate crops. In the southern Amargosa Desert, however, evaporites from lacustrine deposits cause the groundwater to have total dissolved solids concentrations in excess of 10,000 ppm (Winograd and Thordarson, 1975). Near the communities of Amargosa Valley and Death Valley Junction, there are small clusters of water wells. Agricultural uses of groundwater are currently confined to the southern Amargosa Desert where depths to water range from 10 to 40 m and the topography is suitable for flood and center pivot irrigation.

The proposed repository at YM would be of an underground facility designed to accommodate 70,000 metric tons of HLW. The waste disposed in the repository is expected to consist of both commercial spent fuel (SF) (~90 percent) and defense and other HLW (~10 percent), with an age between 5 and 50 yr. The specific layout of the underground facility is based on the DOE new enhanced design alternative (EDA) II, also referred to as Hot Drift Cool Pillar design (Civilian Radioactive Waste Management System, Management and Operating Contractor, 1999a). The EDA II design specifications are presented in table 1-1. Through the thermal loading strategy that includes an 81-m drift spacing, the DOE intends to limit the heating of rock between drifts (i.e., pillars) so that a significant portion of the pillars may remain below the boiling temperature for water. Thus, infiltrating and thermally driven water above the repository may flow through the cool pillars. The rock in the immediate vicinity of the drifts may be heated above boiling, which may reduce seepage into the drift during the thermal period. The cool pillars and dry drifts are created using wide drift spacing (table 1-1), close WP spacing, proper blending of the HLW to reduce variation in WP heat outputs, and active ventilation from the time of waste emplacement through the 50–150- yr period before closure. Reducing the spacing between WPs will require fewer drifts, and thus allow for the larger drift spacing compared to the previous design, without significantly increasing repository area.

The key engineered barriers for EDA II include the WP, drip shield, and backfill. The WP design for HLW disposal consists of a large cylinder (i.e., approximately 1.8-m diameter and 5.6-m length) that includes a 20-mm-thick Alloy 22 outer overpack and a 50-mm-thick stainless steel (SS) type 316L inner overpack.

The inner overpack is designed to provide structural strength during the lifetime of the WP to prevent mechanical failure as a result of rockfall. The WP will be emplaced in the drift on v-shaped supports. A steel ground support and invert with sand or gravel ballast replaces the concrete liner specified in the VA design. A drip shield, made of Ti grade 7, covers the top and side of the WP and extends over the length of the emplacement drift. The drip shield is intended to protect the WP from dripping on the WP surface, especially during the thermal reflux period when the environmental conditions could be conducive to crevice corrosion of the Alloy 22 outer overpack. After repository closure, the backfill covering the drip

**Table 1-1. Comparison TSPA-VA and EDA II Designs**

| Design Characteristics | TSPA-VA | EDA II |
|---|---|---|
| Total access drift length | — | 33,400 m |
| Areal mass loading | 85 MTHM/acre | 60 MTHM/acre |
| Emplacement in upper block | — | ~1,050 acres |
| Drift spacing | 28 m | 81 m (center-to-center) |
| Drift diameter | 5.5 m | 5.5 m |
| Invert | Concrete liner | Steel with sand or gravel ballast |
| Number of waste packages (WP) | 10,500 | 10,039 |
| Total length of emplacement drifts | 107 km | 54 km |
| WP materials | 10-cm carbon steel over 2-cm Alloy-22 | 2-cm Alloy-22 over 5-cm SS 316L |
| Maximum WP capacity | 21 pressurized water reactor (PWR) assemblies | 21 PWR assemblies |
| Peak WP power (blending) | 95% above average PWR WP power | 20% above average PWR WP power |
| Drip shield | None | 2 cm Ti-7 |
| Backfill | None | Yes (may become an option) |
| WP heat output at emplacement Maximum Average (PWR WP) | — | 20 percent blending used to reduce maximum |
| Preclosure period | 50 yr | 50–150 yr |
| Preclosure ventilation rate | 0.1 $m^3/s$ | 2–10 $m^3/s$ air flow in emplacement drifts over 50-yr period |

shield will prolong hot, dry conditions in the drifts and provide added protection to the WP against rockfall. Prior to repository closure, the EDA II design relies on active ventilation of the loaded emplacement drifts to remove a substantial fraction of the heat emitted by the waste and thus limit temperature-induced cladding failure. Ventilation may also control the RH during the preclosure period.

## 1.3 REPORT CONTENT

This user's guide was prepared as the reference document for the TPA Version 4.0 code and provides information on the system parameters, conceptual models, and code outputs essential to interpretation of calculational results. Additionally, the user's guide presents the developers' perspectives on the degree of conservatism adopted in the modeling approaches, major assumptions, input parameters, and the TPA code structure and model implementations.

Chapter 2 provides an overview to the modeling approach and describes the primary conceptual models and their interrelationships. Chapter 3 describes the execution of the TPA Version 4.0 code explaining how data are read, consequence modules are invoked, and various utility modules (e.g., parameter sampling and radionuclide inventory calculations) are used. Chapter 3 also provides an introduction to the consequence modules presented in the following 15 chapters. Chapters 4 to 18 describe the conceptual and mathematical models implemented in the 15 TPA consequence modules. These chapters also delineate the major assumptions and conservatisms of each module. Chapter 19 describes the input files and parameters for the TPA Version 4.0 code, and chapter 20 describes the full set of code outputs. In chapter 21, program installation and execution on UNIX-based workstations are chronicled. Chapter 22 presents the postprocessing routine used to combine the CCDFs to obtain the overall risk curve and a description of the provision built into the code (partially developed) to conduct generalized importance analysis. Chapter 23 outlines future TPA Version 4.0 code developments. In chapter 24, the technical references for this report are listed. Finally, a set of appendixes is provided that contain the reference data set including the basis for the selected values, auxiliary input data files, utility module descriptions, probability distribution function descriptions, the methodology used to calculate the net amount of water infiltrating from the ground surface, intermediate data transfer files, and derivation of empirical flow factors used in the source term module.

Appendix A (the reference data set) provides a road map to the primary TPA input file (*tpa.inp*) and may be most helpful to new users. The reference data set is subdivided by module and provides a description of the parameters and the basis for values selected for the reference case. This information and tabular format of appendix A is different from the format of the *tpa.inp* file, which mostly contains parameter names and values. To further assist the users, the parameter descriptions in appendix A are in the same order as in the *tpa.inp* file. Additional supporting data are presented in appendix B. Data presented in appendixes A and B reflect a reference case (also called a basecase) that will be modified when new data would be available. The code, however, provides flexibility to use values that differ from the reference data set.

## 1.4 UPGRADING TPA VERSION 3.1.4 TO TPA VERSION 3.2 CODE

Several versions of the TPA code have been released since IPA Phase 2 (Wescott et al., 1995). Major releases include the TPA Versions 3.1.4[2] and the TPA Version 3.2 code (Mohanty and McCartin, 1998). The development of the TPA Version 3.1.4 code was a major step forward in making the code accessible to all CNWRA staff and all NRC staff in the HLW program by improving the code's ease of use. The code also made use of the up to date site data, conceptual models, and improved computational

[2]Mohanty, S., and T.J. McCartin, coords. NRC Sensitivity and Uncertainty Analyses for a Proposed HLW Repository at Yucca Mountain, Nevada, Using TPA 3.1. Volume I: Conceptual Models and Data. NUREG–1668. Washington, DC: U.S. Nuclear Regulatory Commission. In press. 2000.

algorithms for implementing these models. Significant improvements were identified based on new information made available by the DOE after the completion of the TPA Version 3.1.4 code. The new information had far-reaching implications for dose calculations and led to the development of the TPA Version 3.2 code. For example, a change in the material selection for the inner overpack of the WP (i.e., from Alloy 625 to Alloy 22) occurred after development and documentation of the TPA Version 3.1.4 code. There are two major effects attributed to the use of Alloy 22. First, Alloy 22 is anticipated to have a service life beyond 10,000 yr while the anticipated service life of Alloy 625 was 3,000–5,000 yr. Second, Alloy 625 degrades through pitting corrosion while, Alloy 22 degrades through general corrosion. This attribute of Alloy 22 required modifications to the TPA Version 3.2 code beyond the simple change to the rate of corrosion. For example, the manner in which water enters, fills, and leaves the WP through corrosion pits in Alloy 625 could be significantly different from Alloy 22 undergoing uniform corrosion. Therefore, the model that uses a bathtub for the mode of water contact with SF and the variable that affects the amount of water entering the WP were evaluated in the context of the mode of corrosion of Alloy 22. Additionally, damage to the WP from events such as rockfall and faulting has the potential to impact the WP through a much longer period for long-lived Alloy 22, than for Alloy 625. Therefore, the conservatism in the SEISMO module and mechanical failure of the WP, not considered significant to performance for WPs with lifetimes of 3,000–5,000 yr, needed to be reexamined for its impact on performance of a longer-lasting WP constructed, in part, from Alloy 22.

## 1.5 UPGRADING TPA VERSION 3.2 TO TPA VERSION 4.0 CODE

The TPA Version 3.2 code was updated to Version 4.0 in response to (i) the new DOE repository design (EDA II), (ii) insights from sensitivity analyses with the TPA Version 3.2 code, and (iii) experience gained from running the TPA Version 3.2 code.

Several code improvements were made necessary by the adoption of the EDA II. For example, the new thermal loading strategy to allow draining of infiltrating water down the pillars rendered the uniform heat distribution assumption for the repository inapplicable. Instead, temperature needs to be computed assuming an array of parallel line sources. Additionally, the drip shield introduced in EDA II has two major effects. First, the drip shield, which is anticipated to have a service life beyond 10,000 yr (current DOE estimate), will prevent water from entering WPs that may have been breached. Second, the time and mode of drip shield failure will control the amount of water contacting the SF after WP failure. These attributes of the drip shield requires additional modifications to the TPA code. For example, the manner in which water enters the WP in the presence of a failed drip shield requires that the factors used to simulate the diversion of water away from the waste be functions of time.

The second basis for improvements made to the TPA Version 4.0 code came from the results of sensitivity analyses, performed at the process level[3] and the system level[4] with the TPA Version 3.2 code. Sensitivity analysis was used to identify the areas for code improvement and refinement prioritization based on importance to performance and deficiencies identified in the code. For example, sensitivity analysis revealed that the peak dose to an average individual in the receptor group is highly sensitive to retardation in alluvium, which controls radionuclides travel time in the SZ to the receptor location. In response to this

[3]Examination of the sensitivity to overall performance due to variation of parameters and models within a specific process.

[4]Examination of the sensitivity to overall performance due to variation of parameters and models within the TPA Version 3.2 code.

sensitivity, the code was made more flexible by providing the option of sampling alluvium length and by developing a technical basis for the range of variation in the thickness based on NRC/CNWRA independent analysis of well bore data and geologic framework model. Additionally, new models not tested in the sensitivity analyses were also included with the anticipation of their importance to sensitivity. For example, to provide flexibility in defining the exposure scenario and allow for probabilistic sampling of the biosphere and exposure scenario parameters, the GENTPA[5] code was incorporated in the TPA code as a stand-alone module for sampling exposure-related parameters. In addition to the technical improvements to the modules, a number of additions to the input options for the code and consistency in parameter sampling were identified to improve the flexibility and provide appropriate data for sensitivity analyses.

The third basis for improvements made to the TPA Version 4.0 code results from experience using the TPA Version 3.2 code. Several shortcomings such as limitations in the use of the code for sensitivity analysis and lack of consistency between dose histories in a $10^4$-yr run and the first $10^4$ yr of a $10^5$-yr run required code improvements.

Specific modifications made to the TPA Version 3.2 code to obtain the Version 4.0 code are summarized below.

- The TPA Version 4.0 code implements the new DOE repository layout (the EDA II design). Because the new layout is designed to reduce peak temperature, several new subareas are added to accommodate the reduced areal loading density.

- Because of the increased drift spacing and decreased WP spacing in the EDA II design, the temperature is computed using line heat sources to simulate a cooler region between the drifts. This modification replaces the uniform thermal source, over the whole repository, used in the TPA Version 3.2 code. The thermal output from the waste has been made consistent with the new design concept, fuel mix, and SF burnup.

- Container life models now account for the presence of the drip shield and the new WP design data. New considerations include the emplacement sequence of outer and inner overpack materials, welds on the WP surface, and radiolysis effects. Weld corrosion is considered not likely to be any faster than that of the nonwelded metal. If necessary, the user can study weld corrosion by changing input parameter values such as the general and localized corrosion rate and the critical potential for the localized corrosion of the weld material. Temperature dependence for the passive corrosion rate and the corrosion potential calculations, which include radiolysis effects (i.e., generation of $H_2O_2$), can be introduced into the TPA code by changing input parameter values in *tpa.inp*. Therefore, no internal changes were made to the code.

- The TPA code accounts for the presence of the drip shield in the prediction of the repository rock and WP temperatures, which in turn affects the time of WP failure and the amount of water entering into the WP. An abstraction of the drip shield failure time is introduced in the form of a distribution function. Preliminary calculations based on data obtained from electrochemical experiments were used in estimating the drip shield failure time distribution used in the TPA Version 4.0 code.

---

[5]GENTPA is a modified version of the GENII code (Napier et al., 1988).

- The effects of the drip shield on the amount of water contacting a WP with and without backfill is evaluated using the time history of the WP wetting parameters, $F_{mult}$ and $F_{ow}$. In the TPA Version 3.2 code, these two parameters were not functions of time and instead were sampled using distributions specified in *tpa.inp*.

- In the previous version of the TPA code, the time-stepping scheme implemented in the reflux model used 1-yr time intervals to compute the flow rate of water during the reflux cycle. Employing 1-yr time intervals necessitates using large arrays when the simulation period is long. To eliminate computer resource problems associated with large arrays, the refluxing period is now limited to 10,000 yr.

- The source term calculation approach has been modified to accommodate uncertainty in the SF dissolution rate and make consistent the mode of failure and the mode of water retention in the failed WP. In the revised SF dissolution rate model 2 (dissolution rate in J-13 water), the preexponential coefficient is a sampled parameter to account for uncertainty. Also, for the source term calculation, a provision is made for the user to specify mode of water retention in the WP (bathtub or flow through) for each failure type. In the previous version of the code, the user was able to select only one water contact model for all failure types.

- The computation of shallow infiltration is modified to incorporate the effects of filled fractures in the bedrock covered by shallow soil and vegetation with spatial variation. The previous version of the code considered only bare soil over unfilled fractures in the bedrock. The regression equation used in the previous version for determining infiltration has been replaced with a digital elevation map (DEM) data file generated by a preprocessor. These changes reflect increased understanding and new data for the infiltration processes at YM as described in chapter 4, appendix A, and appendix H.

- The distribution and range of the present-day area-averaged mean annual infiltration (MAI) has been updated to reflect results from recently conducted process-level modeling.

- The thicknesses of the Calico Hills nonwelded vitric and Upper Crater Flat units for each subarea in the UZ beneath the repository have been changed to reflect new data collected from boreholes in the vicinity of the proposed repository.

- The lengths of the SZ tuff and alluvium units have been modified from fixed values to ones that can be sampled to account for the uncertainty in the location of the tuff/alluvium interface. This change has been incorporated because of the uncertainty in the location of the transition from the tuff aquifer system to the alluvium aquifer system for the groundwater flowing through the repository footprint.

- The diffusion rate and immobile phase porosity of the tuff have been introduced to model matrix diffusion in the SZ. Although the previous version of the TPA code possessed the capability to account for matrix diffusion, the calculations were performed using a first-order rate equation in the NEFTRAN code (Olague et al., 1991). Changes have been incorporated to use more standard parameters (i.e., diffusion coefficient, and fracture density).

- To represent variability in the dose conversion factors (DCFs), provide flexibility in defining the exposure scenario including consideration of age-specific dose calculations, and allow for probabilistic sampling of the biosphere and exposure scenario parameters, the GENTPA code is incorporated as a new stand-alone code. GENTPA code, which is a modification of the GENII code (Napier et al., 1988), estimates radiation dose to humans arising from radionuclides in the environment. In the previous version of the TPA code, dose to the receptor group was computed deterministically using data files with mean values for the DCFs in an off-line analysis performed with the GENII code.

- To increase transparency in the determination of the number of WPs that are affected by an igneous event, the TPA code now samples the number of WPs that are (i) entrained and (ii) impacted by magma flow into the drift. Thus, the number of WPs failed by these two mechanisms is externally constructed and specified as a parameter in the *tpa.inp* file. The sampled values for the number of WPs failed in an igneous event by these two mechanisms are assigned to a subarea that is user-specified. In the previous version of the TPA code, the number of WPs disturbed in an igneous event was calculated using the dimensions of the conduit and the associated dike.

- The resuspension of ash (or mass loading) used to evaluate the consequence of a volcanic event has been made time-dependent by using a functional relationship (e.g., exponentially decreased to a long-term value) between mass loading and time. These time-varying values for the mass loading provide a more realistic representation of how ash resuspension is expected to decrease over time. The previous version of the code assumed a constant mass loading factor.

- Two new distribution functions (log beta and integer uniform) were added to the Latin Hypercube Sampling (LHS) to match the capability of the Monte Carlo sampler in the TPA code. As an alternative to the internal sampling, the code now provides the flexibility of using an externally generated sampled parameter file that is useful for several sensitivity analysis applications.

- The sequence of events occurring during the simulation of seismic events for the first $10^4$-yr in a $10^5$-yr time period of interest (TPI) run is made consistent with that of the $10^4$-yr TPI run. In the previous version of the TPA code, the event sequences (i.e., time and magnitude) were different which made comparing runs and conducting sensitivity analyses difficult.

- Flexibility has been added to the code so that the user is able to define the fraction of the SZ radionuclide plume captured by a pumping well and the dilution volume by changing input parameters. In the previous version, these values were internally calculated in the code.

- The TPA Version 4.0 code uses variable time steps to accurately resolve the peak in release rates occurring immediately after the failure of WPs. The fixed time steps used in the previous version for the source term computation resulted in spuriously large peaks in the release rates.

- The code uses an expanded dilution table to enable the user to select pumping rates that are smaller than those previously allowed in the TPA code.

# 2 OVERVIEW OF THE TPA CONCEPTUAL MODELS

Analysis of repository performance is anticipated to be complex with substantial uncertainties because of the first-of-a-kind nature of the repository, the extended period of performance (at least 10,000 yr), and reliance on engineered and natural barriers. Detailed simulation models that include all the couplings, heterogeneities, and complexities cannot be incorporated into PA models and still maintain reasonable computer execution times and meet hardware requirements. Therefore, a key part in developing the TPA Version 4.0 code is determining the level of detail in the processes, design, and attributes of the site necessary to produce a credible analysis that provides meaningful insights on performance without an unreasonable computational burden. The TPA Version 4.0 code includes the repository system description (e.g., representation of the site and repository design within the TPA Version 4.0 code), conceptual models, and parameter values. A discussion of the repository system description and conceptual models is presented in this section to provide a general overview of the TPA Version 4.0 code. Chapters 4–18 contain more detailed information on the conceptual and mathematical models. The TPA input parameter values and the basis for their selection are presented in appendix A.

## 2.1 CONCEPTUALIZATION OF REPOSITORY AND GEOLOGIC SETTING

For ease of use and computational efficiency, the TPA Version 4.0 code replaces the intricate repository layout and the complex geologic setting with relatively simple conceptual representations. The repository layout, for example, is represented by an idealized planar feature discretized into a set of subareas, while the geology is replaced by a sequence of layers, each of which is homogenous. Properties and conditions for each subarea are assumed to be uniform. Except for the influence of the thermal load, flow and transport processes in and below a given subarea are assumed to be independent of those processes in other subareas. Thus, flow is entirely vertical with no lateral diversion in the UZ.

As illustrated in figure 2-1, quadrilateral subareas of uniform thickness are used to represent individual subregions of the repository. In the current application, the repository is divided into eight subareas;[1] however, the TPA Version 4.0 code has the capability to use much finer discretizations of both the repository and the geologic setting beneath it. The number of WPs in each subarea is assumed to be proportional to the fraction of total repository area represented. Radionuclide releases from the EBS are calculated by modeling a single prototypical WP for each subarea and for each failure type. Performance characteristics of the WP in each subarea are calculated by considering the evolution of such characteristics as water flux, thermal and chemical conditions, and geologic processes [e.g., seismicity, fault displacement, and igneous activity (IA)].

The geologic setting is composed of the UZ (i.e., geologic media between the land surface and the water table) and the SZ (i.e., groundwater aquifer beneath the repository and extending to the location of the receptor group). For simplicity, the stratigraphy is assumed to be laterally continuous and uniform within a subarea to represent the UZ in a separate hydrostratigraphic sequence for each subarea. This simplification is consistent with the assumption that, in general, flow in the UZ is primarily vertical, there is, little or no lateral diversion of flow along hydrostratigraphic units. The geologic setting also includes

[1]The TPA Version 4.0 code divides the EDA II repository boundary into 10 subareas. However, with the specified waste inventory, drift spacing, and WP spacing, only eight subareas are filled.

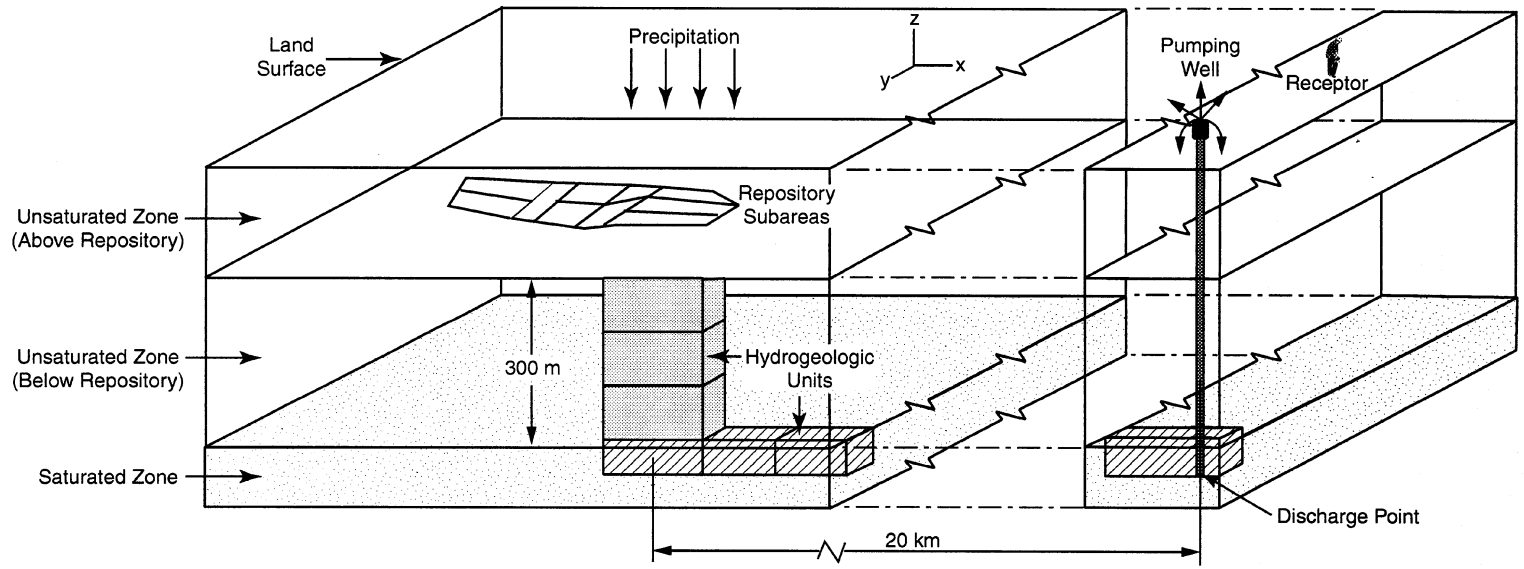


**Figure 2-1. Repository system (not to scale)**

FEPs such as seismicity, tectonism, and volcanism, that may adversely affect the performance of the repository.

The TPA conceptual model of flow and transport in the SZ consists of three distinct streamtubes over the width of the repository footprint normal to UZ flow (figure 2-2). Each of the eight subareas in the UZ is connected to one of the three streamtubes in the SZ. Radionuclide releases from each of the UZ streamtubes provide the source term to the SZ streamtubes. The SZ streamtubes are treated as separate conduits and have flow velocities that vary along the individual flow paths. The mass flow rate of radionuclides exiting all SZ streamtubes is used to compute the average concentration at the well head. This, in turn, is used in calculating annual dose to the average member of the receptor group. The average concentration accounts for all releases, from the groundwater pathway to the location of the receptor group, spatial extent of the releases in the SZ at the location of the receptor group, extent of the production zone containing the radionuclides (all radionuclides are assumed to be released in one production zone), and the influence of the pumping rate attributed to water use by the receptor group.

Direct release of radionuclides to the accessible environment due to a volcanic eruption is also modeled in the TPA Version 4.0 code. The physical characteristics of the eruption and complex magma-repository interactions considered outside the TPA code are used to determine the number of WPs affected by the event. Radionuclides are transported to the receptor location, based on characteristics of the eruption and meteorological conditions, where the concentration of radionuclides in soil, resulting from the deposition of volcanic ash containing SF particles, is calculated. This soil concentration is used in calculating the annual dose to the average member of the receptor group.

## 2.2 CONCEPTUAL MODELS IMPLEMENTED IN THE TPA COMPUTER CODE

In developing the TPA Version 4.0 code, several conceptual models were formulated, integrated, and implemented in various abstracted mathematical models. These basic conceptual models, which describe the interactions/couplings of physical and chemical processes believed to be present in a proposed geologic repository (at YM), can be grouped into the following generic categories:

- Infiltration and deep percolation
- Near-field environment
- Radionuclide releases from the EBS
- Aqueous-phase radionuclide transport (RT) through the UZ and SZ
- Airborne transport from direct radionuclide releases
- Exposure scenario and reference biosphere

These conceptual models are designed to apply to the current DOE repository design and specific site characteristics of the YM area and provide flexibility for examining alternative designs and uncertainties in site and engineered material performance. In some of these generic categories, alternative conceptual models have also been incorporated into the code.

These conceptual models are used to represent a range of system states including disruptive events. The consequences of disruptive events (e.g., seismicity, fault displacement, and IA) are evaluated with the TPA Version 4.0 code by first conducting consequence calculations and then weighting the results with the

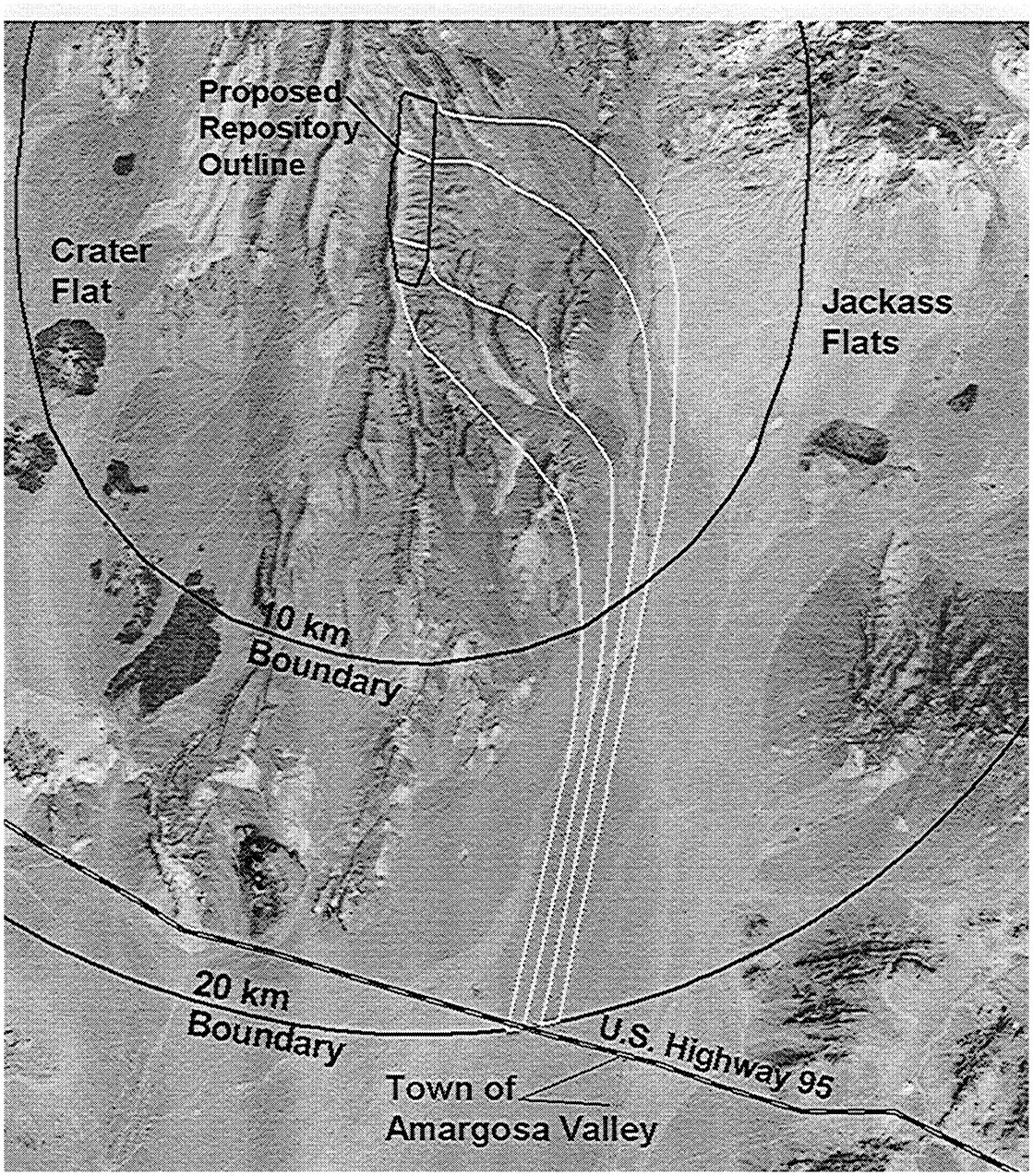


**Figure 2-2. Saturated zone conceptual model representation showing the 20-km receptor location and boundaries of the three saturated zone streamtubes**

probability of a disruptive event impacting the repository to calculate a risk curve as explained in chapter 22.

The following discussion provides a general overview of the key aspects of the major conceptual models implemented in the TPA Version 4.0 code. More detailed descriptions of these models, including the mathematical basis, assumptions, and calculational methodologies, are presented in chapters 4–18.

### 2.2.1 Infiltration and Deep Percolation

A one-dimensional (1D) modeling approach is used in the TPA Version 4.0 code (Chapter 4—UZFLOW Module Description) to describe how meteoric water at the land surface moves vertically downward (i.e., without lateral flow) through the UZ, to the repository horizon, and ultimately to the water table. In the 1D conceptual model, the deep percolation flux ($q_{perc}$) is constrained to be equal to the shallow infiltration rate ($q_{infil}$). The annual average $q_{infil}$ is estimated based on

- Present-day shallow-infiltration rate
- Change in climate with time
- Elevation, vegetation, and soil depth over the repository subarea

Uncertainty in the present-day infiltration rate estimate is accounted for in the TPA Version 4.0 code by treating it as a statistically sampled input parameter. Temporal variations are incorporated by varying the present-day infiltration rate over the 100,000-yr period assumed for long-term climatic changes. The effects of site-specific soil cover thickness (over bedrock and fracture-filled continuum), vegetation, and elevation are used to reflect the spatial variation over each of the subareas.

The variation of $q_{infil}$ because of changes in climate was developed through consideration of paleo-climatic information and a process-level auxiliary analysis (Stothoff et al., 1997; Stothoff, 1999). The $q_{infil}$ response function depends on two independent variables, present-day mean annual precipitation (MAP) and temperature, as well as the present-day infiltration rate. After computing $q_{infil}$, the water flux at the repository horizon is then partitioned into

- Water flux diverted around the failed WP
- Water flux entering the failed WP

Thus, for the purposes of the TPA Version 4.0 code, the net water flux carrying dissolved radionuclides is a fraction of the total water flux arriving at the repository. It is this net water flux that is used in the TPA Version 4.0 code (Chapter 8—EBSREL Module Description) to calculate the radionuclide source term for each subarea.

### 2.2.2 Near-Field Environment

Physical and chemical processes in the near field of the repository, such as heat transfer, water-rock geochemical interactions, and refluxing of condensate water, are expected to affect WP performance. In the TPA Version 4.0 code, a range of near-field characteristics is depicted in the abstracted mathematical

models for heat and water flow and table look-ups for chemical parameters (Chapter 5—NFENV Module Description). For the purpose of estimating WP failure times and radionuclide release rates, the near-field environment is characterized by

- Drift wall rock and WP surface temperatures
- RH (i.e., ratio of vapor pressure at the WP surface to the vapor pressure at the drift rockwall)
- Water chemistry (e.g., pH, chloride concentration, and carbonate ion concentration)
- Water reflux during the thermal phase

The average rock temperature in the repository horizon is calculated assuming a conduction-only model (i.e., the time history of temperature for each subarea is calculated accounting for the amount of emplaced waste). The WP surface temperature is calculated using a multimode heat transfer (i.e., conduction, convection, and radiation) model based on thermal output from the WP and the repository horizon temperature. Temperature calculations account for ventilation during the preclosure period (that could potentially reduce peak WP temperature), backfill during the postclosure period, and the presence of the drip shield. Vapor pressure is computed using the standard thermodynamic equation relating vapor pressure to temperature.

Estimates of the pH and chloride concentration histories of water films on the WP surface were developed in a separate process-level auxiliary analysis using the multicomponent geochemical module of the MULTIFLO code (Lichtner et al., 2000). MULTIFLO was applied to calculate the pH and chloride concentration for water percolating through the matrix of the tuffaceous rock. Because the chloride concentration in the water film is likely to be higher than that in the rock mass, the chloride history is scaled by a statistically sampled parameter. The TPA Version 4.0 code provides the option of either using a look-up table that uses the temperature-dependent pH (not currently used) and chloride concentration generated with the MULTIFLO code or specifying constant values in the input file. In general, the user selects code options by changing flag and variable values in the input file (appendix A).

The amount of water percolating through the drifts varies over time primarily because of the coupled processes of heat transfer and fluid flow (e.g., vaporization, condensation, and refluxing). Water refluxing produced by these thermohydrologic effects is important over the first few thousand years, after which natural percolation determines the rate of water flow into the repository. Three lumped-parameter water reflux models are included in the TPA Version 4.0 code, each based on bulk flow balances. The first model considers episodic reflux associated with time-dependent perching above the repository. The second model assumes that the volume of refluxing water will always be sufficient to depress the boiling isotherm in fractures and reach the WP during times when the surface temperature exceeds the boiling point of water. In the third model, the degree to which the boiling isotherm is depressed is a function of the temperature, the thickness of the dry out zone, and the volume of reflux water. These functions vary with time. Each reflux model produces estimates of the total water flux into the repository during the thermal period.

### 2.2.3 Radionuclide Releases from the Engineered Barrier System

In the TPA Version 4.0 code, the performance of a prototypical WP (including the presence of a drip shield) is modeled for each repository subarea considering the failure time and radionuclide release rates for each of the WP failure categories (Chapter 6—EBSFAIL Module Description). When this prototypical WP fails, all WPs in that subarea under a specified failure category are assumed to have failed.

The estimation of both WP failure times and liquid releases is dependent on the nature and extent of corrosion, effectiveness of the drip shield, near-field environment, percolation flux in the drift, and external processes that may impose static loads, dynamic loads, or both. WP failures are grouped into three basic categories: (i) corrosion and mechanical failure, (ii) disruptive event, and (iii) initially defective WP failures. After determining the WP failure time, the TPA Version 4.0 code calculates the aqueous-phase radionuclide releases from the WP by considering the dissolution of radionuclides from the SF matrix, advective transport from the WP (based on the amount of water contacting and entering the WP, which can be influenced by assumptions for the drip shield), and advective and diffusive transport through the invert directly to the UZ beneath the repository.

Corrosion failure of the WP is defined to occur at the time when the inner overpack is fully penetrated by a single pit and the waste form is therefore accessible to water. The abstracted corrosion model uses a conceptual framework that assumes the formation of a water film containing a salt solution but does not explicitly consider water dripping on the container. The corrosion processes considered in the model abstraction consist of

- Dry air oxidation
- Humid air corrosion
- Aqueous corrosion

Dry air oxidation and humid air oxidation are potential failure mechanisms for the carbon steel overpack of the WP design proposed in the VA (U.S. Department of Energy, 1998). However, for other design alternatives, such as the EDA II, these two corrosion modes have negligible contribution to the failure of the WPs. The only relevant WP failure mechanism for the EDA II design is aqueous corrosion of the Alloy 22 outer overpack. Nevertheless, the TPA Version 4.0 code has retained the capability to evaluate dry air oxidation and humid air oxidation. WP surface temperature and the chloride concentration in the water film influence the mode, and hence, the rate of corrosion. The predominant mode of corrosion (uniform or localized in the form of pitting or crevice corrosion) depends on those environmental factors and on the container material. Mechanical failure of the WP, included in TPA Version 3.2, is considered to be the result of fracture of the outer steel overpack due to thermal embrittlement arising from prolonged exposure at temperatures sufficiently elevated to cause substantial degradation of mechanical properties (it is assumed conservatively that the inner overpack is fractured when the outer overpack is fractured). With the design adopted in EDA II, the consideration of mechanical failure of both the outer and inner overpacks is still incorporated in TPA Version 4.0 code, even if the average WP temperature is relatively low compared to the VA design.

Failure of the drip shield is not mechanistically modeled in TPA Version 4.0 code. The failure time of the drip shield is an input parameter that can be represented by either a constant or by a distribution.

Disruptive event failures are taken into account by modeling the impact of events such as seismicity (Chapter 7—SEISMO Module Description), fault displacement (Chapter 13—FAULTO Module Description), and IA (Chapter 14–15—VOLCANO and ASHPLUME Module Description). In the case of seismicity, WP failures are caused by rockfalls that mechanically load and deform the WP. The drift is assumed not to be backfilled for rockfall to damage the WP. Displacements along yet undetected faults or new faults (because the DOE will not emplace the WPs within a setback distance from known and well-characterized faults) that exceed a preestablished threshold are assumed to fail WPs within the fault zone. For IA, WPs intersected by magma are assumed to fail. WPs within a drift but outside the volcanic conduit are assumed to fail and expose the SF to water while those within the conduit are assumed to be

entrained in the magma and released directly to the biosphere. For fault displacement, failures are modeled by superimposing the physical dimensions of the perturbation (i.e., length, width, and orientation of the fault) on the repository footprint to determine the total number of WPs potentially affected in each repository subarea. Alternatively, a geometric approach can be used to simulate the effects of an igneous dike, TPA Version 4.0 code allows the user to specify the range of WP failure resulting from a complex igneous process. Separate failure times are calculated for seismicity, fault displacement, and IA. Because multiple seismic events occur during the compliance and simulation periods, seismic failure occurrences are collected into four distinct failure times.

In most applications of the TPA Version 4.0 code, it is assumed that a small number of WPs are failed at the time of repository closure. These initially failed WPs are attributed to fabrication defects or damage to the WP as a result of improper emplacement. For conservatism, the number of initially defective WPs is typically assumed to be 0.1 percent[2] of the total number of containers.

Radionuclide releases from the WP are calculated by considering the alteration rate of SF (i.e., rate at which radionuclides in fuel become available for release), radionuclide solubility limits, and transport mechanisms out of the WP. The TPA Version 4.0 code incorporates a number of parameters (e.g., fraction of SF that is wet, particle size of the SF, alteration rate of $UO_{2+x}$, and credit for cladding) that control the release of radionuclides from the SF matrix. The effects of the formation of secondary minerals such as schoepite on SF dissolution are treated separately. After radionuclides are leached from the SF waste form, the calculated releases are adjusted to ensure consistency with the radioelement solubility limits. The gap fraction inventory of radionuclides is available for instantaneous release and therefore, may be a major contributor to peak dose.

A parameter value is used to specify the fraction of failed WPs in the subarea that is wetted—the number of failed WPs available to contribute to the source term (auxiliary calculations are typically done to justify parameter selection). To compute the time-dependent source term, the TPA Version 4.0 code provides two alternative conceptual models: (i) a bathtub model—the WP must fill with water before the radionuclides are released and (ii) a flow-through model—radionuclides are released by water dripping on the waste form. For the bathtub model, the WP is treated as a stirred tank, with the tank capacity dependent on the statistically sampled water outlet height. Water will fill the WP until the capacity (height) is reached and, thereafter, the amount of water entering the WP will equal the amount of water flowing out. Water leaving the WP transports dissolved radionuclides into the UZ below the repository. The water capacity of the bathtub is assumed to be unique to the failure modes and to subareas (except for faulting and IA failures). Releases from WPs will travel through the invert before exiting the EBS. If the physical properties of the construction material for invert are conducive, the radionuclide species could be sorbed, thus providing an additional barrier to the radionuclide release. The flow-through model is a variant of the bathtub model except water does not have to first fill the bathtub before release and the fraction of fuel wetted is independent of the water level. The user has the option of selecting the mode of water retention in the WP (bathtub or flow-through) for each failure type.

[2]Tschoepe et al. (1994) suggests fabricated metallic component reliabilities of 99.9 to 99.99 percent.

### 2.2.4 Treatment of Aqueous-Phase Transport in the Unsaturated and Saturated Zones

Movement of aqueous-phase radionuclides from the repository horizon, through the UZ and SZ, and ultimately to the receptor group, is modeled in the TPA Version 4.0 code (Chapter 9—UZFT Module Description) using the previously described streamtube approach. Each streamtube encompasses one or more repository subareas and is composed of a vertical section from the repository to the water table and horizontal sections in the SZ. The transport module NEFTRAN II (Olague et al., 1991) simulates the spectrum of processes (e.g., advection, dispersion, matrix diffusion, sorption, and decay) occurring within individual streamtubes. For any set of radionuclides from a list of 43, this module simulates vertical transport through the UZ and horizontal transport through the SZ.

Time-dependent flow velocities in the UZ are calculated using the hydraulic properties of each major hydrostratigraphic unit. The transport module simulates the transport of radiocontaminants through either the porous rock matrix or fractures.[3] Radionuclide retardation by chemical sorption in the rock matrix can significantly reduce the transport rates and is therefore included in the model. Retardation on fracture surfaces, however, is neglected for conservatism because the significance of this mechanism has yet to be demonstrated.

Although groundwater flow in the SZ is assumed to be at steady state, RT within individual streamtubes is time-dependent because the source term varies with time. Streamtubes in the SZ exhibit variable cross sections along the flow path; this variable streamtube geometry was based on a separate two-dimensional (2D) modeling study of the subregional flow. The conceptual model of the SZ assumes that flow in the tuff aquifer is in localized conductive zones (i.e., permeable fracture zones) while flow in the alluvium is presumed uniformly distributed in the alluvial aquifer. Although the streamtube approach neglects dilution effects arising from lateral dispersion, credit is taken for sorption in the alluvium, which is likely to retard aqueous phase transport of many radionuclides. The length of the flow path for the alluvium can have a significant effect on the effectiveness of the alluvium in retarding RT. The TPA Version 4.0 code uses a variable distance for the length of the alluvium flow path because presently there are limited data for a precise value. Additionally, matrix diffusion from flowing pores and fractures into the more-or-less stagnant matrix pore water within the rock is included in the SZ transport model.

### 2.2.5 Airborne Transport for Direct Releases

Radiologic risks associated with the volcanic component of IA are calculated in the TPA Version 4.0 code by modeling airborne releases of radionuclides for simulated volcanic eruptions. The volcanism modules assume that the magma intercepts WPs, moves upward to the land surface, and then ejects the tephra and SF mixture into the atmosphere. The physical characteristics of each simulated eruption (e.g., vent size and event power and duration) and atmospheric conditions are treated as statistical parameters in calculations of tephra dispersal and deposition patterns, tephra deposit thickness, and radionuclide soil concentrations. Three primary factors determining the tephra plume geometry and transport rates include

---

[3]Transport though rock matrix takes place if the percolation rate ($q_{perc}$) is less than the hydraulic conductivity of the rock matrix ($K_{matrix}$) or through fractures when $q_{perc}$ exceeds $K_{matrix}$.

- Power and duration of the eruption
- Wind speed and direction
- SF particle sizes

The ash transport model developed by Suzuki (1983) was modified by Jarzemba et al. (1997) and incorporated into the TPA Version 4.0 code to calculate distribution of the released radionuclides. The time-dependent radionuclide areal densities are calculated taking into account the thickness of the tephra deposit leaching and erosion rates, and radionuclide decay rates. The calculated doses attributed to direct releases are strongly influenced by the time of the event (early events result in larger doses due to, in part, the contribution to the estimated doses from short-lived fission products present in the SF).

### 2.2.6 Exposure Pathways and Reference Biosphere

Dose calculations are performed in the TPA Version 4.0 code for exposure pathways that consider an average person of a designated receptor group. These calculations are expressed by the total effective dose equivalent (TEDE). Alternative receptor groups are currently included in the exposure scenario. One receptor group is a farming community 20 km from the repository location while the second is a residential community at a specified distance typically less than 20 km. The average member of the designated receptor group is assumed to be exposed to radionuclides transported through the groundwater pathway, air pathway or both as a result of direct releases arising from the volcanic component of IA.

Geographic location and lifestyle characteristics assigned to each receptor group are two primary aspects defining the receptor group and are specified in the TPA Version 4.0 code by selection of appropriate input options (appendix A). In addition, the farming community receptor group is assumed to include persons that use the contaminated water for

- Drinking (i.e., 2 L/day)
- Agriculture, typical of Amargosa Valley area practices (e.g., growing alfalfa, gardening, and raising livestocks)

The farming community receptor group is assumed to be exposed to surface contamination through

- Consumption of contaminated farm products (i.e., ingestion)
- Breathing air with ash-SF particles (i.e., inhalation)
- Direct contact

In contrast, the residential receptor group is assumed to be composed of persons who use contaminated groundwater only for drinking, but are also exposed to surface contamination (created by ash-SF particle deposition from volcanic eruptions) through inhalation and direct exposure.

Site-specific DCFs for each radionuclide and pathway are used to convert radionuclide concentrations in the groundwater and soil to TEDE values. The individual DCFs are generated through separate pathway calculations using the GENTPA code. A variety of parameters (e.g., irrigation rates, diet, etc.) are used to provide flexibility in the definition of the biosphere and exposure scenario. Two separate sets of parameters are included to represent two distinct reference biospheres associated with the present arid climate and the projected future pluvial climate. In addition to computing the TEDE history for each stochastic simulation, the TPA Version 4.0 code scans these dose calculations to identify the magnitude and timing of the peak dose.

# 3 TPA CODE STRUCTURE AND MODULES

The TPA computer code, which is written in the FORTRAN 77 language (SunPro, 1992), was specifically developed for conducting system-level analyses of the proposed HLW repository. The basic code design is consistent with standard software engineering practices (Liskov and Guttag, 1986) that emphasize the use of a highly modular structure. The architecture of the computer code comprises an executive module, several consequence modules, an extensive set of utility modules, libraries, and a combination of static and dynamic data files. As a result of using this approach, the TPA source code includes a group of process simulation programs, numerous calculational subroutines, data storage and retrieval modules, and a set of table look-up libraries. This modular approach, while having the disadvantage of producing many more code components, has the important advantage of permitting more detailed component testing and easier coding revisions. The TPA source code, which has in excess of 70,000 lines of FORTRAN, was originally written for execution on a SUN workstation using the Solaris UNIX-based operating system (SunSoft, Inc., 1995) and it has also been modified to execute on a personal computer using the NT operating system with Service Pack 5.

The primary use of the TPA code is to conduct probabilistic calculations of doses for specified time periods (e.g., regulatory compliance time period, and TPI) and for designated receptor group locations (e.g., 20 km downgradient of YM). In performing these calculations, system-level simulations of repository performance take into account such aspects as

- Essential features of the engineered and natural barriers
- Natural chemical and physical processes affecting barrier degradation and radionuclide releases to the biosphere
- Uncertainties and spatial variabilities of system attributes, model parameters, and future system states (i.e., scenario classes)
- Lifestyle characteristics of the designated receptor group

As explained in Wescott et al. (1995), the NRC TSPA methodology leads to an overall risk curve (i.e., individual dose versus probability) formed through the calculation of the weighted average of the conditional CCDFs for individual scenario classes. One important departure from the original NRC methodology is that the new TPA code includes climate change and seismicity as parts of the natural evolution of the site (i.e., basecase) and, therefore, these are not considered scenario classes. Also, the new TPA code, like its predecessor, is designed to simulate or analyze scenario classes in a separate run. Thus, two scenario classes, each with binary outcomes, require $2^2$ or a total of four separate TPA runs. The combination of conditional CCDFs for the full set of scenario classes is performed as a separate postprocessing step.

The main objective of this chapter is to describe the overall structure of the TPA computer code, explain the function of selected utility modules, delineate the types of module implementations, and provide an outline for the description of consequence modules in the next 15 chapters (i.e., chapters 4–18). This information is presented to ensure that a new code user develops an understanding of the essential features for using the TPA code. More detailed descriptions of the consequence modules are given in the next chapter and the full set of utility modules is explained in appendix C.

## 3.1 OVERVIEW OF THE TPA COMPUTER CODE

As shown in figure 3-1, the TPA code consists of an executive module (EXEC) that serves as the program driver, an input module (READER) for reading the input file (designated *tpa.inp*), and a set of consequence modules for (i) the engineered barriers (EBSFAIL, EBSREL), (ii) natural barriers (UZFLOW, UZFT, SZFT), (iii) scenario classes (FAULTO, VOLCANO), (iv) direct releases from IA (ASHPLUMO, ASHRMOVO), and (v) receptor group doses (DCAGW, DCAGS). In addition, the processes of climate change (i.e., precipitation history) and seismicity (SEISMO) (i.e., earth motions producing rockfalls and, in turn, WP damage and failure) are treated as part of the natural evolution of the site. Seismicity, however, is only included in the simulation for the case of unbackfilled repository drifts at time of closure. For the backfilled repository design, the TPA code has the user option to exclude consideration of seismicity in the simulation of the natural evolution.

The EXEC module of the TPA code controls the sequences of consequence and utility module executions. For example, the EXEC module begins the computational process sequence by calling the READER module, which in turn reads the *tpa.inp* file and checks the file for errors such as zero time intervals, unqualified flag specifications, and improper range specifications for distribution functions. If errors are detected, the READER module writes diagnostic output, identifies the location of the error(s) in the *tpa.inp* file, and sends a flag to EXEC to terminate the run. If no errors are detected by READER, the EXEC module checks the scenario class to be simulated and determines the ordered sequence of module executions required for that particular scenario class. At this point, EXEC initiates a set of probabilistic calculations for the specified simulation period (e.g., 50,000 yr) typically requiring about 13 hr.[1]

Before initiating the probabilistic simulation, the EXEC calls the statistical sampling utility module (SAMPLER) (not shown in figure 3-1) to generate random values for the input parameters with assigned probability distributions (e.g.,uniform, Gaussian, and lognormal). The SAMPLER module produces the requisite number of random vectors (typically 200–400), with each vector consisting of a collection of the random independent variables drawn from their specified distributions for a given trial. The TPA Version 4.0 code permits the user to select either LHS (Iman and Shortencarier, 1984) or standard Monte Carlo Sampling (MCS) or the use of externally generated LHS files for sensitivity analyses. Generally, LHS is favored over MCS (Iman and Shortencarier, 1984) because it requires fewer trials for the same level of statistical convergence.[2] The procedure used in TPA also allows multiple correlations among variables, whereas the MCS method allows only correlations between two variables at a time. The required number of samples is arbitrary, but generally must be greater than the number of stochastic variables. Statistical convergence should be tested by comparing results for different numbers of samples.

Prior to the random trials, the EXEC module invokes the calculation of the initial radionuclide inventories and thermal loading for the SF characteristics defined in the *nuclides.dat* and *burnup.dat* data files. This calculation is performed by the INVENT utility module (not shown in figure 3-1) which, based on the specified age of the waste, computes the inventory at the time of repository closure for 43 radionuclides. Although only a limited set of these 43 radionuclides is considered in the groundwater

---

[1]Based on 1.3 min/realization/100,000-yr simulation period and 400 random trials on a dedicated SUN Ultra Enterprise workstation.

[2]Note: The Monte Carlo Sampling (MCS) method generally requires less computer memory than the Latin Hypercube Sampling (LHS) method. Also, implementing new distribution functions is easier in MCS than in LHS.

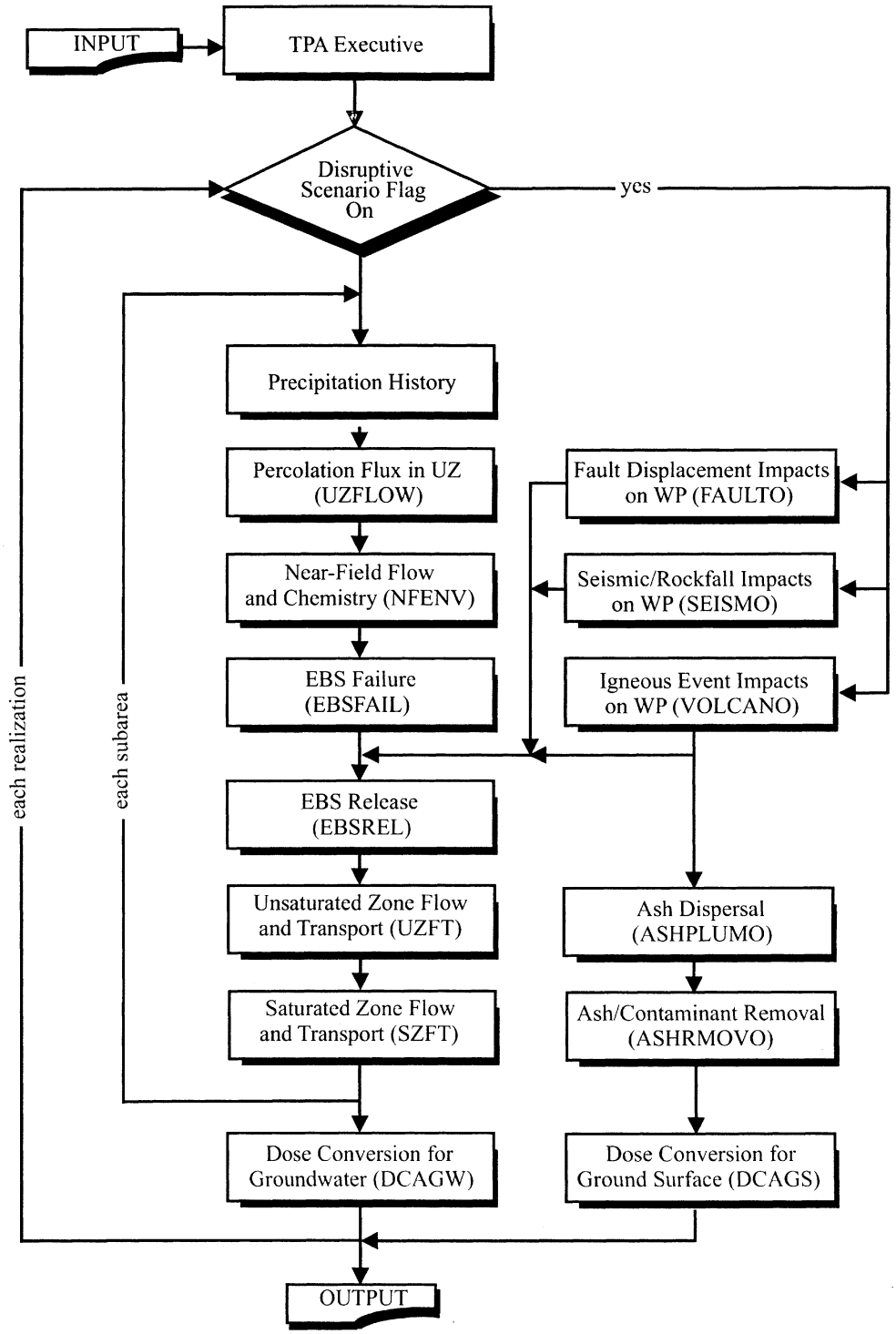


**Figure 3-1. Flow Diagram for TPA Version 4.0 code**

pathway calculations to reduce computation time, the full set is considered in the IA scenario release class. In the current version of TPA, the radionuclide source term is computed assuming only an SF inventory, although the proposed nuclear waste repository is expected to consist of both commercial SF and vitrified defense HLW.

Another preparatory step to initiating the random trials involves setting up the spatial discretization of the repository region and the UZ and SZ flow fields. The repository is divided into a number of subareas (typically eight or more) using the coordinates specified in the *tpa.inp* file. In contrast, the UZ and SZ are discretized prior to the simulation in the flow tube sections with the geometry of the SZ sections being specified by the user in static data files (designated as **.dat*). Similarly, the simulation period (e.g., 10,000 or 100,000 yr) is discretized by the user into two intervals and each interval is subdivided as specified by the user. Results are thus produced at two specified intervals.

After the full set of parameters and data files are assembled, EXEC executes the consequence modules (i.e., modules that simulate physical and chemical processes). The basecase WP degradation and contaminant release and transport process consequence modules include

- UZFLOW—computes time varying percolation flux through the UZ for each subarea
- NFENV—provides thermohydrologic and hydrochemical history in the near field
- EBSFAIL—simulates the corrosion and mechanical failure phenomena and computes the container lifetime
- SEISMO—estimates the number of containers affected by seismically induced rockfall
- EBSREL—computes the radionuclide release rate from the EBS
- UZFT—simulates flow and transport through the UZ using the NEFTRAN II code (Olague et al., 1991) (not shown in figure 3-1)
- SZFT—simulates flow and transport through the SZ using the NEFTRAN II code
- DCAGW—computes radionuclide concentrations at the well head, DCFs, and resulting doses

During the TPA simulation, the EXEC module may invoke other consequence modules. For example, if a particular disruptive event scenario class is specified, the EXEC module will add to the previous sequence of execution one or more of the following consequence modules:

- FAULTO—simulates faulting events and computes number of WPs affected
- VOLCANO—simulates magmatic intrusions and computes amount of waste released
- ASHPLUMO—simulates airborne transport and contaminated ash particle deposition
- ASHRMOVO—computes radionuclide concentrations in soil
- DCAGS—converts soil concentrations into dose

The previously listed consequence modules are implemented in the FORTRAN source code in one or more of the following ways: (i) table look-up, (ii) module/subroutine implementation, and (iii) stand-alone codes.

Table look-up is an implementation in which the consequence module reads from one or more static data files [see figure 3-2(a)]. A table look-up code has been used for those consequence modules where a simulation of features, events, and processes was not computationally feasible (i.e., module requires large execution times for individual random trials). The appropriate process-level code or codes are run offline for selected cases and the results are abstracted and stored in a static data file. SEISMO is an example of a consequence module using a table look-up. The SEISMO module accesses data files generated separately with the Universal Distinct Element Code (UDEC) (Itasca Consulting Group, Inc., 1996). The UDEC program typically requires many hours of CPU time to complete a single 2D simulation of an emplacement drift subjected to a particular seismic load.

Another coding implementation approach embedded directly into the consequence modules is illustrated in figure 3-2(b). In this case, calculations are performed without reliance on static data files or stand-alone programs. Two consequence modules using this type of coding are UZFLOW and ASHRMOVO, which implement numerical algorithms to solve mathematical representations of abstracted process models. Because of the simplicity of these particular models and the fast calculational algorithms, UZFLOW and ASHRMOVO were implemented as subroutines rather than as table look-up modules.

The third code implementation is execution of a stand-alone computer program illustrated in figure 3-2(c). Stand-alone codes do not require any component of the TPA code for execution, although data required for execution are passed to them in the proper format when called by the TPA code. This particular implementation requires a nonstandard FORTRAN call within the TPA code spawning an external process that runs the stand-alone program. Although this feature is not part of FORTRAN 77, it is an option provided by all compilers (SunSoft, Inc., 1996). This method of computer execution is currently used in modules such as EBSREL, UZFT, SZFT, and ASHPLUME. EBSREL executes the release portion of the EBSPAC code (Mohanty et al., 1997) and both UZFT and SZFT execute the NEFTRAN II program (Olague et al., 1991). ASHPLUMO executes the ASHPLUME program (Jarzemba et al., 1997). A summary of the current implementation for consequence modules is provided in table 3-1.

## 3.2 EXEC MODULE OPERATION

This section briefly describes the sequence of operations in the EXEC module including the individual calls to the consequence modules. The user begins TPA execution by typing *tpa.e* (UNIX) or *tpa.exe* (NT) at the keyboard. EXEC then copies files from the data and code subdirectories into the working directory and either reads the data files or runs the stand-alone code executables. A listing and description of the files contained in the data and codes subdirectories are provided in chapter 19 and appendix B.

The first subroutine call in EXEC is to READER. The READER utility module reads data from the *tpa.inp* file and stores the information in variables and arrays. After calling READER, EXEC opens and writes a five-line header to the output files. The headers contain the two-line title specified in the *tpa.inp* file, a two-line description of the output file contents, and a single line with the simulation starting time and date that uniquely identify one execution of the TPA code. A discussion of the contents for each output file is presented in chapter 20. Before calculations are performed, EXEC prints to the screen selected input data specified in the *tpa.inp* file. This information allows the user to verify that certain critical values have been properly set in the input file *tpa.inp* (e.g., repository design, simulation time, and disruptive scenario flags).

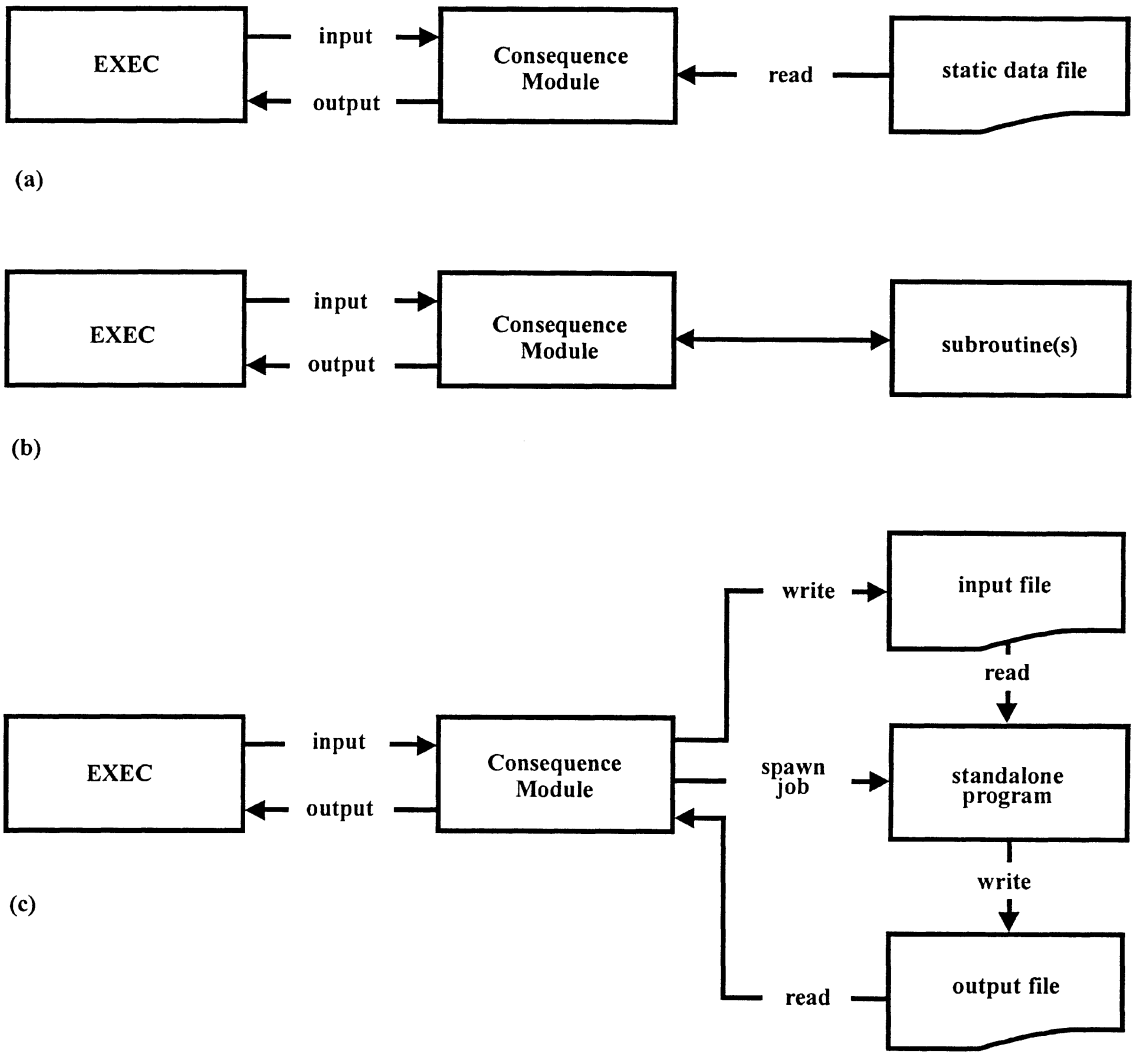


**Figure 3-2. Examples of the three consequence module implementations used in the TPA Version 4.0 code: (a) table look-up, (b) subroutines(s), and (c) external stand-alone program**

### 3.2.1 Realization Loop

Once the output file headers are written, EXEC enters a loop that is executed one time for each realization. In the realization loop, EXEC continues to write results to the screen. These screen prints serve to (i) provide a quick synopsis of global parameter setup, (ii) identify the path for the primary input file, and (iii) present program execution progress and status. Figure 3-3 is an excerpt of the screen output produced during execution of the TPA Version 4.0 code.

At the beginning of each realization, EXEC calls the SAMPLER subroutine *newrealization* to obtain values of all sampled parameters defined in the *tpa.inp* file and assigns the values to an array. Additionally, arrays are initialized at the start of the realization loop. These values may be used by EXEC or any of the consequence modules.

Depending on the sampling methodology (LHS, MCS, or external file), values are either read from the LHS output file, sampled using the RAN utility module, or read from a user-supplied file. If the LHS option is selected in the *tpa.inp* file, EXEC calls the SAMPLER subroutine *newrealization*, which spawns the process for LHS (*snllhs.f*). The LHS program is executed only once in the simulation. The output from LHS provides values for the sampled parameters in *tpa.inp* for all realizations. LHS samples all parameters irrespective of whether the parameters are used or not as long as they are specified as sampled parameters in the input file. If selected, MCS is performed when the EXEC calls the subroutine *newrealization*, typically within the modules on an as-needed basis. In contrast to LHS, MCS occurs at the beginning of each realization and values are then stored in an array. As with LHS sampling, values from MCS may be used by EXEC or any of the consequence modules. In the TPA Version 4.0 code, it is recommended the user exercise only the LHS option because MCS is limited to specifying correlation between only two parameters at a time. For the option of reading from a user-supplied file, which is especially useful in sensitivity analyses, the external file is treated in the same manner as the LHS generated file.

### 3.2.2 Subarea Loop

EXEC next enters a loop executed one time per realization for every subarea. Using sampled parameter values, constants specified in *tpa.inp*, and static data, EXEC proceeds to call the consequence modules and pass the required intermediate results to subsequent modules. The subarea loop begins with a call to UZFLOW. The results from UZFLOW consist of the time-varying flow rate of water into the subarea. Using the total number of WPs in the subarea and the UZFLOW output, EXEC generates time-dependent flow rate per WP, which is the primary input to NFENV. The NFENV module provides values for WP temperature, RH, chloride concentration, and the time-varying flow rate of water contacting the WP.

EXEC then calls the consequence module EBSFAIL. The principal input to EBSFAIL is the NFENV outputs: WP temperature, RH, and chloride concentration. EBSFAIL spawns the process *failt.f* that computes the failure time for all WPs in the subarea, which is written to the screen.

If SEISMO, FAULTO, or VOLCANO flags are set (i.e., the flag in the *tpa.inp* file set equal to 1), EXEC will call the module. Individual scenario modules are not executed when their module specific flag is 0. The scenario modules perform calculations for all subareas. Consequently, these modules are executed only once per realization in the first pass through the subarea loop.

**Table 3-1. Current implementation for consequence modules in the TPA Version 4.0 code**

| Consequence Module | Table Look-Up | Subroutine(s) | External Stand-Alone Program |
|---|---|---|---|
| UZFLOW | X | X | — |
| NFENV | X | X | — |
| EBSFAIL | — | — | X (*failt.f*) |
| EBSREL | X | — | X (*releaset.f and ebsfilt.f*) |
| UZFT | — | X | X (*nefmks.f*) |
| SZFT | X | X | X (*nefmks.f*) |
| DCAGW | X | X | X (GENTPA) |
| FAULTO | — | X | — |
| SEISMO | X | X | — |
| VOLCANO | — | X | — |
| ASHPLUMO | — | — | X (*ashplume.f*) |
| ASHRMOVO | — | X | — |
| DCAGS | X | — | — |

When the SEISMO flag is 1, EXEC calls the SAMPLER subroutine *samplehazardcurve*. This subroutine uses the hazard curve defined in the *tpa.inp* file to determine the number and type of seismic events occurring during the simulation time. EXEC then calls SEISMO, which uses the seismic event data from the hazard curve to calculate the cumulative fraction of WPs failed by seismic activity assuming no WP failures due to initial defects or from processes evaluated in EBSFAIL.

When module flags are set to 1, EXEC calls the FAULTO and VOLCANO modules. FAULTO does not utilize any values calculated in other consequence modules. The output from FAULTO is an array with the fraction of WPs failed by faulting events for each subarea. As with FAULTO, VOLCANO does not utilize any values calculated in other consequence modules. VOLCANO output is an array with the fraction of WPs failed by the dike associated with the volcanic event for each subarea and the mass [in metric tons of uranium (MTU)] of waste ejected from the volcanic cone.

After executing EBSFAIL and the selected disruptive consequence modules, the number of WPs failed by initial defects, corrosion, faulting, IA, and seismicity are determined for the entire subarea. The times of failure are determined and the number of failed WPs are computed for each failure type. There are four seismic failure time intervals (counted as four failure types) specified in the *tpa.inp* file. Thus, there are a total of eight failure types, each with the associated time of event and number of failed WPs. These values are used by the EBSREL module for computing source term.

```
================================================================================
          exec: Welcome to TPA Version 4.0
        Job started: Tue Mar 30 17:55:09 2000
================================================================================
 REPOSITORY DESIGN INFORMATION
 Subarea    Area       Waste    Number of WP
    #      [m^2]      [MTU]
    1    723591.3    14200.8         1455
    2    784763.0    15303.7         1568
    3    390372.0     7564.0          775
    4    207581.3     4157.8          426
    5    378972.8     7417.6          760
    6    424872.5     8305.8          851
    7    163938.3     3152.5          323
    8    393468.9     7944.6          814

 Total Area [acre]          =     856.82238463061
 Total Buried Waste [MTU]   =     68046.720000000
 Repository AML [MTU/acre]  =     79.417532992367

 Specified Global Parameters:

               Compliance Period =  10000.0 (yr)
          Maximum Simulation Time =  10000.0 (yr)
           Number Of Realizations =      1
               Number Of Subareas =      8
               Volcanism scenario =      0 (yes=1, no=0)
                Faulting scenario =      0 (yes=1, no=0)
                 Seismic scenario =      1 (yes=1, no=0)
       Distance to Receptor Group =     20.0 (km)

  **>>> CAUTION: CHECKING OF NUCLIDES AND CHAINS IS DISABLED <<<**
 **>>> You may not be using the standard chains specified   <<<**
 **>>> in the invent module.                                <<<**
 **>>> (see "CheckNuclidesAndChains(yes=1,no=0)" in tpa.inp)<<<**

 The specified path for data  = $TPA_DATA
 The specified path for codes = $TPA_TEST

 **To modify global parameters or the path, stop code execution using
control-C**
--------------------------------------------------------------------------------
     subarea   1 of   8           realization    1 of    1
--------------------------------------------------------------------------------
 exec: calling uzflow
 exec: calling nfenv
```

**Figure 3-3. TPA Version 4.0 code screen output**

The next consequence module called by EXEC, EBSREL, uses the number of initially defective WPs, and the time and number of WPs failed by corrosion, faulting, IA, and seismicity to write the *ebsrel.inp* file, which is an input file for the stand-alone code *releaset.f*. The argument list for EBSREL also includes the flow rate of water potentially hitting the WP before diversion which is written to the *ebsflo.dat* file. Also written to the *ebsflo.dat* file, is the time history of the two factors ($F_{ow}$ and $F_{mult}$) from the *wp flow.dat* data file. These two factors are used to determine the flow rate of water into the WP. The EBSREL consequence module passes to the stand-alone code *ebsfilt.f* the time evolution of radionuclide release rates from the WP for the computation of radionuclide transport through the invert material. The EBSREL consequence module then passes the EBS release rates calculated in the stand-alone code *ebsfilt.f* to EXEC.

EXEC then calls UZFT to compute the release rates from the UZ. Inputs in the UZFT argument list include the flow rate of water into the subarea from UZFLOW and the EBS release rates from EBSREL. UZFT spawns the stand-alone code process *nefmks.f* and maps the release rates calculated in *nefmks.f* to the TPA time steps. These release rates are passed back to EXEC in the UZFT argument list.

The final consequence module called by EXEC in the subarea loop is SZFT. The SZFT module uses release rates from UZFT to determine the SZ release rates at the receptor location (at or less than 20 km). The receptor group is specified in the TPA input file *tpa.inp*. The primary input and output in the SZFT argument list are the UZ release rates from UZFT and SZ release rates, respectively. Just as with UZFT, the SZFT module spawns the *nefmks.f* process, which calculates release rates and maps these release rates to TPA time steps.

Within the subarea loop, arrays store intermediate results that may be subsequently written to output files or summed for calculations performed later in the program execution outside of the subarea loop. In the subarea loop, the consequence modules UZFLOW, NFENV, EBSFAIL, EBSREL, UZFT, and SZFT are executed once for each subarea and the disruptive modules selected in the *tpa.inp* file are called by EXEC on the first pass through the subarea loop.

### 3.2.3 Release Consequence

After completing the subarea loop, EXEC calls the consequence module DCAGW. The principal input to DCAGW in the argument list consists of the release rates from SZFT summed for all subareas. The module DCAGW spawns the execution of the GENTPA code which computes DCFs using exposure-related data specified in the *tpa.inp* file. The DCAGW module used these DCFs to calculate the dose from the groundwater pathway for the current realization. The calculated groundwater dose is passed back to EXEC in the DCAGW argument list.

If the VOLCANO consequence module was executed in the subarea loop, EXEC calls the remaining modules ASHPLUMO, ASHRMOVO, and DCAGS to evaluate the ground surface dose. Otherwise, following the call to DCAGW, EXEC has finished calculations for the current realization. EXEC then returns to the beginning of the realization loop and repeats calculations in the subarea loop for the next realization.

When evaluating the ground surface pathway, EXEC will have already executed VOLCANO. Output from VOLCANO includes the mass of SF ejected from the volcanic cone. After being called by EXEC, the ASHPLUMO module spawns the process for *ashplume.f*, which computes the areal density of SF and ash deposited on the ground surface at the receptor location. Input and output variables in the

ASHPLUMO argument list include the mass of SF ejected and the areal densities of SF and ash. ASHRMOVO is then called and uses the output from ASHPLUMO to determine the SF deposition on the ground surface at the receptor location.

The final ground surface module called by EXEC in the realization loop is DCAGS. The DCAGS module argument list contains the ASHRMOVO output for the ground surface SF deposition. Using these values and DCFs in static data files, DCAGS calculates the ground surface dose, which is passed back to EXEC in the DCAGS argument list.

After DCAGS execution, EXEC has finished the realization loop. The number of realizations performed by EXEC is specified in the *tpa.inp* file. When all realizations are complete, there are no other calls to consequence modules. Throughout the program execution, EXEC writes headers and results to the output files. The TPA output file have names with *res*, *tpa*, *hdr*, *abb*, *rlt*, *ech*, and *cum* extensions. A detailed description of the TPA output files and their contents is provided in chapter 20.

## 3.3 UTILITY MODULES

The TPA Version 4.0 code performs various initializations, input and output processing, and intermediate calculations. There are six primary utility modules: SAMPLER, INVENT, READER, MODULE VARIABLE, SUBAREA, and ARRAY. There are another six secondary utility modules: FILEUNIT, FINDELEV, NUMRECIP, PEAKFIND, RAN, and SNLLHS. Each of these utility modules is composed of a variety of subroutines and function routines that provide centralized support to the algorithms in the consequence modules. Descriptions of SAMPLER and INVENT and their support functions are presented in this section. Appendix C contains more in-depth information on the distributions included in SAMPLER, and descriptions of other individual utility modules including information about specific functions and subroutines for each utility module.

### 3.3.1 SAMPLER

The SAMPLER utility module dynamically stores and retrieves information for model input parameters with assigned statistical distributions. Probability density functions (PDFs) are defined in and read from the *tpa.inp* file during program execution. Although SAMPLER supports either MCS, LHS, or the use of externally generated LHS files, LHS is the primary sampling scheme used in the TPA Version 4.0 code. The user selects the sampling scheme in the *tpa.inp* file. If LHS is selected, the SNLLHS utility module develops the required random variates using a program modified from Iman and Shortencarier (1984). Changes to the LHS code are discussed in section 3.3.1.2.

#### 3.3.1.1 Parameter Sampling

In addition to the option of using externally generated LHS files, there are two sampling options available in the TPA Version 4.0 code: (i) LHS using the code developed by Iman and Shortencarier (1984) modified by the addition of several more distributions, and (ii) MCS. The main advantage of LHS over straight MCS is that the parameter ranges are covered more evenly and, in general, fewer vectors are necessary to achieve statistical convergence in the results when large numbers of parameters are sampled. The output of LHS is written to a file whose size depends upon the number of samples (or vectors) and the number of values in each sample. For instance, if there are $n$ random variables and $N$ samples are required,

then the output file will contain $N$ vectors, each containing $n$ values. One vector at a time is read from this file to provide all the necessary random input to the TPA code.

Table 3-2 lists the distribution functions available for LHS along with examples to guide the user to the correct parameter specifications. A great many distributions can be approximately represented by choosing appropriate combinations of $p$ and $q$ for the beta distribution. Figure 3-4 illustrates how various distribution functions can be approximated using the beta distribution.

If MCS is selected, then samples are drawn from the various distributions using well established algorithms (e.g., Press et al., 1986; Ripley, 1987; Ang and Tang, 1984). The calculations to develop random variates are performed in the RAN utility module.

#### 3.3.1.2 Modifications to the Latin Hypercube Sampling Routine

The computer code LHS, developed by Iman and Shortencarier (1984), was modified substantially for the present TPA code. This included the addition of five new distribution types: log-triangular, exponential, finite exponential, integer uniform, and log-beta as well as modifications to the user-defined and beta distributions. These distributions are described in appendix D.

Although the original LHS code included the beta distribution, it did not work reliably and there were no integer uniform or log-beta distributions. A replacement algorithm was installed for the beta distribution. The new algorithm employs an acceptance-rejection technique (Press et al., 1986) to generate the beta samples efficiently. New algorithms were also added for the integer uniform and log-beta distributions.

#### 3.3.1.3 Distributions

The statistical distributions included in the SAMPLER utility module are

- Constant
- Uniform
- Loguniform
- Normal
- Lognormal
- Triangular
- Log-triangular
- Beta
- Exponential
- Finite exponential
- Integer uniform
- Log-beta

Mathematical representations of these distribution functions are presented in appendix D. A brief description of the input data formats for various distribution functions is presented in table 3-2 and in chapter 19. Figures 3-5 and 3-6 illustrate the distributions listed previously, with the exception of the constant distribution.

**Table 3-2. Latin Hypercube Sampling distribution functions**

| Distribution | Parameter Specifications for LHS | Example |
|---|---|---|
| beta | A B p q<br>A and B are distribution endpoints; (A < B), p, and q are shape parameters | beta<br>NWFaultZoneWidth[m]<br>0.5, 275.0, 1.25, 15.0 |
| exponential | λ<br>λ is recurrence rate | exponential<br>WindSpeed[cm/s]<br>0.002 (here λ is specified in s/cm) |
| finite-exponential | A B λ<br>User must specify recurrence rate λ, upper and lower limits A and B; A < B | finiteexponential<br>TimeOfNextFaultingEventInRegionOfInterest[yr]<br>100.0, 10000.0, 1.0e-4 |
| integer-uniform | A B<br>User must specify endpoints A and B as integers; A < B | iuniform<br>SubareaOfVolcanicEvent[]<br>1, 8 |
| log-beta | A B p q<br>A and B are distribution endpoints; (A < B), p, and q are shape parameters; user must specify A >0 and B >0 | logbeta<br>NWFaultZoneWidth[m]<br>0.5, 275.0, 1.25, 15.0 |
| lognormal | A B<br>User must specify A > 0, B > 0 such that P(X < A) = 0.001 and P(X < B) = 0.999 | lognormal<br>MatrixPermeability_TSw_[m2]<br>2.6e-20, 7.3e-17 |
| log-triangular | A B C<br>A and C are endpoints of the range; B is x-coordinate distribution apex; allows for A < B < C or A = B < C or A < B = C; user must specify A >0, B>0, and C >0 | logtriangular<br>AshMeanParticleLogDiameter[d_in_cm]<br>0.01, 0.1, 1.0 |
| loguniform | A B<br>User must specify end points A > 0 and B > 0; A < B | loguniform<br>SolubilityTh[kg/m3]<br>2.3e-7, 2.3e-1 |
| normal | A B<br>User must specify A and B such that P(X < A) = 0.001 and P(X < B) = 0.999; A < B | normal<br>MetalGrainRadius[micrometer]<br>7.5, 20.0 |
| triangular | A B C<br>A and C are endpoints of the range; B is x-coordinate of the distribution apex; Allows A < B < C or A = B < C or A < B = C | triangular<br>SolubilityNp[kg/m3]<br>1.2e-3, 3.4e-2, 2.4e-0 |

**Table 3-2. Latin Hypercube Sampling distribution functions (cont'd)**

| Distribution | Parameter Specifications for LHS | Example |
|---|---|---|
| uniform | A B<br>User must specify endpoints A and B; A < B | uniform<br>NWCumulativeDisplacementRate[mm/yr]<br>0.0, 0.00005 |
| userdistribution | N x(1), x(2), x(3),....., x(N)<br>Used for sampling from distribution whose distribution is not built into the program; N is number of sample data points and x(i) are equiprobable sample data | userdistribution<br>ThresholdDisplacementForFaultDisruptionOf WP[m]<br>4<br>0.1<br>0.2<br>0.3<br>0.4 |
| correlateinputs | Correlates parameters sampled from two different distributions; correlation value must be greater than or equal to -0.9999 and less than or equal to 0.9999; no more than 50 pairs of correlated inputs can be provided | Input structure for correlated inputs are specified as:<br>correlateinputs (keyword)<br>First correlated parameter (name)<br>Second correlated parameter (name)<br>Correlation value |

In addition to those listed above, the log-beta distribution is supported when MCS is used. Two other options for distribution specification exist that allow sampling from user supplied data and forcing a correlation among parameters. These two options are described in the following sections.

### 3.3.1.4 User-Defined Distribution

SAMPLER also allows the input of user-supplied data for defining and sampling from an empirical distribution. If the information for an input variable is only available in the form of sample data, then the user-defined distribution option provides the means to accommodate these data and sample from them. This is accomplished by sampling directly from the empirical distribution function formed from available data. For example, suppose there are eight equally probable sample data points: 0.3, 0.7, 1.3, 1.8, 2.0, 2.6, 3.0, and 3.3. The CDFs for these example data are shown in figure 3-6b. The step heights (probabilities) are all the same and in this case equal 1/8. Samples from this distribution will be one of the eight input values, and neither interpolation nor extrapolation of the data is performed. Hence, the CDF has a stair-step profile.

### 3.3.1.5 Specified Correlation

SAMPLER contains a feature that allows correlation among multiple variables when using LHS, or between two variables when using MCS. Using an algorithm described by Iman and Shortencarier (1984), the analyst must select the LHS scheme when correlation among more than two variables at a time is required.

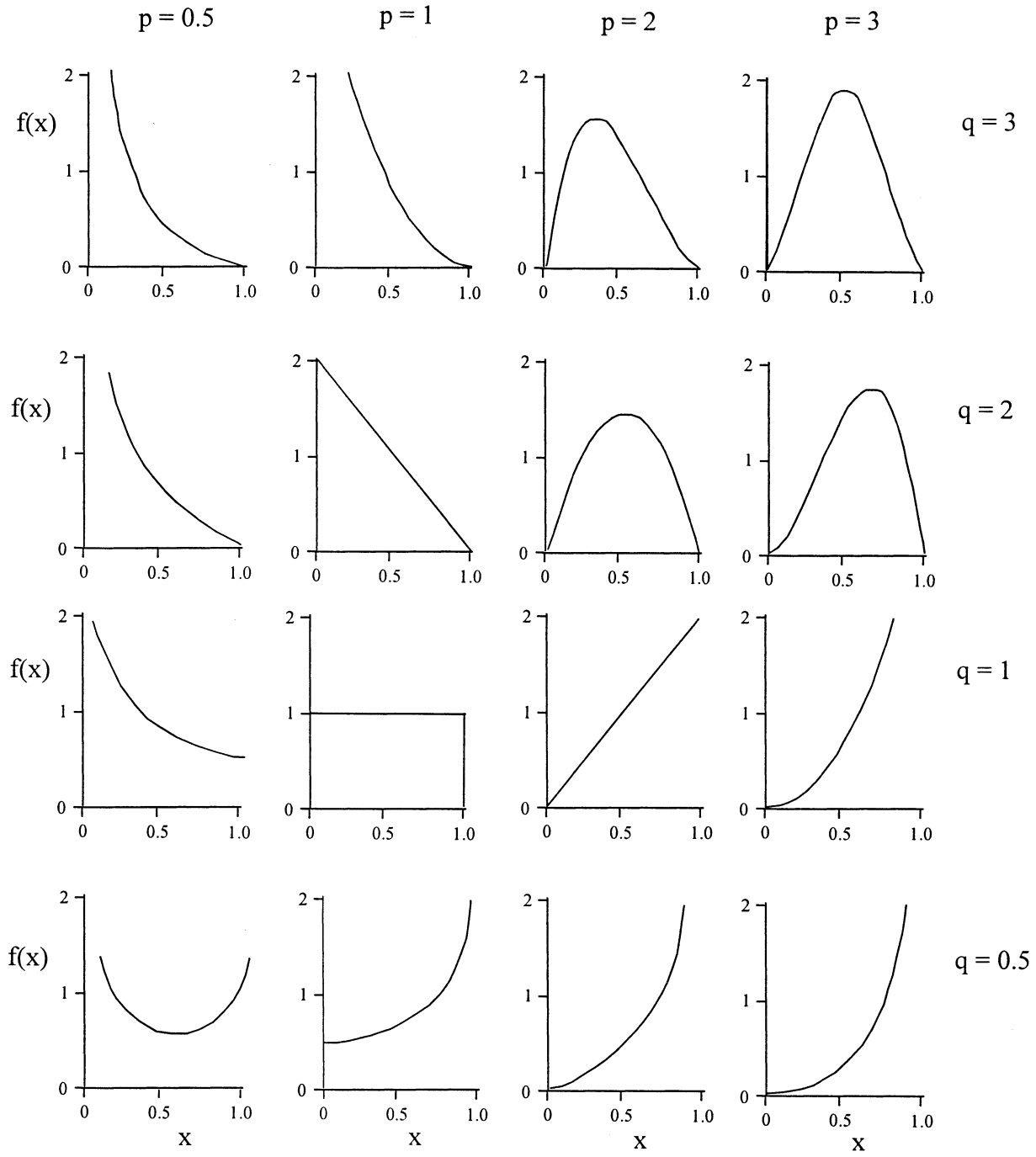


**Figure 3-4. Beta densities for various choices of the parameters *p* and *q* (Iman and Shortencarier, 1984)**

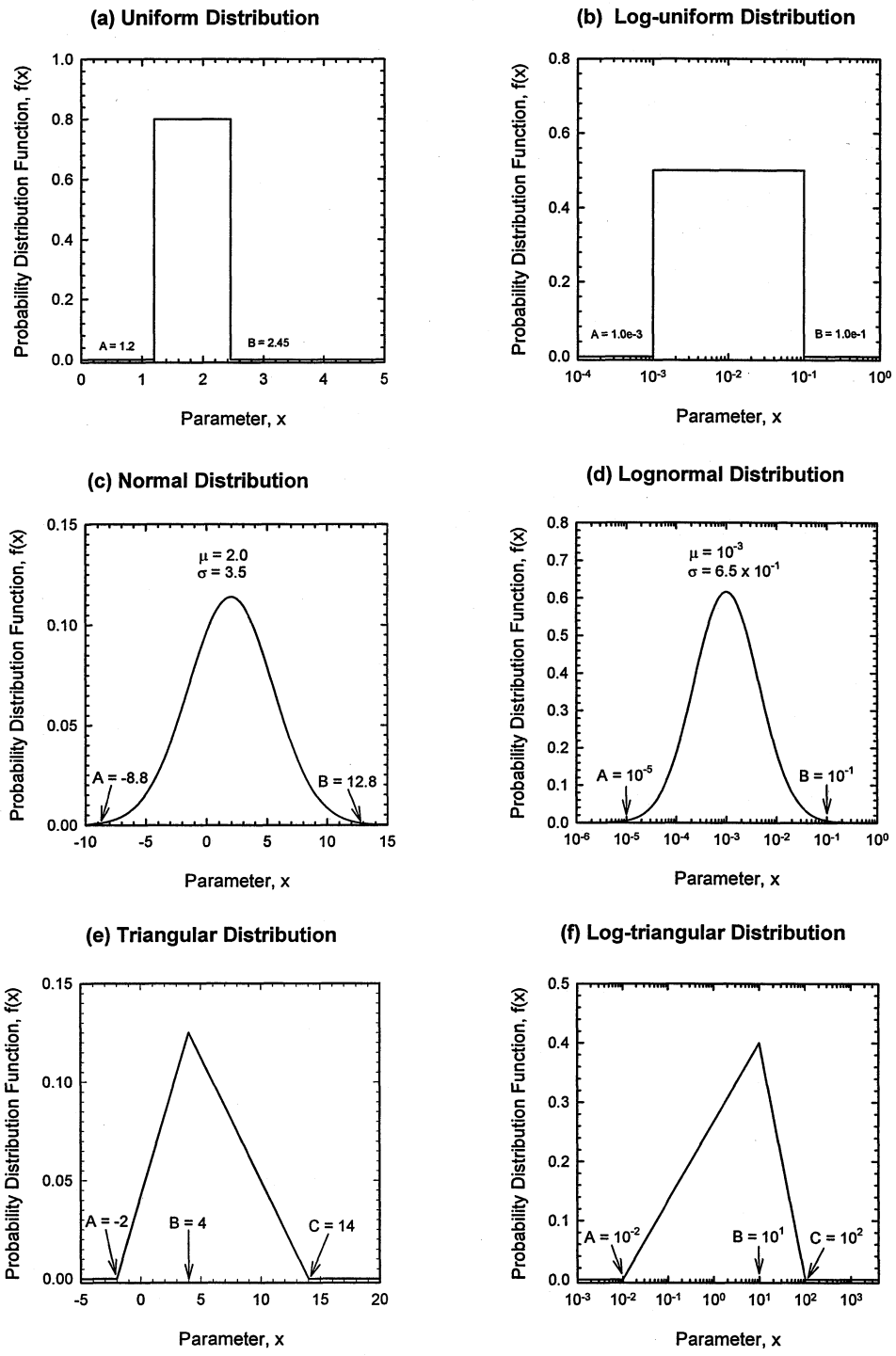


**Figure 3-5. Examples of (a) uniform, (b) loguniform, (c) normal, (d) lognormal, (e) triangular, and (f) log-triangular distributions**

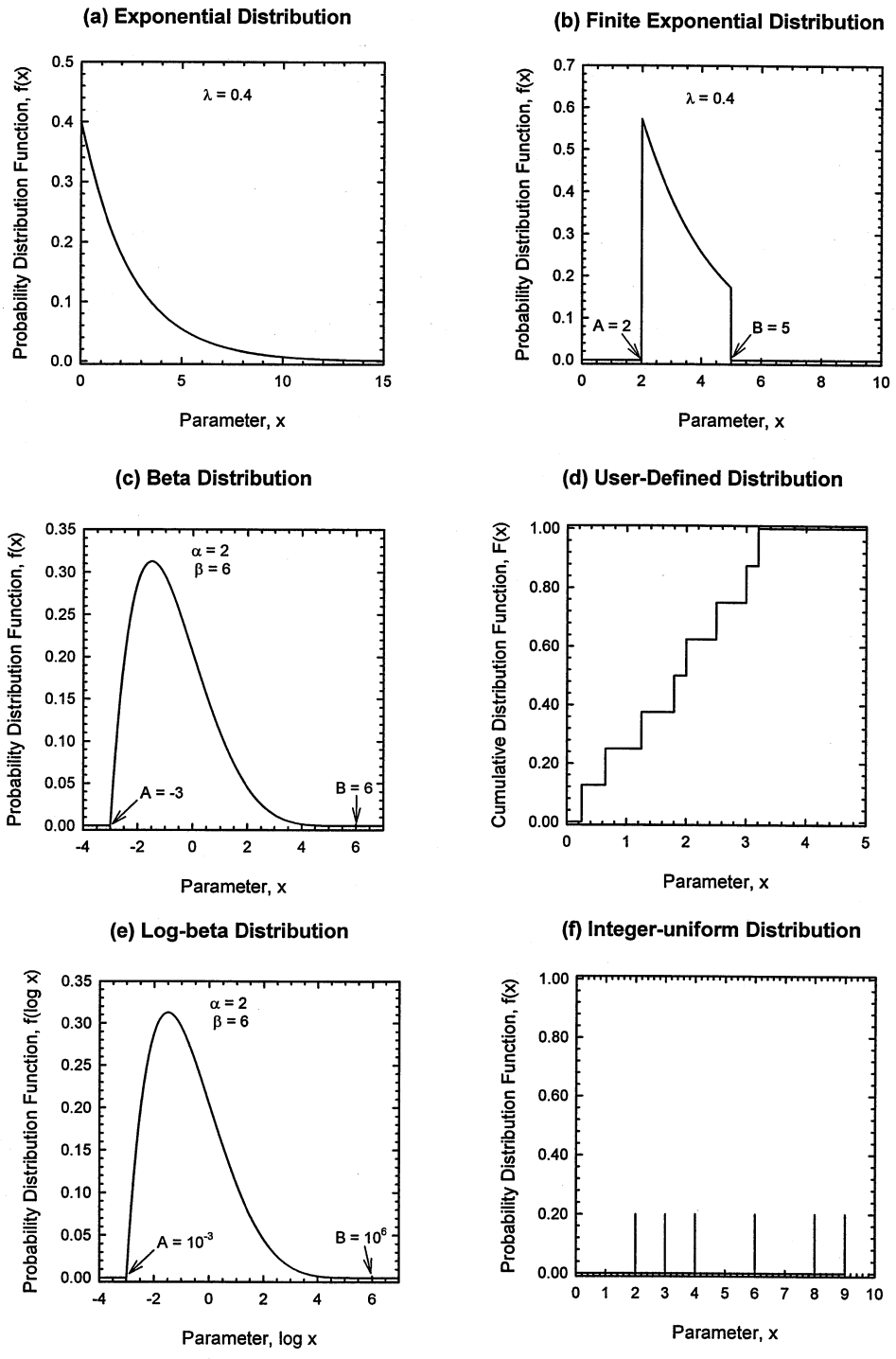


**Figure 3-6. Examples of (a) exponential, (b) finite exponential, (c) beta, (d) user-defined, (e) log-beta, and (f) integer-uniform distributions**

The correlation coefficient, $\rho$, specifies the statistical relationship among sampled variables. When $\rho = 1$, there is a perfect positive correlation. When $\rho = 0$, the two variables are independent. When $\rho = -1$, there is perfect negative correlation.

An example of a user-specified correlation is shown in figure 3-7. On the left side, scatter plots of the $z$'s, $u$'s, and $x$'s are shown between two parameters when $\rho = 0.0$ (i.e., no correlation). On the right side, similar scatter plots are shown for $\rho = 0.9$ (parameters highly positively correlated). These plots visually demonstrate how the algorithm correlates the $z$'s (samples from unit normal distributions), transforms them into $u$'s (quantiles), and then converts these into $x$'s (sampled values). The first parameter has a normal distribution that is the same as shown in figure 3-5.

### 3.3.2 INVENT

INVENT is a utility module that centralizes the computation and storage of radionuclide-specific information and inventory, data for use throughout the TPA Version 4.0 code. This module builds upon and extends the work of Lozano et al. (1994). The subroutines provide the inventory (in Ci/MTU) of 43 radionuclides accounting for chain decay and ingrowth of daughters. The time history of the thermal output of the average waste [MTU weighted average of boiling water reactor (BWR) and pressurized water reactor (PWR) SF] is also provided by the INVENT module.

During the execution of the TPA Version 4.0 code, radionuclide inventories repeatedly must be calculated and queried. For example, in the IPA Phase 2 exercise (Wescott et al., 1995), the inventories of 20 radionuclides were tracked from 10 yr out-of-core (assumed age at emplacement) up to 10,000 yr. From experience with the TPA Version 2.0 code, computation of the nuclide inventories was centralized to ensure data consistency between modules, and to allow for variability of the initial nuclide inventories because of prolonged aging of the waste from reactor to repository and the composition of the waste. The INVENT utility module was developed to centralize the calculation of radionuclide inventories for the SF and to create an efficient storage and retrieval interface for other modules to access this information.

The governing ordinary differential equation for predicting radionuclide inventories as a function of time is

$$\frac{dN_i(t)}{dt} = \lambda^P_{i-1} N_{i-1}(t) - \lambda^T_i N_i(t) \tag{3-1}$$

where

| | | |
|---|---|---|
| $N_i(t)$ | — | radionuclide population as a function of time [mol] |
| $\lambda^P_{i-1}$ | — | radioactive decay constant for the parent radionuclide [1/yr] |
| $N_{i-1}(t)$ | — | parent radionuclide population as a function of time [mol] |

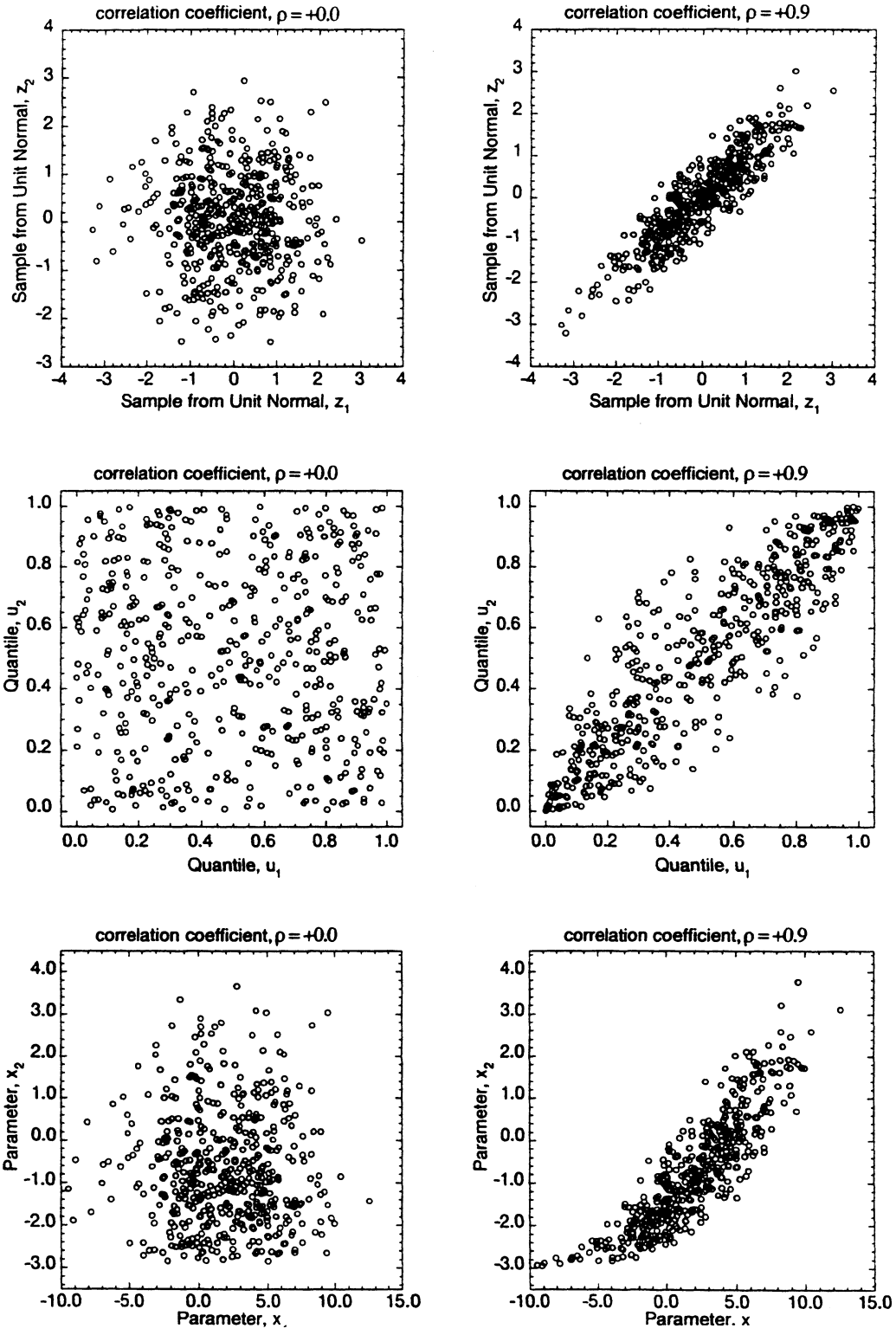


**Figure 3-7. Example of specified correlation between two sampled parameters**

$\lambda_i^T$ — total removal constant, which is a combination of radioactive decay and any other removal processes whose rate of removal is proportional to the population of the nuclide

The analytic solution to the above differential equation is (Jarzemba and Manteufel, 1997)

$$N_i(t) = \sum_{j=1}^{i} \left[ \frac{\sum_{n=1}^{j} \left[ \prod_{m=1}^{i-1} \left( \text{TERM}_m \right) \right] \left( N_{n,0} \right)}{\prod_{\substack{k=1 \\ k \neq j}}^{i} \left( \lambda_k^T - \lambda_j^T \right)} \right] \exp\left( -\lambda_j^T t \right) - \frac{\sum_{u=1}^{i} \left[ \prod_{s=1}^{i-1} \left( \text{TERM}_s \right) \right]}{\prod_{q=1}^{i} \lambda_q^T} \tag{3-2}$$

$$\text{TERM}_m = \begin{cases} \lambda_{n-m}^T - \lambda_j^T & m < n \\ \lambda_m^P & m \geq n \end{cases}$$

$$\text{TERM}_s = \begin{cases} \lambda_s^T - \lambda_j^T & s < u \\ \lambda_s^P & s \geq u \end{cases}$$

where

$N_{n,0}$ — initial population of radionuclide $n$

In the current implementation of the INVENT utility module, $\lambda_i^T$ is equal to $\lambda_i^P$. Equation (3-2) was originally derived for calculating radionuclide leaching from contaminated volcanic ash blankets.

The initial inventories and thermal outputs are read by the INVENT utility module from data files *nuclides.dat* and *burnup.dat*. The thermal outputs are presented for 21 PWR and 44 BWR WPs in *burnup.dat* data files. Although the INVENT module waste inventories are currently based on the default assumptions of an average of PWR waste with a 39.56-GWd/MTU burnup and 35-percent BWR waste with a 32.24-GWd/MTU burnup, 3 percent can be changed if desired. These default assumptions provide an average waste burnup of 37-percent GWd/MTU. The typical age of the waste at the time of emplacement is set at 26 yr (i.e., default value), the average age of the waste at the time of emplacement, unless specified otherwise in the *tpa.inp* file. INVENT uses this information to determine the activity of each of the 43 radionuclides of interest in the HLW projected to the time of interest. The set of 43 radionuclides shown in table 3-3 was selected after reviewing the literature and finding 43 as the largest set of radionuclides being considered in other TSPA efforts (Barnard et al., 1992; Wilson et al., 1994; TRW Environmental Safety Systems, Inc., 1995). The NRC IPA Phase 2 effort tracked 20 radionuclides, hence the database has been expanded.

Details on the physical properties and inventory can be found in table 19-1. The order of the nuclides shown in table 3-3 is used throughout the TPA Version 4.0 code including the DCF tables presented in appendix B. As will be presented later in this user's guide, the direct release calculation uses

**Table 3-3. List of 43 nuclides in the INVENT database**

| Nuclide Number | Nuclide Name | Nuclide Number | Nuclide Name |
|---|---|---|---|
| 1 | $^{238}U$ | 23 | $^{240}Pu$ |
| 2 | $^{246}Cm$ | 24 | $^{236}U$ |
| 3 | $^{242}Pu$ | 25 | $^{232}U$ |
| 4 | $^{242m}Am$ | 26 | $^{151}Sm$ |
| 5 | $^{238}Pu$ | 27 | $^{137}Cs$ |
| 6 | $^{234}U$ | 28 | $^{135}Cs$ |
| 7 | $^{230}Th$ | 29 | $^{129}I$ |
| 8 | $^{226}Ra$ | 30 | $^{126}Sn$ |
| 9 | $^{210}Pb$ | 31 | $^{121m}Sn$ |
| 10 | $^{243}Cm$ | 32 | $^{108m}Ag$ |
| 11 | $^{243}Am$ | 33 | $^{107}Pd$ |
| 12 | $^{239}Pu$ | 34 | $^{99}Tc$ |
| 13 | $^{235}U$ | 35 | $^{93}Mo$ |
| 14 | $^{231}Pa$ | 36 | $^{94}Nb$ |
| 15 | $^{227}Ac$ | 37 | $^{93}Zr$ |
| 16 | $^{245}Cm$ | 38 | $^{90}Sr$ |
| 17 | $^{241}Pu$ | 39 | $^{79}Se$ |
| 18 | $^{241}Am$ | 40 | $^{63}Ni$ |
| 19 | $^{237}Np$ | 41 | $^{59}Ni$ |
| 20 | $^{233}U$ | 42 | $^{36}Cl$ |
| 21 | $^{229}Th$ | 43 | $^{14}C$ |
| 22 | $^{244}Cm$ | | |

all 43 nuclides, whereas a smaller set of nuclides (similar to IPA Phase 2) is used for groundwater releases, though the code has the capability to use any number of nuclides from the list of 43.

The 43 radionuclides considered in the INVENT module for direct releases contain four major actinide element decay chains. These chains are shown in figure 3-8. The specific nuclides being tracked are boxed in the decay chains. Additional radionuclides are tracked in the INVENT module that are not chain decay members; they are handled through simple decay equations. These radionuclides are typically fission or activation products and include $^{232}U$, $^{151}Sm$, $^{137}Cs$, $^{135}Cs$, $^{129}I$, $^{126}Sn$, $^{121m}Sn$, $^{108m}Ag$, $^{107}Pd$, $^{99}Tc$, $^{93}Mo$, $^{94}Nb$, $^{93}Zr$, $^{90}Sr$, $^{79}Se$, $^{63}Ni$, $^{59}Ni$, $^{36}Cl$, and $^{14}C$.

Radionuclide inventory calculations performed by INVENT have been verified by comparing the results with other published results and plotting the inventories for times from 10 to 1,000,000 yr (figure 3-9). The trends in the inventories were compared with those published elsewhere (e.g., Roxburgh, 1987). As expected, most radionuclide inventories decrease with increasing time, some remain relatively constant over long periods of time (those with long half-lives), and others increase with time (daughters in a decay chain). For example, $^{238}Pu$ has an 87.7-yr half-life, and its inventory can be observed to continuously decrease with time. Another example is $^{234}U$, which has a 244,500-yr half-life, and remains relatively constant up to about 100,000 yr. An example of daughter ingrowth can be seen with $^{230}Th$, $^{226}Ra$, and $^{210}Pb$, which are in the $^{246}Cm$ decay series of radionuclides (figure 3-7). Hence, the inventories of these daughters increase with time. In summary, the INVENT module was developed to facilitate the calculation

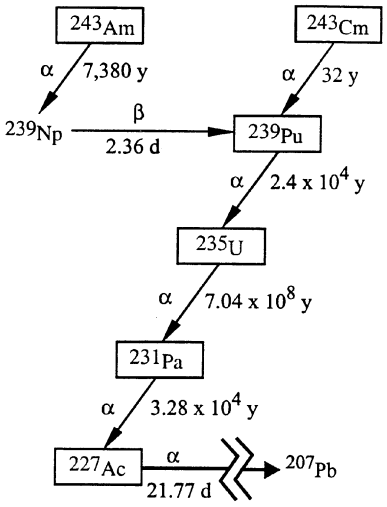


*Cm-243*

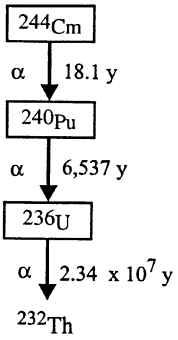


*Cm-244*

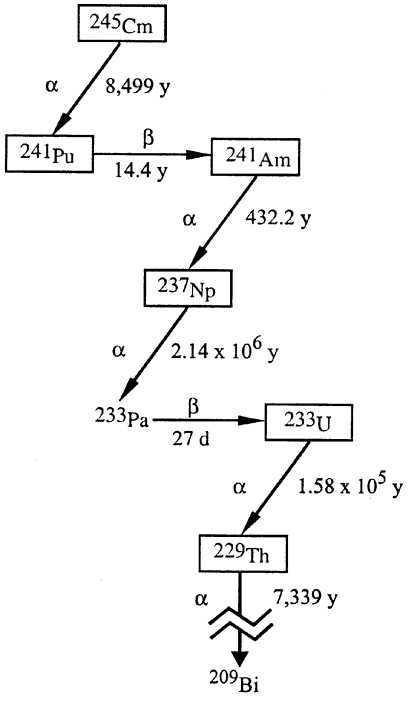


*Cm-245*

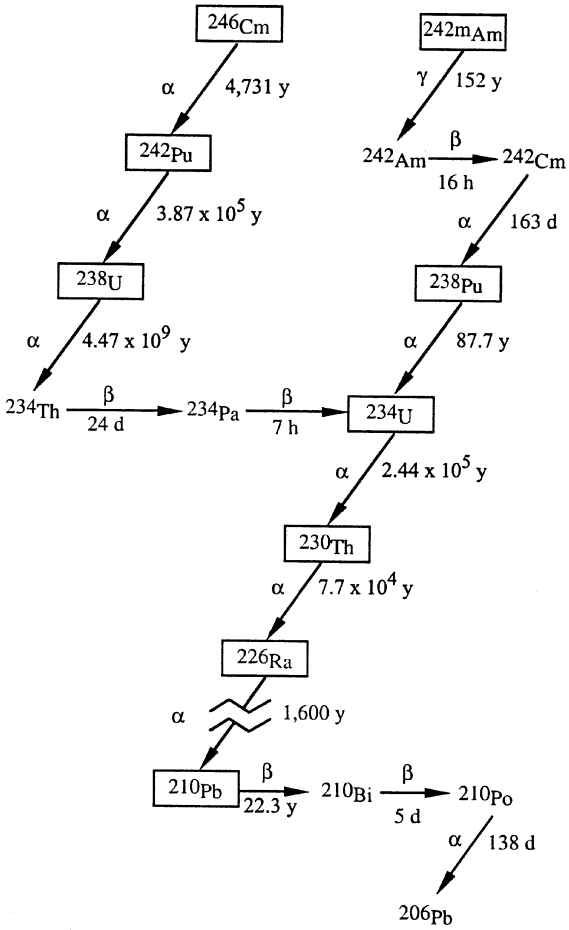


*Cm-246*

**Figure 3-8. $^{243}$Cm, $^{244}$Cm, $^{245}$Cm, and $^{246}$Cm decay chains**

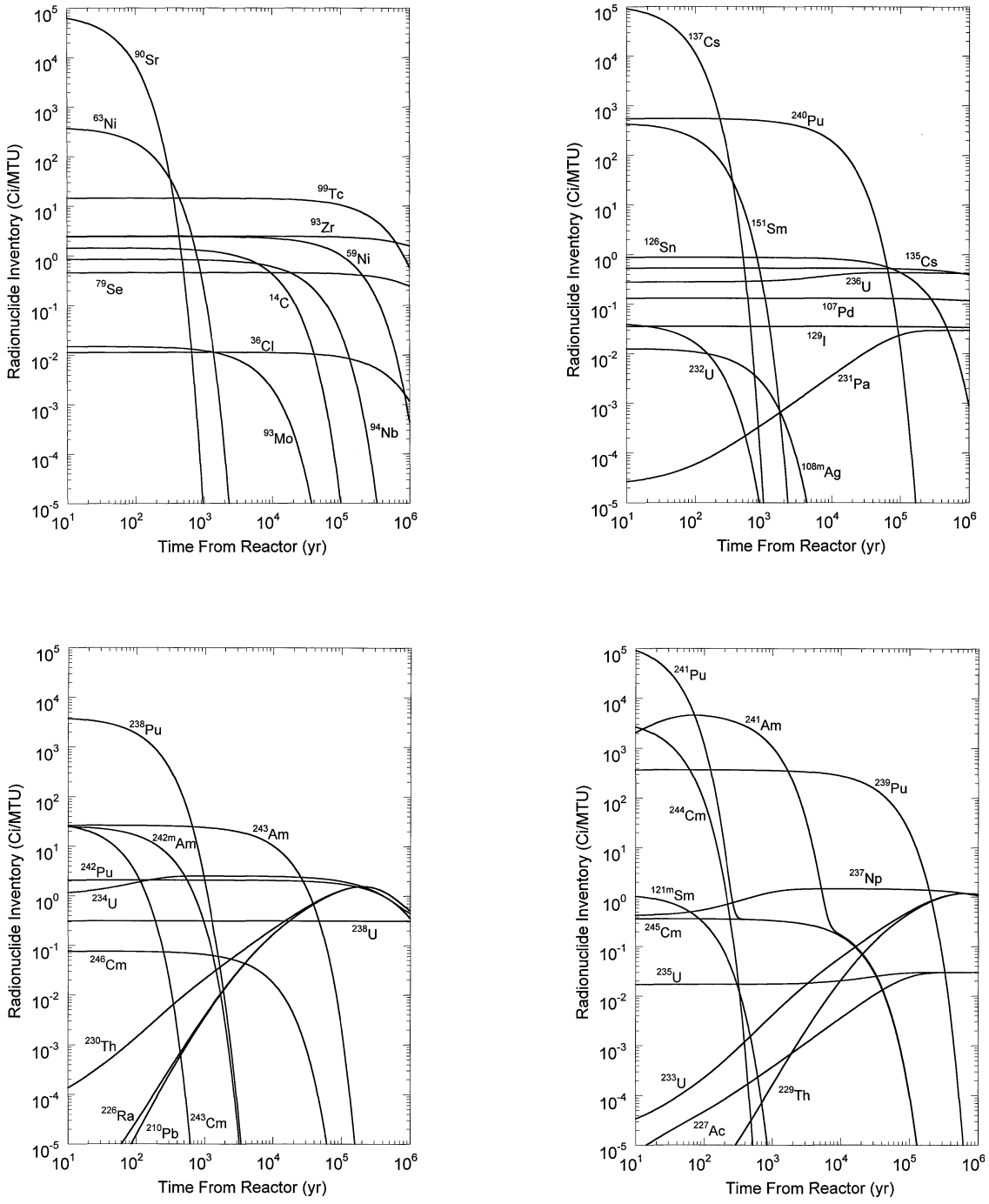


**Figure 3-9. Radionuclide inventories as a function of time (calculated by the INVENT module)**

of radionuclide inventories and the thermal output of the HLW that is used by various consequence modules of the TPA Version 4.0 code.

## 3.4 CONSEQUENCE MODULES

This section presents an outline of the information provided in chapters 4–18 for each of the consequence modules associated with the TPA Version 4.0 code. A description of the conceptual model and its implementation in each consequence module are presented via the following four sections

(i) Information Flow
(general identification of the input supplied by the user and information supplied by other modules, and the information that this module provides to other modules)

(ii) Intermediate Results
(identification of the kinds of intermediate results that are available to provide insight on the calculational results of a particular module that are intermediate to the overall performance measure; examples of intermediate results are WP lifetime and release rates from the UZ)

(iii) Conceptual Model
(description of the technical approach and implementation within the code)

(iv) Assumptions
(listing of some of the important assumptions and, where appropriate, their effect on conservatism in the final results)

The information in chapters 4–18 is intended to allow a potential user of the code to either develop or modify the input files of the TPA Version 4.0 code based on an understanding of the relationship of the input parameters to the calculational approach in the code, and to know the types of results available for analyzing performance.

Execution of the TPA Version 4.0 code requires a variety of input. The primary input file, *tpa.inp*, is used to control the attributes of the simulation (e.g., inclusion of disruptive events, number of realizations in the probabilistic analyses, and length of simulation) and specification of parameters. It is anticipated that the TPA Version 4.0 code will typically be used in a probabilistic mode (i.e., performing a large number of trials based on MCS or LHS of the input parameters) due to uncertainty and variability in describing the repository system (e.g., porosity, retardation, and solubility limits). The input parameters included in the *tpa.inp* file are the only input that can be sampled. Other inputs, not considered appropriate for sampling, are used to specify constants of the analysis (e.g., elevation of the subarea and radionuclide half-life) or abstractions of detailed models (e.g., definition of streamtube characteristics based on a 2D analysis). A variety of data files, generally designated by *.dat* at the end of the file name, are used to supply the deterministic information. For completeness, chapters 4–18 identify input relevant to a particular module; however, the user should only modify the values in the *tpa.inp* file. Chapter 19 and appendixes A and B contain additional information on the input structure for the TPA Version 4.0 code.

Two general types of consequence modules are incorporated in the TPA Version 4.0 code: (i) basecase modules primarily associated with the groundwater pathway—UZFLOW, NFENV, EBSFAIL,

SEISMO, EBSREL, UZFT, SZFT, and DCAGW; and (ii) disruptive event modules associated with damage to the WP and direct release of radionuclides in the air pathway from the extrusive component of IA—FAULTO, VOLCANO, ASHPLUMO, ASHRMOVO, and DCAGS. Overall, the consequence modules described in chapters 4–18 estimate

- Water infiltration from the land surface to the subsurface and, subsequently, into the emplacement drifts onto WPs
- Environment around the WPs (temperature, humidity, pH, chloride ion concentration, and carbonate ion concentration) that affects WP degradation or radionuclide release
- WP failure times due to corrosion and mechanical processes, seismicity induced rockfall, faulting, IA, and WPs assumed to be initially defective
- Release of radionuclides from failed WPs through the invert to the groundwater transport pathway
- Release of radionuclides from the extrusive component of IA to the air pathway
- Transport of radionuclides in groundwater through the UZ and SZ
- Transport of radionuclides in volcanic ash
- Doses to receptors through the radiological contamination in groundwater
- Doses to receptors through the radiological contamination of the ground surface (released from the repository by an extrusive volcanic event)

# 4 UZFLOW MODULE DESCRIPTION

The UZFLOW module calculates the amount of water infiltrating from the ground surface into the UZ above the repository. Water that has infiltrated the subsurface affects the repository near-field environment and is potentially available for WP corrosion, dissolution of material in the WP, and transport of material released from WPs. Specifically, UZFLOW determines the temporal and spatial variation of percolation water flux at the repository horizon in the absence of thermal effects from the repository. The NFENV module, which simulates the near-field environment, accounts for the effect of repository heating on percolation through the repository. The calculation of percolation flux includes the effect of changes in precipitation and temperature that may occur at the ground surface throughout the life of the repository. Additional information on modeling of climate change and its effect on percolation flux can be found in Stothoff et al. (1997).

## 4.1 INFORMATION FLOW WITHIN TPA

### 4.1.1 Information Supplied to UZFLOW

Input provided to the UZFLOW module consists of detailed information on ground surface elevation, soil thickness, and the future climatic conditions (provided via external files, see chapter 19), and parameters that specify the present infiltration and the variation in climate (provided in *tpa.inp*). Ground surface elevation is supplied as a DEM in the data file entitled *elevdem.dat*. A DEM with the same discretization, *soildem.dat*, provides soil thicknesses. The input files *climato1.dat* and *climato2.dat* provide data for representing time-dependent future climatic conditions. Data file *climato1.dat* provides noise data (normally distributed random numbers) used in computing time-varying *MAP* and mean annual temperature (*MAT*). Data file *climato2.dat* provides a time history of glaciation expressed as a fraction of the full glacial maximum in temperature and precipitation. The estimated *MAI* for specified *MAP* and *MAT* is supplied as a table of DEMs in the data file *maidtbl.dat*, which is generated using a preprocessor code. Appendix B gives additional detail on the structure of these data files. All other input parameters to UZFLOW specifying present infiltration and the magnitude of climate variation are in the UZFLOW section of the *tpa.inp* file.

### 4.1.2 Information Provided by UZFLOW

UZFLOW passes to EXEC the time-varying volumetric flow rate of water infiltrating toward the repository, which then provides these values to the NFENV module for use in estimating groundwater reflux during the repository thermal phase and the UZFT module for determining transport velocities.

## 4.2 INTERMEDIATE RESULTS

The intermediate outputs from UZFLOW are available in the *infilper.res* file. For all realizations, the *infilper.res* file provides the deep percolation rate averaged over all subareas for every tenth-time step used in the TPA run. The *infilper.res* file is detailed in tables 20-1 and 20-2.

When the append option is turned on by the user in the *tpa.inp* file to create additional intermediate outputs, UZFLOW inputs and outputs are written to the *uzflow.ech* and the *uzflow.rlt* files. The time intervals specified by EXEC are included in the *uzflow.ech* file. The volumetric flow rates into each

subarea for all time steps are provided in the *uzflow.rlt* file. A complete description of these files is presented in chapter 20.

## 4.3 CONCEPTUAL MODEL

The UZFLOW module has three sections: (i) a climate model for specification of the time history of climatic change, (ii) a model for calculation of shallow infiltration rate under different climates, and (iii) a deep percolation model for calculation of spatially averaged percolation flux at the repository level.

The climate model assumes that climate variables change in response to a glacial cycle, with a period of roughly 100,000 yr, with shorter-term perturbations superimposed upon the cycle. Two climate variables, precipitation and temperature, have the dominant impact on infiltration (Stothoff et al., 1997). The time evolution of the dominant variables is calculated in the TPA Version 4.0 code using input specifications from the *climato1.dat* and *climato2.dat* data files (see table 19-2) and the UZFLOW section of the *tpa.inp* file. The elevation-dependent spatial variability of these variables, is superimposed on the glacial perturbations using the elevations in the *elevdem.dat* data file. Elevation-dependent vapor density, based on RH and temperature data from meteorologic stations that bracket the elevations at YM, is also incorporated into estimates of *MAI* but the elevation dependency is held constant across changes in climate.

Figure 4-1 illustrates the shallow infiltration conceptual model, including water and energy balances for a system of shallow surficial soil above a fractured impermeable bedrock. Water and heat enter and exit the soil at the ground surface. After a precipitation event, evaporation removes a portion of the water and the remaining portion of the water infiltrates and moves into the deep subsurface (below the root zone) via fracture and bedrock flow. Thus, water escaping evaporation becomes deep percolation. Offline simulations of shallow infiltration using this conceptual model were performed for a simulated time period of at least a decade using hourly time steps (Stothoff et al., 1997; Stothoff, 1999). The resulting time-varying infiltration, accounting for short-term variability in climatic parameters, is abstracted into relationships between *MAI* and decade-scale average climate (i.e., *MAP* and *MAT*). In a preprocessor code (section 4.3.2), these relationships are used to estimate the expected value of *MAI* for several combinations of *MAP* and *MAT*, yielding a table of estimates for each grid block in a DEM overlying the repository footprint. In the UZFLOW module, all grid blocks within each subarea are aggregated to yield a table of *MAI* averaged over the subarea. The time history of *MAI* is thus obtained from the time history of *MAP* and *MAT*, with individual *MAI* values calculated for each grid block lying within the repository footprint in the *elevdem.dat* data file.

The gridblock values of *MAI* are used to determine the total deep percolation for each repository subarea (figure 4-2). The time interval for computing deep percolation is specified in the *tpa.inp* file; it is typically on the scale of centuries. The deep-percolation time scale is much longer than for shallow infiltration simulations, justified by the assumption of strong temporal smoothing of fluxes as waters pass from the ground surface to the repository horizon. The smoothing is conceived of as a local process, so that fluxes generally pass vertically to the repository without systematic lateral diversion.

### 4.3.1 Climate Model

Infiltration rates are strongly affected by precipitation and evapotranspiration (which in turn is strongly affected by air temperature). Over the period of repository performance, it is anticipated that average precipitation and air temperature will change. At the last full glacial maximum, available evidence

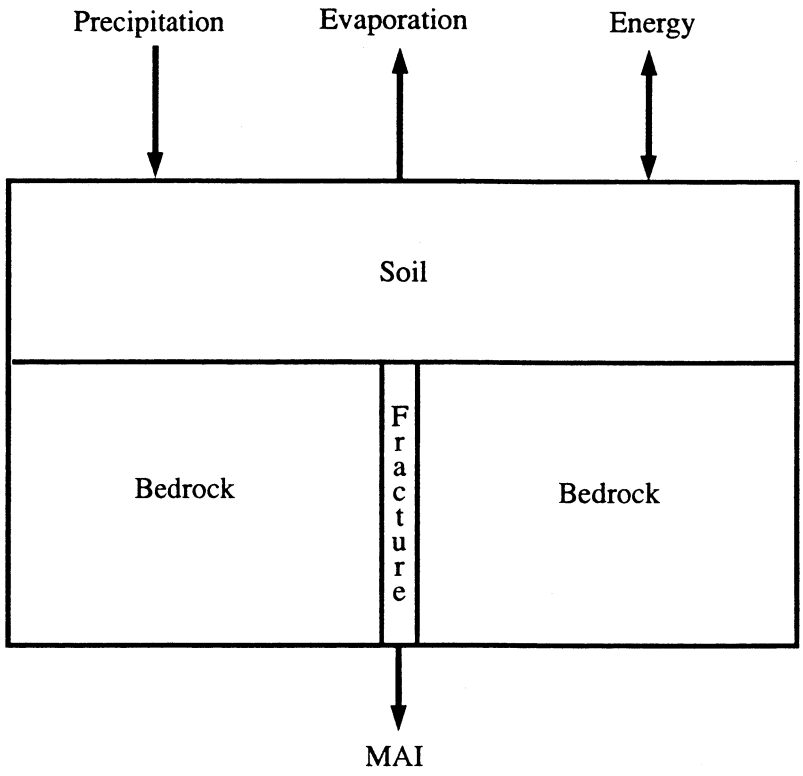


**Figure 4-1. UZFLOW conceptual model**

suggests that *MAP* at YM may have been 1.5–3 times larger than under current climatic conditions, while *MAT* may have been cooler by 5–10 °C (U.S.Nuclear Regulatory Commission, 1997). The effect of such large climatic changes can be examined using the UZFLOW module.

The shallow infiltration model uses the time evolution of *MAP* and *MAT* to calculate *MAI*. In arid environments such as exist at YM, interannual variability in precipitation can vary by a factor of 10, so that the concepts of *MAP* and *MAT* implicitly require averaging over several decades or more. The detailed analysis performed to develop the regression equations for shallow infiltration incorporates climatic variability at time scales shorter than a decade through the use of a 15-yr record from a meteorological station that includes a complete set of the required variables. Climatic variability on scales longer than decades is treated directly in the TPA Version 4.0 code as described in the following paragraphs.

The climate model assumes that the bulk effects of climatic change can be represented by a glacial-change cycle, with shorter time-scale climate changes (century-to-century variability in precipitation and temperature) superimposed on the overall change in climate (bulk signal). The timing of bulk climatic change is felt to be more certain than the magnitude of climatic changes, with a full cycle of climatic

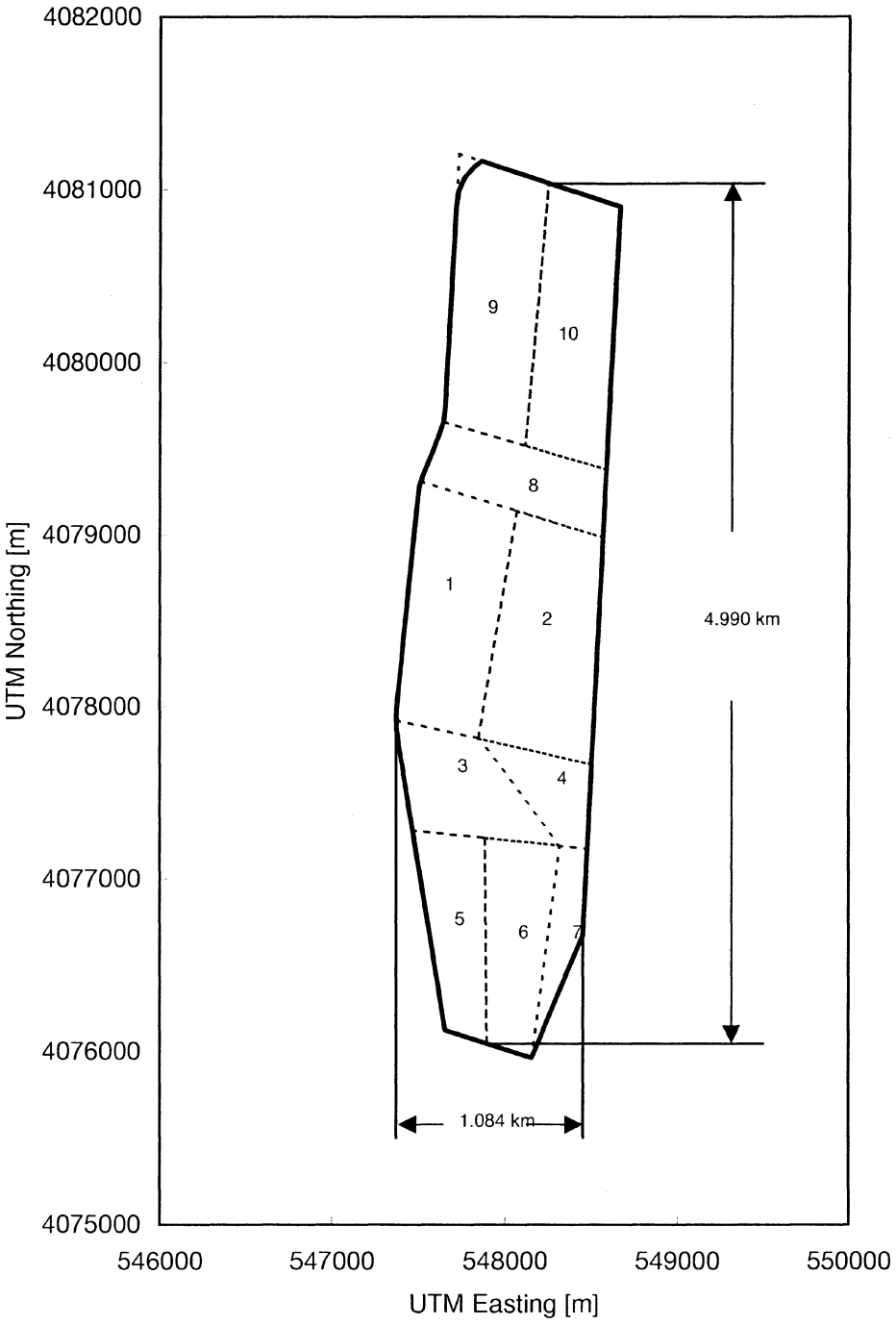


**Figure 4-2. Boundary of proposed Yucca Mountain repository with only eight subareas (1–8) filled**

changes occurring roughly during 100,000 yr. For purposes of this analysis, *MAP* and *MAT* are assumed to be known at the start of the simulation (i.e., the present day), while changes in *MAP* and *MAT* during full glacial conditions are considered quite uncertain.

The UZFLOW model incorporates the effects of climate change by sampling only those parameters that have the greatest uncertainty for each TPA realization. For example, climate change can be characterized by changes in *MAP* as a multiplier of current conditions (e.g., 1.5–3 times current values) and changes in *MAT* as a difference from current conditions (e.g., 5–10 °C cooler). Accordingly, the *MAP* multiplier at full glacial maximum and the *MAT* offset at full glacial maximum are specified in *tpa.inp*. A function describing the temporal variation of bulk climatic change is obtained from the file *climato2.dat*. As the simulation proceeds from the start through the climate change cycle, *MAP* and *MAT* cycle from current values through full glacial maximum conditions and back to current conditions. *MAP* and *MAT* have the same formula for bulk climatic change, so they vary at the same rate over the glacial cycle.

The bulk climatic change file (*climato2.dat*) supplies the code with data generated using the following formula, determined by matching the last several Milankovich cycles

$$p = 1 - \frac{1}{4}\left[1 - \sin\left(\frac{\tau}{14.33 - 1.22}\right)\right]^2 \tag{4-1}$$

$$f = \frac{p - p_0}{1 - p_0} \tag{4-2}$$

where $\tau$ is time (ky) before present (in the Milankovich cycles used to develop the formula), $f$ is the relative change between the current climate and the full glacial maximum, $p$ is a periodicity function, and $p_0$ represents the present-day value of *MAP* or *MAT* (i.e., at $\tau = 0$). The input file has values at each 1,000 yr, which are linearly interpolated to obtain intermediate values. Note that Eqs. ( 4-1) and (4-2) predict that conditions are more than halfway to full glacial maximum (i.e., $f > 0.5$) for roughly 2/3 of the total climatic cycle, as shown in figure 4-3a, although conditions may be slightly drier and hotter than present for about 10 ky.

The climatic history generated from the data file is evaluated for uniform time intervals, with length specified in the *tpa.inp* file as TimeStepForClimate[yr]. At the midpoint for each interval, *MAP* and *MAT* are evaluated using

$$MAP(t) = MAP_0 + f(t)\left(MAP_{\text{fgm}} - MAP_0\right) \tag{4-3}$$

$$MAT(t) = MAT_0 + f(t)\left(MAT_{\text{fgm}} - MAT_0\right) \tag{4-4}$$

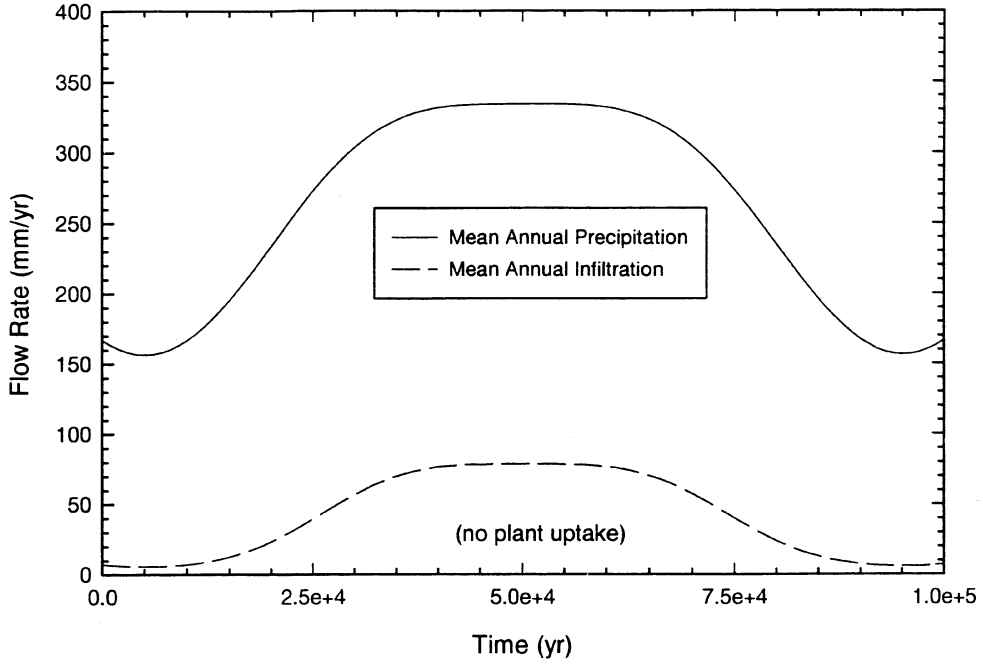


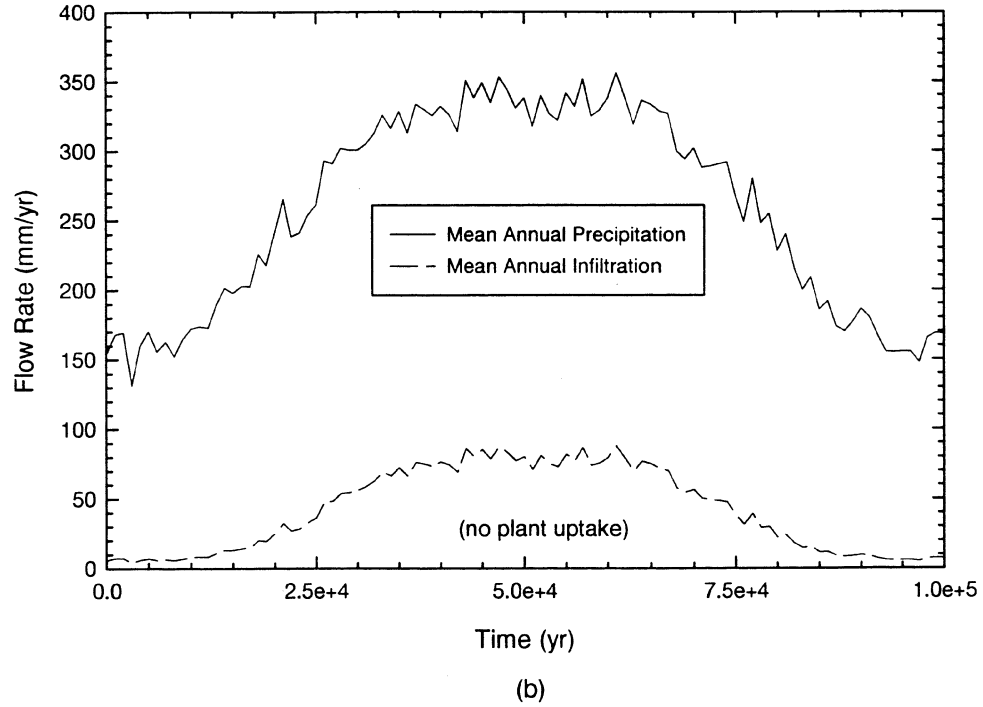


**Figure 4-3. Variation of mean annual infiltration with changes in mean annual precipitation during a climate cycle: (a) mean climate signal only and (b) with perturbation**

where $t$ is time from start of simulation; $MAP_0$ and $MAT_0$ represent *MAP* and *MAT* at the start of the simulation; and $MAP_{fgm}$ and $MAT_{fgm}$ represent *MAP* and *MAT* at full glacial maximum.

**Variation in Climate Change Cycle**

Relatively short-term climatic changes can significantly change the climate from the bulk predictions (e.g., mini-glacial periods), thereby causing periods of higher or lower *MAI*. As *MAI* is exponentially dependent on climate (Section 4.3.2—Shallow Infiltration Model), the expected long-term average infiltration is larger if these mini-glacial periods are considered, even if the climatic changes are evenly distributed above and below the mean cycle. If the variability is small, it may be adequate to use the bulk climate formula to predict infiltration. During relatively short simulations, these departures from the bulk conditions can provide substantial portions of the total infiltration.

The UZFLOW module provides a mechanism to examine the importance for repository performance of short-term climatic perturbations. A perturbation to the bulk value of both *MAP* and *MAT* (developed as described previously) is calculated for each of the uniform time intervals. It is assumed that the *MAP* and *MAT* perturbations are correlated with each other within a time interval, but perturbations are not correlated between successive intervals (i.e., *MAP* and *MAT* variations in one time interval are not affected by variations in previous intervals and do not affect variations in future time intervals). Within a time period, $k$, perturbations are generated using

$$\chi^k = L\varepsilon \tag{4-5}$$

where

| | | |
|---|---|---|
| $\chi^k$ | — | a vector of correlated perturbations in time step k |
| $\varepsilon$ | — | a vector of independent standard normal perturbations |
| $L$ | — | Cholesky decomposition f the correlation matrix |

The correlation between *MAP* and *MAT* perturbations is represented by CorrelationBetweenMAPandMAT in the *tpa.inp* file. The correlation must lie between −1 and 1, and a reasonable value is about −0.8 (i.e., wetter conditions are generally associated with cooler conditions).

The actual values for *MAP* and *MAT* within time step $k$ are calculated using

$$v_j^k = \chi_j^k \sigma_j + m_j \tag{4-6}$$

where $j$ represents *MAP* or *MAT*, $v_j^k$ is the calculated value of variable $j$, $\sigma_j$ the standard deviation of variable $j$, and $m_j$ the value of variable $j$ using the bulk climatic interpolation. For *MAP*, standard deviation values are called StandardDeviationOfMAPAboutMeanInOneTimePeriod[mm/yr] and for *MAT*, they are termed StandardDeviationOfMATAboutMeanInOneTimePeriod[degC] in the *tpa.inp* file. Both standard deviation values are assumed constant over the length of the TPA simulation.

It is important to note that the time variability in the *MAI* formula is for time periods of less than a decade. Within the preprocessor code, time variability of *MAP* and *MAT* may be considered using the same procedure to predict expected *MAI* for a given climate state. In the preprocessor (section 4.3.2), the standard deviations for *MAP* and *MAT* used in Eq. (4-6) should capture variability of 10-yr average climate. Reasonable standard deviation values might be 20–30 mm/yr for *MAP* and 0.4–0.5 °C for *MAT*, based on a 50-yr sequence of daily meteorologic observations at Beatty, Nevada. In the TPA code, the standard deviations for *MAP* and *MAT* used in Eq. (4-6) should capture variability of average climate on a longer time scale, such as centuries or millenia. The variability of climate likely leads to an increased average infiltration as illustrated in the example presented in figure 4-3. If only the bulk climatic behavior is wanted, the two standard deviation values should be set to zero. [Note: constant infiltration rates through all time can be obtained by setting the values of MeanAverageTemperatureIncreaseAtGlacialMaximum to 0 as well as setting the two standard deviations to 0 in the *tpa.inp* file; $MAP_{fgm}$ in Eq. (4-3) is equal to the multiplier times the $MAT_0$.]

## 4.3.2 Shallow Infiltration Model

The shallow infiltration model in UZFLOW calculates the mean annual UZ net-infiltration flux leaving the root zone for the deeper subsurface. The net-infiltration flux is directly linked to the *MAP* and *MAT* climatic parameters, that are calculated as described above.

Infiltration in a semiarid zone, such as exists at YM, tends to occur during particularly wet years possibly separated by years to decades of drier years. Simulations of bare-soil infiltration conducted by Stothoff et al. (1997) and Stothoff (1999) indicate that *MAI* is strongly dependent on soil thickness when the soil thickness is less than 50 cm, and that different soil thicknesses exhibit different sensitivities to changes in *MAP* and *MAT*. Generally, thin soil layers allow infiltration to quickly reach fractures and thus percolate below the root zone into the deeper subsurface. At YM, most of the repository footprint is overlain by thin soils (i.e., less than 50 cm) with significant variability across the site. Accordingly, to calculate *MAI* over the repository footprint, the shallow infiltration model uses a fine scale grid compared to a typical subarea. The fine-scale calculations are averaged to the larger subarea scale within the UZFLOW module.

The UZFLOW module does not explicitly consider any of the processes involved in calculating *MAI*. Rather, an input file *(maidtbl.dat)* provides estimates of expected *MAI* for tabulated values of expected *MAP* and *MAT* for each of the fine grid cells in a DEM. Within UZFLOW, the grid cells within each repository subarea are aggregated before any TPA realization to provide a table of expected subarea-average *MAI* elevation.

During each TPA realization, the history of *MAP* and *MAT* calculated by the CLIMATO module is passed to UZFLOW. These values are used to look up expected *MAI* for each subarea, thus providing a time-history of expected *MAI*.

As the simulations and abstractions used to create the expected *MAI* values do not and cannot capture all of the detail of infiltration-affecting processes across the repository footprint, there are inevitable inaccuracies in estimated *MAI* values. Potential inaccuracies include (i) estimates of present-day *MAI,* (ii) future precipitation and temperature conditions, and (iii) estimates of future shallow infiltration for each predicted future climate condition. For the present-day conditions, the UZFLOW module compensates for these inaccuracies by scaling all estimated *MAI* values by the ratio of a TPA-sampled

estimate of repository-average *MAI* [AreaAverageMeanAnnualInfiltrationAtStart (mm/yr)] to the corresponding estimated values derived from the *maidtbl.dat* input file.

The scaling procedure provides a direct mechanism to examine uncertainty in present-day *MAI*, with the field of expected-*MAI* values providing the mechanism to distribute the sampled *MAI* both in space and in time. For future conditions, the *tpa.inp* parameters MeanAveragePrecipitationMultiplierAtGlacialMaximum and MeanAverageTemperatureIncreaseAtGlacialMaximum [degree C] account for both uncertainty in climate conditions and for inaccuracies in estimating *MAI* at those conditions. The uncertainty in climate conditions was discussed in section 4.3.1. Inaccuracies in estimating *MAI* during future climate conditions may be caused by changes in plant, soil, and bedrock properties brought on by the different climatic conditions.

A preprocessor code, Infiltration Tabulator for Yucca Mountain (ITYM), creates the *maidtbl.dat* input file. The preprocessor explicitly considers processes involved in calculating *MAI*, as well as uncertainty and both spatial and temporal variability in the *MAI*-affecting factors. The ITYM preprocessor and *maidtbl.dat* file are described in appendix B.

### 4.3.3 Deep Percolation Model

Deep percolation at the repository horizon within each subarea is assumed to be the average value of *MAI* within the subarea, with fluxes throughout the repository equilibriating rapidly relative to climatic change. The deep percolation model assumes that redistribution of percolating water from the root zone to the repository level occurs in each subarea. It is generally accepted that percolating water will tend to move vertically in the UZ unless capillary or permeability barriers force lateral redistribution. The resulting model conservatively neglects lateral diversion away from the repository and assumes the subareal-average shallow-infiltration flux moves vertically down to the repository level.

## 4.4 ASSUMPTIONS AND CONSERVATISM OF THE UZFLOW APPROACH

The UZFLOW module is an abstraction of the processes controlling *MAI* and redistribution of infiltrating waters above the repository horizon. The main processes that control infiltration are (i) climatic conditions or variation of precipitation and temperature, (ii) near-surface processes such as evapotranspiration and runoff, and (iii) lateral diversion of subsurface flow.

Annual infiltration is expected to vary over the long term (i.e., thousands of years) because of variation in temperature and precipitation. Based on historical data and paleoclimatic markers, a full cycle of climatic changes is assumed to occur roughly every 100,000 yr and conditions may be slightly drier and hotter than present for about the next 10,000 yr, after which conditions can be expected to become cooler and wetter. This approach is considered a reasonable representation of the long-term evolution of climate. Although short-term perturbations of climate will occur (i.e., some years wetter and cooler and some years drier and hotter than expected), the net effect on estimated doses at a receptor location will be significantly damped by the long transport times from the repository to the receptor location (travel times would be on the order of hundreds to thousands of years or longer).

Estimates of infiltration are sensitive to a number of factors affecting near-surface conditions, such as temperature, precipitation, soil depth, evaporation, plant transpiration, and surface water runoff. Results of detailed 1D simulations of mass and energy fluxes under a range of conditions representative of the

surface of YM were used to develop abstracted, predictive equations for *MAI* as a function of *MAP*, *MAT*, soil thickness, soil and bedrock hydraulic properties, and other climatic inputs. These predictive equations are embodied in a preprocessor code. The detailed model simulations do not account for plant transpiration, which tends to reduce net infiltration. Plant transpiration can be considered in the ITYM preprocessor using a heuristic formula; however, the formula has not been examined in detail and is considered quite uncertain. Neglecting plant transpiration will cause infiltration estimates to become increasingly overestimated as the climate becomes wetter and cooler with resultant increases in vegetation and plant transpiration. Lateral redistribution due to surface runoff is neglected in the detailed model simulations and in the ITYM preprocessor. Neglect of redistribution results in relatively over-predicted *MAI* along ridges and relatively underpredicted *MAI* in areas with significant runon, particularly stream channels. Net runon tends to occur in areas with larger storage capacity and concomitant low *MAI.* Further, under current climatic conditions total channel infiltration is expected to be small relative to distributed infiltration (Woolhiser et al., 1999). Although the spatial distribution of *MAI* may be biased towards ridgetops, it is not clear that areal-average *MAI* at the subarea scale is strongly biased. Finally, the abstractions do not account for temporal variation in soil depth and composition; both respond to climate change in a complex way and both influence infiltration (Stothoff, 1999).

After penetrating to the subsurface, infiltrating water is assumed to pass in pulses vertically through the fracture system of the Tiva Canyon welded unit to the Paintbrush Tuff nonwelded unit, where the pulses spread and dissipate, passing through uniformly to the underlying Topopah Springs welded unit and continuing vertically to the repository horizon. It is assumed that contacts between the welded units and the nonwelded unit do not cause systematic lateral diversion, because of the existence of numerous small faults in the nonwelded unit; diversion would tend to reduce fluxes on the western portion of the repository and might increase fluxes on the eastern portion of the repository. The current approach, which neglects lateral diversion of infiltrating water, is considered conservative because lateral diversion could be expected to reduce the number of containers that encounter dripping water.

There are specific assumptions related to the UZFLOW module and preprocessor:

- It is assumed that the future climate at YM will follow the general form of the paleoclimatic record, with shorter variations imposed on the general trend.

- Both *MAP* and *MAT* are assumed to vary according to the same formula derived from Milankovich cycle data.

- Infiltration is assumed to be directly related to climatic influences, increasing as precipitation increases and temperature decreases. The linkage between climate and infiltration is calculated assuming that infiltration occurs under bare-soil conditions. Bare-soil conditions conservatively overpredict infiltration that are more appropriate for present-day climate than for the future climate conditions. Vegetation density is expected to increase under cooler and wetter climate conditions, thus predictions will become increasingly conservative. A heuristic formula may be used to account for transpiration.

- For the computation of shallow infiltration, the geometric and hydrologic properties of the soil and bedrock will not change during the simulation. It is assumed that hydrologic properties of near surface materials will not change because of faulting or

repository-induced thermal widening of fractures and rock dilation; nor will soil genesis change because of variations in climate.

- It is assumed that *MAT* decreases linearly with increasing elevation, while both *MAP* and atmospheric vapor density vary exponentially with elevation, and the gradients remain the same over time.

# 5 NFENV MODULE DESCRIPTION

The NFENV module calculates the time-dependent hydrothermal environment of the WP such as

- Representative repository-horizon rock temperature
- WP surface and SF temperatures
- RH at the WP surface
- Flow rate of groundwater into the near field
- pH and chloride concentrations of groundwater flowing onto the WP

The near-field environment includes areas inside the drift and those portions of the geologic setting that the repository modifies and that may affect repository performance. Background information on calculation of the pH and chemistry of groundwater flowing onto WPs can be found in Mohanty et al. (1997).

## 5.1 INFORMATION FLOW WITHIN TPA

### 5.1.1 Information Supplied to NFENV

The NFENV module uses input data specified in *tpa.inp* and other data files (*burnup.dat, repdes.dat,* and *multiflo.dat*) for computing temperature, groundwater reflux, and groundwater chemistry. In addition, for each subarea and realization, EXEC passes to NFENV the time-varying volumetric flow rate of water infiltrating toward the repository calculated by UZFLOW for the computation of groundwater reflux. The *repdes.dat* file provides to NFENV the coordinates (in 2D) for the repository boundary and angle of inclination of drifts with respect to the East-West axis for the computation of repository-horizon average rock temperatures in subareas. Other input parameters to NFENV for computing temperature and RH, such as thermal diffusivities, effective thermal conductivities, material emissivities, and time of backfill, are specified in the NFENV section of *tpa.inp*. Temperature and RH values computed external to the TPA Version 4.0 code can be used via the *tefkti.dat* file when the appropriate flag is set in *tpa.inp*. Chloride concentrations are read from the data file *multiflo.dat*. Appendix B gives additional details on the structure of these data files. In *tpa.inp*, the user also selects the reflux model (from REFLUX1, REFLUX2, or REFLUX3) and specifies parameter values for use by REFLUX1, REFLUX2, or REFLUX3.

### 5.1.2 Information Provided by NFENV

The NFENV module passes to EXEC the values for time-dependent WP temperature, RH, pH, and the chloride concentration for use in EBSFAIL. NFENV also provides the time history of percolation flux at the repository level to EBSREL through EXEC.

## 5.2 INTERMEDIATE RESULTS

The intermediate outputs from NFENV are available in *infilper.res* and *nearfld.res*. The reflux of groundwater averaged over all subareas for every tenth time step is presented in *infilper.res* for all realizations. The subarea-averaged near-field conditions (i.e., temperature, RH, and chloride concentration) from each realization for every tenth time step are provided in *nearfld.res*. The *infilper.res* and *nearfld.res* files are detailed in tables 20-1 and 20-2.

When the append option is turned on in *tpa.inp* to create additional intermediate outputs, NFENV inputs and outputs are written to *nfenv.ech* and *nfenv.rlt*. These files allow the user to examine outputs at all time steps instead of subarea-averaged values at every tenth time step. The volumetric flow rate toward the repository per the WP as a function of time is included in *nfenv.ech* for all time steps. The volumetric flow rates corresponding to the cross-sectional areal of the WP and otherwise (i.e., hitting and missing), WP temperature, RH, and chloride concentration for each subarea and all times can be accessed in *nfenv.rlt*. A complete description of these files is provided in section 20.3.

## 5.3 CONCEPTUAL MODEL

The NFENV conceptual model description is divided into three portions: (i) heat transfer and temperature calculation on a mountain and drift scale, (ii) chemical composition of groundwater flow in the near field, and (iii) calculation of thermally driven refluxing of groundwater.

### 5.3.1 Heat Transfer and Temperature Calculation

#### Mountain-Scale Heat Transfer

The repository-horizon average rock temperature is computed using an analytic conduction-only model for mountain-scale heat transfer. The model is based on line thermal sources, representing drifts, separated by the drift spacing specified in the *tpa.inp* file and residing in a semi-infinite medium. The modeled repository region has line sources laid out parallel to each other to cover the proposed repository (figure 5-1). Each line source is at a depth of $H$ below the ground surface and is represented as a high aspect-ratio rectangular element with a length of 2L and width of 2B (the drift diameter) (figure 5-2). Because more than one line source exists, the temperature increase in the semi-infinite medium is the sum of contributions from each line source. The general solution for the temperature increase at any point in space and time is given by Claesson and Proberts (1996) and Carslaw and Jaeger (1959)

$$\Delta T(x,y,z,t) = \int_0^t \frac{\alpha q''_{\text{rep}}(t')}{4k\sqrt{\pi}} \frac{1}{\sqrt{4\alpha(t-t')}} \left[ \text{erf}\left( \frac{L-x}{\sqrt{4\alpha(t-t')}} \right) + \text{erf}\left( \frac{L+x}{\sqrt{4\alpha(t-t')}} \right) \right]$$
$$\left[ \text{erf}\left( \frac{B-y}{\sqrt{4\alpha(t-t')}} \right) + \text{erf}\left( \frac{B+y}{\sqrt{4\alpha(t-t')}} \right) \right] \left[ \exp\left( \frac{-z^2}{4\alpha(t-t')} \right) - \exp\left( \frac{-(z-2H)^2}{4\alpha(t-t')} \right) \right] dt' \quad (5\text{-}1)$$

where

| | | |
|---|---|---|
| $\Delta T(x,y,z,t)$ | — | increase in temperature at time $t$ at point ($x$, $y$, $z$) in the semi-infinite medium due to one line source [°C] |
| $q''_{\text{rep}}(t)$ | — | time-dependent repository heat flux [W/m$^2$] |
| $\alpha$ | — | thermal diffusivity of the semi-infinite medium [m$^2$/s] |
| $k$ | — | thermal conductivity of the semi-infinite medium [W/(m - °C)] |
| $L$ | — | half-length of a line source [m] |

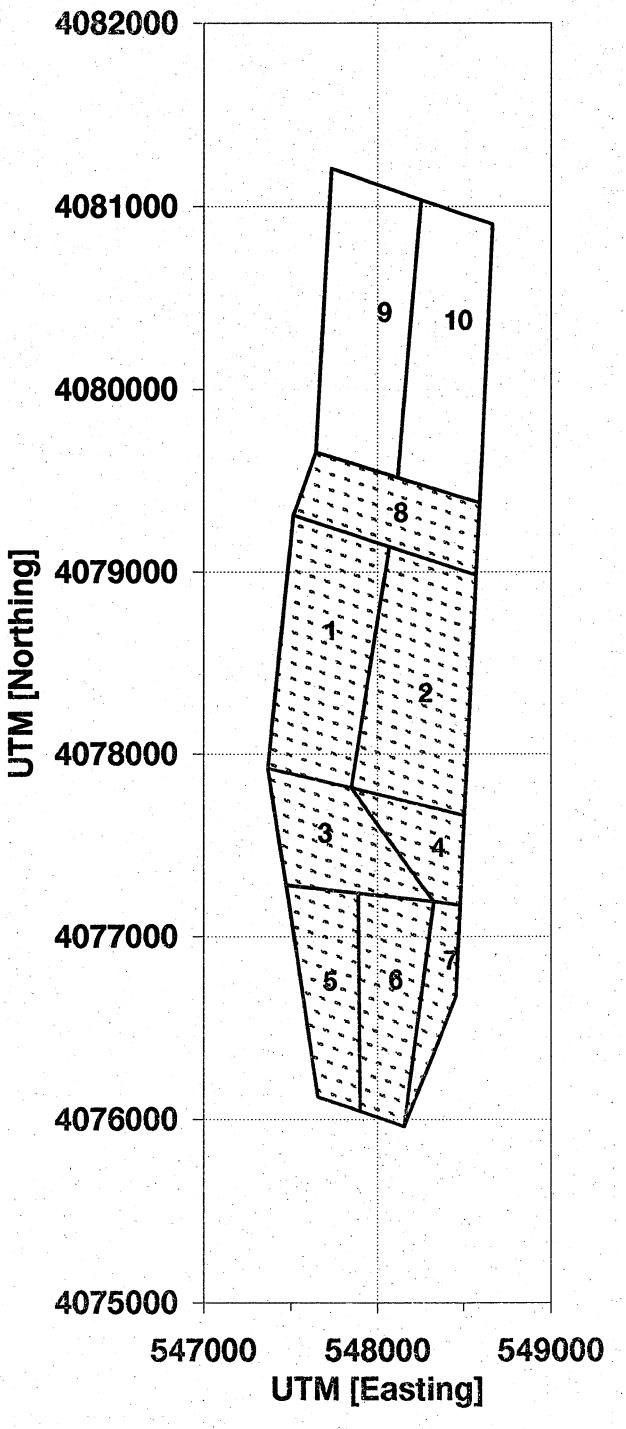


**Figure 5-1. Heat sources represented as parallel lines in the modeled repository region for the NFENV module**

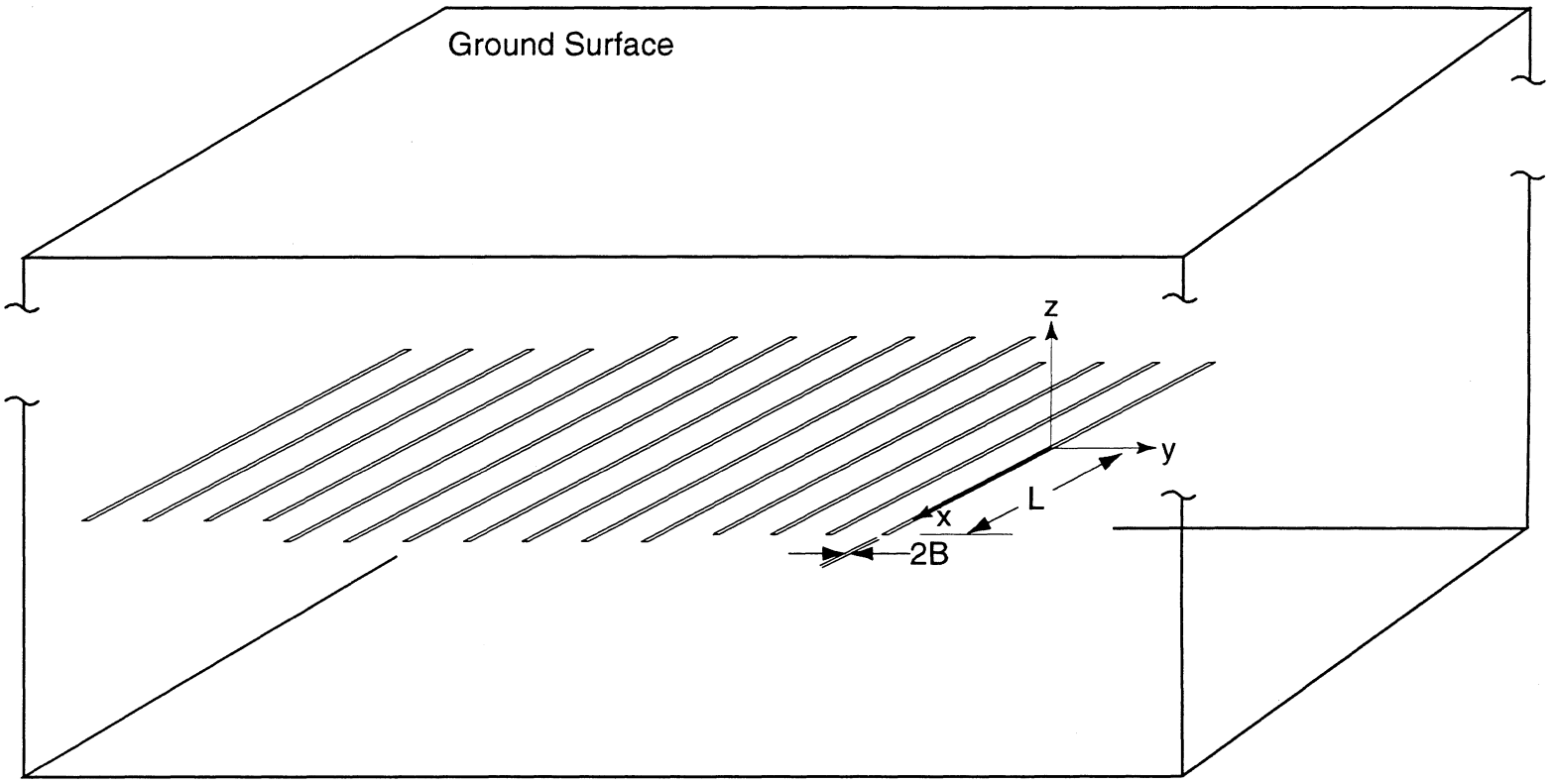


**Figure 5-2. Mountain-scale heat transfer model with line sources**

| | | |
|---|---|---|
| $B$ | — | half-width of a line source [m] |
| $H$ | — | depth of a line source below the ground surface [m] |
| $t$ | — | actual time after activation of heat flux [s] |
| $t'$ | — | time of integration [s] |
| $x,y,z$ | — | location of interest [m] |

The ground surface is assumed to be exposed to atmospheric conditions and has a constant temperature (currently not affected by climate change). The analytic equation is valid below the ground surface, $z < H$. The repository-scale heat flux is related to the AML and heat output per MTU of waste:

$$q''_{\text{rep}}(t) = AML\, Q_{\text{mtu}}(t) \tag{5-2}$$

Likewise, the thermal output for a single WP is related to the WP payload:

$$Q_{\text{wp}}(t) = MTU_{\text{wp}}\, Q_{\text{mtu}}(t) \tag{5-3}$$

where

| | | |
|---|---|---|
| $AML$ | — | areal mass loading for the area occupied by the drifts [MTU/m$^2$] |
| $MTU_{\text{wp}}$ | — | metric tons of uranium in a representative WP |
| $Q_{\text{mtu}}(t)$ | — | time-dependent heat output per MTU of waste [W/MTU]; available using a function subroutine in the INVENT utility module |

Waste is assumed to be emplaced in WPs, in drifts so close to each other that there is no spatial variation in the waste heat output along the drift but there is significant variation in heat output between the drifts. Figure 5-3 shows a plan view of the repository with parallel emplacement drifts with WPs periodically spaced. Because of the variation in heat losses, the temperature varies significantly between drifts (i.e., between the line sources). The temperature increase at any point is due to the contribution from all line sources. For each subarea, the average rock temperature is computed at an elevation of half the drift diameter in the drift nearest to the center of the subarea and is used consistently throughout the TPA Version 4.0 code as a common basis for transferring and calculating information. The analytic mountain-scale conduction model predicts the drift-temperature $T_{\text{rock}}$ as a function of time. Having computed $T_{\text{rock}}$ for the subarea, the WP surface temperature can be calculated.

**Ventilation**

Ventilation during the preclosure period could impact the temperature field computed by the conduction-only model presented above. Ventilation is expected to keep the temperature low at the WP surface and drift wall. To account for ventilation, the heat flux from the line sources are adjusted by the ventilation factor $f_v$:

$$q''_{\text{rep}}(t) = f_v\, q''(t)\big|_{\text{nv}} \tag{5-4}$$

where $q''(t)\big|_{\text{nv}}$ represents no-ventilation thermal output.

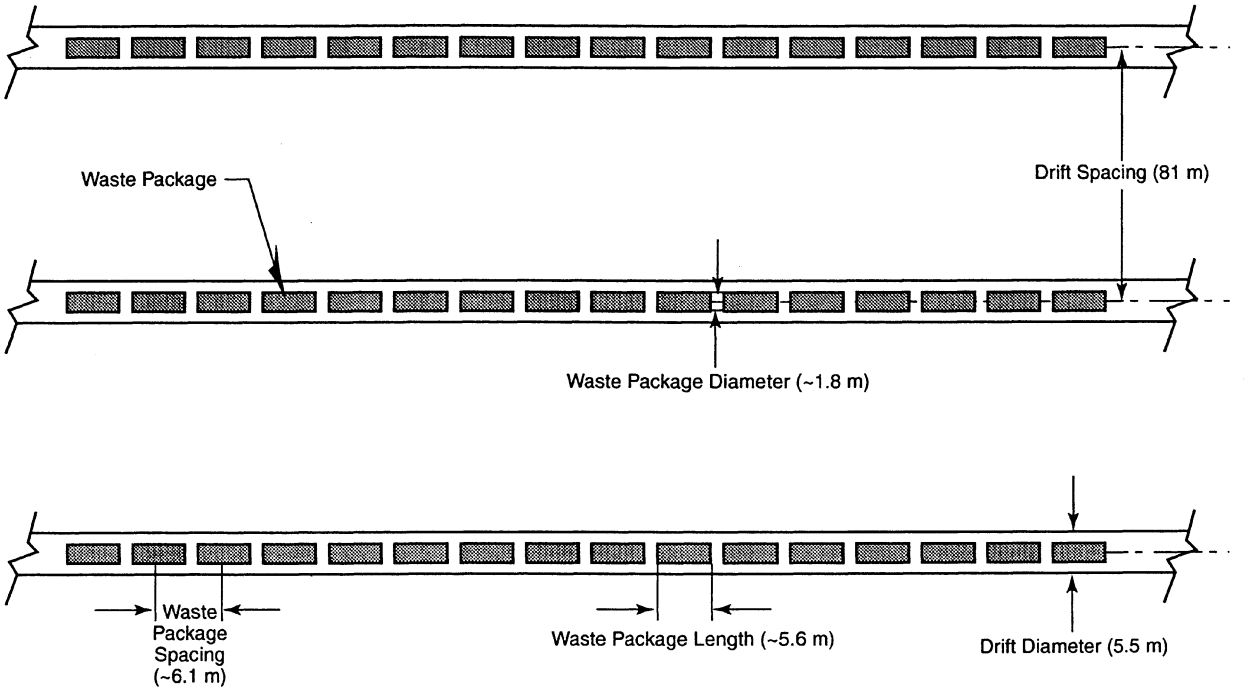


**Figure 5-3. Plan view of repository showing emplacement drifts and waste packages**

### Drift-Scale Heat Transfer

A multimode (i.e., conduction, convection, and radiation) heat transfer model is used for modeling drift-scale heat transfer. Figure 5-4a shows the cross section of a drift with a WP, dripshield, backfill, and invert. Figure 5-4b represents an idealization of these drift components for computing drift-scale heat transfer. A simplified thermal network is used to predict the WP surface temperature and the maximum SF temperature given $T_{rock}$ (from the mountain-scale model described previously) and $Q_{wp}(t)$, and is described in the following sections.

### Waste Package Surface Temperature

Equation (5-5) is used to solve for WP surface temperature, given the rock temperature, thermal output of the WP, and thermal conductances. Heat is transferred by thermal radiation and natural convection

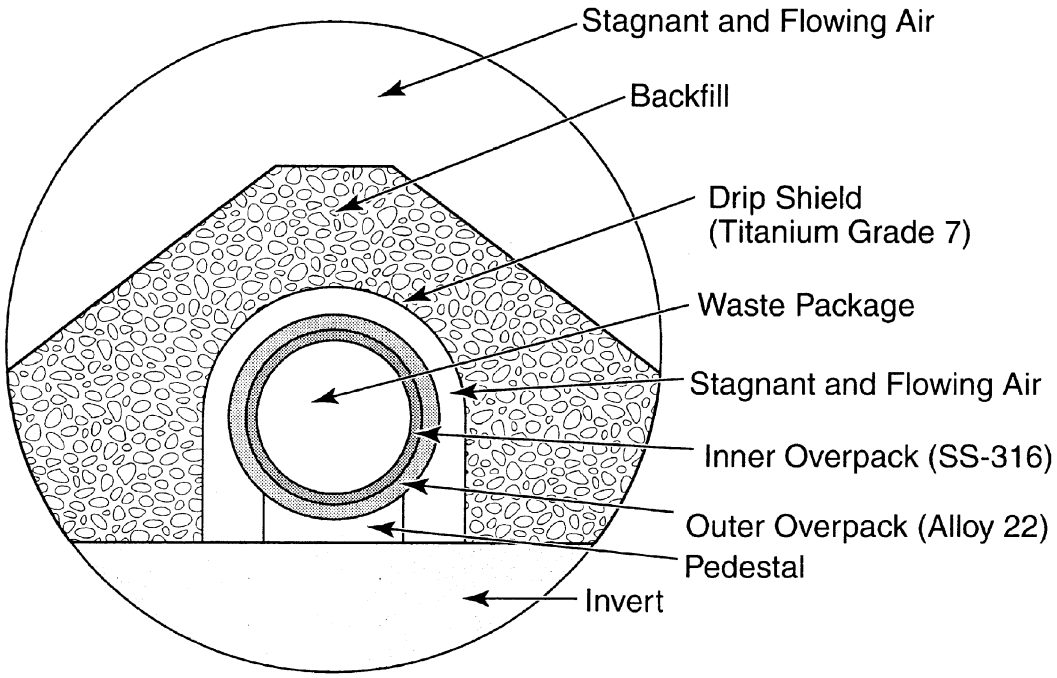


(a)

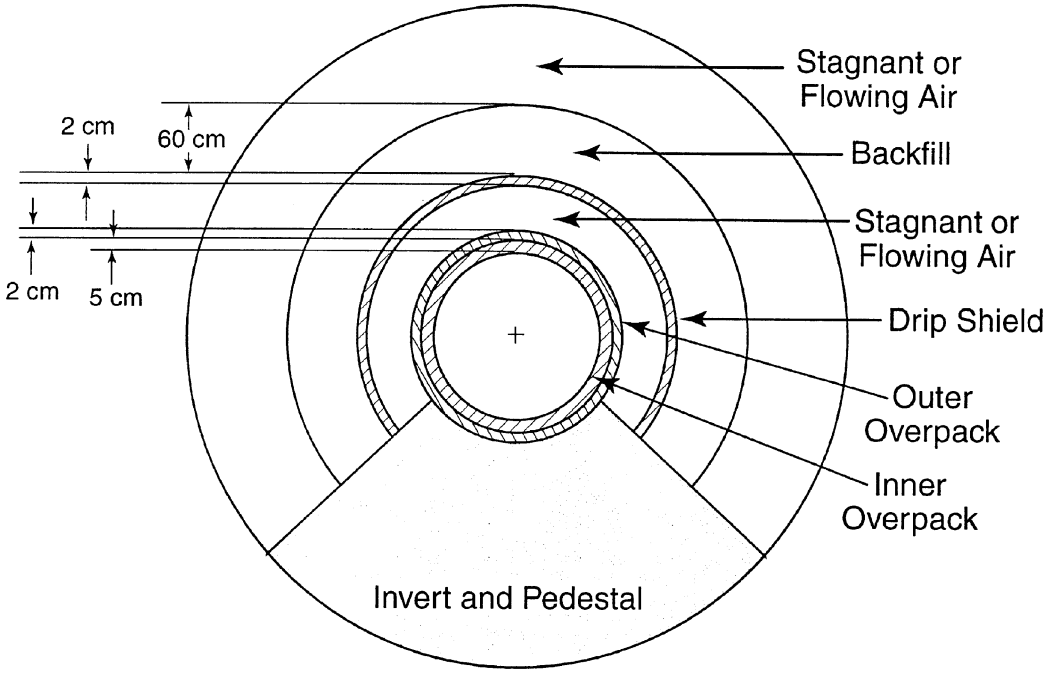


(b)

**Figure 5-4. Schematic showing (a) waste package, drip shield, and backfill emplacement in a drift (2D cross-section) and (b) idealization of the emplacement for performing thermal calculations**

in the unbackfilled region around a WP, and by conduction through the package support and floor material (e.g., invert) as:

$$Q_{wp} = \left(G_{rad} + G_{conv} + G_{cond}\right)\left(T_{wp,surf} - T_{rock}\right) \tag{5-5}$$

where

$Q_{wp}$ — time-dependent thermal output for a WP adjusted for ventilation during the preclosure period [W]
$G_{rad}$ — effective thermal conductance for radiative heat transfer [W/°C]
$G_{conv}$ — effective thermal conductance for convective heat transfer [W/°C]
$G_{cond}$ — effective thermal conductance for conductive heat transfer [W/°C]
$T_{rock}$ — drift wall temperature [°C]
$T_{wp,surf}$ — WP surface temperature [°C]

The thermal conductance for radiative heat transfer above the WP is based on a linearization of the Stefan-Boltzmann law and accounts for the emissivity of the WP and drift rock wall (Incropera and DeWitt, 1990):

$$G_{rad}\Big|_{pre} = f_c \frac{4\sigma\left(273.15 + T_{rock}\right)^3}{\frac{1-\varepsilon_{wp}}{\varepsilon_{wp}\,\pi\,D_{wp}L_{wp}} + \frac{1}{F_{wp\text{-}rw}\pi\,D_{wp}\left(L_{wp}+2\delta\right)} + \frac{1-\varepsilon_{rw}}{\varepsilon_{rw}\pi\,D_{rw}\left(L_{wp}+2\delta\right)}} \tag{5-6}$$

$$G_{rad}\Big|_{post} = f_c \frac{4\sigma\left(273.15 + T_{rock}\right)^3}{\frac{1-\varepsilon_{wp}}{\varepsilon_{wp}\pi\,D_{wp}L_{wp}} + \frac{1}{F_{wp\text{-}ds}\pi D_{ds}\left(L_{wp}+2\delta\right)} + \frac{1-\varepsilon_{ds}}{\varepsilon_{ds}\pi D_{ds}\left(L_{wp}+2\delta\right)}} \tag{5-7}$$

where

$f_c$ — fraction of the WP surface contributing to radiative/convective heat transfer [unitless]
$\sigma$ — Stefan-Boltzmann constant [=5.67 × $10^{-8}$ W/($m^2K^4$)]
$\varepsilon_{wp}$ — emissivity of the WP surface [unitless]
$D_{wp}$ — diameter of the WP [m]
$L_{wp}$ — length of the WP [m]
$F_{wp\text{-}rw}$ — radiative view factor from the WP either to the rock wall or the internal surface of the drip shield (=1) [unitless]
$F_{wp\text{-}ds}$ — radiative view factor from the WP to the drip shield (=1) [unitless]
$\varepsilon_{rw}$ — emissivity of the drift rock wall (or the internal surface of the drip shield surface [unitless]
$D_{rw}$ — diameter of the drift wall [m]

$L_{rw}$ — equivalent length of drift wall per WP drift for heat losses calculation [m]
$2\delta$ — gap between WPs along a drift [m]
$D_{ds}$ — diameter of the drip shield [m]
$\varepsilon_{ds}$ — emissivity of the drip shield (specified same as $\varepsilon_{rw}$) [unitless]

Suffixes "pre" and "post" in the above two and subsequent equations represent conditions before and after closure (i.e., backfilling). A fraction of the WP area is available for the radiative/convective heat transfer and the remainder (i.e., the bottom of the package) participates in conduction through the pedestal/floor. Thermal conductances for convective transfer above the WP and conductive transfer below the package are computed from

$$G_{conv}\Big|_{pre} = f_c \frac{2\pi\, k_{eff,nc}\left(L_{wp} + 2\delta\right)}{ln\dfrac{D_{rw}}{D_{wp}}} \tag{5-8}$$

$$G_{cond} = \left(1 - f_c\right)\frac{2\pi k_{floor}\left(L_{wp} + 2\delta\right)}{\ln\dfrac{D_{rw}}{D_{wp}}} \tag{5-9}$$

where

$k_{eff,nc}$ — effective thermal conductivity representation of natural convection [W/(m–°C)]
$k_{floor}$ — thermal conductivity of the concrete pedestal/floor material [W/(m–°C)]

The effective axial length for conductive and convective transfer from the WP to the drift wall should be larger than the length of the WP. A reasonable value for this length is chosen as the WP spacing (i.e., $L_{wp} + 2\delta$).

For backfilled drifts, conductive and convective heat transfer through the space above the floor (i.e., invert) quarters can be predicted using an effective conductivity for the backfill material

$$G_{conv}\Big|_{post} = f_c \frac{2\pi\, k_{eff,nc}\left(L_{wp} + 2\delta\right)}{\left(\ln\dfrac{D_{dsi}}{D_{wp}} + \ln\dfrac{D_{rw}}{D_{bfo}}\right)} \tag{5-10}$$

$$G_{cond}\Big|_{bfds} = f_c \frac{2\pi\left(L_{wp} + 2\delta\right)}{\dfrac{1}{k_{eff,bf}}\ln\dfrac{D_{rw}}{D_{dso}} + \dfrac{1}{k_{ds}}\ln\dfrac{D_{dso}}{D_{dsi}}} \tag{5-11}$$

where

| | | |
|---|---|---|
| $G_{cond/bfds}$ | — | effective thermal conductance after this backfill emplacement outside of the drip shield [W/°C] |
| $k_{eff,bf}$ | — | effective thermal conductivity of backfill material [W/(m–°C)] |
| $k_{ds}$ | — | thermal conductivity of drip shield [W/(m–°C)] |
| $D_{dso}$ | — | external diameter of the drip shield [m] |
| $D_{dsi}$ | — | internal diameter of the drip shield [m] |
| $D_{bfo}$ | — | equivalent diameter of backfill emplacement [m] |

**Waste Package Inner Wall Temperature**

After computing the outer WP surface temperature, the inner surface temperature of the wall is calculated. The wall of the WP consists of two cylindrical layers for the inner and outer overpacks. The thicknesses and properties of the walls are parameters specified in the *tpa.inp* file. The inner wall temperature is related to the WP heat according to

$$Q_{wp} = G_{shell}\left(T_{in,surf} - T_{wp,surf}\right) \tag{5-12}$$

where

| | | |
|---|---|---|
| $G_{shell}$ | — | thermal conductance for WP shell [W/°C] |
| $T_{in,surf}$ | — | inner surface temperature of the WP wall [°C] |

A schematic of the internals of a WP is shown in figure 5-5. The shell conductance consists of a contribution from the outer and inner overpack layers and is calculated according to:

$$G_{shell} = \frac{L_{wp}}{\frac{t_{iop}}{\pi D_{iop} k_{iop}} + \frac{t_{oop}}{\pi D_{oop} k_{oop}}} \tag{5-13}$$

where

| | | |
|---|---|---|
| $t_{iop}$ | — | thickness of the inner overpack [m] |
| $D_{iop}$ | — | diameter of the inner overpack layer [m] |
| $k_{iop}$ | — | thermal conductivity of inner/overpack material [W/(m°C)] |
| $t_{oop}$ | — | thickness of the outer overpack[m] |
| $D_{oop}$ | — | diameter of the outer overpack [m] |
| $k_{oop}$ | — | thermal conductivity of the outer overpack material [W/(m°C)] |

**Maximum Spent Fuel Temperature**

Using the WP inner surface temperature, the maximum SF temperature is calculated using a conduction shape factor formula that accounts for the volumetric heat generation in the interior region of the package, which includes the SF assemblies and the basket assembly (Manteufel and Todreas, 1994):

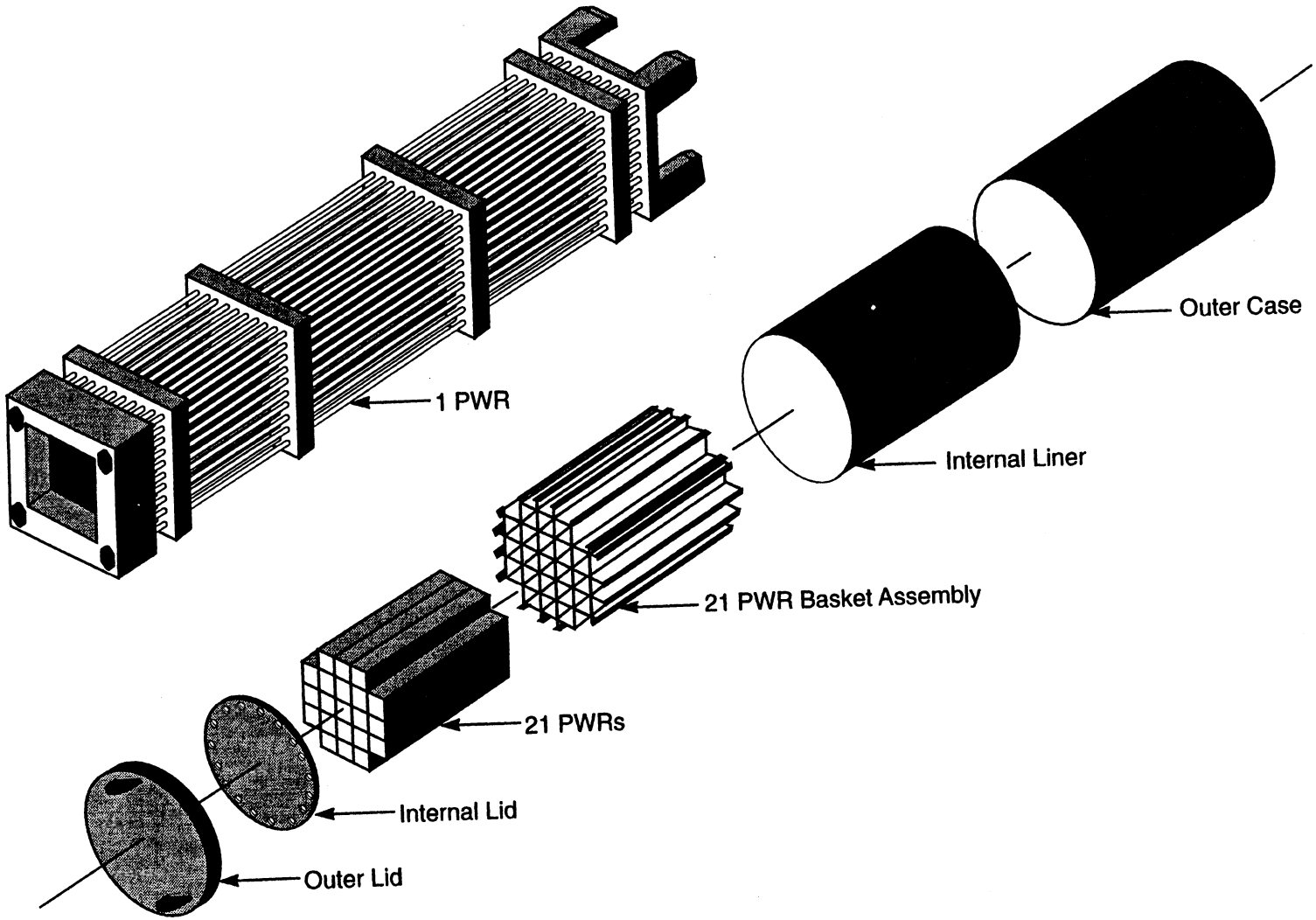


**Figure 5-5. Internals of a large waste package**

$$Q_{wp} = G_{int}\left(T_{max,sf} - T_{in,surf}\right) \tag{5-14}$$

where the conductance of the cylindrical interior region is computed from

$$G_{int} = k_{sf} S L_{wp} \tag{5-15}$$

where

| | | |
|---|---|---|
| $k_{sf}$ | — | effective thermal conductivity of the basket and SF in the WP [W/(m–°C)] |
| $S$ | — | conduction shape factor for a heated cylindrical region [=4π] |

The effective thermal conductivity of the SF accounts for the region between the inner wall and the basket material, the basket material, and the individual assemblies. There are multiple modes of heat transfer including thermal radiation, buoyant convection primarily in the larger void regions, and conduction in the basket material, fuel rods, and regions with primarily stagnant gas. At high temperatures, the heat transfer is dominated by radiative transfer. At lower temperatures, heat transfers can be dominated by conduction. Effective thermal conductivity is a function of temperature, and is a parameter specified in the *tpa.inp* file.

**Relative Humidity**

The WP temperature and RH are required inputs for the corrosion and release models. The RH is defined as the ratio of the actual vapor pressure to the vapor pressure at the WP surface:

$$\mathrm{RH} = \frac{P_v\left[\min\left(T_b, T_w\right)\right]}{P_v\left(T_{wp}\right)} \tag{5-16}$$

where

| | | |
|---|---|---|
| $P_v$ | — | vapor pressure that is a function of temperature [Pa] |
| min ($T_b$, $T_w$) | — | minimum of $T_b$ and $T_w$ |
| $T_b$ | — | boiling point temperature [~370 K at repository] |
| $T_w$ | — | drift wall temperature [K] |
| $T_{wp}$ | — | WP surface temperature [K] |

Below boiling conditions, the definition of RH used in Eq. (5-16) is equivalent to the mole fraction definition of RH frequently found in thermodynamic textbooks (e.g., Van Wylen and Sonntag, 1978; Moran and Shapiro, 1992). RH is generally defined as the actual mole fraction of water vapor in the air divided by the maximum or saturation mole fraction of water vapor in the air at the same temperature and pressure. Below boiling conditions, mole fractions are related to the vapor partial pressures so that this definition is equivalent to Eq. (5-16). Above boiling conditions, the vapor partial pressure cannot exceed the atmospheric pressure within the drift, even in the presence of backfill, because of its high porosity. When the WP surface temperature exceeds the boiling point, it is preferable to define RH as a ratio of the two vapor pressures specified previously, which is consistent with the technical literature (Hartman, 1991; Bejan, 1988; Fyfe, 1994).

As an alternative to the temperature and RH models described previously, use of tabular input of the temperature and RH into the TPA Version 4.0 code can be selected in the *tpa.inp* file, whereupon this information is obtained from an external data file, *tefkti.inp*. Results from detailed 2D and three-dimensional (3D) modeling that can more accurately predict repository edge heat losses can be incorporated as tabular data.

## 5.3.2 Near-Field Chemical Composition

The chemical composition of fluid able to come in contact with the WP is an important consideration in the modeling of WP integrity and RT in the TPA Version 4.0 code. NFENV is designed to provide the chemical composition of the environment as a function of time in the immediate neighborhood of the WP. Chemistry parameters, which include solution pH, oxygen fugacity, chloride and bicarbonate concentration, dissolved silica, and alkalinity, among other environmental factors, can have important consequences on the rate of corrosion of the WP, dissolution of SF, and formation of alteration products. Of special concern in the chemical composition in a partially saturated environment are evaporative effects produced by the heat released from the WP. Chemistry can also be affected by refluxing of evaporated water and by deep percolation at long time periods.

The maximum silica concentration estimated from equilibrium with quartz, chalcedony, and cristobalite gives, respectively, $a_{SiO_2}$ = 0.000835, 0.00137, and 0.00218 molal. By contrast, J-13 well water has a silica concentration of 0.0011 molal (table 5-1). Bounds on the pH are more difficult to obtain. Likewise, calcium and carbonate have no obvious upper bounds since their concentrations will be pH-dependent. Turner (1998) screened available groundwater chemistry data compiled by Perfect et al. (1995), which may provide some limits for current ambient conditions in the vicinity of YM.

To provide a more detailed calculation of the near-field fluid composition, the MULTIFLO Version 1.2 code (Lichtner et al., 2000; Seth and Lichtner, 1996) is used to provide quantitative data in tabular form to the TPA Version 4.0 code. MULTIFLO simulates the transport of reacting chemical constituents coupled to evaporation and condensation processes involving two-phase fluid flow. The code sequentially couples two-phase fluid flow of liquid water, water vapor, and air with reactive transport of aqueous and gaseous species. Homogeneous reactions in the aqueous phase and heterogeneous reactions between the aqueous and gaseous phases are assumed to be in local equilibrium. Mineral reactions are treated irreversibly through prescribed kinetic rate laws.

The MULTIFLO simulates temperature and the associated moisture redistribution as a function of time using a 2-D drift-scale model. An unstructured grid is used to track the detailed geometry near the drift. The fractured YM tuff host rock is described using the dual continuum model (DCM) in which fracture and matrix systems are represented as separate interacting continua. Model predictions indicate the formation of a zone near the drift where the temperature is above the boiling point of water, when the heat load on the drift wall is not reduced significantly by ventilation. In the EDA II design, this boiling zone does not coalesce between drifts, as it did for the TSPA-VA repository design.

The aim of the MULTIFLO calculations is to estimate the chloride concentration of the fluid at the drift wall which, as a first approximation, may be considered to be similar to the fluid that comes in contact

**Table 5-1. Initial fluid composition and pH corresponding to J-13 well water (adapted from Harrar et al., 1990)**

| Species | Molarity × $10^4$ | Species | Molarity × $10^4$ |
|---|---|---|---|
| $Ca^{+2}$ | 2.90–3.70 | $SiO_2$(aq) | 9.50–11.40 |
| $Na^+$ | 18.30–21.70 | $Cl^-$ | 1.78–2.37 |
| $K^+$ | 1.00–1.40 | pH | 6.8–8.3 |
| $HCO_3^-$ | 1.93–2.34 | — | — |

with the surface of the WP. The chloride concentration may be directly or indirectly affected by evaporation, mineral precipitation, aqueous reactions, and $CO_2$ degassing. However, evaporation caused by repository heating is considered the dominant process controlling chloride concentration. In the initial phase of the work to provide input to the TPA Version 4.0 code, the simulation is limited to a single nonreacting chemical (chloride) with detailed representation of the hydro-thermal system to estimate the change in chloride concentration due to evaporation. More detailed multi-component calculations may be undertaken in future work, if needed. The heat load and drift geometry for the MULTIFLO Version 1.2 code calculations are consistent with those of the EDA II design, with no reduction in heat load by ventilation. Neglecting ventilation tends to over-estimate chloride concentration in the repository nearfield and hence provides a bounding estimate. The simulation region spans four hydrostratigraphic units (TSw33–TSw37) as shown in the UZ site model (Civilian Radioactive Waste Management System, Management Operating and Contractor, 1998). The initial chloride concentration corresponds to J-13 well water, as given in table 5-1.

The temperature at the drift wall is shown in figure 5-6. The fractures dry out quickly and remain dry until about 1,200 yr. During this dryout period and within the context of a continuum model, it is not possible to represent the return of liquid water to the WP and the associated chloride concentration, as this flow would presumably take place along open fractures in the form of gravity-driven flow manifested as dripping. To estimate the expected changes in chloride concentrations caused by evaporation, a simple upper bound on the chloride concentration may be derived by assuming equilibrium with halite (NaCl), for example. As evaporation occurs, the sodium and chloride concentrations must remain approximately proportional to one another. Therefore, assuming that the activity coefficients of $Na^+$ and $Cl^-$ are similar at high ionic strength

$$a_{Na^+} = \alpha\, a_{Cl^-} \tag{5-17}$$

where $\alpha$ is the constant of proportionality and $a_{Na+}$ and $a_{Cl}^-$ are sodium and chloride activities. Equilibrium with halite implies

$$K = a_{Na^+} a_{Cl^-} = \alpha\, a_{Cl^-}^2 \tag{5-18}$$

where $K$ is the equilibrium constant. Therefore,

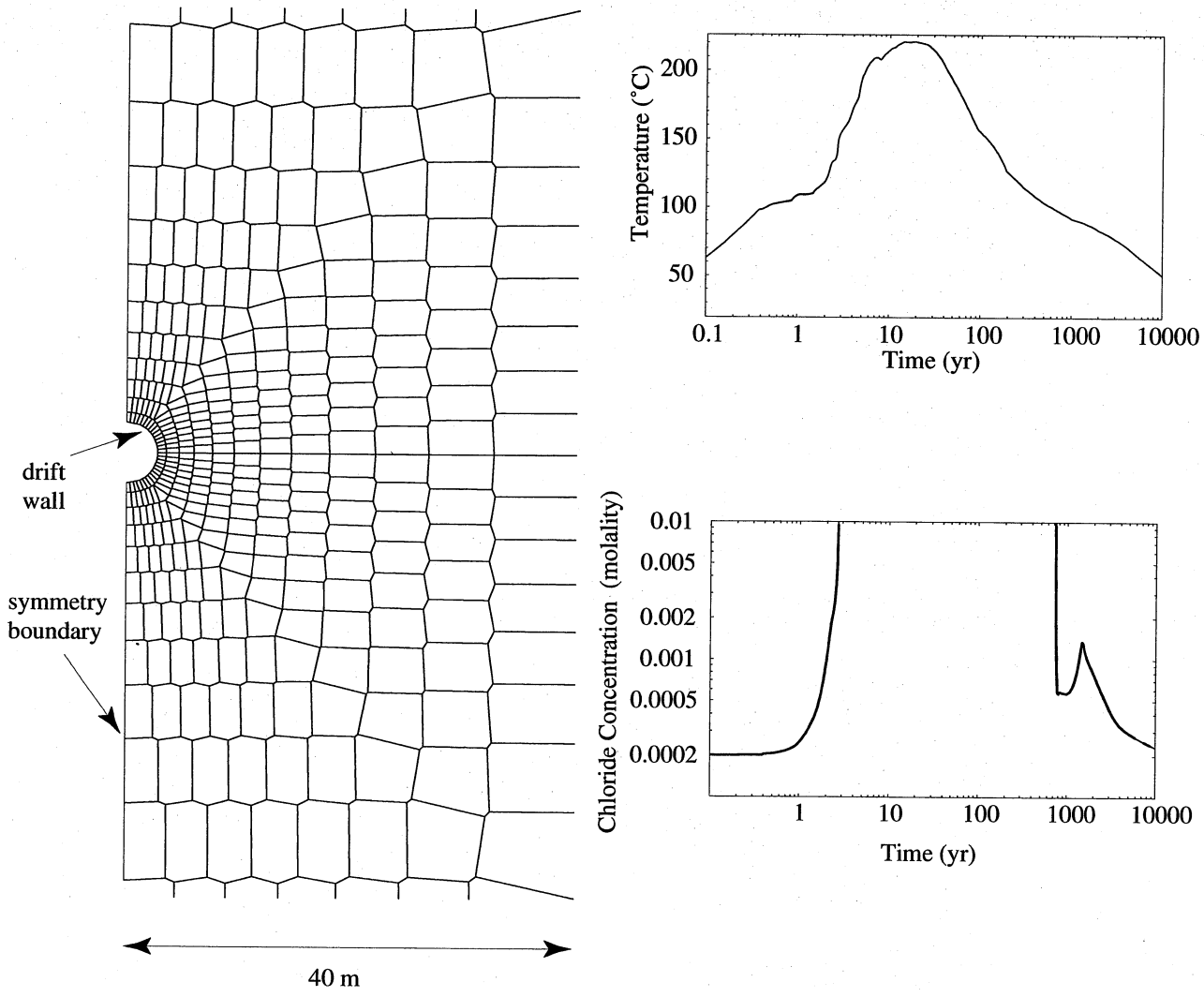


**Figure 5-6. Time evolution of chloride concentration at the drift wall computed by the MULTIFLO code. Also shown are part of the computational model near emplacement drift and temperature at the drift wall used in computing chloride concentration.**

$$a_{Cl^-} = \sqrt{\frac{K}{\alpha}} \tag{5-19}$$

The log $K$ for halite at 100 °C is equal to 1.578 (Wolery, 1992). Taking $\alpha$ = 11.11, derived from J-13 well water (see table 5-1), it follows that $a_{Cl^-}$ = 1.85 molal and $a_{Na+}$ = 20.5 molal. To estimate concentrations, activity coefficient corrections must be included. If the sodium concentration is lowered by precipitation of other Na-bearing solids, the chloride concentration in equilibrium with halite could be substantially increased and the concentration of sodium reduced.

As shown in figure 5-6, when the fracture system above the drift becomes wet again at about 1,000 yr, the chloride concentration is approximately four times its initial value and then decays in a nearly exponentially fashion to the initial value. Chloride concentrations during the rewetting period are provided in tabular form for input into the TPA Version 4.0 code. During the dryout phase, the chloride concentration is assumed to be in equilibrium with respect to halite.

In principle, MULTIFLO would be able to provide chloride concentration, pH, and oxygen fugacity as time-dependent functions; such multi-component calculations may be undertaken in the future, if they are found to be necessary. Currently, only chloride concentration is used in the TPA Version 4.0 code as a function of time. The pH value is currently set at a constant value of 9. Chloride concentrations, as provided by MULTIFLO, are multiplied by a *tpa.inp* parameter representing uncertainties and limitations in the MULTIFLO results (i.e., MULTIFLO results are representative of groundwater chemistry in the porous matrix and chloride concentration on a WP) and could be higher than predicted by MULTIFLO due to evaporation on the WP.

### 5.3.3 Near-Field Groundwater Infiltration

NFENV also provides estimates of groundwater reflux and percolation rates. The amount of water percolating through the near field is different from the infiltration computed in UZFLOW because of thermohydrologic effects resulting from decay heat. WP temperatures may exceed the boiling point of water and vaporize water in the rock surrounding the WPs. The vapor will flow away from the WPs and condense where temperatures are below boiling. The condensate may then flow back toward the WPs. This return flow of condensate is called refluxing.

The area between the WPs and the condensate zone is called the boiling or dryout zone. Although dryout and condensate zones would form both above and below the repository, only the zones that form above the repository are considered in the reflux models. Water that fully penetrates the dryout zone would be available to contact the WPs, possibly accelerating the corrosion of WP materials and facilitating transport of radionuclides released from failed WPs.

Three reflux models have been developed: REFLUX1, REFLUX2, and REFLUX3. Figure 5-7 is a schematic illustrating the movement of water above the repository. Although figure 5-7 and the following discussion refers primarily to REFLUX1, in general, the concepts apply to all three models. Differences are noted in the relevant sections.

Figure 5-7 illustrates the vaporization of ambient rock water in the area above the boiling point temperature, $T_{boil}$. The $T_{boil}$ isotherm is at an elevation $Z_{boil}$ whose location depends on the rate at which

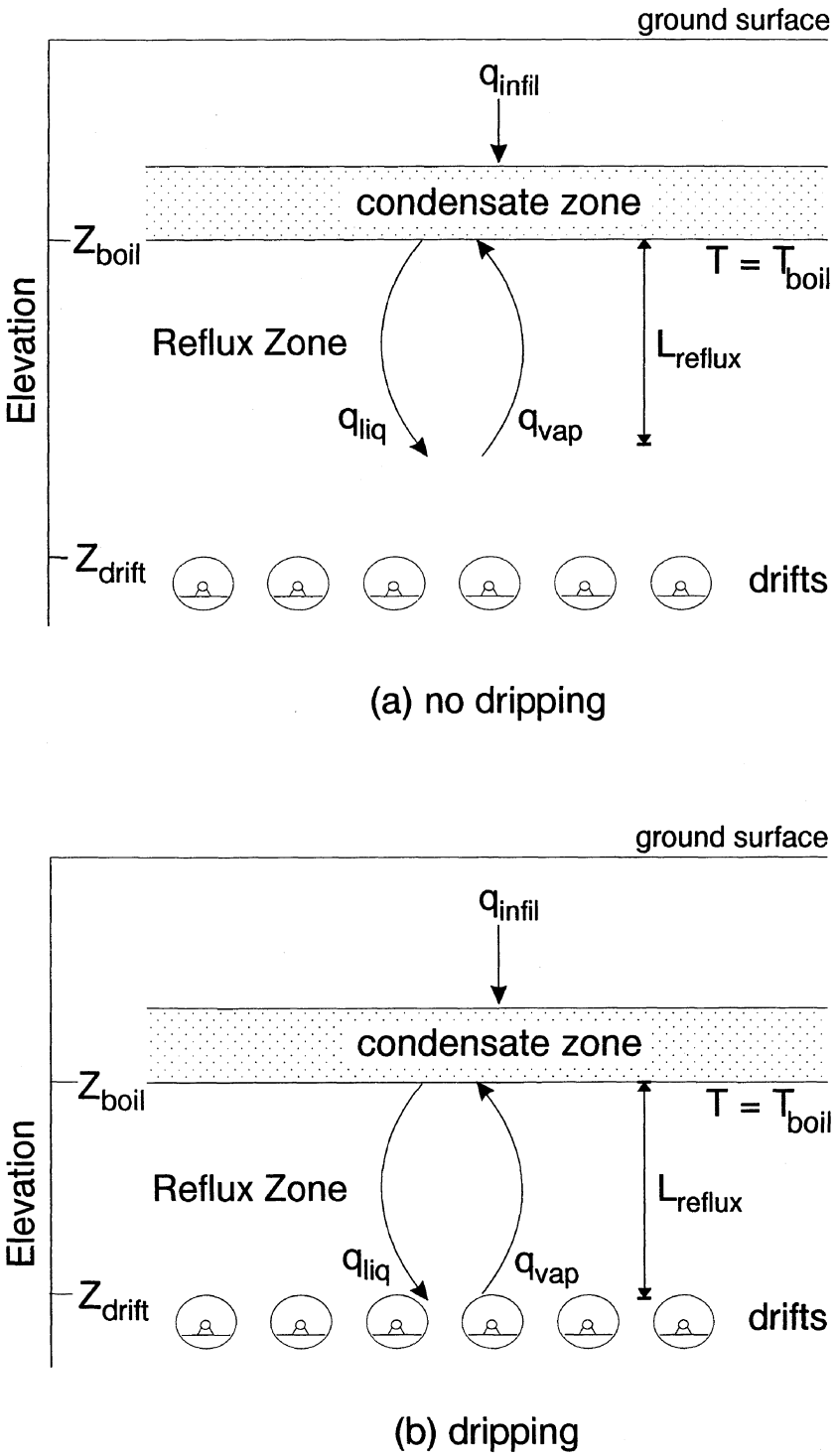


**Figure 5-7. Conceptualization of drift-scale thermal hydrologic model**

heat is generated by the waste and the heat loss away from the near-field environment (calculated in the mountain-scale heat transfer model). Above the $T_{boil}$ isotherm is the condensate zone where water vapor condenses to a liquid that is available to move down toward the repository. Below the $T_{boil}$ isotherm is a boiling zone through which liquid water from the condensate zone flows until it is heated to the point of vaporization and subsequently rises back to the condensate zone.

Together the condensate and boiling zones constitute a perched reflux zone containing water driven from the rock surrounding the repository by heat generated in the repository. No refluxing of groundwater into the repository can occur when the bottom of the reflux zone is at or above the elevation of the top of the drift (which can be the case early in the heating phase) (figure 5-7a). As heat generated by the WPs diminishes over time, the elevation of the $T_{boil}$ isotherm and reflux zone move closer to the elevation of the repository, and dripping in fractures or reflux can occur at the repository. The thickness of the reflux zone, $L_R$, is dependent on $q_{infil}$ and the local heat flux (i.e., the temperature gradient). When $(Z_{boil} - L_R)$ is below the elevation of the top of the drift, $Z_{drift}$, water begins to drip into the drift (figure 5-7b). Any liquid passing below the level of the repository is assumed to continue to the water table. The thermal load reflux is calculated in the NFENV module using one of three models. The source of water in REFLUX1 is only the water infiltrating from the surface while the sources of water for REFLUX2 and REFLUX3 are both infiltrating water and water from the dryout zone surrounding the repository.

NFENV uses the time-dependent temperature profiles generated by the heat transfer models previously described, along with time-dependent water flux $(q_{infil})$ from UZFLOW, to calculate time-dependent flux $(q_{drip})$ in fractures entering the near-field environment and available for dripping onto one WP. In the development of $q_{drip}$, NFENV considers the time-dependent amount of perching caused by thermal pulsing and the time-dependent refluxing of liquid and vapor. The REFLUX models are intended to determine $q_{drip}$ for matrix flow and fracture flow. NFENV partitions percolation flux from the reflux zone, $q_{perc}$, from all the models on a per WP cross-sectional area basis to obtain $q_{drip}$.

**REFLUX1 Methodology**

The REFLUX1 subroutine of NFENV is used to model redistribution of water in the near-field environment owing to heat from emplaced WPs. Vaporized water is assumed to move away from the repository until conditions are cool enough for condensation (i.e., conditions are cooler than boiling). Although a condensate zone would form on either side of the repository, only the zone above the repository is considered in REFLUX1. Above the boiling isotherm, a saturated condensate zone forms, bounded below by the boiling isotherm. Cool water from the condensate zone is assumed to percolate within fractures toward the repository within a reflux zone, with the liquid boiling and returning to the condensate zone as vapor, as shown in figure 5-7.

A mass balance model is used to model the thickness of the condensate zone above the repository:

$$\frac{\partial V_c}{\partial t} = q_{infil} - q_{perc} \tag{5-20}$$

where

| | | |
|---|---|---|
| $V_c$ | — | volume of the condensate zone per unit area [$m^3/m^2$] |
| $t$ | — | time [yr] |
| $q_{infil}$ | — | infiltration flux entering the condensate zone [m/yr] |
| $q_{perc}$ | — | percolation flux leaving the reflux zone [m/yr] |

When $V_c = 0$ (no condensate zone exists) and when $V_c$ is at a maximum value (set in the *tpa.inp* file with the parameter PerchedBucketVolumePerSAarea[m3/m2]) $q_{perc}$ is directly set to $q_{infil}$. A reasonable value for the maximum perched-water volume might be the fracture porosity times the thickness of the Welded Topopah Spring unit above the repository.

Although the condensate zone is intermediate between the two limiting cases, the position of the bottom of the reflux zone determines $q_{perc}$. If the reflux zone is completely above the drifts, all infiltration flux is stored in the condensate zone and $q_{perc} = 0$. Within the reflux zone, the liquid flux, $q_{liq}$, is everywhere balanced by the vapor flux, $q_{vap}$. If the reflux zone intercepts the repository horizon, $q_{perc}$ is determined by evaluating $q_{liq}$ at the repository horizon, assuming that $q_{liq}$ decreases linearly from the boiling isotherm to the bottom of the reflux zone:

$$q_{perc} = q_{reflux}\left(1 - \frac{Z_{boil} - Z_{drift}}{L_{reflux}}\right) \tag{5-21}$$

where

| | | |
|---|---|---|
| $q_{reflux}$ | — | downward liquid flux at the bottom of the condensate zone [m/s] |
| $L_{reflux}$ | — | thickness of the reflux zone [m] |
| $Z_{boil}$ | — | elevation of the boiling isotherm [m] |
| $Z_{drift}$ | — | elevation of the drifts [m] |

The maximum thickness of the reflux zone, $L_{reflux}$, is a parameter in *tpa.inp* called LengthOfRefluxZone[m], while the downward liquid flux at the boiling isotherm, $q_{reflux}$, is named MaximumFluxInRefluxZone[m/s]). Offline calculations are required to define these parameters.

The elevation of the boiling isotherm, $Z_{boil}$, which defines the bottom of the condensate zone and the top of the reflux zone, is determined by assuming that temperature varies linearly near the repository. Alteration of the temperature field because of moisture redistribution and the effects of salt concentration and capillarity on $T_{boil}$ is neglected. The temperature gradient is calculated by assuming the heat generated by the repository is carried by conduction within the boiling isotherm; knowing the thermal conductance of the matrix and the thermal flux due to the repository (obtained from NFENV calculations), the temperature gradient can be determined. The temperature at the repository (obtained from NFENV heat transfer calculations) is projected according to

$$Z_{boil} = \left(Z_{drift} + T_{boil} - T_{repos}\right)\left(\frac{K_{therm}}{0.5q_{heat}}\right) \quad (5\text{-}22)$$

where

$Z_{boil}$ — elevation of the boiling isotherm [m]
$Z_{drift}$ — elevation of the drifts [m]
$T_{repos}$ — temperature of the repository [°C]
$K_{therm}$ — thermal conductivity [W $K^{-1}$ $m^{-1}$]
$q_{heat}$ — thermal flux due to the repository [W/$m^2$]

During much of the boiling phase for the repository, $q_{infil}$ will exceed $q_{perc}$ and liquid (condensate) will accumulate in the condensate zone. If the condensate zone grows beyond the user-specified limit ($L_{reflux}$), the condensate zone overflows and this is added to any fluxes in $q_{perc}$ caused by the reflux zone contacting the drifts.

Once boiling around the repository stops, the reflux zone ceases to exist and any water contained in the condensate zone is released over a few time steps. During this post-boiling period, at each time step $q_{perc}$ is set to $q_{infil}$ plus one-half of the water remaining in the condensate zone. After a few time steps, $q_{perc}$ approaches $q_{infil}$. Note that if $q_{reflux}$ is significant, the condensate zone may empty as the boiling isotherm returns to the drift level.

Although dripping in a drift can occur $(q_{perc}>0)$, the dripping flux is calculated on a per-WP basis (i.e., $q_{perc}$ is multiplied by the fraction of the subarea occupied by WPs) and passed to EBSREL for determination of the amount of water that contacts and enters the WP.

**REFLUX2 Methodology**

REFLUX2 was created as an alternate to REFLUX1 to calculate the amount of water able to contact the WPs based on thermal and gravity driven refluxing. Conceptually, in REFLUX2 the quantity of refluxing water can be sufficient to penetrate the boiling isotherm in the fractures and reach the WP during times when the surface temperature of the WP exceeds boiling. The primary difference between REFLUX1 and REFLUX2 is that in REFLUX2 some condensate return flow may penetrate the boiling isotherm no matter how far the boiling isotherm is located above the WP. In addition, unlike REFLUX1, REFLUX2 considers rock (matrix) water as well as deep percolation of infiltration. As such, REFLUX2 is intended to determine flow toward the repository considering both infiltration from the surface and water originating in the matrix of the dryout zone surrounding the repository in the boiling phase.

Similar to REFLUX1, REFLUX2 is based on a reflux cycle located above the WPs. A particular parcel of water may participate in the reflux cycle many times. With every cycle, however, some portion of the refluxing water may escape as either vapor or liquid and flow away from the heat source, possibly toward the water table. Alternatively, the refluxing cycle can gain water from two sources: infiltration from ground surface (from UZFLOW) and water vaporized from the dryout zone in rock surrounding the near field.

The amounts of water contributed to the refluxing cycle by infiltration and from vaporized ambient rock pore water are calculated separately. The total amount of refluxing water derived from both infiltration and rock pore water vaporization in year $N$ is

$$R_T = R_I + R_D \tag{5-23}$$

where

$R_I$ — the amount of infiltration-derived water [$m^3/m^2$]
$R_D$ — the amount of refluxing ambient rock pore water [$m^3/m^2$]

***Reflux Derived from Infiltration***

The amount of $R_I$ that refluxes during year $N$ is

$$R_I = \sum_{j=0}^{N-1} \frac{q_{\text{infil}_{N-j}}}{A_{\text{sa}}} (1 - L_I)^j \tag{5-24}$$

where

$q_{\text{infil}_{N-j}}$ — infiltration for a given subarea from UZFLOW for the year $(N-j)$ [$m^3/yr$]
$A_{\text{sa}}$ — area for a given subarea [$m^2$]

$N$ — years after start of refluxing [unitless]
$L_I$ — fraction of infiltration that escapes the reflux cycle each year, user input [unitless]

The variable $L_I$ (Reflux2LossI) is specified in the *tpa.inp* file. Note that for large $N$, $R_I$ converges to $1/L_I$.

***Reflux Derived from the Rock Pore Water***

The total amount of water, $D$ [$m^3/m^2$] vaporized from prewaste-emplacement ambient rock pore water and available for refluxing is defined by

$$D = (T)(n)(S - S_r) \tag{5-25}$$

where

$T$ — thickness of dryout zone [m]
$n$ — porosity of rock [unitless]
$S$ — liquid saturation [unitless]
$S_r$ — residual saturation [unitless]

The thickness of the dryout zone (Reflux2Thickness), porosity (Reflux2Porosity), liquid saturation (Reflux2SatInit), and residual saturation (Reflux2SatResid) are specified in the *tpa.inp* file.

A portion of refluxing water may escape the refluxing cycle each year ($L_D$) lowering the amount of refluxing ambient rock pore water, $R_D$ [$m^3/m^2$]. The time required to complete one water reflux cycle may vary from one year to several hundreds to thousands of years. The amount of rock pore water that refluxes in a given year is

$$R_D = \frac{\left[D(P - L_D)^{N-1}\right]}{P^N} \tag{5-26}$$

where $P$ is the number of years required for water to complete one reflux cycle. The variables $L_D$ (Reflux2LossD) and $P$ (Reflux2Period) are specified in the *tpa.inp* file.

The predominant source of refluxing water may change with time. At early times, refluxing water may be dominated by water derived from the rock pore water. At later times, water derived from infiltration may dominate if rock pore water near the WPs has been vaporized and removed from the refluxing cycles. In this case, the amount of refluxing water will converge to the value of $R_I$. If no losses from the refluxing cycle are experienced, the amount of refluxing water will grow at a rate equal to infiltration. In REFLUX2 the temperature and thickness of the dryout zone do not vary with time. The temperature is assumed to be above boiling at all times.

Water exiting the reflux cycle and entering the repository near-field environment is then computed from

$$R_{WP} = (R_I L_I + R_D L_D) A_{sa} \tag{5-27}$$

These values are then converted from a subarea basis to a WP basis by multiplying the flow out of the reflux zone by the fraction of the subarea associated with a WP, passed to EBSREL, to determine the amount of water that contacts the waste form and enters the WP.

**REFLUX3 Methodology**

Like REFLUX1 and REFLUX2, REFLUX3 incorporates a procedure to estimate the amount of water flowing in fractures below the boiling isotherm. There are major differences between REFLUX3 and REFLUX2: in REFLUX3 the thickness of the dryout zone varies with time and REFLUX3 estimates the depth that water will penetrate the boiling isotherm as a function of dryout zone thickness and the volume of water flowing from the condensate zone.

As in REFLUX2, refluxing water originates from two sources: infiltration from ground surface and water vaporized from the dryout zone surrounding the WPs. The amount of water available for refluxing by infiltration is determined by the UZFLOW module outside of the REFLUX3 module. The time-varying dryout zone thickness is read from a table calculated by MULTIFLO. The dryout zone thickness is converted to an equivalent depth of water as shown in Eq. (5-25). The volume of water in the condensate zone is the sum of the water from the dryout zone and infiltration. The REFLUX3 module calculates the volume of water above a single WP. This time-varying volume of water is available to flow to the WPs.

Water flowing down a fracture will penetrate a distance below the boiling isotherm before it is completely vaporized. If the penetration distance is greater than the thickness of the dryout zone above the

drifts, refluxing water will reach the drifts and be available to contact the WPs. The penetration distance is calculated with an expression developed by Phillips (1996):

$$L = \left[ \frac{Qh\rho_w}{k_r \nabla T} \right] \tag{5-28}$$

where

| | | |
|---|---|---|
| $L$ | — | penetration distance [m] |
| $\rho_w$ | — | density of boiling water [kg/m$^3$] |
| $Q$ | — | flow from condensate zone [m$^3$/s] |
| $h$ | — | enthalpy of phase change for water [J/kg] |
| $k_r$ | — | thermal conductivity of rock [W/m-K] |
| $\nabla T$ | — | temperature gradient in vicinity of boiling isotherm [K/m] |

The variables $\rho_w, h, k_r$, and $\nabla T$ are specified in the *tpa.inp* file.

When the penetration distance is less than the thickness of the dryout zone, all of the flow vaporizes and is returned to the condensate zone. When the penetration is greater than the thickness, some portion of the flow reaches the drifts. The rest of the flow vaporizes and returns to the condensation zone. The fraction of flow that vaporizes is proportional to the ratio of the dryout zone thickness to the penetration distance. Thus, if the ratio is 0.8, 80 percent of the flow vaporizes and 20 percent reaches the drift.

REFLUX3 uses several additional variables specified in the *tpa.inp* file: the fraction of water that flows from the condensate zone toward the drifts (FractionOfCondensateTowardRepository), the fraction of water in the condensate zone permanently removed from the system by some unspecified mechanism (e.g., shed along edges of the repository or through pillars between drifts (FractionOfCondensateRemoved), and the fraction of water flowing from the condensate zone toward the drift that is removed by an unspecified mechanism (e.g., flowpaths that bypass drifts, FractionOfCondensateTowardRepositoryRemoved). Refluxing occurs only while WP temperatures are above boiling. The output of REFLUX3 is the amount of water that reaches the drift. The amount of water that actually contacts the WPs is determined in the module EBSREL.

## 5.4 ASSUMPTIONS AND CONSERVATISM OF THE NFENV APPROACH

The near-field environment will affect the corrosion of the WP and the dissolution of SF and will affect the amount of water entering the drift and WP. The NFENV module is an abstraction of the physical and chemical processes in the near field of the repository and includes the determination of (i) temperature of the WP and waste, (ii) RH, (iii) refluxing of condensed water, and (iv) evolution of near-field chemistry.

NFENV has two methods, from which the user must select one, for determining the temperature of the WP and the waste form. One method determines the temperatures through an analytic conduction-only heat transfer model at the mountain-scale and an analytic, steady-state heat transfer model at the drift-scale that accounts for conduction, convection, and radiation in the vicinity of the WP. The analytic solutions simplify the problem by using uniform thermal properties and uniform heat loading at the repository level,

and line sources to represent the heat output at the repository level (drift wall). The second method is a numerical approach performed by using a finite difference algorithm outside the TPA code. The thermal output from the WPs is adjusted by a factor to represent excess heat losses associated with this ventilation during the preclosure period. This second method allows the user to supply WP and waste temperatures in tabular form (temperature predictions would presumably be based on the results of a more detailed model that would include conductive, convective, and advective heat transfer in rocks). Both of these methods provide a single temperature for a representative WP in each repository subarea. Because of the nonuniformity in the temperature field at the repository horizon, the temperature at the wall of the drift nearest to the center of the subarea is used as the representative temperature for the subarea. From the drift wall temperature, the representative WP temperature is back-calculated. The use of a single temperature and a representative WP for each subarea should provide a conservative result because all WPs in a subarea will simultaneously corrode and have the potential for simultaneous release of radionuclides (actual release will depend on the number of packages that get wet).

The NFENV module also implements two methods for determining the RH. One method determines the RH through an analytic expression based on vapor pressure as a function of temperature while the second method allows the user to supply the RH in tabular form. Both these methods provide a single RH value for a representative WP (at the WP surface) in each repository subarea. This approach is considered reasonable based on the reasons discussed previously for temperature.

Water will be redistributed in the near field by evaporation caused by heat from the emplaced waste. Estimating the redistribution of water is highly uncertain because of the complicated two-phase flow processes, variations in the thermal gradient, and heterogeneities in the fracture and matrix hydrologic properties. Refluxing water is assumed to penetrate the boiling isotherm in the vicinity of a WP, allowing liquid water to contact the package even when temperatures exceed the boiling point of water. Reflux of water is represented by three different models (one specifies a reflux zone and the other two specify either a constant or a time-dependent dryout zone with a fraction of infiltration escaping the reflux cycle each year). These models have the flexibility to produce conditions varying from a long dryout period to a short dryout period. Detailed numerical analysis and heater experiments are continuing to determine the effect of the redistribution of water. The degree of conservatism of any particular approach is uncertain at this time.

The chemical composition of the water contacting the WP can affect corrosion of the WP and dissolution of the waste. The evolution of the chemistry of the water is the result of a variety of complicated processes associated with, but not limited to, mineral reactions, evaporation, and condensation. These types of complicated processes cannot be accommodated in a system code while maintaining reasonable execution times. The chemical composition of water in a partially saturated environment is affected by evaporative effects produced by the heat released from the waste. For use in the NFENV module, changes in liquid saturation and temperature at the drift wall and associated changes in chloride concentration are computed using the MULTIFLO numerical model. When the drift wall is above the boiling point of water, the chloride concentration of fluid contacting the WP is calculated by assuming equilibrium with respect to halite. Because of the uncertainty in estimating the water chemistry, the parameter value for the chloride concentration is varied between bounding values to obtain conservative estimates of performance.

There are specific assumptions related to thermohydrologic conditions:

- The mountain-scale conduction model assumes the ground surface is at a constant temperature and is not affected by climate change.

- The repository has enough numbers of ventilation shafts and drifts that a sharp increase in temperature along the drift will not develop in the direction of ventilation.

- The radiation heat loss between the top of the backfill and the drift wall is negligible.

- The thermohydrologic conceptual model implemented in NFENV assumes there are both matrix and fracture flow continua. The hydrologic regime in the near field is assumed dominated by, and in equilibrium with, the thermal regime during the thermal pulse.

- All infiltrating water participates in the reflux cycle.

- In REFLUX1, matrix waters are assumed to be immobile during the thermal pulse, so that refluxing only accounts for fracture waters. This assumption will tend to underpredict fluxes at the repository level at early and intermediate times, as thermally driven matrix water will contribute to fluxes in the fracture.

- REFLUX1 tends to return to ambient conditions almost immediately after the repository drops below boiling, with water in the halo above the boiling isotherm flushing through the system just before the boiling isotherm reaches the repository. As removal of mobilized matrix water would leave a large amount of empty matrix storage and refilling the matrix would tend to strongly attenuate fluxes as the boiling isotherm returns to the repository horizon, REFLUX1 would tend to overpredict fluxes at the repository level.

- REFLUX1, REFLUX2, and REFLUX3 do not consider elevation of the boiling point caused by salt concentration and capillarity.

- In REFLUX2 and REFLUX3, all matrix water in the dryout zone is vaporized.

- In REFLUX2 and REFLUX3, all water vaporized from the rock matrix above the WP participates in the reflux cycle. Vaporized rock water below the WP does not participate in the reflux cycle.

- REFLUX2 always assumes that the near-field temperature is above boiling until all the water in the pores leave the dryout zone.

- In REFLUX2 and REFLUX3, it is assumed that no resaturation takes place when the pores are dry and temperature is below boiling.

There are specific assumptions with water chemistry:

- For the computation of chloride concentration, any fluid which penetrates the boiling isotherm to contact the WP is in equilibrium with halite.

- When the temperature at the drift wall is below the boiling point of water, the chloride concentration in the tuff rock at the drift wall is representative of that contacting the WP.

- MULTIFLO results adequately describe the temperature, liquid saturation, and chloride concentration at the drift wall.

- Uncertainties and limitations of MULTIFLO chloride concentration results can be accounted for by use of a multiplication factor (appendix A) representing differences between groundwater chemistry in the porous matrix (calculated by MULTIFLO) and chloride concentration on a WP, which could be higher through evaporation from the WP surface.

# 6 EBSFAIL MODULE DESCRIPTION

The engineered barrier system failure (EBSFAIL) module calculates the failure time of the WPs caused by various modes of degradation such as dry air oxidation, humid air corrosion, uniform and localized (pitting and crevice) aqueous corrosion, and mechanical failure. Other degradation modes, such as stress corrosion cracking and microbially influenced corrosion, are not currently considered in EBSFAIL. Failures caused by seismicity-induced rockfall are calculated in SEISMO, while disruptive event failures are calculated in FAULTO and VOLCANO. These disruptive event failures are relevant to TPA calculations only if the events occur prior to the time of failure calculated in EBSFAIL.

## 6.1 INFORMATION FLOW WITHIN TPA

### 6.1.1 Information Supplied to EBSFAIL

Inputs required by EBSFAIL, provided by EXEC, include the temperature and RH as a function of time and position in the repository (i.e., subarea) and the chemical composition of the aqueous phase (e.g., pH and chloride concentration) in contact with the WP (calculated by NFENV). Relevant mechanical properties of the WP, corrosion parameters, and other input parameters supplied to EBSFAIL are specified in the EBSFAIL section of the *tpa.inp* file.

### 6.1.2 Information Provided by EBSFAIL

EBSFAIL passes the WP failure time caused by corrosion or mechanical failure, or both, back to EXEC for use in EBSREL for release calculation.

## 6.2 INTERMEDIATE RESULTS

The intermediate outputs from EBSFAIL are provided in the *wpsfail.res* file. For all realizations and subareas, the *wpsfail.res* file contains the failure time and the number of WPs failed because of corrosion. The *wpsfail.res* file is described in detail in tables 20-1 and 20-2.

When the append option is turned on in the *tpa.inp* file to create additional intermediate outputs, EBSFAIL inputs and outputs are written to *ebsfail.ech*, *ebsfail.rlt*, and *failt.cum* files. The time evolution of the WP temperature, RH, chloride concentration, and volumetric flow rates per WP (not used in TPA Version 4.0) are included in the *ebsfail.ech* file. The fraction of WPs failed by corrosion for all times is provided in the *ebsfail.rlt* file. The output from the stand-alone code *echofail.dat* for all subareas and realizations is available in the *failt.cum* file. A complete description of these files is provided in section 20.3.

The EBSFAIL module generates intermediate input and output data transfer files while executing the *failt.f* stand-alone code. These files contain information only for the final realization and subarea available at the end of the TPA code execution. EBSFAIL intermediate output transfer files include *ebsfail.inp* and *ebstrhc.inp*. All corrosion-related parameters specified in the *tpa.inp* file are passed on to the *failt.f* file through the intermediate data transfer file *ebsfail.inp*. The temperature and RH data are available in the *ebstrhc.inp* file. Intermediate output data transfer files from EBSFAIL are *chlrdmf.dat*, *corrode.out*, *ebstrh.dat*, and *echofail.dat*. The time evolution of chloride concentration from the *multiflo.dat*

file is contained in the *chlrdmf.dat* file. Corrosion potentials, critical potentials, and WP wall thickness for both metallic overpacks are listed at given time steps in the *corrode.out* file. The file *ebstrh.dat* contains the temperature, RH, and the corrosion failure time. The file *echofail.dat* echoes the *failt.f* file input data that is read from the *ebsfail.inp* file. Contents of the EBSFAIL intermediate data transfer files are further described in appendix B.

## 6.3 CONCEPTUAL MODEL

EBSFAIL executes the stand-alone FAILT program, which was originally assembled as part of the EBS performance assessment code (EBSPAC) (Mohanty et al., 1997). Three different types of WP failures are considered in TPA: initial (Type 1), disruptive scenario (Type 2), and corrosion and mechanical (Type 3). In Type 1 failure, a portion of the WPs in a subarea is specified to have failed at time t = 0 as a result of initial defects produced before repository closure. These WPs are assumed to have been defective or damaged prior to or during emplacement and are specified in the input data as a fraction of the total containers in a subarea. The number of WPs undergoing Type 1 failure is read from the input file. In Type 2 failure, WPs fail as a result of some disruptive event. The timing and number of WPs affected by Type 2 failures are calculated by consequence modules (e.g., SEISMO, FAULTO, VOLCANO). Type 2 failure is a distribution of scenario failures over time, unlike Types 1 and 3. The TPA Version 4.0 code considers only a limited number of discrete failure times to simplify radionuclide release calculations. Failure corresponding to faulting and volcanic events are treated using two distinct failure times. The multiple failure times from seismic events are collapsed into four distinct failure intervals: 0–2,000 yr; 2,000–5,000 yr; 5,000–10,000 yr; and 10,000–minimum (maximum simulation time, corrosion failure time). For release calculations, the midpoint of these intervals represents the failure time for all failures in that time interval. The number of failed WPs attributed to Type 2 failure is the number of WPs that failed because of disruptive events prior to the corrosion failure of WPs. In other words, all WPs in a subarea that have not undergone Type 1 and Type 2 failures are potentially subject to Type 3 failure. This assumption implies that Type 3 failure affects all WPs equally in a subarea so that all WPs in the same subarea that have not already failed under Types 1 and 2 will fail simultaneously.

### 6.3.1 Corrosion and Mechanical Failures

For simplicity, failure of the WP is defined as the through-wall penetration of the outer and inner overpacks by a single pit, by uniform corrosion, or by brittle fracture caused by mechanically dominated processes in the presence of residual stresses. Depending on the thermohydrological conditions and the near-field environment, three different WP degradation processes are assumed to occur as determined by the interaction of the changing environment with the container materials. The first process is oxidation of the outer container by interaction with gaseous oxygen in dry air at relatively elevated temperatures (100°C to the maximum temperature of the WP surface). The second process is humid-air corrosion of the outer container as a result of the air containing water vapor at intermediate RH values, and the third process is aqueous corrosion that occurs at higher RHs values. An additional degradation process is mechanical failure caused by brittle fracture that may occur as a result of the concurrent effect of thermal embrittlement of the container materials and residual stresses produced by welding during fabrication or WP closure. No allowance for extending WP lifetimes is given to the protection ability of the inner canisters (e.g., pour canister for the vitrified defense reprocessed waste) or the fuel cladding against corrosion or mechanical failure. After the outer and inner overpacks are penetrated by corrosion or failed by fracture, the SF is considered to be exposed to the near-field environment.

At each time step, a calculation is performed to determine if the RH has reached a critical value. If the RH of the environment surrounding the WP is below a lower critical value, the corrosion is treated as dry-air oxidation (and the penetration of the dry-air oxidation front is calculated). In the same time interval, a mechanical failure test is conducted for the new thickness resulting from metal oxidation to evaluate if failure by mechanical fracture occurs. If the WP does not fail by fracture, then the time is advanced, and the RH critical value test is repeated. If RH reaches the lower critical value at any time step, then the calculation of dry-air oxidation is interrupted and the calculation of metal penetration by corrosion in humid air begins. If the RH reaches a higher threshold, the calculation of metal penetration by aqueous corrosion is initiated. The mechanical failure test is performed at all time intervals until failure occurs, regardless of the type of corrosion the WP is undergoing (e.g., dry air, humid air, or aqueous corrosion). The initial time of the time step at which full penetration occurs is computed as the failure time.

In the TPA Version 4.0 code, it is assumed that dry-air oxidation and humid-air corrosion do not contribute to the degradation of the WPs because Alloy 22, the material proposed in EDA II for the outer container, exhibits negligible or almost null penetration as a result of dry-air oxidation and humid-air corrosion. Furthermore, this material does not experience thermal embrittlement, as opposed to carbon steel (the outer overpack in the VA design), and it is not expected that thermal exposure at temperatures below 350°C will lead to mechanical fracture as a result of a significant decrease in fracture toughness. The only feasible mechanism that can cause failure of the outer overpack to contain radionuclides is aqueous corrosion, either as general or localized (crevice) corrosion.

### 6.3.2 Dry-Air Oxidation

Dry-air oxidation is a negligible contributor to the failure of the WPs for design alternatives such as EDA II. The dry-air oxidation model implemented in the TPA Version 4.0 code was originally developed to address the WP design discussed in the VA (U.S. Department of Energy, 1998), which included the use of carbon steel as an outer overpack. The discussion that follows applies to materials such as carbon steel (this degradation mechanism is not valid for materials such as Alloy 22) with the exception of exposures to relatively high temperatures—a situation not considered in the EDA II.

Oxidation of steel in dry air takes place at low RHs and temperatures ranging from ambient to the maximum temperature of the WP surface. The thin oxide layers formed at such temperatures are assumed to protect the container against further oxidation. Oxide growth, however, may become localized and lead to deeper penetration of the oxidation front, adversely affecting long-term container integrity. Localized dry oxidation includes internal oxidation and intergranular oxidation. In the case of internal oxidation, the oxide forms as islands in the metal underneath the uniform oxide layer. In intergranular oxidation, the oxide forms preferentially along metal grain boundaries. Localized dry oxidation takes place by mass transport through short-circuit diffusion paths, such as interfaces between metal and oxide, other inclusions and precipitates, or grain boundaries.

In the EBSFAIL module, it is assumed that localized dry oxidation occurs intergranularly by enhanced diffusion of oxygen anions along grain boundaries. For the calculations of intergranular oxide formation, a mathematical model developed by Oishi and Ichimura (1979) is used, in which oxygen diffusion in the matrix and along the grain boundary can be calculated simultaneously in an infinite 1D body (Ahn, 1995). The main assumptions in the calculations are (i) the effect of the external oxide layer is negligible, (ii) oxygen diffuses into metallic phases (near the interface between grain boundary oxide and metal), and (iii) oxygen also diffuses into the metallic matrix from grain boundaries. The distance of oxygen penetration in the metal at time, $t$, is

$$Y_P = \left[ \frac{4 D_l}{r_g \delta D_g} \sum_{n=1}^{\infty} exp\left( - \frac{D_l n^2 \pi^2 t}{r_g^2} \right) \right]^{-1/2} \quad (6\text{-}1)$$

where

| | | |
|---|---|---|
| $Y_P$ | — | penetration distance by intergranular oxidation [cm] |
| $D_l$ | — | matrix diffusivity [$cm^2/s$] |
| $D_g$ | — | grain boundary diffusivity [$cm^2/s$] |
| $\delta$ | — | the thickness of grain boundary [$\approx 0.7 \times 10^{-7}$ cm, based on Lobnig et al. (1992)] |
| $r_g$ | — | the grain radius [ $\approx 1 \times 10^{-3}$ cm for cast steel, based on Ahn and Soo (1983, 1984)] |
| $t$ | — | time [s] |

Using diffusivities defined by the user in the *tpa.inp* file, Eq. (6-1) yields the penetration distance of oxygen along grain boundaries and is used as a surrogate for oxide formation.

### 6.3.3 Humid-Air Corrosion

Humid-air corrosion is a feasible mechanism contributing to the failure of the WPs under the VA design (U.S. Department of Energy, 1998). Other design alternatives, such as the EDA II, however, have decreased or nullified the relevance of humid-air corrosion. The discussion that follows applies to a material such as carbon steel; this degradation mechanism is not valid for materials such as Alloy 22.

Corrosion of the steel container in air at moderately high RHs, as expected under certain repository conditions after the initial dry period, bears certain similarities to atmospheric corrosion, as discussed elsewhere (Cragnolino et al., 1998). However, significant differences exist. Atmospheric corrosion occurs when a metal surface is covered by a water film of sufficient thickness to sustain electrochemical reactions. Water can be physically adsorbed to the metal surface in molecular form or it can be chemically bonded in a dissociated form that results in the formation of metal-hydroxyl bonds (Leygraf, 1995). The thickness of the water film increases with increasing RH. The critical RH above which atmospheric corrosion of most metals occurs corresponds to the formation of a water film of multiple monolayers that displays properties similar to bulk water. During these conditions, corrosion is governed by the same electrochemical laws applicable to corrosion of metals immersed in an aqueous electrolyte.

Atmospheric corrosion studies reveal that iron and steel exhibit a primary critical RH of approximately 60 percent, similar to most metals (Fyfe, 1994). Above 60 percent RH, corrosion proceeds at a slow rate, but at 75–80 percent RH, the corrosion rate sharply increases for materials such as carbon steel. This secondary critical RH is attributed to capillary condensation of water in the pores of the solid corrosion products.

In the case of carbon steel there is experimental evidence of the existence of two threshold values for the RH; when the threshold values are exceeded, the dissolution rate noticeably increases. For corrosion resistant material, such as Alloy 22, this experimental information is not available. In this case, a threshold RH value of approximately 60–65 percent is adopted for the onset of uniform passive corrosion (assuming further conditions explained in the next section are fulfilled). This value of RH is the value at which a liquid film of sufficient thickness can be formed to sustain electrochemical reactions as in bulk electrolyte solutions.

It is assumed in the EBSFAIL module that humid air corrosion occurs above a primary critical value of RH, whereas aqueous corrosion takes place above a secondary critical value. If the RH is higher than the primary critical value, humid-air corrosion is evaluated using a constant rate set by the user in the *tpa.inp* file, which is assumed to be independent of temperature and time.

### 6.3.4 Aqueous Corrosion

Aqueous corrosion of container materials could be uniform or localized depending on the composition of the near-field environment. If the corrosion potential is higher than the critical potential for the initiation of localized corrosion, the calculation of metal penetration in the form of pit growth begins immediately without an initiation or induction time. When the depth of the pit is greater than the initial thickness of the WP outer overpack, the potential of the galvanic couple formed by the outer and inner containers is calculated. For EDA II design it is considered that there is no galvanic coupling between the outer and the inner overpack. If the corrosion or galvanic potential of the inner container is lower than the critical potential for localized corrosion, penetration of the inner container is computed as uniform corrosion under passive dissolution conditions. Otherwise, pit growth of the inner overpack begins and continues until the depth of the pit becomes equal to the inner overpack wall thickness.

If the RH is higher than the secondary critical value, aqueous corrosion of the container materials is evaluated. It is assumed that a water layer defined by an arbitrary specified thickness on the order of a few millimeters is formed, and its thickness is considered to be the same regardless of the presence or absence of backfill around the WP. Water films that form on the metal surface usually contain a variety of contaminants. Soluble species such as $CO_2$ increase the electrical conductivity and decrease the pH of the film. In the VA design, these species could potentially lead to an increase in the iron or steel dissolution rate (Leygraf, 1995). Anionic species such as $Cl^-$ may escalate the rate of dissolution or promote a more localized form of corrosion.

In the presence of an aqueous phase, corrosion of steel is an electrochemically controlled process. This process could be in the form of uniform active dissolution at pH close to or lower than neutral, or in the form of localized passive dissolution under the alkaline conditions induced by anions present in groundwater such as $HCO_3^-$. Localized corrosion of the carbon steel may be promoted by the simultaneous presence of $Cl^-$ anions at concentrations higher than a minimum critical value in the pH range within which passivation occurs.

On the other hand, experiments at the CNWRA indicate that Alloy 22, the outer overpack material in the EDA II, is an alloy highly resistant to localized corrosion with a passive dissolution rate that seems to be independent of environmental factors such as pH and chloride concentration over wide pH (0.7 to 8.4) and chloride concentration (0.028 to 4.0 M) ranges and only slightly dependent on the temperature (within the 25–95 °C range) (Dunn et al., 1999). In general, Ni-Cr-Mo alloys exhibit localized corrosion in the form of pitting and crevice corrosion above certain critical potentials, which are dependent on the alloy composition (Cragnolino et al., 1999).

At any given time, the mode of aqueous corrosion depends on the corrosion potential and the appropriate critical potential required to initiate a particular localized (pitting or crevice) corrosion process. The corrosion potential is the mixed potential established at the metal/solution interface when a metal is immersed in a given environment. Corrosion potentials are calculated on the basis of a kinetic expression for the cathodic reduction of oxygen and water and the passive current density for the anodic dissolution of the metals.

Empirically derived equations are used in EBSFAIL for the dependence of critical potentials on environmental parameters. Pit initiation and repassivation potentials are assumed to depend only on the chloride concentration and temperature. The dependence of the critical potential on chloride concentration and temperature is given by

$$E_{\text{crit}} = E^{0}_{\text{crit}}(T) + B(T)\log\left[\text{Cl}^{-}\right] \tag{6-2}$$

where $E^{0}_{\text{crit}}(T)$ and $B(T)$, which depend on the material, are linear functions of temperature. The equation is valid above a minimum $Cl^-$ concentration required to promote localized corrosion that also depends on the material. It should be noted that $E_{\text{crit}}(T)$ is the value of $E^{0}_{\text{crit}}(T)$ for a $Cl^-$ concentration equal to 1 M. Both $E^{0}_{\text{crit}}(T)$ and $B(T)$ were evaluated for A516 steel and Alloy 825 for initiation and repassivation potentials for both pitting and crevice corrosion (Sridhar et al., 1993; Dunn et al., 1996). Data for Alloy 625 is available only at temperatures close to the boiling point of water (95 °C) because, at temperatures lower than 60 °C, it is resistant to localized corrosion over a wide range of $Cl^-$ concentrations (Gruss et al., 1998). Because of the insufficiency of the current database, both $E^{0}_{\text{crit}}(T)$ and $B(T)$ are conservatively considered to be independent of temperature until more data are available.

$E_{\text{crit}}(T)$ was also identified as the critical potential for the localized corrosion of Alloy 22. In this case, Eq. (6-2) is valid for the repassivation potential for crevice corrosion at $Cl^-$ concentrations above 0.5 molar and temperatures ranging from 95 to 125 °C (Dunn et al., 1999). However, at temperatures above 125 °C, $E^{0}_{\text{crit}}(T)$ and $B(T)$ are not linear functions of temperature. Nevertheless, the linear dependence is valid for the temperature range of interest in the proposed repository. Equation (6-2) is used to compute the critical potential for localized corrosion in TPA Version 4.0 code provided that the chloride concentration is above 0.5 molar as specified in the *tpa.inp* file as CritChlorideConcForFirstLayer[mol/L].

In the EBSFAIL module, the repassivation potential, $E_{rp}$, is conservatively adopted as the critical potential for the initiation of localized corrosion. The same approach is applied to the outer and inner containers. If the corrosion potential is higher than the repassivation potential, pits are assumed to grow without an initiation time. If the corrosion potential falls below the repassivation potential, previously growing pits are presumed to cease growing, and the material passivates, corroding uniformly at a low rate through a passive film. The metal penetration or remaining thickness is calculated at each time step using rates of uniform and localized corrosion as appropriate.

The propagation of pits is considered in a simplified manner by introducing an empirical equation developed by Marsh and Taylor (1988) for carbon steel in chloride containing bicarbonate/carbonate solutions using an extreme values statistics approach. In Eq. (6-3) pit penetration is time-dependent and given by

$$P = At^{n} \tag{6-3}$$

where

| | | |
|---|---|---|
| $P$ | — | pit penetration [m] |
| $t$ | — | time [yr] |
| $A$ | — | experimentally determined constant specified in the *tpa.inp* file |

Equation (6-3) has also been found to describe the pit penetration depth in a Fe-12Cr steel in 0.1 M NaCl solution at 0.0 $V_{SCE}$ and 60°C. (Zhou and Turnbull, 1999). The coefficient, $A$ (CoefForLocCorrOfOuterOverpack and CoefForLocCorrOfInnerOverpack), and the exponent, $n$ (ExponetForLocCorrOfOuterOverpack and ExponetForLocCorrOfInnerOverpack), are specified in the *tpa.inp* file for both the outer and inner overpack materials. For carbon steel, $n$ is approximately equal to 0.5, which is consistent with a pit growth process controlled by diffusional mass transport and a rate that decreases with time. For Alloy 22 and SS type 316(L or NG), it is considered that pit growth is governed by a constant rate of penetration (i.e., $n = 1$). Experimental results (Dunn et al., 1996), however, suggest that this is a conservative approach since a parabolic rate law ($n$=½) was found to apply to the crevice growth rate of SS type 316L in 1.0 M NaCl solution at 95°C, as discussed in comparison to field data for Alloy 625 (Dunn et al., 1999).

If the corrosion potential is lower than $E_{rp}$, uniform penetration caused by corrosion under passive conditions is calculated by using experimentally available values for the passive current density specified in the *tpa.inp* file.

In the TPA Version 4.0 code, the passive current density, $i$, is transformed into a corrosion rate, $CR$, by

$$CR = \frac{iE_w}{F\rho} \tag{6-4}$$

where

| | | |
|---|---|---|
| $i$ | — | passive current density [C/(m$^2$ yr)] |
| $E_w$ | — | equivalent molecular weight [kg/mol] |
| $F$ | — | Faraday's constant, 96486.7 C/mol |
| ρ | — | Material density [kg/m$^3$] |

The parameters $i$ (AA_1_1 and AA_2_1), $E_w$ (EquivalentWeightOuterOverpack and EquivalentWeightInnerOverpack), and ρ (DensityOuterOverpack and DensityInnerOverpack) are defined by the user in the *tpa.inp* file for both the inner and outer overpack materials. The equivalent molecular weight is defined as a function of the alloy composition as

$$E_w = \frac{1}{\sum_j \frac{z_j f_j}{W_j}} \tag{6-5}$$

where

| | | |
|---|---|---|
| $f_j$ | — | weight fraction of element j |
| $z_j$ | — | oxidation state of element $j$ in the alloy |
| $W_j$ | — | molecular weight of element $j$ [kg/mol] |

The sum in Eq. (6-5) spans throughout the relevant elements in the alloy (i.e., those with compositions above 1 percent). In case of uncertainty in selecting the oxidation state, $z_j$, the user should consider the conservative approach by selecting the smallest stable oxidation state for the element which would lead to high corrosion rates. This approach is taken in the definition of the basecase for the TPA Version 4.0 code. In the derivation of Eq. (6-4), it is assumed that the alloy displays perfect congruent or stoichiometric dissolution.

Following penetration of the outer container, electrical contact of the inner and outer containers through the presence of an electrolyte path (such as that provided by modified groundwater) could promote galvanic coupling, assuming that metallic contact always exists between both containers.

In the case of the VA WP design (U.S. Department of Energy, 1998), and particularly for alloys less resistant to localized corrosion than Alloy 22, such as Alloys 825 and 625, galvanic coupling to the carbon steel after its penetration by pitting corrosion can avoid localized corrosion of the inner overpack material by decreasing the corrosion potential below the repassivation potential. On the other hand, for recent design alternatives, such as EDA II, the issue of galvanic coupling is moot. Alloy 22, as the outer container material, is extremely resistant to localized corrosion, and, if penetrated by a pit, the driving force for galvanic coupling with SS type 316L will be negligible because both alloys form stable passive films enriched in chromium oxide. Nonetheless, the TPA Version 4.0 code has the potential to evaluate galvanic coupling, and the model is next described.

The effect of galvanic coupling between the inner and outer overpacks on the failure time of the WP is evaluated by a simplified approach (Mohanty et al., 1997). The corrosion potential of the inner container in the galvanic couple, $E_{corr}^{wp}$, formed when the wall of the outer container is penetrated by a pit, is estimated using experimentally measured values of the potential bimetallic couple, $E_{couple}$, for a well-defined area ratio between both components, assuming perfect electrical contact (Dunn and Cragnolino, 1997, 1998). If $E_{corr}^{wp}$ is greater than the repassivation potential of the inner overpack material, localized corrosion occurs. Otherwise, uniform corrosion takes place. The $E_{corr}^{wp}$ is determined through a linear combination of corrosion potential, $E_{corr}$, of the inner overpack, in the absence of galvanic coupling at the time of the through-wall penetration of the outer overpack, and $E_{couple}$ according to the empirical expression:

$$E_{corr}^{wp} = (1-\eta)\, E_{corr} + \eta\, E_{couple} \tag{6-6}$$

where $0 \le \eta \le 1$ is the efficiency of the galvanic coupling.

The parameters $\eta$ and $E_{couple}$ are defined in the *tpa.inp* file by the user. For the evaluation of the EDA II, both have been set equal to zero.

### 6.3.5 Mechanical Failure

Mechanical failure of the outer overpack induced by thermal embrittlement of carbon steel was a feasible mechanism contributing to the failure of the WPs considered in the VA design (U.S. Department of Energy, 1998). Other design alternatives, such as the EDA II, however, have decreased the relevance of this failure mode. Mechanical failure caused by brittle fracture may not be feasible for Alloy 22 and SS type 316L because of the high ductility of both materials. It is unlikely that the embrittlement process will induce

mechanical failure at the WP temperatures expected in EDA II. The exception could be high loads that result from seismic events that may promote plastic collapse. Nonetheless, the TPA Version 4.0 code incorporates the existing mechanical failure model used in prior versions of the code. The discussion that follows applies to a material such as carbon steel; this degradation mechanism may not be valid for EDA II materials.

Mechanical failure of WPs in the EBSFAIL module is considered to be the result of fracture of the outer overpack. As a first approximation, other mechanical failure processes such as buckling or yielding were not regarded plausible in the VA design of the WP because of the relatively large thickness of the container wall. Active uniform corrosion of the carbon steel overpack was not expected under the passivating conditions in the near-field environment of the VA design and, therefore, failure modes, such as buckling or yielding, that would require significant generalized thinning of the container wall in the presence of external loads were not included.

The possibility of mechanical failure as a result of thermal embrittlement of the alloy promoted by long-term exposure to temperatures above 150°C is evaluated at each time step. Thermal embrittlement of low-alloy steels occurs as a consequence of prolonged exposure at elevated temperatures and results in a substantial degradation of specific mechanical properties.

One of the important mechanical properties of the WP materials is toughness, which is the ability to absorb energy in the form of plastic deformation without fracture. Toughness, however, is significantly affected by thermal embrittlement, a phenomenon closely related to temper embrittlement. Thermal embrittlement is characterized by an upward shift in the ductile-brittle transition temperature, measured by the variation of the impact fracture energy for notch specimens as a function of test temperature (Vander Voort, 1990). Segregation of impurities, such as Sb, P, Sn, and As, along prior austenite grain boundaries is the main cause of temper embrittlement (Briant and Banerji, 1983). The segregation of P, which in the case of commercial steels is the predominant impurity, promotes fracture of notched specimens upon impact and leads to a change in the low-temperature fracture mode from transgranular cleavage to intergranular fracture (Cragnolino et al., 1996).

A simple fracture model, developed on the basis of linear-elastic fracture mechanics, is used in EBSFAIL. This model is based on a generalized expression for the stress intensity factor ($K_I$). For the case of a cylinder with a surface flaw located on its outer surface, the following equation is applicable:

$$K_I = Y\sigma(\pi a)^{0.5} \tag{6-7}$$

where

| | | |
|---|---|---|
| $K_I$ | — | stress intensity factor for the crack opening mode (I), [MPa $m^{0.5}$] |
| $Y$ | | geometry factor to account for the shape of the crack and the load configuration [unitless] |
| $\sigma$ | — | applied stress [MPa] |
| $a$ | — | depth of crack [m] |

It is assumed that applied stresses are caused by only residual stresses associated with the circumferential weld used for overpack closure. It is also presumed that the maximum value attainable by

residual stresses produced by welding is the yield strength of the material. The depth of the crack increases with time and is conservatively inferred to be equal to that of a pit resulting from localized corrosion. Values of Y are calculated as $Y = M_K Q^{-0.5}$, as discussed by Rolfe and Barsom (1977). The geometry factor, $Y$, corresponds to a part-through thickness thumbnail crack with a length $2c$ equal to two times its depth, $a$, for a hollow cylinder of wall thickness, $t$, in which the crack shape parameter, $Q$, is a function of $a/2c$. The magnification factor, $M_K$, varying from 1.0 to 1.6, is introduced for deep cracks with depths ranging from $t/2$ to $t$. For simplicity, the WP is considered composed of a single shell with the combined thickness of both the outer and the inner overpacks, but with the mechanical properties of the outer overpack.

In addition, a safety factor of 1.4 was applied to calculate the value of $K_I$ by assuming that the yield strength of the material in the vicinity of the welds is higher than the base material. This value is compared at each time step with the critical stress intensity or fracture toughness of the material, $K_{Ic}$, to determine if failure by fracture takes place. By definition, fracture occurs instantaneously if $K_I$ is greater than $K_{Ic}$. Because of the lack of data, no decrease in the value of $K_{Ic}$ with time is assumed in the present analysis. If thermal embrittlement of the alloy occurs through prolonged exposure (thousands of years) to temperatures above 250°C, however, a substantial decrease in the value of $K_{Ic}$ may be expected (Cragnolino et al., 1998).

### 6.3.6 Drip Shield

The EDA II considers the presence of a drip shield extended over the length of the emplacement drifts and enclosing the top and sides of the WPs. The purpose of the drip shield is to avoid water seepage or dripping during the thermal pulse period (when environmental conditions leading to localized corrosion of Alloy 22 may be attained) and presumably to attenuate the direct impact of rockfall of the WPs. The material choice for the drip shield is Ti grade 7 (Ti-0.2Pd) with a thickness of 1.5 or 2 cm.

The TPA Version 4.0 code has limited capability to evaluate the effect of the drip shield on the radionuclide release after WP failure. Uncertainties in the chemical composition of the aqueous environment in contact with the drip shield, insufficiency of parameters needed to describe the degradation processes of the drip shield material, incompleteness of experimental data, and lack of a definite EBS design have precluded the formulation of a detailed model. It is accepted, however, that the drip shield can control the amount of water available for radionuclide release. The drip shield can also affect the presence and composition of salts (e.g., chlorides and carbonates) on the surface of the WP. On the other hand, it is assumed that the drip shield does not have any influence on the relative humidity, which may be considered as a conservative assumption provided that there is no substantial accumulation of airborne materials during the ventilation period. These concepts have been implemented in the TPA Version 4.0 code as next explained.

During the environmental conditions expected in the emplacement drifts, the drip shield will exhibit passive uniform corrosion. The possibility of localized corrosion or hydrogen embrittlement caused by delayed hydride cracking seems to be negligible. Therefore, the failure time is estimated on the basis of experimental data and literature data and introduced as an input parameter in the code. The failure time (PDF) of the drip shield is defined in the *tpa.inp* file (as DripShieldFailureTime[yr]). The drip shield controls the amount of water seeping onto the WP. Thus, radionuclide release cannot be produced until both the WP and the drip shield have failed. A discussion of the radionuclide release model and the implementation of the limitation in the availability of water by the drip shield for radionuclide release can be found in chapter 8.

The drip shield may control the amount of chloride on the WP surface. In the TPA Version 4.0 code, the chloride concentration on the WP surface is computed as the near-field chloride concentration times an appropriate factor defined in the *tpa.inp* file (ChlorideMultFactor and ChlorideMultFactorIntactDripShield). Let $t_{DS}$ represent the drip shield failure time and $t$ an arbitrary time. For $t < t_{DS}$, the chloride factor selected is ChlorideMultFactorIntactDripShield, and for $t > t_{DS}$, ChlorideMultFactor. In the TPA Version 4.0 code, it is defined as ChlorideMultFactorIntactDripShield $\leq 1$ and ChlorideMultFactor $> 1$. That is to say, the chloride concentration is assumed to be less than or equal to the near-field chloride concentration while the drip shield has not failed and assumed to be higher after failure of the drip shield. See appendix A for the basecase values of the chloride multiplication factors. See also appendix A for a definition of the PDF for the failure time of the drip shield, assuming that the construction material is Ti grade 7 and based on the experimental determination of the passive current density.

### 6.3.7 Radiolysis

Radiation from the SF ($\alpha$ and $\gamma$) affecting the WP environment may cause the production of oxidizing species such as $H_2O_2$, $O_2$, and short-lived oxidizing radicals (i.e., HO, $HO_2$). The presence of these oxidizing species may cause an increase in the corrosion potential, which may suffice to change the corrosion mode from general to localized. Uncertainties in the near-field environment, incomplete experimental data, and lack of understanding of the details of the phenomenon have precluded the formulation of a detailed radiolysis model. No matter how complicated this phenomenon may be from the point of view of the degradation of the WP materials, one of the most important issues is the increase in the corrosion potential. This increase in the corrosion potential decays with time (possibly exponentially) because the radiation level decays exponentially with time. In the TPA Version 4.0 code, the increase in the corrosion potential, $\Delta E$, is modeled by

$$\Delta E = \Delta E_o e^{-\lambda t} \tag{6-8}$$

where

| | | |
|---|---|---|
| $\Delta E_o$ | — | increase in the corrosion potential at $t = 0$ [V] |
| $\lambda$ | — | decaying constant [1/yr] |
| $t$ | — | time variable [yr] |

The parameters $\Delta E_o$ and $\lambda$ are specified in the *tpa.inp* file as DeltaPotentialDueToRadiolysis[V] and DecayingConstantRadiolysis[1/yr], respectively. The corrosion potential, $E_{\text{corr}}$, is computed as

$$E_{\text{corr}} = E_{\text{corr}}^{\text{no radiolysis}} + \Delta E \tag{6-9}$$

where

| | | |
|---|---|---|
| $E_{\text{corr}}^{\text{no radiolysis}}$ | — | corrosion potential calculated on the basis of a kinetic expression for the cathodic reduction of oxygen and water and the passive current density for the anodic oxidation of the metal [V] |

Prior to the failure of the WP, α radiation is totally confined within the WP. Thus, radiation effects on the environment outside of the WP are mainly the result of γ radiation. Because of the heat generated by the SF for the first several hundreds of years after the emplacement, there is only air and water vapor surrounding the WP. Because the radiation yield for $H_2O_2$ is low in the moist-air gas system, the concentration of $H_2O_2$ is expected to be negligible in the gas-phase environment (Reed and Van Konynenburg, 1993). Furthermore, the radiation yield of $H_2O_2$ in water vapor is zero (Spinks and Woods, 1990), and $H_2O_2$ is unstable and decays into more stable species such as $H_2O$, $OH^-$, and $O_2$. Therefore, $H_2O_2$ cannot accumulate in the environment in the proximity of the WP during the dry and humid period. After the long dry-air and humid-air periods, water will condense on the surface of the WP and form a thin film. Under this condition, $H_2O_2$ may be formed by irradiation. The irradiation level must be high enough to guarantee a continuous supply of oxidizing species and increase the corrosion potential. By the time of the formation of the water film, however, the energy absorption rate on the environment in the proximity of the WP will be so low (computed to be less than 0.005 J/kg-hr after 1,000 yr in the EDA II) that the production of $H_2O_2$ is expected to be negligible. For this reason, in the basecase for TPA Version 4.0 code, it is considered that $\Delta E_o = 0$ (a dummy value is assigned to the parameter λ). Parameter values can be found in appendix A.

## 6.4 ASSUMPTIONS AND CONSERVATISM OF THE EBSFAIL APPROACH

The EBSFAIL model is an abstraction of failure of the WP that considers (i) dry-air oxidation, (ii) humid-air corrosion, (iii) aqueous corrosion, (iv) mechanical failure, (v) drip-shield failure, (vi) radiolysis, (vii) disruptive-scenario failure, (viii) juvenile failure, and (ix) failure time.

Oxidation of steel can occur in dry air at low RH and temperatures ranging from ambient to the maximum temperature of the WP surface. It is assumed that localized dry-air oxidation occurs intergranularly by enhanced diffusion of oxygen anions along grain boundaries. Because this effect is expected only for a short period at the beginning of the postclosure period when the RH may be lowered by thermal output, it is not anticipated to significantly affect the WP lifetime. With more current design alternatives, such as EDA II, dry-air oxidation does not contribute to failure of the WPs. This process is included because the code was originally developed to evaluate the VA design where this degradation process had some minor significance.

Corrosion of steel in air at moderately high RH, expected after the initial dry period, bears certain similarities to atmospheric corrosion. Humid-air corrosion is assumed to occur when the RH is above a primary RH value and below a secondary critical RH above which aqueous corrosion takes place. Atmospheric corrosion studies for iron and steel indicate a slow rate of corrosion occurring between a primary RH of 60 percent and a secondary RH of 75–80 percent. Humid-air corrosion is not considered to have a significant effect on WP lifetime. For more current design alternatives, such as EDA II, humid-air corrosion does not contribute to failure of the WPs. This process is included because the code was originally developed to evaluate the VA design where this degradation process had some minor significance.

Among dry-air oxidation, humid-air corrosion, and aqueous corrosion, degradation of the WP will be most affected by the aqueous corrosion process. Aqueous corrosion will occur when the secondary RH is exceeded. Aqueous corrosion can occur in the form of uniform or localized corrosion. Localized (pitting or crevice) corrosion will breach the WP in a much shorter time than uniform corrosion. The corrosion potential is the driving force required to promote the occurrence of various corrosion processes under natural environmental conditions. Once the corrosion potential exceeds the repassivation potential, localized corrosion begins, and pit growth rates are calculated by using an empirical expression. Failure of the WP

is defined conservatively as penetration of both overpacks by a single pit or by general dissolution. Because the repassivation potential depends on the temperature and chloride concentration through an empirical expression, the degree of conservatism depends on the approach used to estimate the temperature and chloride concentration. The corrosion potential may also be increased by the presence of additional oxidizing species created by water radiolysis, as later explained.

Mechanical failure of the WP is assumed to occur as a result of fracture of the outer steel overpack. Fracture of the overpack, as a result of thermal embrittlement, is an important consideration in the VA design because the fracture toughness of the steel can be affected by the repository thermal environment (i.e., long-term exposure to temperatures above 150°C). However, for other design alternatives, such as EDA II, this failure mechanism may be irrelevant. Mechanical fracture due to thermal embrittlement may not be feasible for both Alloy 22 and SS type 316L because of the high ductility of both materials. It is unlikely that the embrittlement process will induce mechanical failure at the WP temperatures expected in EDA II. The exception could be high loads that result from seismic events that may promote plastic collapse. Mechanical failure by brittle fracture is included because the code was originally developed to evaluate the VA design, where this degradation process had some significance. In the implemented methodology, the stress intensity arising from residual stresses at the tip of a crack or pit is compared to the fracture toughness of the WP to determine if failure by fracture takes place. This approach is nonconservative because the applied stress considered excludes other stresses (e.g., from seismicity and faulting). However, the overall approach can be conservative depending on the value for fracture toughness specified in the *tpa.inp* file. In the VA design, fracture toughness is affected by the prolonged exposure to high temperatures (above 250°C) and thus is dependent on repository design (e.g., backfill versus no backfill and thermal load).

The drip shield regulates the amount of water for radionuclide release. It is assumed that it also decreases the chloride concentration of the environment in the proximity of the WP. After failure of the drip shield, the chloride concentration could increase because of the presence of salts in the seeping water. The degree of conservatism in the drip shield model depends on the conservatism associated with the drip shield failure time distribution, specified in the *tpa.inp* file. In the current corrosion model that does not consider deposition of airborne substances during the preclosure ventilation period, the assumption that the relative humidity is not affected by the presence of the drip shield is conservative. Because the onset of corrosion degradation is assumed to be governed by the RH, both the drip shield and the WP degrade in a parallel manner. The assumption that the chloride concentration in the proximity of the WP is equivalent to the near-field concentration, while the drip shield is intact, is also a conservative approach.

The effect of $\gamma$ and $\alpha$ radiation on the environment in the proximity of the WP is simulated by assuming an increase in the corrosion potential that decays exponentially with time. The basecase, however, does not take into account this possible increase in the corrosion potential. The reason for this selection is the consideration by CNWRA staff that the radiation levels after the formation of the film of water on the surface of the WP will be so small that it will not be possible to sustain a continuous supply of radiolytic species (unstable on their own). Furthermore, the change in the corrosion potential is not expected to be large enough to change the corrosion mode from general passive corrosion to localized corrosion.

Disruptive scenario failure of the WP is the failure of the WP caused by seismicity, faulting, or igneous activity (further details on the disruptive scenario failures are provided in their respective sections). Seismic activity can cause rockfall from the roof of the emplacement drifts that will cause deformation and, in some cases, failure of the WP. Fault displacement is assumed to fail all WPs intercepted by the fault zone when a given fault displacement is exceeded. Intrusive IA is assumed to fail all WPs in an effective area

intercepted by an intrusive event calculated by an intrusion orientation, length, and width (this assumes that contact between magma and the WP results in failure of the WP).

Juvenile failures of the WP may occur because of manufacturing defects and emplacement accidents. The TPA Version 4.0 code includes a parameter to specify the fraction of WPs assumed to be damaged either at the beginning or at a nonzero simulation time. There is limited data to determine an appropriate value for juvenile failures.

Unique failure times are assigned to each failure type: (i) juvenile failure, (ii) failure by degradation (dry oxidation, humid-air corrosion, and mechanical fracture failure), (iii) faulting disruptive scenario failure, (iv) intrusive IA scenario failure, and (v) seismicity disruptive event scenario. Only one time is used for each of the these categories to represent the failure time of the WPs with the exception of the seismicity disruptive event scenario failure. Because of the frequent occurrence of seismic events that could lead to WP failure, four different time intervals are used to group seismic failures, and the midpoint of these intervals is used as the seismic failure time. The conservative nature of this approach depends on the distribution of failures within the simulation period.

There are specific assumptions and conservatisms of EBSFAIL:

- There is no coupling of the EBSFAIL module for mechanical failure with failure of WPs because of disruptive events calculated outside the EBSFAIL module. This lack of coupling may result in conservative estimates of the number of failed WPs and the time of occurrence computed by the SEISMO module. No inputs from FAULTO and SEISMO modules in the form of applied stresses are used in EBSFAIL to calculate mechanical failure. Only residual stresses arising from weld closures are considered.

- Corrosion failure of all the WPs contained in a subarea occurs simultaneously and is determined by the penetration of both overpacks by a single pit or by general corrosion. These assumptions do not take into consideration the full range of spatial variations in environmental, material, and electrochemical conditions that can be expected for different WPs and on different areas of a single WP.

- Mechanical failure is calculated assuming an intact WP (i.e., no weakening of the WP owing to uniform corrosion), which may yield nonconservatively long times to mechanical failure. For the EDA II, however, this failure mode is considered to be irrelevant.

- For dry-air oxidation of the WP, the rate of oxidation is controlled by oxygen transport into grain boundaries, which is a slow process. This failure mechanism is negligible for the VA design and assumed null for the EDA II.

- Aqueous corrosion occurs through formation of an alkaline and saline water film on the WP surface at high RH. Dripping of modified groundwater on the WP is not considered. This limitation may lead to nonconservative results if there are significant spatial and temporal variations in the flow and chemistry of the water.

- The drip shield is assumed not to have any influence on the relative humidity, and thus it does not delay the degradation of the WP. If there are prior surface deposition of dust or

other chemically aggressive materials, condensates from the inside of the drip shield wall dripping on the WP could accelerate the degradation of the WP.

- The possibility of enhanced corrosion rates occurring along the WP closure weld areas is neglected, which may lead to nonconservative estimates of the failure times. The WP weld area, however, is small compared to the base metal area and located in one of the vertically emplaced ends of the WP. Thus, a limited surface is available for water to seep inside the WP and promote the release of the radionuclides.

# 7 SEISMO MODULE DESCRIPTION

SEISMO determines the number of WPs ruptured by seismically induced rockfalls. The number of ruptured WPs determined from this module, is made available to EBSREL for release calculation. SEISMO is considered a basecase WP failure module, but, because of the uncertainties in the effect of seismicity on WP failure, the TPA Version 4.0 code allows the user to operate the code with or without the SEISMO module. Like disruptive event modules VOLCANO or FAULTO, SEISMO is activated by a flag in the *tpa.inp* file.

## 7.1 INFORMATION FLOW WITHIN TPA

### 7.1.1 Information Supplied to SEISMO

The user selects the seismic disruptive process module in the *tpa.inp* file. EXEC passes to SEISMO the TPA time steps and the number, magnitude, and time of the seismic events that are sampled using the seismic hazard curve data set in the *tpa.inp* file. The vertical extent of rockfall associated with different categories of seismic events and rockfall area determined by joint spacing are used to compute rockfall volume. The vertical extent of rockfall and the fractional rockfall area are provided in the *tpa.inp* file. With the new design, the rockfall is likely to damage WPs only prior to the emplacement of backfill if the backfill is sufficiently designed to eliminate effects of rockfall on WPs. To account for backfill at the postclosure, the SEISMO module has an option to turn rockfall assessment off at a desired simulation time.

### 7.1.2 Information Provided by SEISMO

SEISMO calculates the cumulative fraction of WPs disturbed by the seismic event for all subareas. These results are passed to EXEC and used in EBSREL for release calculations.

## 7.2 INTERMEDIATE RESULTS

The intermediate outputs from SEISMO are accessed in the *wpsfail.res* file. The seismic event time and the number of WPs failed by the seismic event are available in the *wpsfail.res* file. The *wpsfail.res* file is described in detail in tables 20-1 and 20-2.

When the append option is turned on in the *tpa.inp* file to create additional intermediate outputs, SEISMO inputs are written to the *seismo.ech* file and outputs to the *seismo.rlt* file. The number, time, and type of seismic event are included in the *seismo.ech* file. The fraction of WPs failed by seismic events for all time steps is provided in the *seismo.rlt* file. A complete description of these files is presented in chapter 20.

## 7.3 CONCEPTUAL MODEL

The SEISMO module evaluates the potential for direct rupture of WPs from rockfall induced by seismicity. The SEISMO code uses the weight of rock falling from the roof of the emplacement drifts to calculate the impact load on a WP. The magnitude of the impact load is assumed to be a function of the size of the falling rock block and the distance the rock falls. The size of the falling rock block is, in turn, a function of rock conditions and the magnitude of a seismic event. The SEISMO conceptual model is divided into (i) computation of falling rock volume and weight, (ii) calculation of impact load and stress,

(iii) determination of WP rupture, and (iv) determination of the number of WPs ruptured. The SEISMO module accounts for the variation of rock conditions, the relationship between falling rock size and magnitude of seismicity, and the timing of the seismic events.

### 7.3.1 Impact Load and Stress Calculation

The SEISMO conceptual model assumes that for impact load and stress calculation

- No energy dissipation takes place at the point of impact because of local inelastic deformation of the WP material
- The deformation of WPs is directly proportional to the magnitude of the dynamically applied force
- The rock body does not fragment on impact
- The inertia of the WP resisting an impact may be neglected
- The WP is treated as an equivalent spring with a spring constant $k_{wp}$ [figure 7-1(a)]

The dynamic or impact loads determined in the SEISMO module for rock falling on a WP are approximated based on the principle of conservation of energy using the weights of the freely falling rocks. For a rock hitting the WP, the impact load is calculated as (Popov, 1970)

$$P_{\text{dyn}} = W\left(1+\sqrt{1+\frac{2h}{\Delta_{st}}}\right) \tag{7-1}$$

where

| | | |
|---|---|---|
| $P_{\text{dyn}}$ | — | impact load [N] |
| $W$ | — | weight of the rock falling [N] |
| $h$ | — | falling distance of rocks to WPs [m] |
| $\Delta_{st}$ | — | spring deformation [m] |

The supports for WPs are treated as flexible supports in the SEISMO module. In the current repository conceptual design, a WP will be supported by four equally spaced, v-shaped thin beams with one vertical cylindrical bar on either side of the v-shaped beam. In the SEISMO module, only the supports at both ends of a WP are considered [figure 7-1(b)]. In Eq. (7-1), $\Delta_{st}$ was the static deflection of a WP impacted, assuming rigid supports. To account for the deformability of WP support,

$$\Delta_{st} = \frac{W}{k_{\text{wp}}} + \frac{W}{2N_p k_b} \tag{7-2}$$

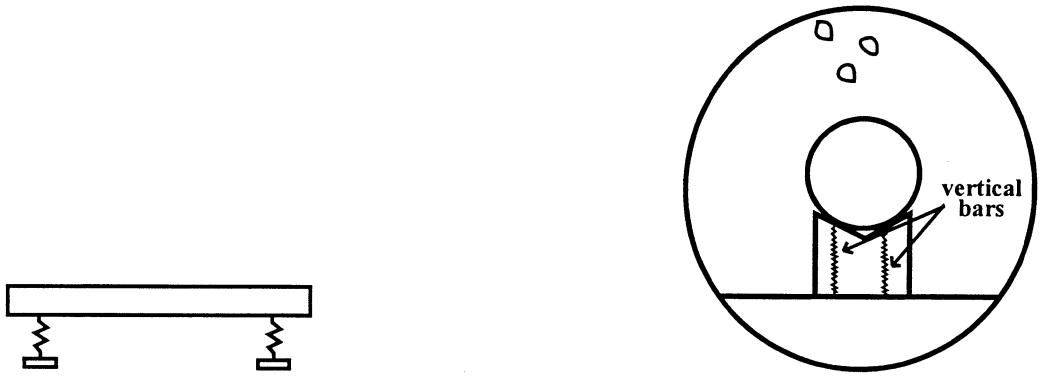


**Figure 7-1. (a) Waste package equivalent beam and (b) waste package vertical supports for SEISMO**

where

$k_{wp}$ — stiffness of the WP determined as unit deflection at the center of a simply supported beam when subjected to a load at the center [N/m].

$N_p$ — number of the supports at each end of the WP (2 in this case)

$k_b$ — stiffness of the vertical WP support bars [N/m]

The WP stiffness, $k_{wp}$, is design dependent and can be calculated by

$$k_{\text{wp}} = \frac{48 E_{\text{wp}} I}{L_{\text{wp}}^3} \tag{7-3}$$

and $k_b$ can be calculated by

$$k_b = \frac{AE}{L} \tag{7-4}$$

where

| | | |
|---|---|---|
| $A$ | — | cross-sectional area of the vertical support bar [$m^2$] |
| $E_{wp}$ | — | equivalent Young's modulus of WP [$N/m^2$] calculated using composite beam theory based on the EDA II design |
| $E$ | — | Young's modulus of the vertical support bar or [$N/m^2$] |
| $L$ | — | height of the vertical support bar [m] |
| $I$ | — | $\pi R_{ave}^3$, where $R_{ave}$ is the average of the outer and inner wall radii of the WP [$m^4$] |
| $L_{wp}$ | — | length of the WP [m] |

No information regarding the shape and dimension of the bar is currently available. In the SEISMO module, the bar is assumed to be a cylinder with a radius of 0.0508 m and height of 0.3048 m.

On obtaining the impact load, the equivalent static stress resulting from the rock impact on a WP can be calculated by adopting a simple concept of two spheres in contact and assuming the pressure is distributed over a small circle of contact (Timoshenko and Goodier, 1987). The impact stress ($p$) in $N/m^2$ can be obtained by

$$p = \frac{3}{2\pi}\left(\frac{16P_{dyn}}{9\pi^2}\frac{1}{\left(C_{wp}+C_{rock}\right)^2 R_{wp}^2}\right)^{\frac{1}{3}} \tag{7-5}$$

where

| | | |
|---|---|---|
| $C_{wp}$ | — | constant for lower sphere or WP [$m^2/N$] |
| $C_{rock}$ | — | constant for upper sphere or rockfall [$m^2/N$] |
| $R_{wp}$ | — | radius of lower sphere or WP [m] |

and

$$C_{wp} = \frac{1-\mu_{wp}^2}{\pi E_{wp}} \tag{7-6}$$

$$C_{\text{rock}} = \frac{1 - \pi^2_{\text{rock}}}{\pi E_{\text{rock}}} \tag{7-7}$$

where

$\mu_{wp}$ — Poisson's ratio of WP [unitless]

$E_{wp}$ — modulus of elasticity of WP [N/m$^2$]

$\mu_{rock}$ — Poisson's ratio of rockfall [unitless]

$E_{rock}$ — modulus of elasticity of rockfall [N/m$^2$]

#### 7.3.1.1 Failure Criterion

To judge the failure of a WP, a maximum allowable strain failure criterion is adopted in the SEISMO module. If the impact stress calculated using Eq. (7-5) induces a plastic strain at the contact of impact exceeding 2 percent (Timoshenko, 1956), the WP is assumed to be ruptured. This assumption should provide a conservative approach for estimating failure of WPs. The potential damage that rockfall can cause to the SF cladding is currently not accounted for in the SEISMO module.

To preserve the conservatism, a failure is allowed to occur when the plastic strain at the point of impact exceeds 2 percent of elongation. Most metals are known to be able to undergo more than 2 percent of elongation without failure. Furthermore, the 2-percent plastic strain at the point of impact constitutes only the initiation of a failure process. More energy will be needed to continue this failure process.

Figure 7-2 shows a schematic of stress versus strain curve for a typical metal under tension. In the figure, the yield strength, $\sigma_Y$, occurs at a point 0.2 percent of the permanent strain (Timoshenko, 1956). ULT represents the ultimate strength at 5 percent of permanent strain (maximum allowable permanent strain). This general stress-strain curve is used in SEISMO. When the energy generated by impact is greater than the energy (area below the stress-strain curve) required to break the WP, the WP is considered failed. The effects of the location of the yield point and the maximum allowable permanent strain can be evaluated by changing their values in *tpa.inp* file.

### 7.3.2 Joint Spacing and Rock Conditions in the TSw2 Unit

It is recognized that not all rocks falling from the roof of the emplacement drifts will rupture the WPs. The effective size of the fallen rock that may impact the WPs is envisioned to be controlled by joint spacing (JS) (width and length of the rock block) and vertical extent of the rock block falling on the WP. Given the wide range distribution of JSs in the TSw2 thermal-mechanical unit, it is convenient to assume five distinct rock conditions exist in the TSw2 unit. These rock conditions are estimated using available JS information (Brechtel et al., 1995) for the TSw2 unit. Since each rock condition represents a range of JS, a normal distribution covering the range of the JS is assumed for the corresponding rock condition (for lack of specific information). The size of the rocks used for each rock condition is then based on the JS distribution condition. The volume of a falling rock can be calculated by JS (width) × JS (length) × vertical

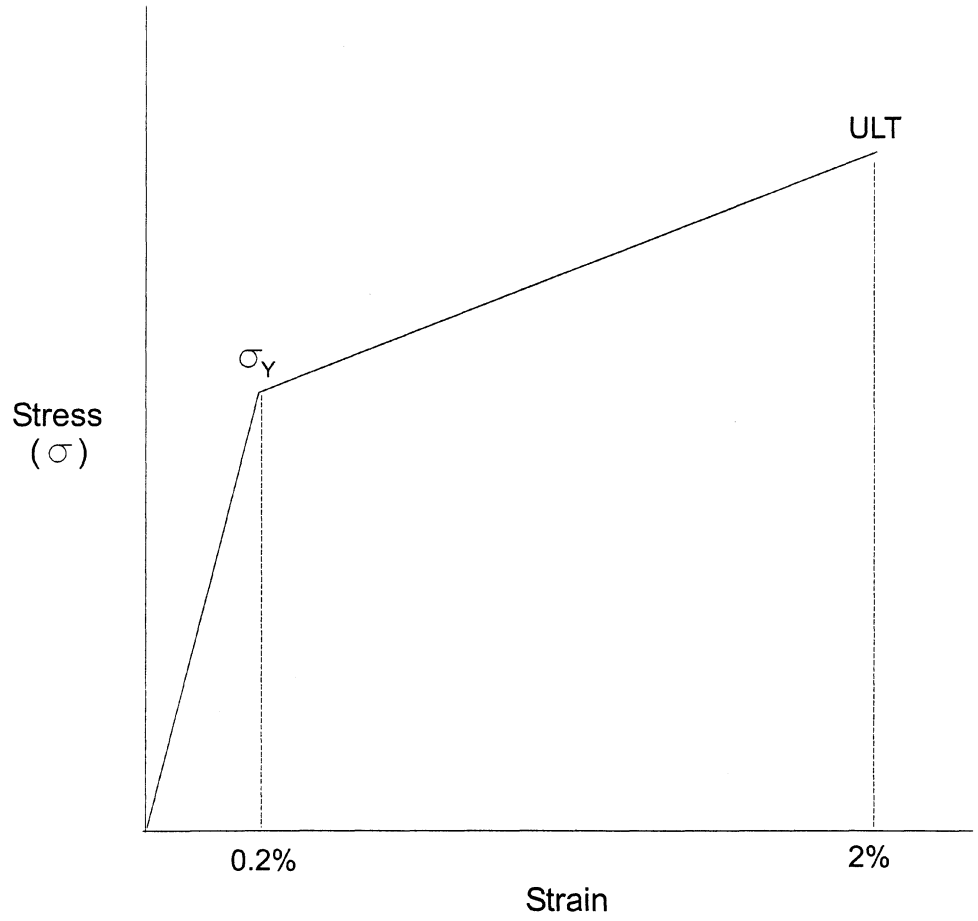


**Figure 7-2. SEISMO stress-strain relationship**

dimension of the falling rock block. At this time, the SEISMO module assumes the width of a falling rock is equal to its length.

#### 7.3.2.1 Fractional Coverage of Rock Conditions and Determination of Number of Waste Packages Ruptured

Based on Brechtel et al. (1995), rock condition 4 appears to contain a large portion of the TSw2 unit. About 62.9 percent of the area can be characterized as rock condition 4, and rock condition 5 occupies roughly 35.6 percent of the area. Rock conditions 1, 2, and 3 account for only 1.5 percent of the total area. Because of the lack of specific information, the 1.5 percent is equally divided into rock conditions 1, 2, and 3.

In the SEISMO module, the percentage of total WPs in each of the rock conditions is assumed to be equal to the fractional coverage of the rock condition. If a seismic event triggers rockfall for a particular rock condition, rockfall is not expected to take place in the entire area of that rock condition. In fact, only a small fraction of the rock will fall in response to a seismic event because of the inherent variation associated with the rocks. Another fraction of the rock may fall at a later time when a separate seismic event, having the same or greater intensity, occurs. Rockfall could also occur in response to a smaller

magnitude event if the rock has been sufficiently weakened by repeated seismic events. The fraction may be related to the event magnitude, joint dip angles, incidence angle of incoming seismic waves, and other parameters.

At this time, there is little information available to determine fractional rockfall area as a function of the previous parameters. Consequently, CNWRA experts developed a continuous function that relates the fractional rockfall area to the magnitude of seismic ground accelerations based on experience in the field. This function is implemented in the SEISMO module for the TPA Version 4.0 code. Currently, this function is independent of the rock condition, that is, the same fraction is applied to all rock conditions in estimating the number of WPs affected by rockfall. Although this function in independent of the rock condition, it is intuitive that, for a particular seismic event, a weaker rock condition should experience a relatively larger area of rockfall compared to a stronger rock condition. This dependency will be incorporated into future versions of the TPA Version 4.0 code.

#### 7.3.2.2 Seismic Hazard Parameters

The SEISMO module requires the generation of a synthetic time history of seismicity over the time period of interest. This estimate is made by using the TPA executive SAMPLER utility module. The required input for generating event history includes ground acceleration sampling points and the corresponding recurrence times, which together form a seismic hazard curve. The horizontal acceleration hazard curve provided in DOE (1995) is used to determine the seismic hazard associated with an earthquake with a given recurrence interval. This hazard curve was specifically developed for surface facilities. A common understanding for YM is that the seismic acceleration at the repository horizon may be half that at the ground surface. In the SEISMO module, half the surface hazard is used as a basecase. The SEISMO module can be used to assess the effects of different hazard curves; however, in changing the hazard curve, the height of rockfall volumes should be modified to reflect the effect of the ground acceleration magnitude.

As discussed earlier, seismic recurrence sampling is handled by the SAMPLER utility module in the TPA Version 4.0 code. The sampling points (accelerations) and the corresponding recurrence time are provided in the *tpa.inp* file. Currently, the SEISMO module allows for an input of up to 10 discrete sampled accelerations in the seismic hazard curve used. Along with the sampling accelerations, the corresponding recurrence times should also be provided to the *tpa.inp* file.

## 7.4 ASSUMPTIONS AND CONSERVATISM OF THE SEISMO APPROACH

The SEISMO module is an abstraction of the effect of seismicity on WP performance. The SEISMO module considers (i) the frequency and magnitude of seismic events, (ii) the quantity of rockfall for each seismic event, and (iii) the effect on the WP.

The SEISMO module does not have the provision to evaluate the effect of the drip shield in mitigating the consequences of rockfall. The SEISMO module currently assumes that no drip shield will be emplaced. Without considering the positive effect of drip shield, the results from the SEISMO module should provide a conservative estimate. Investigation is under way to assess the contribution of drip shield in reducing rockfall effect on WP performance. The analysis results will be included in the SEISMO module in future revisions.

The SEISMO module does not take into account the potential effect of WP vertical movement during vibratory ground motion at the time of rockfall impact. The vibratory ground motion could cause a WP to move up or down during impact. The current assumption that a WP is stationary during impact underestimates the impact load if a WP is moving upward during impact and overestimates the impact load for conditions that a WP is moving downward during impact.

In assessing rockfall effect, the residual stresses arising from WP closure welds and the differential thermal expansion between the WP inner and outer barriers are not considered. The potential effects of not considering those aspects are not clear.

The frequency and magnitude of the seismic events are based on a seismic hazard curve provided as input to the TPA Version 4.0 code. The seismic hazard curve provides accelerations and recurrence frequencies for seismic events over the time period of interest. The seismic hazard curve is based on historical information for surface facilities and is considered a reasonable approach for the underground facility.

The volume of rock that falls for a given event is determined based on properties related to the TSw2 thermal-mechanical unit. Five distinct rock conditions have been identified to characterize the variability in rock properties within the TSw2 unit. The abstraction for rock volume uses JS information (as width and length) and height of yield zone (as vertical extent). The height of yield zone was estimated from dynamic numerical modeling of coupled thermal-mechanical effects. The height of the yield zone has been conservatively set as an upper bound such that the volume of the rockfall represents a maximum value.

If a seismic event triggers a rockfall, it is assumed to equally affect the whole area of the repository irrespective of rock conditions. In other words, fractional areal coverage of rockfall is the same under all five rock conditions. In actuality, a seismic event may trigger more rockfall for one rock condition than for another. Intuitively, for a given seismic ground acceleration, a weaker rock condition should experience a relatively large area of rockfall compared to a stronger rock condition. In the current implementation, the fractional rockfall area is a function of seismic ground acceleration not a function of rock condition. Whether or not this assumption is conservative cannot be determined at this time.

Rockfall may affect the WP lifetime through rupture of the WP by the impact produced by the falling rock and acceleration of corrosion at the location of the impact. Only the first aspect is considered in SEISMO. The key components of the SEISMO module include determination of the impact load and failure. In computing the impact load, the WP is treated as a simply supported beam. In converting impact load to impact stress, all energy generated through dynamic impact of the rockfall is transferred to the WP. A conservative assumption is that the WP will rupture if plastic strain at the point of impact exceeds 2 percent. The analysis assumes, nonconservatively, that rockfall occurs on an intact WP (i.e., corrosion of the WP does not reduce WP strength, and cumulative damage caused by consecutive rockfalls is not considered). Overall the approach is considered conservative over a 10,000-yr compliance period.

There are specific assumptions and conservatisms of SEISMO:

- A WP can be treated as a simply supported beam.
- No energy dissipation takes place at the point of impact because of local inelastic deformation of the WP material.

- Deformation of WPs is directly proportional to magnitude of the impact.
- Inertia of the WP resisting an impact may be neglected.
- Estimate of the impact stress assumes a contact area based on a spherical geometry. This assumption yields a conservative estimate because the actual contact area would be larger.
- In converting impact load to impact stress, falling rocks are assumed to have infinite strength (i.e., all energy generated through impact is transferred to the WPs). If rock is allowed to break, the effective impact stress to the WP should be smaller since some impact energy will be absorbed by the rock breaking.

# 8 EBSREL MODULE DESCRIPTION

The EBSREL module calculates the time-dependent release of radionuclides from the EBS to the UZ. Infiltrating water and refluxed water could reach the drift wall and subsequently the WP. If the container is breached, infiltrating water enriched with chloride and other minerals could enter the WP, coming in contact with the SF. If the cladding has failed, the infiltrating water could dissolve the SF and then carry the radionuclides out of the WP to the geosphere.

## 8.1 INFORMATION FLOW WITHIN TPA

### 8.1.1 Information Supplied to EBSREL

EBSREL obtains values from EXEC for (i) WP temperature by reading in a file created in EBSFAIL, (ii) volumetric flow rate of water in the near field (calculated in NFENV), and (iii) the number of failed WPs and corresponding failure times for all failure modes (corrosion failure, disruptive event failure, and initial defective failure). Radionuclide decay chains, half-lives, initial inventories, and molecular (isotopic) weights in INVENT are passed to EBSREL by EXEC. Data for the time evolution of factors determining the amount of water entering the WP are available in the *wpflow.def* file. Other values, such as WP dimensions, nuclide-specific solubilities, retardation coefficients, fractions of SF wet, and SF dissolution model parameters, are specified in the *tpa.inp* file.

### 8.1.2 Information Provided by EBSREL

EBSREL calculates the radionuclide releases from the EBS for all subareas and passes these results to EXEC for subsequent use in UZFT. EBSREL provides release rates as a function of time for all radionuclides specified in the *tpa.inp* file for groundwater dose calculations.

## 8.2 INTERMEDIATE RESULTS

The cumulative release of nuclides from the EBS (summed over all repository subareas for the simulation period) is available for each radionuclide in the *cumrel.res* and *cumrel_c.res* files. The peak release rate of each radionuclide from each subarea is provided in the *pkreltim.res* and *pkrltm_c.res* files. These four files are described in tables 20-1 and 20-2.

When the append option is turned on in the *tpa.inp* file to create additional intermediate outputs, EBSREL inputs and outputs are written to the *ebsrel.ech*, *ebsrel.rlt*, and *releaset.cum* files. For all times, the flowrate of water hitting a WP and the number and time of WPs failed by all events are included in the *ebsrel.ech* file. The time evolution of EBS releases for all groundwater radionuclides is available in the *ebsrel.rlt* file. The screen output from the stand-alone code *releaset.f* for all subareas and realizations can be accessed in the *releaset.cum* file. A complete description of these files is provided in chapter 20.

The EBSREL module generates intermediate input and output data transfer files while executing the *releaset.f* and *ebsfilt.f* stand-alone codes. These files are overwritten for each realization and subarea and contain information only for the final realization and subarea; those files are available on completion of TPA Version 4.0 code execution. EBSREL intermediate input data transfer files are *ebsrel.inp*, *ebsflo.dat*, *ebspac.nuc*, *ebstrh.dat*, *ebsfilt.inp*, and *wpflow.dat*. All EBS release-related parameters specified

in the *tpa.inp* file are accessed through the *ebsrel.inp* and *ebsfilt.inp* files. The factors determining the amount of water entering the WP in the *wpflow.def* file are mapped to TPA time steps in EBSREL and written to the *wpflow.dat* file. The file *ebsflo.dat* consists of four columns of information containing time, the product of the volumetric flow rate into the drift from NFENV, the WP flow multiplication factor specified in the *tpa.inp* file, and the two flow factors from the *wpflow.dat* file. Nuclide-specific information is located in the *ebspac.nuc* file as well as in the *ebsfilt.inp* file. WP temperature, RH, and corrosion failure time are available in the *ebstrh.dat* file. Intermediate output data transfer files from the EBSREL execution of the *releaset.f* and *ebsfilt.f* files include the *ebsnef.dat*, *ebsnef2.dat*, and *echofilt.dat* files. The file *ebsnef.dat* provides the release rates from the WP for all groundwater radionuclides, whereas the *ebsnef2.dat* file provides the release rates from the EBS. The file *echofilt.dat* echoes input data read from the *ebsfilt.inp* file. The contents of all EBSREL intermediate data transfer files are further described in appendix E.

## 8.3 CONCEPTUAL MODEL

Using WP failure information from EBSFAIL and near-field chemistry, temperature, and liquid flow rate information from NFENV, EBSREL [derived from EBSPAC (Mohanty et al., 1996)] calculates release of radionuclides from a WP. Conceptual models used in EBSREL are described in the succeeding sections. Only advective release from the WP is considered because the diffusive release is found to be orders of magnitude smaller than advective release. In calculating releases, EBSREL takes into account radionuclide decay, generation of daughter products in the chains, temporal variation of inventory in the WP, and temporal variation in water flow. Once the container is breached, the SF may be exposed to aqueous conditions as determined by the near-field calculations. Like EBSFAIL, EBSREL looks at processes affecting an individual WP representative of all WPs in the subarea. Releases calculated by EBSREL from this breached WP are then scaled to account for the total number of WPs breached from a particular failure type (i.e., initially defective, scenario failure, and corrosion failure). Releases from all failure modes are then summed as presented in section 8.3.8.

### 8.3.1 Radionuclide Inventory and Mass Transfer

Two models for aqueous release of nuclides are available for selection by the user: the bathtub model and the flow-through model. In the bathtub model, it is assumed that at the time of failure there are at least two holes in a horizontally emplaced WP that act as inlet and outlet for water. The holes are located such that water enters through one pit and exits through the other. Another presumption is that at least one of the holes is located on the side of the WP at a level lower than that of the water entrance hole, which is situated at the top of the horizontally emplaced WP. After the water level in the WP rises to the specified outflow position (a sampled parameter), water begins to flow from the WP along with the dissolved radionuclides. The flow-through model is a variant of the bathtub model, for which the flow out is assumed to be immediately equal to the flow in and the fraction of fuel wetted is not a function of water level inside the WP.

Figure 8-1 presents a schematic representation of a horizontally emplaced WP with holes representing the inlet and outlet. In this schematic, the conduit for liquid entry is shown on the upper half of the WP and the hole for the liquid exit is shown on one of the sides. Liquid water will accumulate in the WP until its level rises to the level of the exit hole, $h$. The height of the exit hole is specified in the *tpa.inp* file via the SFWettedFraction parameter; 0 implies an outlet at the bottom, and 1 implies an outlet at the

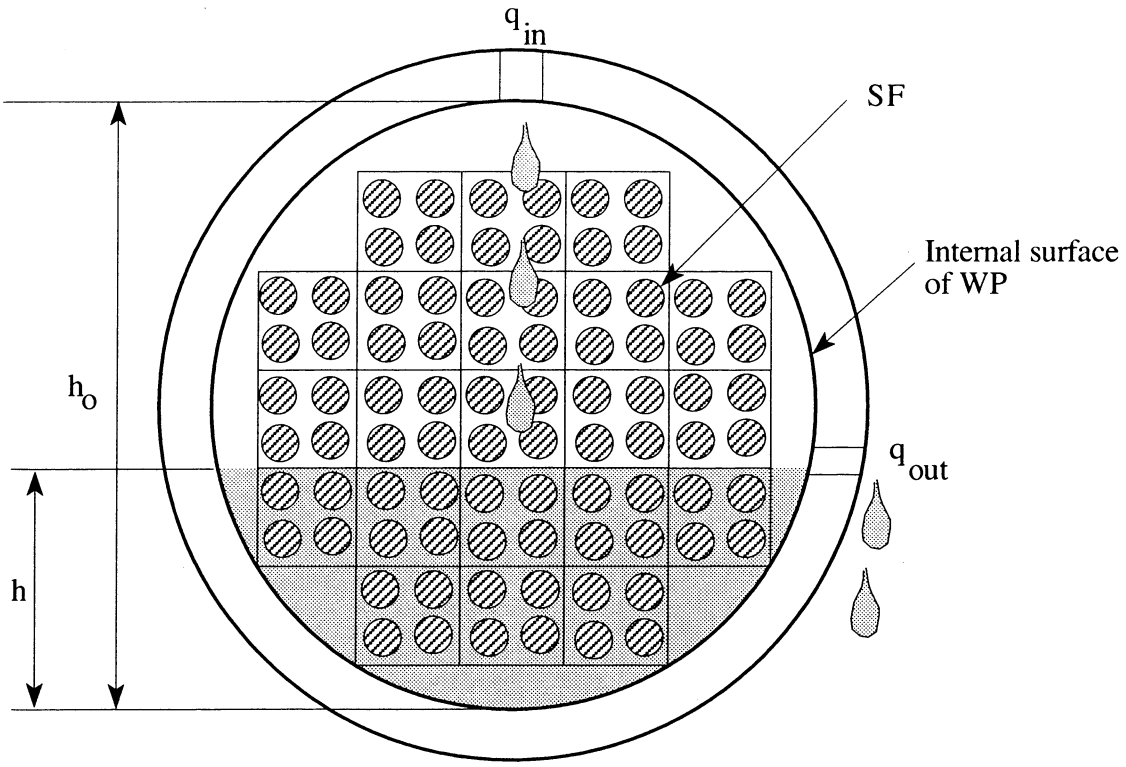


**Figure 8-1. Schematic of bathtub model with incoming and outgoing water conduits**

top of the WP.[1] In the bathtub model, all SF above this level is assumed to remain dry and does not contribute to radionuclide transfer out of the WP.

When liquid water enters the WP following its failure, the overall mass balance model for the radionuclide inventory in liquid water contacting SF in a failed WP is

$$\frac{dm_i}{dt} = w_{li}(t) - w_{ci}(t) - m_i\lambda_i + m_{i-1}\lambda_{i-1} \tag{8-1}$$

where

$m_i$ — amount of radionuclide, $i$, in the WP water at time, $t$ [mol]

[1]The bathtub height varies from subarea to subarea for corrosion, initially defective, and seismic failures. For faulting and volcanic failures, the bathtub height is specified for the whole repository.

$w_{1i}$ — rate of transfer from the SF into the resident water in the WP because of or through leaching of the SF [mol/yr]

$w_{ci}$ — rate of advective transfer out of the WP [mol/yr]

$\lambda_i$ — decay constant of radionuclide, [1/yr]

$m_{i-1}$ — amount of the parent at time, $t$ [mol]

$\lambda_{i-1}$ — decay constant of the parent [1/yr]

The product, $m_i\lambda_i$, is the amount lost due to decay, and $m_{i-1}\lambda_{i-1}$ represents the amount generated by the decay of the parent radionuclide.

### 8.3.2 Advective Mass Transfer

The advective mass transfer out of the WP, $w_{ci}$, can be represented by (Wescott et al., 1995)

$$w_{ci}(t) = C_i(t)q_{\text{out}}(t) \tag{8-2}$$

where

$C_i$ — concentration of radionuclide, $i$, in the WP water [mol/m$^3$]

$q_{\text{out}}$ — water leaving the WP at time, $t$ [m$^3$/yr]

The concentration, $C_i$, is determined by dividing the mass of element $i$, $m_i$, by the volume, $V$ of water in the WP. For the bathtub model, $q_{\text{out}}$ is zero if the volume of water in the WP has not exceeded the WP volume below the exit hole, $V_{\text{max}}$, or is equal to the input flow rate, $q_{\text{in}}$, if the volume of water exceeds $V_{\text{max}}$. The volume of water, $V$ in the WP is determined by integrating the flow rate, $q_{\text{in}}$, with respect to time until it reaches $V_{\text{max}}$, where

$$V = \int_0^t q_{\text{in}}(\tau)d\tau \tag{8-3}$$

For the flow-through model, the flow out of a WP is equal to the flow in for all times. Calculation of the flow in, $q_{\text{in}}$, is described later in this section.

For stability and efficiency in the numerical integration algorithm, $V$ may not be smaller than $V_{\text{min}}$, a quantity used to accelerate convergence of the integration routine, which is defined as

$$V_{\text{min}} = aq_{\text{max}} \tag{8-4}$$

where

$q_{max}$ — maximum flow rate into the WP [$m^3$/yr]
$a$ — constant currently set at 5 yr

In the bathtub model, the fraction of fuel wetted is proportional to the water level. There is no release from the WP until the actual water level exceeds the maximum water level. The flow-through model is implemented by specifying the fraction of the SF wetted and selecting the flow-through option in the *tpa.inp* file. Because water does not have to fill to a certain level inside the WP, release of radionuclides occurs as soon as water enters the WP. The exit hole height parameter [SFWettedFraction] of the bathtub model is used indirectly to specify the fraction of SF wetted in the flow-through model.

Advective mass transfer is considered to occur from the inside to the outside of the WP instantaneously through a nonmechanistic connection to the outside surface of the WP with the EBS-host rock interface, as shown in figure 8-2.

### 8.3.3 Waste Package Inventory

The inventory in the failed WP is calculated by a material balance, Eq. (8-1), accounting for depletion caused by decay, generation of radioactive progeny, and mass depletion from diffusive and advective releases. For the case in which no mass leaves the WP, Eq. (8-1) reduces to

$$\frac{dm_i}{dt} = -m_i\lambda_i + m_{i-1}\lambda_{i-1} \tag{8-5}$$

$$m_i\big|_{t-0} = m_{i0} \tag{8-6}$$

These differential equations are solved to determine the remaining solid mass of the radionuclides in a chain at a given time, $t$. The analytical solution (Bateman, 1910) to this initial value problem is given by

$$N_{ij} = N_{i0}\prod_{k=1}^{j-1}\lambda_k \sum_{L=1}^{j}\frac{e^{-\lambda_L t}}{\prod_{\substack{m=i \\ m\neq L}}^{j}(\lambda_m - \lambda_L)} \tag{8-7}$$

where

$N_{ij}$ — contribution from the $i^{th}$ chain member to the $j^{th}$ chain member [mol]
$N_{i0}$ — initial mass of $i^{th}$ member of chain [mol]
$\lambda_j$ — decay coefficient of $j^{th}$ member of the chain [1/yr]

The total amount of the $j^{th}$ chain member at any time is

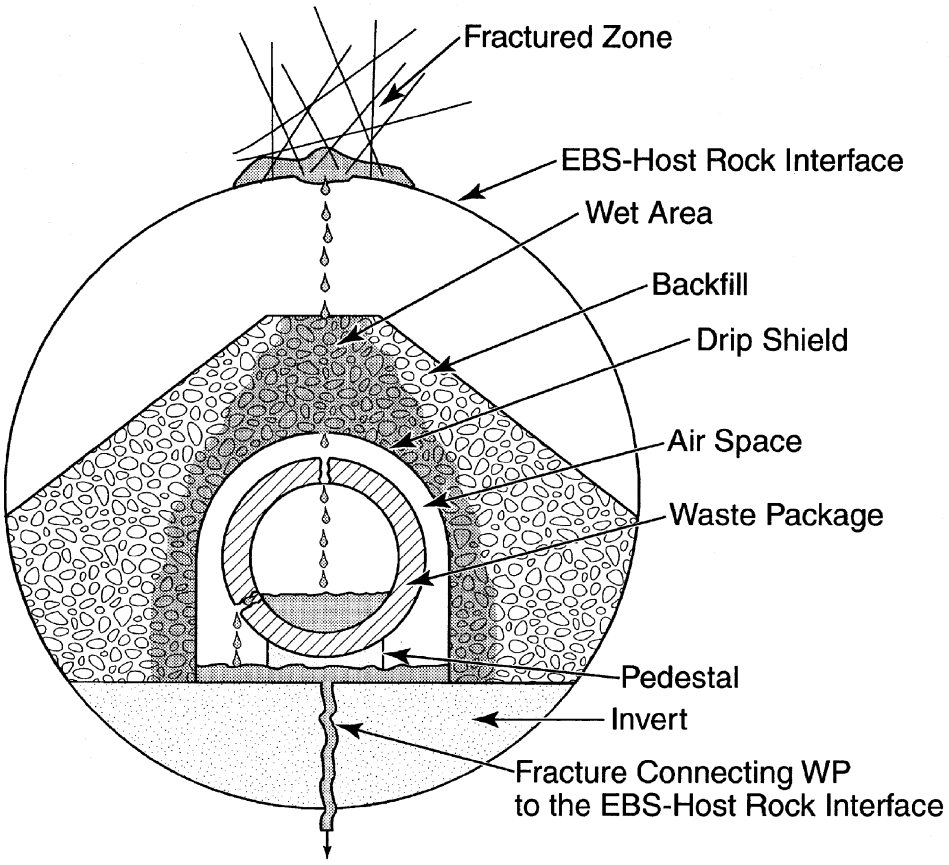


**Figure 8-2. Schematic drawing for advective mass transfer from the waste package to the host rock**

$$N_j = \sum_{i=1}^{j} N_{ij} \tag{8-8}$$

In the previous equations, $m_i = N_i$ except that $N_i$ is used to represent radionuclide mass under conditions of zero mass transport from the container.

## 8.3.4 Spent Fuel Dissolution Rate

The rate of radionuclide transfer from the SF into water in the WP [ $w_{1i}$ in Eq. (8-1)] is a function of the flow rate of water, the composition of water in which the SF is in contact, and the element solubility in that water. Fission and activation product radionuclides normally have high solubility limits that do not limit the release of these radionuclides from a WP. These radionuclides include $^{99}$Tc, $^{129}$I, $^{135}$Cs, $^{14}$C, and $^{36}$Cl. $^{237}$Np may belong to this category also, depending on the chemistry and the flow rate of water in contact with the SF. These radionuclides are understood to be released congruently with the dissolving SF matrix for immersed fuel. Gray and Wilson (1995) determined the intrinsic dissolution rate of the SF matrix

from flow-through tests. The flow-through tests use artificially high flow rates to eliminate the precipitation of secondary phases on the SF surface. Secondary phases may modify the intrinsic dissolution rate of the SF matrix by altering the area of the reactive surface or may otherwise affect radionuclide release by secondary solubility limits and coprecipitation.

The dissolution rate in solutions containing carbonate anions (model 1), which are representative of altered groundwaters present in the near field, was expressed by Gray and Wilson (1995) as

$$\log r = 9.310 + 0.142 \log\left[CO_3^{2-}\right] - 16.7 \log\left(p_{O_2}\right) + 0.140 \log\left[H^+\right] - \frac{2130}{T} + 6.81 \log [T] \log\left(p_{O_2}\right) \quad (8\text{-}9)$$

where

| | | |
|---|---|---|
| $r$ | — | dissolution rate [mg $m^{-2}$ $d^{-1}$] |
| $\left[CO_3^{2-}\right]$ | — | total carbonate concentration [mol/L] |
| $p_{O_2}$ | — | oxygen partial pressure [atm] |
| $\left[H^+\right]$ | — | concentration of hydrogen ions [mol/L] |
| $T$ | — | temperature [K] |

Normally, the groundwater at the YM repository site contains Si and Ca ions. In the presence of these species, the dissolution rate decreases about 100 times (Gray and Wilson, 1995). The dissolution rate in the batch tests (under immersion) is about 10 times lower than that in flow-through tests (Gray, 1992). The dissolution rate in mineral well water containing these ions can be described by (model 2)

$$r = r_0 \exp\left[-\frac{E_a}{RT}\right] \quad (8\text{-}10)$$

where

| | | |
|---|---|---|
| $E_a$ | — | activation energy [kJ/mol] |
| $r_0$ | — | preexponential coefficient [mg/$m^2$-d] |
| $R$ | — | universal gas constant [kJ/mol-K] |
| $T$ | — | WP temperature [K] |

The coefficient $r_0$ varies between 1.2 × ($10^3$–$10^6$) mg $m^{-2}$ $d^{-1}$. These values were selected to simulate dissolution rates in the range 0.01–10 mg/($m^2$d) at room temperature and in mineral waters reported in Forsyth (1997); Bruno et al. (1995); Casas et al. (1993); Gray and Wilson (1995); Gray (1992); Stroes-Gascoyne et al. (1997); Tait and Luht (1997); Wilson (1990); Garcia-Serrano et al. (1996). The activation energies were obtained from tests at 25–85 °C in J-13, and carbonate solutions. An activation energy value of 29 kJ/mol-K has been chosen from the range 20–41 kJ/mol-K (Wilson, 1990; Gray et al., 1992) for use in the TPA Version 4.0 code (see appendix A).

Model 3 is another release rate model that allows the user to specify the dissolution rate, $r$, as a fixed value for each simulation. This option is used for simulating release rates based on other models not considered explicitly, such as models based on natural analog data.

Models 1 and 2 calculate the maximum radionuclide release rate based on the alteration rate of the SF under oxidizing conditions. These conditions do not provide for other mechanisms that might keep the high release rates in check. For example, dissolution of the fuel may lead to the formation of secondary minerals like schoepite under vapor-phase conditions or uranyl silicates under dripping conditions with silica present (e.g., Buck et al., 1998; Finn et al., 1998; Wronkiewicz et al., 1992). Recent data from Argonne National Laboratory (Buck et al., 1998) show significant incorporation of neptunium and other radionuclides into schoepite under conditions favorable to vapor-phase alteration of SF.

The TPA Version 4.0 code permits use of an alternate model (model 4) that accounts for the formation of secondary minerals. Model 4 assumes that all radionuclides contained in the SF matrix, except those in the grain boundary and gap inventories, become incorporated in the secondary uranyl phase, schoepite. Radionuclides contained in schoepite are assumed to be released from this waste form at a rate proportional to the flow rate through the WP and related to the equilibrium concentration of uranium in contact with schoepite. The concentration of uranium is calculated by a speciation model for aqueous uranium species likely to exist in the WP under moist oxidizing conditions in the presence of carbonate and as a function of pH and temperature but neglecting effects of other species such as silica and calcium.

Total uranium concentration in solution is assumed to be the sum of the concentrations of five aqueous species:

$$\left[\mathrm{U(Total)}\right] = \left[\mathrm{UO_2^{2+}}\right] + \left[\mathrm{UO_2CO_3}\right] + \left[\mathrm{UO_2(OH_2)}\right] + \left[\mathrm{UO_2(CO_3)_2^{2-}}\right] + \left[\mathrm{UO_2(CO_3)_3^{4-}}\right] \quad (8\text{-}11)$$

where brackets denote molality. Each of the five aqueous species can be related chemically to schoepite (nominally $UO_3 \cdot 2H_2O$) through coupled reactions with $H^+$, $HCO_3^-$, and $H_2O$ according to the reactions and corresponding mass action relations given in table 8-1. The temperature dependence of the equilibrium constants ($K_i$ in table 8-1) is given by the Van't Hoff equation:

$$\ln K_i = \ln K_{i0} + \frac{\Delta H_i^0}{R}\left[\frac{1}{T_0} - \frac{1}{T}\right] \quad (8\text{-}12)$$

where

$K_i$ — the equilibrium constant for reaction $i$
$K_{i0}$ — equilibrium constant at the reference temperature, $T_0$
$\Delta H_i^0$ — standard molar enthalpy of reaction $i$ (which is assumed to be constant)
$T$ — absolute temperature

Values for parameters in this equation are given in table 8-2, which are taken from or derived from data reported in Grenthe et al. (1992). For calculation of the total uranium concentration according to

**Table 8-1. Reactions and mass action relations**

| Number | Reaction | Mass Action Relation |
|---|---|---|
| 0 | $UO_2(OH)_2 + 2H^+ \Leftrightarrow UO_2^{2+} 2H_2O$ | $[UO_2(OH)_2] \Leftrightarrow [UO_2^{2+}] / K_0 [H^+]^2$ |
| 1 | $UO_2CO_3 + H^+ \Leftrightarrow UO_2^{2+} 2HCO_3^-$ | $[UO_2CO_3] \Leftrightarrow [UO_2^{2+}][HCO_3^-] / K_1 [H^+]$ |
| 2 | $UO_2(CO_3)_2^{2-} + 2H^+ \Leftrightarrow UO_2^{2+} 2HCO_3^-$ | $[UO_2CO_3]_2^{2-} \Leftrightarrow [UO_2^{2+}][HCO_3^-]^2 / K_2 [H^+]^2$ |
| 3 | $UO_2(CO_3)_3^{4-} + 3H^+ \Leftrightarrow UO_2^{2+} 3HCO_3^-$ | $[UO_2CO_3]_3^{4-} \Leftrightarrow [UO_2^{2+}][HCO_3^-]^3 / K_3 [H^+]^3$ |
| 4 | $UO_3 2H_2O + 2H^+ \Leftrightarrow UO_2^{2-} 3H_2O$ | $[UO_2^{2+}] \Leftrightarrow K_4 [H^+]^2$ |

Eq. (8-11), the five mass-action relations in table 8-1 are solved using calculated values of the equilibrium constants for specified temperature, bicarbonate concentration, and pH, assuming that activities of schoepite and $H_2O$ differ negligibly from 1.0 and that ratios of activity coefficients in mass action relations are equal to 1.0. In this sensitivity study, the flux of uranium out of the system is assumed to be given by the product of the water flux and the calculated uranium concentration at equilibrium with schoepite. Fluxes of other radioelements contained in schoepite are assumed to be released according to their proportion relative to uranium in SF. Release from the gap and grain boundary inventories are discussed in the subsequent sections.

EBSREL allows the user to choose from among four release rate models: (i) Eq. (8-10); (ii) Eq. (8-11); (iii) a constant rate of release; or (iv) the schoepite equilibrium model. The $w_{1i}(t)$ term in Eq. (8-1) is calculated by multiplying the SF dissolution rates obtained from Eq. (8-10), Eq. (8-11), or the constant rate option by the SF surface area for models 1, 2, and 3. For model 4, the SF dissolution rate is calculated as the product of uranium concentration in kg $m^{-3}$ and flow rate through the WP in $m^3$ $yr^{-1}$.

For all four release rate models, a portion of the radionuclide inventory is assumed to be held loosely on the grain boundaries, cladding/fuel gap, and cladding, referred to collectively as gap inventories. These inventories are available for instantaneous release, which could be a major contributor to peak dose. The gap and grain boundary inventories for each radionuclide are specified by the user as an input parameter in the *tpa.inp* file.

### 8.3.5 Spent Fuel Surface Area

Two models for determining the SF surface area are available in the *tpa.inp* file. The first model determines surface area using fragmented pellets (i.e., particles), and the second model uses SF grain size

**Table 8-2. Parameters for the Van't Hoff equation**

| Reaction Number | $\Delta H^0$ (kJ mol$^{-1}$) | $Log_{10}K_0$ |
|---|---|---|
| 0 | -50.46 | 10.30 |
| 1 | -19.70 | 0.65 |
| 2 | -47.90 | 3.71 |
| 3 | -4.90 | 9.38 |
| 4 | -50.39 | 4.81 |

criterion. The particle model assumes that SF in a WP is fragmented into small spherical particles (~1 mm diameter), and the intergranular porosity does not contribute to the surface area. The total surface area for the particle model is then computed as

$$A_p = \left( \frac{M_{SF}}{M_p} \times 4\pi r_{po}^2 \right) f_{\text{wet}} \tag{8-13}$$

where

$M_p$ — $\frac{4}{3}\pi r_{po}^3 \rho_{go}$ (particle mass [kg])

$A_p$ — particle surface area [m$^2$]

$M_{SF}$ — SF inventory/WP [kg]

$r_{po}$ — particle radius [m]

$\rho_{go}$ — density of oxidized SF [kg m$^{-3}$]

$f_{\text{wet}}$ — volume fraction of SF immersed in the WP water

If subgranular fragmentation of the SF takes place through fuel conversion from $UO_2$ to $UO_{2.4}$ and $U_3O_8$, a smaller particle size (i.e., equivalent) can be considered in the SF particle model to represent additional exposed surface area. In the case of the second model, in which SF grains are exposed, the following expression is used to compute the total surface area:

$$A_g = 4x10^{-12}\pi \left( \frac{M_{SF}}{M_p} \right) \left[ \left( r_g - w \right)^2 + \frac{3}{r_g} \left( 3r_g^2 w - 3r_g w^2 + w^3 \right) \right] f_{\text{wet}} \tag{8-14}$$

where

$A_g$ — grain surface area [m$^2$]

$r_g$ — SF grain radius [$\mu$m]

$w$ — width of the oxidized zone [$\mu$m]

The surface area available for leaching is held constant throughout the leaching period even though the radius of the unoxidized fuel grains or particles would diminish with time. In addition, preferential attacks of grain boundaries in the fuel particles were not considered.

In deriving these equations, the effects of ionizing radiation have not been considered explicitly. These effects are complex, potentially leading to higher release rates. Factors such as the age of the waste, thickness of water films, cladding protection, and protectiveness of secondary mineral layers on the fuel would have to be considered to take ionizing radiation into account.

### 8.3.6 Cladding

SF cladding may protect the bare SF matrix from exposure to water in the WP and reduce release rates significantly. The failure mechanisms of cladding include (i) mechanical failure by external forces such as rockfalls, (ii) localized corrosion, (iii) creep, (iv) hydrogen-induced failure, (v) splitting by matrix volume expansion, and (vi) stress corrosion cracking.

It is assumed that cladding reduces the fraction of the total SF surface exposed to water entering the WP. In the TPA Version 4.0 code, the fraction of SF surface area affected by cladding protection is controlled by a factor in the *tpa.inp* file, which specifies the fraction of fuel that is unprotected by cladding, and thus does not inhibit release (CladdingCorrectionFactor = 1 indicates no cladding protection, and 0 indicates complete cladding protection and no release). Currently, cladding protection is assumed to remain constant and unaffected by additional failure mechanisms or disruptive events.

### 8.3.7 Water Dripping Abstraction

The dripping abstraction determines the quantity of liquid water, $q_{\text{in}}$, eventually entering the WP. It is assumed that there is a net downward percolation of meteoric water at the site after thermal reflux and that water will flow in fractures within the emplacement unit.

The dripping abstraction is represented by sampled distributions rather than a model embedded in the code. This approach is computationally efficient and is more easily and transparently factored into sensitivity analysis than an embedded model. Furthermore, this approach allows incorporation of alternative conceptual flow models such as structural control of wetting along faults or fracture zones without requiring code changes.

The WP infiltration flow rate is

$$q_{\text{in}} = qF_{\text{ow}}\ F_{\text{mult}} \tag{8-15}$$

where

$q$ — groundwater flow rate at the repository horizon after thermal reflux of water from deep percolation and reflux [$m^3$/yr]

$F_{ow}$ — factor to account for large-scale focusing/diversion

$F_{mult}$ — factor to account for near- and in-drift flow diversion

When the factor, $F_{ow}$, is multiplied by the groundwater flux, $q$, and the plan area of the WP, the resulting product defines the flow rate that potentially reaches a wetted WP. $F_{ow}$ represents focusing of flow when it is assigned a value greater than one and diverging of flow when less than one. $F_{ow}$ is correlated with another factor, $F_{wet}$, which is the fraction of a WP receiving a dripping flux greater than zero. This approach assumes the number of WPs wetted is invariant in a given run and does not take into consideration that dripping locations may change with time. The dripping of water on the WP is delayed (i.e., $q_{in} = 0$) until after the failure of the drip shield. The time of drip shield failure is a sampled parameter specified in the *tpa.inp* file (DripShieldFailureTime[yr]).

The flow diversion factor, $F_{mult}$, which ranges from 0 to 1, is defined as the fraction of potentially dripping water that will enter the WP and contribute to the release and transport of radionuclides. Only a fraction of the water intercepting the drifts is expected to come into direct contact with the WPs. Only a portion of the water dripping onto the WPs is expected to get inside where it can interact with the waste form. The effect of the size of the through-going hole on the drip shield controls the amount of water entering the WP, which is factored into the calculation while deriving the $F_{mult}$ factor presented in appendix F. Elements considered in $F_{mult}$ include

- The reduction in flow to a WP because water is diverted around a drift is based on the presence of a capillary barrier. Water flow into the drift will face a capillary barrier if the fractures are small enough and the fracture network has adequate connectivity. Water cannot easily move across the capillary barrier and can be diverted in the fracture around the drift opening.

- Water flow crossing the capillary barrier into the drift can drip from the ceiling or from protuberances along the drift. Some of the water, however, is likely to be diverted as sheet flow along the drift walls rather than drip from the ceiling onto the containers. The closer to the crest of the tunnel, the greater the propensity to drip. Away from the crest, the slope of the tunnel walls would divert water to sheet flow along the walls.

- With the drip shield as an added barrier to flow, water dripping from the ceiling would have to fall onto the drip shield and the WP in such a way that it could enter the co-axial, open holes. If a drop of water is directly in the path of co-axial open holes (e.g., such as those resulting from corrosion by dripping water), then this condition would be fulfilled.

- A few drops could enter a corrosion hole but may be unable to enter the canister because of the presence of corrosion products. These corrosion products may be flaky, porous, or gel-like, and their densities will be considerably less than the alloy itself. Without a high rate of water flux, there will be no mechanism to remove them from the location where they form. If the corrosion products remain in place, then water dripping into the corrosion hole would have difficulty entering the canister and would simply flow off. Holes at the crest will have a higher probability that water would enter because there would be a smaller

propensity for water to flow off. Holes on the side will have higher probability that the water would flow off rather than enter.

A more detailed explanation of the derivation of $F_{mult}$ and $F_{ow}$ (and appropriate values for them) is contained in appendix F.

### 8.3.8 Computational Approach

The first step in the calculation is to determine when a liquid release starts. The release calculation includes the computation of the radionuclide inventory in the solid mass, radionuclide releases from the solid mass into the liquid surrounding the waste form, the generation of the new radionuclide inventory in the liquid because of radioactive ingrowth, advective release of mass from water leaving the WP, and diffusive losses into the medium surrounding the WP.

At each time step, the inventory of the elements is computed as the sum of the mass of all the isotopes of that element. At any given time, the concentration of an element in the WP water is calculated by dividing the element inventory by the volume of water in the WP. If the concentration of that element in the WP water exceeds its solubility limit, then the calculated concentration value is discarded and the solubility limit is assigned to the concentration of the element. Release of an individual nuclide occurs at a rate proportional to the mass fraction of all the isotopes of the element.

The number of WPs undergoing initially defective failure is read from the *tpa.inp* file, while the number of WPs actually being considered for faulting, IA, and seismic failure are determined in the consequence modules. The times of initially defective, faulting, IA, and seismic failure are specified in the *tpa.inp* file, whereas the time of corrosion failure is calculated in EBSFAIL. If the corrosion failure occurs before the faulting, IA, or seismic failure, then the number of WP undergoing faulting, IA, or seismic failure is reset to zero. If the corrosion failure occurs after the faulting, IA, or seismic failure, then calculations of release from the faulting, IA, or seismic failure are performed.

Liquid release of contaminants arises only from the wetted fraction of the SF in a WP. Radionuclides are released from the waste form at a rate proportional to the dissolution rate of the fuel (congruent release), into the volume of water present in the WP. Release of radionuclides from the WP by advection and diffusion may be limited subsequently by the elemental solubility of the radionuclides in the WP water.

At the end of this calculation, the cumulative release is recorded for each nuclide. After advancing the time, the calculation is repeated for the next time step. The calculation continues until all radionuclides are depleted from the solid SF and the water in the WP or the end of the simulation is reached, whichever occurs first. Release calculations focus on release from a single WP for each WP failure category; thus, to obtain the total release in the final calculations, the release from one WP is multiplied by the total number of wetted WPs for each failure category in a subarea.

### 8.3.9 EBSFILT Model for Transport of Radionuclides through the Invert

EBSFILT (EBS FILTer) works in conjunction with the EBSREL module to simulate transport by advection and diffusion of radionuclides in the near field, especially through the invert and backfill.

EBSFILT takes the output of the EBSREL code and passes it through a filter, or transfer function, derived from an analytical model of advection and diffusion in 1D steady flow.

Releases from the WP will travel through the invert before entering the tunnel wall. Current design shows the WP on steel supports over a porous invert made of steel with sand or gravel ballast (see table 1-1). Water running off or passing through the WP would fall onto the invert. The invert material could sorb some of the radionuclide species, thereby providing an additional barrier to their release into the geosphere proper.

If flow of groundwater through the invert can be considered to be at steady state and the material properties of the invert constant and uniform, then the transport flux of a single nuclide by advection and molecular diffusion at the end of the invert from an instantaneous impulse release of one unit at $t = 0$ at the top would be

$$F(t) = \frac{x + ut / R_d}{4\sqrt{D\pi t^3 / R_d}} \exp\left[ -\frac{\left(x - ut / R_d\right)^2}{4Dt / R_d} - \lambda t \right] \tag{8-16}$$

where

| | | |
|---|---|---|
| $F(t)$ | — | transfer function [$yr^{-1}$] |
| $x$ | — | distance of flow through the invert [m] |
| $u$ | — | pore velocity of water through invert [m/yr] |
| $t$ | — | time [yr] |
| $R_d$ | — | retardation coefficient [unitless] |
| $D$ | — | diffusion coefficient [$m^2$/yr] |
| $\lambda$ | — | decay coefficient [$yr^{-1}$] |

For an arbitrary release of radionuclides at the top of the invert, Eq. (8-16) can be generalized using convolution:

$$W(t) = \int_0^t f(\tau) F(t - \tau) d\tau \tag{8-17}$$

where $W$ is the release rate at the bottom of the invert [Ci/yr] and $f$ is the release rate from the WP [Ci/yr]. For each value of time, $t$, Eq. (8-17) is integrated using Simpson's rule. For maximum efficiency and precision, the integration range is narrowed to take advantage of the kernel being close to zero over much of the range.

EBSFILT is invoked in the TPA Version 4.0 code by specifying the parameter InvertBypass(0=ebsfilt,1=bypass_ebsfilt) in the *tpa.inp* file equal to 0. Parameters that must be specified in the *tpa.inp* file are InvertRockPorosity, InvertThickness[m], InvertMatrixPermeability[m^2], and the

retardation coefficients of the invert material (e.g., RD_Invert_Cm). The pore velocity through the invert material, $u$, is calculated from the average water flux, $Q_i$, divided by the porosity. At present, $Q_i$ is defined as the flux of infiltrating water per WP averaged over the time period of interest chosen for the run (e.g., 10,000 yr) divided by the plan area of the WP. The code has the provision that, if $Q_i$ exceeds the hydraulic conductivity of the invert material, the invert model will become a simple pass-through with no holdup or retardation. Under the current design, with a porous medium invert, this bypass is unlikely.

## 8.4 ASSUMPTIONS AND CONSERVATISM OF THE EBSREL APPROACH

EBSREL is an abstraction of the processes that will take place in a failed waste container. The main processes that control releases of radionuclides from the SF to the boundary with the geosphere are (i) protection of the SF by cladding, (ii) degradation of the SF by air and water vapor, (iii) contact of the SF by liquid water, (iv) mobilization of radionuclides from the SF to the liquid water, (v) transport of dissolved or otherwise mobilized (colloids) radionuclides in the water to the outside of the WP, and (vi) transport of dissolved radionuclides in the water through the invert material to the outside of the EBS.

There is no mechanistic model for cladding protection. Instead, cladding protection is specified as a factor between zero and one, representing the fraction of the surface area of the fuel exposed to dissolution. In most cases, it is conservatively assumed that no cladding protection exists. Some runs have considered substantial protection by cladding with only 0.5 percent of the available surface area of the fuel exposed. These values were derived empirically from laboratory leaching studies with deliberately failed fuel-rod samples (Wilson, 1990).

EBSREL does not consider degradation of fuel by air and water vapor explicitly. There are no mechanistic models of degradation by air and water vapor in the model. The SF is assumed to be in a degraded state upon contact with liquid water. It is assumed there can be no transport of radionuclides from the SF until liquid water contacts the fuel. This is a conservative yet reasonable approach, because it is expected that most exposed fuel will degrade in the period between exposure to air and liquid water contact.

The contact of exposed fuel by liquid water is assumed to be controlled by either the bathtub or the flow-through model. In the bathtub model, the fraction of fuel exposed is presumed to be controlled by the water height in the container. In the flow-through model, contact is independent of the water level. It seems clear that if water were to pool in the container, the submerged fuel would be in contact with liquid water. Aside from submersion, contact of fuel with liquid water would be controlled by complex and ill-defined processes occurring inside the container, such as dripping, water films on the fuel controlled by surface tension, evaporation, and thermal reflux.

The fraction of fuel contacted may or may not be important, depending if the radionuclides contributing most to the dose are limited by solubility. If solubility controls the release, the fraction of fuel contacted is unimportant and the flow rate of water in contact with the fuel is important. Conversely, if solubility is not the limiting factor, the fraction of fuel exposed to liquid water is important.

The amount of water that a WP can contain (i.e., bathtub height) is uniquely assigned to each failure type (in some cases, for each subarea) and is treated as a sampled parameter. EBSREL assumes the nature of the openings for water to enter the WP are the same for all failure types and subareas. This implies that if the corrosion failure results in a pinhole, then other failures will also result in pinholes for water entry.

Thus the flow diversion factor, as specified by $F_{mult}$, is the same for all failure types. This could be nonconservative for some failure types, such as from seismicity or faulting.

Released radionuclides are assumed to be transported by advection to the geosphere by water leaving the WP except when the option for flow through the invert is turned on, in which case both advective and diffusive transport takes place. There is no accounting for the possibility that radionuclides in the water might be captured along the liquid-water pathway by precipitation or sorption on material inside the WP. If backfill is considered part of the EBSREL model, sorption of radionuclides from the flowing water might offer a significant reduction in releases. Molecular diffusion through backfill or rock is considered a minor factor and may be eliminated in future versions of the TPA code.

There are specific assumptions and conservatism related to the EBSREL module:

- Liquid release calculations focus on release from a representative WP in each subarea. It is assumed that the release environment within the subarea is not affected by the location or the geometric configuration of other WPs. Therefore, to obtain the total release in the final calculations, the release from a representative WP is multiplied by the number of WPs for each applicable WP failure category in the subarea.

- EBSREL considers only radionuclide releases from SF; no consideration is given to radionuclide releases from vitrified waste or the DOE SF.

- Colloidal transport is not explicitly considered, which could be nonconservative.

- The surface area of SF exposed to water during the leaching process is constant even if shrinking of particles takes place with time. Preferential attacks of grain boundaries have not been considered.

- For the bathtub model, all fuel below the water level is assumed to come in contact with water uniformly.

- No new pits are formed with time that would alter the volume of the bathtub. Once the water reaches the level of the exit hole, it can leave the WP unimpeded.

- There is no radionuclide release from SF above the water level, which could be nonconservative.

- The change in water chemistry in the WP caused by corrosion of container material is not explicitly considered, but can be taken into account by adjusting the parameters of the leaching rate equation.

- Gaseous release occurs only from dry SF, but is not used in dose calculations because gaseous contributions to dose are negligible.

- The congruent release mode is considered for SF leaching with the exception of model 4 in which radionuclide release is tied to the dissolution of schoepite and not to the SF matrix.

- In *ebsfilt.f*, the transfer function model requires the pore velocity, $u$, to be steady. The model cannot accommodate a time-varying flow rate because transfer functions must be time-invariant. Although a numerical integration solution such as finite difference or finite element could accommodate time-varying properties, the increased complexity and execution times accompanying these approaches were not considered justifiable at this time.

- The transfer function model, as presented in *ebsfilt.f*, is for a single radionuclide and does not accommodate chain decay. There are some other close-form and Laplace transform domain solutions available for chain decay, but they are more complicated. The approach is nonconservative because ingrowth is negligible; however, it is believed that most of the radionuclides important to dose (e.g., $^{129}I$, $^{99}Tc$, and $^{237}Np$) will not be significantly affected by this simplification.

# 9 UZFT MODULE DESCRIPTION

The UZFT module determines the release rate of radionuclides into the SZ below the repository footprint by simulating the transport of radionuclides in the UZ between the repository and the water table taking into account fracture versus matrix flow and retardation because of adsorption and ion exchange.

## 9.1 INFORMATION FLOW WITHIN TPA

### 9.1.1 Information Supplied to UZFT

EXEC passes to UZFT the time-varying release rates computed in EBSREL of all groundwater pathway nuclides and the time history of the volumetric flow rate from UZFLOW into the subarea. Other inputs to UZFT, such as hydrologic properties of stratigraphic units and retardation coefficients, are specified in the UZFT section of the *tpa.inp* file.

### 9.1.2 Information Provided by UZFT

UZFT outputs for the time-varying groundwater release rates of all groundwater pathway nuclides as a function of time from the UZ are passed back to EXEC along with the groundwater travel time (GWTT) for the UZ. Although GWTT values are used only for reporting purposes, the release rate histories are provided as input to SZFT.

## 9.2 INTERMEDIATE RESULTS

The UZFT intermediate outputs provide information on the flow field and the overall transport of radionuclides. An averaged UZ GWTT (averaged over time) is computed for each repository subarea and accessed in the *gwttuzsz.res* output file. The cumulative release of radionuclides from the UZ (summed over all repository subareas and the simulation period) for each radionuclide is available in the *cumrel.res* and *cumrel_c.res* files. The *gwttuzsz.res*, *cumrel.res*, and *cumrel_c.res* files are described in detail in tables 20-1 and 20-2.

When the append option is turned on in the *tpa.inp* file to create additional intermediate outputs, UZFT inputs and outputs are written to the *uzft.ech*, *uzft.rlt*, and *nefiiuz.cum* files. The deep percolation from UZFLOW and the EBS releases from EBSREL for all times are included in the *uzft.ech* file. The time history of UZ releases for all groundwater radionuclides is provided in the *uzft.rlt* file. The output from the stand-alone code *nefmks.f* for all subareas and realizations is available in the *nefiiuz.cum* file. A complete description of these files is provided in section 20.3.

The UZFT module generates intermediate input and output data transfer files while executing the *nefmks.f* stand-alone code. These files contain information only for the final realization and subarea available at the end of the TPA Version 4.0 code execution. UZFT intermediate input data transfer files are *nefiiuz.inp*, *nefiiuz.vel*, and *nefiiuz.src*. All UZFT parameters specified in the *tpa.inp* file are accessed through the *nefiiuz.inp* file. The file *nefiiuz.vel* contains the groundwater flow velocity for each *nefmks.f* transport leg. The EBS release rates from EBSREL are available in the *nefiiuz.src* file. Intermediate output data transfer files from UZFT include *nefiiuz.dis* and *nefiiuz.out*. The UZ release rates for all groundwater

radionuclides can be accessed in the *nefiiuz.dis* file. The file *nefiiuz.out* provides the *nefmks.f* output file. Contents of all UZFT intermediate data transfer files are further described in appendix E.

## 9.3 CONCEPTUAL MODEL

The UZFT module provides the temporal and spatial variation of deep percolation and radionuclide transport from the repository horizon to the water table. UZFT uses the stand-alone code NEFTRAN II (Olague et al., 1991) to track contaminant transport through the UZ below the repository.

UZ flow and RT are complicated by geologic heterogeneities, at a variety of spatial scales, in the hydrologic and geochemical properties of the fractures and matrix and in temporal variation in deep percolation. Although these complications affect accurate predictions at the small scale (on the order of meters), the emphasis is on estimating performance of the overall behavior of the repository. Therefore, an approach is used that considers flow and transport at a larger scale which is on the order of tens to hundreds of meters. The effect of large-scale heterogeneities is included only to the extent that different stratigraphic layers are uniquely identified via thickness and unique hydrologic and transport properties that vary among the ten modeled subareas. Although the approach neglects the spatial and temporal heterogeneities at smaller scales, it is assumed to be appropriate owing to the conservativeness in the conceptual modeled. The UZFT module captures a sufficient level of detail in the properties of the UZ such that performance calculations will provide insight on how variations in hydrologic and geochemical properties of the UZ affect overall performance.

### 9.3.1 Unsaturated Zone Flow Model

UZ flow is the primary mechanism for transporting dissolved radionuclides from the repository to the water table below the repository. Fracture versus matrix flow, groundwater velocity, and moisture content are the characteristics of the UZ flow used in UZFT. Spatial and temporal variability of these characteristics are considered using a simplified approach: spatial variability is accounted for by using 10 repository subareas where each subarea has a distinct stratigraphy and deep percolation, and each stratigraphic unit has its own hydrologic and geochemical properties (see table 9-1 for stratigraphic thicknesses for each of the ten repository subareas), and temporal variation is accounted for by using the time-varying deep percolation determined in UZFLOW. This simplified approach assumes there is no lateral diversion between the repository and the water table (i.e., flow is 1D and vertical), the UZ flow field is in equilibrium (i.e., time variations in the flow field occur rapidly in the UZ), and thermal perturbations on UZ flow do not affect the deep percolation below the repository (the waste containers are considered to be mostly intact at early times when this assumption is most in question).

The hydrostratigraphic layer thicknesses (table 9-1) used in the UZFT module are derived from the Geologic Framework Model 3.1 [Civilian Radioactive Waste Management System, Management and Operating Contractor, (1999) (Integrated Site Model Process Model Report)] by aggregating thicknesses of thermal-mechanical stratigraphic layers of similar hydrologic properties. The thicknesses are taken from a representative location (i.e., center) in each subarea. Conversions are made from the UTM NAD27 (m) projection used for the subarea outlines in TPA Version 4.0 code to the State Plane NAD27 (ft) projection used by the Geologic Framework Model 3.1. Calico Hills nonwelded vitric and nonwelded zeolitic thicknesses are estimated from the interpolation of thicknesses from borehole interpretations that consider zeolite percent and degree of welding (Winterle et al., 1999a,b). There are uncertainties in vitric thickness variations across the repository footprint. Estimates of minimum vitric thicknesses (minimum of all

**Table 9-1. Hydrostratigraphic thicknesses (m) for each of the 10 repository subareas extending from the repository horizon to the water table**

| Subareas | 1 | 2 | 3 | 4 | 5 | 6 | 7 | 8 | 9 | 10 |
|---|---|---|---|---|---|---|---|---|---|---|
| Topopah Springs, welded | 100 | 161 | 79 | 144 | 58 | 85 | 138 | 163 | 91 | 138 |
| Calico Hills, vitric | 19 | 2 | 24 | 17 | 31 | 37 | 44 | 0 | 10 | 0 |
| Calico Hills, zeolitic | 72 | 108 | 55 | 88 | 49 | 58 | 63 | 120 | 128 | 137 |
| Prow Pass, welded | 50 | 50 | 52 | 56 | 65 | 66 | 66 | 25 | 28 | 0 |
| Upper Crater Flat | 57 | 18 | 68 | 61 | 71 | 81 | 67 | 0 | 9 | 0 |
| Bullfrog, welded | 22 | 0 | 81 | 0 | 101 | 51 | 0 | 0 | 0 | 0 |
| TOTAL | 320 | 339 | 359 | 366 | 375 | 379 | 377 | 308 | 267 | 275 |

interpolated values within a subarea) are provided in table 9-1; these estimates are considered reasonably conservative with regard to dose estimates. Provision also exists in the TPA code to sample these parameters. The upper and lower boundaries of UZ transport are the drift elevations and the water table. EDA II lays out drifts horizontally in the east-west direction but sloping downward to the north 75 m; this slope is incorporated in the estimation of the thicknesses of the Topopah Springs welded layer. Based on borehole data (Farrell et al., 1999), the water table elevation varies across the drift footprint by at least 45 m. The southeasterly slope of the water table is taken into account for the calculation of the bottom layer thicknesses.

Determination of fracture versus matrix flow is considered the most important aspect of the UZ flow model because water velocity in fractures tends to be large relative to velocity in the matrix because of differences in porosity (generally one to two orders of magnitude) and retardation of radionuclides within fractures is generally considered to be much smaller than retardation in the matrix because of the much larger surface area available for sorption in the matrix compared to the fracture. For each stratigraphic unit in the UZ, a determination is made in the UZFT module if fracture or matrix flow properties will be used by comparing the deep percolation with the saturated hydraulic conductivity of the matrix. Fracture flow properties are used for transporting radionuclides when the deep percolation exceeds the saturated hydraulic conductivity of the matrix. This conceptualization assumes that the flow conditions (fracture versus matrix flow) remain the same within a particular stratigraphic unit and that any transition between matrix and fracture flow occurs only at the interface between stratigraphic units. Thus, each stratigraphic sequence has its own associated velocity and saturation characteristic of either the fracture or the matrix continuum.

Calculation of the water velocity and moisture content uses the van Genuchten (1980) characteristic curve to represent the relationship between saturation and hydraulic conductivity:

$$K_r = \sqrt{S}\left[1-\left(1-S^{1/\lambda}\right)^{\lambda}\right]^2 \tag{9-1}$$

where

$K_r$ — relative hydraulic conductivity [unitless]

$S$ — saturation [unitless]

$\lambda = 1 - \frac{1}{\beta}$

$\beta$ — fitting parameter [unitless] specified in the *tpa.inp* file.

The velocity and saturation calculation assumes that deep percolation is occurring in either the matrix or the fracture, but not both. This approach represents a simplification of the approach used in the NRC IPA Phase 2 effort (Wescott et al., 1995), which accounted for the partitioning of fracture and matrix flow. The simplification was done to improve efficiency in the UZ flow and transport module to accommodate other improvements considered more important (e.g., time-varying deep percolation and simulation periods beyond 10,000 yr). Additionally, the partitioning of fracture and matrix flow is not considered as important to performance given the higher estimates for deep percolation (stratigraphic units will be either primarily fracture flow or matrix flow).

As mentioned previously, time-varying deep percolation is determined in UZFLOW. A time-varying velocity is calculated for each stratigraphic unit from the time-varying deep percolation using

$$v(t) = \frac{Q(t)}{AnS} \tag{9-2}$$

where

$v(t)$ — time-varying velocity for the stratigraphic unit [m/yr]

$Q(t)$ — time-varying deep percolation rate [$m^3$/yr]

$n$ — porosity of the stratigraphic unit corresponding to either the matrix porosity or the fracture porosity [unitless]

$S$ — saturation of the stratigraphic unit corresponding to either the matrix saturation or the fracture saturation [unitless]

$A$ — cross-sectional area of subarea [$m^2$]

To aid in the computational efficiency of the NEFTRAN II code, the velocities are artificially limited to an upper bound corresponding to a 5-yr residence time for a given stratigraphic unit. This restriction should not have a significant effect on the dose calculation.

From the time-varying velocities, the time-varying residence times are determined for each stratigraphic unit using:

$$t_I(t) = \frac{x}{v(t)} \tag{9-3}$$

where

| | | |
|---|---|---|
| $t_t(t)$ | — | time-varying residence time [yr] |
| $x$ | — | thickness of the stratigraphic unit [m] |
| $v(t)$ | — | time-varying velocity for the stratigraphic unit [m/yr] |

The mean residence time, $T_T$, for each stratigraphic unit is determined as a weighted average of the time-varying residence times over the time period of interest. A simple trapezoidal integration of the residence time is used for the calculation. In addition, the sum of the mean residence time for each stratigraphic unit is summed to obtain the total residence time for the UZ (i.e., $\Sigma\ T_T$). The mean residence time of a stratigraphic unit is used to select which stratigraphic units satisfy a set of criteria that maintains the computational efficiency of the NEFTRAN II code. That is, stratigraphic units where $\Sigma\ T_T$ is less than 10 yr or that have a $T_T$ less than $\Sigma\ T_T/10$ are removed from consideration for the transport of radionuclides. These criteria should not have a significant effect on the dose calculation.

The time-varying velocities for each contributing stratigraphic unit are output to file *nefii.vel* for input to NEFTRAN II. The UZ residence time, $\Sigma\ T_T$, for each subarea is written to the file *gwttuzsz.res* as an intermediate result. The content of this file is described further in chapter 20.

### 9.3.2 Unsaturated Transport

Transport of radionuclides in geologic media is often retarded relative to the water velocity because of geochemical reactions (e.g., adsorption and ion exchange) between the dissolved radionuclides and the geologic materials. Retardation factors (ratio of the water velocity to the velocity of a dissolved radionuclide) are determined for the matrix using the following distribution coefficient or $K_d$ approach:

$$R_f = 1.0 + \frac{\rho(1-n)}{\theta} K_d \tag{9-4}$$

where

| | | |
|---|---|---|
| $R_f$ | — | retardation factor [unitless] |
| $\rho$ | — | grain density of porous matrix [kg/m$^3$] |
| $n$ | — | porosity of matrix [unitless] |
| $\theta$ | — | moisture content of matrix [unitless] |
| $K_d$ | — | distribution coefficient (radionuclide and stratigraphic unit specific) [m$^3$/kg] |

Retardation within fractures in the UZ is considered constrained by the limited surface area available for ion exchange and adsorption. Therefore, the $K_d$ approach noted previously was not considered appropriate for fracture flow and a retardation factor is used to characterize retardation in fractures in the *tpa.inp* file. The use of a retardation factor for fracture transport was included in UZFT for completeness in the event that sufficient evidence becomes available that supports retardation of radionuclides within fractures. It is expected, however, the retardation factor would typically be set for no retardation (value of 1.0).

**NEFTRAN II**

NEFTRAN II (Olague et al., 1991) uses the following three files: (i) the standard NEFTRAN II input file that specifies the radionuclides, transport path lengths, and transport path properties (*nefii.inp* file); (ii) the time history of the transport velocity developed in UZFT using hydrologic parameters specified in the *tpa.inp* file and time history of deep percolation determined in UZFLOW (*nefii.vel* file); and (iii) the time history of radionuclide releases from the repository provided by EBSREL (*sotnef.dat* file). NEFTRAN II uses a series of 1D transport paths or legs (each representing a particular stratigraphic unit) that are defined by their length, velocity, saturation, porosity, dispersion length, and retardation. (Note: matrix diffusion is a process contained in the NEFTRAN II program, however, this process was not included in the UZ transport because of the uncertainty in assigning parameter values that determine the magnitude of its effect.) As described in the previous sections, UZFT calculates velocity, saturation, and retardation factors. NEFTRAN II uses this information as well as input parameters (porosity and dispersion length) to simulate advection and hydrodynamic dispersion of dissolved radionuclides using a distributed velocity method (DVM). DVM is similar to a particular tracking approach where discrete particles are used to simulate contaminant movement; however, DVM calculates a distribution of velocities for each radionuclide and each leg, based on the mean velocity and the dispersion length, and uses the velocity distribution to transport groups or packets of particles. The formulation used in calculating the velocity distribution is

$$v_j = \varepsilon_j \sqrt{\frac{2dv_m}{t R_f}} + \frac{v_m}{R_f} \tag{9-5}$$

where

| | | |
|---|---|---|
| $v_j$ | — | $j^{th}$ interval of the velocity distribution (seven intervals are used to represent the distribution) [m/yr] |
| $\varepsilon_j$ | — | $j^{th}$ abscissa from a standard normal distribution [unitless] |
| $d$ | — | dispersion length [m] |
| $v_m$ | — | mean velocity (velocity calculated in UZFT and used as input to NEFTRAN II is assumed to be the mean velocity) [m/yr] |
| $R_f$ | — | retardation factor [unitless] |
| $t$ | — | time to exit the leg[1] [yr] |

Figure 9-1 illustrates the implementation of the 1D legs or transport paths in NEFTRAN II to represent the UZs and SZs at YM. The UZFT module provides the radionuclide releases to the water table at discrete times. This information is then used by the SZFT module for the SZ transport calculation.

[1]The use of the exit time is a departure from the original NEFTRAN II formula that used the value for the time step. When used in conjunction with time-varying velocity field, the time step approach led to unrealistic velocity distributions—the mean velocity was small, the time step was small, and a velocity distribution was dependent on the time step of the simulation rather than the physical properties of the leg. The revised formula, using the time to exit the leg, corrected these deficiencies and is considered a more appropriate approach for determining the velocity distribution.

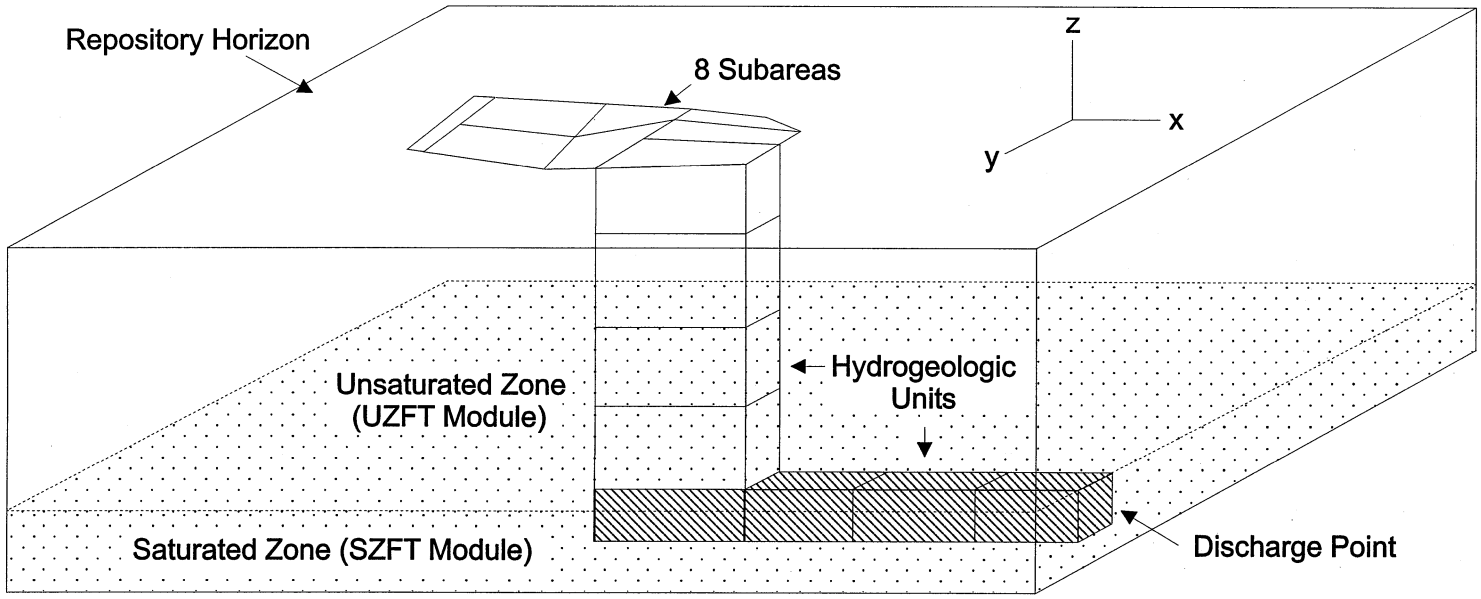


**Figure 9-1. UZFT contaminant transport legs**

### 9.3.3 Efficiency of Simulating Flow and Transport

Efficiency in simulating flow and transport in the UZ were considered in development of the UZFT module owing to potentially long run times associated with long-term performance periods (much greater than 10,000 yr) together with additional processes such as matrix diffusion. Long simulation times can occur when the transport velocity is such that the use of a small time step over the simulation period is required. A resolution to this problem was to bypass consideration of stratigraphic units that had short residence times (less than 10 yr or less than 10 percent of the residence time of all legs). When the velocity in a particular leg results in a short residence time, the leg is not included in the NEFTRAN II simulation. If all the legs for a particular subarea are bypassed, the entire UZ transport calculation is bypassed, and releases from the repository are provided directly to the SZ transport module, SZFT.

Additionally, the time intervals over which the velocity varies, as provided by UZFLOW, can affect simulation times (e.g., short intervals resulting in long run times). Therefore, the UZFT module varies the velocity over a time interval dictated by a minimum change in the velocity field (an input parameter specifies the UZ minimum velocity change factor), where a small fractional change will result in shorter time intervals and associated longer simulation time.

## 9.4 ASSUMPTIONS AND CONSERVATISM OF THE UZFT APPROACH

The UZFT module is an abstraction of groundwater flow and RT from the repository to the SZ. The main attributes of the UZ that control transport of radionuclides are (i) the transport velocity of radionuclides in groundwater, (ii) radionuclide sorption, (iii) matrix diffusion, and (iv) the hydrologic stratigraphy. The transport velocity of radionuclides in groundwater is influenced by the presence or absence of fracture flow. Because of differences in porosity between the fracture and matrix, transport velocities can be much larger (up to 2–3 orders of magnitude) in the fractures than in the matrix for the same flux. The transport velocity within a specific hydrostratigraphic unit (e.g., Calico Hills zeolitic) is determined by assuming vertical flow below the repository and comparing the vertical flow to the saturated hydraulic conductivity of the matrix (if the vertical flow exceeds the saturated conductivity any time during the simulation, fracture transport velocities are used). This approach is considered a reasonable representation for the bulk behavior of a number of hydrologic units at YM because saturated hydraulic conductivity of the matrix is either significantly above or below the net flux (e.g., Calico Hills zeolitic, Calico Hills vitric, and Topopah Springs welded). While this approach does not account for spatial variability of flow caused by heterogeneities in the hydrologic properties of the fractures and matrix, or the episodic nature of the infiltration, the approach generally yields short travel times to the SZ, using the current hydraulic properties and infiltration estimates. Short travel times are considered consistent with the presence of $^{36}Cl$ at multiple locations in the Exploratory Studies Facility (ESF) at YM. The degree of conservatism in these travel times cannot be determined until site investigations including the $^{36}Cl$ data are complete.

Transport of radionuclides can be significantly slowed by the sorption of radionuclides on mineral and rock surfaces. Retardation of radionuclides is considered limited within fractures relative to the matrix because retardation of radionuclides is assumed largely affected by the surface area available for sorption, while flow through the matrix encounters significantly more surface area than fracture flow. Although the TPA Version 4.0 code has the capability to represent retardation of radionuclides within fractures, fracture retardation factors have been set to 1.0 (i.e., no retardation) in the data set. This is a conservative approach

considered to have limited impact on the results, given the assumption that sorption of radionuclides within fractures will be limited.

Transport of radionuclides within fractures can be delayed by diffusion of radionuclides within the fractures into the matrix. The rate of diffusion of radionuclides is affected by the variation in fracture and matrix flow, the concentration gradient between the fracture and matrix water, and the nature of the fracture surface (e.g., permeability of fracture coatings). Within the TPA Version 4.0 code, it is conservatively assumed that matrix diffusion does not occur in the UZ. Overall, this assumption in UZFT is consistent with little, if any, delay of radionuclides moving large distances in the UZ over short time scales, as evidenced by the presence of $^{36}Cl$ at multiple locations in the ESF at YM. Moreover, the observed differences in water chemistry between matrix and fracture water would not be present if matrix diffusion was significant. The degree of conservatism in this assumption will be determined based on the ongoing site investigations.

It is obvious from the previous discussions that transport in the UZ will be sensitive to the occurrence of fracture flow. Fracture flow will dominate in a unit with low matrix conductivity (e.g., Calico Hills zeolitic), while matrix flow will dominate in a unit with high matrix hydraulic conductivity (e.g., Calico Hills vitric). Thus, the presence or absence of particular units below the repository and the assumption that the flow is primarily vertical has a strong influence in determining the occurrence of fracture flow. The abstraction for stratigraphy uses 10 subareas to account for the spatial variability in the thickness of the hydrostratigraphic units (primarily based on the spatial variability of the Calico Hills vitric and zeolitic units). This approach was used to provide a general representation of the UZ and does not represent thin stratigraphic units (i.e., on the order of a few meters). Although the inclusion of some of these thin units could increase travel times, through lateral diversion or matrix-only flow, they are not included in the current approach.

There are specific assumptions related to unsaturated flow:

- Spatial heterogeneities are accounted for at the scale of the stratigraphic units. Although smaller scale heterogeneities are neglected, the approach is considered appropriate because of the conservatisms built into the conceptual model.

- Flow is downward toward the water table with no lateral diversion.

- The UZ flow field is time varying but in equilibrium (temporal variation in the near surface infiltration, because of climate variation, equilibrates rapidly in the UZ).

- Deep percolation between the repository and the water table is not affected by thermal reflux. During the highest thermal period, when this assumption is most uncertain, it is reasonable to assume that few, if any, containers will fail.

- Fracture flow occurs only when the percolation exceeds the saturated conductivity of the matrix; when this occurs, it is assumed the interconnected fractures are capable of conducting the remaining flow.

- Transition between matrix and fracture flow occurs only at the interface between stratigraphic units (the amount of fracture and matrix flow is uniform within a stratigraphic unit).

There are specific assumptions related to UZ transport:

- It is assumed that radionuclides are transported in either the fractures or the matrix and are not partitioned when flow occurs in the fractures and the matrix (fracture flow is used when the deep percolation exceeds the saturated matrix hydraulic conductivity of the matrix). This transport does not account for the partitioning of flow between the fractures and the matrix and will be conservative when fracture flow is a small percentage of matrix flow

- Retardation within fractures does not significantly delay RT in the UZ.

- Matrix diffusion does not significantly delay RT in the UZ.

# 10 SZFT MODULE DESCRIPTION

The SZFT module describes RT in the SZ from the location at which radionuclides enter the water table immediately below the repository to a receptor location. The SZ transport model consists of an array of 1D streamtubes originating at the water table below the repository and terminating at a receptor location. RT in the SZFT module is simulated using the NEFTRAN II code (Olague et al., 1991), which calculates the radionuclide release rate (Ci/yr) at the down-gradient receptor location. In the SZFT module, there are three SZ streamtubes each connecting to one or more UZ streamtubes (Figure 10-1).

## 10.1 INFORMATION FLOW WITHIN TPA

### 10.1.1 Information Supplied to SZFT

From EXEC, the SZFT receives the radionuclide release rate as a function of time from the UZ as computed by the UZFT module. Other inputs to SZFT are specified in the SZFT section of the *tpa.inp* file or in the *strmtube.dat* file. The *strmtube.dat* file provides the streamtube widths as functions of position and the flow rates for each streamtube. Data provided by the *tpa.inp* file include hydrologic properties, retardation factors, matrix diffusion parameters, and the fraction of the flow path through fractured volcanic tuff versus alluvium. The user selects either 10 km or 20 km as the distance to the receptor group in the *tpa.inp* file.

### 10.1.2 Information Provided by SZFT

SZFT computes estimates of the total activity of the radionuclides transported to the receptor location as a function of time in Ci/yr. SZFT results for the time-varying release rates from the SZ are passed to EXEC along with the GWTT for the SZ for subsequent use in DCAGW for dose calculations.

## 10.2 INTERMEDIATE RESULTS

The SZFT intermediate outputs provide information on the flow field and the overall transport of radionuclides. An averaged SZ GWTT (averaged over time) is computed for each repository subarea and written to the *gwttuzsz.res* output file. The cumulative release of radionuclides from the SZ (summed over all repository subareas and the simulation period) is calculated for each radionuclide and is available in the *cumrel.res* and *cumrel_c.res* files. Additionally, the normalized SZ releases presented as a CCDF are contained in the *gwccdf.res* and *gwccdf_c.res* files. The *gwttuzsz.res*, *cumrel.res*, *cumrel_c.res, gwccdf.res*, and *gwccdf_c.res* files are described in detail in tables 20-1 and 20-2.

When the append option is turned on in the *tpa.inp* file to create additional intermediate outputs, SZFT inputs are written to the *szft.ech* file and outputs to the *szft.rlt* file. The UZFT releases for all times and groundwater radionuclides are included in the *szft.ech* file. The time history of SZ releases for all groundwater radionuclides is available in the *szft.rlt* file. A complete description of these files is provided in section 20.3.

The SZFT module generates intermediate input and output data transfer files while executing the *nefmks.f* stand-alone transport code. These files contain information only for the final realization and subarea available at the end of the TPA Version 4.0 code execution. SZFT intermediate input data transfer

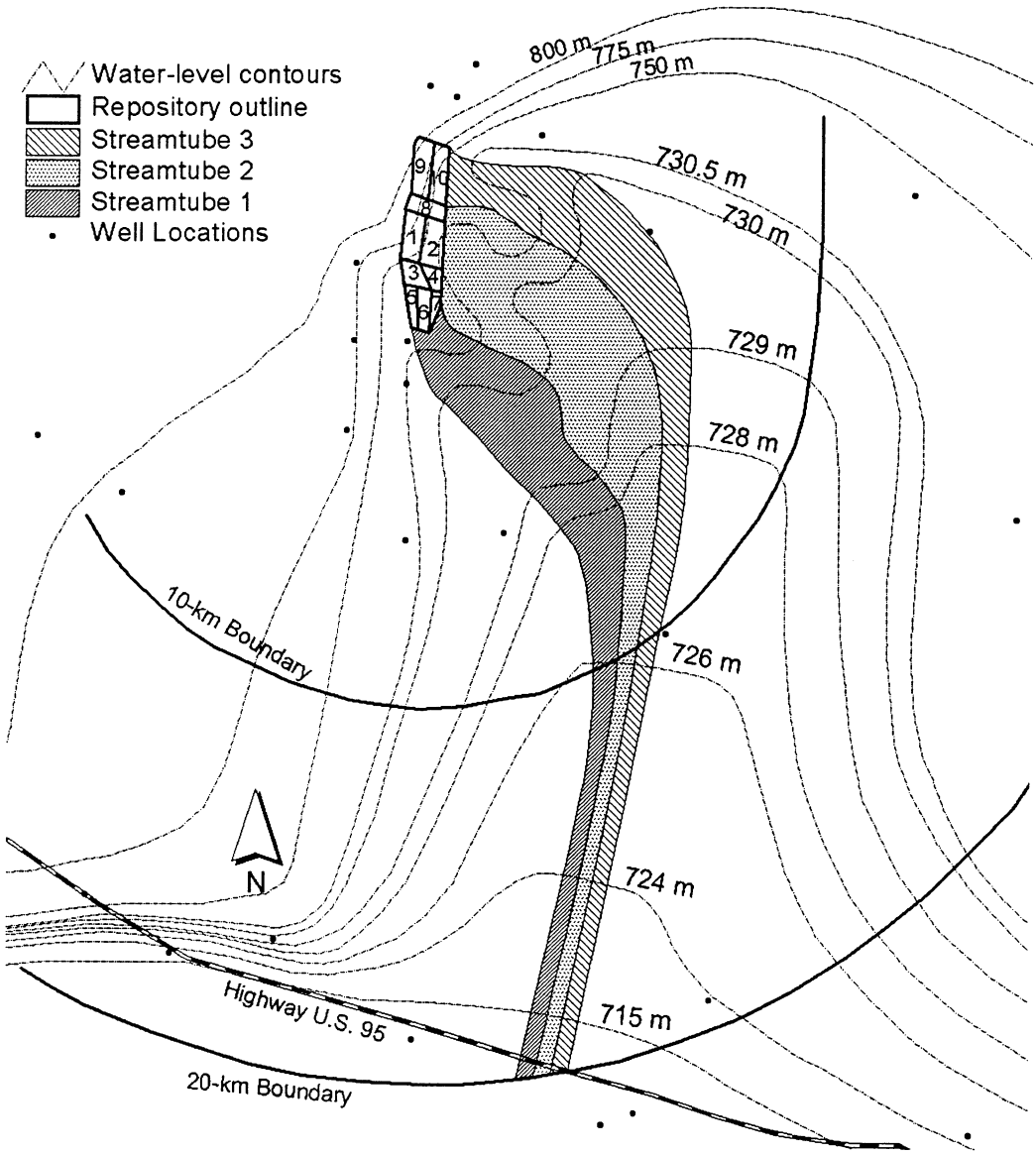


**Figure 10-1. Saturated zone streamtubes model showing three streamtubes from just upgradient of the repository footprint southward to the proposed 20-km compliance boundary**

files are *nefiisz.inp* and *nefiisz.src*. All SZFT parameters specified in the *tpa.inp* file are accessed through the *nefiisz.inp* file. Inputs to SZFT are the UZ groundwater release rates from UZFT and are available in the *nefiisz.src* file. Intermediate output data transfer files from SZFT include the *nefiisz.dis* and *nefiisz.out* files. The SZ release rates for all groundwater radionuclides are accessed in the *nefii.dis* file. The file *nefiisz.out* provides the *nefmks.f* output file. Contents of all SZFT intermediate data transfer files are further described in appendix E.

## 10.3 CONCEPTUAL MODEL

The SZFT module describes the temporal and spatial variation of radionuclide mass transport from the water table at a location immediately below the repository to the receptor location. SZFT uses the stand-alone code NEFTRAN II (Olague et al., 1991) to track radionuclide mass transport.

Transport of radionuclides in the SZ is complicated by (i) spatial variability in the geochemical properties of the fracture surfaces and rock matrix, (ii) heterogeneity of pore-scale to formation-scale transport pathways, (iii) temporal variations in the flow field caused by climatic change and pumping for water use, and (iv) variability in the rate at which radionuclides transiting the UZ reach the water table. The extent to which these features and processes are incorporated into predictive models affect the accuracy of point estimates of radionuclide concentrations in the aquifer. The approach adopted in DCAGW (chapter 11) for determining the radionuclide concentration of water consumed at the receptor location allows the SZFT model to neglect many of the high-resolution spatial and temporal variations in transport processes.

Radionuclide mass (activity) release rates at the receptor location are converted into radionuclide concentrations by multiplying the mass release rate by the fraction of mass captured by a well or well field and then dividing this product by the volume of water that is pumped. In DCAGW, simplified well capture zone relationships are used to determine the fraction of mass captured by low-discharge wells or well fields. At high-discharge well fields used to supply irrigation water, it is assumed that all radionuclides are captured. Therefore, SZFT does not need to accurately describe the 3D distribution of radionuclide concentrations at the receptor location. The SZFT module needs only to predict the mean trajectory and travel times of radionuclides in the SZ and take into account the variation in geochemical properties along the transport path. Although temporal changes in the flow field caused by climatic change and variations in pumping rates may affect transport, in SZFT it is assumed that a steady-state representation of the flow field is sufficient.

### 10.3.1 Saturated Zone Flow Model

For the TPA Version 4.0 code, a 2D horizontal flow-net approach was used to abstract the steady-state velocity field used in the SZFT module for the SZ region from below the repository to the receptor location. The abstraction is made by constructing three streamtubes that emanate from the vertical projection of the repository lateral boundary onto the water table and terminate at the appropriate receptor location. Differences in the mean travel time along each of the four streamtubes arise from differences in streamtube input fluxes, lengths, and three sampled values: effective porosity of the tuff, effective porosity of the alluvium, and the fraction of the streamtube occupied by each.

The flow net approach is based on an interpretation by Winterle et al. (2000) of horizontal hydraulic gradients in the uppermost aquifer between the repository and the 20-km compliance boundary. The

potentiometric surface map, shown in figure 10-1, was obtained by hand drawing lines of equal hydraulic head to match static well-water levels in the YMR reported by DOE and Nye County investigators (e.g., Czarnecki et al., 1997; Graves et al., 1997; Graves, 1998; Nye County, 1999). This hand-contouring approach allows use of judgement and consideration of structural and stratigraphic features. Additionally, this approach avoids the need to calibrate a model to observed hydraulic heads, as done in the previous version of the TPA code, which used a 2D numerical-modeling approach (Baca et al., 1996). The greatest uncertainty in the interpretation of the potentiometric surface lies in areas of sparse data west of Fortymile Wash and along the southern portion of the distance between the repository and the 20-km compliance point.

Streamtube boundaries were drawn assuming that groundwater flow is in the direction of the hydraulic gradient, which is true only in the case of a horizontally isotropic aquifer. The northernmost and southernmost streamtube boundaries were selected to be tangential to the respective ends of the repository footprint. Between these two boundaries occur two ridges of higher water-level elevations, just east of the repository, forming groundwater divides, which act as logical and convenient delineations for two additional streamtube boundaries. These four streamtube boundaries form three adjacent streamtubes. All water passing beneath the repository must flow through one of these streamtubes.

Streamtube fluxes were calculated based on the hydraulic gradient and transmissivity. In the area from 3–5 km east of the repository, reliable transmissivity estimates for the scale of interest have been obtained from testing at the C-Holes Complex (Winterle and La Femina, 1999), and there are numerous monitor wells to constrain the local hydraulic gradient. Aquifer transmissivity in this vicinity is on the order of 1,000 $m^2/d$, and the hydraulic gradient is on the order of 0.0003. Based on streamtube widths in this area and an estimated 400-m aquifer thickness,[1] calculated volumetric flow in the three streamtubes, from south to north, is calculated to be 600, 730, and 470 $m^3/yr$ per meter of aquifer thickness. Because steady-state groundwater volumetric flow rate is constant throughout the length of a 1D streamtube, the groundwater volumetric flow rate calculated from data near the C-holes can be extended to areas along the streamtubes where fewer data are available. For the basecase *strmtube.dat* file, it is conservatively assumed that radionuclide release rate calculated by the UZFT module is diluted only by the water in the top 1 m of aquifer thickness.

Because a constant volumetric flow rate is specified for each streamtube, variations in streamtube widths cause Darcy velocities to vary from about 0.25 to 1.9 m/yr. This variability is abstracted in TPA by specifying streamtube widths at 20 points along each path line in the *strmtube.dat* file. The greatest Darcy velocities would occur to the south, where all three streamtubes narrow to about 400 m. It should be noted, however, that streamtube widths in this area are poorly constrained for lack of water-level data in southern portion of the compliance area. Darcy velocities are translated into mean transport velocities by dividing by the kinematic (effective) porosities. Thus, uncertainty in Darcy velocity estimates is incorporated into the range and distribution of effective porosities specified in the *tpa.inp* file. Sampled effective porosity varies from 0.001 to 0.01 for the fractured-tuff portion of the streamtube, and from 0.10 to 0.15 for the alluvial portion.

A new feature of the TPA Version 4.0 code is that the projected radionuclide transport path-length from the repository footprint to the tuff-alluvium contact (via the fractured tuff aquifer) is now a sampled

[1]Calculated mean distance from the water table to the top of the Tram bedded tuff layer, which is believed to be approximately at the top of the lower volcanic confining layer

parameter with a distribution specified in the *tpa.inp* file. The remainder of the transport path-length to the compliance boundary is assumed to occur through the alluvial aquifer system. This change was incorporated because of the existing uncertainty regarding the zone where groundwater (and hence transported radionuclides) flowing through the repository footprint transitions from the tuff aquifer system to the alluvial aquifer system.

## 10.3.2 Saturated Zone Transport Model

Sampled transport parameters whose probability distribution or sampling range is defined in the *tpa.inp* file include (i) longitudinal dispersivity, sampled as a fraction of the transport path length; (ii) retardation coefficients for each radionuclide; (iii) a diffusion coefficient for matrix diffusion in saturated tuffs; (iv) effective flow porosities for saturated tuff and alluvium; (v) matrix (immobile) porosity of the saturated tuff unit; (vi) an immobile porosity penetration fraction for the saturated tuff unit; and (vii) porosity of saturated alluvium.

Longitudinal macrodispersivity is generally assumed to increase with the scale of the contaminant plume until an asymptotic upper bound is attained (Gelhar, 1993). As such, it is incorrect to assign a separate dispersivity value to each NEFTRAN II transport leg. Consequently, a single value is sampled, the value of which is dependant on the distance to the critical group location. The retardation coefficients set in the *tpa.inp* file depend on the dominant mineralogy of the medium in the transport leg as well as the particular radionuclide being transported.

NEFTRAN II has the capability to account for the migration of dissolved contaminants from flowing pores and fractures into the more-or-less immobile water within the rock matrix pores. The governing equation used in NEFTRAN II to account for the rate of change of concentration in the immobile phase is (Olague et al., 1991)

$$\theta_s \, R_s \frac{\partial C_s(x,t)}{\partial t} = \beta\left[C_d(x,t) - C_s(x,t)\right] \tag{10-1}$$

where

| | | |
|---|---|---|
| $\theta_s$ | — | immobile (stagnant) porosity [unitless] |
| $R_s$ | — | retardation factor [unitless] |
| $C_s$ | — | volume-averaged solute concentration in stagnant region [mass per unit volume] |
| $x$ | — | distance in direction of flow [length] |
| $t$ | — | time [yr] |
| $\beta$ | — | mass-transfer rate coefficient [1/yr] |
| $C_d$ | — | dynamic (mobile) solute concentration [mass per unit volume] |

This process is commonly referred to as matrix diffusion. However, the mass transfer rate coefficient ($\beta$) is not so much a fundamental physical parameter but rather a parameter somewhat unique to the NEFTRAN II computer code. Therefore, the *tpa.inp* file contains parameters that are more commonly used to describe

matrix diffusion. These parameters are used to calculate the mass transfer rate coefficient and effective immobile porosity using the following formula:

$$\beta = \frac{\theta_s D}{0.28\left(\frac{f}{2n}\right)^2} \tag{10-2}$$

where

| | | |
|---|---|---|
| $D$ | — | diffusion coefficient [length$^2$ per time] |
| $f$ | — | fraction of immobile porosity in which matrix diffusion occurs [unitless] |
| $n$ | — | number of fractures per meter [1/length] (measured perpendicular to the fracture assuming regular spaced fractures) |
| 0.28 | — | shape factor used for parallel planar matrix blocks [unitless] |

Equation (10-2) is based on a formula derived by van Genuchten (1985) for estimating first-order, mass-transfer coefficients according to rates of diffusion and flow system geometry. The original formula of van Genuchten was modified to include the factor $f$, an immobile porosity penetration fraction. This fraction accounts for the fact that matrix blocks may not be fully permeated by diffusing solutes if time scales for transport to the receptor location are short relative to the time scale for diffusion to the matrix block center. The fraction $f$ is also used to scale the effective immobile porosity to a lower value using the formula

$$\theta_s = f\theta_m \tag{10-3}$$

where $\theta_m$ is total rock matrix porosity [unitless]

The immobile porosity penetration fraction, $f$, is a difficult parameter to estimate because it is a nonlinear function of several variables, including matrix block size, advection velocity, and solute-specific diffusion rates. Accordingly, for purposes of the TPA basecase abstraction, this penetration fraction is sampled from a loguniform distribution over a range of conservatively low values from 0.01 to 0.1.

## 10.4 ASSUMPTIONS AND CONSERVATISM OF THE SZFT APPROACH

The abstracted model implemented in the SZFT module is assumed to adequately capture the range of processes and features that control and affect the transport of dissolved radionuclides from the SZ below the repository to the receptor location. Processes simulated by the SZFT module include (i) advective transport through the tuff and alluvial aquifers, (ii) longitudinal dispersion during transport, (iii) chemical sorptive processes that retard the transport of radionuclides in the alluvial aquifer and in the matrix of the tuff aquifer, and (iv) diffusion of radionuclides from the fractures to the matrix in the tuff aquifer.

Because the estimated magnitude of water-well pumping for irrigation at the receptor location is sufficient to capture most radionuclides emanating from the repository (Fedors and Wittmeyer, 1998), a

relatively simple 1D model can be used to convey radionuclides directly from the repository to the receptor location. Transport velocities along the flow tubes are equal to the ratio of the Darcy velocity to the effective porosity. Uncertainty regarding estimated groundwater velocities is addressed by performing TPA calculations over a range of effective porosities from 0.001 to 0.01 in the tuff aquifer and from 0.10 to 0.15 in the alluvial aquifer.

The effects of lateral dispersion on vertical spreading of the plume are not explicitly accounted in the streamtube approach. Since vertical dispersion would likely reduce *in situ* radionuclide concentrations or reduce the fraction of mass captured by the pumping well, neglecting its effects is conservative. The effects of longitudinal dispersion are included in the model; however, the value of longitudinal dispersivity used in the SZFT abstraction is conservatively assumed to be 0.01 of total transport distance for saturated tuff and 0.1 for saturated alluvium.

Transport of radionuclides can be significantly retarded by sorption of radionuclides on mineral surfaces. Retardation of radionuclides is considered to be much more limited in fractures than in the matrix because sorption is assumed to be primarily controlled by the mineral surface area, which is much greater in the rock matrix. Although the TPA Version 4.0 code has the capability to represent retardation of radionuclides within fractures, fracture retardation factors have been set to 1.0 (i.e., no retardation) in the data set. This is a conservative approach considered to have a limited impact on the results assuming that sorption of radionuclides within fractures will be limited. Retardation caused by sorption of radionuclides on the abundant clays and iron minerals in the alluvium is assumed to be significant and is included in the SZFT model abstraction.

Transport of radionuclides in the tuff aquifer can be delayed by diffusion of radionuclides from the fractures into the matrix. The rate of diffusion of radionuclides is affected by variations in fracture and matrix flow, the concentration gradient between the fracture and matrix water, and the permeability of mineral coatings on the fracture surface. Matrix diffusion can be accounted for in the tuff aquifer; however, it is conservatively limited to a small fraction of the total matrix porosity. The degree of conservatism in this assumption cannot be assessed until ongoing site investigations are complete.

Because of the significant differences between the radionuclide transport properties of the fractured tuff and alluvium, the relative transport distance through each aquifer system has been recognized as important to repository performance. Limited data, however, are available to identify the zone of transition between the tuff and alluvial aquifers. This uncertainty is increased by the fact that the abstracted streamtubes do not account for possible horizontal anisotropy in the fractured tuff aquifer, caused by the predominant north-northeast trend of fractures and faults in the area. Horizontal anisotropy could reasonably be expected to divert flow in the tuff aquifer more to the south, which would result in a greater fraction of the transport distance through fractured tuff. To account for this uncertainty, the TPA Version 4.0 code includes the fraction of transport distance through tuff versus alluvium as a new sampled parameter in the *tpa.inp* file.

The flow-net analysis used to abstract the three SZ transport streamtubes is based on several assumptions:

- Differences in water levels in wells are representative of changes in hydraulic head and can be used to infer horizontal hydraulic gradients in the uppermost parts of the tuff and alluvial aquifers.

- Flow in the tuff and alluvial aquifer systems occurs in the direction of the horizontal hydraulic gradient.

- Climate change during the period of repository performance has no effect on the regional groundwater flow.

There are also several assumptions regarding transport in the SZ:

- The velocity field can be adequately modeled by dividing the region into three flow tubes whose lateral boundaries are defined by streamlines emanating from either edge of the repository.

- Within the tuff aquifer, advective transport takes place primarily through interconnected fractures.

- Radionuclides entering a flow tube are uniformly mixed across the width of the flow tube.

- The longitudinal dispersivity is related to the length of the transport path.

There are conservatisms adopted in SZFT:

- Use of relatively small longitudinal dispersivities reduces mixing during transport.

- Assumption of steady-state flow precludes dispersion of the radionuclide plume caused by changes in the magnitude and direction of the mean velocity field through pumping and climatic change.

# 11 DCAGW MODULE DESCRIPTION—FARMING RECEPTOR GROUP

The DCAGW module calculates the annual TEDE to an average member of a receptor group from exposure to radionuclide concentrations in groundwater. The receptor group can be either a farming group or a residential group. The primary differences in the calculation of the dose to these two groups is that a different model is used to determine the concentration of radionuclides in the well water and that more pathways are considered for the farming group. The models and assumptions used to calculate the dose to the farming receptor group are described in this chapter, while the models and assumptions used to calculate the dose to the residential receptor group are described in chapter 12.

## 11.1 INFORMATION FLOW WITHIN TPA

### 11.1.1 Information Supplied to DCAGW

DCAGW receives information passed from the EXEC and various data files so dilution and dose conversion calculations can be executed. For dilution calculations, time-varying release rates computed in SZFT for each radionuclide released through groundwater are passed to DCAGW by EXEC. Radionuclide groundwater concentrations are calculated from the release rates using the dilution volume. For the dose calculations, important reference biosphere and receptor group parameters are sampled in EXEC from the *tpa.inp* file and passed to DCAGW. The remaining dose parameters are constants but can be modified by editing the *ggenii.def* and *gdefault.def* files (shown in appendix G). A list of default parameter values for the *tpa.inp* file is provided in appendix A.

A number of default data files provide important information for the calculations in the GENTPA Version 1.0 code. For the multiple pathway DCF calculations applicable to a farming receptor, these files include: *gftrans.def* (food transfer factors and leaching factor), *gdefault.def* (default parameters), *ggamen.dat* (gamma energies), *ggrdf.dat* (external dose coefficients), *gbioac1.dat* (bioaccumulation factors for fresh and salt water organisms), *ggenii.def* (primary input parameter file), *grmdlib.dat* (radionuclide library), *gnewdf.dat* (inhalation and ingestion dose coefficients), *gdosinc2.dat* (header file), and *filename.dat* (data file directory structure). These files relate to data files used for the GENII Version 1.485 code (remove the initial letter of each filename to determine the applicable GENII file name) (Napier et al., 1988).

Modifications to these data files for TPA use include populating the *gftrans.def* file with the transfer factors described in LaPlante and Poor (1997), updating the leaching factors in the *gftrans.def* file by recalculation using the *tpa.inp* file input, adding $^{108m}$Ag and the relevant physical information to the *grmdlib.dat* and *ggamen.dat* files, and updating external dose coefficients in the *ggrdf.dat* file using values from Federal Guidance Report (FGR) 12 (U.S. Environmental Protection Agency, 1993). The use of a new dose coefficient data file, *gnewdf.dat*, to calculate DCFs from intakes provided by the *env.exe* program replaces the use of the *dosinc.dat* file and the *dose.exe* program (from GENII Version 1.485 code). Unlike the *dosinc.dat* file, the data file *gnewdf.dat* can be read and edited by the user when updates are needed, and the *gnewdf.dat* file contains age-dependent dose coefficients from ICRP Publication 72 (International Commission on Radiological Protection, 1996) as well as adult (default) dose coefficients from FGR 11 (U.S. Environmental Protection Agency, 1988). The *filename.dat* and *gdosinc2.dat* files are necessary for the GENTPA Version 1.0 code to execute correctly; however, it is not anticipated the user will need to view or modify these files for TPA use.

### 11.1.2 Information Provided by DCAGW

The groundwater pathway dose for each radionuclide as a function of time is passed to EXEC. The dose results are applicable to the receptor age group selected in the *tpa.inp* file: infant, toddler, preteen, teen, or adult based on ICRP Publication 72 (International Commission on Radiological Protection, 1996) or an alternate adult selection based on FGR 11 (U.S. Environmental Protection Agency, 1988).

## 11.2 INTERMEDIATE RESULTS

Groundwater pathway DCFs, output from DCAGW and used in determining doses from radionuclide concentrations for a farming receptor group located 20 km from YM coincident with the location of the groundwater releases, are contained in two data files: *gw_cb_ad.dat* and *gw_pb_ad.dat*. Each file pertains to different climatic conditions (either current biosphere designated by *cb* or pluvial biosphere designated by *pb* in the file names). These files contain separate DCFs for direct exposure, inhalation, and ingestion of animal products, terrestrial products, drinking water, and milk.

The groundwater doses for all radionuclides are accessed in the *npkdoset.res, npkdst_c.res, gwpkdos.res,* and *gwpkdos_c.res* files. The *npkdoset.res* and *npkdst_c.res* files provide the peak groundwater dose and the time of the peak dose for each radionuclide. The overall peak groundwater dose from all nuclides, the time of the peak dose, and the contribution to the peak groundwater dose from each radionuclide are contained in the *gwpkds.res* and *gwpkdos_c.res* files. Also, the time history of total dose from the groundwater is included in the *totdos.res* and *totdose_c.res* files along with the pumping volume used in calculating the radionuclide concentration at the wellhead. The *npkdoset.res, npkdst_c.res, gwpkdos.res, gwpkds_c.res, totdose.res,* and *totdos_c.res* files are described in detail in tables 20-1 and 20-2.

When the append option is turned on in the *tpa.inp* file to create additional intermediate outputs, DCAGW inputs are written to the *dcagw.ech* file and outputs to the *dcagw.rlt* file. The SZ releases from SZFT for all times are included in the *dcagw.ech* file. The time history of groundwater doses for all radionuclides and the plume mass fraction captured are available in the *dcagw.rlt* file. Additionally, groundwater doses can be accessed in the *rgwna.tpa, rgwnr.tpa, rgwsa.tpa, rgwsr.tpa,* and *rgwgssa.tpa* files. The file *genv.cum* provides radionuclide specific intakes (Ci/yr) for each realization by pathway including leafy vegetables, other vegetables, soil, fruit, grain, beef, poultry, milk, eggs, drinking water, and inhalation. The *genv.cum* file also provides information on external exposure. The file *ggenii.cum* contains the input parameter echo from GENTPA Version 1.0 code for all realizations. This input parameter echo can be used to verify the parameters used in the DCF calculations for each realization. The *dcf.cum* file echos the contents of the *gw_cb_ad.dat* and *gw_pb_ad.dat* files for each realization. A complete description of these files is provided in section 20.3 and table 20-6.

## 11.3 CONCEPTUAL MODEL

The dilution volume at the pumping well is calculated using intermediate results and parameters specified in the *tpa.inp* file. However, the user has the option of specifying a value for the dilution volume by activating a flag in the *tpa.inp* file. In the dilution volume calculations, the DCAGW module utilizes the water use characteristics of the farming receptor group. The receptor group, a farming community at distances at least 20 km from YM, is to be consistent with draft 10 CFR Part 63. Once the dilution volume

is determined, the module converts the activity released from the saturated zone per unit time values calculated by SZFT to activity per unit volume of water by dividing by the pumping rate. DCFs are then calculated and used to determine dose to the average member of the receptor group. The streamtube information used in SZFT and the DCF files are tied to the location of the receptor group. Therefore, any change to the location of the receptor group must be consistent with the streamtube data files.

For each time step, the product of each radionuclide concentration and DCF are summed within and among groundwater pathways and radionuclides to calculate total doses. In addition to summary doses, selected output is stratified by realization, time step, and radionuclide. The EXEC uses results from all realizations to identify and report peak doses. The output files indicate which age group has been selected for the calculations.

### 11.3.1 Development of Radionuclide Concentrations in Water for a Farming Receptor Group

For the farming receptor group, the volume of water into which the released radionuclides are diluted is the greater of the flow rate of water within the uppermost producing horizon in the pumped aquifer and the volumetric flow rate of water pumped for household and agricultural needs of the receptor group location. The flow rate of water within the uppermost horizon is set to the greater of the UZ flow rate and SZ flow rate. This condition sets a reasonable lower limit for the dilution volume consistent with the assumption that the combined well discharge rates at the farming location are large enough to capture all released radionuclides. Borehole concentrations at the farming location are computed by dividing the radionuclide release rate by the appropriate dilution flow rate. Although the well discharge rates are assumed to be large enough to capture the entire radionuclide plume, the user may specify the fraction of the radionuclide plume captured by activating a flag in the *tpa.inp* file.

For the farming receptor group location, there are no readily available data that can be used to assess the variation in hydraulic conductivity or borehole inflow with depth. The nearest wells completed in alluvium from which there is detailed lithologic information are located in the northwestern Amargosa Valley near the Beatty low-level waste facility. The soil texture varies from clay to gravel in this area; however, drillers' logs indicate that the predominant soil texture classes are sands and gravels. Data compiled from drillers' logs by Oatfield and Czarnecki (1991) show that the fraction of coarse-grained sediments in the Amargosa Farms area ranges from 0.50 to 0.70. Since sands and gravels are the predominant alluvial facies, it is reasonable to assume wells are screened over their entire depth. In fact, statistics on water well screen depths and lengths suggest that the typical well in the Amargosa Farms region is continuously screened over the lower 75 percent of the saturated section penetrated by the borehole. The mean and standard deviation of the thickness of the uppermost producing horizon, which here is defined as extending from the water table to the bottom of the well screen, are 55 and 32 m. The minimum and maximum values of the producing horizon thickness are 8.5 and 158 m.

The distribution of the producing horizon thickness for the farming receptor group is positively skewed and may be suitably represented by a lognormal or gamma distribution; however, it is assumed to be uniform. For producing horizon thicknesses of 20, 80, and 140 m, the flow rates in the uppermost producing horizon in the alluvial aquifer are 40,940, 163,760, and 286,580 $m^3$/yr. Expected flow rates for farming are much greater than those for residential use. Assuming that the primary water use is for center-pivot irrigation of quarter-section alfalfa fields, a reasonable range of consumptive water use is 6,222,230 to 17,973,330 m $^3$/yr (13 and 27 quarter-section alfalfa fields, 126 irrigated acres per

quarter-section, and 3.1–4.38 ft of water applied each growing season).[1,2] Clearly, the volumetric flow rate of water pumped exceeds the flow rate of water within the uppermost producing horizon.

## 11.3.2 Development of Dose Conversion Factors

The DCAGW module contains the executable pathway dose code GENTPA Version 1.0, which is based on the GENII Version 1.485 code (Napier et al., 1988) that generates radionuclide and pathway-specific annual intake rates for the selected receptor age group. DCAGW uses the intake rates to calculate DCFs designed to convert groundwater concentrations to TEDEs for the average member of the receptor group. DCAGW multiplies the intake rates from GENTPA Version 1.0 code to the applicable dose coefficients in the *gnewdf.dat* file to generate the DCFs. Selection of the desired age category in the *tpa.inp* file (i.e., by using the ReceptorAgeGroup parameter) ensures the correct age-dependent input parameters (e.g., consumption rates) and dose coefficients (from the *gnewdf.dat* file) are used to calculate DCFs.

The default age group is an adult based on inhalation and ingestion dose coefficients provided in FGR 11 (U.S. Environmental Protection Agency, 1988). All other receptor age group calculations involve inhalation and ingestion dose coefficients from ICRP Publication 72 (International Commission on Radiological Protection, 1996). ICRP Publication 72 (International Commission on Radiological Protection, 1996) provides inhalation and ingestion dose coefficients for the following age groups: 3 months, 1 yr, 5 yr, 10 yr, 15 yr, and adult. For TPA modeling , the coefficients were assumed to relate to the midpoints of following age ranges, respectively: <1 yr, 1–3 yrs, 3–7 yrs, 7–12 yrs, 12–17 yrs, and >17 yrs. Considering the age stratification of available age-dependent consumption rate information (discussed below), the ICRP based age groups were collapsed into five groups: <1 yr, 1–7 yrs, 7–12 yrs, 12–17 yrs, and >17 yrs. Dose coefficients for 1–3 yr and 3–7 yr were averaged to combine the categories into one. The resulting age groups were given the following titles: Infant, Toddler, Pre-Teen, Teen, and Adult. Information on the age group classifications is summarized in table 11-1. Based on ICRP Publication 72, (International Commission on Radiological Protection, 1996) the adult age category (greater than 17 yr) dose coefficients are provided to allow for comparison of adult doses with pre-adult age group doses using consistent dosimetry methodology and intake rates. For all other adult dose calculations, the FGR 11 dose coefficients (U.S. Environmental Protection Agency, 1988), used for the adult FGR 11 age category, are recommended.

A new feature for DCF calculation in the TPA Version 4.0 code is the ability to account for buildup of radionuclides in the soil from prior years of irrigation. This feature is controlled by an input parameter in the *tpa.inp* file which represents the number of years of irrigation water deposition prior to the intake period. The user specifies how many years prior to the year of intake (i.e., the year of the DCF calculation) that irrigation with contaminated groundwater is expected to occur, and GENTPA Version 1.0 code calculates the additional soil radionuclide concentration from the deposition, decay, and leaching that occurred during the number of prior years specified. It is assumed that the concentration of radionuclides in the water during prior years of irrigation is the same as the concentration in the current year. Because of the transient nature of farming in the Amargosa Valley region, it is assumed to be unlikely that farming will occur on the same plot of land continuously for more than 15 or 20 yr.

---

[1]3.1 ft/yr near Los Angeles, California [table 14-2, p. 377 (Linsley and Franzini, 1979)]

[2]4.38 ft/yr in Mesa, Arizona [table 2-50, p. 99 (van der Leeden et al., 1990)]

**Table 11-1. Categories used for age-dependent dose calculations for farming receptor group**

| Age Group | Age (y) |
|---|---|
| Infant | <1 |
| Toddler | 1–7 |
| Pre-Teen | 7–12 |
| Teen | 12–17 |
| Adult | greater than 17 |

The DCAGW module calculates DCFs designed to convert groundwater concentrations to TEDEs for the average member of the receptor group. A farming receptor group is reasonable because site-specific information indicates farms exist down-gradient of YM. Two climate regimes are assumed for the biosphere, one based on the present climatic conditions in the Amargosa Valley area and a second based on a future pluvial climate (i.e., a cooler and wetter climate). DCAGW switches from use of current (nonpluvial) condition DCFs to pluvial condition DCFs at a time specified by the user in *tpa.inp*. DCAGW stores the climate conditions (*MAP* and *MAT*) that exist when this transition to pluvial conditions takes place. If future climate conditions (*MAP* and *MAT*) fall below this transitional threshold, DCAGW automatically reverts to using the nonpluvial DCFs.

Pluvial DCFs reflect estimated changes to the biosphere as described in LaPlante and Poor (1997). Estimated pluvial conditions do not change receptor groups or exposure pathways considered in DCF calculations (i.e., similar types of farming activities are expected under both estimated climate states). Pluvial conditions include a reduced well pumping rate, based on the reduced pumping rate at analog sites described in LaPlante and Poor (1997).

The exposure pathways considered in the farming scenario are depicted in figure 11-1 and include ingestion (of contaminated water, crops, animal products, and soil), inhalation (from resuspension of contaminated soil), and direct exposure. The following assumptions apply to the farming receptor group. The farmer grows alfalfa (for beef and milk cow feed), vegetables, fruits, and grains for personal consumption and feed for egg-laying hens. Drinking and irrigation water is pumped from a groundwater well at the farm. Water is consumed at a rate of 2 L/d pumped from a groundwater well; however, TPA provides the flexibility for the user to sample or change the value of this parameter. The mass load above soil in Amargosa Valley is sampled in the DCAGS module, but it is also used to calculate dose from the inhalation pathway in DCAGW. Additional details of methods and assumptions used in the exposure scenarios for DCF calculations are provided in the succeeding sections and in LaPlante and Poor (1997).

## 11.4 ASSUMPTIONS AND CONSERVATISM OF DCAGW APPROACH

DCAGW is an abstraction of complex and uncertain processes occurring in the biosphere. The conversion of groundwater concentrations to receptor dose involves assumptions about (i) the location of the receptor group, (ii) the lifestyle characteristics of the receptor group that form the basis for exposure pathways, (iii) processes that determine fate and transport of contaminants in the biosphere, (iv) calculation of human doses from factors that convert exposure to contaminated media to effective dose equivalents, and (v) well pumping rates.

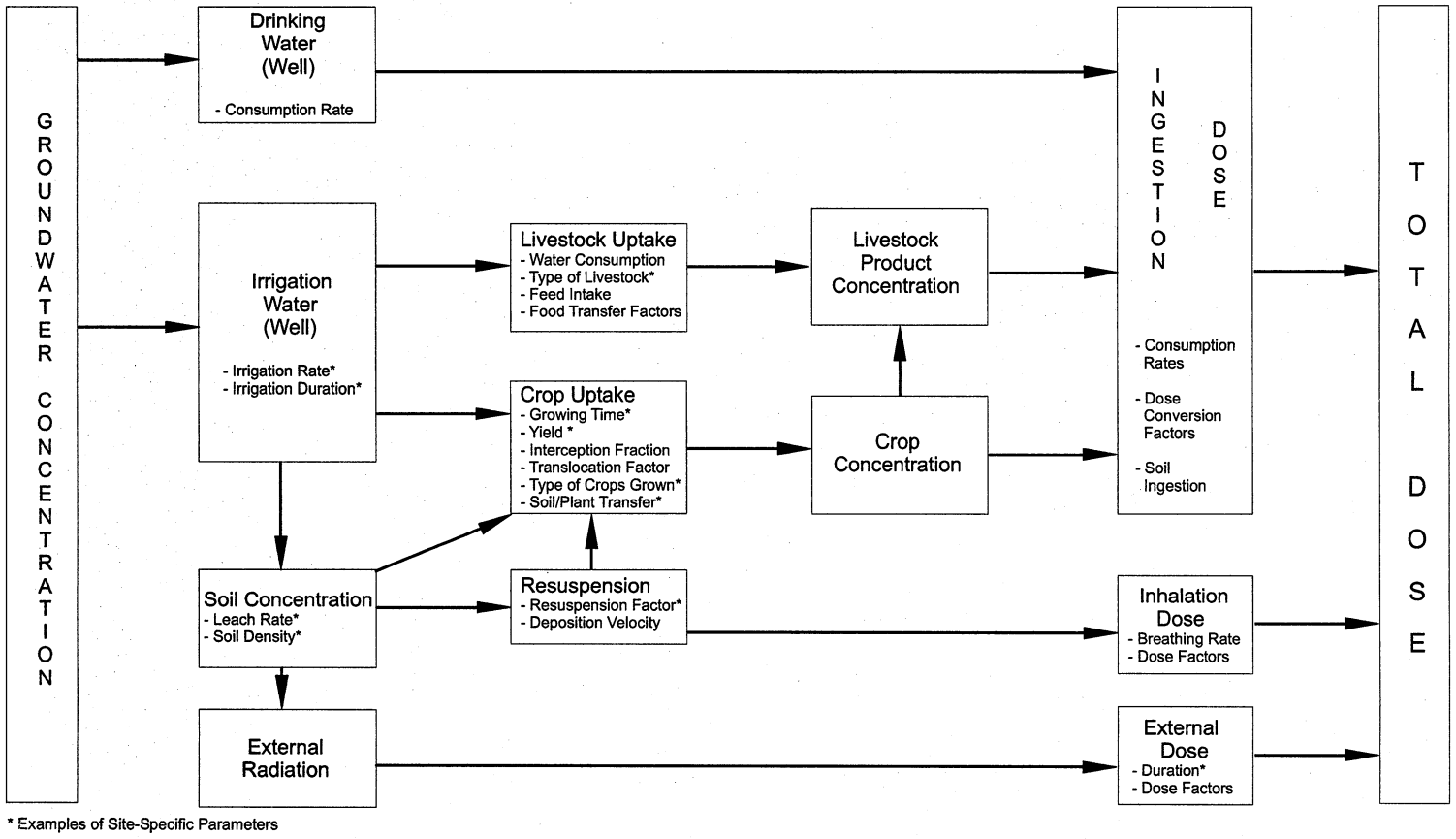


**Figure 11-1. Farmer exposure pathways**

Receptor location is based on the assumption that present physical constraints (i.e., topography, depth to water table, and soil conditions) that limit present farming to the Amargosa Valley area will continue to limit farming south of YM to within approximately 20 km from the proposed repository site. Because the receptor location and lifestyle assumption relates to potential human behavior, it is speculative but considered reasonably conservative for PA calculations.

The conversion of groundwater concentrations to receptor dose requires conceptualization of potential exposure pathways based on the site-specific characteristics of the release pathway, YM biosphere, and receptor group. When groundwater is the source of contamination, the potential exposure pathways are assumed to be those resulting from pumping (including dilution) and agricultural use of water consistent with present farming conditions south of YM. These pathways include ingestion (of contaminated water, crops, and animal products), inhalation (from resuspension of soil contaminated by irrigation), and direct exposure to contaminated soil.

The assumed diet of locally produced food is important to estimating the dose for a farming receptor group. The farmer is assumed to grow alfalfa (for beef and milk cow feed), vegetables, fruits, and grains for personal consumption and feed for egg-laying hens. The practices the farmer is presumed to engage in have been confirmed to exist in areas south of YM; however, it appears unlikely that all activities identified would be practiced by a single individual. Therefore, the doses calculated from such assumptions are expected to be greater than might occur under current conditions. Since bartering is known to exist among community members,[3] it is reasonable to project that for the most highly exposed group, a significant portion of diet could be obtained from local sources. Thus, the assumption is conservative, but not excessively so. These assumptions may change when additional information on local consumption patterns is made available.

Modeling the fate and transport of radionuclides in the biosphere involves consideration of radionuclide deposition (from groundwater) to soil using local irrigation rates, determination of crop concentrations using soil/plant uptake factors, determination of air concentrations from resuspended contamination using a mass load model, and accounting for feed intake and transfer of contamination to livestock.

Radionuclide deposition from irrigation of crops is calculated from the irrigation rate, irrigation duration, and radionuclide concentration in groundwater. The irrigation rate and duration are relevant to local conditions in the Amargosa farms area of Nye County. Loss of contaminants to deeper soil layers from leaching is accounted for by a $K_d$ based model that includes factors that contribute to infiltration, such as rainfall and evapotranspiration. Rainfall and evapotranspiration rates are obtained from local or regional information sources, and $K_d$ values are relevant to the general soil texture classification reported for Amargosa farming soils. Full documentation of parameters is provided in LaPlante and Poor (1997). Additional details are provided in the (bulleted) list of assumptions.

Crop concentrations are based on transfer factors that represent the ratio of plant and soil concentrations for a class of crops grown in contaminated soil. Food transfer factors are generic values based primarily on a large survey of the literature (International Atomic Energy Agency, 1994) or supplemental sources when needed (Baes et al., 1982). Because of the lack of site-specific information, it

---

[3]Eisenberg, N.A. *Staff Visit to Amargosa Valley: Trip Report.* Memorandum (May 14) to M. Federline, U.S. Nuclear Regulatory Commission. Washington DC: U.S. Nuclear Regulatory Commission. 1996.

is reasonable to use generic values; however, they may not be representative of arid conditions that exist in southern Nevada. The selected factors are expected values and have not been arbitrarily increased for conservatism. The transfer coefficients are varied by the use of scale factors that account for variation and uncertainty in the expected values.

Air concentrations from resuspended contamination are calculated by applying a mass loading model. This model uses a mass loading factor that is the amount of airborne dust in the air and assumes that the concentration of radionuclides in the airborne dust is equal to the concentration of the radionuclides in the surface soil. The resuspension process is highly uncertain and is influenced by a number of factors including wind speed, surface roughness, resuspended particle size and density, and the moisture content of soil. Because the GENTPA Version 1.0 code does not provide a mass loading model for crop deposition, a resuspension model was used with an adjusted mass loading factor.

Determination of radionuclide concentrations in livestock products is done by quantifying the intake of contaminated feed and applying a transfer coefficient. The animal transfer coefficients are based on studies that measure radionuclide concentrations in livestock based on measured intake. The coefficients are element and livestock specific and are based on a large survey of available literature (International Atomic Energy Agency, 1994) or a supplemental source (Baes et al., 1982). The transfer coefficients are varied by the use of scale factors that account for variation and uncertainty in the expected values.

Calculation of human dose is accomplished through the use of dose coefficients that convert the estimated concentrations in water, food, air, and soil, together with the corresponding intakes and residence times to TEDE. The dosimetry models that form the basis for the default adult dose coefficients are consistent with those described in the ICRP Publication 30 (International Commission on Radiological Protection, 1979). The dosimetry models represent state-of-the-art techniques and methodologies at the time the publication was released. Refinements to dosimetry models have since been published by the ICRP but have not yet been adopted by the U.S. Government and are, therefore, not used in DCAGW. Age-dependent dose coefficients for alternative receptors are from ICRP Publication 72 (International Commission on Radiological Protection, 1996). The source materials (International Commission on Radiological Protection, 1996) should be consulted for a detailed description of dosimetry assumptions used for the age-dependent dose coefficients.

For the farming receptor group, sampled cumulative well discharge rates are based on assumed ranges of irrigated acreage (13–27 quarter-sections) and consumptive water use (3.1–4.38 ft of water per year for alfalfa). It is assumed that the radionuclide plume emanating from the repository would be completely captured by any configuration of wells whose total discharge equals the sample discharge rate. Borehole concentrations at the farming receptor locations are calculated by dividing the radionuclide mass release rate by the cumulative well discharge rate.

More specific assumptions for DCAGW are provided in the following list and in LaPlante and Poor (1997).

- The dose calculation from consumption of crops does not account for washing of fruits and vegetables prior to consumption and is, therefore, conservative.

- Food transfer factors are generic values based primarily on a large survey of the literature (International Atomic Energy Agency, 1994). Because of the lack of site-specific information, it is reasonable to use generic values; however, they may not be representative

of arid conditions that exist in southern Nevada. The selected factors are expected values and have not been arbitrarily increased for conservatism. These factors are varied by using scale factors derived from a review of the applicable uncertainty factors provided in relevant reference material (International Union of Radioecologists, 1989) as discussed in LaPlante and Poor (1997). For a given realization, the sampled value for each scale factor (plant uptake scale factor, animal uptake scale factor) adjusts the tabulated expected values of transfer coefficients by the same amount. Because transfer coefficients vary across radioelements and food product types to different degrees, the implementation of the scaling approach in DCAGW is a simplification that implicitly assumes correlations among transfer coefficients, which may result in higher estimated doses.

- Food consumption rates for the default adult receptor are based on a survey of Amargosa Valley residents (Civilian Radioactive Waste Management System, Management & Operations, 2000). The survey provides the best available information on local food consumption practices. The consumption rates are representative of average consumption practices of residents who have food gardens that supply a portion of the food consumed annually. Consumption rates applicable to the default adult receptor are provided in appendix A. Age-dependent consumption rates are also provided in appendix A. It is recommended that the age-dependent values be used for comparison purposes only. Comparison dose calculations should not be done between the adult based in ICRP Publication 72 (International Commission on Radiological Protection, 1996) and the default adult based on FGR 11 (U.S. Environmental Protection Agency, 1998) because the dosimetry models employed for these receptors are not comparable.

- For human dosimetry modeling, the average member of the receptor group is an adult consistent with the EPA proposed Federal Radiation Protection Guidance for Exposure of the General Public (U.S. Environmental Protection Agency, 1994). The individual is presumed to have physiology consistent with the assumptions of reference man (International Commission on Radiological Protection, 1975). Age-dependent dose coefficients for alternative receptors are from ICRP Publication 72 (International Commission on Radiological Protection, 1996). The source materials (International Commission on Radiological Protection, 1996) should be consulted for a detailed description of dosimetry assumptions used for the age-dependent dose coefficients.

- Internal DCFs for DCAGW are calculated using dose coefficients consistent with Federal FGR 11 (U.S. Environmental Protection Agency, 1988) for the default adult receptor and ICRP Publication 72 (International Commission on Radiological Protection, 1996) for all other age-dependent receptor groups. Where choices for lung classes and blood uptake fractions exist, dose coefficients that result in the highest doses are used. The rationale for using the highest internal dose coefficient values for DCAGW is that, in general, the contaminant chemical species most soluble in water, and thus most likely to transport in groundwater to the receptor group, fall within the same chemical classes associated with the greatest internal dose coefficients. Therefore, the high-dose coefficients are based on chemical classes that are generally consistent with expected chemistry of transportable radioactive contaminants. External DCFs are calculated using dose coefficients that are consistent with FGR 12 (U.S. Environmental Protection Agency, 1993).

- Inhalation and external exposure times are based on generic information provided in Kennedy and Strenge (1992). For the farming group, 55 percent of total time is assumed to be spent inside the residence, 20 percent outside of residence, 24 percent at offsite work, and 1 percent gardening and farming alfalfa, which is not a labor intensive crop to farm. These activity times are considered conservative for a common residential setting (Kennedy and Strenge, 1992) but may not be for a more active farming resident.

- Resuspension of contaminated soil applies to crop deposition, inhalation, and external dose modeling. A mass loading model is applicable to a homogeneously mixed layer of contamination in the soil, and, therefore, a reasonable mass loading factor from a review of applicable literature is used (Rognon, 1991; Tegen and Fung, 1994; Anspaugh et al., 1975; Soldat et al., 1973; and Sehmel, 1977). For crop deposition, the GENTPA Version 1.0 code uses a resuspension model with the selected mass loading factor being converted to a resuspension factor using an equation presented in the GENII-S user manual (Napier et al., 1988). The mass loading and resuspension models are abstractions of complex and varying processes. Thus, considerable uncertainty exists in applying them to YM conditions.

- For pluvial climate conditions, the biosphere is assumed similar to that of northern Nevada and southeastern Idaho. These areas have average annual rainfall and monthly temperature profiles similar to predictions of future YM climate made from analysis of local paleoclimatic studies (U.S. Nuclear Regulatory Commission, 1997).

- Use of a concentration of radionuclides uniformly mixed in water for household and agricultural needs of the critical group is assumed appropriate for estimating doses to the average member of the critical group. Although some variation in concentrations would be expected between specific locations and well characteristics, assuming all crops within the farming community are irrigated with water containing radionuclides, a concentration uniformly mixed in the volume pumped by the farming community is considered a reasonable approach for estimating average exposure conditions.

- Age-dependent consumption rates and ranges were derived from information provided in the EPA Exposure Factors Handbook (U.S. Environmental Protection Agency, 1997), which summarizes a large amount of information on U.S. food consumption. The handbook draws on information from peer-reviewed, scientific literature and nationwide population surveys conducted by the U.S. Department of Agriculture (1992). Because food consumption patterns change over time, values were selected from the most recent data sources reported in the EPA Exposure Factors Handbook. In some cases, the reported age ranges in the handbook did not exactly match the age groups used for this analysis. The data, however, were found to be generally consistent with the age groups. For some reported values, age categories were collapsed by averaging the rates for two or three groups to correspond to the required age range for the analysis. Selected consumption rates are mean values except for drinking water, where a median was reported in the source data. Where information was presented by gender, the more conservative (higher) male values were selected. Standard errors were provided for a limited number of data sets, often not for the most recent data, therefore, the best available information was selected for determining distribution ranges. While EPA provides no information on the population distributions from the survey data, all were assumed lognormal because reported arithmetic

means were always well above the median, and other studies suggest consumption rates are lognormally distributed (Hoffman et al., 1982).

- Age-dependent intake parameters, provided in appendix A, assume that an infant does not eat solid food during the first 12 months of life. Most of the diet is assumed to be from consumption of baby formula mixed with water and milk. When any pre-adult receptor group is selected, all behaviors other than intake of foods and liquids (and air) are assumed to be similar to adult behaviors unless the user makes additional parameter changes. This will not affect most parameters; however, the external dose calculations are based on adult outdoor activity fractions, and these calculations are applied to all age groups unless changed. Because the external dose is a small fraction of the internal doses, using adult outdoor activity fraction should not bias results to any significant degree.

- DCAGW uses ground surface external dose coefficients directly from FGR 12 (U.S. Environmental Protection Agency, 1993). The original GENII Version 1.485 code divides the dose coefficients read from the *grdf.dat* file by 0.15 m (the depth of the contaminated soil layer) for use with volume-based dose coefficients (Napier et al., 1988). The new external dose coefficients from FGR 12 (U.S. Environmental Protection Agency, 1993) used for the TPA Version 4.0 Code are area based (ground surface). Therefore, the 0.15-m value was removed from the calculations.

# 12 DCAGW MODULE DESCRIPTION—RESIDENTIAL RECEPTOR GROUP

The DCAGW module calculates annual TEDE to an average member of a receptor group from exposure to radionuclide concentrations in groundwater. The receptor group can be either a farming group or a residential group. The primary differences in the calculation of the dose to these two groups are that a different model is used to determine the concentration of radionuclides in the well water, and more pathways are considered for the farming group. The models and assumptions used to calculate the dose to the residential receptor group are described in this section, while the models and assumptions used to calculate the dose to the farming receptor group are described in chapter 11.

## 12.1 INFORMATION FLOW WITHIN TPA

### 12.1.1 Information Supplied to DCAGW

DCAGW receives information passed from the EXEC and various data files so dilution and dose calculations can be executed. For dilution calculations, time-varying release rates computed in SZFT for each radionuclide released through groundwater are passed to DCAGW by EXEC. Radionuclide concentrations in groundwater are calculated from the release rates using the dilution volume and the mass fraction of the groundwater contaminant plume captured by an average member of the residential receptor group. For the dose calculations, important reference biosphere and receptor group parameters are sampled in EXEC from the *tpa.inp* file and passed to DCAGW. The remaining dose parameters are constants but can be modified by editing the *ggenii.def* and *gdefault.def* files (shown in appendix G). A list of default parameter values for the *tpa.inp* file is provided in appendix A.

For less than 20 km from the site, a detailed calculation is used to determine the portion of the plume that enters the residential receptor group water supply. Parameters that specify the pumping rates of the residential receptor group, location of the receptor group, location of the conductive zone being pumped, and plume thickness are specified in the *tpa.inp* file. Other input parameters are read from the DCAGW section of the *tpa.inp* file. Residential receptor parameters entered in the *tpa.inp* file are written to the *ggenii.inp* file.

A number of default data files provide important information for the calculations in GENTPA Version 1.0 code. For the drinking water calculations applicable to a residential receptor, these files include: *ggenii.def* (primary input parameter file), *grmdlib.dat* (radionuclide library), *gnewdf.dat* (inhalation and ingestion dose coefficients), and *filename.dat* (data file directory structure). These files relate to the following files used for the GENII Version 1.485 code: *genii.in*, *rmdlib.dat*, *dosinc.dat*, and *filename.dat* (Napier et al., 1988). Modifications to these data files for TPA include the addition of $^{108m}$Ag and the relevant physical information to the *grmdlib.dat*. file. The dose coefficient data file *gnewdf.dat* to calculate DCFs from intakes provided by the *env.exe* program replaces the use of the *dosinc.dat* file and the *dose.exe* program from GENII Version 1.485 code. Unlike the *dosinc.dat* file, the data file *gnewdf.dat* can be read and edited by the user when updates are needed. The *gnewdf.dat* file contains age-dependent dose coefficients as well as adult (default) dose coefficients. The *filename.dat* file is necessary for GENTPA Version 1.0 code to execute correctly; however, it is not anticipated the user will need to modify this file for TPA use.

### 12.1.2 Information Provided by DCAGW

The groundwater pathway dose for each radionuclide as a function of time is passed to EXEC. The dose results are applicable to the receptor age group selected in the *tpa.inp* file: infant, toddler, pre-teen, teen, or adult based on ICRP Publication 72 (International Commission on Radiological Protection, 1996) or an alternate adult selection based on FGR 11 (U.S. Environmental Protection Agency, 1988).

## 12.2 INTERMEDIATE RESULTS

Groundwater pathway DCFs used in determining doses from radionuclide concentrations for a residential receptor group located less than 20 km from YM, coincident with the location of the groundwater releases, are contained in two data files: *gw_cb_ci.dat* and *gw_pb_ci.dat*. Each file pertains to different climatic conditions (either current biosphere, designated by *cb*, or pluvial biosphere, designated by *pb* in file names).

The groundwater doses for all radionuclides can be accessed in the *npkdoset.res, npkdst_c.res, gwpkdos.res,* and *gwpkdos_c.res* files. The *npkdoset.res* and *npkdst_c.res* files provide the peak groundwater dose and the time of the peak dose for each radionuclide. The overall peak groundwater dose from all nuclides, the time of the peak dose, and the contribution to the peak groundwater dose from each radionuclide are contained in the *gwpkdos.res* and *gwpkds_c.res* files. Also, the time history of total dose from the groundwater is included in the *totdose.res* and *totdos_c.res* files along with the dilution volume used in calculating concentration at the wellhead. The *npkdoset.res, npkdst_c.res, gwpkdos.res, gwpkds_c.res, totdose.res,* and *totdos_c.res* files are described in detail in tables 20-1 and 20-2.

When the append option is turned on in the *tpa.inp* file to create additional intermediate outputs, DCAGW inputs are written to the *dcagw.ech* file and outputs to the *dcagw.rlt* file. The SZ releases from SZFT for all times are included in the *dcagw.ech* file. The time history of groundwater doses for all radionuclides and the plume mass fraction captured are available in the *dcagw.rlt* file. Additionally, groundwater doses can be accessed in the *rgwna.tpa, rgwnr.tpa, rgwsa.tpa, rgwsr.tpa,* and *rgwgssa.tpa* files. The file *genv.cum* provides radionuclide specific intakes (Ci/yr) for each realization by pathway including leafy vegetables, other vegetables, fruit, grain, beef, poultry, milk, eggs, drinking water, and inhalation. For the residential receptor, only the drinking water pathway applies. The file *ggenii.cum* contains the input parameter echo from GENTPA for all realizations. This input parameter echo can be used to verify the parameters used in the DCF calculations for each realization (note in the current implementation the default data file echo will not be correct). The *dcf.cum* file echoes the contents of the *gw_cb_ad.dat* and *gw_pb_ad.dat* files for each realization. A complete description of these files is provided in section 20.3 and table 20-6.

## 12.3 CONCEPTUAL MODEL

The dilution volume at the pumping well is calculated using intermediate results and parameters specified in the *tpa.inp* file. However, the user has the option of specifying a value for the dilution volume by activating a flag in the *tpa.inp* file. In the dilution volume calculations, the DCAGW module uses the water use characteristics of the residential receptor group. The receptor group is represented by a residential community at a distance less than 20 km from YM. Once the pumping volume is determined, the module converts the activity per unit time values calculated by SZFT to activity per unit volume of water using a

site-specific mass fraction of radionuclides captured by the receptor group. DCFs are then calculated and used to determine dose to the average member of the residential receptor group. The streamtube information used in SZFT and the DCF files are tied to the location of the receptor group. Therefore, any change to the location of the receptor group must be consistent with the streamtube data files.

For each timestep, the products of each radionuclide concentration and DCF are summed within and among groundwater pathways and radionuclides to calculate total doses. In addition to summary doses, selected output is stratified by realization, timestep, and radionuclide. The EXEC uses results from all realizations to identify and report peak doses. The output files indicate which age group has been selected for the calculations.

### 12.3.1 Development of Radionuclide Concentrations in Water for a Residential Receptor Group

At the residential receptor group location (assumed between 5 and 20 km from YM), the fraction of the radionuclide plume captured in the well withdrawal is either calculated or specified by the user when a flag is activated in the *tpa.inp* file. The calculation for determining the fraction of the radionuclide plume captured uses sampled values of well discharge, aquifer thickness, and plume thickness, steady-state well hydraulics equations are solved to determine the fraction of the radionuclide plume that is captured. Borehole concentrations at the residential location are computed by multiplying the radionuclide release rate by the capture fraction and dividing the product by the volumetric flow rate for the well.

It is assumed the tuff aquifer extends from below the repository to the residential receptor location, and is homogenous and isotropic with a hydraulic conductivity of 1 m/d and a regional gradient of 0.00125. The radionuclide plume in the SZ below the repository is assumed to have a width equal to the width of the four streamtubes described in section 10.7. It is also assumed that all wells have an effective radius of 0.254 m.

After sampled values are obtained for the volumetric flow rate at the well and the thickness of the aquifer, an estimate of the appropriate well screen length is interpolated from a table of values determined using Thiem's equations for steady state, confined radial flow (Lohman, 1972), and Muskat's adjustment for partially penetrating wells (McWhorter and Sunada, 1977). Using the analytic element model GFLOW (Haitjema, 1995), tables of capture zone thickness and capture zone width, as functions of pumping rate and aquifer thickness, were constructed. After interpolated values of capture zone thickness and width are obtained from the look-up tables for the sampled pumping rate and aquifer thickness, the fraction of mass captured is determined using one of three procedures listed.

- If the screen length is greater than the sampled plume thickness, or if the capture zone thickness is greater than 90 percent of the aquifer thickness, the fraction of mass captured is equal to the ratio of the capture zone width to the plume width.

- If the screen length is less than the plume thickness, but the capture zone thickness is greater than the plume thickness, the fraction of mass captured is equal to the ratio of the capture area within the plume to the cross-sectional area of the plume. The capture area within the plume is composed of two parts: (i) that portion of the plume lying above the bottom of the well screen and (ii) that portion of the half-elliptical section of the capture

zone that lies below the bottom of the well screen and above the lower vertical extent of the plume.

- If the screen length and capture zone thickness are less than the plume thickness, the fraction of the mass captured is equal to the ratio of the cross-sectional area of the capture zone to the cross-sectional area of the plume. The capture area within the plume is composed of two parts: (i) that portion of the plume lying above the bottom of the well screen and (ii) the area of the half-elliptical section of the capture zone that lies below the bottom of the well screen.

The radionuclide concentration at the wellhead is computed by multiplying the radionuclide activity release rate by the fraction of mass captured and dividing this product by the volumetric pumping rate.

It is assumed that all water at the residential receptor group location is supplied by a single, partially penetrating well in an aquifer of specified thickness. Pumping rates are sampled from a uniform distribution with a range of $1.5 \times 10^4$ to $2.64 \times 10^5$ gal. per day (gpd). The minimum value for the distribution is based on a community with a population of 100 persons with a per capita daily water use of 150 gal., while the maximum value is based on a community of 880 persons with a daily per capita water use of 300 gal.[1,2] The range of 150–300 gpd encompasses local estimates of per capita water use: (i) 210 gpd for Nye County (Basse, 1990); (ii) 182 gpd from 1995 metering for Beatty, Nevada (Buqo, 1996); and (iii) 319 gpd by assuming 1 ac-ft/yr and 2.8 people per household for Amargosa Valley, Nevada (Buqo, 1996).

Data from flowmeter surveys conducted at boreholes penetrating the saturated tuffs at YM indicate that flow is confined to a few, relatively thin, interconnected fracture zones. In conformance with the assumptions underlying the vertically averaged, 2D flow model used to define the flow tubes in SZFT, it is assumed these highly conductive fracture zones can be represented by an equivalent aquifer. At YM the saturated tuffs are divided into two fractured tuff aquifers separated by an aquitard composed of bedded ash-fall tuffs. The upper volcanic aquifer is composed of the Topopah Spring member of the Paintbrush Group and is underlain by the upper volcanic confining unit composed of the Calico Hills Formation, which is, in turn, underlain by the lower volcanic aquifer composed of the Prow Pass, Bullfrog, and Tram members of the Crater Flat Group (Luckey et al., 1996). These hydrogeologic units are separated from the underlying Paleozoic carbonate aquifer by the lower volcanic confining unit composed of the Lithic Ridge tuff and older tuffs (Luckey et al., 1996).

As noted in Luckey et al. (1996), the upper volcanic aquifer is present east of YM at water supply wells J-12 and J-13, where 70 percent of the aquifer is saturated, south of YM near boreholes USW WT#11 and UE-25 WT#12, where the lower 8–15 percent of the aquifer is saturated, and in Crater Flat at VH-1 where the aquifer is fully saturated. In the region immediately below the proposed repository, only the lower volcanic aquifer is saturated. Therefore, radionuclides released from the repository will most likely be transported within the lower volcanic aquifer until they encounter major north-trending faults across which there is significant offset of hydrostratigraphic units. Although site-scale transport modeling studies (Baca et al., 1996; Cohen et al., 1997) indicate that faults may have a significant effect on the vertical and horizontal spreading of the radionuclide plume, these effects were not incorporated into the SZFT or

---

[1]Per capita daily water use for Tucson, Arizona, is 149 gal. [table 5-16, p. 319 (van der Leeden et al., 1990)].

[2]Per capita daily water use for Las Vegas, Nevada, is 300 gal. [table 5-16, p. 319 (van der Leeden et al., 1990)].

DCAGW modules. It is assumed, however, that the upper and lower volcanic aquifers function as a single composite aquifer. It is also presumed that vertical mixing in this composite tuff aquifer is greater than would be expected in a relatively homogeneous sand and gravel aquifer owing to heterogeneities at a variety of scales.

Data from Luckey et al. (1996) indicate that the composite saturated thickness of the upper and lower volcanic aquifers ranges from 337 to 719 m. It is therefore assumed that the aquifer thickness is uniformly distributed with a minimum of 300 m and a maximum of 700 m.

Compilations of dispersivity values estimated from laboratory and field data suggest that longitudinal dispersivity is approximately equal to one-tenth of the distance traveled by the contaminant plume (de Marsily, 1986). Data compiled by Gelhar et al. (1992) suggest that horizontal transverse dispersivities are an order of magnitude smaller than longitudinal dispersivities, and vertical transverse dispersivities are one to two orders of magnitude smaller than horizontal transverse dispersivities. The length of the mean particle trajectory from the repository to a 5-km boundary is approximately 7 km. Using the empirical method suggested previously, the estimated vertical transverse dispersivity ranges from 7 to 70 m. In the final report of the Saturated Zone Flow and Transport Expert Elicitation Project (Geomatrix Consultants, Inc., 1998), one member of the expert panel (Lynn Gelhar) estimated a mean (geometric) longitudinal dispersivity of 50 m, but estimated that the mean (geometric) horizontal transverse dispersivity is 0.5 m and the vertical transverse dispersivity is 0.005 m. Gelhar's estimates of transverse dispersivity were primarily based on data from the Cape Cod and Borden test site experiments, which were both conducted in relatively homogeneous sand and gravel aquifers (Geomatrix Consultants, Inc., 1998) and may be too small to apply to the complex fractured and faulted tuff units at YM.

Assuming a mean Darcy velocity of 0.46 m/yr, kinematic porosities ranging from 0.001 to 0.01, a plume trajectory 7 km in length, and vertical transverse dispersivities ranging from 7 to 70 m, the one standard deviation vertical spreading thickness ($\sigma_z$) of a point source Gaussian plume at a 5-km receptor location varies from 104 m to 330 m.[3] Using the same calculational procedure but substituting the vertical transverse dispersivity estimate of 0.005 m provided by Gelhar, the one standard deviation vertical spreading thickness is 8.4 m. Because there are no site-specific data for vertical transverse dispersivities, it is extremely difficult to select an appropriate distribution for the thickness of the plume at the receptor location. Although it may appear to be conservative to select a distribution of plume thicknesses that maximizes the likelihood that a low-discharge well captures the entire plume, even the smallest pump discharge rate considered ($1.5 \times 10^4$ gpd) creates a capture zone more than 150 m thick. Based partly on the bounding calculations described previously and on a need to account for variability in this important parameter, plume thickness was assumed to be uniformly distributed between 10 and 100 m. Although this analysis at 5 km was used in determining *tpa.inp* parameters, the same methodology applies to all distances of the residential group in the TPA Version 3.2 code.

## 12.3.2 Calculation of Dose Conversion Factors

The DCAGW module contains an executable pathway dose code GENTPA Version 1.0 code based on the GENII Version 1.485 code (Napier et al., 1988) that generates radionuclide and pathway specific

---

[3] $3\sigma_z = \left(2\alpha_z vT\right)^{1/2}$, where $\alpha_z$ is the vertical dispersivity, $v$ the linear groundwater velocity, and $T$ the mean travel time.

annual intake rates for the selected receptor age group. DCAGW uses the intake rates to calculate DCFs designed to convert groundwater concentrations to TEDEs for the average member of the receptor group. DCAGW multiplies the intake rates from GENTPA Version 1.0 code to the applicable dose coefficients in the *gnewdf.dat* file to generate the DCFs. Selection of the desired age category in the *tpa.inp* file ensures the correct age-dependent input parameters (e.g., consumption rates from the *tpa.inp* file) and dose coefficients (from the *gnewdf.dat* file) are used to calculate DCFs.

The default age group is an adult based on inhalation and ingestion dose coefficients provided in FGR 11 (U.S. Environmental Protection Agency, 1988). All other receptor age group calculations use inhalation and ingestion dose coefficients from ICRP Publication 72 (International Commission on Radiological Protection, 1996). ICRP Publication 72 (International Commission on Radiological Protection, 1996) provides inhalation and ingestion dose coefficients for the following age groups: 3 mo, 1 yr, 5 yr, 10 yr, 15 yr, and adult. For TPA modeling , the coefficients were assumed to relate to the midpoints of following age ranges: <1 yr, 1–3 yrs, 3–7 yrs, 7–12 yrs, 12–17 yrs, and >17 yrs. Considering the age stratification of available age-dependent consumption rate information (discussed below), the ICRP-based age groups were collapsed into five groups: <1 yr, 1–7 yrs, 7–12 yrs, 12–17 yrs, and >17 yrs. Dose coefficients for 1–3 yrs and 3–7 yrs were averaged to combine the categories into one. The resulting age groups were given the following titles: Infant, Toddler, Pre-Teen, Teen, and Adult. Information on the age group classifications is summarized in table 12-1. Based on ICRP Publication 72 (International Commission on Radiological Protection, 1996), the adult age category (17 yr and above) dose coefficients are provided to allow comparison of adult doses with pre-adult age group doses using consistent dosimetry methodology. For all other adult dose calculations, the FGR 11 dose coefficients (U.S. Environmental Protection Agency, 1988) are recommended.

Site-specific information indicates that residential dwellings exist down-gradient of YM. Two climate regimes are assumed for the biosphere in the TPA Version 4.0 code. For the residential exposure group, the exposure pathway (drinking water) is not expected to be affected by the predicted biosphere changes. Thus, no biosphere variations are included in the exposure pathway calculations for this receptor group. The following assumptions apply to the residential receptor group. The residential exposure pathways are limited to groundwater consumption. Water pumped from a well is consumed at a rate of 2 L/d; however, TPA provides the flexibility for the user to sample or change the value of this parameter. Additional details of methods and assumptions used in the exposure scenarios for DCF calculations are provided in the succeeding sections and in LaPlante and Poor (1997).

## 12.4 ASSUMPTIONS AND CONSERVATISM OF DCAGW APPROACH

The DCAGW module for the residential receptor group converts groundwater radionuclide concentrations to residential receptor dose. Therefore, the module involves assumptions about (i) the location of the receptor group, (ii) the lifestyle characteristics of the receptor group that form the basis for exposure pathways, (iii) the conversion of intake to dose, and (iv) well pumping rates.

The residential receptor is based on an assumption that local topography and the economics of groundwater extraction allows for a potential nonfarming residential receptor group to exist closer to the potential repository site than a farming receptor group. Because this assumption relates to potential human behavior, it is speculative.

**Table 12-1. Categories used for age-dependent dose calculations for residential receptor group**

| Age Group | Age (y) |
|---|---|
| Infant | <1 |
| Toddler | 1–7 |
| Pre-Teen | 7–12 |
| Teen | 12–17 |
| Adult | greater than 17 |

Dose calculation involves consideration of only the drinking water ingestion dose pathway because this pathway is the primary route of exposure for residential uses. Other household uses are not included in the dose calculation because it is assumed the ingestion dose will far exceed that caused by bathing and other uses.

The drinking water dose is calculated from the well head concentration, drinking water consumption rate, and the ingestion dose conversion factor. The consumption rate is assumed conservatively to be 2 L/d and the default adult dose coefficient is from FGR 11 (U.S. Environmental Protection Agency, 1988). Age-dependent dose coefficients for alternative receptors are from ICRP Publication 72 (International Commission on Radiological Protection, 1996).

The source materials (International Commission on Radiological Protection, 1996) should be consulted for a detailed description of dosimetry assumptions used for the age-dependent dose coefficients.

The range of pumping rates for the residential community is based on a population assumed to vary from 100 to 880 persons, having a per capita daily water use that varies from 150 to 300 gal. Corresponding daily well discharge rates for the residential receptor location vary from 57 to 1,000 $m^3/d$. Analytical methods are used to calculate the fraction of the radionuclide plume of a given thickness that would be captured by a single well having the sampled daily discharge rate. Borehole radionuclide concentrations are calculated by dividing the product of the radionuclide mass release rate and the fraction captured by the well discharge rate.

There are specific assumptions and conservatism in DCAGW:

- For human dosimetry modeling, the average member of the receptor group is an adult consistent with the EPA proposed Federal Radiation Protection Guidance for Exposure of the General Public (U.S. Environmental Protection Agency, 1994). The individual is presumed to have physiology consistent with the assumptions of reference man (International Commission on Radiological Protection, 1975). Age-dependent dose coefficients for alternative receptors are from ICRP Publication 72 (International Commission on Radiological Protection, 1996). The source materials (International Commission on Radiological Protection, 1996) should be consulted for a detailed description of dosimetry assumptions used for the age-dependent dose coefficients.

- Internal DCFs for DCAGW are calculated using dose coefficients consistent with FGR 11 (U.S. Environmental Protection Agency, 1988) for the default adult receptor and ICRP Publication 72 (International Commission on Radiological Protection, 1996) for all other age-dependent receptor groups. For radionuclides where choices for blood uptake fractions exist, the dose coefficients that result in the highest doses are used. The rationale for using the highest internal dose coefficients for DCAGW is that, in general, the contaminant chemical species most soluble in water and, thus, most likely to transport in groundwater to the receptor group, fall within the same chemical classes associated with the greatest internal dose coefficients. Therefore, the high dose factors are based on chemical classes generally consistent with expected chemistry of mobile radioactive contaminants. External DCFs are calculated using dose coefficients that are consistent with FGR 12 (U.S. Environmental Protection Agency, 1993).

- Use of a uniform radionuclide concentration in drinking water is assumed to be appropriate for estimating doses to the average member of the critical group. Although some variation in concentrations would be expected between specific locations and well characteristics, a uniform concentration in the volume pumped by the residential community is considered a reasonable approach for estimating average exposure conditions.

- Age-dependent drinking water consumption rates and ranges were derived from information provided in the EPA Exposure Factors Handbook (U.S. Environmental Protection Agency, 1997), which summarizes a large amount of information on U.S. consumption behaviors. The information on tap water consumption rates was primarily from peer reviewed scientific literature. Reported age ranges in the handbook did not exactly match the age groups used for this analysis but were generally consistent. Selected consumption rates for tap water are median values reported in the source data. Tap water consumption was assumed to be distributed lognormally among the population as reported in the source literature (Roseberry and Burmaster, 1992).

# 13 FAULTO MODULE DESCRIPTION

The FAULTO module determines the number of WP failures from direct fault disruption of the proposed repository block. The number, location, and time of WP failures are made available to EBSREL. Additional information about FAULTO and the stand-alone FAULTING code can be found in Ghosh et al. (1997, 1998). As described in chapter 2, a faulting event does not disturb the thermohydrological characteristics of the proposed repository.

## 13.1 INFORMATION FLOW WITHIN TPA

### 13.1.1 Information Supplied to FAULTO

The user selects the faulting disruptive event module in the *tpa.inp* file. Other FAULTO input parameters, including time of the event and fault length and width, are specified in the FAULTO section of the *tpa.inp* file.

### 13.1.2 Information Provided by FAULTO

FAULTO passes a time history of WP failure from faulting events for all subareas to EXEC for subsequent use in radionuclide release calculations in EBSREL.

## 13.2 INTERMEDIATE RESULTS

Information on WP failures caused by faulting and the time of the event are available in the *wpsfail.res* file. The *wpsfail.res* file is described in detail in tables 20-1 and 20-2.

When the append option is turned on in the *tpa.inp* file to create additional intermediate outputs, FAULTO inputs are written to the *faulto.ech* file, and outputs are written to the *faulto.rlt* file. The TPA time steps are set in the *tpa.inp* file, and the number of subareas are included in *faulto.ech*. The fraction of WPs failed by faulting events for all time steps is provided in the *faulto.rlt* file. A complete description of these files is presented in section 20.3.

## 13.3 CONCEPTUAL MODEL

FAULTO evaluates the potential for direct WP rupture from fault displacement along planar decoupled faults. In the code, faults are considered zones or bands of deformation with a finite width. WPs within these zones are assumed damaged, provided the fault slip exceeds a threshold displacement value. It is assumed that WP emplacement in the proposed repository will be appropriately set back from those faults known to present a potential hazard and that a minimum amount of fault displacement is needed to disrupt a WP. Thus, FAULTO is designed to evaluate hazards related to faults not accounted for in the proposed repository design such as (i) new faults, those that may form during the period of concern; (ii) hidden faults, those within the proposed repository presently unknown and unmapped; or (iii) underestimated faults, those mapped faults not considered significant during design or construction that pose a significant risk over the lifetime of the proposed repository.

The code initiates a new fault zone within the proposed repository based on geometric and recurrence parameters sampled from a series of PDFs. Geometric parameters include fault-zone location, orientation, strike, length, width, and displacement. Recurrence parameters include recurrence rate, time of faulting event, and cumulative displacement rate. Although in nature these geometric and recurrence properties may be related (i.e., longer faults seem to correlate with wider deformation zones or bigger faults tend to be more active), for simplicity they are specified as independent parameters in the TPA Version 4.0 code.

In FAULTO, parameters describing future faulting events in the repository are sampled independently and the effective recurrence rate is sampled from a single exponential distribution. Calculating the effective recurrence interval within the repository boundary is not straightforward because, unlike point-source events, fault zones are tabular volumes with planar boundaries that have orientation, length, and width. Moreover, both fault orientation, fault length, and fault width have their own PDFs. Recurrence rate, therefore, does not scale directly with change in simulation area. There is a critical simulation region (CSR) below which the recurrence interval does not increase in proportion to the reduction in the size of the simulation area. If the simulation region is smaller than the critical area, a fault could still initiate outside the area and have the necessary length and orientation to intersect the proposed repository. To overcome this problem, an empirical solution uses an area of interest larger than the repository footprint. This approach is described in the following paragraphs.

The CSR for faulting was developed to include the range of fault orientations and length of faults (e.g., the fault map of Simonds et al., 1995). Approximately 90 percent of the faults have lengths of 30 km or shorter or half lengths of 15 km or shorter. In addition, fault orientations range between N55 ° W (azimuth 305°) and N25° E (azimuth 25°). Given these constraints, the size of the CSR is 15.2 km × 32.8 km. The ratio of the CSR area to the area used to estimate faulting recurrence from paleoseismic studies is 2.2 (498.6 divided by 225.0). Thus, the scaled recurrence of the CSR is 5,909 yr (13,000 divided by 2.2) yielding a conditional probability for faulting of $1.69 \times 10^{-4}$/yr.

The recurrence value was then scaled to only the repository footprint using the FAULTING stand-alone code (not a part of the TPA Version 4.0 code) to empirically estimate what percentage of faults generated in the CSR would actually intersect the proposed repository given a 5,909-yr recurrence interval for the CSR. Modeling results show that an average of 3 percent of all simulated faults intersect the repository, based on a number of different realizations between 500 and 1,000,000. Thus, the recurrence for faults within the repository itself is 197,000 yr (5,909 divided by 0.03), or an annual probability (referred to as absolute probability) of $5.0 \times 10^{-6}$.

Some parameters normally used to fully describe faulting events were not used in FAULTO, including fault dip angle, number of slip surfaces, partition of fault slip among different slip surfaces, cumulative displacement rate, and cumulative displacement rate partitioned among slip surfaces. These parameters were excluded for the following reasons:

- Fault dip angle is not important because the WPs are assumed to be emplaced within a single almost horizontal horizon. Fault dips at the surface at YM are rarely less than 45°. Therefore, the problem essentially reduces to two dimensions. Variations in fault dip angle over the vertical thickness of the emplacement drifts will not affect the consequence.

- Number of slip surfaces of a fault does not affect performance because the area affected is constant and the entire fault has the same maximum displacement. The fault slip is either divided among the slip surfaces or allowed on one surface. Because the WPs are assumed

to be uniformly distributed, the area affected (fault width times the trace length of the fault within the footprint of the proposed repository)—not the exact location of the slip surface(s)—is important.

- Cumulative displacement rates for faults at YM (see table 2-4 of Ghosh et al., 1997) are too small to affect significantly the performance of the proposed repository given a 10,000-yr or even 20,000-yr period of concern.

Using the effective recurrence interval for the repository, FAULTO samples midpoint location, orientation, length, width, and displacement slip of a fault in the repository. The displacement slip is sampled from the user supplied distribution for maximum slip and is the same for the entire fault. With the orientation and width known, FAULTO calculates the intersection area of the fault with the repository. If the sampled displacement slip exceeds the threshold displacement specified by the user, all WPs in the intersection area are reported to EBSREL as having failed. Figure 13-1 illustrates a simulated fault within the proposed repository boundary. Time for WP failure is the instant the fault is generated.

## 13.4 ASSUMPTIONS AND CONSERVATISM OF THE FAULTO APPROACH

The FAULTO module is an abstracted model of the failure of WPs from instantaneous fault displacement along deep dipping, new, or inadequately characterized faults. The FAULTO module considers the (i) distribution of WPs within the emplacement drifts, (ii) fault recurrence parameters, (iii) fault geometric parameters, and (iv) fault-slip displacement and threshold displacement.

WPs are assumed to be spread uniformly throughout the repository as a first order approximation. Repository design could influence the extent to which this assumption is acceptable, but using a uniform density of emplaced WPs is acceptable to estimate the significance of fault displacement without speculating on repository design.

The time for the next faulting event is calculated from the effective recurrence rate. The effective recurrence rate has been estimated by taking into consideration the length and orientation of the mapped faults in the YM region. The critical simulation region concept, described in section 13.3, was used to estimate the annual probability of faulting in the proposed repository region at $5.0 \times 10^{-6}$. Fifty percent of faulting is assumed to occur on new faults or faults where WPs are not set back in the repository design. This assumption is conservative because most geological observations infer that large faulting events in YM will occur on known and mapped faults. For example, paleoseismic studies show that nearly all the large faults at YM produce evidence for repeated earthquake ruptures (e.g., U.S. Geological Survey, 1996; chapter 4).

The fault geometric parameters include fault midpoint location, orientation, length, and width. These parameters are generated from PDFs developed from field data. Most of the faults mapped in the YM region predominantly strike in the north-northeast direction (about 95 percent) with dip angle rarely less than 45°. As a result, variations in fault dip angle over the vertical thickness of the emplacement drifts will not significantly affect the performance. Therefore, fault dip angle was not considered in the FAULTO module.

Similarly, other parameters, such as number of slip surfaces of a fault and cumulative displacement, were ignored. It is considered a reasonable approach to drop these parameters from the module as their effects on the consequence were found to be insignificant. Mapped faults in the YMR tend to have widths

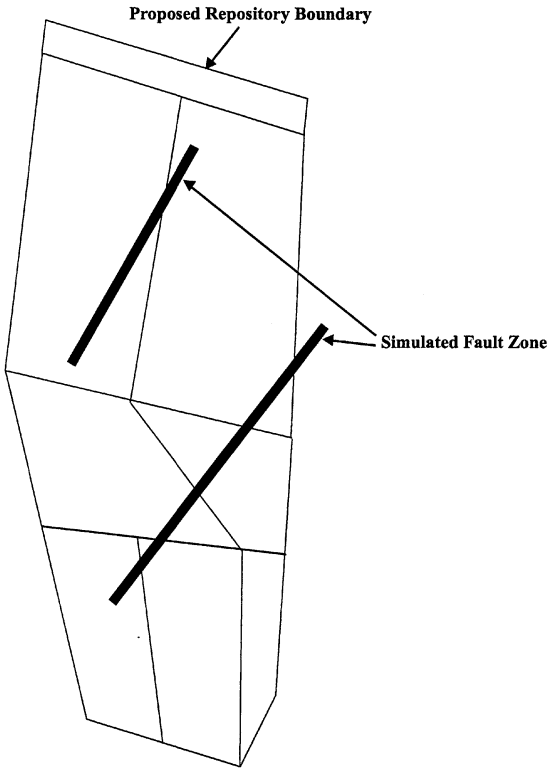


**Figure 13-1. Simulated faults within the repository boundary**

clustered around small values, although a fault may have a large width at least on the surface. A beta distribution with a small median value is considered reasonable to approximate the fault width distribution.

The fault slip displacement is sampled from the lognormal distribution of maximum slip and is considered the same for the entire fault plane. A lognormal distribution is considered a reasonable assumption to describe the distribution of fault slips observed in the YMR. In the absence of both a model transferring forces from fault displacement to emplaced WPs and a well-developed WP design, assumptions are made about the amount of fault displacement that leads to WP failure. The threshold fault displacement directly affects the WP disruption. If the fault slip exceeds the threshold value, all WPs within the repository block along the fault zone (fault length within the repository boundary multiplied by the fault width) are considered failed. The threshold displacement is an input parameter supplied by the user that reflects lack of understanding of the WP disruption process. Although the TPA Version 4.0 code does not couple the degradation of WP strength caused by corrosion and other phenomena with the threshold displacement, the approach is considered conservative because a small threshold of displacement leading to WP failure (specified in the reference data set) is believed to provide a conservative estimate of WP failure. Although WP disruption is assumed to occur only within the fault zone boundary, the assumption that all WPs within the boundary fail—if the fault displacement threshold is exceeded—is believed to provide a conservative estimate of WP failure in the absence of more sophisticated modeling.

Specific assumptions of faulting disruption effects in the FAULTO module of the TPA Version 4.0 code are listed below.

- Fifty percent of faulting is assumed to occur on new faults or faults where WPs are not set back in the repository design. This assumption is conservative.

- In FAULTO there is assumed to be no link between faulting, seismicity, and volcanism. In nature, volcanic eruptions are always accompanied by numerous pre- and syn-eruption earthquakes (Luhr and Simkin, 1993; Fedotov and Markhinin, 1983). Likewise, all faulting events that would affect the proposed repository would be accompanied by significant seismicity.

- The emplacement drifts are assumed to be randomly oriented. Most YM faults are oriented roughly north-south. If the actual emplacement drifts are subparallel to the fault trend, a much greater number of WPs will be affected by each faulting event than currently estimated in the code.

- The TPA Version 4.0 code is limited to one faulting event per realization, regardless of the selected recurrence interval. This simplification is acceptable as long as the estimate of recurrence intervals on the order of $10^5$ yr is correct, and the time period of interest is 10,000–20,000 yr. Otherwise, this limitation reduces the potential consequence of faulting and is, therefore, not conservative if the WP has not already failed by other mechanisms.

- There is no correlation among fault length, fault zone width, fault orientation, and probable displacement along the fault plane. In nature, longer faults have undergone larger displacements. Observations of fault zone widths in the YMR show that fault zone widths seem to be large for incipient faults and narrow as the fault zone matures. In the FAULTO module, fault zone widths are sampled from a broad range, including a few wider than 100 m.

- Faulting could weaken WPs and make them more susceptible to corrosion over time. To compensate for not accounting for this effect, a small threshold displacement for WP failure was used.

- WP failure in FAULTO is not linked to a WP mechanical failure approach as used in EBSFAIL. This simplification is conservative because the WP is always assumed to fail when the fault displacement exceeds a threshold value.

- All WPs intersected by the fault zone are considered failed. This conservative assumption is necessary at present because the forces WPs could encounter in fault zones are poorly understood.

- The module assumes the damage zone caused by slip along a fault is entirely restricted within the fault zone boundaries (i.e., no diffuse deformation outside the fault zone). This assumption is not conservative.

- The module does not take into account the effects of slip on a new or an uncharacterized fault caused by rupture on an existing fault in the repository region.

# 14 VOLCANO MODULE DESCRIPTION

The VOLCANO module simulates key IA processes such as (i) timing of future igneous events, (ii) subsurface area affected by a volcanic event, (iii) type of event (i.e., intrusive only or intrusive and extrusive), and (iv) number of WPs affected by intrusions extending laterally from the volcanic conduit.

## 14.1 INFORMATION FLOW WITHIN TPA

### 14.1.1 Information Supplied to VOLCANO

The VOLCANO disruptive event module is selected by the user in the *tpa.inp* file. The VOLCANO input parameters, including the minimum and maximum times of the event (the maximum specified time for volcanic events should be the same as the maximum simulation time), distributions for the number of WPs likely to fail during volcanic and intrusive events, number of possible volcanic conduits that form during an event, and number of drifts potentially affected, are specified in the VOLCANO section of the *tpa.inp* file. When only the results for the direct releases are of interest, an option is available to bypass groundwater release calculations to substantially gain computational efficiency.

### 14.1.2 Information Provided by VOLCANO

VOLCANO passes WP failure time from a volcanic event for all subareas to EXEC. VOLCANO also passes the mass of waste (in MTUs) ejected by the volcanic event for ground surface radionuclide release calculations in ASHPLUMO, and it passes the number of WPs disrupted by magma flow into repository drifts by igneous intrusions for all subareas to EXEC for groundwater source-term calculations in EBSREL.

## 14.2 INTERMEDIATE RESULTS

The volcanic event WP failure history is provided in the *wpsfail.res* file. The normalized ground surface releases presented as a CCDF are contained in the *gsccdf.res* and *gsccdf_c.res* files. The *wpsfail.res, gsccdf.res,* and *gsccdf_c.res* files are detailed in tables 20-1 and 20-2.

When the append option is turned on in the *tpa.inp* file to create additional intermediate outputs, VOLCANO inputs are written to the *volcano.ech* file and outputs written to the *volcano.rlt* file. The TPA time steps set in the *tpa.inp* file and the number of subareas are included in the *volcano.ech* file. The fraction of WPs failed by volcanic events for all time steps and the MTUs of waste ejected are available in the *volcano.rlt* file. A complete description of these files is provided in section 20.3.

## 14.3 CONCEPTUAL MODEL

Occurrence of IA is a disruptive scenario with a relatively low annual probability of occurrence but potentially high radiological dose consequences. Event processes can be broadly categorized as volcanic processes that disrupt WPs and directly transport HLW into the accessible environment via the airborne pathway and intrusive processes that enhance WP degradation but do not directly transport HLW from the repository.

In the TPA Version 4.0 code, a volcanic center is assumed to form randomly within a specified area that commonly is restricted to the center of the proposed repository block. This ensures igneous disruption is evaluated during each modeled realization. The annual probability of volcanic disruption of the proposed repository site is bounded by $10^{-7}$, which represents a reasonably conservative value based on independent analyses (U.S. Nuclear Regulatory Commission, 1999a). Probabilities at least one order of magnitude higher and lower than this value can be derived from the reviewed literature (U.S. Nuclear Regulatory Commission, 1999a). The probability of igneous intrusion, however, is likely larger by a factor of 2–5 than the probability of volcanic disruption alone (U.S. Nuclear Regulatory Commission, 1999a). The user can select the appropriate annual probability for the event being modeled in the TPA Version 4.0 code. Timing of the igneous event is determined by sampling a finite exponential distribution between 100 and 10,000 yr postclosure, using a recurrence probability of $10^{-7}$.

Two types of igneous events may be modeled in the TPA Version 4.0 code. These types are either a volcanic eruption, which intersects the repository and ejects HLW in the WPs into the air and affects other WPs through magma flow into repository drifts, or an igneous intrusion that disrupts WPs but does not directly release HLW to the accessible environment. A volcanic event always is associated with a subsurface igneous intrusion, however, an intrusive event does not require formation of a volcano at the ground surface. The user can specify the number of WPs erupted from the volcanic conduit and number of additional WPs disrupted in a drift by magma flow but not erupted directly (i.e., intrusive event). This parameterization allows the user to readily evaluate consequences for changes in repository design, in contrast to the TPA Version 3.2 code approach that calculated the number of WPs disrupted using average repository loading and simplified igneous event geometries. The user also can consider the number of drifts intersected by an igneous event or if multiple volcanic conduits are possible during a single igneous event. The user identifies what fraction of the events are volcanic with associated intrusive effects or what fraction are exclusively intrusive. In resulting risk calculations, the user will need to use the appropriate probability for intrusive or volcanic events.

Volcanic centers in nondisturbed geologic settings disrupt a finite volume of subsurface material during the emplacement and eruption of ascending basaltic magma. Work conducted at an analog volcano site in Kamchatka, Russia (Doubik and Hill, 1999), demonstrated that the roughly circular subsurface conduits associated with YMR-type volcanoes may widen to a 50±7-m diameter during late-stage disruptive events (figure 14-1a). Several of the youngest YMR volcanoes have near-vent evidence of similar, late-stage disruptive events (Doubik and Hill, 1999). In addition, the phenomenology associated with the interaction of an ascending magma with a drift(s) is a highly complex process that is incompletely understood (figure 14-1). The range of potentially impacted WPs could range from 0, when the conduit is completely within an intervening pillar, to some number greater than or equal to 1 and less than or equal to the number of WPs in the drift. The TPA code has been revised to consider a range of potential scenarios for the interaction of the magma with WPs. The user needs to consider appropriate probabilities of such interactions. The user can assume a single geometric relationship exists between conduit size and number of WP disrupted, which is the approach specified in the basecase dataset. As an alternative, the user can select how many WPs can be transported during this complex interaction process by considering (i) available number of WPs in a single drift, (ii) WP response to rapid influx of basaltic magma, (iii) timing and dimensions of resulting volcanic conduits, (iv) magma flow paths through the disrupted drift, and (v) number of WPs entrained in the flowing magma versus number of WPs disrupted but remaining in the magma-filled drift (e.g., U.S. Nuclear Regulatory Commission, 1999a). For example, using the EDA II design of 150 WPs per drift, the user can consider that ascending magma will only entrain WPs located between the point of magma intersection and the nearest end of the drift, giving 1–75 WPs potentially erupted during

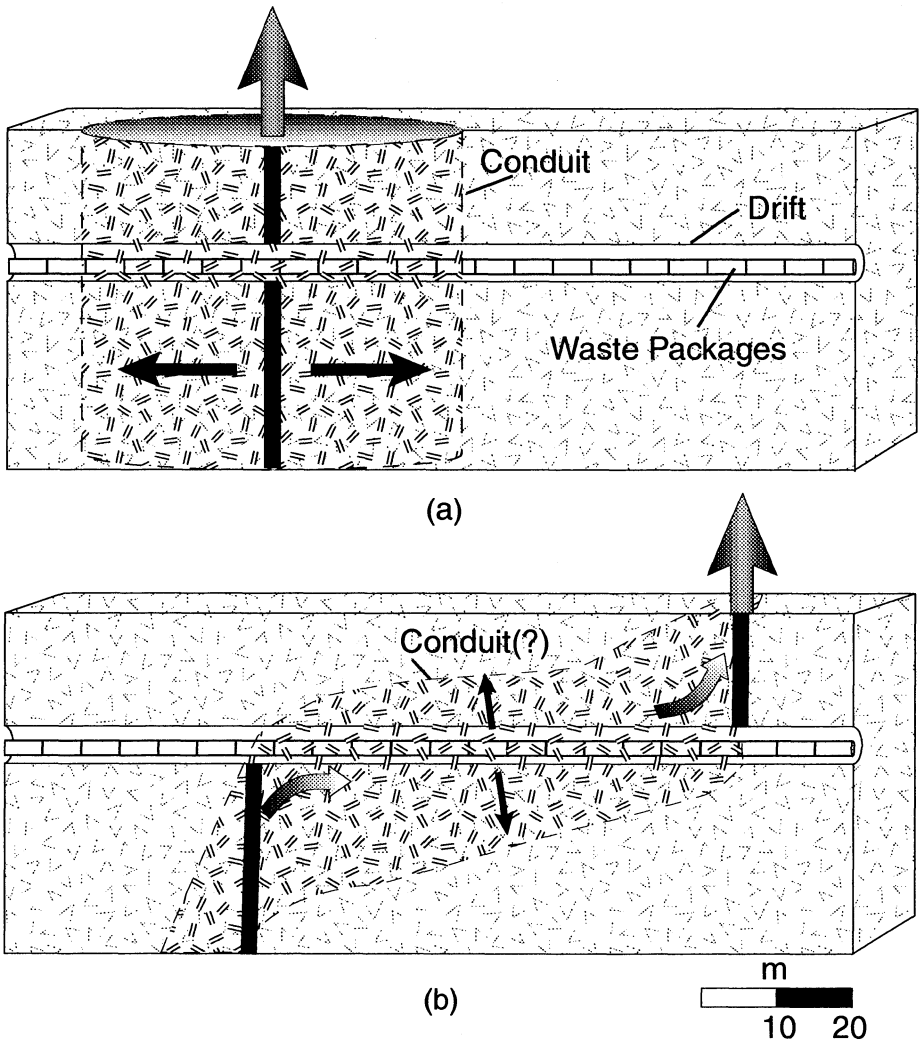


**Figure 14-1. Schematic of subsurface disruption associated with extrusive volcanic events. (a) Undisturbed geologic setting, where ascending dike (thick line) begins a cylindrical conduit that expands up to 50 m in diameter during eruption (black arrows) and entrains up to 10 waste packages. (b) Ascending dike intersects open repository drift and magma flows into drift until magma pressure exceeds strength of drift roof. Magma fractures roof and flows to surface (graded arrows), entraining waste packages along flow path. Deflected conduit may develop as eruption progresses (black arrows). Note that distance between lower and upper dike segments can range conceptually from coincident [as in schematic (a)] to opposite ends of a repository drift.**

the event, with the resulting difference from 150 equaling the number of WPs disrupted but remaining in the drift (i.e., figure 14-1b).

Subsurface igneous intrusions may extend for many kilometers from the central volcanic conduit. These intrusions may penetrate farther into the repository than the area disrupted by the volcanic conduit. Because of the significant pressure differences between ascending magma and open repository drifts, magma intersecting a drift will flow into that drift (U.S. Nuclear Regulatory Commission, 1999a). The current volume of the EDA-II repository drifts is about $4 \times 10^6$ m$^3$. In contrast, YMR Quaternary volcanoes

have eruptive volumes from about $2 \times 10^6$ m$^3$ to $1 \times 10^8$ m$^3$, with most volcanoes $\geq 10^7$ m$^3$ (U.S. Nuclear Regulatory Commission, 1999a). Thus, most prior YMR eruptions appear capable of completely filling the proposed repository drifts with basaltic magma using <10 percent of the available magma. The TPA Version 4.0 code allows the user to evaluate the effects of this process by considering a user-selected distribution of the number of WPs failed, but not erupted directly, by a repository-penetrating igneous event through multiple drifts.

Many of the <5 Ma basaltic volcanoes of the YMR are preserved sufficiently to determine that multiple conduits formed during a single igneous event (e.g., U.S. Nuclear Regulatory Commission, 1999a). In addition, multiple conduits commonly are observed during historical eruptions (e.g., 1975 Tolbachik, Doubik and Hill, 1999), and many prehistorical volcanic fields have evidence for the close spatial and temporal association of conduits during volcanic events (e.g., Conway et al., 1997). For YMR volcanoes <5 Ma with reasonable evidence of multiple conduits during a single event (i.e., Sleeping Butte, Crater Flat, Amargosa Anomaly "a"), the average spacing between conduits is 2.5 ± 1.4 km (n=8). Because the north-trending orientation of the proposed 3.7-km-long repository is coincident with the expected direction of future conduit alignment, some fraction of repository-penetrating igneous events could form at least two conduits within the repository footprint. The TPA Version 4.0 code allows the user to evaluate the effects of this process by considering a user-selected distribution of the number of WPs intersected by a volcanic conduit.

## 14.4 ASSUMPTIONS AND CONSERVATISM OF THE VOLCANO APPROACH

The VOLCANO module defines the source term for HLW transport by a basaltic volcanic eruption. The VOLCANO module determines (i) timing of the volcanic event, (ii) amount of HLW available for airborne transport by the eruption column, and (iii) number of WPs disrupted by magma but not erupted during the igneous event.

Timing of igneous events follows a temporally homogeneous Poisson distribution with a $10^{-7}$ annual probability of volcano formation for the proposed repository site. This distribution is represented in the VOLCANO module by using an exponential distribution, which is not significantly different from a Poisson distribution, for the probabilities and time-scales being considered.

The number of WPs available for airborne transport is a key parameter to evaluating risk to the critical group. Users can specify explicit probability distribution functions to represent different conceptual models for HLW dispersal. For example, assuming that a cylindrical volcanic conduit would form essentially undisturbed by the presence of open repository drifts could be represented by a uniform distribution of 1–10 WPs. In contrast, conduit disruption of some additional portion of a drift half-length could be represented by a lognormal distribution of 1–75 WP. For any distribution represented, all HLW in the disrupted WP is assumed to be available for transport, because staff have concluded that a WP likely will fail during a basaltic volcanic event (U.S. Nuclear Regulatory Commission, 1999a).

Additional WPs are likely to be disrupted by basaltic magma flowing for some distance into open or partially backfilled repository drifts. Although these additional WPs are not available for extrusive volcanic transport, HLW in these WPs are assumed to be available for subsequent groundwater release.

There are specific assumptions and conservativism in the VOLCANO module:

- Volcanic conduit is assumed to form in the center of the repository block and the stated probabilities are for volcano formation within the repository footprint.

- Timing of the volcanic event follows a Poisson distribution with a $10^{-7}$ annual probability of volcano formation for the proposed repository site, which is a reasonably conservative value (U.S. Nuclear Regulatory Commission, 1999a). This model does not consider the potential effects of repository construction and thermal loading on the distribution of rock stress, which may affect how ascending magma interacts with the local repository setting.

- Based on conservative interpretations of data and analyses presented in reports by the U.S. Nuclear Regulatory Commission (1999a) and DOE (1998, TSPA-VA), all WPs are assumed to fail when intersected by basaltic magma.

- The number of WPs disrupted during a volcanic event can be adjusted to reflect conduit formation in an essentially undisturbed geologic setting (i.e., 1–10 WPs) or to account for magma flow into repository drifts and significant modification of the conduit geometry (e.g., 1–75 WPs). Current analyses indicates the latter conceptual model may be more realistic, but the number of WPs directly erupted remains poorly constrained (U.S. Nuclear Regulatory Commission, 1999a).

- Multiple conduits may form during a single igneous event, which appears possible based on characteristics of YMR volcanoes and analogous volcanoes elsewhere (U.S. Nuclear Regulatory Commission, 1999a). Currently the basecase, however, assumes that only one conduit forms.

- Magma can flow into numerous open or partially backfilled drifts and fail an additional number of WPs. HLW from these failed WPs is not erupted during the volcanic event, but is available for subsequent hydrologic release. This process appears reasonably conservative given the large volume of basalt present during most YMR igneous events, relative to the volume of proposed repository drifts.

- In the case of an intrusive volcanic event, all WPs intersected by magma are assumed to fail simultaneously and contribute to groundwater releases.

- Consequences of intrusive processes are assumed limited to the area directly occupied by basaltic magma. The extent of processes that will likely enhance WP degradation or affect nondisturbed repository performance, such as increasing temperatures and dry out zones around intrusions (e.g., Connor et al., 1997), are not considered in the current module.

# 15 ASHPLUMO MODULE DESCRIPTION

The purpose of the ASHPLUMO code module is to estimate the deposition of both tephra (i.e., ash) and incorporated SF in mass per unit area at the point of compliance after an extrusive volcanic event has penetrated the proposed repository. The ASHPLUMO module invokes execution of the ASHPLUME stand-alone code (Jarzemba et al., 1997) in deterministic mode using input from EXEC or other modules (e.g., VOLCANO) that describe characteristics of the eruption, such as volcanic power and durations together with the size distribution of the ash particle.

## 15.1 INFORMATION FLOW WITHIN TPA

### 15.1.1 Information Supplied to ASHPLUMO

The mass of SF ejected in the volcanic event (i.e., ground surface radionuclide source term), as estimated by the VOLCANO code module, is provided by EXEC. Additionally, the ASHPLUMO module uses input values from the ASHPLUMO section of the *tpa.inp* file, including height of the eruption column, wind speed, and ash particulate characteristics, to determine the transport and deposition of radionuclides in volcanic ash.

### 15.1.2 Information Provided by ASHPLUMO

ASHPLUMO estimates the areal deposition of both ash and SF at the receptor group location that is passed to EXEC for subsequent use by the ASHRMOVO module.

## 15.2 INTERMEDIATE RESULTS

The ASHPLUMO intermediate outputs are provided in the *ashout.res* file. The contents of *ashout.res* include the time of volcanic event and the number of WPs exhumed. The *ashout.res* files are described in detail in tables 20-1 and 20-2.

When the append option is turned on in the *tpa.inp* file to create additional intermediate outputs, ASHPLUMO inputs are written to the *ashplumo.ech* file and outputs are written to the *ashplumo.rlt* file. The *ashplumo.ech* and *ashplumo.rlt* files contain the information passed between the EXEC and ASHPLUMO. The MTUs of waste ejected by the volcanic event passed from EXEC to ASHPLUMO is included in the *ashplumo.ech* file. The contents of the *ashplumo.rlt* file are values passed from ASHPLUMO to EXEC and consist of the ash and SF areal densities. A complete description of these files is provided in section 20.3.

The ASHPLUMO module generates intermediate input and output data transfer files while executing the *ashplume.f* stand-alone code. These files contain information only for the final realization available at the end of the TPA Version 4.0 code execution. The ASHPLUMO intermediate input data transfer file is *ashplume.in*. The ASHPLUMO parameters specified in the *tpa.inp* file are accessed through the *ashplume.in* file. The intermediate output data transfer file from ASHPLUMO includes the *ashplume.out* file. The ASHPLUMO outputs for the ash and SF areal densities are available in the *ashplume.f* output file, *ashplume.out*. Contents of all ASHPLUMO intermediate data transfer files are further described in appendix E.

## 15.3 CONCEPTUAL MODEL

The ASHPLUME code calculates the areal density of SF (in grams of SF per square centimeter) at points on the surface of the earth after an extrusive volcanic event penetrates the repository and exhumes SF. Using published data for wind speed at the YM site and the estimate of pertinent volcanic parameters of events similar to those that may have occurred at YM in the past, the ASHPLUME code simulates the transport of contaminated particles (composed of SF and ash) to surface points downwind. The SF concentration from deposition is provided to the ASHRMOVO code module and subsequently to the DCAGS code module for the dose calculation.

Basaltic volcanism can encompass a variety of eruption styles depending on the eruption energy. The energy of basaltic eruptions varies from effusive activity, where the predominant product is lava flows, to explosive activity, resulting in fragmentation of the magma into scoria fragments and transport of scoria in the atmosphere as pyroclasts. This latter style of activity generally results in the formation of cinder cones such as those found in the YMR. Explosive volcanic activity of this kind has the potential to cause dispersal of radionuclides through the biosphere. This dispersion of radionuclides resulting from volcanic activity is modeled in the ASHPLUME code using approaches originally developed by Suzuki (1983) to model the dispersal of ash after volcanic eruptions.

Figure 15-1 shows the exposure scenario investigated with the ASHPLUME code. The exposure scenario analyzed can be divided into four subprocesses:

(i) Magma enters the repository and becomes contaminated with SF particles

(ii) Tephra forms from the magma and SF is incorporated into the tephra (Jarzemba and LaPlante, 1996)

(iii) Eruption column and contaminant plume form and produce fallout at various distances downwind from the volcano (Suzuki, 1983; Jarzemba, 1996)

(iv) Radionuclide contamination causes doses to be incurred at receptor locations (LaPlante et al., 1995; Jarzemba and LaPlante, 1996)

Specifically, ASHPLUME addresses (ii) and (iii) from the previous list.

To assess the hypothetical radiation doses that would occur after a basaltic eruption, the distribution of SF (and, hence, radionuclides) in the biosphere after such an event needs to be estimated. It is assumed that the ash particles from the eruption are the carrier of the SF particles. Methods used previously to estimate radionuclide dispersal by volcanism (Wescott et al., 1995) theorize that the ash cloud travels in a Gaussian plume, released at a stack height of one-half of the volcanic column height. Application of the Gaussian plume model presumes that a plume of contaminants travels in the same direction as the prevailing wind (x-direction), but may be somewhat depressed toward the earth surface owing to gravitational settling. Contaminants in the plume follow a Gaussian distribution in the dimensions perpendicular to the direction of travel (y- and z-directions).

The Gaussian plume model is suitable for modeling airborne and ground concentrations of contaminants for a point source release of contaminants above the surface of the earth (i.e., the stack

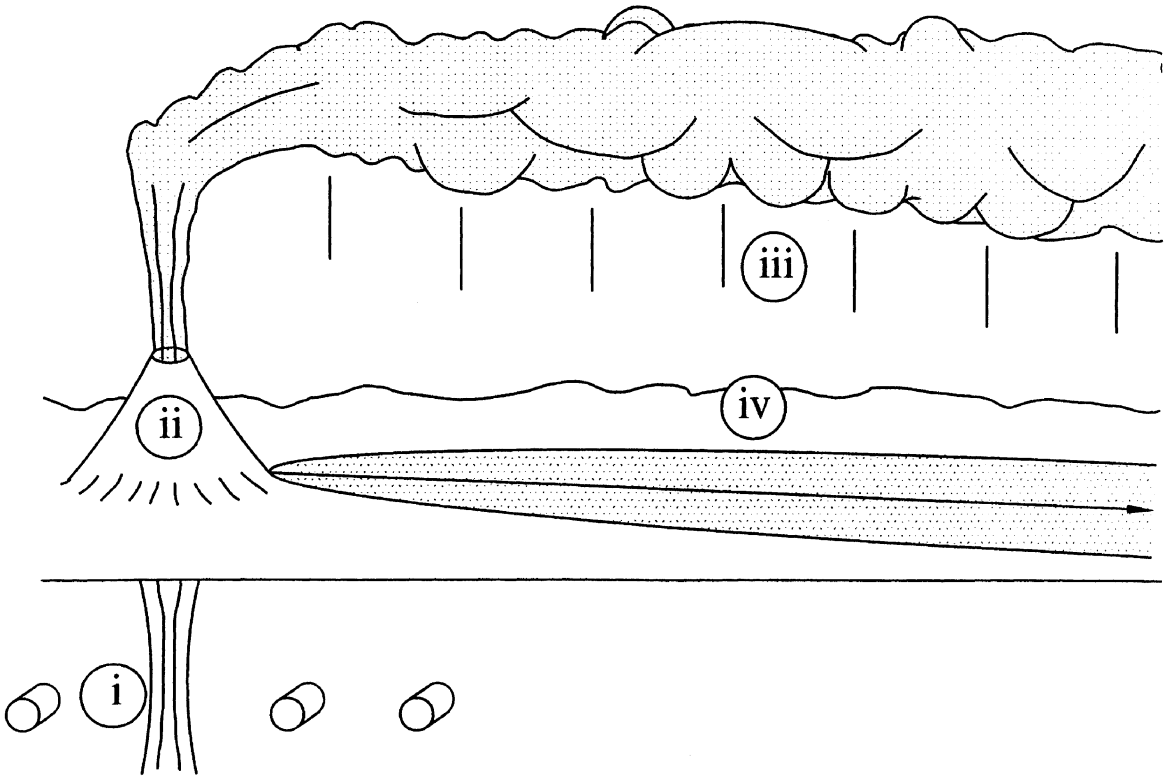


**Figure 15-1. ASHPLUMO contaminant release and deposition**

height). A point source approximation may not be appropriate for a volcanic eruption because a volcanic eruption column is a line source of contaminants in the upward direction. Also, the Gaussian plume model does not accurately account for the effects of gravitational settling of volcanic particles with large diameters (i.e., centimeters). This shortcoming may lead to the Gaussian plume model predicting much greater particle ranges than would be the case in reality and, hence, wider radionuclide distributions than would normally be expected after a basaltic eruption. This wider distribution of radionuclides may tend to underestimate the radiation exposure of persons in a receptor group.

Models to predict the distribution of ash after an eruption have been developed with the intention of relating eruption magnitude to ash dispersion (Suzuki, 1983; Hopkins and Bridgeman, 1985; Glaze and Self, 1991). The ASHPLUME code uses the model described in Suzuki (1983) that relates eruption magnitude to ash distribution, which is modified to relate eruption magnitude to SF distribution for YM based on a few simple assumptions. The model uses the power and duration of the eruption, along with other properties of the ash particulates, and develops a SF distribution from those sampled parameters. The SF distribution can be translated into the radionuclide distribution that can then be used to model dose-to-man.

The model described in Suzuki (1983) can be summarized by the equation that describes the areal density of accumulated ash on the earth surface after an eruption:

$$X(x,y) = \int_{\rho=\rho_{min}}^{\rho_{max}} \int_{z=0}^{H} \frac{5QP(z)f(\rho)}{8\pi C(t+t_s)^{5/2}} \exp\left[\frac{5\{(x-ut)^2+y^2\}}{8C(t+t_s)^{5/2}}\right] d\rho\, dz \qquad (15\text{-}1)$$

where

| | | |
|---|---|---|
| $X(x,y)$ | — | mass of ash per unit area accumulated at location $(x,y)$ [g/cm$^2$] |
| $\rho_{max}$ | — | maximum value of $\rho$ |
| $\rho$ | — | common logarithm of particle diameter d [cm] |
| $\rho_{min}$ | — | minimum value of $\rho$ |
| $H$ | — | height of the eruption column above the vent [km] |
| $z$ | — | vertical distance from the ground surface [km] |
| $Q$ | — | total quantity of erupted material [g] |
| $P(z)$ | — | function for particle diffusion at height within $dz$ about $z$ [unitless] |
| $f(\rho)$ | — | distribution function for particles with a log-diameter within $d\rho$ about $\rho$ normalized per unit mass [unitless] |
| $C$ | — | constant relating the eddy diffusivity and the particle fall time [cm$^2$/s$^{5/2}$] |
| $t$ | — | particle fall time [s] |
| $t_s$ | — | particle diffusion time in the eruption column [s] |
| $x$ | — | x-coordinate on the surface of the earth [cm]; coordinate oriented in the same direction as the prevailing wind |
| $u$ | — | wind speed [cm/s] |
| $y$ | — | y-coordinate on the surface of the earth [cm]; coordinate oriented perpendicular to the direction of the prevailing wind |

For calculation of dose, the necessary quantity to track is the mass of SF per unit area at the compliance point after ash released from the eruption that penetrates the proposed repository settles on the surface of the earth. To calculate this quantity, a model for SF incorporation into ash was created. This model requires the introduction of a function to determine the mass of fuel per unit mass of volcanic ash as a function of the log-diameter of the ash after the ash has been contaminated with SF, $[FF(\rho)]$. The volcanic ash mass is assumed to be distributed log normally:

$$f(\rho^a) = \frac{1}{\sqrt{2\pi}\sigma d} \exp\left(-\frac{(\rho^a - \rho^a_{mean})^2}{2\sigma_d^2}\right) \qquad (15\text{-}2)$$

where

$f(\rho^a)$ — normalized (per unit mass) probability distribution of ash mass as a function of $\rho^a$

$\sigma_d$ — standard deviation of the log-particle size

$\rho^a$ — log-diameter of ash particle size [cm]

$\rho^a_{mean}$ — mean of the log-diameter of ash particle size [cm]

To determine $FF[\rho^a]$, the fuel fraction (ratio of fuel mass to ash mass) as a function of $\rho^a$, one must consider that all fuel particles of a size smaller than $(\rho^a - \rho_c)$ have the ability to simultaneously be incorporated into volcanic ash particles of size $\rho^a$ or larger, where $\rho_c$ is the incorporation ratio. The fuel fraction as a function of $\rho^a$ is determined by summing all the incremental contributions of fuel mass to the volcanic ash mass from fuel sizes smaller than $(\rho^a - \rho_c)$. An expression for the fuel fraction is given as

$$FF(\rho^a) = \frac{U}{Q}\int^{\rho^a} \frac{m(\rho - \rho_c)}{1 - F(\rho)} d\rho \qquad (15\text{-}3)$$

where

$FF(\rho^a)$ — fuel fraction as a function of particle size [unitless]

$Q$ — total mass of ash ejected in the event [g]

$U$ — total mass of fuel ejected in the event [g]

$F(\rho)$ — cumulative distribution of ash mass with $\rho$

$m(\rho - \rho_c)$ — normalized probability distribution of fuel mass with $(\rho - \rho_c)$

This equation assumes the resulting contaminated particles follow the same size distribution as the original volcanic ash particles. This assumption seems reasonable because, for most events sampled in these analyses, the total mass of volcanic ash is on the order of $10^{13}$–$10^{15}$ g and for most events, only several WPs are disrupted ($10^7$ g of fuel each). For each simulation, Eq. (15-3) is numerically integrated to calculate the distribution of the SF and volcanic ash on the Earth's surface resulting from a basaltic eruption assumed to disrupt the repository. The integrand of Eq. (15-3) is multiplied by $FF(\rho^a)$ and then recalculated to find the SF density at location ($x$,$y$).

The model developed by Suzuki (1983) is appropriate for particles of mean diameter greater than about 15–30 µm. This cutoff is generally accepted to be the lower limit for the importance of gravitational settling of particles (Cember, 1983; Heffter and Stunder, 1993). For particle sizes less than about 15 µm, atmospheric turbulence is great enough to keep the particle aloft for a longer time than would be predicted

by the model. Since the typical mean diameter of ash particles after an eruption is generally much larger than 15 μm (Suzuki, 1983), this model is useful for calculating the distribution for the vast majority of ash and, hence, radionuclides released. Jarzemba and LaPlante (1996), Jarzemba (1996), and Jarzemba et al. (1997) contain more complete descriptions of the derivation, structure, and use of the ASHPLUME code and its algorithms.

## 15.4 ASSUMPTIONS AND CONSERVATISM OF THE ASHPLUMO APPROACH

The ASHPLUMO module is an abstraction of the transport of radioactively contaminated ash (i.e., tephra) from the repository located to points downwind from the event. The main processes that control the transport of SF in the ash are (i) SF particulate incorporation in the ash, (ii) dispersion in the eruption column and plume, and (iii) wind blowing ash downwind from the event.

The model in ASHPLUME for SF incorporation in ash assumes that all SF particles are eventually incorporated into larger (by a preset factor) ash particles. Actually, it is likely that only a percentage of the SF particles may be incorporated in this fashion, and some of the SF may be transported as bare particles. The conservatism of this approach is not yet known.

The transport model in ASHPLUME uses a dispersion-advection transfer function type solution, which is empirical (e.g., eddy diffusivity constant and column shape parameter). Because the solution uses empirical constants defined based on observations at analogous volcanoes, it requires that future eruptions that may occur at the repository site be similar to those observed at the present time at other locations.

The transport model in ASHPLUME as implemented in the TPA Version 4.0 code assumes the wind speed and direction do not vary during the course of the event. This is clearly a conservative assumption because variances in wind velocity during the event will lead to a wider distribution of SF than those predicted with a single velocity. The level of conservatism is unknown at this time.

In addition to those assumptions described before, the derivation of Eq. (15-1) assumes the following, which are reiterated here from Suzuki (1983):

- The distribution of the diameter of the released particles is well described by a lognormal distribution
- All particles fall at the terminal velocity and finally accumulate on the ground
- The particles have a probability of diffusing out of the column during upward travel such that the probability density distribution, *P(z)*, has the following form:

$$P(z) = \frac{\beta\, W_0\, Y \exp\left(-Y\right)}{V_0\, H\left[1-\left(1+Y_0\right)\exp\left(-Y_0\right)\right]} \tag{15-4}$$

where

$$Y = \frac{\beta W(z)}{V_0} \text{ [unitless]}$$

$Y_0$ = $\frac{\beta W_0}{V_0}$ [unitless]

$\beta$ — constant controlling the diffusion of particles out of the eruption column [unitless]

$W_0$ — volcanic eruption velocity at the vent exit [cm/s]

$W(z)$ — particle velocity as a function of height equal to $W_0(1-z/H)$ [cm/s]

$V_0$ — particle terminal velocity at sea level [cm/s]

The terms $Y$ and $Y_o$ have been modified from Suzuki (1983) where they were equal to $\beta(W(z)-V_0)/V_0$ and $\beta(W_0-V_0)/V_0$ because with the former definition of $Y$, $P(z)$ has a negative value at heights approaching the top of the column. The definition of $Y_0$ has been altered to maintain identity as the value of $Y(z)$ at $z = 0$. The modified model has been benchmarked against actual eruptions with good agreement (Hill et al., 1998)

- The distribution of SF particle diameter is well described by a log-triangular distribution
- The size distribution of contaminated ash particles is unaffected by the incorporation of SF particles

# 16 ASHRMOVO MODULE DESCRIPTION

The purpose of the ASHRMOVO module of TPA is to calculate areal radionuclide densities at the compliance point for times after a volcanic event has deposited a contaminated ash blanket. The radionuclide areal densities are greatest at the time of the event and decrease thereafter through surface erosion, leaching of radionuclides from the blanket, and radioactive decay. Ingrowth of radionuclides is also accounted for but, in general, ingrowth is more than compensated by the removal processes.

## 16.1 INFORMATION FLOW WITHIN TPA

### 16.1.1 Information Supplied to ASHRMOVO

The areal deposition of both SF and ash at the compliance point generated by ASHPLUMO is passed to ASHRMOVO from EXEC. The radionuclide inventory of the SF at times after the volcanic event (generated by INVENT) is also provided by EXEC. Additionally, the ASHRMOVO code module reads input values such as ash blanket characteristics and decay parameters from the ASHRMOVO section of the *tpa.inp* file.

### 16.1.2 Information Provided by ASHRMOVO

For all ground surface radionuclides, ASHRMOVO transfers the areal radionuclide density in activity per unit area as a function of time at the compliance point back to EXEC for subsequent use in DCAGS for dose calculation.

## 16.2 INTERMEDIATE RESULTS

There are no ASHRMOVO intermediate outputs in files with *.res* extensions.

When the append option is turned on in the *tpa.inp* file to create additional intermediate outputs, ASHRMOVO inputs are written to the *ashrmovo.ech* file and outputs to the *ashrmovo.rlt* file. The TPA time steps set in the *tpa.inp* file and the SF areal density are included in the *ashrmovo.ech* file. The areal radionuclide density is available in the *ashrmovo.rlt* file. A complete description of these files is provided in section 20.3.

## 16.3 CONCEPTUAL MODEL

The ASHRMOVO module models the time-dependent radionuclide areal densities of contaminated soil surface layers subject to removal by leaching, erosion, and radioactive decay. ASHRMOVO is used in concert with ASHPLUMO, which establishes initial radionuclide areal densities for extrusive volcanic events at the time of the event that intersects the waste repository. ASHRMOVO uses the INVENT utility module to decay the inventory for succeeding times. The subsequent time history of radionuclide surficial contamination is converted to dose by the DCAGS module.

ASHRMOVO uses generalized analytical solutions to calculate dynamic serial radioactive decay, including nonradioactive decay losses by leaching or erosion. For the volcanic exposure scenario previously described in ASHPLUMO, ASHRMOVO calculates the time history of radionuclide surficial contamination

following the event by using analytical solutions to the following differential equations (i.e., INVENT utility modules):

$$\frac{dN_i(t)}{dt} = \lambda_{i-1}^P N_{i-1}(t) - \lambda_i^P N_i(t) - \lambda_i^L N_i(t) - \lambda^B N_i(t)$$
$$= \lambda_{i-1}^P N_{i-1}(t) - \lambda_i^T N_i(t) \qquad (16\text{-}1)$$

where

| | | |
|---|---|---|
| $\lambda_i^T$ | = | $\lambda_i^P + \lambda_i^L + \lambda^B$ |
| $N_i(t)$ | — | time-dependent areal density of radionuclide $i$ [mol/m$^2$] |
| $N_{i-1}(t)$ | — | time-dependent areal radionuclide density of the parent [mol/m$^2$] |
| $\lambda_i^P$ | — | removal (or generation) of a contaminant through radioactive decay [1/yr] |
| $\lambda_i^L$ | — | relative leach rate of radionuclide $i$ from the ash blanket [1/yr] |
| $\lambda^B$ | — | bulk removal of the blanket through surface erosion [1/yr] |
| $\lambda_i^T$ | — | total loss rate of radionuclide $i$ from physical decay, leaching, and surface erosion [1/yr] |

The initial conditions for the system of equations are the areal densities of the radionuclides at the time of the event. These densities have been estimated by ASHPLUME.

The relative leach rate of radionuclide $i$ is based on a model equation in Napier et al. (1988). The relative leach rate has an upper limit, $\lambda_i^{L\max}$ dependent on the solubility limit of the radionuclide and the amount of radionuclide present. When the processes are leach rate limited, the relative leach rate of radionuclide $i$ is given by

$$\lambda_i^L = \lambda_i^{L\max} \qquad N_i \langle \frac{S_i R_a}{\lambda_i^{L\max}} \qquad (16\text{-}2)$$

and when the leach processes are solubility limited it is given by

$$\lambda_i^L = \frac{S_i R_a}{N_i} \cong \frac{S_i R_a}{\overline{N_i}} \qquad N_i \langle \frac{S_i R_a}{\lambda_i^{L max}} \qquad (16\text{-}3)$$

where

| | | |
|---|---|---|
| $S_i$ | — | solubility limit of radionuclide $i$ [mol/m$^3$] |

$R_a$ — areal recharge of water [$m^3/(m^2\ yr)$]

$\overline{N}_i$ — average radionuclide areal density over the time step [$mol/m^2$]

The quantity $\lambda_i^{L\max}$ is a combination of more basic parameters and is given by

$$\lambda_i^{L\max} = \frac{P\left(1-f_e^P\right)f_{sat}^P + I\left(1-f_e^i\right)f_{sat}^i}{d\left(1+(\rho/\theta)K_{d_i}\right)} \tag{16-4}$$

where

$P$ — annual precipitation rate [m/yr]

$f_e^P$ — fraction of precipitation water lost to evapotranspiration

$f_{sat}^P$ — fraction of year blanket is saturated because of precipitation

$I$ — annual irrigation rate [m/yr]

$f_e^i$ — fraction of irrigation water lost to evapotranspiration

$f_{sat}^i$ — fraction of year blanket is saturated because of irrigation

$d$ — depth of the blanket [m]

$\rho$ — soil bulk density [$g/cm^3$]

$\theta$ — soil volumetric water content

$K_{d_i}$ — distribution coefficient for radionuclide $i$ [$cm^3/g$]

The bulk removal rate of the blanket, $\lambda^B$, is a constant value of 0.0001/yr based on preliminary estimates of ash blanket lifetimes, but may be sampled by specifying a distribution in the *tpa.inp* file (appendix A). A complete demonstration of the model in ASHRMOVO, including plots of time-dependent radionuclide areal densities for an example case is given in Jarzemba and Manteufel (1997), however, a demonstration for the $^{245}Cm$ decay chain is provided here as an example. Tables 16-1 and 16-2 provide a listing of the data used in this example. Using these data and the model described in this section, the areal radionuclide densities as a function of time [$N_i(t)$] are estimated and shown graphically in figure 16-1.

## 16.4 ASSUMPTIONS AND CONSERVATISM OF THE ASHRMOVO APPROACH

The ASHRMOVO module is an abstraction of the leaching and removal of radionuclides from a contaminated soil/ash surface layer after an extrusive volcanic event has distributed radionuclides on the Earth's surface. The three main processes modeled by ASHRMOVO are removal of radionuclides from the contaminated ash blanket by solubilization and leaching by infiltrating water, radioactive decay, and blanket erosion.

Infiltrating water has the ability to dissolve radionuclides in the ash blanket and transport them to deeper soil/ash layers. Because only the contamination in the top 15 cm of ash is considered in dose

**Table 16-1. A listing of the nonradionuclide specific data used in estimating the surficial radionuclide areal density for members of the $^{245}Cm$ decay chain**

| Parameter | Value |
|---|---|
| Initial spent fuel areal density | 1 $kg/m^2$ |
| Annual precipitation rate | 0.15 m/yr |
| Annual irrigation rate | 1.52 m/yr |
| Fraction of precipitation lost by evapotranspiration | 0.68 |
| Fraction of irrigation lost by evapotranspiration | 0.5 |
| Fraction of year soil is saturated by precipitation | 0.0054 |
| Fraction of year soil is saturated by irrigation | 0.2 |
| Soil bulk density | 2 $g/cm^3$ |
| Soil porosity | 0.4 |
| Fractional blanket erosion rate | 0.001 |
| Depth of the rooting zone | 1 m |

**Table 16-2. A listing of the radionuclide-specific data used in estimating the surficial radionuclide areal density for members of the $^{245}Cm$ decay chain**

| Nuclide | Initial Inventory ($Bq\ m^{-2}Kg^{-1}$) | Physical Decay Constant ($yr^{-1}$) | Solubility (atoms/L) | $K_d$ ($cm^3\ g^{-1}$) |
|---|---|---|---|---|
| $^{245}Cm$ | $4.6 \times 10^{6}$ | $8.2 \times 10^{-5}$ | $6.0 \times 10^{17}$ | $4.0 \times 10^{3}$ |
| $^{241}Pu$ | $2.8 \times 10^{12}$ | $4.8 \times 10^{-2}$ | $3.0 \times 10^{18}$ | $5.5 \times 10^{2}$ |
| $^{241}Am$ | $6.1 \times 10^{10}$ | $1.6 \times 10^{-3}$ | $3.0 \times 10^{18}$ | $1.9 \times 10^{3}$ |
| $^{237}Np$ | $1.1 \times 10^{7}$ | $3.2 \times 10^{-7}$ | $9.5 \times 10^{19}$ | $5.0 \times 10^{0}$ |
| $^{233}U$ | $8.9 \times 10^{2}$ | $4.4 \times 10^{-6}$ | $2.7 \times 10^{19}$ | $3.5 \times 10^{1}$ |
| $^{229}Th$ | $5.1 \times 10^{0}$ | $9.5 \times 10^{-5}$ | $1.9 \times 10^{15}$ | $3.2 \times 10^{3}$ |

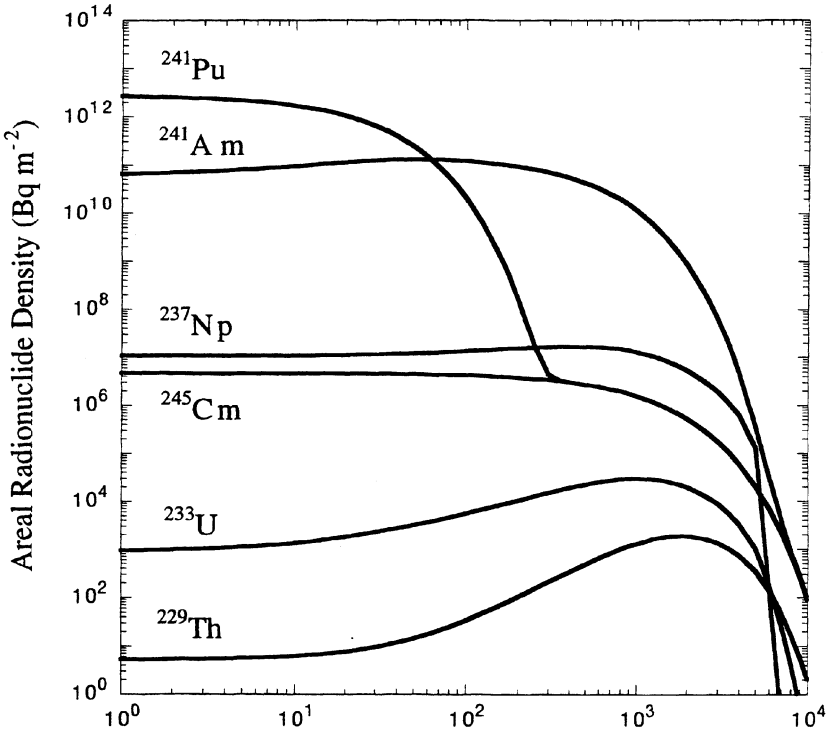


**Figure 16-1. A plot of the areal radionuclide density as a function of time for radionuclides in the $^{245}$Cm decay chain**

calculations, the effect of this transport is to remove leached radionuclides from the biosphere. Contamination of groundwater from this source is not considered.

Radioactive decay of nuclides in the blanket is accounted for in this model. Any radioactive daughters formed from parent decay are also considered.

Blanket erosion is accounted for in the model as a first order process. The blanket erosion term should be considered as net erosion (deposition from ash eroded from other sections of the blanket minus that eroded from the current location). Mechanical redistribution of ash is not specifically accounted for in the ASHRMOVO model.

# 17 DCAGS MODULE DESCRIPTION—FARMING RECEPTOR GROUP

The purpose of the DCAGS module is to convert the areal radionuclide activity densities (in $Ci/m^2$) calculated by the ASHRMOVO module into annual TEDEs (in rem).

## 17.1 INFORMATION FLOW WITHIN TPA

### 17.1.1 Information Supplied to DCAGS

Time-varying areal concentrations computed in ASHRMOVO for each ground surface radionuclide and the ash areal density calculated in ASHPLUMO are provided to DCAGS by the EXEC from which ground surface radionuclide dose (an annual TEDE) is obtained using ground surface DCFs in two data files: *gs_cb_ad.dat*, and *gs_pb_ad.dat* consistent with the lifestyle of the receptor group and the climatic conditions specified in the *tpa.inp* file. The two data files are identified by the following nomenclature: *cb*—current biosphere, *pb*—pluvial biosphere, and *ad*—farming group. The time evolution of average annual precipitation and temperature from UZFLOW are passed by the EXEC to DCAGS to determine the time when the current condition will switch to pluvial conditions. Other DCAGS input parameters such as the resuspendable depth and values for the airborne mass load and occupancy factor are specified in the DCAGS section of the *tpa.inp* file.

### 17.1.2 Information Provided by DCAGS

The ground surface doses as a function of time for each radionuclide computed in DCAGS at every TPA time step are passed to EXEC.

## 17.2 INTERMEDIATE RESULTS

The ground surface doses for all radionuclides are accessed in the *airpkds.res, arpkds_c.res, totdose.res,* and *totdos_c.res* files. The overall peak ground surface dose from all nuclides, the time of the peak dose, and the contribution to the peak ground surface dose from each radionuclide are contained in the *airpkdos.res* and *arpkds_c.res* files. Also, the time history of total dose from the groundwater and ground surface are included in the *totdos.res* and *totdose_c.res* files. The contents of the *airpkdos.res, arpkds_c.res, totdose.res,* and *totdos_c.res* files are described in detail in tables 20-1 and 20-2.

When the append option (see appendix A) is turned on in the *tpa.inp* file to create additional intermediate outputs, DCAGS inputs are written to the *dcags.ech* file and outputs to *dcags.rlt* file. The ground surface areal radionuclide activity densities for all times and the ash areal density are included in *dcags.ech* file. The time history of ground surface doses for all radionuclides are available in the *dcags.rlt* file. Additionally, ground surface doses can be accessed in *rgsna.tpa, rgsnr.tpa, rgssa.tpa, rgssr.tpa,* and *rgwgssa.tpa.* A complete description of these files is provided in section 20.3 and table 20-6.

## 17.3 CONCEPTUAL MODEL

The conceptual framework for DCAGS includes processes occurring subsequent to airborne transport and deposition of radiological contamination, released from the repository by an extrusive volcanic

event to the ground surface where the farming receptor group is located. Processes included in the conceptual model for DCAGS at the 20-km receptor location include resuspension of deposited contamination with subsequent inhalation, direct exposure, and ingestion of contaminated plant and animal products. This model is implemented in DCAGS (with the exception of the inhalation pathway, which is explained next) by using databases of DCFs that convert unit radionuclide areal densities to annual TEDEs. DCFs were calculated using a deterministic approach in the GENII-S pathway/dose assessment code (Leigh et al., 1993; Napier et al., 1988). These calculations were based on unit radionuclide concentrations in the soil and a combination of site-specific and generic input parameters discussed in LaPlante and Poor (1997). The average member of the farming receptor group is approximated by use of average or median values (depending on the distribution type) for input parameters that describe the habits of the group.

For each TPA realization, DCAGS multiplies ground surface radionuclide concentrations generated from the ASHRMOVO module by the exposure pathway/climate and radionuclide-specific DCFs. For each time step, the products of each radionuclide concentration and DCF are summed within and among exposure pathways and radionuclides to calculate total doses. The reporting of peak doses and applicable exposure pathways is the same as described in chapter 11 for the DCAGW module. The only exceptions are that surface contamination, not groundwater, is the source of radionuclides, and DCAGS does not include the ingestion of contaminated water.

For inhalation, a mass loading model was developed that is more applicable to expected site conditions than available models in GENII-S (Leigh et al., 1993; Napier et al., 1988). The mass loading model estimates the airborne concentration of radionuclides above the ash blanket after the volcanic event. The model multiplies the airborne mass load by the concentration of radionuclides in the ash being resuspended. The concentration in ash is calculated from the output of the ASHPLUMO and ASHRMOVO modules. The model also accounts for the effect of blanket thickness on the amount of material that is available for resuspension. The areal concentration of the $i$th radionuclide, $C_{a(i)}$, in Ci/m$^3$ is

$$C_{a(i)} = S\,\eta_i\,f_R \tag{17-1}$$

where

| | | |
|---|---|---|
| $S$ | — | airborne mass load [g/m$^3$] |
| $\eta_i$ | — | activity of radionuclide $i$ per mass of ash [Ci/g] |
| $f_R$ | — | fraction of resuspended mass that emanated from the contaminated volcanic ash layer [unitless] |

Immediately following the deposition of the material, the airborne mass load will be significantly larger than under normal conditions. The mass load will then decrease as the smaller particles are removed from the surface soil due to wind transport, transport to deeper levels of the soil, or agglomeration of particles. Anspaugh (1985) and Garger, et al. (1995) indicate that the mass load following deposition of material will decrease exponentially in time until it reaches a long-term stable value. The model accounts for this time dependence in the airborne mass load using the following formula:

$$S = \left(S_0 - S_\infty\right)\exp\left(-\lambda_r t\right) + S_\infty \tag{17-2}$$

where

$S_0$ = airborne mass load in year following deposition (g/m$^3$)
$S_\infty$ = airborne mass load at long times after event (g/m$^3$)
$\lambda_r$ = rate of reduction of airborne mass load (1/yr)

The activity of radionuclide *i* per mass of ash at the receptor location is estimated from quantities already calculated by the TPA Version 4.0 code modules as follows:

$$\eta_i = \frac{R_i(x,y)}{C X(x,y)} \tag{17-3}$$

where

$R_i(x,y)$ — quantity of radioactivity per unit area accumulated at location $(x,y)$ [Ci/m$^2$]
$X(x,y)$ — mass of ash per unit area accumulated at location $(x,y)$ [g/cm$^2$]
$C$ — factor to convert g/cm$^2$ to g/m$^2$

The fraction of resuspended mass that emanated from the contaminated volcanic ash deposit depends upon the thickness of the ash deposit ($T_B$) and the thickness of the resuspendible layer ($T_R$). The thickness of the resuspendible layer is the depth from the surface below which no resuspended ash can emanate over the course of one year. For blankets thicker than $T_R$, $f_R$ is unity. For blankets thinner than $T_R$, $f_R$ is given by

$$f_R = \frac{T_B}{T_R} \tag{17-4}$$

Situations where $f_R$ is equal to unity and where $f_R$ is less than unity are shown in figure 17-1.

The blanket thickness is a function of time and is given by

$$T_B = T_{B-0} \exp\left[-\lambda_B\left(t - t_{\text{event}}\right)\right] \tag{17-5}$$

where

$T_{B-0}$ — blanket thickness at the compliance point immediately following the event (estimated from $X(x,y)$ from ASHPLUMO) [cm]
$\lambda_B$ — net blanket erosion rate from ASHRMOVO [1/yr]
$t_{\text{event}}$ — time of the volcanic event from VOLCANO [yr]

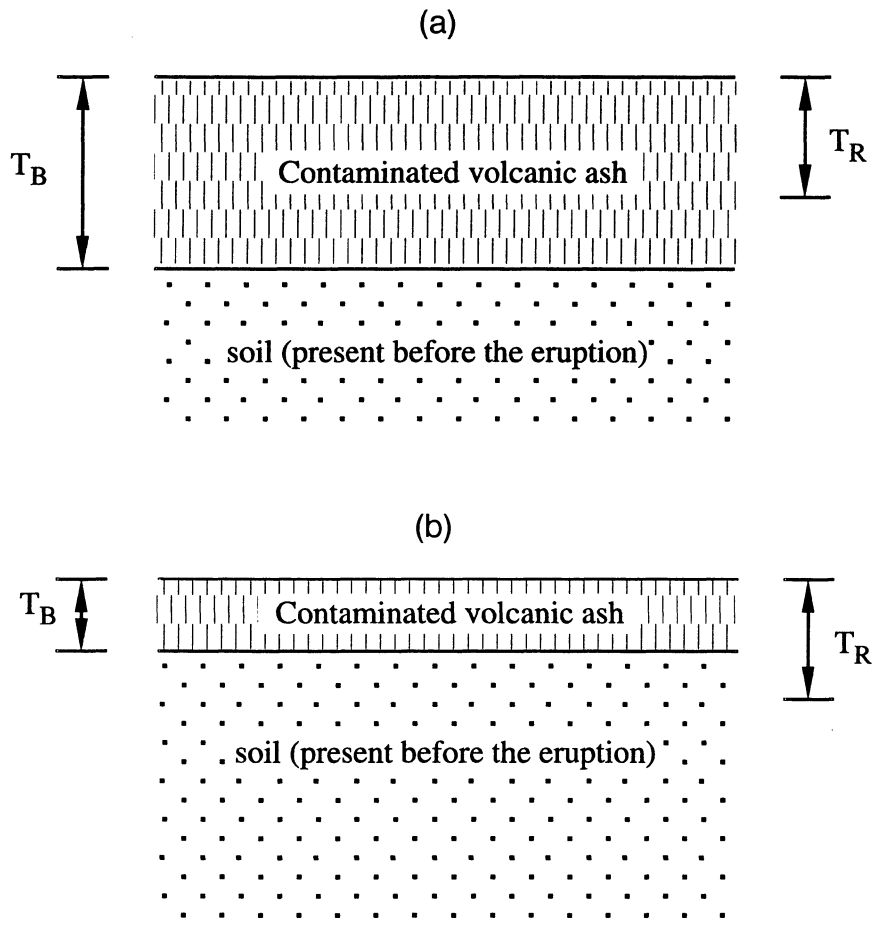


**Figure 17-1. Cases where fraction of resuspended mass emanated from the contaminated volcanic ash layer $(f_R)$: (a) is unity and (b) is less than unity**

Once the airborne radionuclide concentration has been estimated, the rest of the dose conversion process is described by the following equation

$$D_i = BI_i C_{a(i)} f_e \tag{17-6}$$

where

$D_i$ — inhalation dose rate due to the airborne pathway for radionuclide $i$ [rem/yr ]

$B$ — breathing rate [$m^3$/yr]

$f_e$ — fraction of the year the individual is exposed to contaminated air

$I_i$ — Inhalation-to-dose conversion factor in rem/Ci (U.S. Environmental Protection Agency, 1988) (choices for removal class are as listed in PNL library)

The quantity $BI_i$ is provided in the DCF tables in the files *gs_cb_ad.dat* and *gs_pb_ad.dat* (inhalation parameter column) to the code as input data where $B$ is assumed to be $1.05 \times 10^4$ m$^3$/yr (20 L/min) (Bureau of Radiological Health, 1970).

For each time step, the products of each radionuclide concentration and DCF are summed within and among ground surface exposure pathways and radionuclides to calculate total doses. In addition to summary doses, selected output is stratified by realization, time step, and radionuclide. The executive model uses results from all realizations to identify and report the peak dose.

## 17.4 ASSUMPTIONS AND CONSERVATISM OF THE DCAGS APPROACH

DCAGS is an abstraction of complex and uncertain processes occurring in the biosphere. The conversion of soil radionuclide concentrations to receptor dose involves assumptions about (i) the location of the receptor group, (ii) the lifestyle characteristics of the receptor group that form the basis for exposure pathways, (iii) the processes that determine fate and transport of contaminants in the biosphere, and (iv) the calculation of human doses from factors that convert exposure to contaminated media to effective dose equivalents.

Receptor location is based on the assumption that present physical constraints (topography, depth to water table, and soil conditions) that limit present farming to the Amargosa Valley area will continue to limit farming south of YM to within approximately 20 km from the proposed repository site. Because the receptor location and lifestyle assumption relates to potential human behavior, it is speculative but considered to be reasonably conservative for PA calculations.

The conversion of soil concentrations to receptor dose requires conceptualization of potential exposure pathways based on the site-specific characteristics of the release pathway, YM biosphere, and receptor group. When soil is the source of contamination, the potential exposure pathways are assumed to be those resulting from agricultural use of land, consistent with present farming conditions south of YM. These pathways include ingestion (of contaminated crops and animal products), inhalation (from resuspension of soil), and direct exposure to contaminated soil.

The assumed diet of locally produced food is important in estimating the dose for a farming receptor group. The farmer is assumed to grow alfalfa (for beef and milk cow feed), vegetables, fruits, and grains for personal consumption, and feed for egg laying hens. The practices the farmer is presumed to engage in have been confirmed to exist in areas south of YM; however, it appears unlikely that all activities identified would be practiced by a single individual. Therefore, the doses calculated from such assumptions are expected to be greater than that which might occur under current conditions. Since bartering is known to exist among community members (Eisenberg, 1996), however, it is reasonable to project that (for the most highly exposed group) a significant portion of diet could be obtained from local sources. Thus, the assumption is conservative, but not excessively so. These assumptions may change when additional information on local consumption patterns is made available.

Modeling the fate and transport of radionuclides in the biosphere involves determination of crop concentrations using soil/plant uptake factors, determination of air concentrations from resuspended contamination using a mass load model, and accounting for feed intake and transfer of contamination to livestock.

Crop concentrations are based on transfer factors that represent the ratio of plant and soil concentrations for a class of crops grown in contaminated soil. Food transfer factors are generic values based primarily on a large survey of the literature (International Atomic Energy Agency, 1994) or supplemental sources when needed (Baes et al., 1982). Because of the lack of site-specific information, it is reasonable to use generic values; however, they may not be representative of arid conditions that exist in Nevada. The selected factors are expected values and have not been arbitrarily increased for conservatism.

Air concentrations from resuspended contamination are calculated by applying a mass loading model. This model uses a mass loading factor that is the ratio of airborne and surface soil radionuclide concentrations. The resuspension process is highly uncertain and is influenced by a number of factors including wind speed, surface roughness, resuspended particle size and density, and the moisture content of soil. Because the GENII-S code does not provide a mass loading model for crop deposition, a resuspension model was used with an adjusted mass loading factor. A separate mass loading model for inhalation is used in DCAGS that was developed to be more applicable to site conditions than the available models in GENII-S (Leigh et al., 1993; Napier et al., 1988). This mass loading model estimates the airborne concentration of radionuclides above the ash deposit after the volcanic eruption. The model accounts for the effect of deposit thickness (as a function of time) on the amount of material available for resuspension and the reduction in the mass load in the years following deposition of the ash deposit.

Determination of radionuclide concentrations in livestock products is done by quantifying the intake of contaminated feed and applying a transfer coefficient. The animal transfer coefficients are based on studies that measure radionuclide concentrations in livestock based on measured intake. The coefficients are element and livestock specific and based on a large survey of available literature (International Atomic Energy Agency, 1994) or a supplemental source (Baes et al., 1982).

Calculation of human dose is accomplished through the use of dose factors that convert the estimated concentrations in food, air, and soil and the corresponding intakes and residence times to total effective dose equivalents. The dosimetry models that form the basis for the dose factors are consistent with those described in the ICRP publication 30. The dosimetry models represent state-of-the-art techniques and methodologies in existence at the time the publication was released. Refinements to dosimetry models have since been published by the ICRP, but have not yet been adopted by the U.S. Government and are therefore not used in DCAGS.

More specific assumptions for DCAGS are provided in the following list and in LaPlante and Poor (1997).

- Contamination spread on the ground surface is the sole source of contamination, as opposed to contamination dissolved in the groundwater used in DCAGW. This assumption means that radionuclides leached from the ash blanket to lower soil layers and possibly the SZ are removed from the biosphere and thus do not contribute to estimated doses. Because, the most significant contributors to dose for this exposure pathway are actinides such as Pu, Am, and Cm and these radionuclides are not expected to be easily leached from ground surface soil/ash layers, this assumption seems valid.

- The dose calculation from consumption of crops does not account for washing of fruits and vegetables prior to consumption and is therefore conservative.

- Food consumption rates for the default adult receptor are based on a survey of Amargosa Valley residents (Civilian Radioactive Waste Management System, Management & Operations, 2000). The survey provides the best available information on local food consumption practices. The consumption rates are representative of average consumption practices of residents who have food gardens that supply a portion of the food consumed annually.

- For human dosimetry modeling, the average member of the receptor group is understood to be an adult consistent with the EPA proposed Federal Radiation Protection Guidance for Exposure of the General Public (U.S. Environmental Protection Agency, 1994). The individual is assumed to have physiology consistent with the reference man model (International Commission on Radiological Protection, 1975).

- Inhalation and external exposure times are based on generic information provided in Kennedy and Strenge (1992). For the farming group, 55 percent of total time is assumed to be spent inside the residence, 20 percent outside of residence, 24 percent at work (indoors within the plume deposition area), and 1 percent gardening and farming alfalfa which is not a labor intensive crop to farm. It is assumed that time spent indoors reduces the airborne mass load by 50 percent and the direct exposure by 67 percent based on NUREG/CR–5512. These activity times are considered to be conservative for a common residential setting (Kennedy and Strenge, 1992), but may not be conservative for a more active farming resident. The 50 percent reduction in inhalation mass loading indoors is based on normal mass loading conditions and may be conservative for the higher outdoor mass loading associated with volcanic ash.

- Resuspension of contaminated soil applies to crop deposition, inhalation, and external dose modeling. A mass loading model is applicable to a homogeneously mixed layer of contamination in the soil and, therefore, a reasonable mass loading factor derived from a review of the literature is used. The mass load in the year following the volcanic eruption is assumed to be the average airborne mass load based on an initial value of 0.1-1 g/m3 (National Council on Radiation Protection and Measurements, 1984; Stewart, 1964) and decreasing with an effective half-life of 55 days (Anspaugh et al., 1975). This value accounts for temporary increases in the airborne mass load when the deposit is mechanically disturbed, such as during plowing. In future years, it is assumed that the airborne mass load approaches the airborne mass load above a desert soil with an effective half-life of 10 yr. Data in Anspaugh et al. (1975) and NRC (1975) would support an effective half-life of 1 yr or less, but to account for the wide distribution of ash in the surrounding area potentially replenshing fine material in the deposit, this value is increased to 10 yr. The airborne mass load above a desert soil is derived from a review of the literature to be between 5e-5 and 3e-4 (Sehmel, 1977; Anspaugh et al., 1975; Soldat et al., 1973; Rognon, 1991; Tegen and Fung, 1994). The airborne mass load is an important parameter in determining the dose from volcanism, and the applicability of these values to a volcanic ash deposit in a farming community will continue to be evaluated. For crop deposition, the GENII-S code includes a resuspension model; therefore, the selected mass loading factor is converted to a resuspension factor using an equation in the GENII-S User Manual (Napier et al., 1988). A mass-load model is used to determine annual TEDEs from the inhalation pathway. Provided that a reasonably conservative value for the airborne mass load is used, a reasonably conservative estimate of dose from the inhalation pathway for

volcanism will be achieved since doses from inhalation are linearly dependent on this factor. The mass loading and resuspension models are abstractions of complex and varying processes. Thus, considerable uncertainty exists in applying them to YM conditions.

- Like DCAGW, DCAGS uses DCFs calculated using internal DCF in FGR 11 (U.S. Environmental Protection Agency, 1988). For radionuclides where choices for lung classes and blood uptake fractions exist, the dose factors that result in the highest doses are used. The rationale for selecting the high values for internal dose factors in DCAGS is that many uncertainties exist in understanding the chemical form of the contaminants (e.g., for SF entrained in the volcanic ash following transport through exposure pathways to the receptor). Given the uncertainty, a reasonable and commonly used assumption is to select the highest values to ensure that potential doses are not being underestimated.

# 18 DCAGS MODULE DESCRIPTION— RESIDENTIAL RECEPTOR GROUP

The purpose of the DCAGS module is to convert the areal radionuclide activity densities (in $Ci/m^2$) calculated by the ASHRMOVO module into annual TEDEs (in rem).

## 18.1 INFORMATION FLOW WITHIN TPA

### 18.1.1 Information Supplied to DCAGS

Time-varying areal concentrations computed in ASHRMOVO for each ground surface radionuclide and ash areal density in ASHPLUMO are provided to DCAGS by the EXEC from which the ground surface radionuclide dose (an annual TEDE) is obtained using ground surface DCFs in two data files: *gs_cb_ci.dat* and *gs_pb_ci.dat* and consistent with the lifestyle of the receptor group and the climatic conditions specified in the *tpa.inp* file. The two data files are identified by the following nomenclature: *cb*—current biosphere, *pb*—pluvial biosphere, and *ci*—residential. Other DCAGS input parameters, such as resuspendable depth and the values for the airborne mass load and occupancy factor, are specified in the DCAGS section of the *tpa.inp* file. The time evolution of average annual precipitation and temperature from UZFLOW is passed by the EXEC to DCAGS to determine the current conditions that occur with the switch to pluvial conditions.

### 18.1.2 Information Provided by DCAGS

The ground surface doses as a function of time for each radionuclide computed in DCAGS at every TPA time step are passed to EXEC.

## 18.2 INTERMEDIATE RESULTS

The ground surface doses for all radionuclides are accessed in the *airpkdos.res, arpkds_c.res, totdose.res,* and *totdos_c.res* files. The overall peak ground surface dose from all nuclides, the time of the peak dose, and the contribution to the peak ground surface dose from each radionuclide are contained in the *airpkdos.res* and *arpkds_c.res* files. Also, the time history of total dose from the groundwater and ground surface are included in the *totdose.res* and *totdos_c.res* files. The contents of the *airpkdos.res, arpkds_c.res, totdose.res,* and *totdos_c.res* files are described in detail in tables 20-1 and 20-6.

When the append option (appendix A) is turned on in the *tpa.inp* file to create additional intermediate outputs, DCAGS inputs are written to the *dcags.ech* file and outputs to the *dcags.rlt* file. The ground surface, areal radionuclide activity densities for all times and the ash areal density are included in the *dcags.ech* file. The time history of ground surface doses for all radionuclides are available in the *dcags.rlt* file. Additionally, ground surface doses can be accessed in the *rgsna.tpa, rgsnr.tpa, rgssa.tpa, rgssr.tpa,* and *rgwgssa.tpa* files. A complete description of these files is provided in section 20.3 and table 20-2.

## 18.3 CONCEPTUAL MODEL

The conceptual framework for DCAGS includes processes occurring subsequent to airborne transport and deposition of radiological contamination (released from the repository by an extrusive volcanic event) to the ground surface where the residential receptor group is located. Processes included in the conceptual model for DCAGS include resuspension of the deposited contamination at the residential receptor location and calculation of dose from inhalation and direct exposure. This model is implemented in DCAGS by using databases of DCFs that convert unit radionuclide activity areal densities to annual TEDEs. DCFs were calculated using a deterministic approach in the GENII-S pathway/dose assessment code (Leigh et al., 1993; Napier et al., 1988). These calculations were based on unit radionuclide concentrations in the soil and a combination of site-specific and generic input parameters discussed in LaPlante and Poor (1997). The average member of the residential receptor group is approximated by use of average or median values (depending on the distribution type) for input parameters that describe the habits of the group.

For each TPA realization, DCAGS multiplies ground surface radionuclide concentrations generated from the ASHRMOVO module by the exposure pathway/climate and radionuclide-specific DCFs. For each time step, the products of each radionuclide concentration and DCF are summed within and among exposure pathways and radionuclides to calculate total doses. The reporting of peak doses and applicable exposure pathways are all the same as described in chapter 12 for the DCAGW module. The only exceptions are that surface contamination, not groundwater, is the source of radionuclides, and DCAGS does not include the ingestion of contaminated water.

For inhalation, a mass loading model was developed that is more applicable to expected site conditions than available models in GENII-S (Leigh et al., 1993; Napier et al., 1988). The mass loading model estimates the airborne concentration of radionuclides above the ash blanket after the volcanic event. The model multiplies the airborne mass load by the concentration of radionuclides in the ash being resuspended. The concentration in ash is calculated from the output from ASHPLUMO and ASHRMOVO modules. The model also accounts for the effect of blanket thickness on the amount of material available for resuspension and the decrease in the mass load above the ash blanket over time. The areal concentration of the *i*th radionuclide, $C_{a(i)}$, in Ci/m$^3$ is computed from Eq. (17-1). The time dependence of the airborne mass load is calculated using Eq. (17-2). The activity of radionuclide $i$ per mass of ash at the receptor location is estimated from quantities already calculated by the TPA Version 4.0 code modules using Eq. (17-3).

The fraction of resuspended mass that emanates from the contaminated volcanic ash deposit depends on the thickness of the ash deposit ($T_B$) and the thickness of the resuspendible layer ($T_R$). The thickness of the resuspendible layer is the depth from the surface below which no resuspended ash can emanate during the course of 1 yr. For deposits thicker than $T_R$, $f_R$ is unity. For deposits thinner than $T_R$, $f_R$ is given by Eq. (17-4). Situations where $f_R$ is equal to unity and where $f_R$ is less than unity are shown in figure 17-1. The blanket thickness is a function of time and is given by Eq. (17-5).

Once the airborne radionuclide concentration has been estimated, the rest of the dose conversion process is described by Eq. (17-6).

For each time step, the products of each radionuclide concentration and DCF are summed within and among ground surface exposure pathways and radionuclides to calculate total doses. In addition to summary doses, selected output is stratified by realization, time step, and radionuclide. The executive model uses results from all realizations to identify and report the peak dose.

## 18.4 ASSUMPTIONS AND CONSERVATISM OF THE DCAGS APPROACH

The DCAGS module for the residential receptor converts soil radionuclide concentrations to both inhalation and external doses. Therefore, the module involves assumptions about (i) the location of the receptor group, (ii) the lifestyle characteristics of the receptor group that form the basis for exposure pathways, and (iii) the conversion of intake to dose.

The residential receptor is based on an assumption that local topography and the economics of groundwater extraction allows for a potential nonfarming residential receptor group to exist closer to the potential repository site than a farming receptor group. While DCAGS does not include the groundwater pathways (those are addressed in DCAGW) the implicit assumption is that access to water is a precondition for the existence of residential dwellings. Because the receptor location and lifestyle assumption relates to potential human behavior, it is only speculative.

Because DCAGS considers the dose from airborne contaminants deposited to soil, exposure pathways are limited to inhalation and direct exposure. The inhalation dose is assumed to be from resuspension of contaminated soil and external dose is due primarily to outdoor human activities in the vicinity of contaminated soils.

Resuspension is modeled in DCAGS by use of a mass loading model that was developed to be more applicable to site conditions than the available models in GENII-S (Leigh et al., 1993; Napier et al., 1988). The mass loading model estimates the airborne concentration of radionuclides above the ash blanket after the volcanic event. The model accounts for the effect of blanket thickness (as a function of time) on the amount of material available for resuspension and the reduction in the mass load in the years following deposition of the ash blanket. The subsequent dose calculation involves the receptor breathing rate, exposure time, and inhalation to DCF. Exposure times for inhalation are obtained from conservative estimates in Kennedy and Strenge (1992) suggesting a resident spends 55 percent of total time inside the residence, 20 percent outside the residence, 24 percent at work (indoors within the plume deposition area), and 1 percent gardening and farming alfalfa. It is assumed that time spent indoors reduces the airborne mass load by 50 percent and the direct exposure by 67 percent based on NUREG–5512. The 50 percent reduction in inhalation mass loading indoors is based on normal mass loading conditions and may be conservative for the higher outdoor mass loading associated with volcanic ash. The inhalation to dose conversion factors are obtained from Federal Guidance Report No. 11 (U.S. Environmental Protection Agency, 1988).

Conversion of soil concentrations to external dose is a simple calculation involving the exposure time and the dose conversion factor for groundshine. The exposure times for external exposure are based on the aforementioned assumptions for inhalation exposure. The dose conversion factors for external exposures are from Federal Guidance Report No. 12 (U.S. Environmental Protection Agency, 1993).

Following are additional details of DCAGS modeling assumptions.

- Provided that a reasonably conservative value for the airborne mass load is used, a reasonably conservative estimate of dose from the inhalation pathway for volcanism will be achieved since doses from inhalation are linearly dependent on this factor.

- Contamination spread on the ground surface is the sole source of contamination, as opposed to contamination dissolved in the groundwater. This assumption means that radionuclides leached from the ash blanket to lower soil layers and possibly the SZ are removed from the biosphere and thus do not contribute to estimated doses. Because, for this exposure pathway, the most significant contributors to dose are actinides such as Pu, Am, and Cm, and these radionuclides are not expected to be easily leached from ground surface soil/ash layers, this assumption seems valid. It is noted that the parameters in the basecase data set that determine leaching of radionuclides out of the contaminated ash blanket are appropriate for a farming receptor group, which may be nonconservative if applied to a residential group.

- For human dosimetry modeling, the average member of the receptor group is understood to be an adult consistent with the EPA proposed Federal Radiation Protection Guidance for Exposure of the General Public (U.S. Environmental Protection Agency, 1994). The individual is presumed to have physiology consistent with the assumptions of reference man (International Commission on Radiological Protection, 1975).

- Like DCAGW, DCAGS uses DCFs calculated using internal DCFs in Federal Guidance Report No. 11 (U.S. Environmental Protection Agency, 1988). For radionuclides where choices for lung classes and blood uptake fractions exist, the dose factors that result in the highest doses are used. The rationale for selecting the high values for internal dose factors in DCAGS is that many uncertainties exist in understanding the chemical form of the contaminants (e.g., for SF entrained in the volcanic ash following transport through exposure pathways to the receptor). Given the uncertainty, a reasonable (and commonly used) assumption is to select the highest values to ensure that potential doses are not being underestimated.

# 19 INPUT DATA

The TPA Version 4.0 code is executed in batch mode using a primary and some auxiliary input data files. Primary input data for the TPA Version 4.0 code are contained in the *tpa.inp* file. Auxiliary input data files are used by some consequence modules; however, these files are static in the sense they were created using external codes. Changes to these files are expected to be made only in special cases. The *tpa.inp* file contains all information necessary for the user to specify the scenarios, number of realizations, simulation time, number of subareas, and parameters to be sampled. The first part of this chapter describes the structure and preparation of the primary input file followed by a brief description of the auxiliary input data files.

## 19.1 STRUCTURE OF THE *tpa.inp* FILE

The *tpa.inp* file defines program flow and variable values for each of the processes modeled in the TPA Version 4.0 code that can be modified by the user. Global parameters are specified in the first several hundred lines of this file. The *tpa.inp* file is organized in the following order:

**Global Parameters**

- Title
- Importance analysis flags
- Disruptive scenario flags
- Subarea specifications, including total number and locations of subareas, radionuclides, and radionuclide chain specifications
- Sampling specifications, including the seed for the random number generator, LHS flag, and number of realizations
- Simulation time, compliance time, and corresponding number of time steps
- Output print options for writing files with intermediate results

**Module-Specific Parameters**

Consequence module variable definitions are grouped by module. The order in which these sections appear in *tpa.inp* matches the order of their presentation in chapters 4–18.

- UZFLOW
- NFENV
- EBSFAIL
- SEISMO
- EBSREL
- UZFT
- SZFT

- DCAGW
- FAULTO
- VOLCANO
- ASHPLUMO
- ASHRMOVO
- DCAGS
- Correlated parameters

Each program execution or variable definition in the *tpa.inp* file starts with a keyword, followed by a variable name, a line of input appropriate for the keyword used. Descriptions of keywords are given in the next section. Exceptions to this three-line input for variable definition are the identification of the subarea coordinates, list of radionuclides, seismic hazard curve definition in SEISMO, and specification of user distribution and correlated input parameters. Explanation and examples of these formats are also provided in the following text.

Although the user can control the operation of the program and change the shape and value of variable distributions, the user must maintain all components and variables in the *tpa.inp* file. **The user should not remove or comment out program execution or variable definition lines in the *tpa.inp* file.** For example, even if a disruptive scenario consequence module flag is set so that a particular module is not run [i.e., VolcanismDisruptiveScenarioFlag (yes = 1, no = 0) set to 0], the *tpa.inp* lines defining variables for that module still must be contained in the *tpa.inp* file. During program execution, each of the variables is checked to assure it is present and has an acceptable value. This helps ensure that the problem definition supplied by the user is complete and is conducted as part of the internal TPA Version 4.0 code quality assurance (QA) checks. Names of variables defined in the *tpa.inp* file can contain up to 60 characters and include units where appropriate. Variable names are meant to be descriptive and must not be modified by the user.

The reference data set presented in appendix A is an example of the data set in the *tpa.inp* file. Columns 1, 2, 4, and 6 from this appendix were used in preparing the *tpa.inp* file.

## 19.2 DEVELOPMENT OF INPUT FILE *tpa.inp*

The *tpa.inp* file is keyword oriented. A keyword is located on a line by itself. Subsequent lines (one or more) describe the data more fully. There are 21 keywords available to the user: **title, iflag, subarea, aqueousnuclides, endoffile, constant, iconstant, uniform, loguniform, iuniform, normal, lognormal, beta, logbeta, triangular, logtriangular, exponential, finiteexponential, hazardcurve, userdistribution,** and **correlateinputs.** All keywords are case sensitive and should be lower case. Some of these keywords are optional and may never be needed in a run, while others are required. Numerous error traps in the READER utility module help detect problems with the input data and provide helpful comments to the analyst. The *tpa.inp* file has all of the description required to execute the TPA code. This file is designed to be the primary source of input information. Because duplicate sources of the same data can become a problem in any large TSPA, the *tpa.inp* file is designed to accommodate the wide variety of input data. Although this file is expected to be the only input data file for the TPA code, other static data files such as the digital elevation maps for the ground surface are more conveniently stored in separate files. These archival files represent data not changeable for an application.

Comment lines can be added to the input file. The first character in a comment line is "*". Comment lines should be placed between groups of input data. For example, three lines may be required to describe one input parameter, and another three for the second parameter. Comment lines can be used after the first parameter is fully described and before the second is described.

Some of the keywords in the *tpa.inp* file are specific to the EXEC parameters, but most are generic and are used to specify consequence module parameters. For example, the title, subarea, and aqueousnuclides keywords are required and used by EXEC. The other keywords are more generic and are included for the consequence module parameters as well as the EXEC. These keywords typically assign values (or statistical distributions) to parameters. Each parameter has a unique name up to 60 characters in length. SAMPLER will produce an error message and stop execution if a parameter is defined more than once. The module developer who introduces the parameter and assigns the name uses that name to query the parameter value from within the consequence module code. Hence, the module developer who has introduced the parameter must also query the value using precisely the same name. In this way, SAMPLER provides values of parameters to consequence modules. Each keyword is described in the following subsections.

## 19.2.1 Problem Definition Keywords

### 19.2.1.1 title

The analyst is required to provide a two-line title that uniquely identifies the simulation case. This requirement is both common practice and provides useful QA documentation. The description should be sufficiently specific for the particular problem being analyzed. The format for the title line is the keyword **title**. The next two lines contain the two, 80-character-long titles. The following is an example of the use of **title** for a code run:

```
**
title
Input file tpa.inp as supplied with TPA Version 4.0 Code.
Base case data set Rev 4.0    3/31/00
**
```

The "**" indicates a comment line, one above and one below the two title lines. The two title lines cannot be separated by comments.

### 19.2.1.2 iflag

The keyword **iflag** is set to either 0 (indicating no or not active) or 1 (indicating yes or active). The flag is used to select an option. For example, the scenarios have been modeled using flags that determine whether the TPA code performs execution of the disruptive event/process (e.g., the user can activate a flag to activate a disruptive scenario evaluation). Next is an example of the use of **iflag**:

```
**
iflag
VolcanismDisruptiveScenarioFlag(yes=1,no=0)
1
**
iflag
FaultingDisruptiveScenarioFlag(yes=1,no=0)
1
```

```
**
iflag
SeismicDisruptiveScenarioFlag(yes=1,no=0)
1
**
```

The previous example would execute the VOLCANO, FAULTO, and SEISMO modules in a TPA Version 4.0 code run.

The **iflag** keyword can pass information to EXEC and other consequence modules. This use of **iflag** makes the most sense when the user has a choice between two options. An example is illustrated here with the selection of either calculating or specifying the dilution volume.

```
**
iflag
DilutionModel
0
**
```

The DCAGW module will query the value of the parameter name DilutionModel. If the value is 0, the DCAGW module will calculate the dilution volume, whereas a user defined dilution volume in the *tpa.inp* file will be used if the value is 1.

### 19.2.1.3 subarea

The analyst is required to specify the total number and locations of the repository subareas using the **subarea** keyword. A subarea is represented by a quadrilateral and defined by specifying coordinates of the four vertices. An example of an eight-subarea discretization of the repository is provided (these eight subareas are plotted in figure 4-2):

```
**
** Number and Location Of SubAreas[m] Based On EDA-II Design.
subarea
8
edaii 1-cw
547514.88,4079310.61
548069.2,4079136.5
547847.3,4077816.2
547370.95,4077922.04
547514.88,4079310.61
edaii 2-cw
548069.2,4079136.5
548569.32,4078981.
548504.06,4077664.24
547847.3,4077816.2
548069.2,4079136.5
edaii 3-cw
547370.95,4077922.04
547847.3,4077816.2
548322.7,4077192.2
547474.7,4077281.6
547370.95,4077922.04
edaii 4-cw
547847.3,4077816.2
```

```
548504.06,4077664.24
548479.71,4077173.06
548322.7,4077192.2
547847.3,4077816.2
edaii 5-cw
547474.7,4077282.6
547887.3,4077238.1
547897.79,4076045.46
547655.97,4076123.07
547474.7,4077282.6
edaii 6-c
547887.3,4077238.1
548322.7,4077192.2
548155.7,4075962.63
547897.79,4076045.46
547887.3,4077238.1
edaii 7-cw
548322.7,4077192.2
548479.71,4077173.06
548455,4076674.51
548155.7,4075962.63
548322.7,4077192.2
edaii 8-cw
547645.27,4079656.06
548588.98,4079377.55
548569.32,4078981
547514.88,4079310.61
547645.27,4079656.06
```

The first line of the example contains the keyword **subarea**. The second line contains the number of subareas being defined, which affects the subsequent lines. The eight subareas overlay the southern most portion of the upper block. For the EDA II WP spacing, drift spacing, and amount of waste contained in each WP that are specified in the *tpa.inp* file, eight subarea are sufficiently large to accommodate about 68,000 MTU of waste. The DOE also has extended the northern boundary of this zone for an additional emplacement area if necessary. The added space in the northern portion of the repository may be needed if the EDA II design is changed.

Following the number of subareas, the location of each subarea is then provided. The format for the subarea vertices is based on the plotting software TECPLOT (Amtec Engineering, Inc., 1993). The next 48 lines of input data are exactly the same lines used in the input file for plotting and visually checking the coordinate locations and repository outline. Although the previous format appears awkward, it avoids the error-prone process of retyping the coordinate data. The format consists of six lines for each subarea. The first line is specific to the postprocessor TECPLOT. The second through fifth lines define the coordinates of the subarea vertices in Universal Transverse Mercator (UTM) coordinates. Easting is the first coordinate, and Northing is the second, and both are in units of meters. The last line echoes the second line (which closes the quadrilateral drawn by connecting points). Here is another example:

```
1
**ZONE T="ONE RECTANGULAR ZONE SUBAREA", F=POINT
          547500.0,         4076000.0
          547500.0,         4079467.56
          548500.0,         4079467.56
          548500.0,         4076000.0
          547500.0,         4076000.0
```

This example defines one rectangular subarea with the area as the total area of the eight subareas. This example is often useful in testing consequence modules where the looping over the number of subareas is minimized (will do only one loop) before proceeding to the next realization.

### 19.2.1.4 aqueousnuclides

The analyst is required to specify the number and names of radionuclides to be considered in the groundwater pathway during the run. The analyst is also required to identify the chains and the order of nuclides in chains. The INVENT utility module recognizes the specific nuclides and from the *nuclides.dat* data file assigns information for each nuclide such as half-life, molecular (isotopic) weight, and initial radionuclide inventory (see table 19-1 for specific values). While any set of nuclides from the 43 listed in table 19-1can be specified for aqueous releases, radio-isotope dependent parameters must be added to the *tpa.inp* file to reflect the new isotopes in the aqueous nuclides list. The following is an example of the use of the **aqueousnuclides** keyword:

```
**
aqueousnuclides
**    number of nuclides, number of chains
20
13
**
**    chain 1
2
Cm246
U238
**    chain 2
3
Cm245
Am241
Np237
**    chain 3
2
Am243
Pu239
**    chain 4
1
Pu240
**    chain 5
4
U234
Th230
Ra226
Pb210
**    chain 6
1
Cs135
**    chain 7
1
I129
**    chain 8
1
Tc99
** chain 9
1
```

```
Ni59
**    chain 10
1
C14
**    chain 11
1
Se79
**    chain 12
1
Nb94
**    chain 13
1
Cl36
**
endofnuclides
**
```

The first line contains the keyword **aqueousnuclides**. The third line provides the number of nuclides and number of chains being selected. The selection of nuclides to be tracked is not a trivial exercise, and several considerations determine the limited set of nuclides for aqueous releases [based on Wescott et al. (1995), with the addition of $^{36}Cl$ because of its importance in the DOE TSPA-95 (i.e., TRW Environmental Safety Systems, Inc., 1995) from the set of 43. Unless the analyst has a clear understanding of how nuclides are handled in the code or a clear rationale to do otherwise, the default set of nuclides presented in the example input file (shown previously) should be used. After the number of nuclides and number of chains have been established, each nuclide is identified on a separate line in a group of lines representing a single chain. The first line in this group contains the number of nuclides in the chain. All nuclide names are provided in the first six spaces of each line. The **endofnuclides** keyword is required to terminate the **aqueousnuclides** section.

#### 19.2.1.5 endoffile

The **endoffile** keyword is used to indicate the last line in the *tpa.inp* file. The analyst must specify this keyword once and only once. If it is used more than once, an error message will be printed, and code execution will stop.

### 19.2.2 Distribution Definition Keywords

Listed are keywords used in the *tpa.inp* file to define distributions described in section 3.2 SAMPLER. Distribution functions available in the LHS code are presented in table 3-2.

#### 19.2.2.1 constant

The **constant** keyword has a wide variety of uses and is one of the simplest inputs. Only three lines are required to define a constant parameter. The first line has the keyword **constant**. The second line includes a name for the parameter that emcompases most of the 60-character length. The third line provides the value of the constant. FORTRAN distinguishes between integer and real types of data; hence, the constant value is a real (floating point) number. The analyst can view the constant as a delta probability density function. In the future, the analyst may want to use a uniform or normal distribution to describe the range of the parameter. It is straightforward to transform a parameter from type constant to another type between runs by editing the *tpa.inp* file. The following two examples are of specific constants currently being used.

**Table 19-1. List of 43 radionuclides in the TPA Version 4.0 code with associated half-lives, isotopic weights, and initial waste package inventories**

| Radionuclide | Half-life (yr) | Mol. Wt. (Isotopic Wt.) | Initial WP Inventory (Ci/MTU at 10 yr) |
|---|---|---|---|
| $^{14}C$ | $5.729 \times 10^{3}$ | 14 | $1.44 \times 10^{0}$ |
| $^{36}Cl$ | $3.010 \times 10^{5}$ | 36 | $1.15 \times 10^{-2}$ |
| $^{59}Ni$ | $8.000 \times 10^{4}$ | 59 | $2.44 \times 10^{0}$ |
| $^{63}Ni$ | $9.200 \times 10^{1}$ | 63 | $3.72 \times 10^{2}$ |
| $^{79}Se$ | $6.496 \times 10^{4}$ | 79 | $4.58 \times 10^{-1}$ |
| $^{90}Sr$ | $2.912 \times 10^{1}$ | 90 | $6.25 \times 10^{4}$ |
| $^{93}Zr$ | $1.530 \times 10^{6}$ | 93 | $2.47 \times 10^{0}$ |
| $^{93}Mo$ | $3.498 \times 10^{3}$ | 93 | $1.51 \times 10^{-2}$ |
| $^{94}Nb$ | $2.030 \times 10^{4}$ | 94 | $8.48 \times 10^{-1}$ |
| $^{99}Tc$ | $2.130 \times 10^{5}$ | 99 | $1.45 \times 10^{1}$ |
| $^{107}Pd$ | $6.496 \times 10^{6}$ | 107 | $1.31 \times 10^{-1}$ |
| $^{108m}Ag$ | $1.270 \times 10^{2}$ | 108 | $1.26 \times 10^{-2}$ |
| $^{121m}Sn$ | $4.997 \times 10^{1}$ | 121 | $1.04 \times 10^{0}$ |
| $^{126}Sn$ | $1.000 \times 10^{5}$ | 126 | $8.85 \times 10^{-1}$ |
| $^{129}I$ | $1.570 \times 10^{7}$ | 129 | $3.57 \times 10^{-2}$ |
| $^{135}Cs$ | $2.300 \times 10^{6}$ | 135 | $5.36 \times 10^{-1}$ |
| $^{137}Cs$ | $3.000 \times 10^{1}$ | 137 | $9.15 \times 10^{4}$ |
| $^{151}Sm$ | $8.999 \times 10^{1}$ | 151 | $4.28 \times 10^{2}$ |
| $^{210}Pb$ | $2.230 \times 10^{1}$ | 210 | $5.67 \times 10^{-8}$ |
| $^{226}Ra$ | $1.600 \times 10^{3}$ | 226 | $4.11 \times 10^{-7}$ |
| $^{227}Ac$ | $2.177 \times 10^{1}$ | 227 | $7.51 \times 10^{-6}$ |
| $^{229}Th$ | $7.339 \times 10^{3}$ | 229 | $2.75 \times 10^{-7}$ |
| $^{230}Th$ | $7.700 \times 10^{4}$ | 230 | $1.37 \times 10^{-4}$ |
| $^{231}Pa$ | $3.277 \times 10^{4}$ | 231 | $2.69 \times 10^{-5}$ |
| $^{232}U$ | $7.200 \times 10^{1}$ | 232 | $3.93 \times 10^{-2}$ |

**Table 19-1. List of 43 radionuclides in the TPA Version 4.0 code with associated half-lives, isotopic weights, and initial waste package inventories (cont'd)**

| Radionuclide | Half-life (yr) | Mol. Wt. (Isotopic Wt.) | Initial WP Inventory (Ci/MTU at 10 yr) |
|---|---|---|---|
| $^{233}U$ | $1.585 \times 10^{5}$ | 233 | $3.44 \times 10^{-5}$ |
| $^{234}U$ | $2.445 \times 10^{5}$ | 234 | $1.18 \times 10^{0}$ |
| $^{235}U$ | $7.038 \times 10^{8}$ | 235 | $1.71 \times 10^{-2}$ |
| $^{236}U$ | $2.341 \times 10^{7}$ | 236 | $2.81 \times 10^{-1}$ |
| $^{237}Np$ | $2.140 \times 10^{6}$ | 237 | $4.34 \times 10^{-1}$ |
| $^{238}Pu$ | $8.774 \times 10^{1}$ | 238 | $3.77 \times 10^{3}$ |
| $^{238}U$ | $4.468 \times 10^{9}$ | 238 | $3.15 \times 10^{-1}$ |
| $^{239}Pu$ | $2.406 \times 10^{4}$ | 239 | $3.69 \times 10^{2}$ |
| $^{240}Pu$ | $6.537 \times 10^{3}$ | 240 | $5.44 \times 10^{2}$ |
| $^{241}Pu$ | $1.440 \times 10^{1}$ | 241 | $9.22 \times 10^{4}$ |
| $^{241}Am$ | $4.322 \times 10^{2}$ | 241 | $2.08 \times 10^{3}$ |
| $^{242}Pu$ | $3.869 \times 10^{5}$ | 242 | $2.10 \times 10^{0}$ |
| $^{242m}Am$ | $1.520 \times 10^{2}$ | 242 | $2.48 \times 10^{1}$ |
| $^{243}Cm$ | $2.850 \times 10^{1}$ | 243 | $2.55 \times 10^{1}$ |
| $^{243}Am$ | $7.380 \times 10^{3}$ | 243 | $2.64 \times 10^{1}$ |
| $^{244}Cm$ | $1.811 \times 10^{1}$ | 244 | $2.68 \times 10^{3}$ |
| $^{245}Cm$ | $8.499 \times 10^{3}$ | 245 | $3.66 \times 10^{-1}$ |
| $^{246}Cm$ | $4.731 \times 10^{3}$ | 246 | $7.62 \times 10^{-2}$ |

```
**
constant
ElevationOfRepositoryHorizon[m]
1072.0
**
constant
WastePackagePayload[MTU]
9.76
**
```

The first value is used in the NFENV module and shows the elevation of the upper block of the repository is 1,072 m above sea level. The second constant, in the EBSREL consequence module, indicates the average WP has a waste payload of 9.76 MTU.

#### 19.2.2.2 iconstant

The **iconstant** keyword is the same as the **constant** keyword, except that the value must be of type integer instead of real. Some compilers are more forgiving and will read noninteger numbers rather then convert them into integer values. For example, the SUN FORTRAN compiler (SunSoft, Inc., 1996) will read the number 200.5 as 200 and will read the number 2.34e3 as 2340, although neither are originally in integer format. The user is encouraged to only use integers to avoid input problems. The user also is encouraged to check the output files (especially *cp.tpa*, which is described in section 20.4) to verify that the data were read properly. Examples of the use of **iconstant** are

```
**
iconstant
NumberOfRealizations
1
**
iconstant
NumberOfTimeStepsInCompliancePeriod
201
**
```

The first example specifies the number of realizations or vectors. The second dictates the number of time steps in the compliance period used by EXEC to synchronize the transfer of data between consequence modules.

#### 19.2.2.3 uniform

The **uniform** keyword specifies the uniform distribution type of PDF for a parameter. This requires three lines consisting of the keyword **uniform**, the unique name of the parameter, and the lower and upper limits of the uniform distribution. The value of the parameter has zero probability outside this range and uniform probability within this range. The TPA code includes many error checking routines such as checking that the minimum value is less than the maximum value. Examples of distributions defined using the keyword **uniform** include:

```
**
uniform
ArealAverageMeanAnnualInfiltrationAtStart[mm/yr]
2.0, 10.0
**
uniform
WellPumpingRateAtReceptorGroup20km[gal/day]
4.5e6, 1.3e7
**
```

The first example, currently used by UZFLOW, varies the initial MAI into the repository horizon. The second example is currently used in the DCAGW module to account for borehole dilution at 20 km and to calculate dose of the groundwater radionuclides.

#### 19.2.2.4 iuniform

The **iuniform** keyword starts the definition of the integer uniform PDF for a parameter. The complete description of the parameter and PDF requires three lines. The first line contains the keyword

**iuniform**. The second identifies the unique name of the parameter (up to 60 characters). The third line presents two integer values representing the low and high values, inclusively. The low value must be less than the high. Each value beginning with the low and including the high are equally probable. An example of the use of **iuniform** is provided:

```
**
iuniform
RandomNumberToSelect1of125GENIIRealizations
1, 125
**
```

This example was used in an earlier version of DCAGW in which one of the 125 stored results for DCFs is selected and used for the realization.

#### 19.2.2.5 loguniform

The **loguniform** keyword begins defining a log-uniform PDF for a parameter. The entire description requires three lines. The first line specifies the keyword **loguniform**. The second contains the unique name of the parameter, using up to 60 characters. The third sets the lower and upper limits of the log-uniform distribution. The values of the lower and upper limits are not log-transformed. The TPA code log-transforms the lower and upper limits. These log-transformed values are considered in the same way as the upper and lower limits of the uniform distribution. As with the uniform PDF, the lower limit must be less than the upper limit. Presented is an example of the log-uniform distribution definition:

```
**
loguniform
VolcanicEventDuration[s]
6.13e+4, 7.24e6
**
```

This example is used in ASHPLUMO for the duration of a volcanic eruption as well as to calculate the ash and SF deposition from an extrusive event.

#### 19.2.2.6 normal

The **normal** keyword assigns the normal PDF to a sampled parameter. This keyword requires three lines. The first line contains the keyword **normal**. The second line specifies the unique name of the parameter to 60 characters. The third line provides two values to identify the normal PDF. Frequently, analysts use the mean and standard deviation to describe the normal PDF, but not here. For this keyword, the normal distribution is defined by the value at 3.09 standard deviations below the mean and 3.09 standard deviations above the mean. Another way of depicting this distribution is that the corresponding CDF have values of 0.001 (0.1 percent quantile) and 0.999 (99.9 percent quantile). This method of describing normal distributions is a continuation of that used by Iman and Shortencarier (1984). Next is an example of a normal distribution being assigned to a parameter.

```
**
normal
InitialRadiusOfSFParticle[m]
7.0e-4, 3.0e-3
**
```

Currently this parameter is being used by the EBSREL module. The distribution for the initial radius of the SF particle has a 0.001 quantile value of $7.0\times10^{-4}$ and a 0.999 quantile value of $3.0\times10^{-3}$ m.

### 19.2.2.7 lognormal

Requiring three lines, the **lognormal** keyword begins the definition of the lognormal PDF for a parameter. The first line presents the keyword **lognormal**. The second provides the unique name of the parameter (up to 60 characters). The third line identifies the lower and upper limits used to describe the lognormal PDF. The values are not log-transformed. The lower and upper limits represent the parameter values where the CDF has a value of 0.001 (0.1 percent quantile) and 0.999 (99.9 percent quantile). This method of describing lognormal distributions is a continuation of that used by Iman and Shortencarier (1984). The following are examples of the lognormal distribution definition:

```
**
lognormal
MatrixKD_CHnzAm[m3/kg]
1.2e+01    1.1e+07
**
lognormal
MatrixPermeability_TSw_[m2]
0.2e-19     0.2e-17
**
```

The first parameter is presently used by the UZFT module. The distribution of the $K_d$ for Am in the Calico Hills (nonwelded zeolitic) stratigraphic unit has a 0.001 quantile of $1.2 \times 10^{1}$ and a 0.999 quantile of $1.1 \times 10^{7}$ $m^3/kg$. The second parameter for the matrix permeability of the Topopah Spring (welded) stratigraphic unit is used in UZFT and has a 0.001 quantile value of $2.0 \times 10^{-20}$ and a 0.999 quantile value of $2.0 \times 10^{-18}$ $m^2$.

### 19.2.2.8 beta

The **beta** keyword starts the definition of the beta PDF for a parameter. This definition requires three lines. The first line contains the keyword **beta**. The second line includes the unique name of the parameter, using up to 60 characters. The third line sets the four values used to describe the beta PDF. The first two input values control the range of the parameter, and the last two, $\alpha$ and $\beta$, control the shape of the beta distribution. The beta distribution has zero probability of having a value less than the lower limit or greater than the upper limit. Two examples are provided:

```
**
beta
NWFaultZoneWidth[m]
0.5, 275.0, 1.25, 15.0
**
beta
NEFaultZoneWidth[m]
0.5, 365.0, 1.25, 15.0
**
```

Currently, this example is employed in FAULTO. The parameters determine the width for northwest- and northeast-trending faults. Northwest fault zone widths range from 0.5 to 275 m, while the

northeast fault zone widths vary from 0.5 to 365 m. Both distributions have the same shape parameters of 1.25 and 15.0.

#### 19.2.2.9 logbeta

The **logbeta** keyword begins definition of the log-beta PDF for a parameter, which requires three lines. The first line consists of the keyword **logbeta**. The second specifies the unique name of the parameter to 60 characters. The third line presents four values used to describe the log-beta PDF. The first two values control the range of the parameters and the last two, $\alpha$ and $\beta$, control the shape of the distribution. The parameter has zero probability of having a value less than the lower limit or greater than upper limit. The values of the lower and upper limits are not log-transformed values. Here is an example:

```
**
logbeta
MaxtixSaturatedHydraulicConductivityOfTSw[from SNL TSPA-93]
2.88e-13, 1.07e-8, 0.980, 1.875
**
```

This example is not currently being used in the simulation of the proposed repository, but is based on data in the Sandia National Laboratories TSPA-93 report (Wilson et al., 1994) for the matrix saturated hydraulic conductivity of the Topopah Spring (welded) rock unit near the repository horizon.

#### 19.2.2.10 triangular

Requiring three lines, the **triangular** keyword begins defining the triangular PDF for a parameter. The first line is the keyword **triangular**. The second line identifies the unique name of the parameter, using up to 60 characters. The third line includes three values used to describe the triangular PDF. The values represent the minimum, peak, and maximum parameter values. An example is presented:

```
**
triangular
SolubilityNp[kg/m3]
1.2e-3, 3.4e-2, 2.4e-0
**
```

This example was used in an earlier version of the EBSREL module for the solubility of Np. Based on experimental observations, geochemists estimated the solubility ranges from $1.2 \times 10^{-3}$ to $2.4 \times 10^{0}$ kg/m$^3$ with a mode of $3.4 \times 10^{-2}$ kg/m$^3$. The distribution was approximated by a triangular distribution.

#### 19.2.2.11 logtriangular

The **logtriangular** keyword starts the definition of the log-triangular PDF for a parameter. To implement this keyword, the user must specify three lines. The first line depicts the keyword **logtriangular**. The second line contains the unique name of the parameter (up to 60 characters). The third line sets the three values used to describe the log-triangular PDF. The values represent the minimum, peak, and maximum parameter. These values are not log-transformed. The following is an example:

```
**
logtriangular
```

```
AshMeanParticleLogDiameter[d_in_cm]
0.01, 0.1, 1.0
**
```

This example is currently being used in the ASHPLUMO module. The mean value for the diameter of an ash particle is approximated by a log-triangular distribution having a range from 0.01 to 1.0 cm and a mode of 0.1 cm.

#### 19.2.2.12 exponential

Specifications for the **exponential** keyword consist of three lines as this keyword starts defining the exponential PDF for a parameter. The first line contains the keyword **exponential**. The second specifies the unique name of the parameter to 60 characters. The third line indicates one value used to describe the exponential PDF. This value represents the decay or recurrence probability (see chapter 3). Here is an example of the exponential PDF:

```
**
exponential
WindSpeed[cm/s]
0.00083
**
```

ASHPLUMO currently uses this parameter. The wind speed is exponentially distributed with a proportionality constant of 0.00083 s/cm.

#### 19.2.2.13 finiteexponential

The **finiteexponential** keyword begins the definition of the finite exponential PDF for a parameter. Three lines are required to use this keyword option. The first line presents the keyword **finiteexponential**. The second identifies the unique name of the parameter, using up to 60 characters. The third includes the three values used. The first two values represent the minimum and maximum acceptable values. The last value represents the decay or proportionality constant (the same as for the exponential PDF). The finite exponential distribution has the advantage of forcing an event to occur within a range, yet the PDF retains the exponential shape. An example is given.

```
**
finiteexponential
TimeOfNextVolcanicEventinRegionOfInterest[yr]
100.0, 10000.0, 1.0e-7
**
```

Currently this parameter is used in VOLCANO. The distribution for this parameter could be used to generate the time of the next volcanic event in the region of interest, given its annual probability to be one in ten million and also requiring that the event occur from 100 yr to 10,000 yr.

#### 19.2.2.14 hazardcurve

Requiring at least five lines, the **hazardcurve** keyword begins the definition of a hazard curve used to generate a time series of events. The first line depicts the keyword **hazardcurve**. The second line indicates the unique name of the parameter (up to 60 characters). The third line contains one integer value

used to describe the number of intervals into which the hazard curve has been discretized. Following this line, there is one line for each hazard curve interval with each line having a magnitude and a corresponding return period. The only requirements for these values are for the periods to be in ascending order and the magnitudes to be monotonic. The following is an example:

```
**
hazardcurve
SeismicHazardCurveforSEISMO
10
0.05 180.0
0.10 500.0
0.15 1200.0
0.20 2400.0
0.25 4400.0
0.30 7800.0
0.35 11000.0
0.40 20000.0
0.45 30000.0
0.50 44000.0
**
```

This example is used to generate a history of seismic events over the TPA simulation for the SEISMO module. The seismic history will have numerous events of the smallest magnitude (0.05 g) and a few of the higher magnitudes. There are 10 magnitudes of events that will be generated in the seismic history (0.05, 0.1, 0.15, 0.20, 0.25, 0.30, 0.35, 0.40, 0.45, and 0.50 g acceleration). The corresponding return periods for these events are 180; 500; 1,200; 2,400; 4,400; 7,800; 11,000; 20,000; 30,000; and 44,000 yr.

#### 19.2.2.15 userdistribution

The **userdistribution** keyword starts the definition of the user-supplied discrete PDF. Use of this keyword requires at least five lines. The first line is the keyword **userdistribution**. The second specifies the unique name of the parameter to 60 characters. The third presents one value to describe the number of user-supplied values. Each subsequent line contains one of the user-supplied values—all having equal probability. An example is provided:

```
**
userdistribution
ThresholdDisplacementforFaultDisruptionOfWP[m]
4
0.1
0.2
0.3
0.4
**
```

This parameter is currently used in the FAULTO module. There are four values for the threshold displacement for faults disrupting WPs (0.1, 0.2, 0.3, and 0.4 m).

#### 19.2.2.16 correlateinputs

The **correlateinputs** keyword is used to introduce correlations between two input parameters. The correlation is based on the rank transformed parameters. This description requires four lines as shown. The

first line gives the keyword **correlateinputs**. The second line contains the unique name of the first parameter (up to 60 characters). The third line includes the unique name of the second parameter, using up to 60 characters. Both the first and second parameters must be defined elsewhere in the input file. The fourth line has one value representing the rank correlation between input parameters. Below is an example.

```
**
correlateinputs
SubAreaWetFraction
ArealAverageMeanAnnualInfiltrationAtStart[mm/yr]
0.631
**
```

This example specifies a rank correlation of 0.631 between the wet fraction of the subarea used in EBSREL and the MAI used in UZFLOW.

## 19.3 AUXILIARY DATA FILES

The primary purpose of auxiliary input files is to provide data to the TPA code in large arrays, especially parameters that vary as functions of time. The user is not expected to change these data files frequently. All auxiliary files are located in the subdirectory *data*. In addition to auxiliary data files, the TPA code has other useful files in the subdirectory *data*. Table 19-2 lists these auxiliary data files and identifies which modules use them. Additional details are presented in appendix B.

## 19.4 DISCUSSION ON GLOBAL PARAMETERS

Aside from choosing all eight subareas or the whole repository as one subarea, the user can also target groundwater release calculations to one subarea by selecting appropriate parameters (i.e., StartAtSubarea and StopAtSubarea) in the *tpa.inp* file.

To obtain results at the compliance time and the maximum simulation time, the user can specify a compliance time smaller than the maximum simulation time and associated time intervals. The user specifies the compliance time and numbers of time intervals at which TPA outputs are to be obtained. The user can also obtain outputs at a time beyond the compliance time in the same TPA code execution. The number of time intervals must be modified so that the sum of pre- and post-compliance time intervals does not exceed the intervals permitted by the dimensioning in the code (appendix A). The pre- and post-compliance periods can have independent and nonuniform time steps.

The user must specify the output mode in the *tpa.inp* file to generate outputs in addition to those contained in the **.res* files (as described in the next chapter). To minimize use of disk space, several options are available for the user to specify in the *tpa.inp* file. The user can generate these outputs only for a limited number of realizations (instead of for all realizations) by specifying starting and ending realization numbers for which the outputs are intended to be stored. Also, the user can select a specific module for which the intermediate outputs are to be stored. The user can select all modules at a time, but not a combination of a few modules. A screen display provides the user an estimate of the disk space requirement at the beginning of the code execution.

The TPA code allows the user to conduct code execution for a subset of realizations for which the parameters are sampled. This option is particularly advantageous if the user needs to repeat the run and only

focus on a particular segment of a long TPA run. Focusing on a particular segment allows the user to specify appropriate append options for additional intermediate output generation.

As presented in chapter 3, the TPA Version 4.0 code uses a database of 43 nuclides. All these nuclides are considered for the direct release calculations; however, for groundwater release calculations one can avoid the computational burden imposed by short-lived nuclides by specifying only a selected list of nuclides. The basecase data set uses the following list of nuclides and chains for the groundwater release calculations (table 19-2). This list is similar to the list used in IPA Phase 2 studies except that $^{137}Cs$, which does not make a significant contribution to dose, has been eliminated.

Inventories for each nuclide can be computed using the initial waste inventories and the total waste emplaced in the repository. Nuclide initial inventories in Ci/MTU are specified in the *nuclides.dat* file (section 3.3.2—INVENT and table 19-1). The total waste emplaced in the repository is specified in the *tpa.inp* parameter TotalWasteEmplacedInRepository[MTU] and is also written to the screen at the beginning of a TPA simulation.

**Table 19-2. Description of auxiliary data files**

| File | Used by | Description |
|---|---|---|
| *burnup.dat* | INVENT | Time history of the thermal output and blend for the pressurized water reactor and boiling water reactor spent fuel |
| *climato1.dat* | UZFLOW | Climatic variation data are a vector of random numbers sampled from a normal distribution with zero mean and unit standard deviation; the vector is internally partitioned into sets of MAP/MAT noise with length equal to the number of climate time steps. |
| *climato2.dat* | UZFLOW | Time history for climatic variation; the *climato2.dat* input file contains<br>Column 1: time instant (yr)<br>Column 2: corresponding fraction of full glacial MAP<br>Column 3: corresponding fraction of full glacial MAT |
| *dilution.dat* | DCAGW | Cross-sectional fraction of radionuclide plume to be captured by the pumping well by the residential lifestyle receptor group |
| *drythick.dat* | *NFENV* | Temporal profile of dryout zone thickness in meters for REFLUX3 module from MULTIFLO |
| *filename.dat* | DCAGW/ GENTPA | Assigns file names to logical unit numbers for input and output files for the GENTPA stand-alone code |
| *gbioac1.dat* | DCAGW/ GENTPA | Bioaccumulation factors (not used, but option is available) |
| *gdosinc2.dat* | DCAGW/ GENTPA | Contains single line header that describes the *gnewdf.dat* data file contents (for tracking file changes) |
| *ggamen.dat* | DCAGW/ GENTPA | Gamma energies (MeV/dis) for six energy groups for each radionuclide; used for finite plume calculations |
| *ggrdf.dat* | DCAGW/ GENTPA | External dose coefficients for all radionuclides for air submersion, water surface, soil surface, deep soil, and buried waste |
| *gnewdf.dat* | DCAGW/ GENTPA | Age-dependent internal dose coefficients for infant, toddler, preteen, teen, adult, and adultFG11 receptor groups |
| *grmdlib.dat* | DCAGW/ GENTPA | Radionuclide master library containing list of all radionuclides and radiological decay data |
| *gs_cb_ad.dat* | DCAGS | Dose conversion factors for ground surface, current biosphere, farming lifestyle receptor group at or beyond 20-km distance (Amargosa Desert) |
| *gs_cb_ci.dat* | DCAGS | Dose conversion factors for ground surface, current biosphere, residential lifestyle receptor group at distance between 5 and 20 km |

**Table 19-2. Description of auxiliary data files (cont'd)**

| File | Used by | Description |
|---|---|---|
| *gs_pb_ad.dat* | DCAGS | Dose conversion factors for ground surface, pluvial biosphere, farming lifestyle receptor group at or beyond 20-km distance (Amargosa Desert) |
| *gs_pb_ci.dat* | DCAGS | Dose conversion factors for ground surface, pluvial biosphere, residential lifestyle receptor group at distance between 5 and 20 km |
| *maidtbl.dat* | UZFLOW | Table of digital elevation models providing expected MAI for different climates; values computed using ITYM preprocessor described in appendix H |
| *multiflo.dat* | NFENV | MULTIFLO output; currently provides chloride history only; read from 12th column; no calculations performed beyond 10,000 yr; values at 100,000 yr are starting values because chloride concentration for times greater than 10,000 yr will approach J-13 well water |
| *nuclides.dat* | INVENT | Nuclide-specific data for 43 radionuclides analyzed in TPA code including isotope name, element name, molecular weight, half-life, EPA limit, and initial inventory 10 yr from the reactor; information also presented in table 19-1 |
| *repdes.dat* | READER | Contains coordinates for repository outline, drift angle, and starting and stopping points of emplacement blocks; information used to determine coordinates and number of waste packages for each drift |
| *strmtube.dat* | SZFT | Streamtube information for generating *nefmks.f* input files; basecase data file contains streamtube definitions only to 20 km |
| *tefkti.inp* | NFENV | Used only when option for using tabular data for temperature and relative humidity is turned on in *tpa.inp* file |
| *tpanames.dbs* | EXEC | Contain eight character abbreviations for parameter names used in *tpa.inp* file; used in *samplpar.hdr* file if parameter sampled |
| *wpflow.def* | EBSREL | Time history of factors that account for flow reaching waste package ($F_{ow}$) and near-drift and in-drift flow diversions ($F_{mult}$) |

**Radionuclides for Groundwater Releases**

| | | | |
|---|---|---|---|
| 1. | $^{246}Cm$ | 11. | $^{226}Ra$ |
| 2. | $^{238}U$ | 12. | $^{210}Pb$ |
| 3. | $^{245}Cm$ | 13. | $^{135}Cs$ |
| 4. | $^{241}Am$ | 14. | $^{129}I$ |
| 5. | $^{237}Np$ | 15. | $^{99}Tc$ |
| 6. | $^{243}Am$ | 16. | $^{59}Ni$ |
| 7. | $^{239}Pu$ | 17. | $^{14}C$ |
| 8. | $^{240}Pu$ | 18. | $^{79}Se$ |
| 9. | $^{234}U$ | 19. | $^{94}Nb$ |
| 10. | $^{230}Th$ | 20. | $^{36}Cl$ |

**Radionuclide Chains for Groundwater Release**

| | | | |
|---|---|---|---|
| 1. | $^{246}Cm \rightarrow {}^{238}U$ | 8. | $^{99}Tc$ |
| 2. | $^{245}Cm \rightarrow {}^{241}Am \rightarrow {}^{237}Np$ | 9. | $^{59}Ni$ |
| 3. | $^{243}Am \rightarrow {}^{239}Pu$ | 10 | $^{36}Cl$ |
| 4. | $^{240}Pu$ | 11. | $^{14}C$ |
| 5. | $^{234}U \rightarrow {}^{230}Th \rightarrow {}^{226}Ra \rightarrow {}^{210}Pb$ | 12. | $^{79}Se$ |
| 6. | $^{135}Cs$ | 13. | $^{94}Nb$ |
| 7. | $^{129}I$ | | |

# 20 OUTPUT FILES

The TPA Version 4.0 code generates a number of output files for later use in sensitivity analyses, evaluation of subsystem performance measures, and total-system performance measures. These output files are summarized in tables 20-1 and 20-2. The files, which are in ASCII format, contain data about sampled parameters, constant parameters, module variables, compliance with the EPA release standard, and time-dependent annual doses. Output files containing values generated in consequence module calculations are described in the intermediate results sections of chapters 4–18 for each module.

## 20.1 DESCRIPTION OF PRIMARY OUTPUT FILES

This section provides the format and structure of the primary TPA output files in tables 20-1 and 20-2. Also, noteworthy aspects of certain primary output files (*samplpar.abb*, *samplpar.hdr*, *wpsfail.res*, *infilper.res*, *nearfld.res*, and the files with EPA release limits) are highlighted in the subsequent sections.

The primary output files are identified by the extension *.res* (for result). Table 20-1 lists the names and a general description of the contents of these files. The primary output files (*res*) have several lines at the beginning of the file that uniquely identify a TPA Version 4.0 code run. The first five lines of each output file are standardized and have the format

```
title1
title2
code version, time and date of start of run
description of file data, first line
description of file data, second line
```

The first two lines are the title lines defined in the *tpa.inp* file. These lines are of type character and are up to 80 characters in length. The third line contains the name and version of the code being used followed by the time and date of the start of the run. The information in these lines provides a unique identification of the run in all of the *.res* files as required by the QA procedure. The fourth and fifth lines provide brief descriptions of the file contents. Following these five identifier lines, there are two column header lines. The first represents the column names and the second provides corresponding units. Subsequent lines indicate the data from the TPA runs.

There are several parameters in the *tpa.inp* file that affect the total size of the output files. The user is advised to set the parameters judiciously to avoid creating enormous amounts of data that can consume all available disk space and cause the TPA run to abort. The parameters to set include

```
VolcanismDisruptiveScenarioFlag(yes=1,no=0)
NumberOfRealizations
StartAtRealization
StopAtRealization
DurationOfCompliancePeriod[yr]
MaximumTime[yr]
NumberOfTimeStepsInCompliancePeriod
NumberOfTimeStepsAfterCompliancePeriod
.
.
.
OutputMode(0=None,1=All,2=UserDefined)
```

**Table 20-1. TPA Version 4.0 code primary output files**

| Files | Description |
|---|---|
| *airpkdos.res* | total ground surface peak dose, time of peak dose, and dose from each nuclide at the time of peak dose |
| *arpkds_c.res* | total ground surface peak dose, time of peak dose, and dose from each nuclide at the time of peak dose for the compliance period |
| *ashout.res* | surface areal ash density and areal fuel density, and some key input parameters, such as plume height, ash mass, and vent velocity |
| *cumrel.res* | engineered barrier system (EBS), unsaturated zone (UZ), and saturated zone cumulative release over all subareas |
| *cumrel_c.res* | EBS, UZ, and SZ cumulative release over all subareas for the compliance period |
| *gsccdf.res* | complementary cumulative distribution function (CCDF) of U.S. Environmental Protection Agency (EPA) normalized release limits for the ground surface release |
| *gsccdf_c.res* | CCDF of EPA normalized release limits for the ground surface release for the compliance period |
| *gwccdf.res* | CCDF of EPA normalized release limits for the groundwater release |
| *gwccdf_c.res* | CCDF of EPA normalized release limits for the groundwater release for the compliance period |
| *gwpkdos.res* | total groundwater peak dose, time of peak dose, and dose from each nuclide at the time of peak dose |
| *gwpkds_c.res* | total groundwater peak dose, time of peak dose, and dose from each nuclide at the time of peak dose for the compliance period |
| *gwttuzsz.res* | groundwater travel time (GWTT) by subarea (UZ, SZ, and total), including averages |
| *infilper.res* | average flow rates for percolation (infiltration), reflux, and diversion |
| *nearfld.res* | average waste package (WP) temperature, relative humidity (RH), and chloride concentration |

**Table 20-1. TPA Version 4.0 code primary output files (cont'd)**

| Files | Description |
|---|---|
| *pkdoset.res* | groundwater peak dose and corresponding time for each nuclide |
| *npkdst_c.res* | groundwater peak dose and corresponding time for each nuclide for the compliance period |
| *pkreltim.res* | EBS peak release rates and corresponding time for each nuclide |
| *pkrltm_c.res* | EBS peak release rates and corresponding time for each nuclide for the compliance period |
| *relccdf.res* | CCDF of EPA normalized release limits for the total release (groundwater + ground surface) |
| *rlccdf_c.res* | CCDF of EPA normalized release limits for the total release (groundwater + ground surface) |
| *relgwgs.res* | EPA normalized release limits for the groundwater, ground surface, and total (groundwater + ground surface) releases |
| *rlgwgs_c.res* | EPA normalized release limits for the groundwater, ground surface, and total (groundwater + ground surface) releases for the compliance period |
| *samplpar.abb* | header file for *samplpar.res* with sampled parameter abbreviations |
| *samplpar.hdr* | header description file for *samplpar.res* with sampled parameter abbreviations accompanying the complete sampled parameter names |
| *samplpar.res* | sampled parameter values for each vector |
| *totdos_c.res* | total dose summed for all nuclides by vector and by time and dilution volume for the compliance period |
| *totdose.res* | total dose summed for all nuclides by vector and by time and dilution volume |
| *wpsfail.res* | number of WPs failed, time of WP failure, and type of event (i.e., volcanic seismic, faulting, and corrosion) |

**Table 20-2. Detailed data structure for the primary output files**

| File | Column | Generating Module | Description |
|---|---|---|---|
| *airpkdos.res* and *arpkds_c.res* | 1 | *exec.f* | vector |
| | 2 | *exec.f* | time of peak total effective dose equivalent (TEDE) (direct release) [yr] |
| | 3 | *dcags.f* | peak TEDE (direct release) [rem/yr] |
| | 4 | *dcags.f* | nuclide 1 TEDE at time of peak TEDE (direct release) [rem/yr] |
| | 5 | *dcags.f* | nuclide 2 TEDE at time of peak TEDE (direct release) [rem/yr] |
| | 6 | *dcags.f* | nuclide 3 TEDE at time of peak TEDE (direct release) [rem/yr] |
| | ... | *dcags.f* | etc., for all nuclides |
| | n+3 | *dcags.f* | nuclide n TEDE at time of peak TEDE (direct release) [rem/yr] |
| | The preceding is repeated for all vectors.<br>number of rows = number of vectors | | |
| *ashout.res* | 1 | *exec.f* | vector |
| | 2 | *volcano.f* | time of volcanic event [yr] |
| | 3 | *exec.f* | number of waste packages (WP) exhumed |
| | 4 | *ashplume.f* | areal ash density [g/cm$^2$] |
| | 5 | *ashplume.f* | areal spent fuel density [g/cm$^2$] |
| | 6 | *ashplume.f* | column height [km] |
| | 7 | *ashplume.f* | ash mass [g] |
| | 8 | *ashplume.f* | vent exit velocity [cm/sec] |
| | The preceding is repeated for all vectors.<br>number of rows = number of vectors | | |
| *cumrel.res* and *cumrel_c.res* | 1 | *exec.f* | vector |
| | 2 | *exec.f* | name of nuclide 1 |
| | 3 | *ebsrel.f* | cumulative release from engineered barrier system, summed over all subareas [Ci] |
| | 4 | *uzft.f* | cumulative release from unsaturated zone (UZ), summed over all subareas [Ci] |

**Table 20-2. Detailed data structure for the primary output files (cont'd)**

| File | Column | Generating Module | Description |
|---|---|---|---|
| | 5 | *szft.f* | cumulative release from saturated zone (SZ), summed over all subareas [Ci] |
| | This is repeated for all vectors for nuclide 1. | | |
| | The foregoing is repeated for all nuclides.<br>number of rows = number of vectors × number of nuclides | | |
| *gsccdf.res* and *gsccdf_c.res* | 1 | *exec.f* | normalized release value for direct release |
| | 2 | *exec.f* | probability |
| | number of rows = number of unique release values | | |
| *gwccdf.res* and *gwccdf_c.res* | 1 | *exec.f* | normalized release value for groundwater |
| | 2 | *exec.f* | probability |
| | number of rows = number of unique normalized release values | | |
| *gwpkdos.res* and *gwpkds_c.res* | 1 | *exec.f* | vector |
| | 2 | *dcagw.f* | time of peak TEDE groundwater release [yr] |
| | 3 | *dcagw.f* | peak TEDE groundwater release [rem/yr] |
| | 4 | *dcagw.f* | nuclide 1 TEDE at time of peak TEDE groundwater release [rem/yr] |
| | 5 | *dcagw.f* | nuclide 2 TEDE at time of peak TEDE groundwater release [rem/yr] |
| | 6 | *dcagw.f* | nuclide 3 TEDE at time of peak TEDE groundwater release [rem/yr] |
| | ... | *dcagw.f* | etc., for all nuclides |
| | n+3 | *dcagw.f* | nuclide n TEDE at time of peak TEDE groundwater release [rem/yr] |
| | n+4 | *exec.f* | time of peak drinking water dose [yr] |
| | n+5 | *exec.f* | peak drinking water dose [rem/yr] |
| | The preceding is repeated for all vectors. | | |
| *gwttuzsz.res* | number of rows = number of vectors | | |
| | 1 | *exec.f* | vector |
| | 2 | *uzft.f* | subarea 1 UZ groundwater travel time (GWTT) [yr] |

**Table 20-2. Detailed data structure for the primary output files (cont'd)**

| File | Column | Generating Module | Description |
|---|---|---|---|
| | 3 | *uzft.f* | subarea 2 UZ GWTT [yr] |
| | ... | *uzft.f* | etc., for all subareas |
| | nsa+1 | *uzft.f* | subarea nsa UZ GWTT [yr] (nsa = number of subareas) |
| | nsa+2 | *exec.f* | repository average UZ groundwater release travel time [yr] |
| | nsa+3 | *szft.f* | subarea 1 SZ GWTT [yr] |
| | nsa+4 | *szft.f* | subarea 2 SZ GWTT [yr] |
| | ... | *szft.f* | etc., for all subareas |
| | 2(nsa)+2 | *szft.f* | subarea nsa SZ GWTT [yr] |
| | 2(nsa)+3 | *exec.f* | repository average SZ GWTT [yr] |
| | 2(nsa)+4 | *exec.f* | subarea 1 total (UZ + SZ) GWTT [yr] |
| | 2(nsa)+5 | *exec.f* | subarea 2 total (UZ + SZ) GWTT [yr] |
| | ... | *exec.f* | etc., for all subareas |
| | 3(nsa)+3 | *exec.f* | subarea nsa total (UZ + SZ) GWTT [yr] |
| | 3(nsa)+4 | *exec.f* | repository average total (UZ + SZ) GWTT [yr] |
| | The foregoing is repeated for all vectors.<br>number of rows = number of vectors | | |
| *infilper.res* | 1 | *exec.f* | vector |
| | 2 | *exec.f* | time (every $10^{th}$ time step) in years |
| | 3 | *exec.f* | infiltration [mm/yr] from UZFLOW averaged over all subareas |
| | 4 | *exec.f* | infiltration after reflux [mm/yr] from NFENV averaged over all subareas |
| | 5 | *exec.f* | infiltration after diversion [mm/yr], using $F_{mult}$ and $F_{ow}$ parameters, averaged over all subareas |
| | The preceding is repeated for every $10^{th}$ time step. | | |
| | The foregoing is repeated for all vectors.<br>number of rows = number of vectors × number of time steps/10 | | |

**Table 20-2. Detailed data structure for the primary output files (cont'd)**

| File | Column | Generating Module | Description |
|---|---|---|---|
| *nearfld.res* | 1 | *exec.f* | vector |
| | 2 | *exec.f* | time (every 10th time step) [yr] |
| | 3 | *exec.f* | WP temp [°C] averaged over all subareas |
| | 4 | *exec.f* | relative humidity in fraction averaged over all subareas |
| | 5 | *exec.f* | chloride concentration [mol/L] averaged over all subareas |
| | The preceding is repeated for every 10th time step. | | |
| | The foregoing is repeated for all vectors.<br>number of rows = number of vectors × number of time steps/10 | | |
| *npkdoset.res* and *npkdst_c.res* | 1 | *exec.f* | vector |
| | 2 | *exec.f* | nuclide 1 time of peak TEDE [yr] |
| | 3 | *dcagw.f* | nuclide 1 peak TEDE [rem/yr] |
| | ... | — | etc., for all nuclides |
| | 2(n) | — | nuclide n time of peak TEDE [yr] |
| | 2(n)+1 | — | nuclide n peak TEDE [rem/yr] |
| | The preceding is repeated for all vectors.<br>number of rows = number of vectors | | |
| *pkreltim.res* and *pkrltm_c.res* | 1 | *exec.f* | vector |
| | 2 | *exec.f* | name of nuclide 1 |
| | 3 | *ebsrel.f* | peak release rate in subarea 1 for nuclide 1 [Ci/yr] |
| | 4 | *exec.f* | peak release time in subarea 1 for nuclide 1 [yr] |
| | ... | — | etc., for all subareas |
| | 2(nsa)+1 | — | peak release rate in subarea nsa for nuclide 1 [Ci/yr] |
| | 2(nsa)+2 | — | peak release time in subarea nsa for nuclide 1 [yr] |
| | The foregoing is repeated for all vectors for nuclide 1. | | |
| | The preceding is repeated for all nuclides.<br>number of rows = number of vectors × number of nuclides | | |

**Table 20-2. Detailed data structure for the primary output files (cont'd)**

| File | Column | Generating Module | Description |
|---|---|---|---|
| *relccdf.res* and *rlccdf_c.res* | 1 | *exec.f* | total EPA normalized releases with duplicate values combined |
| | 2 | *exec.f* | cumulative probability |
| | number of rows = number of unique total EPA normalized release values | | |
| *relgwgs.res* and *rlgwgs_c.res* | 1 | *exec.f* | vector |
| | 2 | *exec.f* | groundwater EPA release (normalized) |
| | 3 | *exec.f* | direct EPA release (normalized) |
| | 4 | *exec.f* | total EPA release (normalized) |
| | The foregoing is repeated for all vectors.<br>number of rows = number of vectors | | |
| *samplpar.abb* | 1 | *exec.f* | abbreviation for sampled parameter |
| | The preceding is repeated for all sampled parameters.<br>number of rows = number of sampled parameters | | |
| *samplpar.hdr* | 1 | *exec.f* | sampled parameter index |
| | 2 | *exec.f* | sampled parameter abbreviation |
| | 3 | *exec.f* | sampled parameter name |
| | The foregoing is repeated for all sampled parameters.<br>number of rows = number of sampled parameters | | |
| | row | — | data are in format for *snllhs.f* output (i.e., five columns) |
| | 1 | *exec.f* | vector |
| | 1 | *exec.f* | number of sampled parameters (nsp) |
| | 2 | *exec.f* | row 2 provides sampled parameters in five columns until number of sampled parameters exhausted |
| | ... | *exec.f* | |
| | nsp/5 +1 | *exec.f* | |
| | The preceding is repeated for all vectors. | | |

**Table 20-2. Detailed data structure for the primary output files (cont'd)**

| File | Column | Generating Module | Description |
|---|---|---|---|
| *totdose.res* and *totdos_c.res* | 1 | *exec.f* | vector |
| | 2 | *exec.f* | time [yr] |
| | 3 | *exec.f* | TEDE [rem/yr] |
| | 4 | *dcagw.f* | dilution volume [$m^3$/yr] |
| | The foregoing is repeated for each time step. | | |
| | The preceding is repeated for all vectors.<br>number of rows = number of vectors × number of time steps | | |
| *wpsfail.res* | 1 | *exec.f* | vector |
| | 2 | *exec.f* | time of container failure [yr] |
| | 3 | *ebsfail.f* | number of WPs failed due to corrosion |
| | 4 | *seismo.f* | number of WPs failed due to seismic activity |
| | 5 | *faulto.f* | number of WPs failed due to faulting |
| | 6 | *volcano.f* | number of WPs failed due to volcanic activity |
| | The foregoing is repeated for each container failure event in a vector. | | |
| | The preceding is repeated for all vectors.<br>number of rows = (depends on number of vectors and number of times with container failures in each vector) | | |

```
UserDefinedLowerRealizationAppended
UserDefinedUpperRealizationAppended
SelectAppendFiles
```

Some of the primary output files have up to 46 columns that render them highly unreadable. Table 20-2 describes the structure of the *.res* files that should help the user identify output data. In addition to supplying the data structure and corresponding units, table 20-2 also lists which module calculates the output values. If output values from other modules are averaged in *exec.f*, then *exec.f* is listed as the module supplying the values.

In addition to the *.res* extension, *.abb* (for abbreviations) and *.hdr* (for header) are also used for the primary output files. The *.abb* file contains only the abbreviations for names of sampled parameters. The *.hdr* file lists the abbreviations and corresponding sampled parameter names. The latter two files are created for easy identification of column headers combined with appropriate *.res* files when conducting sensitivity analysis using S-plus. A more in-depth description of the files is provided later in this section.

To limit the size of *infilper.res* and *nearfld.res* files, the TPA Version 4.0 code only writes output at every $10^{th}$ time step. The number of lines skipped cannot be adjusted by the user and is fixed at 10.

The normalized EPA cumulative release limits at the receptor compliance boundary are computed in the EXEC and written to the *relgwgs.res* and *rlgwgs_c.res* files for each vector. These release limits do not apply anymore in Part 63, but are maintained in the code for data analysis proposes only. To facilitate data analysis, the EXEC also uses these data. The CCDFs are presented in the same format in each of these files. For example, in the files *relccdf.res* and *rlccdf_c.res*, the first five lines are consistent with the general format described previously. On each subsequent line, the realization number and the summed normalized cumulative release are output, as shown here:

```
Input file tpa.inp as supplied with TPA Version 4.0 Code
Basecase data set Rev 4.0    4/3/00
TPA 4.0, Job started: Tue Apr 14 14:43:45 2000
Total release CCDF for one scenario.
Release Probability
0.34305000E+01    0.00000000E+00
```

## 20.2 DESCRIPTION OF SECONDARY OUTPUT FILES

The TPA Version 4.0 code provides an option to generate additional files with intermediate outputs. When the append option is activated in the *tpa.inp* file, secondary output files are created with *.cum, .rlt,* and *.ech* extensions. Files with *.cum* extensions are output from the stand-alone codes *ashplume.f, failt.f,* GENTPA, *nefmks.f* (for the UZ only), and *releaset.f.* Table 20-3 provides a description of the *.cum* file contents and appendix E discusses each stand-alone code output file listed in this table.

The *.rlt* and *.ech* files are the outputs and inputs passed in the argument list of the consequence modules. Tables 20-4 and 20-5 describe the contents of the *.rlt* and *.ech* files. A further explanation is available in chapter 4, Information Flow, and the Intermediate results in chapters 4–18.

In the *tpa.inp* file, the user selects either all realizations or a range of realizations. For the specified realizations, information is written each time the stand-alone code and consequence module are executed.

The user is cautioned that with the append option on, disk space problems or a "too many files open" condition may arise that will terminate the TPA Version 4.0 code execution. While the disk space problem may not be evident immediately, the error message for too many files open occurs at the beginning of code execution. Section 21.6 provides further discussion of these and other error conditions and some suggestions to eliminate them.

## 20.3 LIST OF OTHER OUTPUT FILES

TPA outputs are presented in another convenient format for data analysis in files with the *.tpa* extension. These files are listed in table 20-6. The files of most frequent interest are *sp.tpa, cp.tpa, rgssa.tpa,* and *rgwsa.tpa.* The files *rgwnr.tpa, rgwsr.tpa, rgwna.tpa, rgwsa.tpa, rgsnr.tpa, rgssr.tpa, rgsna.tpa, rgssa.tpa,* and *rgwgssa.tpa* contain time-dependent annual effective dose equivalent data at the receptor location. The files represent the pathway (either groundwater, ground surface, or both), the realization (either per realization or averaged over all realizations), and the nuclide (either per nuclide or summed over all nuclides).

Files with a time history for each realization can be used to generate hair diagrams of dose as a function of time. These files have an 'r' as the last letter before the file name extension.

The format of the files varies because of the need to report data per realization (or averaged among all realizations) and data per nuclide (or summed among all nuclides). The first few lines of the *rgwsa.tpa* file are provided as an example.

```
Input file tpa.inp as supplied with TPA Version 4.0 Code.
Basecase data set Rev 4.0    4/13/00
TPA 4.0, Job started: Tue Apr 14 14:43:44 2000
TEDE[rem/yr], GroundWater Pathway
summed over all nuclides, averaged over all realizations
0.231E+01   0.100E-14
0.467E+01   0.100E-14
0.709E+01   0.100E-14
0.957E+01   0.100E-14
```

The data have two columns representing the time and annual dose. The first few lines of this example file show no annual dose (the value has been set to a small value of $10^{-15}$ so these data can be plotted using a log scale).

Model input parameters with statistical distributions (i.e., sampled parameters) are designated by the user in the *tpa.inp* file using PDFs such as uniform, normal, lognormal, or beta. Depending on the option selected in the *tpa.inp* file whether LHS is selected, these parameters are either computed with the SNLLHS utility model (LHS), are sampled within the SAMPLER utility module once for each realization (MCS), or are read from a user supplied file. The *exec.f* module writes the values of each sampled parameter for each realization to the file *sp.tpa*. An example of the first few lines of *sp.tpa* is

```
Input file tpa.inp as supplied with TPA Version 4.0 Code.
Basecase data set Rev 4.0    4/3/00
TPA 4.0, Job started: Tue Apr 1 14:43:45 2000
      Sampled Parameters for each realization
      Sampled Parameters change each realization
         0        244
      ArealAverageMeanAnnualInfiltrationAtStart[mm/yr]
      MeanAveragePrecipitationMultiplierAtGlacialMaximum
      MeanAverageTemperatureIncreaseAtGlacialMaximum[degC]
      FractionOfCondensateRemoved[1/yr]
      FractionOfCondensateTowardRepository[1/yr]
      ....etc....
        1        244
        0.6711709E+01
        0.2405849E+01
       -0.7990369E+01
        0.8220503E-05
        0.8044294E+00
```

The first five lines of the example *sp.tpa* are consistent with the general format described previously. The sixth line contains two numbers, the first is the realization count (initially zero to indicate a text section for names rather than a data section) and the second is the number of sampled parameters. In this example, the number of parameters is 244. Next, the name of each sampled parameter is output, one name per line. These names are the same as given in the *tpa.inp* file. Next is a line having two integer numbers representing the realization number and the number of sampled parameters. The second number is the same as provided prior to the listing of names. It is included again as a helpful reminder to the user. Next, the numeric information is provided for all parameters. This is a column of 244 numbers representing

**Table 20-3. Stand-alone cumulative files**

| File | Description |
|---|---|
| *ashplume.cum* | all *ashplume.out* files by realization |
| *failt.cum* | all *failt.out* files by subarea and by realization |
| *ggenii.cum* | all *ggenii.out* files by realization |
| *genv.cum* | all *genv.out* files by realization |
| *dcf.cum* | all *gw_cb_ad.dat* and *gw_pb_ad.dat* files by realization. These files result from postprocessing of the GENTPA *genv.out* files during each realization. |
| *nefiiuz.cum* | all *nefiiuz.out* files (i.e., *nefii.out* from *nefmks.f*) for the unsaturated zone by subarea and by realization |
| *releaset.cum* | all *releaset.out* files by subarea and by realization |

**Table 20-4. Consequence module output files**

| File | Description |
|---|---|
| *ashplumo.rlt* | output from *ashplumo.f*: surface areal spent fuel and ash density |
| *ashrmovo.rlt* | output from *ashrmovo.f*: ground surface releases by time and by nuclide |
| *dcags.rlt* | output from *dcags.f*: ground surface doses by time and by nuclide |
| *dcagw.rlt* | output from *dcagw.f*: groundwater doses by time and by nuclide and the fraction of plume mass captured by pumping well |
| *ebsfail.rlt* | output from *ebsfail.f*: fraction of waste packages (WPs) failed from corrosion by time |
| *ebsrel.rlt* | output from *ebsrel.f*: engineered barrier system releases including *ebsfilt.f* by time and by nuclide |
| *faulto.rlt* | output from *faulto.f*: fraction of WPs failed from faulting by time and by subarea |
| *nfenv.rlt* | output from *nfenv.f*: repository temperature, WP temperature, relative humidity, pH, chloride concentration, downward flow rate in subarea proportional to SA cross-sectional area not occupied by WPs and not directly above a WP, and downward flow rate in SA proportional to cross-sectional area of a WP and directly above a WP |
| *seismo.rlt* | output from *seismo.f*: fraction of WPs failed from seismic activity by time |
| *szft.rlt* | output from *szft.f*: saturated zone releases by time and by nuclide |
| *uzflow.rlt* | output from *uzflow.f*: subarea flow rates by time |
| *uzft.rlt* | output from *uzft.f*: unsaturated zone releases by time and by nuclide, and UZ flow rates by subarea |
| *volcano.rlt* | output from *volcano.f*: inventory ejected, inventory in failed WPs by subarea, and fraction of WPs failed from volcanic activity by time and by subarea |

**Table 20-5. Consequence module input echo files**

| File | Description |
|---|---|
| *ashplumo.ech* | input to *ashplumo.f*: metric tonnes of uranium ejected |
| *ashrmovo.ech* | input to *ashrmovo.f*: time step and surface areal spent fuel density |
| *dcags.ech* | input to *dcags.f*: ash areal density, mean annual precipitation, mean annual temperature, time step, and ground surface releases by time and by nuclide |
| *dcagw.ech* | input to *dcagw.f*: mean annual precipitation, mean annual temperature, time step, and saturated zone releases by time and by nuclide |
| *ebsfail.ech* | input to *ebsfail.f*: time step, repository temperature, waste packages (WPs) temperature, relative humidity, pH, chloride concentration, and flow rate of water hitting the WPs |
| *ebsrel.ech* | input to *ebsrel.f*: time and number of WPs failed by event type, time step, repository temperature, pH, chloride concentration, and flow rate of water hitting the WPs |
| *faulto.ech* | input to *faulto.f*: time step and number of subareas |
| *nfenv.ech* | input to *nfenv.f*: time step and flow rate per WP by subarea |
| *seismo.ech* | input to *seismo.f*: number of seismic events and time and type of each event |
| *szft.ech* | input to *szft.f*: time step and unsaturated zone releases by time and by nuclide |
| *uzflow.ech* | input to *uzflow.f*: time step |
| *uzft.ech* | input to *uzft.f*: engineered barrier system releases by time and by nuclide and subarea flow rates by time |
| *volcano.ech* | input to *volcano.f*: time step and number of subareas |

a vector of sampled parameters for the first realization. The line with two integers (indicating realization number and total number of sampled parameters) follows with the next vector of sampled parameters. This information is repeated for all realizations.

Constant model parameters are specified by the user in the *tpa.inp* file using keywords such as **constant**, **iflag,** and **iconstant**. The output file *cp.tpa* provides the convenience of reviewing all parameters kept constant during a TPA run. Maintaining a distinction between a constant parameter and a sampled parameter is helpful for the analyst who desires to perform a sensitivity analysis. These parameters are not sampled within the SAMPLER utility module, and the values remain fixed for all realizations in the simulation. The *exec.f* module writes the *cp.tpa* file. An example of the first few lines of the *cp.tpa* file is shown here:

```
Input file tpa.inp as supplied with TPA Version 4.0 Code.
     Basecase data set Rev 4.0    4/3/00

TPA 4.0, Job started: Tue Apr 1 14:43:45 2000
Constant Parameters for the run
Constant Parameters do not change during run
```

**Table 20-6. Other useful output files**

| File | Description |
|---|---|
| *cp.tpa* | total-system performance assessment (TPA) *exec.f* output file of the constant parameters in *tpa.inp* |
| *mv.tpa* | TPA *exec.f* output file of module variables |
| *rgsna.tpa* | TPA *exec.f* output file with the time history dose by direct release pathways by nuclide averaged among all realizations |
| *rgsnr.tpa* | TPA *exec.f* output file with the time history dose by direct release pathways by nuclide for all realizations |
| *rgssa.tpa* | TPA *exec.f* output file with the time history dose by direct release pathways summed for all nuclides averaged among all realizations |
| *rgssr.tpa* | TPA *exec.f* output file with the time history dose by direct release pathways summed for all nuclides and for all realizations |
| *rgwgssa.tpa* | TPA *exec.f* output file with the time history dose by groundwater plus dose by direct release pathways summed for all nuclides averaged among all realizations |
| *rgwna.tpa* | TPA *exec.f* output file with the time history of groundwater dose by nuclide averaged among all realizations |
| *rgwnr.tpa* | TPA *exec.f* output file with the time history of groundwater dose by nuclide for all realizations |
| *rgwsa.tpa* | TPA *exec.f* output file with the time history of groundwater dose summed for all nuclides averaged among all realizations |
| *rgwsr.tpa* | TPA *exec.f* output file with the time history of groundwater dose summed for all nuclides and for all realizations |
| *sp.tpa* | TPA *exec.f* output file with the sampled parameter values |
| *spquery.tpa* | TPA *exec.f* output file with the number of times a sampled parameter value was requested for each realization (only available with the append flag on) |

```
1 = VolcanismDisruptiveScenarioFlag(yes=1,no=0)

1 = FaultingDisruptiveScenarioFlag(yes=1,no=0)

1 = SeismicDisruptiveScenarioFlag(yes=1,no=0)

1 = StartAtSubarea

2 = StopAtSubarea

0 = CheckNuclidesAndChains(yes=1,no=0)

0 = DirectReleaseOnlyFlag(yes=1,no=0)
```

The first five lines are consistent with the general format described previously. Next, the values and the names of each of the constant parameters are provided with both the value and the parameter name on the same line. The parameter names match the names defined in the *tpa.inp* file.

The analyst may change the parameter value assignment in the *tpa.inp* file. For example, in one run the parameter may be a constant; in another run, it may be described by a uniform PDF. The *exec.f* module writes the parameter to either the *cp.tpa* file (if it is a constant) or to *sp.tpa* (if described by a PDF). By separating *cp.tpa* and *sp.tpa*, file sizes are reduced significantly.

Module variables are introduced by the code developers and almost always are used to report subsystem performance measures. These variables are identified within the consequence modules and represent important output information useful for sensitivity and importance analyses. The module variables are calculated by the consequence modules for each realization and then are stored in arrays using the MODULE VARIABLE utility module. The *exec.f* prompts the MODULE VARIABLE utility module to write the values at the end of each realization to the file *mv.tpa*. The following is an example of the first few lines of *mv.tpa*:

```
Input file tpa.inp as supplied with TPA Version 4.0 Code.

Basecase data set Rev 4.0    4/3/00
      TPA 4.0, Job started: Tue Apr 1 14:43:45 2000
Module Variables for each realization
Module Variables are stored for each realization
  401
     1   WPCorrosionFailTime[yr]Subarea 1
     2   WPCorrosionFailTime[yr]Subarea 2
     3   WPCorrosionFailTime[yr]Subarea 3
     4   WPCorrosionFailTime[yr]Subarea 4
      ....etc.....
     1         401
     1              0.10000E+05
     2              0.10000E+05
     3              0.00000E+00
     4              0.00000E+00
```

The first five lines are consistent with the general format described previously. Next, the number of module variables is specified. In this example, the number of variables is 401. The names of the module variables follow, one per line. These names are the same as introduced by the consequence modules. The next line has two integer values for the realization number and the number of variables (the number of module variables remains the same during a run and is repeated for each realization as an aid to the user). The specific values for the variables follow, one per line.

Some information in files with a *.tpa* extension is contained in other TPA output files. The *sp.tpa* file provides the nonconstant parameter names defined in the *tpa.inp* file and the sampled values. The same information is also available in the *samplpar.res* and *samplpar.hdr* files. For all realizations, time histories of groundwater and ground surface doses by radionuclide are accessed in the *rgwnr.tpa* and *rgsnr.tpa* files. Instead of containing the entire time histories for the groundwater and ground surface doses, the *gwpkdos.res*, *gwpkds_c.res*, *npkdoset.res*, *npkdst_c.res*, *airpkdos.res,* and *arpkds_c.res* files provide peak dose and the time of the peak dose for all nuclides. Additionally, certain output, including the fraction of WPs failed by disruptive scenario events, UZ and SZ GWTTs by subarea, and groundwater and ground surface peak dose and time of the peak dose by nuclide are presented in *mv.tpa*. This information is also available in *wpsfail.res* (WPs failed), *gwttuzsz.res* (GWTT), and *gwpkdos.res, gwpkds_c.res, npkdoset.res*, and *npkdst_c.res* (peak dose and peak time).

# 21 PROGRAM INSTALLATION AND EXECUTION

The TPA Version 4.0 code was developed on a Sun Microsystems, Inc., SPARC 20 workstation running SunOS Version 5.5.1 (UNIX) and compiled with Sun FORTRAN Version 5.0 (f77). This chapter provides information for the system administrator or the user of the TPA Version 4.0 code regarding installation, customization, and execution. Portability, user support, QA, and troubleshooting are also reviewed.

## 21.1 SYSTEM ADMINISTRATION

### 21.1.1 Installing Source Code from an 8-mm Tape

Because of the size of the source code, the TPA Version 4.0 code generally is supplied for installation on an 8-mm data cartridge tape created using the *tar* command in the UNIX operating system environment. FORTRAN source code, associated data files, and stand-alone programs have been written to the tape. The following command (possibly with some small variation) has been used to prepare the tape:

```
tar -cvf /dev/rmt/0 tpa
```

This command copies the *tpa* directory with all its files and subdirectories onto the tape (see table 21-1 for a list of all files in the *tpa* directory, table 21-2 for a list of all files in subdirectory *tpa/data*, table 21-3 for a list of all files in subdirectory *tpa/codes*, table 21-4 for a list of all files in subdirectory *tpa/ccdf*, and table 21-5 for a list of all files in subdirectory *tpa/ccdf/gentpa*).

At the site (defined by the path $TPA_CODE) where the program is to be installed, (e.g., tpa40) the administrator will type the following commands (possibly with some small system-specific variation) to install the code:

```
mkdir tpa40
setenv TPA_CODE    $HOME/tpa40
cd $TPA_CODE
tar -xvpf /dev/rmt/0
```

This command unloads the tape and creates the *tpa* directory with all the necessary files, subdirectories, and programs relative to the $TPA_CODE directory. For example, at the CNWRA, $TPA_CODE refers to the path /solapps/cnwra/A_tpa4.0 where the TPA Version 4.0 code is installed. Tables 21-1, 21-2, 21-3, 21-4, and 21-5 list files that should be present after executing the *tar* command to unload the tape.

### 21.1.2 Customizing the Code for a Specific Host Machine

After installing the TPA Version 4.0 code on a computer, the installation should be customized to the user system environment. Two methods are suggested to link the FORTRAN input/output with the user system environment. One method involves setting UNIX environment variables (see section 21.1.2.1) and the other requires editing a FORTRAN *include* file employed by the TPA source code (see section 21.1.2.2). The former method is favored more than the latter as a general approach that can be applied in all cases.

**Table 21-1. TPA Version 4.0 code *tpa* directory files**

| Code Files | Include Files | | | | Other Files |
|---|---|---|---|---|---|
| *array.f* | *driftsa.i* | *mva.i* | *sampler0.i* | *stop.i* | *tpa.inp* |
| *ashplumo.f* | *execa.i* | *mvb.i* | *sampler1.i* | *subareaa.i* | *Makefile* |
| *ashrmovo.f* | *execb.i* | *mvc.i* | *sampler2.i* | *subareab.i* | |
| *condxyzt.f* | *fu1.i* | *mvd.i* | *sampler3.i* | *subareac.i* | |
| *dcags.f* | *fu2.i* | *mve.i* | *samplera.i* | *subaread.i* | |
| *dcagw.f* | *ia.i* | *mvf.i* | *samplerb.i* | *subareae.i* | |
| *ebsfail.f* | *inventa.i* | *nintv.i* | *samplerc.i* | *subareaf.i* | |
| *ebsrel.f* | *inventb.i* | *path.i* | *samplerd.i* | *subareag.i* | |
| *exec.f* | *inventc.i* | *reader.i* | *samplere.i* | *szft.i* | |
| *faulto.f* | *inventd.i* | *reader1.i* | *samplerf.i* | *uz_climi.i* | |
| *fileunit.f* | *invente.i* | *reader2.i* | *samplerg.i* | *uz_climr.i* | |
| *findelev.f* | *inventf.i* | *reader3.i* | *samplerh.i* | *uz_climz.i* | |
| *ia.f* | *inventg.i* | *reader4.i* | *sampleri.i* | *uz_flowi.i* | |
| *invent.f* | *inventh.i* | *reflux2.i* | *samplerj.i* | *uz_flowr.i* | |
| *mv.f* | *inventi.i* | | *samplerk.i* | *uz_flowz.i* | |
| *nfenv.f* | *inventj.i* | | *samplerl.i* | *uz_parms.i* | |
| *numrecip.f* | *inventk.i* | | *samplerm.i* | | |
| *peakfind.f* | *inventl.i* | | *samplern.i* | | |
| *ran.f* | *inventm.i* | | *samplero.i* | | |
| *reader.f* | *inventn.i* | | *samplerp.i* | | |
| *sampler.f* | *invento.i* | | *samplerq.i* | | |
| *seismo.f* | *max500yr.i* | | *samplerr.i* | | |
| *subarea.f* | *maxchain.i* | | *samplers.i* | | |
| *szft.f* | *maxnnucl.i* | | *samplert.i* | | |
| *uzflow.f* | *maxnsuba.i* | | *sampleru.i* | | |
| *uzft.f* | *maxntime.i* | | *samplerv.i* | | |
| *volcano.f* | | | *samplerw.i* | | |
| *zportunx.f* | | | *samplerx.i* | | |
| | | | *samplery.i* | | |
| | | | *samplerz.i* | | |

**Table 21-2. TPA Version 4.0 code *tpa/data* directory files**

| Data Files | | |
|---|---|---|
| *FILENAME.DAT* | *gftrans.def* | *nuclides.dat* |
| *burnup.dat* | *ggamen.dat* | *repdes.dat* |
| *climato1.dat* | *ggenii.def* | *soildem.dat* |
| *climato2.dat* | *ggrdf.dat* | *strmtube.dat* |
| *dilution.dat* | *gnewdf.dat* | *tefkti.inp* |
| *drythick.dat* | *grmdlib.dat* | *tpanames.dbs* |
| *ebsfail.def* | *gs_cb_ad.dat* | *wpflow.def* |
| *ebsfilt.def* | *gs_cb_ci.dat* | |
| *ebsrel.def* | *gs_pb_ad.dat* | |
| *elevdem.dat* | *gs_pb_ci.dat* | |
| *gbioac1.dat* | *maidtbl.dat* | |
| *gdefault.def* | *multiflo.dat* | |
| *gdosinc2.dat* | | |

**Table 21-3. Files associated with the TPA Version 4.0 code *tpa/codes* directory**

| Code Files | Include Files | Other Files |
|---|---|---|
| *ashplume.f* | *SIZES.INC* | *Makefile* |
| *ebsfilt.f* | *SIZES2.INC* | |
| *failt.f* | | |
| *nefmks.f* | | |
| *releaset.f* | | |
| *snllhs.f* | | |

**Table 21-4. Files associated with the TPA Version 4.0 code *tpa/ccdf* directory**

| Code Files | Include Files | Other Files |
|---|---|---|
| *tccdf.f* | *tccdf.i* | *Makefile* |
| | | *tccdf.inp* |

**Table 21-5. Files associated with the TPA Version 4.0 code *tpa/codes/gentpa* directory**

| Code Files | | Include Files | Other Files |
|---|---|---|---|
| *accmod.f* | *headng.f* | *AFPPAR.CMN* | *Make.bat* |
| *acute1.f* | *idnuc.f* | *AIRPAR.CMN* | *Makefile* |
| *acutea.f* | *inhcal.f* | *ANMPAR.CMN* | *Mkenv.fig* |
| *acutec.f* | *initnv.f* | *AQUPAR.CMN* | *Mkenvin.fig* |
| *aircal.f* | *intpol.f* | *CONC.CMN* | |
| *anmcal.f* | *invmol.f* | *DAYPC.CMN* | |
| *aqucal.f* | *makda2.f* | *DECAY.CMN* | |
| *biocal.f* | *opnfil.f* | *DFPAR.CMN* | |
| *blockd.f* | *order.f* | *DOSALL.CMN* | |
| *bsort.f* | *packag.f* | *ENVPAR.CMN* | |
| *candh.f* | *plmriz.f* | *EXPALL.CMN* | |
| *chain.f* | *prior.f* | *EXTPAR.CMN* | |
| *check.f* | *prob.f* | *FILES.CMN* | |
| *cronmod.f* | *profile.f* | *FODPAR.CMN* | |
| *crpcal.f* | *readin.f* | *INVIN.CMN* | |
| *dkharv.f* | *redcas.f* | *LABELS.CMN* | |
| *dose.f* | *redcha.f* | *MTBPAR.CMN* | |
| *drfbiv.f* | *redflt.f* | *OPT.CMN* | |
| *drfsec.f* | *redist.f* | *ORGMAS.CMN* | |
| *drkcal.f* | *ritenv.f* | *ORGPAR.CMN* | |
| *dumred.f* | *ritexp.f* | *RAD.CMN* | |
| *edranm.f* | *ritmed.f* | *RADIN.CMN* | |
| *edrcrp.f* | *ritqa.f* | *RMD.CMN* | |
| *edrnon.f* | *rlibin.f* | *RMD2.CMN* | |
| *edrres.f* | *rwake.f* | *SOLPAR.CMN* | |
| *env.f* | *sigma.f* | *SWPAR.CMN* | |
| *envin.f* | *swcal.f* | *TIMES.CMN* | |
| *envlib.f* | *trnspt.f* | *TITL.CMN* | |
| *exposr.f* | *ustar.f* | | |
| *extcal.f* | *xqcal.f* | | |
| *filerr.f* | *xqin.f* | | |
| *fntdrf.f* | | | |

#### 21.1.2.1 Customizing Using Environment Variables

The preferred approach uses environment variables TPA_TEST and TPA_DATA. (Note that in the UNIX environment the $ is required when using an environment variable as a target of most command line commands with the exception of the `setenv` command.) TPA_TEST should be set to the directory in which the TPA Version 4.0 code was placed by the *tar* command (i.e., to the $TPA_CODE directory as described in section 21.1.1). TPA_DATA should be set to a path within the home directory of the user (e.g., to the working directory $HOME/TPARUN in which the user will execute the TPA Version 4.0 code). A subdirectory (e.g., $TPA_DATA/*data*) should be defined to store the files that will be copied from $TPA_TEST/data. The following commands may be used (possibly with some small variation):

```
cd $HOME
mkdir TPARUN

setenv TPA_TEST $TPA_CODE/tpa
setenv TPA_DATA $HOME/TPARUN
```

The user's *.cshrc* file should then be modified to incorporate the correct definition of the environment variables.

Note that the user may want to edit some or all of the data files (i.e., *tpa.inp* and the files downloaded to $TPA_TEST/data). These files should be copied into the directory $TPA_DATA and read/write permissions set for the user. Note that the file *tpa.inp* must be in the directory in which the code will be executed. The following commands may be used:

```
cd $TPA_TEST
cp tpa.inp $TPA_DATA
cp data/* $TPA_DATA/data
```

After the environment has been customized, the TPA Version 4.0 code executable file, called *tpa.e*, and all the object files should be deleted and the *Makefile* executed via the *make* command to generate a new *tpa.e* executable. This procedure is described in section 21.1.3.

The user *.cshrc* file should then be modified to incorporate the correct definition of the environment variables. After setting these variables, the TPA executable file, *tpa.e*, and all of the object files should be deleted and the *Makefile* executed via the *make* command to generate a new TPA Version 4.0 code executable. This procedure is described in section 21.1.3.

#### 21.1.2.2 Customizing by Changing Path References in the Source Code

The other approach to customize an installation involves modifying the source code file *path.i,* which maintains references to the main TPA directory with subdirectories for data files and stand-alone programs. The TPA Version 4.0 code is delivered with the following *path.i* file:

```
character*10 path
data path / '$TPA_TEST/' /
character*10 dpath
data dpath / '$TPA_DATA/' /
```

The *path.i* file may be changed to specify the working directory used to run the TPA Version 4.0 code. For example, if the working directory is /dates/home/nmss2/ymipa3/, the user may change the *path.i* file to the following

```
character*25 path
data path / '/dates/home/nmss2/ymipa3/' /
character*25 dpath
data dpath / '/dates/home/nmss2/ymipa3/' /
```

Note that both the length of the character type declaration and the data statements require modification. After the environment has been customized, the TPA executable file, called *tpa.e* and all the object files should be deleted and the *Makefile* executed via the *make* command to generate a new TPA Version 4.0 code executable. This procedure is described in the next section.

### 21.1.3 Program Setup

The TPA Version 4.0 code is written in FORTRAN 77 and designed to run using the Sun Microsystems, Inc., SunOS Version 5.5.1 operating system. The Sun/OS operating system supports many features to assist code developers. One feature is the *Makefile*, which allows the developer to automatically link the object files of many subroutines. The following is an example of a *Makefile* (also provided on the 8-mm tape):

```
FFLAGS = -O4

OBJECTS = array.o      \
          ashplumo.o   \
          ashrmovo.o   \
          dcagw.o      \
          dcags.o      \
          ebsfail.o    \
          ebsrel.o     \
          faulto.o     \
          ia.o         \
          invent.o     \
          mv.o         \
          nfenv.o      \
          szft.o       \
          reader.o     \
          sampler.o    \
          seismo.o     \
          subarea.o    \
          uzflow.o     \
          uzft.o       \
          volcano.o    \
          ran.o        \
          numrecip.o   \
          condxyzt.o   \
          peakfind.o   \
          fileunit.o   \
          findelev.o   \
          zportunx.o
```

```
all :       tpa
      cd codes; make
      cd codes/gentpa; make

tpa :       $(OBJECTS)
      f77 exec.f -o tpa.e $(OBJECTS)

clean:
      rm *.o
      rm *.e
```

After unloading the TPA Version 4.0 code from the tape and either changing environmental variables or modifying the *path.i* file, the administrator can generate an executable version of the code by typing

```
cd $TPA_TEST
make
```

This command will prompt the SunOS system to compile the *exec.f* file and link with the 27 listed object files. The *Makefile* also has the handy feature of ensuring the object files are up to date. The *Makefile* checks the time and date of the last change made to the 27 FORTRAN source code files used to create the object files. If any of the FORTRAN source code files have been modified since the object files were made, then the object files are considered out of date. The *Makefile* begins a compilation of the FORTRAN source code to generate a new object file. This procedure is performed on a file-by-file basis, making it an efficient process. Only the changed files are compiled. The *Makefile* then generates a TPA Version 4.0 code executable file named *tpa.e*.

Some consequence modules spawn jobs that execute stand-alone programs (e.g., NEFTRAN). The source code for these stand-alone programs is provided in the subdirectory *codes*. These programs are compiled with the main TPA code in the *Makefile* procedure described previously. The *Makefile* need only be executed once for complete installation.

The user is cautioned not to make changes to the stand-alone source code files because these are part of the TPA Version 4.0 code. If alterations are needed, these must be coordinated with the software QA code custodian.

## 21.2 PROGRAM EXECUTION

Before running the TPA Version 4.0 code, the user should verify with the system administrator that the installation was performed as described in this chapter. If variations were made to this procedure, the user should obtain a modified program execution procedure from the system administrator.

### 21.2.1 Input Preparation

The setup for running the TPA Version 4.0 code has been revised to add flexibility for data input. Presently, the user can modify input data in the subdirectory *$TPA_DATA/data* in addition to changing the *tpa.inp* file. The user must not alter files in *$TPA_DATA/data* without knowing the impact the modification

will have on the executionof the TPA code. The user will not be able to vary any of the *$TPA_DATA/data* files unless the system administrator has set the privileges to write access for the files.

### 21.2.2 Editing Basic Files in the User Work Space

An example of how the user may *telnet* from a personal computer (PC) to the accessible SUN workstation via the *telnet* utility is

```
telnet vulcan
username: jdoe
password: *********
```

After accessing a SUN workstation (presumably at the default directory level $HOME), the user should switch to the subdirectory TPARUN.

The TPA Version 4.0 code is designed to permit specification of all user-supplied parameters in the *tpa.inp* file. In addition, the user can change the auxiliary data files. The files in the data subdirectory can be listed with the following command:

```
ls $TPA_DATA/data
```

With the proper file access permissions set (see section 21.1.2.1), the *tpa.inp* file in the $TPA_DATA directory and *$TPA_DATA/data/** files in the $TPA_DATA/data directory can be changed. The *vi* editor or any text editor may be used to modify the TPA files. Alternatively, the user can *ftp* the files to a PC or MacIntosh Computer (MAC) for alterations and then *ftp* the files back into the appropriate directories.

### 21.2.3 Execution of the TPA Version 4.0 Code

If the installation procedure described in this chapter has been performed, the TPA Version 4.0 code can be executed with the following commands:

```
cd ~/TPARUN
$TPA_TEST/tpa.e
```

During execution, the TPA Version 4.0 code will generate a number of output files with *.res*, and *.tpa* extensions. These files are overwritten every time the TPA Version 4.0 code is run. The output files are described in chapter 20.

## 21.3 PORTABILITY LIMITATION OF THE TPA VERSION 4.0 CODE

The TPA Version 4.0 code is written in FORTRAN 77 as implemented in the Sun FORTRAN Version 5.0. The subroutines have been designed and written to be as portable as possible, recognizing that some nonstandard FORTRAN features are supported on many computer platforms, while some features are not. For example, the time and date functions are not standard for the FORTRAN 77 language specification, but are required for QA documentation. Fortunately, many FORTRAN compilers on a variety of computer platforms have the built-in nonstandard feature of time and date. Similarly, many compilers support variable and array names longer than six characters. This feature is used throughout the TPA Version 4.0 code with long variable names that serve to add clarity to the source code. It is not anticipated that other major

FORTRAN compatibility issues exist. The TPA Version 4.0 code has been ported to the Windows/NT platform. The details of the porting process can be found in Muller et al. (1998).

## 21.4 USER SUPPORT

For technical assistance, users may contact

Dr. Sitakanta Mohanty
Center for Nuclear Waste Regulatory Analyses
Southwest Research Institute
P.O. Box Drawer 28510
San Antonio, TX 78228-0510
(210) 522-5185
email: smohanty@swri.org

Mr. Ronald Janetzke
Center for Nuclear Waste Regulatory Analyses
Southwest Research Institute
P.O. Box Drawer 28510
San Antonio, TX 78228-0510
(210) 522-3318
email: rjanetzke@swri.org

## 21.5 SOFTWARE QUALITY ASSURANCE

Software QA has been an integral part of the TPA Version 4.0 code development process. Many of the software QA recommendations made in Wescott et al. (1995) were implemented in developing the TPA Version 4.0 code. Testing was conducted in an independent manner by staff who did not contribute to the module development. Module testing was performed not only to probe for the correct implementation and determine the limitations of computational algorithms, but also to assess code capabilities to detect user input errors. The *exec.f* module and the consequence and utility modules were put through a broad spectrum of tests considered appropriate for each module. Specific types of tests performed included

- Verification of utility modules through comparisons with calculations made with MCAD (MathSoft Inc., 1995) and Mathematica (Wolfram, 1991)
- Verification of module outputs through comparison of results from the stand-alone module and the same module integrated into the TPA Version 4.0 code
- Verification of selected modules through hand calculations and published results, where deemed feasible
- Line-by-line check of libraries containing static data for parameters such as radionuclide half-lives, specific activities, inventories, and EPA limits
- Line-by-line check of selected consequence modules (e.g., NFENV), where deemed feasible

- Compilation of module source code using different FORTRAN compilers

In addition, complete runs were made with the TPA Version 4.0 code, and the results (i.e., subsystem and total-system performance measures) checked for reasonableness. The TPA Version 4.0 code currently adheres to software configuration control in accordance with the CNWRA Technical Operating Procedure (TOP) 018.

## 21.6 TROUBLESHOOTING

The user may obtain various kinds of error messages during the execution of the TPA Version 4.0 code as a result of computer resource limitations and incorrect format in the TPA Version 4.0 code input file *tpa.inp*. The TPA Version 4.0 code was designed with numerous error traps that provide helpful diagnostic information to the user. It is recommended that the user observe the successful completion of the first realization to develop a reasonable assurance the code is configured correctly before running hundreds of realizations that may take more than a day to run. Most problems related to set up related are encountered during the first few minutes of code execution. Some of the commonly encountered problems and actions to avoid execution errors are described in the following sections.

**Problem:**

The code stops executing after the following message is printed to the screen:

```
exec: calling uzft
Killed
   ***>>> Error in UZFT <<<***
   NEFTRAN failure. Status =    35072
```

**Solution:**

This problem occurs when there is not enough memory available to execute the TPA Version 4.0 code. The user or other users may be running processes that could cause this problem. It is recommended the user cancel processes, ask others to terminate processes, or wait until the processes are complete. This will make resources available for the TPA Version 4.0 code.

**Problem:**

When the append option is turned on in the *tpa.inp* file, the TPA Version 4.0 code stops after the following message:

```
exec: calling ebsfail
open: [24] Too many open files
logical unit 8, named 'corrode.out'
Abort
   ***>>> Error in ebsfail <<<***
   istatus .ne. 0
   istatus = sh( "failt.e" )
   istatus =    34304
```

**Solution:**

The user should type the word *unlimit* at the UNIX prompt and run the TPA Version 4.0 code again. This error message arises because the allowed number of open files has been exceeded (default is 64). By typing *unlimit*, the maximum allowed number of open files is increased to 1,024. When the append option is turned on, the TPA Version 4.0 code creates 33 additional output files that result in greater than 64 open files.

**Problem:**

The TPA Version 4.0 code will not use information from data files the user has modified. The user may elect to change values in a data file, but after TPA Version 4.0 code execution, the original data file is present in the working directory. Additionally, it is evident by examining results that the TPA Version 4.0 code did not use the modified data file.

**Solution:**

The user may not have set the environment variables correctly. The user should follow the exact procedure described in section 21.1.2. When these steps are followed and the problem persists, the user should consult the system administrator or code custodian.

**Problem:**

A common problem that causes the TPA Version 4.0 code execution to terminate or use incorrect data files is the path not being set properly. The path setup can be checked in the first few lines of the screen output:

```
================================================================================
          exec: Welcome to TPA Version 4.0
        Job started: Fri Feb 18 10:57:58 2000
================================================================================
REPOSITORY DESIGN INFORMATION
Subarea    Area        Waste    Number of WP
   #       [m^2]       [MTU]
   1     723591.3     13605.4         1394
   2     784763.0     15049.9         1542
   3     390372.0      7827.5          802
   4     207581.3      3904.0          400
   5     378972.8      7573.8          776
   6     424872.5      8452.2          866
   7     163938.3      3279.4          336
   8     393468.9      8344.8          855

Total Area [acre]           =      856.822384630614
Total Buried Waste [MTU]    =     68036.9600000000
Repository AML [MTU/acre]   =     79.4061420668083

Specified Global Parameters:

                Compliance Period =  10000.0 (yr)
          Maximum Simulation Time =  20000.0 (yr)
           Number Of Realizations =       2
                Number Of Subareas =       8
```

```
              Volcanism scenario =       0 (yes=1, no=0)
               Faulting scenario =       0 (yes=1, no=0)
                Seismic scenario =       1 (yes=1, no=0)
      Distance to Receptor Group =    20.0 (km)


**>>> CAUTION: CHECKING OF NUCLIDES AND CHAINS IS DISABLED <<<**
**>>> You may not be using the standard chains specified   <<<**
**>>> in the invent module.                                  <<<**
**>>> (see "CheckNuclidesAndChains(yes=1,no=0)" in tpa.inp)<<<**

The specified path for data  = $TPA_DATA/
The specified path for codes = $TPA_TEST/
  .
  .
```

**Solution:**

The user should verify with the code custodian that the path is correctly set in the file *path.i.*

**Problem:**

TPA Version 4.0 code execution time is too long and it is desirable to obtain results quickly.

**Solution:**

In some applications, the user is not interested in the numerical accuracy of dose results. For example, the user may want to run many vectors to test sampling algorithms. The user can increase the speed of the code execution time by bypassing the UZFT calculations. This can be achieved by setting all UZ leg lengths to zero in the *tpa.inp* file.

**Problem**:

The input file *tpa.inp* is modified and the TPA Version 4.0 code execution terminates at the beginning of the run. Three examples of this type of error message written to the screen are provided:

*Example 1:*

```
=========================================================================
exec: Welcome to TPA Version 4.0
Job started: Tue Apr 14 14:41:11 2000
=========================================================================

  ***>>> Error in Reader <<<***
  for uniform distribution
  name = ArealAverageMeanAnnualInfiltrationAtStart[mm/yr]
  xmax .le. xmin
  xmax =      1.0000000000000
  xmin =     10.0000000000000
  Look on Line Number =    165
```

*Example 2:*

```
================================================================================
exec: Welcome to TPA Version 4.0
Job started: Tue Apr 14 14:43:45 2000
================================================================================

   ***>>> Error in Reader <<<***
   for logtriangular distribution
   name = SolubilityNp[kg/m3]
   xmin  =      1.2000000000000D-03
   xpeak =      3.4000000000000
   xmax  =     0.24000000000000
   Look on Line Number =    1367
```

*Example 3:*

```
================================================================================
exec: Welcome to TPA Version 4.0
Job started: Tue Apr 14 14:45:12 2000
================================================================================

   ***>>> Error in ispquery <<<***
   cannot find name of parameter
   dump of first 15 PDFs defined
   ipdf, description
    1   VolcanismDisruptiveScenarioFlag(yes=1,no=0)
    2   FaultingDisruptiveScenarioFlag(yes=1,no=0)
    3   Seismic DisruptiveScenarioFlag(yes=1,no=0)
    4   StartAtSubarea
    5   StopAtSubarea
    6   SeedForRandomNumber
    7   LatinHypercubeSampling(yes=1,no=0)
    8   NumberOfRealizations
    9   StartAtRealization
    10   StopAtRealization
    11   MaximumTime[yr]
    12   NumberOfTimeSteps
    13   RatioOfLastToFirstTimeStep
    14   OutputMode(0=None,1=All,2=UserDefined)
    15   UserDefinedLowerRealizationAppended

   ***>>> Error in ispquery <<<***
   cannot find name of parameter
   in above list of all PDF names
   name =Seismic DisruptiveScenarioFlag(yes=1,no=0)
```

**Solution:**

These three examples are typical messages written to the screen when the user has made an error in editing the TPA input file *tpa.inp*. The message echoes the incorrect information specified in *tpa.inp* and may provide the user with the line number in *tpa.inp* where the error occurred. In example 1, the user specified a uniform distribution with the first value greater than the second. The required format in the *tpa.inp* file for the uniform distribution lower and upper limits must be the lower limit followed by the upper limit. The second example illustrates the error message generated when the peak value for a triangular

distribution is outside the minimum and maximum values. The order for values describing the triangular distribution must be the lower limit, the peak value, and the upper limit. The last example shows the user modified the name of the seismic flag parameter in *tpa.inp* by adding a space. The user must not modify the *tpa.inp* file parameter names. The TPA Version 4.0 code searches through the parameter names in the *tpa.inp* file, and if a name has been altered, the TPA Version 4.0 code execution stops, and an error message is written to the screen.

**Problem:**

The TPA Version 4.0 code execution terminates at the beginning of the run and the following message is written to the screen:

```
list read: [-1] end of file
logical unit 40, named 'lhs.out'
lately: reading sequential list external IO
part of last format: ext list io
part of last data: |
```

**Solution:**

The user should view the diagnostic output file *lhse.out* to read the error message written by the *snllhs.f* file. An example of information contained in *lhse.out* is provided:

```
1      FOR THE UNIFORM DISTRIBUTION THE LOWER LIMIT A      0.1000000015
       IS GREATER THAN OR EQUAL TO THE UPPER LIMIT B      0.1000000015
```

In this example, an error message was written because the user specified in the *tpa.inp* file the lower limit for a uniform distribution as 0.1 and the upper limit for a uniform distribution as 0.1000001. These are read in *snllhs.f* as the same value. This condition occurs because *snllhs.f* uses six significant digits.

It is strongly recommended that on completion of a TPA run, the user examines the *lhse.out* file for messages. Two examples of messages in the *lhse.out* file for cases with one realization and 200 realizations are presented here. In both cases, the TPA Version 4.0 code execution is normal.

*Example 1:*

```
1

     TITLE - Created for tpa execution


     RANDOM SEED =   -188910452

     NUMBER OF SAMPLED VARIABLES = 157

     NUMBER OF CONSTANT VARIABLES =    0

     NUMBER OF OBSERVATIONS =    10
0    AN INPUT CORRELATION MATRIX HAS BEEN SPECIFIED
1TITLE - Created for tpa execution

0INPUT RANK CORRELATION MATRIX
                                                                PAGE    1
```

```
0     1  1.0000
0    43 -0.2240  1.0000
0    45  0.6310 -0.3660  1.0000
0   122  0.0000  0.1300 -0.6230  1.0000
0              1       43       45      122
0VARIABLES
0*********  CAUTION  USER  PLEASE  NOTE  *********  CAUTION  USER  PLEASE  NOTE
********* CAUTION USER PLEASE NOTE **********

 SINCE THE SAMPLE SIZE IS LESS THAN OR EQUAL TO THE NUMBER OF VARIABLES
 THIS IS NOT A FULL RANK CASE SO THE REQUESTED
 CORRELATION STRUCTURE, SHOWN ABOVE, CANNOT BE GENERATED
 THEREFORE THE INPUT MATRIX WILL BE GENERATED AS IF THE
 INPUT VARIABLES WERE INDEPENDENT


**********************************************************************************
**********************************
```

*Example 2:*

```
1

     TITLE - Created for tpa execution


     RANDOM SEED =   -188910452

     NUMBER OF SAMPLED VARIABLES = 157

     NUMBER OF CONSTANT VARIABLES =    0

     NUMBER OF OBSERVATIONS =   200
0    AN INPUT CORRELATION MATRIX HAS BEEN SPECIFIED
1TITLE - Created for tpa execution

0INPUT RANK CORRELATION MATRIX
                                                                      PAGE    1
0     1  1.0000
0    43 -0.2240  1.0000
0    45  0.6310 -0.3660  1.0000
0   122  0.0000  0.1300 -0.6230  1.0000
0              1       43       45      122
0VARIABLES
```

In example 1, the user selected fewer realizations than sampled parameters. This generates a caution message from the *snllhs.f* file stating the input parameters were not correlated. The second example provides an *lhse.out* file with no error or caution messages.

**Problem:**

The TPA Version 4.0 code execution stops after the following message is printed to the screen:

```
------------------------------------------------------------------------
      subarea    1 of    8            realization     1 of     1
------------------------------------------------------------------------
  cp: ./climato1.dat: write: No space left on device
```

```
exec: calling uzflow
cp: ./elevdem.dat: write: No space left on device
unexpected end of DEM file <elevdem.dat>!
```

**Solution:**

This type of error message occurs when there is not enough disk space available to write TPA results to output files. The user may determine the available disk space using the following command:

```
df -k
```

It is strongly recommended that the user check the amount of free disk space prior to beginning a TPA run. The disk space required for a TPA run depends on the options specified in the *tpa.inp* file. Chapter 20 provides a discussion of factors affecting the disk space required for a TPA run. After running the TPA Version 4.0 code, the user will become familiar with the disk space requirements. For runs that have been completed, the user may check the disk space occupied by the TPA files by typing the following command:

```
du
```

This UNIX command lists the disk space consumed by all files in the current directory and all subdirectories.

# 22 TOOLS FOR SUPPLEMENTARY ANALYSES

Various tools have been, or are being, prepared to augment the TPA Version 4.0 code to provide supplementary analyses. These tools include auxiliary codes and importance analyses features. The auxiliary codes are stand alone and separate from the modules that make up the TPA Version 4.0 code. These auxiliary codes manage information passed to or from the TPA Version 4.0 code to aid in the analysis of results. Importance analyses features are a part of the main TPA modules and involve the removal of barriers from analyses.

## 22.1 TOTAL COMPLEMENTARY CUMULATIVE DISTRIBUTION FUNCTION CODE

At the present time, total complementary cumulative distribution function (TCCDF) is the only operational supplementary analyses tool in the TPA Version 4.0 code. This code requires outputs from multiple TPA code executions for certain calculations.

### 22.1.1 Complementary Cumulative Distribution Function

For the purposes of analyzing TPA output, the CCDF provides a mechanism to evaluate the probability of an output data value exceeding a given limit. A given output data (e.g., cumulative release or peak dose) value has a probability associated with it because the simulations are nondeterministic and many vectors or realizations of sampled parameters are usually executed per run. Each output data value has a probability of 1/N, where N is the number of vectors or realizations used for a particular run. These probabilities are cumulative when presented in a regular CDF. The complementary CDF differs from the regular CDF in that it represents 1 minus the CDF. This gives the CCDF its characteristic monotonically decreasing upper-left to lower-right shape.

Figure 22-1 is an example of CCDF curves showing peak dose at 10,000 and 50,000 yr. The data in this example were taken from a run of 400 vectors. Each result is considered an equally likely outcome, so each point will have a probability of 1/400. The complementary cumulative curve begins at the upper left with a value of 1.0 and proceeds to the lower right with a complementary cumulative probability of 0.0025. The curve is disturbed from a strict interpretation of the algorithm by forcing the left-most point to be plotted at 1.0 rather then 0.9975. This adjustment is somewhat capricious, but permits the use of a log scale on the y-axis because the right-most point would otherwise have a y value of 0.0. Inspection of figure 22-1 provides a hint that the generation of the CCDF is greatly eased if the data are sorted from low value to high rather than remaining in an array indexed by vector number.

The use of a CCDF was required in previous TPA exercises to compare the results with the EPA limits for normalized release. The EPA limit specification is a step function indicating that normalized release values less than 1.0 were not restricted, that the probability of normalized release values occurring between 1.0 and 10.0 was to be less than 0.01, and that the probability of normalized release values greater than 10.0 was to be less than 0.001. So, by displaying the normalized release output data on a CCDF plot, the probability of each point (each representing one vector) could be checked to see if it exceeded the EPA standard for its respective value step. If any point exceeded its respective limit, the curve as a whole was said to indicate noncompliance. CCDF plots used in this manner are called exceedance probability curves.

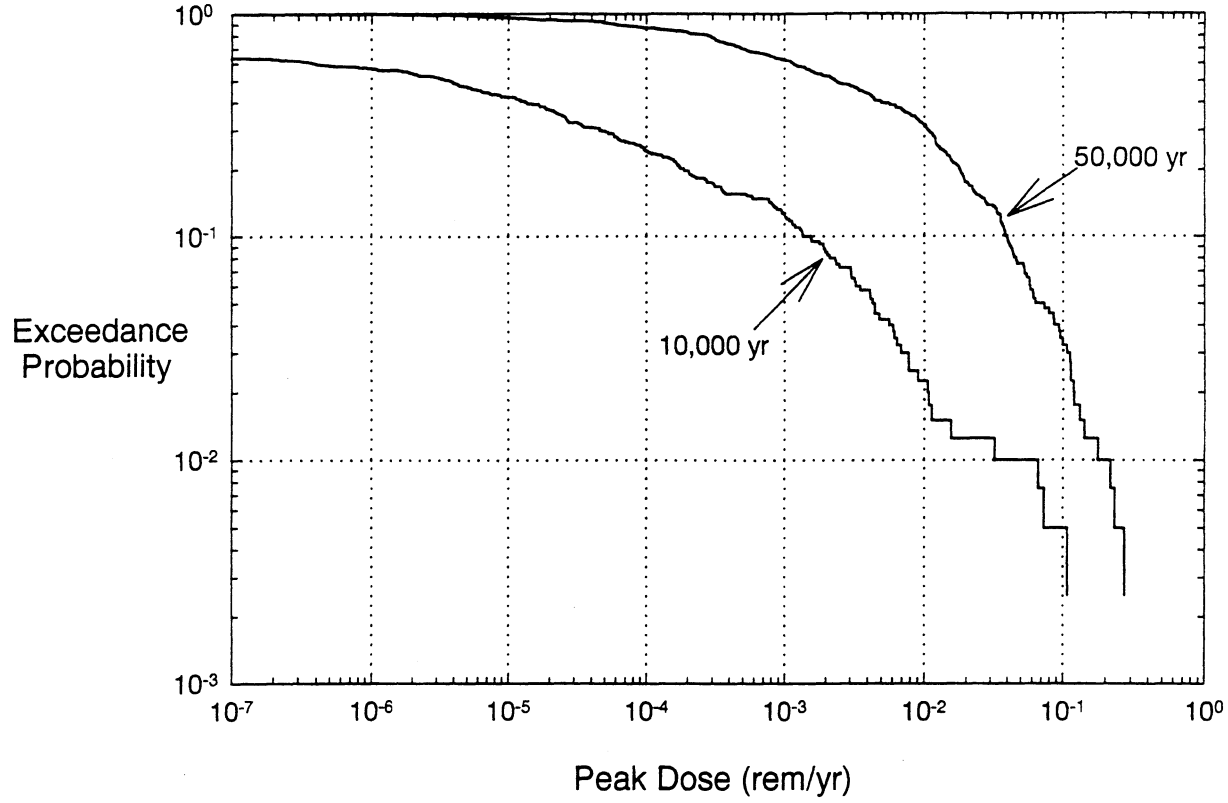


**Figure 22-1. Example complementary cumulative distribution function**

### 22.1.2 Conditional Complementary Cumulative Distribution Function

CCDF curves generated from the output of one scenario, thus ignoring all other scenarios in the problem domain, are called conditional CCDFs. Conditional CCDFs assume that the selected scenario has a probability occurrence of 1.0 and are constructed in the following manner:

- A vector represents a single realization of all of the sampled variables
- Each vector is assigned an equal probability within the scenario (i.e., for 400 vectors, each vector has a probability $p_i = 1/400$)
- The set of vectors is sorted from lowest to highest value $X$
- The exceedance probability $E$ of the sorted values is calculated by the following formula:

$$E_1 = 1.0;$$
$$E_k = 1.0 - \sum_{i=1}^{k-1} p_i, \text{ for } k = 2 \ldots N \tag{22-1}$$

where $p_i$ is the probability of the $i^{th}$ vector of the sorted set, $N$ is the number of vectors in the set, and $k$ is an individual vector number of the set

- The CCDF is the graph of $E$ versus its sorted values $X$.

### 22.1.3 Total Complementary Cumulative Distribution Function

TCCDF is generated by considering all scenarios in the problem domain. Each scenario is not required to be equally probable, so the vector probabilities associated with a given scenario must be weighted by the probability of the scenario occurrence. The sum of all scenario probabilities must equal 1.0.

The weighted probability of each vector $p_i$ is taken as the scenario probability $p_j$ divided by the number of vectors $N_j$ in the scenario:

$$p_i = \frac{p_j}{N_j} \tag{22-2}$$

The $X$ values are then sorted, as before, from lowest to highest. The exceedance probability is then defined as

$$E_1 = 1.0$$
$$E_k = 1 - \sum_{i=1}^{k-1} p_i, \text{ for } k = 2 \ldots N \tag{22-3}$$

where $N'$ is the total number of vectors in all scenarios and $p_i$ is the weighted probabilities for the sorted $X$ values.

### 22.1.4 Total Complementary Cumulative Distribution Function Code

The auxiliary code TCCDF produces a total CCDF for multiple scenarios. The TPA code is limited by the *tpa.inp* input file to accept input for only one scenario at a time. The TPA code must be reexecuted for each additional scenario desired. Any number of additional scenarios can be run that can contribute to the generation of a total CCDF of all scenarios. A probability must be assigned to each scenario such that the total probability of all scenarios equals 1.

The TPA Version 4.0 code produces four files for each scenario that can be used as input to the TCCDF code to generate a TCCDF. The release data are in the files *relgwgs.res* and *rlgwgs_c.res* with one release entry per realization for each data value of groundwater, ground surface, and total release. Only the total release value is used for the TCCDF. The dose data are in the files *totdose.res* and *totdos_c.res* with many total dose entries per realization. The entry of interest is the peak dose rate for each realization. This value is located automatically by the TCCDF code so the file does not have to be edited for use as an input file.

Because each run (scenario) of the TPA code produces *.res* files with the same name, the user must move these files to the *./ccdf* subdirectory with unique names. The following scheme is suggested to easily identify the contents of the files. Move the *relgwgs.res* to files with a name such as

*relnnn.dat*

Move the *totdose.res* files to files with a name such as

*dosnnn.dat*

where *nnn* is as shown in table 22-1.

Typically, a complete set of eight scenarios is generated, however, other combinations are possible with appropriate adjustments to the probabilities, (i.e., sum of the scenario probabilities should be one). The TCCDF input file is *tccdf.inp*, and it is the mechanism by which the user identifies files and associated probabilities. With the input file created, the TCCDF program can be executed by the command

>tccdf.e

This command produces three new files containing the TCCDFs for all scenario files for the release, peak dose rate, and dose rate at end of simulation. The TCCDF for release is in the *trelccdf.res* file, the total CCDF for peak dose rate is in the *tpkdccdf.res* file, and the TCCDF for final dose rate is in the *tdosccdf.res* file.

### 22.1.5 Total Complementary Cumulative Distribution Function Input Description

The TCCDF input file consists of three sections: header, release, and dose. All three sections must be present in the file for proper operation. The header section is three lines long: two title lines (for run identification) and one blank line.

The release section contains information about the release files to be used in generating the total release CCDF. The first line presents the number of release files to be identified. The next three lines are header lines for the two columns of data values. The first column is Probability and the second is File_name. These are immediately followed by one line for each release file, identifying the probability associated with the file and the file name. The number of files specified must match the value supplied in the first line of the release section. At least one release file must be stipulated. The section is closed with a blank line.

**Table 22-1. Possible values for *nnn***

| *nnn* | Faulting | Seismic* | Volcanic |
|---|---|---|---|
| *000* | no | no | no |
| *00v* | no | no | yes |
| *0s0* | no | yes | no |
| *0sv* | no | yes | yes |
| *f00* | yes | no | no |
| *f0v* | yes | no | yes |
| *fs0* | yes | yes | no |
| *fsv* | yes | yes | yes |

*Seismicity is considered part of the basecase and is always on

The dose section provides information about the dose files to be used in generating the peak dose CCDF. The first line contains the number of dose files to be identified. The next three lines are header lines for the two columns of data values. The first column is Probability and the second is File_name. These are immediately followed by one line for each dose file displaying the probability associated with the file and the file name. The number of dose files specified must match the value supplied in the first line of the dose section. At least one dose file must be defined.

## 22.2 IMPORTANCE ANALYSES

The TPA code has been modified to perform importance analysis of the proposed repository system. Importance analysis is the process of neutralizing a component, barrier, or subsystem from the analysis. Neutralization of a barrier does not imply simply to bypass a module in the TPA code. Typically, the neutralization of a barrier requires modifications to more than one TPA module. For example, if backfill is neutralized as a barrier, the heat transfer model is adjusted as well as the diversion of flow away from drifts. This requires modifications to the modules that compute near-field temperature and the amount of water entering the WP.

To perform importance analysis, the barriers likely to be neutralized have been identified. For each barrier, a flag has been introduced in the *tpa.inp* file so that when that particular flag is turned ON, all relevant adjustments consistent with the neutralization of the barrier are made to the various modules in the code. The importance analysis flags have been identified at the beginning of the *tpa.inp* input file. Although, the importance analysis was operational in a previous version of the TPA code, modifications have not been made to make it operational in the TPA Version 4.0 code. Importance analysis options will be made operational in a future version of the TPA code.

# 23 FUTURE IMPROVEMENTS TO THE TPA CODE

The TPA Version 4.0 code adds an essential element to the capability of the NRC staff to review the DOE TSPA using independent analyses. While the TPA Version 4.0 code was developed to provide the NRC a flexible tool for analyzing a variety of approaches and conceptual models consistent with current data and scientific understanding, modifications to the TPA Version 4.0 code are being considered to improve its overall capabilities. Refinements are anticipated to reduce conservatism in conceptual models and parameter values, include additional processes in the conceptual models, and increase efficiencies in the calculations. The refinements will improve the capability of the NRC to review the DOE TSPA. There are several specific areas to be considered for future improvements to the TPA code and its parameters.

Correlated parameters were introduced in a previous version of the TPA code to address coupling between processes. An increase in the coupling of system components is desirable so that potential synergisms are not neglected. The introduction of correlated parameters was a computationally efficient method to increase system coupling. However, achieving coupling through the introduction of correlated parameters creates difficulty for some of the sensitivity analysis techniques. In general, future versions of the TPA code will attempt to reduce the number of correlated parameters but increase the overall system coupling. For example, the dependence of distribution coefficients on the mineralogy and geochemistry of the system is handled through the correlation of distribution coefficients. Future versions of the TPA code will attempt to sample the pH and other properties, then calculate distribution coefficients.

Specific improvements to be made to the TPA Version 4.0 code in the future may include (i) incorporation of a mechanistic basis for the failure of SF cladding, (ii) development of a model for the environment inside the WPs, (iii) consideration of colloidal transport in the UZ and SZ, (iv) improvement of the abstraction of dripping on the WPs based on detailed process-level simulations, and (v) addition/development of increased coupling/interaction of engineered system components (e.g., drip shield, waste package, and backfill) with each other and near-field processes (i.e., geochemistry, corrosion, thermohydrology, mechanical failure, radiation damage). The importance of specific improvements is continually evaluated with sensitivity studies, process-level modeling, and level of conservatism of abstracted models by NRC technical staff. Future versions of the TPA code may have the flexibility to assess the contribution of individual barriers in meeting the performance objective.

# 24 REFERENCES


Ahn, T.M. *Long-Term Kinetic Effects and Colloid Formations in Dissolution of LWR Spent Fuels.* NUDOC Accession Number 9508030112. Washington, DC: Nuclear Regulatory Commission. 1995.

Ahn T., and P. Soo. *Container Assessment—Corrosion Study of HLW Container Materials, Quarterly Progress Report, October–December 1983.* BNL–NUREG–34220. Upton, NY: Brookhaven National Laboratory. 1983.

Ahn T., and P. Soo. *Container Assessment—Corrosion Study of HLW Container Materials, Quarterly Progress Report, January–March 1984, April–June 1984.* Upton, NY: Brookhaven National Laboratory. 1984.

Amtec Engineering, Inc. *TECPLOT Interactive Data Visualization for Scientists and Engineers, Version 6 Users Manual.* Bellevue, WA: Amtec Engineering, Inc. 1993.

Ang, A.H-S., and W.H. Tang. *Probability Concepts in Engineering Planning and Design. Volume II: Decision, Risk, and Reliability.* New York: John Wiley and Sons. 1984.

Anspaugh, L.R., J.H. Shinn, P.L. Phelps, and N.C. Kennedy. Resuspension and redistribution of plutonium in soils. *Health Physics* 29: 571–582. 1975.

Baca, R.G., G.W. Wittmeyer, and R.W. Rice. Analysis of contaminant dilution in groundwater. *Scoping Calculations for Revisions to the EPA Standard.* NUREG–1538. Washington, DC: Nuclear Regulatory Commission. 1996.

Baes, C.F., III, R.D. Sharp, A.L. Sjoreen, and R.W. Shor. *A Review and Analysis of Parameters for Asessing Transport of Environmentally Released Radionuclides Through Agriculture.* ORNL–5876. Oak Ridge, TN: Oak Ridge National Laboratory. 1982.

Barnard, R.W., M.L. Wilson, H.A. Dockery, J.W. Gauthier, P.G. Kaplan, R.R. Easton, F.W. Bingham, and T.H. Robey. *TSPA 1991: An Initial Total-System Performance Assessment for Yucca Mountain.* SAND91–2795. Albuquerque, NM: Sandia National Laboratories. 1992.

Basse, B. *Water Resources in Southern Nevada.* San Antonio, TX: Center for Nuclear Waste Regulatory Analyses. 1990.

Bateman, H. The solution of a system of differential equations occurring in the theory of radioactive transformation. *Proceedings of the Cambridge Philosophical Society.* 15: 473. 1910.

Bejan, A. *Advanced Engineering Thermodynamics.* New York: John Wiley and Sons. 1988.

Brechtel, C.E., M. Lin, E. Martin, and D.S. Kessel. *Geotechnical Characterization of the North Ramp of the Exploratory Studies Facility. Volume I: Data Summary.* SAND95–0488/1, UC–814. Albuquerque, NM: Sandia National Laboratories. 1995.

Briant, C.L., and S.K. Banerji, eds. Intergranular fracture in ferrous alloys in nonaggressive environments. *Treatise on Materials Science and Technology. Volume 25: Embrittlement of Engineering Alloys.* C.L. Briant and S.K. Banerji, eds. New York, NY: Academic Press: 21–58. 1983.

Bruno, J., I. Casas, E. Cera, J. De Pablo, J. Giménez, and M.E. Torrero. Uranium (IV) dioxide and SIMFUEL as chemical analogues of nuclear spent fuel matrix dissolution—A comparison of dissolution results in a standard $NaCl/NaHCO_3$ solution. *Materials Research Society Symposium Proceedings.* Pittsburgh, PA: Materials Research Society 353: 601–608. 1995.

Buck, E.C., R.J. Finch, P.A. Finn, and J.K. Bates. Retention of neptunium in uranyl alteration phases formed during spent fuel corrosion. *Material Research Society Symposium Proceedings.* Pittsburgh, PA: Materials Research Society 506: 87–123. 1998.

Buqo, T.S. *Baseline Water Supply and Demand Evaluation of Southern Nye County, Nevada.* Nye County, NV: Nye County Nuclear Waste Repository Office. 1996.

Bureau of Radiological Health. *Radiological Health Handbook.* Rockville, MD: U.S. Department of Health, Education, and Welfare. 1970.

Carslaw, H.S., and J.C. Jaeger. *Conduction of Heat in Solids.* London, United Kingdom: Oxford University Press. 1959.

Casas, I., J. Giménez, J. De Pablo, and M.E. Torrero. Dissolution of $UO_2(s)$ in $MgCl_2$ brines under different redox conditions. *Material Research Society Symposium Proceedings.* Pittsburgh, PA: Materials Research Society 294: 67–72. 1993.

Cember, H. *Introduction to Health Physics.* New York: Permagon Press. 1983.

Civilian Radioactive Waste Management System, Management and Operating Contractor. Chapter 2: Unsaturated zone hydrology model. *Total System Performance Assessment—Viability Assessment (TSPA-VA) Analyses Technical Basis Document.* B00000000–01717–4301–00002. Las Vegas, NV: TRW Environmental Safety Systems, Inc. 1998.

Civilian Radioactive Waste Management System, Management and Operating Contractor. *License Application Design Selection Report.* B00000000–01717–4600–00123. Revision 01. Las Vegas, NV: Civilian Radioactive Waste Management System, Management and Operating Contractor. 1999a.

Civilian Radioactive Waste Management System, Management and Operating Contractor. *Integrated Site Model Progress Model Report.* TDR–NBS–GS–000002. Revision 00. Las Vegas, NV: Civilian Radioactive Waste Management System, Management and Operating Contractor. 1999b.

Civilian Radioactive Waste Management System, Management and Operating Contractor. *Identification of Critical Group (Consumption of Locally Produced Food and Tap Water).* ANL–MGR–MD–000005. Revision 0. Las Vegas, NV: Civilian Radioactive Waste Management System, Management and Operating Contractor. 2000.

Claesson, J., and T. Proberts. *Temperature Field Due to Time-Dependent Heat Sources in a Large Rectangular Grid—Derivation of Analytical Solution.* SKB 96-12. Stockholm, Sweden: Swedish Nuclear Fuel and Waste Management Co. 1996.

Codell, R.B., N.A. Eisenberg, D.J. Fehringer, W.H. Ford, T.S. Margulies, T.J. McCartin, J.R. Park, and J.D. Randall. *Initial Demonstration of the NRC's Capability to Conduct a Performance Assessment for a High-Level Waste Repository.* NUREG–1327. Washington, DC: Nuclear Regulatory Commission. 1992.

Cohen, A.J.B., C.M. Oldenburg, A.M. Simmons, A.K. Mishra, and J. Hinds. *$S^4Z$: Sub-Site Scale Saturated Zone Model for Yucca Mountain.* SP25UM4. Berkeley, CA: Lawrence Berkeley National Laboratory. 1997.

Connor, C.B., S. Magsino, J. Stamatakos, R. Martin, P. La Femina, B. Hill, and S. Lieber. Magnetic surveys help reassess volcanic hazards at Yucca Mountain. *EOS, Transactions, American Geophysical Union* 74(7): 73–78. 1997.

Conway, M.F., D.A. Ferrill, C.M. Hall, A.P. Morris, J.A. Stamatakos, C.B. Connor, A.N. Halliday, and C. Condit. Timing of basaltic volcanism along the Mesa Butte fault in the San Francisco volcanic field, Arizona, from $^{40}Ar/^{39}Ar$ dates: Implications for longevity of cinder cone alignments. *Journal of Geophysical Research* 102: 815–824. 1997.

Cragnolino, G.A., H.K. Manaktala, and Y-M. Pan. *Thermal Stability and Mechanical Properties of High-Level Radioactive Waste Container Materials: Assessment of Carbon and Low-Alloy Steels.* CNWRA 96-004. San Antonio, TX: Center for Nuclear Waste Regulatory Analyses. 1996.

Cragnolino, G.A., D.S. Dunn, P. Angell, and N. Sridhar. Factors influencing the performance of carbon steel overpacks in the proposed high-level nuclear waste repository. *Proceedings of the CORROSION '98 Conference.* Paper No. 147. Houston, TX: NACE International. 1998.

Cragnolino, G. A., D.S. Dunn, C.S. Brossia, V. Jain, and K.S. Chan. *Assessment of Performance Issues Related to Alternate Engineered Barrier System Materials and Design Options.* CNWRA 99-003. San Antonio, TX: Center for Nuclear Waste Regulatory Analyses. 1999.

Czarnecki, J.B., and R.K. Waddell. *Finite-Element Simulation of Groundwater Flow in the Vicinity of Yucca Mountain, Nevada–California.* WRI–84–4349. Denver, CO: U.S. Geological Survey. 1984.

Czarnecki, J.B., C.C. Faunt, C.W. Gable, and G.A. Zyvoloski. *Hydrogeology and Preliminary Calibration of a Preliminary Three-Dimensional Finite-Element Groundwater Flow Model of the Site Saturated Zone, Yucca Mountain, Nevada.* Yucca Mountain Project Milestone Report SP23NM3. Denver, CO: U.S. Geological Survey. 1997.

D'Agnese, F.A., C.C. Faunt, A.K. Turner, and M.C. Hill. *Hydrogeologic Evaluation and Numerical Simulation of the Death Valley Regional Ground-Water Flow System, Nevada and California.* Water Resources Investigations Report 96-4300. Denver, CO: U.S. Geological Survey. 1997.

de Marsily, G. *Quantitative Hydrogeology.* Orlando, FL: Academic Press, Inc. 1986.

Doubik, P., and B.E. Hill. Magmatic and hydromagmatic conduit development during the 1975 Tolbachik eruption, Kamchatka, with implications for hazards assessment at Yucca Mountain, Nevada. *Journal of Volcanology and Geothermal Research* 91: 43–64. 1999.

Dunn, D.S., and G.A. Cragnolino. *An Analysis of Galvanic Coupling Effects on the Performance of High-Level Nuclear Waste Container Materials.* CNWRA 97-010. San Antonio, TX: Center for Nuclear Waste Regulatory Analyses. 1997.

Dunn, D.S., and G.A. Cragnolino. *Effects of Galvanic Coupling Between Overpack Materials of High-Level Nuclear Waste Containers—Experimental and Modeling Results.* San Antonio, TX: Center for Nuclear Waste Regulatory Analyses. 1998.

Dunn, D.S.; Y-M. Pan, and G.A. Cragnolino. *Effects of Environmental Factors on the Aqueous Corrosion of High-Level Radioactive Waste Containers—Experimental Results and Models.* CNWRA 99-004. San Antonio, TX: Center for Nuclear Waste Regulatory Analyses. 1999.

Dunn, D.S., G.A. Cragnolino, H.K. Manaktala, P. Angell, Y.-M. Pan, and N. Sridhar. Factors influencing the performance of carbon steel overpacks in the proposed high-level nuclear waste repository. *Proceedings of the CORROSION '97 Conference.* Paper No. 99. Houston, TX: NACE International: 1996.

Farrell, D.A., A. Armstrong, J.R. Winterle, D.R. Turner, D.A. Ferrill, J.A. Stamatakos, N.M. Coleman, M.B. Gray, and S.K. Sandberg. *Structural Controls on Groundwater Flow in the Yucca Mountain Region.* San Antonio, TX: Center for Nuclear Waste Regulatory Analyses. 1999.

Fedors, R.W., and G.W. Wittmeyer. *Initial Assessment of Dilution Effects Induced by Water Well Pumping in the Amargosa Farms Area.* San Antonio, TX: Center for Nuclear Waste Regulatory Analyses. 1998.

Fedotov, S.A., and Ye. K. Markhinin. *The Great Tolbachik Fissure Eruption.* Cambridge, United Kingdom: Cambridge University Press. 1983.

Finn, P.A., R. Finch, E. Buck, and J. Bates. Corrosion mechanisms of spent fuel under oxidizing conditions. *Materials Research Society Symposium Proceedings.* Pittsburgh, PA: Materials Research Society 506: 123–131. 1998.

Flint, L.E. *Characterization of Hydrogeologic Units Using Properties, Yucca Mountain Nevada.* Water-Resources Investigations Report 97-4243. Denver, CO: U.S. Geological Survey. 1998.

Flint, A.L., J.A. Hevesi, and L.E. Flint. *Conceptual and Numerical Model of Infiltration for the Yucca Mountain Area, Nevada.* Milestone 3GUI623M. Las Vegas, NV: U.S. Department of Energy. 1996.

Forsyth, R. *An Evaluation of Results from the Experimental Programme Performed in the Studsvik Hot Cell Laboratory.* SKB TR 97-25. Stockholm, Sweden: Swedish Nuclear Fuel and Waste Management Company. 1997.

Fyfe, D. *Corrosion.* R.A. Jarman and G.T. Burstein, eds. Oxford, United Kingdom: Butterworth Heinmann. 1: 2:31–2:42. 1994.

García-Serrano, J., J.A. Serrano, P.P. Díaz-Arocas, J. Quiñones, and J.L.R. Almazan. SIMFUEL leaching studies in granitic groundwater under oxidizing conditions. *Materials Research Society Symposium Proceedings.* Pittsburgh, PA: Materials Research Society 412: 83–90. 1996.

Geldon, A.L. *Preliminary Hydrogeologic Assessment of Boreholes UE–25c#1, UE–25c#2, and UE–25c#3, Yucca Mountain, Nye County, Nevada.* WRI–92–4016. Denver, CO: U.S. Geological Survey. 1993.

Gelhar, L.W. *Stochastic Subsurface Hydrology.* Englewood Cliffs, NJ: Prentice-Hall, Inc. 1993.

Gelhar, L.W., C. Welty, and K.R. Rehfeldt. A critical review of data on field-scale dispersion in aquifers. *Water Resources Research* 28(7): 1,955–1,974. 1992.

Geomatrix Consultants, Inc. *Saturated Zone Flow and Transport Expert Elicitation Project.* San Francisco, CA: Geomatrix Consultants, Inc. 1998.

Ghosh, A., R.D. Manteufel, and G.L. Stirewalt. *FAULTING Version 1.0—A Code for Simulation of Direct Fault Disruption: Technical Description and User's Guide.* CNWRA 97-002. San Antonio, TX: Center for Nuclear Waste Regulatory Analyses. 1997.

Ghosh, A., J. Stamatakos, S. Hsiung, R. Chen, A.H. Chowdhury, and H.L. McKague. *Key Technical Issue Sensitivity Analysis with SEISMO and FAULTO Modules within the TPA (Version 3.1.1) Code.* San Antonio, TX: Center for Nuclear Waste Regulatory Analyses. 1998.

Glaze, L.S., and S. Self. Ashfall dispersal for the 16 September 1986 eruption of Lascar, Chile, calculated by a turbulent diffusion model. *Geophysical Research Letters* 18: 1,237–1,240. 1991.

Graves, R.P. *Water Levels in the Yucca Mountain Area, Nevada, 1996.* U.S. Geological Survey Open File Report 98-169. 1998.

Graves, R.P., P. Tucci. and G.M. O'Brien. *Analysis of Water Level Data in the Yucca Mountain Area, Nevada, 1985–95.* Water Resources Investigations Report 96-4256. Denver, CO: U.S. Geological Survey. 1997.

Gray, W.J. Dissolution testing of spent fuel. *Presentation to Nuclear Waste Technical Review Board.* October 14–16, Las Vegas, Nevada. Richland, WA: Pacific Northwest National Laboratory. 1992.

Gray, W.J., H.R. Leider, and S.A. Steward. Parametric Study of LWR Spent Fuel Dissolution Kinetics. *Journal of Nuclear Materials* 190: 46–52. 1992.

Gray, W.J., and C.N. Wilson. *Spent Fuel Dissolution Studies FY 1991 to 1994.* PNL–10540. Richland, WA: Pacific Northwest National Laboratory. 1995.

Grenthe, I., J. Fuger, R.J.M. Konings, R.J. Lemire, A.B. Muller, C. Nguyen-Trung, and H. Wanner. *Chemical Thermodynamics of Uranium.* New York: North-Holland. 1992.

Gruss, K.A., G.A. Cragnolino, D.S. Dunn, and N. Sridhar. Repassivation potential for localized corrosion of Alloys 625 and C22 in simulated repository environments. *Proceedings of the CORROSION '98 Conference.* Paper No. 149. Houston, TX: NACE International. 1998.

Haitjema, H.M. *Analytic Element Modeling of Groundwater Flow.* New York: Academic Press. 1995.

Harrar, J.E., J.F. Carley, W.F. Isherwood, and E. Raber. *Report of the Committee to Review the Use of J-13 Well Water in Nevada Nuclear Waste Storage Investigations.* UCID–21867. Livermore, CA: Lawrence Livermore National Laboratory. 1990.

Hartman, H.L. *Mine Ventilation and Air Conditioning.* Malabar, FL: Krieger Publishing Company. 1991.

Heffter, J.L., and B.J.B. Stunder. Volcanic ash forecast transport and dispersion (VAFTAD) model. *Weather and Forecasting* 8: 533–541. 1993.

Hill, B.E., C.B. Connor, M.S. Jarzemba, P.C. La Femina, M. Navarro, and W. Strauch. 1995 eruptions of Cerro Negro volcano, Nicaragua, and risk assessment for future eruptions. *Geological Society of America Bulletin.* 10: 1,231–1,241. 1998.

Hoffman, F.O., R.H. Gardner, and K.F. Eckerman. *Variability in Dose Estimates Associated with the Food Chain Transport and Ingestion of Selected Radionuclides.* NUREG/CR–2612. Washington DC: Nuclear Regulatory Commission. 1982.

Hopkins, A.T., and C.J. Bridgeman. A volcanic ash transport model and analysis of Mount St. Helens ashfall. *Journal of Geophysical Research* 90: 10,620–10,630. 1985.

Iman, R.L., and M.J. Shortencarier. *A FORTRAN 77 Program and User's Guide for the Generation of Latin Hypercube and Random Samples for Use with Computer Models.* NUREG/CR–3624. Washington, DC: Nuclear Regulatory Commission. 1984.

Incropera, F.P., and D.P. DeWitt. *Fundamentals of Heat and Mass Transfer.* 3rd Edition. New York: John Wiley and Sons. 1995.

International Atomic Energy Agency. *Handbook of Parameter Values for the Prediction of Radionuclide Transfer in Temperate Environments.* Technical Report Series No. 364. Vienna, Austria: International Atomic Energy Agency. 1994.

International Commission on Radiological Protection. *Reference Man: Anatomical, Physiological, and Metabolic Characteristics.* ICRP 23. Annals of the International Council on Radiation Protection. New York: Pergamon Press. 1975.

International Commission on Radiological Protection. *Limits for Intakes of Radionuclides by Workers.* ICRP 30, Parts 1–3 (including agenda and supplements). Annals of the International Council on Radiation Protection. New York: Pergamon Press. 1979–1982.

International Commission on Radiological Protection. *Age-Dependent Doses to Members of the Public from Intake of Radionuclides. Part 5: Compilation of Ingestion and Inhalation Dose Coefficients.* ICRP 72. Annals of the International Council on Radiation Protection. Tarrytown, NY: Elsevier Science Inc. 118(2): 132–141. 1996.

International Union of Radioecologists. *Sixth Report of the Working Group on Soil-to-Plant Transfer Factors.* Biltoven, The Netherlands: RIVM. 1989.

Itasca Consulting Group, Inc. *UDEC–Universal Distinct Element Code, Version 3. Volume I: User's Manual.* Minneapolis, MN: Itasca Consulting Group, Inc. 1996.

Jarzemba, M.S. Stochastic radionuclide distributions after a basaltic eruption for performance assessments of Yucca Mountain. *Nuclear Technology.* 1997.

Jarzemba, M.S., and P.A. LaPlante. *Preliminary Calculations of Expected Dose from Extrusive Volcanic Events at Yucca Mountain.* San Antonio, TX: Center for Nuclear Waste Regulatory Analyses. 1996.

Jarzemba, M.S., and R.D. Manteufel. An analytically based model for the simultaneous leaching-chain decay of radionuclides from contaminated ground surface soil layers. *Health Physics* 73(6): 919–927. 1997.

Jarzemba, M.S., P.A. LaPlante, and K.J. Poor. *Ashplume Code Version 1.0 Model Description and User's Guide.* CNWRA 97-004. San Antonio, TX: Center for Nuclear Waste Regulatory Analyses. 1997.

Kennedy, W.E., and D.L. Strenge. *Residual Radioactive Contamination from Decommissioning: Technical Basis for Translating Contamination Levels to Annual Total Effective Dose Equivalent.* NUREG/CR–5512. Volume 1. Washington, DC: Nuclear Regulatory Commission. 1992.

LaPlante, P.A., and K. Poor. *Information and Analyses to Support Selection of Critical Groups and Reference Biospheres for Yucca Mountain Exposure Scenarios.* CNWRA 97-009. San Antonio, TX: Center for Nuclear Waste Regulatory Analyses. 1997.

LaPlante, P.A., S.J. Maheras, and M.S. Jarzemba. *Initial Analysis of Selected Site-Specific Dose Assessment Parameters and Exposure Pathways Applicable to a Groundwater Release Scenario at Yucca Mountain.* CNWRA 95-018. San Antonio, TX: Center for Nuclear Waste Regulatory Analyses. 1995.

Leigh, C.D., B.M. Thompson, J.E. Campbell, D.E. Longsine, R.A. Kennedy, and B.A. Napier. *User's Guide for GENII-S: A Code for Statistical and Deterministic Simulation of Radiation Doses to Humans from Radionuclides in the Environment.* SAND91–0561. Albuquerque, NM: Sandia National Laboratories. 1993.

Leygraf, C. Atmospheric corrosion. *Corrosion Mechanisms in Theory and Practice.* P. Marcus and J. Oudar, eds. New York: Marcel Decker, Inc.: 421–455. 1995.

Lichtner, P.C., M.S. Seth, and S. Painter. *MULTIFLO User's Manual MULTIFLO Version 1.2—Two-Phase Nonisothermal Coupled Thermal-Hydrologic-Chemical Flow Simulator.* Revision 2. Change 1. San Antonio, TX: Center for Nuclear Waste Regulatory Analyses. 2000.

Linsley, R.K., and J.R. Franzini. *Water-Resources Engineering.* New York: McGraw-Hill Book Company. 1979.

Liskov, B., and J. Guttag. *Abstraction and Specification in Program Development.* Cambridge, MA: MIT Press. 1986.

Lobnig, R.E., H.P. Schmidt, K.Hennesen, and H.J. Grabke. Diffusion of cations in chromia layers grown on iron-base alloys. *Oxidation of Metals* 37: 81–93. 1992.

Lohman, S.W. *Ground-Water Hydraulics.* U.S. Geological Survey Professional Paper 708. 1972.

Lozano, A.S., H. Karimi, J.P. Cornelius, R.D. Manteufel, and R.W. Janetzke. *INVENT: A Module for the Calculation of Radionuclide Inventories, Software Description, and User Guide.* CNWRA 94-016. San Antonio, TX: Center for Nuclear Waste Regulatory Analyses. 1994.

Luckey, R.R., P. Tucci, C.C. Faunt, E.M. Ervin, W.C. Steinkampf, F.A. D'Agnese, and G.L. Patterson. *Status of Understanding of the Saturated-Zone Ground-Water Flow System at Yucca Mountain, Nevada, as of 1995.* WRI–96–4077. Denver, CO: U.S. Geological Survey. 1996.

Luhr, J.F., and T. Simkin. *Parícutin, the Volcano Born in a Mexican Cornfield.* Phoenix, AZ: Geoscience Press, Inc. 1993.

Manteufel, R.D., and N.E. Todreas. Effective thermal conductivity and edge conductance model for a spent fuel assembly. *Nuclear Technology* 105(3): 421–440. 1994.

Marsh, G., and K. Taylor. An assessment of carbon steel containers for radioactive waste disposal. *Corrosion Science* 28: 289–320. 1988.

MathSoft Inc. *MathCad Plus 5.0 Users Guide.* Cambridge, MA: MathSoft Inc. 1995.

McWhorter, D.B., and D.K. Sunada. *Ground-Water Hydrology and Hydraulics.* Fort Collins, CO: Water Resources Publications. 1977.

Mohanty, S., and T.J. McCartin, coords. *Total-system Performance Assessment (TPA) Version 3.2 Code: Module Description and User's Guide.* San Antonio, TX: Center for Nuclear Waste Regulatory Analyses. 1998.

Mohanty, S., G.A. Cragnolino, T. Ahn, D.S. Dunn, P.C. Lichtner, R.D. Manteufel, and N. Sridhar. *Engineered Barrier System Performance Assessment Code: EBSPAC Version 1.0 β, Technical Description and User's Manual.* CNWRA 96-001. San Antonio, TX: Center for Nuclear Waste Regulatory Analyses. 1996.

Mohanty, S., G.A. Cragnolino, T. Ahn, D.S. Dunn, P.C. Lichtner, R.D. Manteufel, and N. Sridhar. *Engineered Barrier System Performance Assessment Code: EBSPAC Version 1.1 Technical Description and User's Manual.* CNWRA 97-006. San Antonio, TX: Center for Nuclear Waste Regulatory Analyses. 1997.

Moran, J.J., and H.N. Shapiro. *Fundamentals of Engineering Thermodynamics.* New York: John Wiley and Sons. 1992.

Muller, M.A., M. Epley, and S. Mohanty. Procedure for Installing and Modifying *Total-system Performance Assessment (TPA) Version 2.3 PCβ Code.* San Antonio, TX: Center for Nuclear Waste Regulatory Analyses. 1998.

Napier, B.A., R.A. Peloquin, D.L. Strenge, and J.V. Ramsdell. *GENII: The Hanford Environmental Radiation Dosimetry Software System. Volumes 1, 2, and 3: Conceptual Representation, User's Manual, and Code Maintenance Manual.* PNL–6584. Richland, WA: Pacific Northwest National Laboratory. 1988.

National Council on Radiation Protection and Measurements. *Radiological Assessment: Predicting the Transport, Bioaccumulation, and Uptake by Manof Radionuclides Released to the Environment.* NCRP 76. Bethesda, MD: National Council on Radiation Protection and Measurements. 1984.

Nevada Division of Water Resources. *Preliminary Special Hydrographic Abstract for Valley Basin No. 230 from the Nevada Division of Water Resources Water Rights Database.* Carson City, NV: Nevada Division of Water Resources. Unpublished reports, 1995.

Nye County. *Phase I–FY 1999 Data Package for Early Warning Drilling Program.* Pahrump, NV: Nye County Nuclear Waste Repository Project Office. 1999.

Oatfield, W.J., and J.B. Czarnecki. Hydrogeologic inferences from drillers' logs and from gravity and resistivity surveys in the Amargosa Desert, southern Nevada. *Journal of Hydrology* 124(1-2): 131–158. 1991.

Oishi, Y., and H. Ichimura. Grain-boundary enhanced interdiffusion in polycrystalline CaO-stabilized Zirconia system. *Journal of Chemical Physics* 71(12): 5,134–5,139. 1979.

Olague, N.E., D.E. Longsine, J.E. Campbell, and C.D. Leigh. *User's Manual for the NEFTRAN II Computer Code.* NUREG/CR–5618. Washington, DC: Nuclear Regulatory Commission. 1991.

Perfect, D.L., C.C. Faunt, W.C. Steinkampf, and A.K. Turner. *Hydrochemical Data Base for the Death Valley Region, California and Nevada.* USGS Open-File Report 94-305. 1995.

Phillips, O.M. Infiltration of a liquid finger down a fracture into superheated rock. *Water Resources Research* 32(6): 1,665–1,670. 1996.

Popov, E.P. *Mechanics of Materials.* New York: Prentice-Hall. 1970.

Press, W.H., B.P. Flannery, S.A. Tekolsky, and W.T. Vetterling. *Numerical Recipes in FORTRAN.* Cambridge, United Kingdom: Cambridge University Press. 1986.

Rautman, C.A., L.E. Flint, A.L. Flint, and J.D. Istok. *Physical and Hydrologic Properties of Rock Outcrop Samples from a Nonwelded to Welded Tuff Transition, Yucca Mountain, Nevada.* WRI–95–4061. Denver, CO: U.S. Geological Survey. 1995.

Reed, D.T., and R.A. Van Konynenburg. *Preliminary Near-Field Report. Volume II: Scientific Overview of Near-Field Environment and Phenomena.* D.G. Widlder, ed. UCRL–LR–107476. Livermore, CA: Lawrence Livermore National Laboratory. 1993.

Ripley, B.D. *Stochastic Simulation.* New York: John Wiley and Sons. 1987.

Rognon, P. Field Measurement of dust near the ground, correlated with surrounding soils in the Sahara and Sahe. *Z. Geomorph.* NF.35(4): 491–501. 1991.

Rolfe, S.T., and J.M. Barsom. *Fracture and Fatigue Control in Structures.* Englewood Cliffs, NY: Prentice-Hall. 1977.

Roseberry, A.M., and D.E. Burmaster. Lognormal distributions for water intake by children. *Risk Analysis* 12: 99–104. 1992.

Roxburgh, I.S. *Geology of High-Level Nuclear Waste Disposal: An Introduction.* New York: Chapman and Hall. 1987.

Sagar, B., ed. *NRC High-Level Radioactive Waste Program Annual Progress Report: Fiscal Year 1996.* NUREG/CR–6513. No. 1. Washington, DC: Nuclear Regulatory Commission. 1997.

Schenker, A.R., D.C. Guerin, T.H. Robey, C.A. Rautman, and R.W. Bernard. *Stochastic Hydrogeologic Units and Hydrogeologic Properties Development for Total System Performance Assessments.* SAND94–0244. Albuquerque, NM: Sandia National Laboratories. 1995.

Sehmel, G.A. *Radionuclide Particle Resuspension Research Experiments on the Hanford Reservation.* BNWL–2081. Richland, WA: Pacific Northwest National Laboratory. 1977.

Seth, M.S., and P.C. Lichtner. *User's Manual for MULTIFLO. Part I: Metra 1.0 β, Two-Phase Nonisothermal Flow Simulator.* CNWRA 96-005. San Antonio, TX: Center for Nuclear Waste Regulatory Analyses. 1996.

Simonds, W.F., J.W. Whitney, K. Fox, A. Ramelli, J.C. Yount, M.D. Carr, C.D. Menges, R. Dickerson, and R.B. Scott. *Map of Fault Activity of the Yucca Mountain Area, Nye County, Nevada.* U.S. Geological Survey Miscellaneous Investigations Series Map, I-2520. Scale 1: 24,000. 1995.

Soldat, J.K, J.G Droppo, Jr., W.H. Rickard, and L.G. Faust. *Assessment of the Environmental Impact of the Retrievable Surface Storage Facility.* BNWL–151–313. Richland, WA: Pacific Northwest National Laboratory. 1973.

Spinks, J.W.T., and R.J. Woods. *Introduction to Radiation Chemistry.* 3rd Edition. New York: John Wiley and Sons. 1990.

Sridhar, N., G.A. Cragnolino, and D.S. Dunn. *Experimental Investigations of Localized Corrosion of High-Level Waste Container Materials.* CNWRA 93-004. San Antonio, TX: Center for Nuclear Waste Regulatory Analyses. 1993.

Stewart, K. The resuspension of particulate material from surfaces. *Proceedings of the Surface Contamination Symposium.* B.R. Fish, ed. New York: Pergaman Press. 1964.

Stothoff, S. Infiltration *Abstractions for Shallow Soil over Fractured Bedrock in a Semiarid Climate.* San Antonio, TX: Center for Nuclear Waste Regulatory Analyses. 1999.

Stothoff, S.A., H.M. Castellaw, and A.C. Bagtzoglou. Simulating the Spatial Distribution of Infiltration at Yucca Mountain, Nevada. San Antonio, TX: Center for Nuclear Waste Regulatory Analyses. 1997.

Stroes-Gascoyne, S., L.H. Johnson, J.C. Tait, J.L. McConnell, and R.J. Porth. Leaching of used CANDU fuel: Results from a 19-year leach test under oxidizing conditions. *Materials Research Society Symposium Proceedings*. Pittsburgh, PA: Materials Research Society 465: 511–518. 1997.

SunPro. *SPARCompiler FORTRAN 2.01 Reference Manual*. Mountain View, CA: Sun Microsystems, Inc. 1992.

SunSoft, Inc. *Solaris Advanced User's Guide*. Mountain View, CA: Sun Microsystems, Inc. 1995.

SunSoft, Inc. *Fortran 77 Language Reference, Compiler 4.2*. Mountain View, CA: SunSoft, Inc. 1996.

Suzuki, T. *A Theoretical Model for Dispersion of Tephra. Arc Volcanism: Physics and Tectonics*. Tokyo, Japan: Terra Scientific Publishing: 95–113. 1983.

Tait, J. C. and J. M. Luht. *Dissolution Rates of Uranium from Unirradiated $UO_2$ and Uranium and Radionuclides from Used CANDU Fuel Using the Single-Pass Flow-through Apparatus*. Ontario Hydro Report No. 06819–REP–01200–0006–ROO. Toronto, Canada: Ontario Hydro. 1997.

Tegen, I. and I. Fung. Modeling of mineral dust in the atmosphere: sources, transport and optical thickness. *J Geophysical Research* 99(11): 22,897–22,914. 1994.

Thompson, B.G.J. *A Method for Overcoming the Limitation of Conventional Scenario-Based Assessments by Using Monte Carlo Simulation of Possible Future Environmental Changes*. PAAG/DOC/88/11. Paris, France: Nuclear Energy Agency/Organization for Economic Cooperation and Development. 1988.

Thompson, B.G.J., and B. Sagar. The development and application of integrated procedures of post-closure assessment, based upon Monte Carlo simulation: the probabilistic systems assessment (PSA) approach. *Reliability Engineering and System Safety* 42: 125–160. 1993.

Timoshenko, S.P. *Strength of Materials Part II: Advanced Theory and Problems*. 3rd Edition. Princton, NJ: D. Van Nostrand Company, Inc. 1956.

Timoshenko, S.P., and J.N. Goodier. *Theory of Elasticity*. New York: McGraw-Hill. 1987.

TRW Environmental Safety Systems, Inc. *Total System Performance Assessment—1995: An Evaluation of the Potential Yucca Mountain Repository*. B00000000–01717–2200–00136. Revision 01. Las Vegas, NV: TRW Environmental Safety Systems, Inc. 1995.

TRW Environmental Safety Systems, Inc. *Total System Performance Assessment—Viability Assessment (TSPA-VA) Plan*. B00000000–01717–2200–00179. Las Vegas, NV: TRW Environmental Safety Systems, Inc. 1996.

Tschoepe, E., III, F. Lyle, Jr., D.M. Dancer, C.G. Interrante, and P.K. Nair. *Field Engineering Experience with Structural Materials*. San Antonio, TX: Center for Nuclear Waste Regulatory Analyses. 1994.

Turner, D.R. *Radionuclide Sorption in Fractures at Yucca Mountain, Nevada: A Preliminary Demonstration of Approach for Performance Assessment.* San Antonio, TX: Center for Nuclear Waste Regulatory Analyses. 1998.

U.S. Department of Agriculture. *Nationwide Food Consumptive Survey, 1987-88: Food and Nutrient Intakes by Individuals in the United States.* NFCS 87–I–1. Washington, DC: U.S. Department of Agriculture, Human Nutrition Information Service. 1992.

U.S. Department of Commerce. *Census of Agriculture: Farm and Ranch Irrigation Survey.* Washington, DC: U.S. Department of Commerce. 1994.

U.S. Department of Energy. *Seismic Design Methodology for a Geologic Repository at Yucca Mountain Topical Report.* YMP–0030NP. Las Vegas, NV: U.S. Department of Energy. 1995.

U.S. Department of Energy. *Viability Assessment of a Repository at Yucca Mountain. Overview* and all five volumes. DOE/RW–0508. Las Vegas, NV: U.S. Department of Energy, Office of Civilian Radioactive Waste Management. 1998.

U.S. Environmental Protection Agency. *Federal Guidance Report No. 11: Limiting Values of Radionuclides Intake and Air Concentration and Dose Conversion Factors for Inhalation, Submersion, and Ingestion.* EPA 520/1-88-020. Washington, DC: U.S. Environmental Protection Agency. 1988.

U.S. Environmental Protection Agency. *Federal Guidance Report No. 12: External Exposure to Radionuclides in Air, Water, and Soil.* EPA 402–R–93–081. Washington, DC: U.S. Environmental Protection Agency, Office of Radiation and Indoor Air. 1993.

U.S. Environmental Protection Agency. *Notice of Proposed Federal Radiation Protection Guidance for Exposure of the General Public.* Federal Register 59: 31618. Washington, DC: U.S. Government Printing Office. 1994.

U.S. Environmental Protection Agency. *Exposure Factors Handbook.* Volumes 1 and 2. EPA/600/P–95/002Fa and b. Washington, DC: U.S. Environmental Protection Agency. 1997.

U.S. Geological Survey. *Seismotectonic Framework and Characterization of Faulting at Yucca Mountain, Nevada.* J.W. Whitney, coord. Denver, CO: U.S. Geological Survey. 1996.

U.S. Nuclear Regulatory Commission. *Issue Resolution Status Report on Methods to Evaluate Climatic Change and Associated Effects at Yucca Mountain.* Washington, DC: Nuclear Regulatory Commission. 1997.

U.S. Nuclear Regulatory Commission. *Issue Resolution Status Report. Key Technical Issue: Igneous Activity.* Revision 2. Washington, DC: Nuclear Regulatory Commission, Division of Waste Management. 1999a.

U.S. Nuclear Regulatory Commission. *Issue Resolution Status Report. Key Technical Issue: Unsaturated and Saturated Flow Under Isothermal Conditions.* Revision 2. Volume 1. Washington, DC: Nuclear Regulatory Commission. 1999b.

Vander Voort, G.F. Embrittlement of steels. *Metals Handbook. Properties and Selection: Irons, Steels, and High-Performance Alloys.* Volume 1: 10th Edition. Materials Park, OH: ASM International: 689–736. 1990.

van Genuchten, M.T. A general approach for modeling solute transport in structured soils. *Hydrogeology of Rocks of Low Permeability. IAH Memorandum 17(2): 513–526.* Ottawa, Ontario: International Association of Hydrogeologists. 1985.

van Genuchten, R. A close-form equation for predicting the hydraulic conductivity of unsaturated soils. *Soil Science Society of America Journal* 44(4): 892–898. 1980.

Van Wylen, G.J., and R.E. Sonntag. *Fundamentals of Classical Thermodynamics.* New York: John Wiley and Sons. 1978.

Wescott, R.G., M.P. Lee, T.J. McCartin, N.A. Eisenberg, and R.G. Baca, eds. *NRC Iterative Performance Assessment Phase 2: Development of Capabilities for Review of a Performance Assessment for a High-Level Waste Repository.* NUREG–1464. Washington, DC: Nuclear Regulatory Commission. 1995.

Wilson, C.N. *Results from NNWSI Series 3 Spent Fuel Dissolution Tests.* PNL–7170. Richland, WA: Pacific Northwest National Laboratory. 1990.

Wilson, M.L., J.H. Gauthier, R.W. Barnard, G.E. Barr, H.A. Dockery, E. Dunn, R.R. Eaton, D.C. Guerin, N. Lu, M.J. Martinez, R. Nilson, C.A. Rautman, T.H. Robey, B. Ross, E.E. Ryder, A.R. Scheneker, S.A. Shannon, L.H. Skinner, W.G. Halsey, J.D. Gansemer, L.C. Lewis, A.D. Lamont, I.R. Triay, A. Meijer, and D.E. Morris. *Total-System Performance Assessment for Yucca Mountain—SNL Second Iteration (TSPA–93).* Volumes 1 and 2. SAND93–675. Albuquerque, NM: Sandia National Laboratories. 1994.

Winograd, I.J., and W. Thordarson. *Hydrogeologic and Hydrochemical Framework, South-Central Great Basin, Nevada-California, with Special Reference to the Nevada Test Site.* U.S. Geological Survey Professional Paper 712–C. 1975.

Winterle, J.R., and P.C. La Femina. *Review and Analyses of Hydraulic and Tracer Testing at the C-Holes Complex Near Yucca Mountain, Nevada.* San Antonio, TX: Center for Nuclear Waste Regulatory Analyses. 1999.

Winterle, J.R., R.W. Fedors, D.L. Hughson, and S. Stothoff. *Update of Hydrologic Parameters for the Total-system Performance Assessment Code.* San Antonio, TX: Center for Nuclear Waste Regulatory Analyses. 1999a.

Winterle, J.R., R.W. Fedors, D.L. Hughson, and S. Stothoff. *Review of the Unsaturated Zone Models Used to Support the Viability Assessment of a Repository at Yucca Mountain.* San Antonio, TX: Center for Nuclear Waste Regulatory Analyses. 1999b.

Winterle, J.R., N.M. Coleman, W.A. Illman, and D. Hughson. *Review of Permeability Estimates Obtained from the Yucca Mountain Project.* San Antonio, TX: Center for Nuclear Waste Regulatory Analyses. 2000.

Wittwer, C., G. Chen, G.S. Bodvarsson, M. Chornack, A. Flint, L. Flint, E. Klicklis, and R. Spengler. *Preliminary Development of the LBL/USGS Three-Dimensional Site Scale Model of Yucca Mountain, Nevada.* LBL–37356, UC–814. Berkeley, CA: Lawrence Berkeley National Laboratory. 1995.

Wolery, T.W. *EQ3/6, A Software Package for Geochemical Modeling of Aqueous Systems: Package Overview and Installation Guide Version 7.0.* UCRL–MA110662. Livermore, CA: Lawrence Livermore National Laboratory. 1992.

Wolfram, S. *Mathematica: A System for Doing Mathematics by Computer.* Redwood City, CA: Addison-Wesley Publishing Company. 1991.

Woolhiser, D., S. Stothoff, and G. Wittmeyer. *Estimating Channel Infiltration from Surface Runoff in the Solitario Canyon Watershed, Yucca Mountain, Nevada. San Antonio, TX: Center for Nuclear Waste Regulatory Analyses. 1999.*

Wronkiewicz, D.J., J.K. Bates, T.J. Gerding, E. Veleckis, and B.S. Tani. Uranium release and secondary phase formation during unsaturated testing of $UO_2$ at 90. *Journal of Nuclear Materials* 190: 107–127. 1992.

Zhou, S., and A. Turnbull. Influence of pitting on the fatigue life of turbine blade steel. *Fatigue and Fracture of Engineering Material and Structure* 22: 1,083–1,093. 1999.

# INDEX


Acceleration Hazard Curve ..... 7-7
Adsorption ..... 9-1, 9-5
Advective Transport ..... 2-7, 10-6, 10-8
Age ..... 1-6, 3-2, 3-18, 3-20, 8-11, 11-2-5, 11-10-11, 12-2-3, 12-6-8
Agriculture ..... 2-10, 11-11
Alkaline ..... 6-5, 6-14
Alloy 22 ..... 1-6, 1-9, 2-7, 6-3-8, 6-10, 6-13
Alluvial ..... 1-6, 2-9, 10-4-8, 11-3
Alluvium ..... 1-9-11, 2-9, 10-1, 10-3, 10-5, 10-7, 11-3
Alteration Rate ..... 2-8, 8-8
Animal Products . 11-2, 11-5, 11-7, 17-2, 17-5
Aqueous Corrosion 2-7, 6-1-3, 6-5, 6-12, 6-14
Aquifer ..... 1-6, 1-11, 2-1, 2-9, 10-3-8, 11-3 ,12-3-5
Ash ..... 1-4, 1-12, 2-3, 2-10, 3-4, 3-10-11, 3-20, 3-25, 15-1-7, 16-1-3, 16-5, 17-1-4, 17-6-8, 18-1-4,19-11, 19-14, 20-2, 20-4, 20-12, 20-13
Ash Blanket ..... 16-1-3, 17-2, 17-6, 18-2-4
ASHPLUMO ..... 3-2, 3-5, 3-8, 3-10-11, 3-25, 14-1, 15-1-3, 15-6, 16-1, 17-1-3, 18-1-2, 19-2, 19-11-14, 20-12, 20-13, 21-2, 21-6
ASHRMOVO ..... 3-2, 3-5, 3-8, 3-10-11, 3-25, 15-1-2, 16-1-3, 16-5, 17-1-3, 18-1-2, 19-2, 20-12, 20-13, 21-2, 21-6

Backfill ..... 1-3, 1-6, 1-7, 1-11, 2-6, 5-1, 5-6-7, 5-9-10, 5-12, 5-25, 6-5, 6-13, 7-1, 8-13, 8-16, 22-5, 23-1
Basaltic Volcanism ..... 15-2
Bathtub Model ..... 2-8, 8-2-5, 8-15-16
Bicarbonate ..... 5-13, 8-9
Bulk Density ..... 16-3, 16-4
Burnup .... 1-10, 3-2, 3-20, 5-1, 19-19, 21-3

Capillary ..... 4-9, 6-4, 8-12
Capillary Barrier ..... 8-12
Capture Zone ..... 10-3, 12-3-5
Carbon Steel ..... 1-7, 2-7, 6-3-9
Carbonate .... 2-6, 3-25, 5-13, 8-7, 8-8, 12-4
CCDF .. 10-1, 14-1, 20-2, 20-3, 20-10, 22-1-5
Chloride Concentration ..... 2-6-7, 3-7, 5-1-2, 5-13-16, 5-24-26, 6-1, 6-5-6, 6-11, 6-13, 19-19, 20-2, 20-7, 20-12, 20-13
Cladding ... 1-7, 2-8, 6-2, 7-5, 8-1, 8-9, 8-11, 8-15, 23-1
Climate Change ... 3-1-2, 4-1, 4-5, 4-7, 4-10, 5-5, 5-24, 10-8
Code .. 1-8-12, 2-1, 2-3, 2-5-10, 3-1-12, 3-18, 3-20, 3-21, 3-24, 4-1-3, 4-5, 4-8-10, 5-1, 5-5, 5-13-16, 5-24, 6-1-3, 6-6-14, 7-1, 7-7, 7-8, 8-1, 8-7, 8-8, 8-11, 8-11-16, 9-1-5, 9-8-9, 10-1, 10-3-5, 10-7, 11-1-2, 11-4, 11-8, 11-10, 11-11, 12-1, 12-5-6, 13-1-2, 13-4-5, 14-2, 14-4, 15-1-3, 15-6, 16-1, 17-2, 17-3, 17-5-7, 18-2, 19-1-4, 19-7-8, 19-10-11, 19-12-19, 20-1, 20-2, 20-9-11, 20-13, 20-15, 21-1-12, 21-14-16, 22-1, 22-4-5, 23-1
Colloidal ..... 8-16, 23-1
Condensate Zone .. 5-16, 5-18-20, 5-22, 5-23
Condensation 2-6, 5-13, 5-18, 5-23, 5-24, 6-4
Conduction .... 2-6, 5-2, 5-5-6, 5-8-10, 5-12, 5-19, 5-23, 5-24
Conductivity ..... 2-9, 5-2, 5-9-10, 5-12, 5-20, 5-23, 6-5, 8-15, 9-3-4, 9-8-10, 11-3, 12-3, 19-13
Congruent Release ..... 8-13, 8-16
Consumption Rates ..... 11-4, 11-9-11, 12-6, 12-8, 17-7
Convection ..... 2-6, 5-6, 5-9, 5-12, 5-23
Correlation .... 3-7, 3-14, 3-18-19, 4-7, 13-5, 19-15-16, 21-14-15, 23-1
Corrosion ..... 1-6, 1-9, 1-10, 2-7, 3-4, 3-8, 3-10, 3-25, 4-1, 5-12-13, 5-16, 5-23-24, 6-1-15, 7-8, 8-1-3, 8-11-13, 8-15-16, 13-4-5, 20-3, 20-9, 20-12, 23-1
Creep ..... 8-11
Crevice Corrosion ..... 1-6, 2-7, 6-5-6
Crops ... 1-6, 11-5, 11-7, 11-8, 11-10, 17-5-6

Darcy Velocity ..... 10-4, 10-7, 12-5

# INDEX


DCAGS .... 3-2, 3-8, 3-10, 3-11, 3-25, 11-5, 15-2, 16-1, 17-1-1, 17-5-6, 17-8, 18-1-4, 19-2, 19-18, 19-19, 20-4, 20-12, 20-13, 21-2, 21-6

DCAGW .... 3-2, 3-8, 3-10, 3-25, 10-1, 10-3, 11-1-2, 11-5, 11-8-9, 11-11, 12-1-2, 12-5-8, 17-2, 17-6, 17-8, 18-2-4, 19-2, 19-4, 19-10-11, 19-18, 20-5, 20-7, 20-9, 20-12, 20-13, 21-2, 21-6

DCF ..... 3-20, 11-1-5, 12-2-3, 12-6, 17-2, 17-5, 17-8, 18-2-3, 20-12

Dike ..... 1-12, 2-8, 3-8, 14-3

Dilution .... 1-3-4, 2-9, 11-1-3, 11-7, 12-1-2, 19-4, 19-10, 19-18, 20-3, 20-9, 21-3

Direct Exposure . 2-10, 11-2, 11-5, 11-7, 17-2, 17-5,17-7, 18-2-3

Dispersion ..... 2-9, 9-6, 10-6-8, 15-2-3, 15-6

Disruptive Event ..... 2-5, 2-7, 3-4, 3-25, 6-1, 6-2, 6-14, 7-1, 8-1, 13-1, 14-1

Distribution Coefficient ..... 9-5, 16-3

Dose Pathway ..... 12-7

Drift .... 1-6-7, 1-10, 1-12, 2-1, 2-6, 2-7, 3-5, 5-1-2, 5-5-9, 5-12-19, 5-20, 5-23-25, 8-1-2, 8-12, 9-3, 14-2-4, 19-5, 19-19

Drinking Water Dose ..... 12-7, 20-5

Drip Shield ... 1-3, 1-6-7, 1-9-11, 2-6, 5-7-10, 6-10-11, 6-13-15, 7-8, 8-12, 23-1

Dripping ..... 1-6, 2-7-8, 4-10, 5-14, 5-18, 5-20, 6-10, 6-14-15, 8-8, 8-11-12, 8-15, 23-1

Dry-air Oxidation ..... 6-3, 6-12, 6-14

Dryout ..... 5-14, 5-16, 5-18, 5-20-25, 19-18

EBS ..... 1-2, 2-1-3, 2-8, 3-4, 3-10, 6-2, 6-10, 8-1-2, 8-13, 9-1, 20-2, 20-3

EBSFAIL ..... 3-2, 3-7-8, 3-10, 3-24, 5-1, 6-1-3, 6-5-6, 6-9, 6-12, 6-14, 8-1-2, 8-13, 13-5, 19-1, 20-9, 20-12, 20-13, 21-2-3, 21-6, 21-10

EBSPAC ..... 3-5, 6-2, 8-1-2

EBSREL ..... 3-2, 3-5, 3-8, 3-10, 3-25, 5-1, 5-20, 5-22, 5-23, 6-1, 7-1, 8-1-2, 8-9, 8-13-16, 9-1, 9-6, 13-1, 13-3, 14-1, 19-1, 19-9, 19-12-13, 19-16, 19-19, 20-4, 20-7, 20-12, 20-13, 21-2-3, 21-6

EDA II ..... 1-6-7, 1-9-10, 2-1, 2-7, 5-13-14, 6-3-5, 6-8-10, 6-12-14, 7-4, 9-3, 14-2, 19-5

Effective Porosity ..... 10-3, 10-4, 10-7

Engineered Barrier System (EBS) .. 1-2, 20-2

Erosion ..... 2-10, 16-1-5, 17-3

Eruption Column ..... 14-4, 15-1-4, 15-6-7

Evaporation ..... 4-2, 4-9, 5-13-14, 5-16, 5-24, 5-26, 8-15

Evapotranspiration .... 4-2, 4-9, 11-7, 16-3-4

EXEC ..... 3-2, 3-4-5, 3-7-8, 3-10-11, 4-1, 5-1, 6-1, 7-1, 8-1, 9-1, 10-1, 11-1-3, 12-1-3, 13-1, 14-1, 15-1, 16-1, 17-1, 18-1, 19-3-4, 19-10, 19-19, 20-4-11, 20-13-15, 21-2, 21-7, 21-9-13, 21-16

Exposure Pathway ..... 12-6, 17-6, 18-4

Exposure Scenario .... 1-10, 1-12, 2-3, 2-10, 5-2, 16-1

Extrusive ..... 3-25, 14-1, 14-3-4, 15-1-2, 16-1, 16-3,17-1, 18-2, 19-11

Farming Group ..... 11-1, 10-12, 12-1, 17-7

Fault ..... 1-6, 2-1-3, 2-7-8, 6-13, 13-1-5, 19-12, 19-13

Fault Slip ..... 13-1-2, 13-4

Fault Displacement ..... 2-1, 2-3, 2-7-8, 6-13, 13-1, 13-3-5

Fault Width ..... 13-2-4

Fault Length ..... 13-1-2, 13-4-5

Faulting ... 1-3, 1-9, 2-8, 3-4, 3-8, 3-10, 3-25, 4-10, 6-2, 6-13-14, 8-3, 8-13, 8-16, 13-1-5, 20-3, 20-9, 20-12, 21-12, 22-5

FAULTO .... 3-2, 3-7, 3-8, 6-1-2, 6-14, 7-1, 13-1-5, 19-2, 19-4, 19-12, 19-15, 20-9, 20-12, 20-13, 21-2, 21-6

Flow Tube ..... 3-4, 10-8

Food Transfer Factors ..... 11-1, 11-7-8, 17-6

Fracture Flow ..... 5-18, 5-25, 9-3-5, 9-8-10

# INDEX


Fractures . . . . . 1-11, 2-6, 2-9, 4-8, 4-11, 5-14, 5-18, 5-20, 5-22, 8-11-12, 9-2-3, 9-5, 9-8-10, 10-5-8, 14-3

Galvanic . . . . . 6-5, 6-8
Gaseous Release . . . . . 8-16
Gaussian Plume . . . . . 12-5, 15-2-3
GENII . . . . . 1-10, 1-12, 11-1, 11-4, 11-10-11, 12-1, 12-5, 17-2, 17-6-7, 18-2-3
GENII-S . . . . . 11-10, 17-2, 17-6-7, 18-2-3
GENTPA . . . . . 1-10, 1-12, 2-10, 3-8, 3-10, 11-1-2, 11-4, 11-8, 11-10, 12-1-2, 12-5-6, 19-18, 20-10, 20-12,
Grain Density . . . . . 9-5
Groundwater Travel Time . . . 9-1, 20-2, 20-5

Hazard Curve . 3-8, 7-1, 7-7-8, 19-2, 19-14-15
Heat Transfer . . . . . 2-5-6, 5-2, 5-4-6, 5-8-9, 5-12, 5-18-19, 5-23-24, 22-5
Heterogeneity . . . . . 10-3
Humid-air Corrosion . . . . . 6-2-5, 6-12, 6-14
Hydraulic Conductivity . . . . . 2-9, 8-15, 9-3-4, 9-8-10, 11-3, 12-3, 19-13

Igneous Intrusion . . . . . 14-2
Impact Load . . . . . 7-1-2, 7-4, 7-8-10
Impact Stress . . . . . 7-4-5, 7-8-9
Index . . . . . 20-8
Infiltration . . . . . 1-3, 1-11, 2-3, 2-5, 3-25, 4-1-3, 4-6-10, 5-16, 5-19-22, 5-24, 8-11, 9-8-9, 11-7, 20-2, 20-6
Ingestion Dose . . . . . 11-1, 11-4, 12-1, 12-6-7
Ingrowth . . . . . 3-18, 3-21, 8-13, 8-17, 16-1
Inhalation Dose . . . . . 17-4, 18-3
Initially Defective WP . . . . . 2-7
Inner Overpack . . . . . 1-6, 1-9, 1-10, 2-7, 5-10, 6-5, 6-7-8
Installation . . . . . 1-1, 1-8, 21-1, 21-5, 21-7-8
Inventory . . . . . 1-8, 2-1, 2-8, 3-2, 3-4, 3-18, 3-20, 3-21, 8-2-3, 8-9, 8-13, 16-1, 16-4, 19-6, 19-8, 19-19, 20-12
Ion Exchange . . . . . 9-1, 9-5
Irrigation . . . . . 1-6, 2-10, 10-3, 10-6, 11-3-5, 11-7, 16-3-4
ITYM . . . . . 4-9-10, 19-19

Joint Spacing (JS) . . . . . 7-5

Kd . . . . . 9-5, 11-7, 16-4, 19-12

Lateral Diversion . . . . . 2-1, 4-2, 4-9, 4-10, 9-2, 9-9
Latin Hypercube Sampling . 1-12, 3-2, 3-12-14
Leaching . . . . . 2-10, 3-20, 8-4, 8-11, 8-15-16, 11-1, 11-4, 11-7, 16-1-3, 18-4
Livestock . . . . . 11-7-8, 17-5-6
Localized Corrosion . . . 1-10, 6-5-6, 6-8, 6-10, 6-12-13, 8-11
Longitudinal Dispersivity . . . . . 10-5, 10-7, 10-8, 12-5

Magma . . . . . 1-4, 1-12, 2-3, 2-7-9, 6-14, 14-1-5, 15-2
MAI 1-11, 4-1-3, 4-7-10, 19-10, 19-16, 19-19
MAP . . . . . 1-5, 1-8, 1-11, 2-5, 4-1-3, 4-5, 4-7-8, 4-10-11, 10-4, 11-5, 13-2, 19-18
MAT . . 4-1-3, 4-5, 4-7-8, 4-10-11, 11-5, 19-18
Matrix Diffusion . . . . . 1-11, 2-9, 9-6, 9-8-10, 10-1, 10-5-7
Matrix Flow . . . 5-18, 9-1, 9-2-4, 9-9-10, 10-7
Mean Annual Temperature (MAT) . . . . . 4-1
Mean Annual Precipitation (MAP) . . . . . 2-5
Mean Annual Infiltration (MAI) . . . . . 1-11
Mechanical Failure . . . . . 1-6, 1-9, 2-7, 3-4, 6-1-3, 6-8-9, 6-12-14, 8-11, 13-5, 23-1
Moisture Content . . . . . 9-2-3, 9-5, 11-8, 17-6
Monte Carlo . . . . . 1-12, 3-2
MULTIFLO . . . . . 2-6, 5-1, 5-13-16, 5-22, 5-24-26, 6-1, 19-18, 19-19, 21-3

Near-field . . . . . 1-3, 2-3, 2-5-7, 4-1, 5-1, 5-13, 5-16, 5-18, 5-22-23, 5-25, 6-2, 6-5, 6-9, 6-11, 6-13, 8-2, 22-5, 23-1
NEFTRAN . . . . . 1-11, 2-9, 3-4-5, 9-2, 9-4-6, 9-8, 10-1, 10-3, 10-5, 21-7, 21-10

# INDEX


Neptunium ..... 8-8
NFENV ..... 3-7-8, 3-10, 3-24, 4-1, 5-1-3, 5-13, 5-16, 5-18, 5-19, 5-23-25, 6-1, 8-1-2, 19-1, 19-9, 19-18-19, 20-6, 20-12, 20-13, 21-2, 21-6, 21-9

Outer Overpack ..... 1-6, 2-7, 5-10, 6-3, 6-5, 6-7-10

Particle Size 15-5, 8-10, 2-8, 11-8, 15-5, 17-6
Particle Diameter ..... 15-4, 15-7
Passivation ..... 6-5
PDF ..... 6-10-11, 20-15, 19-10-15, 21-13,
Peak Dose ..... 1-3, 1-9, 2-8, 2-10, 8-9, 11-2, 12-2, 17-1, 17-5, 18-1, 18-3 20-2, 20-3, 20-15, 22-1, 22-4-5,
Percolation .... 2-3, 2-5-7, 2-9, 3-4, 4-1, 4-2, 4-9, 5-1, 5-13, 5-16, 5-18-20, 8-11, 9-1-4, 9-6, 9-9-10, 20-2
Permeability ..... 4-9, 9-9, 10-7, 19-12
pH ..... 2-6, 3-25, 5-1, 5-13-14, 5-16, 6-1, 6-5, 8-8-9, 20-12-13, 23-1
Pitting ..... 1-9, 2-7, 6-1, 6-5-6, 6-8, 6-12
Plume Trajectory ..... 12-5
Plume Thickness ..... 12-1, 12-3-5
Pluvial Climate ..... 2-10, 11-5, 11-10
Porosity ..... 1-11, 3-24, 5-12, 5-19, 5-21, 8-10, 8-15, 9-3-6, 9-8, 10-3-7, 16-4
Progeny ..... 8-5
Pumping Well ..... 12-2
Pumping ..... 1-4, 1-6, 1-12, 2-3, 10-3, 10-6-8, 11-2-3, 11-5, 11-7, 12-1-4, 12-6-7, 19-18, 20-12
Pumping Volume ..... 11-2, 12-2
Pumping Well . 1-12, 10-7, 11-2, 19-18, 20-12

Radiation ..... 1-3, 1-12, 2-6, 5-6, 5-12, 5-23, 5-25, 6-11-13, 8-11, 11-9, 12-7, 15-2, 15-3, 17-8, 18-1, 23-1
Radiolysis ..... 1-10, 6-11-13
Receptor Group ..... 1-2, 1-4, 1-9, 1-12, 2-1, 2-3, 2-9, 2-10, 3-1, 3-2, 3-10, 10-1, 11-1-5, 11-7-9, 11-11, 12-1-4, 12-6-8, 15-1, 15-3, 17-1, 17-2, 17-5, 17-7, 21-12, 18-1-4, 19-18, 19-19
Receptor Location 1-9, 2-3-4, 3-10, 3-11, 4-9, 10-1, 10-3, 10-6-7, 11-7-8, 12-3, 12-5, 12-7, 15-2, 17-2, 17-3, 17-5, 18-2, 18-3, 20-10
Recurrence Rate ..... 3-13, 13-2-3
Reference Biosphere .... 2-3, 2-10, 11-1, 12-1
Reflux ..... 1-6, 1-11, 2-6, 4-1, 5-1, 5-16, 5-18-20, 5-21, 5-22, 5-24-25, 8-11, 8-15, 9-9, 20-2, 20-6
Relative Humidity ... 1-3, 5-13, 6-10, 6-13-14, 19-19, 20-2, 20-7, 20-12, 20-13
Repassivation ..... 6-6, 6-8, 6-12-13
Residential Group ..... 11-1, 12-1, 12-5, 18-4
Resuspension Factor ..... 9-5, 9-6, 9-8, 10-1, 10-5, 11-10, 17-7
Rock Impact ..... 7-4
Rock Conditions ..... 7-1, 7-2, 7-5-8
Rockfall ..... 1-6-7, 1-9, 2-7, 3-2, 3-4, 3-27, 6-1, 6-10, 6-13, 7-1, 7-4-8, 8-11

SAMPLER ..... 3-2, 3-7-8, 3-11-12, 3-14, 7-7, 19-3, 19-7, 20-11, 20-13
Saturated Zone (SZ) ..... 1-3, 1-6, 1-9, 2-1, 2-3, 2-9, 3-4, 3-10, 3-27, 9-1, 9-6, 9-8, 10-1-3, 10-5-8, 11-2-3, 12-2-3, 17-6, 18-4, 20-2, 20-5-6, 20-15, 23-1
Saturation .... 5-12, 5-21, 5-24-25, 9-3-4, 9-6
Scoria ..... 15-2
Screen Length ..... 12-3-4
Seismic Hazard ..... 7-1, 7-7-8, 19-2
Seismicity .... 1-3, 2-1, 2-3, 2-7-8, 3-1-2, 3-8, 3-10, 3-27, 6-1, 6-13-14, 7-1, 7-2, 7-7, 8-16, 13-5, 22-5,
SEISMO ..... 1-9, 2-7, 3-2, 3-4-5, 3-7-8, 3-27, 6-1-2, 6-14, 7-1-8, 19-1-2, 19-4, 19-15, 21-3, 21-7
Soil Depth ..... 2-5, 4-9-10

# INDEX


Soil Concentration . . . . . 2-3, 2-9, 3-4, 11-7, 17-5-6, 18-3
Solubility . . . . . 2-8, 3-13, 3-26, 8-6-7, 8-13, 8-15, 16-2, 16-4, 19-13
Spatial Variability . . . . . 3-1, 4-2, 4-9, 9-2, 9-8-9, 10-3
Spent Fuel Surface Area . . . . . 8-11
Spent Fuel Dissolution . . . . . 8-1, 8-6, 8-9
Spent Fuel (SF) . . . . . 1-3, 1-6, 1-9-11, 2-3, 2-7-10, 3-2, 3-4, 3-10-11, 3-20, 5-1, 5-6, 5-10, 5-12-13, 5-23, 6-2, 6-11-12, 7-5, 8-1-11, 8-13, 8-15-16, 16-1, 17-8, 18-4, 19-1-2, 23-1
Stainless Steel (SS) . . . . . 1-6-7, 6-7-8, 6-13
Stratigraphy . . . . . 1-4, 2-1, 9-2, 9-8-9
Stress Intensity . . . . . 6-9-10, 6-13
Subareas . . . . . 1-10-12, 2-1, 2-3, 2-5-6, 2-8-9, 3-4, 3-7-8, 3-10-11, 3-13, 3-26, 5-1-2, 5-5, 5-20-22, 5-24, 6-1-2, 6-14, 7-1, 8-1-3, 8-13, 8-15-16, 9-1-5, 9-8-9, 10-1, 13-1, 14-1, 19-1-6, 19-16, 20-2, 20-4-7, 20-12-13, 20-15, 21-11, 21-15
SZFT . . . . . 3-2, 3-4-5, 3-8, 3-10, 3-27, 9-1, 9-6, 9-8, 10-1, 10-3, 10-6-8, 11-1-3, 12-1-4, 19-1, 19-19, 20-5, 20-6, 20-12, 20-13, 21-3, 21-7

Tectonism . . . . . 2-3
TEDE . . . . . 2-10, 11-1, 11-4-5, 11-8, 12-1, 12-6, 17-1-2, 17-7, 18-1-2, 20-4, 20-5, 20-7, 20-9
Temper Embrittlement . . . . . 6-9
Tephra . . . . . 2-9-10, 15-1-2, 15-6
Thermal Embrittlement . . . . . 2-7, 6-2-3, 6-8, 6-10, 6-13
Thermal Conductivity . . . 5-1-2, 5-9-10, 5-12, 5-20, 5-23
Total Dose . . . . 11-2-3, 12-2-3, 17-1-2, 17-5, 18-1-3, 20-3, 22-4
Transport Path . . . . . 1-3, 9-6, 10-3-5, 10-8
Transverse Dispersivity . . . . . 12-5

Uniform Corrosion . . . . 1-9, 6-2, 6-5, 6-8-10, 6-12, 6-14
Uranium . . . . . 3-8, 5-5, 8-8-9, 20-13
Unsaturated Zone (UZ) . . . . . 1-4, 1-11, 2-1, 2-3, 2-5, 2-7-9, 3-4, 3-10, 3-26, 3-27, 4-1, 4-8-9, 5-14, 8-2, 9-1-6, 9-8-10, 10-1, 10-3, 11-3, 21-12, 20-2, 20-4-6, 20-10, 20-12, 20-15, 23-1
UZFLOW . . . . 2-5, 3-2, 3-4-5, 3-7, 3-8, 3-10, 3-26, 4-1-3, 4-5, 4-7-10, 5-1, 5-16, 5-18, 5-20-22, 9-1-2, 9-4, 9-6, 9-8, 17-1, 18-1, 19-1, 19-10, 19-16, 19-18-19, 20-6, 21-3, 21-7, 21-17
UZFT . . . . . 2-9, 3-2, 3-4-5, 3-8, 3-10, 3-27, 4-1, 8-1, 9-1-3, 9-5-9, 10-1, 10-3, 10-4, 19-1, 19-12, 21-10, 21-12

Velocity Field . . . . . 9-6, 9-8, 10-3, 10-8
Volcanic Power . . . . . 15-1
Volcanism . . . . . 2-3, 2-9, 13-5, 15-2, 17-7-8, 18-4, 21-12
VOLCANO . . . . . 2-7, 3-2, 3-4, 3-7-8, 3-10, 3-27, 6-1-2, 7-1, 14-1–2, 14-4-5, 15-1, 17-3, 19-2, 19-4, 19-14

Waste Package Inventory . . . . . 8-6, 19-8
Water Dripping . . . . . 2-7-8, 8-11-12
Water Table . . . . . 2-1, 2-5, 2-9, 5-18, 5-20, 9-1-3, 9-6, 9-9, 10-1, 10-3-4, 11-3, 11-7, 17-5
Well Pumping . . . . . 1-6, 10-6, 11-5, 12-5
Well Field . . . . . 10-3
Waste Package (WP) . . . . . 1-1, 1-3, 1-6-7, 1-9, 1-12, 2-1, 2-5-9, 3-2-4, 3-7-8, 3-10, 3-26-27, 4-2, 5-1, 5-2, 5-5–6, 5-8, 5-10, 5-12, 5-14-15, 5-18, 5-20, 5-22-26, 6-1-5, 6-8-15, 7-1-9, 8-1-16, 13-1-5, 14-1-5, 15-1, 15-5, 19-5, 19-8-9, 19-15, 20-2-4, 20-7, 20-9, 20-12-13, 20-15, 21-11, 22-5, 23-1
WP Failure Time . . . . 2-6-7, 3-8, 3-27, 6-1-2, 6-10, 6-14, 14-1, 20-3

# APPENDIX A

# APPENDIX A
# REFERENCE DATA SET

The base case (reference) data set (i.e., *tpa.inp*) is presented in the following tables. This section is presented in such a format that by making a table-to-text conversion and a slight manipulation, a *tpa.inp* input file can be created in a format usable by the TPA Version 4.0 code. Various columns in this table represent flags or distribution functions, parameter names, parameter descriptions, data ranges, and descriptions of the source of data. The initials and asterisks used in the last column of the tables are described at the end of the appendix. This input data set includes information provided by various key technical issues (KTIs). However, it is expected that the base case data set will evolve further as KTIs begin using the code and analyzing results. The format of the following text matches the format in the *tpa.inp* file.

| Distribution Type | Parameter Name | Description | Parameter Range | Remarks | Provided by |
|---|---|---|---|---|---|
| ** title Input file *tpa.inp* as supplied with TPA Version 4.0 code Base case** ** ** ***>>> GLOBAL PARAMETERS <<<*** ** ** ***>>> Importance Analysis Flags ** | | | | | |
| iflag | ImportanceAnalysisFlag(yes=1,no=0) | Flag to activate importance analysis. | 0 | The importance analysis for TPA Version 4.0 code has not been thoroughly tested. It is recommended not to use the importance analysis features until the implementation is tested and refined. The flags in this section are used to nullify the protective action of the designated barrier. They are used only if the flag ImportanceAnalysisFlag equals one. | ** |
| iflag | InnerContainerPresenceFlag(yes=1,no=0) | Self-explanatory | 1 | Used if ImportanceAnalysisFlag equals 1 | ** |
| iflag | OuterContainerPresenceFlag(yes=1,no=0) | Self-explanatory | 1 | Used if ImportanceAnalysisFlag equals 1 | ** |
| iflag | CladdingPresenceFlag(yes=1,no=0) | Self-explanatory | 1 | Used if ImportanceAnalysisFlag equals 1 | ** |

| Distribution Type | Parameter Name | Description | Parameter Range | Remarks | Provided by |
|---|---|---|---|---|---|
| iflag | SoilPresenceFlag(yes=1,no=0) | Soil layer presence | 1 | Used if ImportanceAnalysisFlag equals 1 | ** |
| iflag | UpperUnsaturatedLayerPresenceFlag(yes=1,no=0) | Self-explanatory | 1 | Used if ImportanceAnalysisFlag equals 1 | ** |
| iflag | TSwPresenceFlag(yes=1,no=0) | Topopah Spring | 1 | Used if ImportanceAnalysisFlag equals 1 | ** |
| iflag | CHnvPresenceFlag(yes=1,no=0) | Calico Hills vitric | 1 | Used if ImportanceAnalysisFlag equals 1 | ** |
| iflag | CHnzPresenceFlag(yes=1,no=0) | Calico Hills zeolitic | 1 | Used if ImportanceAnalysisFlag equals 1 | ** |
| iflag | PPwPresenceFlag(yes=1,no=0) | Prow Pass | 1 | Used if ImportanceAnalysisFlag equals 1 | ** |
| iflag | UCFPresenceFlag(yes=1,no=0) | Upper Crater Flat | 1 | Used if ImportanceAnalysisFlag equals 1 | ** |
| iflag | BFwPresenceFlag(yes=1,no=0) | Bull Frog | 1 | Used if ImportanceAnalysisFlag equals 1 | ** |
| iflag | STFFPresenceFlag(yes=1,no=0) | Saturated tuff | 1 | Used if ImportanceAnalysisFlag equals 1 | ** |
| iflag | SAVPresenceFlag(yes=1,no=0) | Saturated alluvium | 1 | Used if ImportanceAnalysisFlag equals 1 | ** |
| iflag | PumpingWellPresenceFlag(yes=1,no=0) | Dilution volume provided by pumping well | 1 | Used if ImportanceAnalysisFlag equals 1 | ** |

| Distribution Type | Parameter Name | Description | Parameter Range | Remarks | Provided by |
|---|---|---|---|---|---|
| ** | | | | | |
| ** | | | | | |
| ** ***>>> Disruptive Scenario flags <<<*** | | | | | |
| ** | | | | | |
| iflag | VolcanismDisruptiveScenario Flag(yes=1,no=0) | Self-explanatory | 0 | — | ** |
| iflag | FaultingDisruptiveScenarioFl ag(yes=1,no=0) | Self-explanatory | 0 | — | ** |
| iflag | SeismicDisruptiveScenarioFla g(yes=1,no=0) | Self-explanatory | 1 | — | ** |
| ** | | | | | |
| ** ***>>> Subarea Size <<<*** | | | | | |
| ** | | | | | |
| ** | | | | | |
| ** Number and Location Of SubAreas[m] Based On EDA-II Design. | | | | | |
| subarea | | | | | |
| 8 | | | | | |
| edaii 1-cw | | | | | |
| 547514.88,4079310.61 | | | | | |
| 548069.2,4079136.5 | | | | | |
| 547847.3,4077816.2 | | | | | |
| 547370.95,4077922.04 | | | | | |
| 547514.88,4079310.61 | | | | | |
| edaii 2-cw | | | | | |
| 548069.2,4079136.5 | | | | | |
| 548569.32,4078981. | | | | | |
| 548504.06,4077664.24 | | | | | |
| 547847.3,4077816.2 | | | | | |
| 548069.2,4079136.5 | | | | | |

| Distribution Type | Parameter Name | Description | Parameter Range | Remarks | Provided by |
|---|---|---|---|---|---|
| edaii 3-cw<br>547370.95,4077922.04<br>547847.3,4077816.2<br>548322.7,4077192.2<br>547474.7,4077281.6<br>547370.95,4077922.04<br>edaii 4-cw<br>547847.3,4077816.2<br>548504.06,4077664.24<br>548479.71,4077173.06<br>548322.7,4077192.2<br>547847.3,4077816.2<br>edaii 5-cw<br>547474.7,4077282.6<br>547887.3,4077238.1<br>547897.79,4076045.46<br>547655.97,4076123.07<br>547474.7,4077282.6<br>edaii 6-c<br>547887.3,4077238.1<br>548322.7,4077192.2<br>548155.7,4075962.63<br>547897.79,4076045.46<br>547887.3,4077238.1<br>edaii 7-cw<br>548322.7,4077192.2<br>548479.71,4077173.06<br>548455,4076674.51<br>548155.7,4075962.63<br>548322.7,4077192.2<br>edaii 8-cw<br>547645.27,4079656.06 | | | | | |

| Distribution Type | Parameter Name | Description | Parameter Range | Remarks | Provided by |
|---|---|---|---|---|---|
| 548588.98,4079377.55<br>548569.32,4078981<br>547514.88,4079310.61<br>547645.27,4079656.06<br>** | | | | | |
| iconstant | StartAtSubarea | | 1 | | |
| iconstant | StopAtSubarea | | 8 | | |
| **<br>** ***>>> Nuclides and Chains <<<***<br>**<br>**<br>** Nuclides can be eliminated from the basecase set.<br>** However, if additional nuclides (Pu242, Am242m, Pu238, Cm243,<br>** U235, Pa231, Ac227, Pu241, U233, Th229, Cm244, U236, U232, Sm151,<br>** Cs137, Sn126, Sn121m, Ag108m, Pd107, Mo93, Zr93, Sr90, or Ni63)<br>** are added to the basecase set, then corresponding RDs, KDs,<br>** solubilities, gap fractions, and correlations must be added.<br>**<br>iflag<br>CheckNuclidesAndChains(yes=1,no=0)<br>0<br>**<br>aqueousnuclides<br>** number of nuclides, number of chains<br>20<br>13<br>**<br>** chain 1 | | | | | |

| Distribution Type | Parameter Name | Description | Parameter Range | Remarks | Provided by |
|---|---|---|---|---|---|
| 2 | | | | | |
| Cm246 | | | | | |
| U238 | | | | | |
| ** chain 2 | | | | | |
| 3 | | | | | |
| Cm245 | | | | | |
| Am241 | | | | | |
| Np237 | | | | | |
| ** chain 3 | | | | | |
| 2 | | | | | |
| Am243 | | | | | |
| Pu239 | | | | | |
| ** chain 4 | | | | | |
| 1 | | | | | |
| Pu240 | | | | | |
| ** chain 5 | | | | | |
| 4 | | | | | |
| U234 | | | | | |
| Th230 | | | | | |
| Ra226 | | | | | |
| Pb210 | | | | | |
| ** chain 6 | | | | | |
| 1 | | | | | |
| Cs135 | | | | | |
| ** chain 7 | | | | | |
| 1 | | | | | |
| I129 | | | | | |
| ** chain 8 | | | | | |
| 1 | | | | | |
| Tc99 | | | | | |
| ** chain 9 | | | | | |
| 1 | | | | | |

| Distribution Type | Parameter Name | Description | Parameter Range | Remarks | Provided by |
|---|---|---|---|---|---|
| Ni59<br>** chain 10<br>1<br>C14<br>** chain 11<br>1<br>Se79<br>** chain 12<br>1<br>Nb94<br>** chain 13<br>1<br>Cl36<br>**<br>endofnuclides<br>**<br>** | | | | | |
| ** ***>>> Parameter Sampling <<<***<br>**<br>** | | | | | |
| iflag | DirectReleaseOnlyFlag(yes=1,no=0) | Option to conduct direct-release only calculation | 0 | — | ** |
| constant | SeedForRandomNumber | Seed for random number generator | 188910452.0 | — | ** |
| iflag | LatinHypercubeSampling(yes=1,no=0) | Latin Hypercube Sampling flag | 1 | — | ** |

| Distribution Type | Parameter Name | Description | Parameter Range | Remarks | Provided by |
|---|---|---|---|---|---|
| iconstant | NsetLatinHypercubeSampling | Number of sets of realizations in the Morris method sensitivity analysis. This value equals the total number of realizations divided by the number of desired realizations in each set analyses using the Morris method. | 1 | — | ** |
| iconstant | NumberOfRealizations | Number of realizations | 1 | — | ** |
| iconstant | StartAtRealization | Realization to start code | 1 | — | ** |
| iconstant | StopAtRealization | Realization to stop code. Should be zero to perform all remaining realizations | 0 | — | ** |
| ** ** ** ***>>> Simulation Times <<<*** ** ** | | | | | |
| constant | DurationOfCompliancePeriod [yr] | Compliance time in years. Specified as ≤ Maximum time. Allows the user to obtain outputs at two periods (compliance period and | 1.0e4 | — | ** |

| Distribution Type | Parameter Name | Description | Parameter Range | Remarks | Provided by |
|---|---|---|---|---|---|
| | | maximum time) simultaneously | | | |
| constant | MaximumTime[yr] | Simulation time period | 1.0e4 | — | ** |
| iconstant | NumberOfTimeStepsInCompliancePeriod | Sum of pre- and post-compliance time steps must not exceed 201 | 201 | — | ** |
| constant | RatioOfLastToFirstTimeStepInCompliancePeriod | Ratio of last to first time step in the compliance period. When the ratio is set as 1, then all time intervals are equal. When the ratio is greater than 1, the time intervals geometrically progress until the end of the compliance period. | 100.0 | — | ** |
| iconstant | NumberOfTimeStepsAfterCompliancePeriod | Parameter ignored if MaximumTime[yr] = DurationOfCompliancePeriod[yr] (sum of pre- and post-compliance time steps must not exceed 201) | 0 | — | ** |
| constant | RatioOfLastToFirstTimeStepAfterCompliancePeriod | Parameters ignored if MaximumTime[yr] = DurationOfCompliancePeriod[yr] | 0.0 | — | ** |

| Distribution Type | Parameter Name | Description | Parameter Range | Remarks | Provided by |
|---|---|---|---|---|---|
| * ** ** ***>>> Output Print Options <<<*** ** ** | | | | | |
| iconstant | OutputMode(0=None,1=All,2 =UserDefined) | Flag for appending intermediate output to files (0 = no files appended, 1 = all files appended, and 2 = all files for specified realizations) | 0 | — | ** |
| iconstant | UserDefinedLowerRealizatio nAppended | For output mode = 2, append files are written beginning with this realization | 1 | — | ** |
| iconstant | UserDefinedUpperRealization Appended | For output mode = 2, append files are written ending with this realization | 1 | — | ** |
| iconstant | SelectAppendFiles | For Select Append Files:<br>0 = append all files<br>1 = *uzflow.ech* and *uzflow.rlt* only<br>2 = *nfenv.ech* and *nfenv.rlt* only<br>3 = *ebsfail.ech* and *ebsfail.rlt* only | 0 | The user can append inputs and intermediate outputs either to all .rlt, .ech, and .cum files or can select such information to be appended for a particular module. For example, when selecting append option 9, the input and intermediate output | ** |

| Distribution Type | Parameter Name | Description | Parameter Range | Remarks | Provided by |
|---|---|---|---|---|---|
| | | 4 = *seismo.ech* and *seismo.rlt* only<br>5 = *faulto.ech* and *faulto.rlt* only<br>6 = *volcano.ech* and *volcano.rlt* only<br>7 = *ebsrel.ech* and *ebsrel.rlt* only<br>8 = *uzft.ech* and *uzft.rlt* only<br>9 = *szft.ech* and *szft.rlt* only<br>10 = *dcagw.ech* and *dcagw.rlt* only<br>11 = *ashplumo.ech* and *ashplumo.rlt* only<br>12 = *ashrmovo.ech* and *ashrmovo.rlt* only<br>13 = *dcags.ech* and *dcags.rlt* only<br>14 = *ashplume.cum* only<br>15 = *failt.cum* only<br>16 = *nefiiuz.cum* only<br>17 = *releaset.cum* only<br>18 = *ggenii.cum* only<br>19 = *genv.cum* only<br>20 = *dcf.cum* only<br>(*gw_cb_ad.dat* and *gw_pb_ad.dat*) | | for only the SZFT module can be appended. In this version of the code, multiple append options cannot be selected at the same time. | |

| Distribution Type | Parameter Name | Description | Parameter Range | Remarks | Provided by |
|---|---|---|---|---|---|
| ** ** ** ***>>> UZFLOW <<<*** ** | | | | | |
| uniform | ArealAverageMeanAnnualInfiltrationAtStart[mm/yr] | Areally averaged mean annual infiltration for the initial (current) climate (mm/yr) | 4.–13 | Current best estimate by Unsaturated and Saturated Flow under Isothermal Conditions (USFIC) team [see Winterle et al., 1999b] | ** |
| uniform | MeanAveragePrecipitationMultiplierAtGlacialMaximum | Mean average precipitation (MAP) multiplier at glacial maximum | 1.5, 2.5 | Best estimate by USFIC team (see Issue Resolution Status Report on climate, Nuclear Regulatory Commission, 1997) | ** |
| uniform | MeanAverageTemperatureIncreaseAtGlacialMaximum[degC] | Mean average temperature (MAT) increase at glacial maximum (°C) | -10, -5 | Best estimate by USFIC team (see IRSR on climate, Nuclear Regulatory Commission, 1997) | ** |
| constant | TimeStepForClimate[yr] | Time step used in the climate model | 500.0 | Value selected on the basis of efficiency of the TPA Version 4.0 code and the rate for climate change | ** |
| constant | StandardDeviationOfMAPAboutMeanInOneTimePeriod[mm/yr] | Standard deviation of MAP about mean in one time period (mm/yr) | 0.0 | Deviation about mean is not considered necessary at this point and allows efficient execution of the code | ** |

| Distribution Type | Parameter Name | Description | Parameter Range | Remarks | Provided by |
|---|---|---|---|---|---|
| constant | StandardDeviationOfMATAboutMeanInOneTimePeriod[degC] | Standard deviation of MAT about mean in one time period (°C) | 0.0 | Deviation about mean is not considered necessary at this point and allows efficient execution of the code | ** |
| constant | CorrelationBetweenMAPAndMAT | Correlation between MAP and MAT | -0.8 | Best estimate by the USFIC team.<br>Derived from climate expert elicitation (DeWispelare et al., 1993). | ** |
| iconstant | ClimatePerturbationSet | Options: 1 and 2; currently both sets are identical | 1 | — | ** |
| **<br>**<br>**  ***>>> NFENV <<<***<br>** | | | | | |
| iflag | TabularTemperatureRHFlag(yes=1,no=0) | Flag to use *tefkti.inp* file containing temperature and relative humidity (RH) data computed external to the TPA Version 4.0 code | 0 | — | ** |
| iconstant | nsetUsedToPickTempRHDataSet | Selects the data set in *tefkti.inp* that has up to four sets of data (options 1 to 4) | 1 | — | ** |

| Distribution Type | Parameter Name | Description | Parameter Range | Remarks | Provided by |
|---|---|---|---|---|---|
| constant | WPLength[m] | Outer length of waste package (WP) (m) | 5.275 | Civilian Radioactive Waste Management System Management & Operating Contractor (1999a) | ** |
| constant | WPDiameter[m] | Outer diameter of WP (m) | 1.579 | Average of the WP diameter containing 21 pressurized water reactor and 44 boiling water reactor WPs | ** |
| constant | EmplacementDriftDiameter[m] | Emplacement drift diameter (m) | 5.5 | Civilian Radioactive Waste Management System Management and Operating Contractor (CNWRA) (1996) | ** |
| constant | CircumferentialFractionNotCoveredByFloor[] | Fraction of the circumference of the drift not covered by floor or invert | 0.75 | CNWRA best estimate | SM 1/24/00 |
| constant | EmplacementBackfillThickness[m] | Equivalent thickness of emplaced backfill (m) | 0.0 | EDA II design. A value of 0.0 indicates that backfill is not present in the drift. | SM 1/24/00 |
| constant | DripShieldThickness[m] | Drip shield thickness (m) | 0.02 | Civilian Radioactive Waste Management System Management & Operating Contractor (1999a) | SM 1/26/00 |
| constant | DripShieldEqvIntDia[m] | Equivalent diameter of drip shield (m) | 2.75 | CNWRA best estimate | SM 1/26/00 |

| Distribution Type | Parameter Name | Description | Parameter Range | Remarks | Provided by |
|---|---|---|---|---|---|
| iconstant | SelectRefluxModel(1,2,3) | Flag to select reflux model (reflux1 = 1, reflux2 = 2, and reflux3 = 3) | 3 | — | ** |
| constant | LengthOfRefluxZone[m] | Length of reflux zone (m) in reflux1 model | 20 | Thermal Effects on Flow (TEF) team best estimate (Not applicable for EDA-II design) | DH 10/30/00 |
| constant | MaximumFluxInRefluxZone[m/s] | Maximum flux in reflux zone (m/s) in reflux1 model | 1.0e-9 | CNWRA best estimate (Not applicable for EDA-II design) | DH 10/30/00 |
| constant | PerchedBucketVolumePerSA area[m3/m2] | Perched bucket volume per subarea ($m^3/m^2$) in reflux1 model | 0.5 | TEF team best estimate (Not applicable for EDA-II design) | DH 10/30/00 |
| constant | Reflux2Thickness | Thickness of dry-out zone (m) in the reflux2 model | 100.0 | 100 m consistent with MULTIFLO simulations of the dry-out zone (Not applicable for EDA-II design) | DH 10/30/00 |
| constant | Reflux2Porosity | Porosity of rock in the reflux zone in the reflux2 model | 0.14 | CNWRA best estimate (Not applicable for EDA-II design) | DH 10/30/00 |
| constant | Reflux2SatInit | Initial water saturation in the reflux zone in the reflux2 model | 0.9 | CNWRA best estimate (Not applicable for EDA-II design) | DH 10/30/00 |
| constant | Reflux2SatResid | Residual water saturation in the reflux zone in the reflux2 model | 0.1 | CNWRA best estimate (Not applicable for EDA-II design) | DH 10/30/00 |

| Distribution Type | Parameter Name | Description | Parameter Range | Remarks | Provided by |
|---|---|---|---|---|---|
| constant | Reflux2Period | Reflux cycle in the reflux2 model; when this factor has a value of 1, dry-out water recycles each year | 100.0 | Best estimate, upper value from MULTIFLO runs (Not applicable for EDA-II design) | DH 10/30/00 |
| constant | Reflux2LossI | Fraction of infiltration derived water that escapes each year | 0.1 | TEF team best estimate (Not applicable for EDA-II design) | DH 10/30/00 |
| constant | Reflux2LossD | Fraction of dry-out zone derived water that escapes the reflux cycle each year | 0.1 | TEF team best estimate (Not applicable for EDA-II design) | DH 10/30/00 |
| constant | EmplacementDriftSpacing[m] | Spacing between drifts | 81 | Design value for Enhanced Design Alternative II Civilian Radioactive Waste Management System Management & Operating Contractor, 1999a. | ** |
| constant | WPSpacingAlongEmplacementDrift[m] | WP spacing (m) | 6.1392 | WP center-to-center distance | SM 2/21/00 |
| constant | TotalWasteEmplacedInRepository[MTU] | Self-explanatory | 68030.0 | The repository is expected to receive 63,000 MTU of CSNF, and 7,000 MTU of vitrified high level waste and defense spent nuclear fuel. Currently, the Total-system Performance Assessment code emplaces a maximum of 68,030 MTU in 8 subareas instead of partially | DD 2/23/00 |

| Distribution Type | Parameter Name | Description | Parameter Range | Remarks | Provided by |
|---|---|---|---|---|---|
| | | | | filling subareas 9 and 10. However, the code assumes all wastes to have the properties of CSNF. | |
| uniform | FractionOfCondensateRemoved[1/yr] | Fraction of water condensate removed in each reflux3 time step. (Parameter specific to reflux3 model.) | 0.0, 0.25 | In the absence of data provided by either models or experiments, these values are estimated by TEF team members. Future results from laboratory- and field-scale tests are anticipated to provide bounds on these estimates | DH 10/12/00 |
| uniform | FractionOfCondensateTowardRepository[1/yr] | Fraction of condensate moving toward the repository. (Parameter specific to reflux3 model.) | 0.05, 1.0 | Same as above | DH 10/12/00 |
| constant | FractionOfCondensateTowardRepositoryRemoved[1/yr] | Fraction of condensate moving toward the repository but escaped before entering the repository. (Parameter specific to reflux3 model.) | 0.0 | Same as above | DH 10/12/00 |
| constant | DensityOfWaterAtBoiling[kg/m^3] | Density of water at the boiling point temperature at the repository ($kg/m^3$). | 960.5 | Weast and Astle (1984) | ** |

| Distribution Type | Parameter Name | Description | Parameter Range | Remarks | Provided by |
|---|---|---|---|---|---|
| | | (Parameter specific to reflux3 model.) | | | |
| constant | EnthalpyOfPhaseChangeForWater[J/kg] | Enthalpy of phase change for water (J/kg). (Parameter specific to reflux3 model.) | 2.4e6 | Weast and Astle (1984) | ** |
| uniform | TemperatureGradientInVicinityOfBoilingIsotherm[K/m] | Temperature gradient in the vicinity of the boiling isotherm (K/m). (Parameter specific to reflux3 model.) | 1.0, 100.0 | Based on MULTIFLO runs, laboratory-scale experiments | ** |
| constant | WastePackagePayload[MTU] | WP payload (MTU/package) | 9.76 | U.S. Department of Energy (1987) | ** |
| constant | AgeOfWaste[yr] | Age of waste at the time of emplacement | 26.0 | Civilian Radioactive Waste Management System Management & Operating Contractor (1999a) | ** |
| constant | AmbientRepositoryTemperature[C] | Ambient repository temperature (°C) | 20.0 | Assumed in TRW Environmental Safety Systems, Inc. (1995) | ** |
| constant | MassDensityofYMRock[kg/m^3] | Mass density of rock ($kg/m^3$) | 2580.0 | U.S. Department of Energy (1990) | ** |
| constant | SpecificHeatofYMRock[J/(kg-K)] | Specific heat of rock (J/kg-K) | 840.0 | U.S. Department of Energy (1990) | ** |
| uniform | ThermalConductivityofYMRock[W/(m-K)] | Thermal conductivity of rock (W/m-K) | 1.8, 2.2 | U.S. Department of Energy (1993) | ** |

| Distribution Type | Parameter Name | Description | Parameter Range | Remarks | Provided by |
|---|---|---|---|---|---|
| constant | EmissivityOfWastePackage[-] | Emissivity of WP surface | 0.87 | Emissivity of Alloy 22 Civilian Radioactive Waste Management System Management & Operating Contractor (1999a) | SM 2/21/00 |
| constant | EmissivityOfDriftWall[-] | Emissivity of drift wall | 0.8 | Incropera & DeWitt (1995) | ** |
| constant | EmissivityOfDripShield[-] | Emissivity of the drip shield internal surface | 0.63 | Civilian Radioactive Waste Management System Management & Operating Contractor (1999a) | SM 1/26/00 |
| constant | ThermalConductivityOfFloor[ W/(m-C)] | Thermal conductivity of floor (W/m-°C) | 0.6 | Incropera & DeWitt (1995) | ** |
| constant | Cond_EqvForNaturalConvect ion[W/(m-C)] | Equivalent conductance representing natural convention [W/m-°C] | 0.90 | Thermal conductance equivalence based on a thermal conductivity 30 times that of air | SM 1/26/00 |
| constant | FactorForVentilationHeatloss es[] | A factor for accounting for ventilation heat losses | 0.7 | Assumed | SM 1/26/00 |
| constant | TimeOfBackfillEmplaced[yr] | Time of backfill emplacement (yr) | 50 | Civilian Radioactive Waste Management System Management and Operating Contractor (1996) | SM 3/22/00 |
| iconstant | NumberOfWeightsForGaussL egendreIntegration[] | Number of weights for Gauss Legendre integration for computing repository scale temperature | 20 | Best estimate for numerical convergence | SM 2/23/00 |

| Distribution Type | Parameter Name | Description | Parameter Range | Remarks | Provided by |
|---|---|---|---|---|---|
| constant | ThermalConductivityOfDripShield[W/(m-C)] | Thermal conductivity of drip shield material (W/m-°C) | 20.77 | Corresponds to the thermal conductivity of Ti Grade 7 at 93.33 °C; varies between 21.95 at 21.11 °C and 19.88 at 204.44 °C Civilian Radioactive Waste Management System Management & Operating Contractor (1999) | SM 1/26/00 |
| constant | ThermalConductivityOfBackfill[W/(m-C)] | Thermal conductivity of the backfill material (W/m-°C) | 0.27 | Quartz sand thermal conductivity Civilian Radioactive Waste Management System Management & Operating Contractor (1999); Thermal conductivity of crushed tuff is 1.20 W/(m-C) | SM 2/21/00 |
| constant | ThermalConductivityOfInnerOverpack[W/m-C] | Thermal conductivity of inner overpack material (W/m-°C) | 15.0 | Corresponds to the thermal conductivity of A 316 stainless steel at 100.0 °C; varies between 15.0 W/m-°C at 100.0 °C and 17.77 W/m-°C at 500.0 °C (Lyman et al., 1960; Brandes, 1983) | SM 2/21/00 |
| constant | ThermalConductivityOfOuterOverpack[W/m-C] | Thermal conductivity of outer overpack material (W/m-°C) | 11.1 | Corresponds to the thermal conductivity of Alloy 22 at 93.33 °C; varies between 10.1 at 48°C and 13.4 at 200 °C Civilian Radioactive Waste Management System Management & Operating Contractor (1999) | SM 1/26/00 |

| Distribution Type | Parameter Name | Description | Parameter Range | Remarks | Provided by |
|---|---|---|---|---|---|
| constant | EffectiveThermalConductivityOfBasket&SFinWP[W/(m-°C)] | Effective thermal conductivity of basket & spent fuel (SF) in WP (W/m-°C) | 1.0 | Assumed based on Manteufel and Todreas (1994) | ** |
| constant | ElevationOfRepositoryHorizon[m] | Elevation of repository horizon above sea level (m) | 1072.0 | Civilian Radioactive Waste Management System Management and Operating System (1996) | ** |
| constant | ElevationOfGroundSurface[m] | Elevation of ground surface above sea level (m) | 1400.0 | Civilian Radioactive Waste Management System Management and Operating Contractor (1996) | ** |
| ** ** ** ***>>>EBSFAIL <<<*** ** | | | | | |
| constant | OuterWPThickness[m] | Thickness of the outer overpack (m) | 0.02 | Snell (1999) | SM 3/22/00 |
| constant | InnerWPThickness[m] | Thickness of the inner overpack (m) | 0.05 | Snell (1999) | SM 3/22/00 |
| constant | MetalGrainRadius[micrometer] | Average radius of the metal grains constituting the WP outer overpack ($\mu$m) | 13.75 | Container Life and Source Term (CLST) meetings 04/11/97, 04/14/97, and 04/17/97. Data not relevant for EDA II. | ** |
| constant | GrainBoundaryThickness[micrometer] | Thickness of grain boundary used in the model for calculating | 7.0e-4 | Range about value assumed in Mohanty et al. (1996); Lobnig et al. (1992). | ** |

| Distribution Type | Parameter Name | Description | Parameter Range | Remarks | Provided by |
|---|---|---|---|---|---|
| | | coupled oxygen diffusion along grain boundaries in metal ($\mu$m) | | Data not relevant for EDA II. | |
| constant | DryOxidationConstant | Constant relating matrix and grain boundary oxygen diffusivities in metal | 9999 | Artificially set at 9999 to suppress corrosion due to dry oxidation. | ** |
| constant | CriticalRelativeHumidityHumidAirCorrosion | Critical relative humidity above which humid-air corrosion may initiate | 0.55 | Data not relevant for EDA II because the corrosion rate under humid air condition (specified as Humid Air Corrosion Rate [m/yr] is set at 1.e-15 m/yr. CLST meeting 04/24/97. | ** |
| normal | CriticalRelativeHumidityAqueousCorrosion | Critical RH above which aqueous corrosion may initiate | 0.6, 0.65 | CNWRA staff best estimate | ** |
| uniform | ThicknessOfWaterFilm[m] | Thickness of water film on WP surface (m) | 0.001, 0.003 | Assumed in Mohanty et al. (1996) | ** |
| constant | BoilingPointOfWater[C] | Boiling point of water at Yucca Mountain (YM) (°C) | 97.0 | Manteufel (1997) | ** |
| constant | OuterOverpackErpIntercept | Outer overpack $E_{rp}$ intercept in $mV_{SHE}$ | 2.006e3 | Dunn et al. (1999) | DD 2/22/00 |
| constant | TempCoefOfOuterPackErpIntercept | Temperature coefficient of outer overpack $E_{rp}$ in $mV_{SHE}/°C$ | -15.2 | Dunn et al. (1999) | DD 2/22/00 |

| Distribution Type | Parameter Name | Description | Parameter Range | Remarks | Provided by |
|---|---|---|---|---|---|
| constant | OuterOverpackErpSlope | Outer overpack $E_{rp}$ slope in $mV_{SHE}$ | -590.7 | Dunn et al. (1999) | DD 2/22/00 |
| constant | TempCoefOfOuterPackErpSlope | Temperature coefficient of outer overpack $E_{rp}$ slope in $mV_{SHE}/°C$ | 4.3 | Dunn et al. (1999) | DD 2/22/00 |
| constant | InnerOverpackErpIntercept | Inner overpack $E_{rp}$ intercept in mVshe | -1.0e4 | Value selected to not grant any protection against corrosion by the inner overpack in the EDA II. CLST meeting 2/15/00. | OPR 2/22/00 |
| constant | TempCoefOfInnerPackErpIntercept | Temperature coefficient of inner overpack $E_{rp}$ intercept in mV/(°C) | 0.0 | Value selected to not grant any protection against corrosion by the inner overpack in the EDA II. CLST meeting 2/15/00. | OPR 2/22/00 |
| constant | InnerOverpackErpSlope | Inner overpack $E_{rp}$ slope in mV | 0.0 | Value selected to not grant any protection against corrosion by the inner overpack in the EDA II. CLST meeting 2/15/00. | OPR 2/22/00 |
| constant | TempCoefOfInnerPackErpSlope | Temperature coefficient of inner overpack $E_{rp}$ slope in mV/(°C) | 0.0 | Value selected to not grant any protection against corrosion by the inner overpack in the EDA II. CLST meeting 2/15/00. | OPR 2/22/00 |
| constant | OuterWPBetaKineticsParameterforOxygen | Transfer coefficient for oxygen reduction reaction ( $\beta O_2$ ) for the WP outer overpack | 0.75 | Assumed based on Calvo and Schriffrin (1988) | ** |

| Distribution Type | Parameter Name | Description | Parameter Range | Remarks | Provided by |
|---|---|---|---|---|---|
| constant | OuterWPBetaKineticsParameterforWater | Transfer coefficient for water reduction reaction ($\beta_{H2O}$) for the WP outer overpack | 0.5 | Assumed based on Bockris and Reddy (1970) | ** |
| constant | InnerWPBetaKineticsParameterforOxygen | Transfer coefficient for oxygen reduction reaction ( $\beta O_2$ ) for the WP inner overpack | 0.75 | Assumed based on Calvo and Schriffrin (1988) | ** |
| constant | InnerWPBetaKineticsParameterforWater | Transfer coefficient for water reduction reaction ($\beta_{H2O}$) for the WP inner overpack | 0.5 | Assumed based on Bockris and Reddy (1970) | ** |
| constant | OuterWPRateConstantforOxygenReduction[coulomb-m/mole/yr] | Rate constant for oxygen reduction for the WP outer overpack (C-m/yr/mol) | 3.0e10 | Assumed based on Bockris and Reddy (1970); Calvo (1979) | GC 2/23/00 |
| constant | OuterWPRateConstantforWaterReduction[coulomb-m/m^2/yr] | Rate constant for water reduction for the WP outer overpack ($C/m^2/yr$) | 3.2 | Assumed based on Turnbull and Gardner (1982) | GC 2/23/00 |
| constant | OuterWPActivationEnergyforOxygenReduction[J/mole] | Activation energy for oxygen reduction for WP outer overpack (J/mol) | 4.0e4 | Assumed based on Calvo (1979) | GC 2/23/00 |
| constant | OuterWPActivationEnergyforWaterReduction[J/mole] | Activation energy for water reduction for WP outer overpack (J/mol) | 25000.0 | Assumed based on Heusler (1976) | ** |

| Distribution Type | Parameter Name | Description | Parameter Range | Remarks | Provided by |
|---|---|---|---|---|---|
| constant | InnerWPRateConstantforOxygenReduction[coulomb-m/mole/yr] | Rate constant for oxygen reduction for WP inner overpack (C-m/yr/mol) | 3.0e10 | Assumed based on Bockris and Reddy (1970); Calvo (1979) | ** |
| constant | InnerWPRateConstantforWaterReduction[coulomb-m/m^2/yr] | Rate constant for water reduction for WP inner overpack ($C/m^2/yr$) | 3.2 | Assumed based on Turnbull and Gardner (1982) | ** |
| constant | InnerWPActivationEnergyforOxygenReduction[J/mole] | Activation energy for oxygen reduction reaction for WP inner overpack (J/mol) | 40000.0 | Assumed based on Calvo (1979) | ** |
| constant | InnerWPActivationEnergyforWaterReduction[J/mole] | Activation energy for water reduction reaction for WP inner overpack (J/mol) | 25000.0 | Assumed based on Heusler (1976) | ** |
| normal | AA_1_1[C/m2/yr] | Passive current density for WP outer overpack ($C/m^2/yr$) | 1.6e3, 1.7e4 | Dunn et al. (1999); Kowaka (1994) | GC 2/23/00 |
| constant | AA_2_1[C/m2/yr] | Passive current density for WP inner overpack ($C/m^2/yr$) | 1e10 | Value selected to not grant any protection against corrosion by the inner overpack in the EDA II. CLST meeting 2/15/00. | OPR 2/23/00 |
| constant | MeasuredGalvanicCouplePotential | Experimentally measured galvanic couple between inner and outer overpack | 0 | Irrelevant data for EDA II | ** |

| Distribution Type | Parameter Name | Description | Parameter Range | Remarks | Provided by |
|---|---|---|---|---|---|
| constant | CoefForLocCorrOfOuterOverpack | Coefficient for localized corrosion rate of outer overpack ($m/yr^n$, n=ExponetForLocCorrOfOuterOverpack) | 2.5e-4 | Assumed in Mohanty et al. (1997). 1997 Sensitivity Analysis indicates low sensitivity. | ** |
| constant | ExponetForLocCorrOfOuterOverpack | Exponent for localized corrosion rate of outer overpack | 1.0 | Assumed constant pit penetration rate | ** |
| constant | CoefForLocCorrOfInnerOverpack | Coefficient for localized corrosion rate of inner overpack ($m/yr^n$, n=ExponetForLocCorrOfInnerOverpack) | 1.0 | Value selected to not grant any protection against corrosion by the inner overpack in the EDA II. CLST meeting 2/15/00. | OPR 2/23/00 |
| constant | ExponentForLocCorrOfInnerOverpack | Exponent for localized corrosion rate of inner overpack | 1.0 | Assumed constant pit penetration rate | OPR 2/23/00 |
| constant | HumidAirCorrosionRate[m/yr] | Humid air corrosion rate (m/yr) | 1e-15 | Assumed | GC 2/23/00 |
| constant | FractionalCouplingStrength | Efficiency factor, varying from 0 to 1, representing galvanic coupling between the outer and inner overpack | 0.0 | Switch: full credit = 1; no credit = 0 | ** |
| constant | FactorForDefiningChoiceOfCritPotential | Factor for defining choice of critical potential (initiation or repassivation) | 0.0 | Mohanty et al. (1997) | ** |

| Distribution Type | Parameter Name | Description | Parameter Range | Remarks | Provided by |
|---|---|---|---|---|---|
| constant | CritChlorideConcForFirstLayer[moL/L] | Critical chloride concentration for localized corrosion of outer overpack (mol/L) | 0.5 | Dunn et al. (1999) | GC 2/23/00 |
| constant | CritChlorideConcForSecondLayer[moL/L] | Critical chloride concentration for localized corrosion of inner overpack (mol/L) | 1e-10 | Value selected to not grant any protection against corrosion by the inner overpack in the EDA II. CLST meeting 2/15/00. | OPR 2/23/00 |
| uniform | ChlorideMultFactor | The chloride concentration in the proximity of the WP is computed as the near field concentration times this chloride factor, after failure of the drip shield. | 1.0, 30.0 | Assumed. Note solubility limit for NaCl = 6 mol/liter. 1997 Sensitivity Analysis indicates high sensitivity. Continue evaluating. | ** |
| constant | ChlorideMultFactorIntactDripShield | Chloride multiplication factor prior to failure of the drip shield | 1.0 | The chloride concentration in the proximity of the WP is computed as the near field concentration times the chloride multiplication factor prior to failure of drip shield | OPR 2/23/00 |
| lognormal | DripShieldFailureTime[yr] | Time of failure of the dripshield (yr) | 3700.0, 27300.0 | CNWRA tests on the passive dissolution rate of Ti Grade 7 suggest passive current densities between $10^{-8}$ and $5\times10^{-7}$ A/cm$^2$. Accurate determination of passive current densities is hindered by the existence of a passive film that grows with | OPR SB 2/23/00 |

| Distribution Type | Parameter Name | Description | Parameter Range | Remarks | Provided by |
|---|---|---|---|---|---|
| | | | | time, decreasing the magnitude of the anodic current density to levels such that the total current density becomes cathodic. Researchers have observed steady-state passive current densities for Ti and Ti alloys ranging from $5\times10^{-8}$ A/cm$^2$ (Kelly, 1982) to $10^{-4}$ A/cm$^2$ (Shibata and Zhu, 1995), depending on the environmental conditions. The range $10^{-8}$ — $5\times10^{-7}$ A/cm$^2$ is in agreement with results by McCright (1998) on immersed coupons of Ti Grades 12 and 16. A corrosion rate range with extreme values $8.7\times10^{-5}$ and $4.3\times10^{-3}$ mm/yr is associated to the chosen range for the passive current density. In computing these corrosion rates it was assumed an alloy density of 4.51 g/cm$^3$, and an equivalent molecular weight of 11.97 g/mol. These corrosion rates do not account for localized corrosion, enhanced dissolution rates in fluoride containing solutions, and hydrogen embrittlement. Further work examining these issues is planned. By assuming | |

| Distribution Type | Parameter Name | Description | Parameter Range | Remarks | Provided by |
|---|---|---|---|---|---|
| | | | | that the probability density function for the corrosion rate reaches 0.1 and 99.9 percent quantile values at $8.7\times10^{-5}$ mm/yr and $4.3\times10^{-3}$ mm/yr, respectively, it can be shown that the failure time for a 20 mm thick drip shield can be approximately described by a log-normal PDF. Its defining parameters are herein listed. See the Scientific Notebook 355, pages 59–64 for further details. | |
| constant | ReferencepH | pH of water (do not change) | 9.0 | Assumed in Mohanty et al. (1997); based on MULTIFLO calculations | ** |
| constant | WPsurfaceScaleThickness[m] | Scale deposit on WP surface | 0.0 | A value of 0.0 implies no scale deposit | ** |
| constant | TortuosityOfScaleonWP | Tortuosity of a porous layer scale deposited on the WP. Thickness does not change with time. | 1.0 | In the case of no deposit, the value is 1.0 | ** |
| constant | PorosityOfScaleonWP | Porosity of the layer deposited on the WP. Porosity does not change with time. | 1.0 | In the case of no deposit, the value is 1.0 | ** |
| constant | YieldStrength[MPa] | Yield strength of outer overpack, MPa | 370 | Alloy 22 manufacturer specifications | GC 2/23/00 |

| Distribution Type | Parameter Name | Description | Parameter Range | Remarks | Provided by |
|---|---|---|---|---|---|
| constant | SafetyFactor | Safety factor for residual stresses | 1.4 | Assumed in Mohanty et al. (1997) | ** |
| constant | FractureToughness[MPa-m**0.5] | Fracture toughness of outer overpack | 1e7 | High value selected to avoid the presence of thermal embrittlement in the computations. The materials in the EDA II are not prone to thermal embrittlement. CLST meeting 2/15/00. | OPR 2/23/00 |
| constant | DensityOuterOverpack[kg/m^3] | Self-explanatory | 8690 | Alloy 22 manufacturer specifications | OPR 2/23/00 |
| constant | DensityInnerOverpack[kg/m^3] | Self-explanatory | 7700 | 316L ss manufacturer specifications | OPR 2/23/00 |
| constant | EquivalentWeightOuterOverpack[kg/mol] | Self-explanatory. See Eq. (6-5) for details. | 0.02597 | In computing the equivalent weight, the following oxidation states for the Alloy 22 components were assumed: Ni–2, Cr–3, Mo–3, W–4, Fe–2, Co–2, Mn–2, V–2. This assumption leads to conservative estimates of corrosion rates. See Eq. (6-5) for details. | OPR 2/23/00 |
| constant | EquivalentWeightInnerOverpack[kg/mol] | Self-explanatory. See Eq. (6-5) for details. | 0.02494 | In computing the equivalent weight, the following oxidation states for the 316L stainless steel components were assumed: Ni–2, Cr–3, Mo–3, Fe–2, Mn–2, Si–2, Cu–2. This assumption | OPR 2/23/00 |

| Distribution Type | Parameter Name | Description | Parameter Range | Remarks | Provided by |
|---|---|---|---|---|---|
| | | | | leads to conservative estimates of corrosion rates. See Eq. (6-5) for details. | |
| constant | DeltaPotentialDueToRadiolysis[V] | Increase in the corrosion potential due to the presence of radiolytic species. See Eq. (6-8) and (6-9). | 0 | The CNWRA staff currently considers that the irradiation levels in the proximity of the WP in EDA II are not sufficiently high to guarantee a continuous supply of oxidizing species, enough to increase the corrosion potential. See section 6.3.7 for further comments on this issue.<br>Sensitivity analyses by Electric Power Research Institute (1998a) using the VA design also suggested that radiolysis does not significantly enhance the corrosion rate. | LY 2/23/00 |
| constant | DecayingConstantRadiolysis[1/yr] | Constant controlling the exponential decay of the *radiolytic potential*. See Eqs. (6-8) and (6-9). | 7e-5 | Dummy value selected to avoid overflow and/or underflow in the computations. | OPR 2/23/00 |
| ** | | | | | |
| ** | | | | | |
| ** ***>>> SEISMO <<<*** | | | | | |
| ** | | | | | |

| Distribution Type | Parameter Name | Description | Parameter Range | Remarks | Provided by |
|---|---|---|---|---|---|
| constant | SeedForRandomNumberForSEISMO | A random number seed for sampling the time and magnitude of seismic events | 505187067.0 | — | ** |
| hazardcurve | SeismicHazardCurveforSEISMO | Minimum peak ground acceleration for bins, return period (yr); number of magnitudes for recurrence of seismic events, magnitude, and recurrence time | 10<br>0.05, 250<br>0.10, 1150<br>0.15, 1800<br>0.20, 3300<br>0.25, 9100<br>0.30, 11000<br>0.35, 14000<br>0.40, 17000<br>0.45, 25000<br>0.50, 40000 | Based on data from probabilistic Hazard Analyses for Fault Displacement and Vibratory Ground motion at Yucca Mountain, Nevada (Civilian Radioactive Waste Management System Management & Operating Contractor, 1998) | SH 10/30/00 |
| constant | WeightPercentageOfRockFallThatHitsWPforSEISMO | Weight percentage of rock fall that hits WP | 1.0 | Not used | ** |
| constant | WeightOfWPforSEISMO[N] | Weight of WP used in impact calculation during free fall (N) | 1.27e05 | Not used | ** |
| constant | WPModulusOfElasticityforSEISMO[Pa] | WP modulus of elasticity (Pa) | 1.76e11 | Estimated based on Ugural and Fenster (1995) | SH 2/23/00 |
| normal | RockModulusOfElasticityforSEISMO[Pa] | Rock modulus of elasticity (Pa) | 2.76e10, 4.14e10 | Brechtel et al. (1995), table 2-4, p. 2-12 | ** |
| constant | WPPoissonRatioforSEISMO[ ] | WP Poisson ratio | 0.2e0 | Popov (1970), p. 36 | ** |

| Distribution Type | Parameter Name | Description | Parameter Range | Remarks | Provided by |
|---|---|---|---|---|---|
| normal | RockPoissonRatioforSEISMO [] | Rock Poisson ratio | 0.15, 0.25 | Brechtel et al. (1995), table 2-4, p. 2-12, supplies the mean value for the parameter. The 25% variation for the assumed normal distribution of this parameter is adopted from table 5.1, p. 5-19, of the Department of Energy Site Characterization Plan (U.S. Department of Energy, 1988) | ** |
| constant | RockFallingDistanceforSEISMO[m] | Rock falling distance gap between the top of WP and the drift crown (m) | 2.0e0 | Estimated based on the diameter of the emplacement drift minus the diameter of the WPs minus the height of the pedestal | ** |
| constant | WPFallingDistanceforSEISMO[m] | WP falling distance for freefall calculations (m) | 0.3e0 | Not currently used in this version of TPA | ** |
| iconstant | WPNumberofSupportPairforSEISMO | Number of support pairs on the WP pedestal | 2 | The conceptual SEISMO module is based on an assumption that WPs can be represented as simply supported beams. Consequently, two support beams are assumed. | ** |
| constant | WPSupportStiffnessforSEISMO[pa*m] | Stiffness of the pedestal | 5.5e09 | Calculated using the following equation:<br>K = A E/L<br>where<br>K is the support stiffness<br>A is the cross-sectional area of the support | ** |

| Distribution Type | Parameter Name | Description | Parameter Range | Remarks | Provided by |
|---|---|---|---|---|---|
| | | | | E is the Young's modulus of the support<br>L is the height of the support<br>No information for the pedestal is available at this time. This data may change when that information is released. | |
| constant | DistributionJointSpacing1forSEISMO | Fractional areal coverage for rock condition 1 | 5.0e-03 | Based on Brechtel et al. (1995), fig. 7-3, p. 7-9, rock conditions 1, 2, and 3 take up only 1.5% of the area in total and are each equally subdivided into 0.5% of the repository | ** |
| constant | DistributionJointSpacing2forSEISMO | Fractional areal coverage for rock condition 2 | 5.0e-03 | Based on Brechtel et al. (1995), fig. 7-3, p. 7-9, rock conditions 1, 2, and 3 take up only 1.5% of the area in total and are each equally subdivided into 0.5% of the repository | ** |
| constant | DistributionJointSpacing3forSEISMO | Fractional areal coverage for rock condition 3 | 5.0e-03 | Based on Brechtel et al. (1995), fig. 7-3, p. 7-9, rock conditions 1, 2, and 3 take up only 1.5% of the area in total and are each equally subdivided into 0.5% of the repository | ** |
| constant | DistributionJointSpacing4forSEISMO | Fractional areal coverage for rock condition 4 | 0.629e0 | Based on Brechtel et al. (1995), fig. 7-3, p. 7-9, about 62.9% of the repository can be | ** |

| Distribution Type | Parameter Name | Description | Parameter Range | Remarks | Provided by |
|---|---|---|---|---|---|
| | | | | characterized as rock condition 4 | |
| constant | DistributionJointSpacing5forSEISMO | Fractional areal coverage for rock condition 5 | 0.356e0 | Based on Brechtel et al. (1995), fig. 7-3, p. 7-9, rock condition 5 occupies about 35.6% of the repository | ** |
| normal | SEISMOJointSpacing1[m] | Joint spacing (JS) for rock condition 1 | 0.466, 0.600 | Not all rocks falling from the roof of the emplacement will impact WPs. The effective size of the rock that impacts WPs will be controlled by JS. For abstraction into the TPA Version 4.0 code, the TSw2 thermomechanical unit was subdivided into five distinct rock conditions. The rock conditions are estimated using available JS (Brechtel et al., 1995) information for the TSw2 provided in Brechtel et al. (1995), which summarizes data collected from North Ramp Geotechnical boreholes. In the report, the JS information is presented in terms of rating of JS (Hoek and Brown, 1982). Three JS ratings are observed in the TSw2 Unit: 5, 8, and 10. JS rating of 5 indicates a JS that is smaller than 0.06 m; JS rating of | ** |

| Distribution Type | Parameter Name | Description | Parameter Range | Remarks | Provided by |
|---|---|---|---|---|---|
| | | | | 8 is for JS between 0.06 m to 0.2 m; and JS rating of 10 represents JS of 0.2 to 0.6 m. For the rock condition scheme used in the SEISMO module, rocks related to JS rating of 10 are further subdivided into three conditions: conditions 1, 2, and 3 respectively. This subdivision is considered reasonable because (i) the range for JS rating of 10 between 0.2 m to 0.6 m is large and (ii) larger JS will induce greater impact failures on WPs. A normal distribution of JS is assumed in each rock condition category because no additional information about the distributions of JSs was compiled when the SEISMO module was coded. Future work will examine the validity of this assumption. | |
| normal | SEISMOJointSpacing2[m] | JS for rock condition 2 | 0.333, 0.466 | Not all rocks falling from the roof of the emplacement will impact WPs. The effective size of the rock that impacts WPs will be controlled by JS. For abstraction into the TPAVersion 4.0 code, the TSw2 | ** |

| Distribution Type | Parameter Name | Description | Parameter Range | Remarks | Provided by |
|---|---|---|---|---|---|
| | | | | thermomechanical unit was subdivided into five distinct rock conditions. The rock conditions are estimated using available JS (Brechtel et al., 1995) information for the TSw2 provided Brechtel et al. (1995), which summarizes data collected from NRG holes. In the report, the JS information is presented in terms of rating of JS (Hoek and Brown, 1982). Three JS ratings are observed in the TSw2 Unit: 5, 8, and 10. JS rating of 5 indicates a JS that is smaller than 0.06 m; JS rating of 8 is for JS between 0.06 to 0.2 m; and JS rating of 10 represents JS of 0.2 to 0.6 m. For the rock condition scheme used in the SEISMO module, rocks related to JS rating of 10 are further subdivided into three conditions: conditions 1, 2, and 3 respectively. This subdivision is considered reasonable because (i) the range for JS rating of 10 between 0.2 m to 0.6 m is large and (ii) larger JS will induce greater impact failures on WPs. A normal distribution of JS is assumed in | |

| Distribution Type | Parameter Name | Description | Parameter Range | Remarks | Provided by |
|---|---|---|---|---|---|
| | | | | each rock condition category because no additional information about the distributions of JSs was compiled when the SEISMO module was coded. Future work will examine the validity of this assumption. | |
| normal | SEISMOJointSpacing3[m] | JS for rock condition 3 | 0.20, 0.333 | Not all rocks falling from the roof of the emplacement will impact WPs. The effective size of the rock that impacts WPs will be controlled by JS. For abstraction into the TPA Version 4.0 code, the TSw2 thermomechanical unit was subdivided into five distinct rock conditions. The rock conditions are estimated using available JS information for the TSw2 provided in Brechtel et al. (1995), which summarizes data collected from NRG holes. In the report, the JS information is presented in terms of rating of JS (Hoek and Brown, 1982). Three JS ratings are observed in the TSw2 Unit: 5, 8, and 10. JS rating of 5 indicates a JS that is smaller than 0.06 m; JS rating of 8 is for JS between 0.06 to 0.2 | ** |

| Distribution Type | Parameter Name | Description | Parameter Range | Remarks | Provided by |
|---|---|---|---|---|---|
| | | | | m; and JS rating of 10 represents JS of 0.2 to 0.6 m. For the rock condition scheme used in the SEISMO module, rocks related to JS rating of 10 are further subdivided into three conditions: conditions 1, 2, and 3 respectively. This subdivision is considered reasonable because (i) the range for JS rating of 10 between 0.2 m to 0.6 m is large and (ii) larger JS will induce greater impact failures on WPs. A normal distribution of JS is assumed in each rock condition category because no additional information about the distributions of JSs was compiled when the SEISMO module was coded. Future work will examine the validity of this assumption. | |
| normal | SEISMOJointSpacing4[m] | JS for rock condition 4 | 0.06, 0.20 | Not all rocks falling from the roof of the emplacement will impact WPs. The effective size of the rock that impacts WPs will be controlled by JS. For abstraction into the TPA Version 4.0 code, the TSw2 thermomechanical unit was | ** |

| Distribution Type | Parameter Name | Description | Parameter Range | Remarks | Provided by |
|---|---|---|---|---|---|
| | | | | subdivided into five distinct rock conditions. The rock conditions are estimated using available JS information for the TSw2 provided in Brechtel et al. (1995), which summarizes data collected from NRG holes. In the report, the JS information is presented in terms of rating of JS (Hoek and Brown, 1982). Three JS ratings are observed in the TSw2 Unit: 5, 8, and 10. JS rating of 5 indicates a JS that is smaller than 0.06 m; JS rating of 8 is for JS between 0.06 to 0.2 m; and JS rating of 10 represents JS of 0.2 to 0.6 m. For the rock condition scheme used in the SEISMO module, condition 4 is assumed to be the rocks with JS rating of 8. A normal distribution of JS is assumed in each rock condition category because no additional information about the distributions of JSs was compiled when the SEISMO module was coded. Future work will examine the validity of this assumption. | |

| Distribution Type | Parameter Name | Description | Parameter Range | Remarks | Provided by |
|---|---|---|---|---|---|
| normal | SEISMOJointSpacing5[m] | JS for rock condition 5 | 0.03, 0.06 | Not all rocks falling from the roof of the emplacement will impact WPs. The effective size of the rock that impacts WPs will be controlled by JS. For abstraction into the TPA Version 4.0 code, the TSw2 thermomechanical unit was subdivided into five distinct rock conditions. The rock conditions are estimated using available JS information for the TSw2 provided in Brechtel et al. (1995), which summarizes data collected from NRG holes. In the report, the JS information is presented in terms of rating of JS (Hoek and Brown, 1982). Three JS ratings are observed in the TSw2 Unit: 5, 8, and 10. JS rating of 5 indicates a JS that is smaller than 0.06 m; JS rating of 8 is for JS between 0.06 to 0.2 m; and JS rating of 10 represents JS of 0.2 to 0.6 m. For the rock condition scheme used in the SEISMO module, condition 5 is assumed to be equivalent to the rock with JS rating of 5. A normal distribution of JS is assumed in each rock condition category | ** |

| Distribution Type | Parameter Name | Description | Parameter Range | Remarks | Provided by |
|---|---|---|---|---|---|
| | | | | because no additional information about the distributions of JSs was compiled when the SEISMO module was coded. Future work will examine the validity of this assumption. | |
| constant | WPUltimateStrength[N/m^2] | Ultimate strength of WP ($N/m^2$) | 6.2e08 | The ultimate strength value of 6.2e08 is measured at 700 °F ASME B&PV Code, Section II, Part D- Properties, Table U.C.,(American Society of Mechanical Engineers, 1998). | SH 2/23/00 |
| constant | GrainDensityforTSw2SEISMO[] | Grain density for Topopah Spring—welded ($g/cm^3$) | 2.55 | Brechtel et al. (1995) table 2-4, p. 2-12. | ** |
| constant | FractionAreaForGroundMotion1 | Fractional rockfall area for ground motion type 1 (i.e., a seismic ground acceleration magnitude of 0.05) listed for the SeismicHazardCurvefor SEISMO parameter | 0.05 | From CNWRA expert elicitation | ** |
| constant | FractionAreaForGroundMotion2 | Same as above except for ground motion type 2 (i.e., seismic ground acceleration magnitude of 0.1) | 0.12 | Same as above | ** |

| Distribution Type | Parameter Name | Description | Parameter Range | Remarks | Provided by |
|---|---|---|---|---|---|
| constant | FractionAreaForGroundMotion3 | Same as above except for ground motion type 3 (i.e., seismic ground acceleration magnitude of 0.15) | 0.17 | Same as above | ** |
| constant | FractionAreaForGroundMotion4 | Same as above except for ground motion type 4 (i.e., seismic ground acceleration magnitude of 0.2) | 0.23 | Same as above | ** |
| constant | FractionAreaForGroundMotion5 | Same as above except for ground motion type 5 (i.e., seismic ground acceleration magnitude of 0.25) | 0.28 | Same as above | ** |
| constant | FractionAreaForGroundMotion6 | Same as above except for ground motion type 6 (i.e., seismic ground acceleration magnitude of 0.3) | 0.34 | Same as above | ** |
| constant | FractionAreaForGroundMotion7 | Same as above except for ground motion type 7 (i.e., seismic ground acceleration magnitude of 0.35) | 0.4 | Same as above | ** |
| constant | FractionAreaForGroundMotion8 | Same as above except for ground motion type 8 (i.e., seismic ground | 0.46 | Same as above | ** |

| Distribution Type | Parameter Name | Description | Parameter Range | Remarks | Provided by |
|---|---|---|---|---|---|
| | | acceleration magnitude of 0.4) | | | |
| constant | FractionAreaForGroundMotion9 | Same as above except for ground motion type 9 (i.e., seismic ground acceleration magnitude of 0.45) | 0.5 | Same as above | ** |
| constant | FractionAreaForGroundMotion10 | Same as above except for ground motion type 10 (i.e., seismic ground acceleration magnitude of 0.5) | 0.54 | Same as above | ** |
| constant | VerticalExtentOfRockFall1_1 [m] | Vertical extent of rock fall for rock condition 1 and ground acceleration 0.05g | 0.0 | Same as above | ** |
| constant | VerticalExtentOfRockFall1_2 [m] | Same as above except ground acceleration 0.10g | 0.0 | Same as above | ** |
| constant | VerticalExtentOfRockFall1_3 [m] | Same as above except ground acceleration 0.15g | 0.0 | Same as above | ** |
| constant | VerticalExtentOfRockFall1_4 [m] | Same as above except ground acceleration 0.20g | 0.0 | Same as above | ** |

| Distribution Type | Parameter Name | Description | Parameter Range | Remarks | Provided by |
|---|---|---|---|---|---|
| constant | VerticalExtentOfRockFall1_5 [m] | Same as above except ground acceleration 0.25g | 0.0 | Same as above | ** |
| constant | VerticalExtentOfRockFall1_6 [m] | Same as above except ground acceleration 0.30g | 0.0 | Same as above | ** |
| constant | VerticalExtentOfRockFall1_7 [m] | Same as above except ground acceleration 0.35g | 0.0 | Same as above | ** |
| constant | VerticalExtentOfRockFall1_8 [m] | Same as above except ground acceleration 0.40g | 0.0 | Same as above | ** |
| constant | VerticalExtentOfRockFall1_9 [m] | Same as above except ground acceleration 0.45g | 0.0 | Same as above | ** |
| constant | VerticalExtentOfRockFall1_10[m] | Same as above except ground acceleration 0.50g | 0.0 | Same as above | ** |
| uniform | VerticalExtentOfRockFall2_1 [m] | Vertical extent of rock fall for rock condition 2 and ground acceleration 0.05g. The lower limit is approximately equivalent to the average rock joint spacing of rock condition 1. The upper limit is estimated from numerical results. | 0.5, 0.6 | Same as above | ** |

| Distribution Type | Parameter Name | Description | Parameter Range | Remarks | Provided by |
|---|---|---|---|---|---|
| uniform | VerticalExtentOfRockFall2_2 [m] | Same as above except ground acceleration 0.10g | 0.5, 1.0 | Same as above | ** |
| uniform | VerticalExtentOfRockFall2_3 [m] | Same as above except ground acceleration 0.15g | 0.5, 1.1 | Same as above | ** |
| uniform | VerticalExtentOfRockFall2_4 [m] | Same as above except ground acceleration 0.20g | 0.5, 1.2 | Same as above | ** |
| uniform | VerticalExtentOfRockFall2_5 [m] | Same as above except ground acceleration 0.25g | 0.5, 1.3 | Same as above | ** |
| uniform | VerticalExtentOfRockFall2_6 [m] | Same as above except ground acceleration 0.30g | 0.5, 1.4 | Same as above | ** |
| uniform | VerticalExtentOfRockFall2_7 [m] | Same as above except ground acceleration 0.35g | 0.5, 1.45 | Same as above | ** |
| uniform | VerticalExtentOfRockFall2_8 [m] | Same as above except ground acceleration 0.40g | 0.5, 1.5 | Same as above | ** |
| uniform | VerticalExtentOfRockFall2_9 [m] | Same as above except ground acceleration 0.45g | 0.5, 1.65 | Same as above | ** |
| uniform | VerticalExtentOfRockFall2_10[m] | Same as above except ground acceleration 0.50g | 0.5, 1.8 | Same as above | ** |

| Distribution Type | Parameter Name | Description | Parameter Range | Remarks | Provided by |
|---|---|---|---|---|---|
| uniform | VerticalExtentOfRockFall3_1 [m] | Vertical extent of rock fall for rock condition 3 and ground acceleration 0.05g | 0.5, 1.0 | Same as above | ** |
| uniform | VerticalExtentOfRockFall3_2 [m] | Same as above except ground acceleration 0.10g | 0.5, 2.0 | Same as above | ** |
| uniform | VerticalExtentOfRockFall3_3 [m] | Same as above except ground acceleration 0.15g | 0.5 2.5 | Same as above | ** |
| uniform | VerticalExtentOfRockFall3_4 [m] | Same as above except ground acceleration 0.20g | 0.5 3.0 | Same as above | ** |
| uniform | VerticalExtentOfRockFall3_5 [m] | Same as above except ground acceleration 0.25g | 0.5 3.5 | Same as above | ** |
| uniform | VerticalExtentOfRockFall3_6 [m] | Same as above except ground acceleration 0.30g | 0.5 4.0 | Same as above | ** |
| uniform | VerticalExtentOfRockFall3_7 [m] | Same as above except ground acceleration 0.35g | 0.5 4.5 | Same as above | ** |
| uniform | VerticalExtentOfRockFall3_8 [m] | Same as above except ground acceleration 0.40g | 0.5 5.0 | Same as above | ** |

| Distribution Type | Parameter Name | Description | Parameter Range | Remarks | Provided by |
|---|---|---|---|---|---|
| uniform | VerticalExtentOfRockFall3_9 [m] | Same as above except ground acceleration 0.45g | 0.5 5.7 | Same as above | ** |
| uniform | VerticalExtentOfRockFall3_10[m] | Same as above except ground acceleration 0.50g | 0.5 6.5 | Same as above | ** |
| uniform | VerticalExtentOfRockFall4_1 [m] | Vertical extent of rock fall for rock condition 4 and ground acceleration 0.05g | 0.5 2.7 | Same as above | ** |
| uniform | VerticalExtentOfRockFall4_2 [m] | Same as above except ground acceleration 0.10g | 0.5 5.5 | Same as above | ** |
| uniform | VerticalExtentOfRockFall4_3 [m] | Same as above except ground acceleration 0.15g | 0.5 6.0 | Same as above | ** |
| uniform | VerticalExtentOfRockFall4_4 [m] | Same as above except ground acceleration 0.20g | 0.5 6.5 | Same as above | ** |
| uniform | VerticalExtentOfRockFall4_5 [m] | Same as above except ground acceleration 0.25g | 0.5 7.0 | Same as above | ** |
| uniform | VerticalExtentOfRockFall4_6 [m] | Same as above except ground acceleration 0.30g | 0.5 7.5 | Same as above | ** |

| Distribution Type | Parameter Name | Description | Parameter Range | Remarks | Provided by |
|---|---|---|---|---|---|
| uniform | VerticalExtentOfRockFall4_7 [m] | Same as above except ground acceleration 0.35g | 0.5 8.0 | Same as above | ** |
| uniform | VerticalExtentOfRockFall4_8 [m] | Same as above except ground acceleration 0.40g | 0.5 8.5 | Same as above | ** |
| uniform | VerticalExtentOfRockFall4_9 [m] | Same as above except ground acceleration 0.45g | 0.5 9.3 | Same as above | ** |
| uniform | VerticalExtentOfRockFall4_10[m] | Same as above except ground acceleration 0.50g | 0.5 10.0 | Same as above | ** |
| uniform | VerticalExtentOfRockFall5_1 [m] | Vertical extent of rock fall for rock condition 5 and ground acceleration 0.05g | 0.5 4.7 | Same as above | ** |
| uniform | VerticalExtentOfRockFall5_2 [m] | Same as above except ground acceleration 0.10g | 0.5 9.33 | Same as above | ** |
| uniform | VerticalExtentOfRockFall5_3 [m] | Same as above except ground acceleration 0.15g | 0.5 9.7 | Same as above | ** |
| uniform | VerticalExtentOfRockFall5_4 [m] | Same as above except ground acceleration 0.20g | 0.5 10.0 | Same as above | ** |

| Distribution Type | Parameter Name | Description | Parameter Range | Remarks | Provided by |
|---|---|---|---|---|---|
| uniform | VerticalExtentOfRockFall5_5 [m] | Same as above except ground acceleration 0.25g | 0.5 10.7 | Same as above | ** |
| uniform | VerticalExtentOfRockFall5_6 [m] | Same as above except ground acceleration 0.30g | 0.5 11.33 | Same as above | ** |
| uniform | VerticalExtentOfRockFall5_7 [m] | Same as above except ground acceleration 0.35g | 0.5 12.0 | Same as above | ** |
| uniform | VerticalExtentOfRockFall5_8 [m] | Same as above except ground acceleration 0.40g | 0.5 12.66 | Same as above | ** |
| uniform | VerticalExtentOfRockFall5_9 [m] | Same as above except ground acceleration 0.45g | 0.5 13.3 | Same as above | ** |
| uniform | VerticalExtentOfRockFall5_10[m] | Same as above except ground acceleration 0.50g | 0.5 14.0 | Same as above | ** |
| constant | WPYieldPoint[] | WP yield point | 0.002 | Estimated from Timoshenko (1956) | ** |
| constant | WPPlasticElongation[] | WP plastic elongation | 0.05 | Estimated from Summers et al. (1998) | SH 2/23/00 |

**
**
**  ***>>> EBSREL <<<***
**

| Distribution Type | Parameter Name | Description | Parameter Range | Remarks | Provided by |
|---|---|---|---|---|---|
| iflag | WaterContactMode_Initial(0=BathTub,1=FlowThrough) | Water contact mode for initial WP failure with iflag = 0 for bathtub and iflag=1 for flowthrough | 0 | Assumed | ** |
| iflag | WaterContactMode_Faulting(0=BathTub,1=FlowThrough) | Water contact mode for WP failure from faulting with iflag = 0 for bathtub and iflag=1 for flowthrough | 1 | Assumed | ** |
| iflag | WaterContactMode_Volcanic (0=BathTub,1=FlowThrough) | Water contact mode for WP failure from igneous activity with iflag = 0 for bathtub and iflag=1 for flowthrough | 1 | Assumed | ** |
| iflag | WaterContactMode_SeismicInterval1(0=BathTub,1=FlowThrough) | Water contact mode for WP failure in seismic interval 1 with iflag = 0 for bathtub and iflag=1 for flowthrough | 0 | Assumed | ** |
| iflag | WaterContactMode_SeismicInterval2(0=BathTub,1=FlowThrough) | Water contact mode for WP failure in seismic interval 2 with iflag = 0 for bathtub and iflag=1 for flowthrough | 0 | Assumed | ** |
| iflag | WaterContactMode_SeismicInterval3(0=BathTub,1=FlowThrough) | Water contact mode for WP failure in seismic interval 3 with iflag = 0 | 0 | Assumed | ** |

| Distribution Type | Parameter Name | Description | Parameter Range | Remarks | Provided by |
|---|---|---|---|---|---|
| | | for bathtub and iflag=1 for flowthrough | | | |
| iflag | WaterContactMode_SeismicInterval4(0=BathTub,1=FlowThrough) | Water contact mode for WP failure in seismic interval 4 with iflag = 0 for bathtub and iflag=1 for flowthrough | 0 | Assumed | ** |
| iflag | WaterContactMode_Corrosion(0=BathTub,1=FlowThrough) | Water contact mode for WP failure from corrosion with iflag = 0 for bathtub and iflag=1 for flowthrough | 0 | Assumed | ** |
| constant | WastePackageFlowMultiplicationFactor | Factor that is multiplied by the flow rate hitting a WP. The resulting flow rates are written to *ebsflo.dat* which is an input file to the *releaset.f* stand-alone code. | 1.0 | Assumed | ** |
| uniform | SubAreaWetFraction | Subarea wet fraction | 0.0, 1.0 | See appendix F | ** |
| constant | InitialFailureTime[yr] | Failure time for initially defective WPs | 0.0 | ** | ** |
| uniform | DefectiveFractionOfWPs/cell | Fraction of total WPs in an SA that fails at time specified for InitialFailureTimeyr | 1.0e-4, 1.0e-2 | No available literature evaluating this problem. The reported range has been estimated based on analogous | OPR 2/25/00 |

| Distribution Type | Parameter Name | Description | Parameter Range | Remarks | Provided by |
|---|---|---|---|---|---|
| | | | | data found in (Electric Power Reseach Institute, 1998a; Nuclear Regulatory Commission, 1973; Nuclear Regulatory Commission, 1979; NRC, 1984; Nuclear Regulatory Commission, 1988b; SKi, 1996; Timmins, 1998, and Tschoepe et al., 1994). | |
| iconstant | NumberOfSEISMOWPFailureIntervals | Number of intervals used for evaluating release from WPs failed due to seismically induced rockfall (4 intervals selected as a reasonable compromise between efficiency and impact of variation over the time of WP failures) | 4 | Nuclear Regulatory Commission (NRC)/CNWRA best estimate | ** |
| constant | BeginningOfSEISMOWPFailureInterval1[yr] | First interval (0–2,000 yr) selected to capture WP failures at the hottest temperatures (note: failure time is 1,000 yr) | 0.0 | NRC/CNWRA best estimate | ** |
| constant | BeginningOfSEISMOWPFailureInterval2[yr] | Second interval (2,000–5,000 yr) selected to capture WP failures at the intermediate | 2000.0 | NRC/CNWRA best estimate | ** |

| Distribution Type | Parameter Name | Description | Parameter Range | Remarks | Provided by |
|---|---|---|---|---|---|
| | | temperatures (note: failure time is 3,500 yr) | | | |
| constant | BeginningOfSEISMOWPFailureInterval3[yr] | Third interval (5,000–10,000 yr) selected to capture WP failures through the cool down phase (note: failure time is 7,500 yr) | 5000.0 | NRC/CNWRA best estimate | ** |
| constant | BeginningOfSEISMOWPFailureInterval4[yr] | Last interval (10,000 until the minimum of the end of the simulation and the corrosion failure time) selected to capture WP failure of long-lived containers (note: failure time is the mean of the 10,000 yr and the minimum of the simulation period and corrosion failure time) | 10000.0 | NRC/CNWRA best estimate | ** |
| constant | WPInternalVolume[m3] | Internal WP volume where water can reside ($m^3$) | 4.83 | Assumed in Mohanty et al. (1996). These data may be updated when EDA II details are available | ** |
| constant | FlowOnsetTemperature[C] | Flow onset temperature | 999 | Deliberately set at a large value to allow flow into the WP, starting at time 0.0 if water is available | ** |

| Distribution Type | Parameter Name | Description | Parameter Range | Remarks | Provided by |
|---|---|---|---|---|---|
| constant | SFDensity[kg/m3] | Spent fuel density ($kg/m^3$) | 10600 | Wilson (1990a); based on $UO_2$ | ** |
| iconstant | SurfaceAreaModel | Selection of model for computing surface area of SF (options 1 and 2) | 1 | Mohanty et al. (1997). 1997 Sensitivity Analysis indicates high sensitivity. Continue evaluating. | ** |
| iconstant | IModel | Selection of model for computing SF dissolution (1=absence of Ca and Si, 2=presence of Ca and Si, 3=user specified, 4=schoepite equilibrium). | 2 | Mohanty et. al. (1997). 1997 Sensitivity Analysis indicates high sensitivity. Continue evaluating. | ** |
| constant | OxygenPartialPressure[atm] | Oxygen partial pressure (over pressure) (atm) | 0.21 | Assumed in Mohanty et al. (1996). 1997 Sensitivity Analysis indicates high sensitivity. Continue evaluating. Based on atmospheric composition. Stockman (1997). | ** |
| constant | NegativeLog10CarbonateConcentration[mol/L] | Negative $\log_{10}$ of carbonate concentration in surrounding water (mol/L) | 3.71 | Revised value that accounts for re-interpretation of literature data. Previous MULTIFLO runs based on only $[CO_3^{-2}]$; new MULTIFLO runs based on the total carbonate concentration. | ** |
| constant | UserLeachRate[kg/yr/m2] | User-provided leaching rate ($kg/yr/m^2$) used if IModel = 3 | 2.5e-6 | Based on a value for the oxidation rate at the Peña Blanca natural analog (Murphy et al., 1997) scaled to the mass | ** |

| Distribution Type | Parameter Name | Description | Parameter Range | Remarks | Provided by |
|---|---|---|---|---|---|
| | | | | of uranium in the repository, basecase surface area per container, and number of containers in the repository | |
| loguniform | Preexponential_SFDissolution Model2 | Pre-exponential factor for spent fuel dissolution rate from (mg $m^{-2}$ $d^{-1}$) | 1.2e3, 1.2e6 | At room temperature the SF dissolution rate ranges from 0.01 to 10 mg $m^{-2}$ $d^{-1}$ (Bruno et al., 1995; Gray et al., 1994; Gray and Thomas, 1992; Shoesmith et al., 1989; Steward and Weed, 1994; Gray et al., 1993; García-Serrano et al., 1996). Three other studies report lower dissolution rates: Sunder et al. (1997, $10^{-6}$ mg $m^{-2}$ $d^{-1}$ ), Casas et al. (1993, $2.7\times10^{-4}$ mg $m^{-2}$ $d^{-1}$), and Thomas and Till (1984, $8\times10^{-7}$ mg $m^{-2}$ $d^{-1}$). As a conservative approach, the lower bound for the SF dissolution rate is considered to be 0.01 mg $m^{-2}$ $d^{-1}$, and the upper bound, 10 mg $m^{-2}$ $d^{-1}$. Further studies supporting this selected range are listed in Cunnane (1999); Finn et al. (1998); Forsyth (1997); Forsyth et al. (1986); Stroes-Gascoyne et al. (1985, 1997); Tait and Luth, (1997); Wilson | TA OPR 2/23/00 |

| Distribution Type | Parameter Name | Description | Parameter Range | Remarks | Provided by |
|---|---|---|---|---|---|
| | | | | (1990a, b), (1990b). The PDF for the SF dissolution rate at any given temperature is uncertain and further analysis is needed to define it. A loguniform PDF is the current staff best estimate. The equation that uses the pre-exponential factor assumes a constant activation energy. Reported values in the literature are 41 kJ/mol (de Pablo et al., 1997), 20 – 30 kJ/mol (Gray and Steward, 1992; Thomas and Till, 1984; Johnson and Joling, 1982), 32.2 and 36.6 kJ/mol (Steward and Weed, 1994), 41 kJ/mol (Gray and Wilson, 1995). Shoesmith et al. (1998) reports an activation energy of 47 kJ/mol for carbonate containing solutions, and a range of 29 – 34 kJ/mol when carbonate is not present. In the TPA code, the activation energy is defined equal to 29 kJ/mol, which is consistent with the values reported by the above authors. | |
| constant | RD_Invert_Cm | Retardation factor of Cm in invert | 6.00e3 | Bradbury and Sarott (1995) | ** |

| Distribution Type | Parameter Name | Description | Parameter Range | Remarks | Provided by |
|---|---|---|---|---|---|
| constant | RD_Invert_Pu | Retardation factor of Pu in invert | 3.00e3 | Campbell and Krupka (1997) | ** |
| constant | RD_Invert_U | Retardation factor of U in invert | 6.01e2 | Same as above | ** |
| constant | RD_Invert_Am | Retardation factor of Am in invert | 3.00e3 | Same as above | ** |
| constant | RD_Invert_Np | Retardation factor of Np in invert | 1.20e3 | Same as above | ** |
| constant | RD_Invert_Th | Retardation factor of Th in invert | 3.00e3 | Same as above | ** |
| constant | RD_Invert_Ra | Retardation factor of Ra in invert | 6.01e2 | Same as above | ** |
| constant | RD_Invert_Pb | Retardation factor of Pb in invert | 3.01e2 | Bradbury and Sarott (1995) | ** |
| constant | RD_Invert_Cs | Retardation factor of Cs in invert | 1.21e2 | Same as above | ** |
| constant | RD_Invert_I | Retardation factor of I in invert | 7.00e0 | Campbell and Krupka (1997) | ** |
| constant | RD_Invert_Tc | Retardation factor of Tc in invert | 1.0 | Same as above | ** |
| constant | RD_Invert_Ni | Retardation factor of Ni in invert | 6.10e1 | Same as above | ** |
| constant | RD_Invert_Cl | Retardation factor of Cl in invert | 1.0 | Same as above | ** |

| Distribution Type | Parameter Name | Description | Parameter Range | Remarks | Provided by |
|---|---|---|---|---|---|
| constant | RD_Invert_C | Retardation factor of C in invert | 6.10e1 | Same as above | ** |
| constant | RD_Invert_Se | Retardation factor of Se in invert | 1.0 | Bradbury and Sarott (1995) | ** |
| constant | RD_Invert_Nb | Retardation factor of Nb in invert | 6.01e2 | Campbell and Krupka (1997) | ** |
| constant | GapFractionForCM246 | Cm-246/kg of SF in grain and pellet cladding gap | 0.0 | Value assumed due to lack of information | ** |
| constant | GapFractionForU238 | U-238/kg of SF in grain and pellet cladding gap | 0.0 | Value assumed due to lack of information | ** |
| constant | GapFractionForCM245 | Cm-245/kg of SF in grain and pellet cladding gap | 0.0 | Value assumed due to lack of information | ** |
| constant | GapFractionForAM241 | Am241/kg of SF in grain and pellet cladding gap | 0.0 | Value assumed due to lack of information | ** |
| constant | GapFractionForNP237 | Np-237/kg of SF in grain and pellet cladding gap | 0.0 | Value assumed due to lack of information | ** |
| constant | GapFractionForAM243 | Am243/kg of SF in grain and pellet cladding gap | 0.0 | Value assumed due to lack of information | ** |
| constant | GapFractionForPU239 | Pu-239/kg of SF in grain and pellet cladding gap | 0.0 | Value assumed due to lack of information | ** |

| Distribution Type | Parameter Name | Description | Parameter Range | Remarks | Provided by |
|---|---|---|---|---|---|
| constant | GapFractionForPU240 | Pu-240/kg of SF in grain and pellet cladding gap | 0.0 | Value assumed due to lack of information | ** |
| constant | GapFractionForU234 | U-234/kg of SF in grain and pellet cladding gap | 0.0 | Value assumed due to lack of information | ** |
| constant | GapFractionForTH230 | Th-230/kg of SF in grain and pellet cladding gap | 0.0 | Value assumed due to lack of information | ** |
| constant | GapFractionForRA226 | Ra-226/kg of SF in grain and pellet cladding gap | 0.0 | Value assumed due to lack of information | ** |
| constant | GapFractionForPB210 | Pb-210/kg of SF in grain and pellet cladding gap | 0.0 | Value assumed due to lack of information | ** |
| constant | GapFractionForCS135 | Cs-135/kg of SF in grain and pellet cladding gap | 0.06 | Best estimate (Johnson and Tait, 1997) | ** |
| constant | GapFractionForI129 | I-129/kg of SF in grain and pellet cladding gap | 0.06 | Best estimate (Johnson and Tait, 1997) | ** |
| constant | GapFractionForTC99 | Tc-99/kg of SF in grain and pellet cladding gap | 0.01 | Best estimate (Johnson and Tait, 1997) | ** |
| constant | GapFractionForNI59 | Ni-59/kg of SF in grain and pellet cladding gap | 0.0 | Value assumed due to lack of information | ** |
| constant | GapFractionForCL36 | Cl-36/kg of SF in grain and pellet cladding gap | 0.12 | Best estimate (Johnson and Tait, 1997) | ** |
| constant | GapFractionForC14 | C-14/kg of SF in grain and pellet cladding gap | 0.1 | Best estimate (Johnson and Tait, 1997) | ** |
| constant | GapFractionForSE79 | Se-79/kg of SF in grain and pellet cladding gap | 0.06 | Best estimate (Johnson and Tait, 1997) | ** |

| Distribution Type | Parameter Name | Description | Parameter Range | Remarks | Provided by |
|---|---|---|---|---|---|
| constant | GapFractionForNB94 | Nb-94/kg of SF in grain and pellet cladding gap | 0.0 | Value assumed due to lack of information | ** |
| normal | InitialRadiusOfSFParticle[m] | Initial radius of $UO_2$ particle (m) | 7.0e-4, 3.0e-3 | Guenther et al. (1991), Belle (1961). 1997 Sensitivity Analysis indicates high sensitivity. Continue evaluating. | ** |
| constant | RadiusOfSFGrain[m] | Radius of $UO_2$ grain (m) | 1.25e-5 | Einziger et al. (1992), Belle (1961). 1997 Sensitivity Analysis indicates low sensitivity. | ** |
| constant | CladdingCorrectionFactor | Cladding correction factor | 1.0 | Assumes no cladding protection | ** |
| normal | SubGrainFragmentRadiusAfterTransFrac[m] | Subgrain fragment radius of $UO_2$ particle after transgranular fracture (m); used only if fuel conversion takes place from $UO_2$ to $UO_{2.4}$ and $U_3O_8$; used only by the SF dissolution models that are dependent on exposed surface area. | 5.0e-7, 2.0e-6 | Mohanty et al. (1997). Distribution based on distribution of grains or particles. 1997 Sensitivity Analysis indicates high sensitivity. Continue evaluating. | ** |
| constant | ThicknessOfCladding[m] | Thickness of cladding (m) | 6.1e-4 | Smith & Baldwin (1989) | ** |
| constant | SFC-14InventoryPerKgSF[ci] | C-14 inventory in SF per kg of SF (Ci) | 7.2e-4 | Not used. Assumed in Mohanty et al. (1996). | ** |

| Distribution Type | Parameter Name | Description | Parameter Range | Remarks | Provided by |
|---|---|---|---|---|---|
| constant | CladC-14InventoryPerKgSF[ci] | C-14 inventory in cladding material per kg of SF (Ci) | 4.89e-4 | Not used. Park (1992). | ** |
| constant | ZyrOxideAndCrudC-14InvPerKgSF[ci] | C-14 inventory in Zirconium Oxide and crud per kg of SF (Ci) | 2.48e-5 | Not used. Park (1992). | ** |
| constant | GapAndGrainBoundaryInventoryPerKgSF[ci] | C-14 inventory in the gap and grain boundary per kg of SF (Ci) | 6.2e-6 | Not used. Park (1992). | ** |
| uniform | SolubilityAm[kg/m3] | Solubility limit for Am | 2.4e-8, 2.4e-4 | TRW Environmental Safety Systems, Inc. (1995), table 6.3-1, based on expert elicitation described in Gauthier (1993), and Nitsche et al. (1993). 1997 Sensitivity Analysis indicates high sensitivity. Continue evaluating. | ** |
| constant | Solubility_I[kg/m3] | Solubility limit for I | 1.29e2 | TRW Environmental Safety Systems, Inc. (1995), p. 6-7. Based on the assumption that there is no solubility controlling phase for iodine. Conservatively assume 1.0 mol/L. | ** |
| constant | SolubilityTc[kg/m3] | Solubility limit for Tc | 9.93e1 | Based on CNWRA assumption that there is no solubility controlling phase for technetium. Conservatively assume 1.0 mol/L. | ** |

| Distribution Type | Parameter Name | Description | Parameter Range | Remarks | Provided by |
|---|---|---|---|---|---|
| constant | SolubilityCl[kg/m3] | Solubility limit for Cl | 3.6e1 | TRW Environmental Safety Systems, Inc. (1995), p. 6-7. Based on assumption that there is no solubility controlling phase for iodine. Conservatively assume 1.0 mol/L. | ** |
| constant | Solubility_C[kg/m3] | Solubility limit for C | 1.4e1 | TRW Environmental Safety Systems, Inc. (1995), p. 6-7. Based on assumption that there is no solubility controlling phase for carbon (Gauthier, 1993). Conservatively assume 1.0 mol/L. | ** |
| constant | Solubility_U[kg/m3] | Solubility limit for U | 7.6e-3 | TRW Environmental Safety Systems, Inc. (1995), table 6.3-1, based on expert elicitation described in Gauthier (1993), and Wanner and Forest (1992). 1997 Sensitivity Analysis indicates low sensitivity. The apex of the logtriangular distribution (2.4e-6 to 2.4e0) used in the sensitivity studies was chosen. | ** |
| constant | SolubilityCm[kg/m3] | Solubility limit for Cm | 2.4e-4 | TRW Environmental Safety Systems, Inc. (1995), table 6.3-1, based on expert elicitation described in Gauthier (1993). Assumed that curium behaves similarly to $Am^{3+}$ (see Fuger, | ** |

| Distribution Type | Parameter Name | Description | Parameter Range | Remarks | Provided by |
|---|---|---|---|---|---|
| | | | | 1992). 1997 Sensitivity Analysis indicates low sensitivity. The maximum value of the uniform distribution (2.4e-8 to 2.4e-4) used in the sensitivity studies was chosen. | |
| uniform | SolubilityPu[kg/m3] | Solubility limit for Pu | 2.4e-6, 2.4e-4 | TRW Environmental Safety Systems, Inc. (1995), table 6.3-1, based on expert elicitation described in Gauthier (1993), Nitsche et al. (1993), and Dyer (1993). 1997 Sensitivity Analysis indicates high sensitivity. Continue evaluating. | ** |
| constant | SolubilityTh[kg/m3] | Solubility limit for Th | 2.3e-4 | Based on solubility data in carbonate containing systems [Östhols et al. (1994), table 3 and fig. 6; Rai et al. (1995), figures 1 & 3 and appendix]. 1997 Sensitivity Analysis indicates low sensitivity. The mean value of the loguniform distribution (2.3e-7 to 2.3e-1) used in the sensitivity studies was chosen. | ** |
| constant | SolubilityRa[kg/m3] | Solubility limit for Ra | 2.3e-5 | TRW Environmental Safety Systems, Inc. (1995), table 6.3-1, based on expert elicitation described in Gauthier (1993), and Kerrisk (1984). 1997 | ** |

| Distribution Type | Parameter Name | Description | Parameter Range | Remarks | Provided by |
|---|---|---|---|---|---|
| | | | | Sensitivity Analysis indicates low sensitivity. The apex of the distribution of the logtriangular distribution (2.3e-7 to 2.3e-3) used in the sensitivity studies was chosen. | |
| constant | SolubilityPb[kg/m3] | Solubility limit for Pb | 6.6e-5 | TRW Environmental Safety Systems, Inc. (1995), table 6.3-1, based on expert elicitation described in Gauthier (1993), Andersson (1988), and Pei-Lin et al. (1985). 1997 Sensitivity Analysis indicates low sensitivity. The apex of the logtriangular distribution (2.1e-6 to 2.1e-3) used in the sensitivity studies was chosen. | ** |
| constant | SolubilityCs[kg/m3] | Solubility limit for Cs | 1.35e2 | Based on CNWRA assumption that there is no solubility controlling phase for cesium. Conservatively assume 1.0 mol/L. | ** |
| constant | SolubilityNi[kg/m3] | Solubility limit for Ni | 1.1e-1 | TRW Environmental Safety Systems, Inc. (1995), table 6.3-1, based on expert elicitation described in Gauthier (1993), Andersson (1988), and Siegel et al. (1993). 1997 Sensitivity Analysis indicates low sensitivity. The apex of the | ** |

| Distribution Type | Parameter Name | Description | Parameter Range | Remarks | Provided by |
|---|---|---|---|---|---|
| | | | | logtriangular distribution (5.9e-5 to 5.9e0) used in the sensitivity studies was chosen. | |
| constant | SolubilitySe[kg/m3] | Solubility limit for Se | 7.9e1 | Based on CNWRA assumption that release of selenium is controlled by waste form dissolution. High value of 1.0 mol/L is used. | ** |
| constant | SolubilityNb[kg/m3] | Solubility limit for Nb | 9.3e-7 | TRW Environmental Safety Systems, Inc. (1995), table 6.3-1, based on expert elicitation described in Gauthier (1993) and Andersson (1988). 1997 Sensitivity Analysis indicates low sensitivity. The mean value of the loguniform distribution (9.3e-8 to 9.3e-6) used in the sensitivity studies was chosen. | ** |
| uniform | SFWettedFraction_Initial_1 | SF wet fraction for initial failures in subarea 1 | 0.0, 1.0 | NRC/CNWRA best estimate | ** |
| uniform | SFWettedFraction_Initial_2 | SF wet fraction for initial failures in subarea 2 | 0.0, 1.0 | Same as above | ** |
| uniform | SFWettedFraction_Initial_3 | SF wet fraction for initial failures in subarea 3 | 0.0, 1.0 | Same as above | ** |

| Distribution Type | Parameter Name | Description | Parameter Range | Remarks | Provided by |
|---|---|---|---|---|---|
| uniform | SFWettedFraction_Initial_4 | SF wet fraction for initial failures in subarea 4 | 0.0, 1.0 | Same as above | ** |
| uniform | SFWettedFraction_Initial_5 | SF wet fraction for initial failures in subarea 5 | 0.0, 1.0 | Same as above | ** |
| uniform | SFWettedFraction_Initial_6 | SF wet fraction for initial failures in subarea 6 | 0.0, 1.0 | Same as above | ** |
| uniform | SFWettedFraction_Initial_7 | SF wet fraction for initial failures in subarea 7 | 0.0, 1.0 | Same as above | ** |
| uniform | SFWettedFraction_Initial_8 | SF wet fraction for initial failures in subarea 8 | 0.0, 1.0 | Same as above | ** |
| uniform | SFWettedFraction_FAULTO | SF wet fraction for faulting failures | 0.0, 1.0 | Same as above | ** |
| uniform | SFWettedFraction_VOLCANO | SF wet fraction for volcanic failures | 0.0, 1.0 | Same as above | ** |
| uniform | SFWettedFraction_SEISMO1_1 | SF wet fraction for seismic failures - seismic interval 1 and subarea 1 | 0.0, 1.0 | Same as above | ** |
| uniform | SFWettedFraction_SEISMO1_2 | SF wet fraction for seismic failures - seismic interval 1 and subarea 2 | 0.0, 1.0 | Same as above | ** |

| Distribution Type | Parameter Name | Description | Parameter Range | Remarks | Provided by |
|---|---|---|---|---|---|
| uniform | SFWettedFraction_SEISMO1_3 | SF wet fraction for seismic failures - seismic interval 1 and subarea 3 | 0.0, 1.0 | Same as above | ** |
| uniform | SFWettedFraction_SEISMO1_4 | SF wet fraction for seismic failures - seismic interval 1 and subarea 4 | 0.0, 1.0 | Same as above | ** |
| uniform | SFWettedFraction_SEISMO1_5 | SF wet fraction for seismic failures - seismic interval 1 and subarea 5 | 0.0, 1.0 | Same as above | ** |
| uniform | SFWettedFraction_SEISMO1_6 | SF wet fraction for seismic failures - seismic interval 1 and subarea 6 | 0.0, 1.0 | Same as above | ** |
| | | | | | |
| uniform | SFWettedFraction_SEISMO1_8 | SF wet fraction for seismic failures - seismic interval 1 and subarea 8 | 0.0, 1.0 | Same as above | ** |
| uniform | SFWettedFraction_SEISMO2_1 | SF wet fraction for seismic failures - seismic interval 2 and subarea 1 | 0.0, 1.0 | Same as above | ** |
| uniform | SFWettedFraction_SEISMO2_2 | SF wet fraction for seismic failures - | 0.0, 1.0 | Same as above | ** |

| Distribution Type | Parameter Name | Description | Parameter Range | Remarks | Provided by |
|---|---|---|---|---|---|
| | | seismic interval 2 and subarea 2 | | | |
| uniform | SFWettedFraction_SEISMO2_3 | SF wet fraction for seismic failures - seismic interval 2 and subarea 3 | 0.0, 1.0 | Same as above | ** |
| uniform | SFWettedFraction_SEISMO2_4 | SF wet fraction for seismic failures - seismic interval 2 and subarea 4 | 0.0, 1.0 | Same as above | ** |
| uniform | SFWettedFraction_SEISMO2_5 | SF wet fraction for seismic failures - seismic interval 2 and subarea 5 | 0.0, 1.0 | Same as above | ** |
| uniform | SFWettedFraction_SEISMO2_6 | SF wet fraction for seismic failures - seismic interval 2 and subarea 6 | 0.0, 1.0 | Same as above | ** |
| uniform | SFWettedFraction_SEISMO2_7 | SF wet fraction for seismic failures - seismic interval 2 and subarea 7 | 0.0, 1.0 | Same as above | ** |
| uniform | SFWettedFraction_SEISMO2_8 | SF wet fraction for seismic failures - seismic interval 2 and subarea 8 | 0.0, 1.0 | Same as above | ** |

| Distribution Type | Parameter Name | Description | Parameter Range | Remarks | Provided by |
|---|---|---|---|---|---|
| uniform | SFWettedFraction_SEISMO3_1 | SF wet fraction for seismic failures - seismic interval 3 and subarea 1 | 0.0, 1.0 | Same as above | ** |
| uniform | SFWettedFraction_SEISMO3_2 | SF wet fraction for seismic failures - seismic interval 3 and subarea 2 | 0.0, 1.0 | Same as above | ** |
| uniform | SFWettedFraction_SEISMO3_3 | SF wet fraction for seismic failures - seismic interval 3 and subarea 3 | 0.0, 1.0 | Same as above | ** |
| uniform | SFWettedFraction_SEISMO3_4 | SF wet fraction for seismic failures - seismic interval 3 and subarea 4 | 0.0, 1.0 | Same as above | ** |
| uniform | SFWettedFraction_SEISMO3_5 | SF wet fraction for seismic failures - seismic interval 3 and subarea 5 | 0.0, 1.0 | Same as above | ** |
| uniform | SFWettedFraction_SEISMO3_6 | SF wet fraction for seismic failures - seismic interval 3 and subarea 6 | 0.0, 1.0 | Same as above | ** |
| uniform | SFWettedFraction_SEISMO3_7 | SF wet fraction for seismic failures - seismic interval 3 and subarea 7 | 0.0, 1.0 | Same as above | ** |

| Distribution Type | Parameter Name | Description | Parameter Range | Remarks | Provided by |
|---|---|---|---|---|---|
| uniform | SFWettedFraction_SEISMO3_8 | SF wet fraction for seismic failures - seismic interval 3 and subarea 8 | 0.0, 1.0 | Same as above | ** |
| uniform | SFWettedFraction_SEISMO4_1 | SF wet fraction for seismic failures - seismic interval 4 and subarea 1 | 0.0, 1.0 | Same as above | ** |
| uniform | SFWettedFraction_SEISMO4_2 | SF wet fraction for seismic failures - seismic interval 4 and subarea 2 | 0.0, 1.0 | Same as above | ** |
| uniform | SFWettedFraction_SEISMO4_3 | SF wet fraction for seismic failures - seismic interval 4 and subarea 3 | 0.0, 1.0 | Same as above | ** |
| uniform | SFWettedFraction_SEISMO4_4 | SF wet fraction for seismic failures - seismic interval 4 and subarea 4 | 0.0, 1.0 | Same as above | ** |
| uniform | SFWettedFraction_SEISMO4_5 | SF wet fraction for seismic failures - seismic interval 4 and subarea 5 | 0.0, 1.0 | Same as above | ** |
| uniform | SFWettedFraction_SEISMO4_6 | SF wet fraction for seismic failures - seismic interval 4 and subarea 6 | 0.0, 1.0 | Same as above | ** |

| Distribution Type | Parameter Name | Description | Parameter Range | Remarks | Provided by |
|---|---|---|---|---|---|
| uniform | SFWettedFraction_SEISMO4_7 | SF wet fraction for seismic failures - seismic interval 4 and subarea 7 | 0.0, 1.0 | Same as above | ** |
| uniform | SFWettedFraction_SEISMO4_8 | SF wet fraction for seismic failures - seismic interval 4 and subarea 8 | 0.0, 1.0 | Same as above | ** |
| uniform | SFWettedFraction_Corrosion_1 | SF wet fraction for corrosion failures in subarea 1 | 0.0, 1.0 | Same as above | ** |
| uniform | SFWettedFraction_Corrosion_2 | SF wet fraction for corrosion failures in subarea 2 | 0.0, 1.0 | Same as above | ** |
| uniform | SFWettedFraction_Corrosion_3 | SF wet fraction for corrosion failures in subarea 3 | 0.0, 1.0 | Same as above | ** |
| uniform | SFWettedFraction_Corrosion_4 | SF wet fraction for corrosion failures in subarea 4 | 0.0, 1.0 | Same as above | ** |
| uniform | SFWettedFraction_Corrosion_5 | SF wet fraction for corrosion failures in subarea 5 | 0.0, 1.0 | Same as above | ** |
| uniform | SFWettedFraction_Corrosion_6 | SF wet fraction for corrosion failures in subarea 6 | 0.0, 1.0 | Same as above | ** |

| Distribution Type | Parameter Name | Description | Parameter Range | Remarks | Provided by |
|---|---|---|---|---|---|
| uniform | SFWettedFraction_Corrosion_7 | SF wet fraction for corrosion failures in subarea 7 | 0.0, 1.0 | Same as above | ** |
| uniform | SFWettedFraction_Corrosion_8 | SF wet fraction for corrosion failures in subarea 8 | 0.0, 1.0 | Same as above | ** |
| iflag | InvertBypass(0=ebsfilt,1=bypass-ebsfilt) | Flag for selecting to perform calculations for transport through the invert. A value of 1 indicates that the transport through invert is skipped. | 0 | — | ** |
| constant | InvertRockPorosity | Porosity of the invert | 0.30 | Green et al. (1995) | ** |
| constant | InvertThickness[m] | Invert thickness (m) | 0.75 | Snell (1997) | ** |
| constant | InvertDiffusionCoefficient[m^2/yr] | Diffusion coefficient for the invert ($m^2/yr$) | 4.4e-5 | Clifton et al. (1991) | ** |
| lognormal | InvertMatrixPermeability[m^2] | Matrix permeability of the invert ($m^2$) | 2.0e-18, 2.0e-16 | Green et al. (1995) | ** |
| ** ** ** ***>>> UZFT <<<*** ** | | | | | |
| constant | UnsaturatedZoneMinimumVelocityChangeFactor[Fraction] | Same velocity is used unless the velocity | 0.4 | Same as in base case. Current best estimate by the USFIC | RWF 2/25/00 |

| Distribution Type | Parameter Name | Description | Parameter Range | Remarks | Provided by |
|---|---|---|---|---|---|
| | | changes by this fraction of the initial velocity. However, the minimum time span over which velocity does not change is 500 yr. | | team. | |
| constant | MatrixLongitudinalDispersivity[FractionOfLayer] | Maximum matrix longitudinal dispersivity specified as a fraction of layer thickness | 0.1 | Same as in base case. Current best estimate by the USFIC team. | RWF 2/25/00 |
| constant | FractureLongitudinalDispersivity[FractionOfLayer] | Maximum fracture longitudinal dispersivity specified as a fraction of layer thickness | 0.1 | Same as in base case. Current best estimate by the USFIC team. | RWF 2/25/00 |
| lognormal | MatrixKD_TSw_Am[m3/kg] | Matrix $K_d$ of Am for Topopah Spring—welded [$m^3$/kg] (UZ) | 4.2e+00, 3.8e+06 | CNWRA best estimate. Calculated using surface complexation models and site specific geochemistry. | DRT 2/25/00 |
| lognormal | MatrixKD_CHnvAm[m3/kg] | Matrix $K_d$ of Am for Calico Hills—nonwelded vitric [$m^3$/kg] (UZ) | 1.3e+01, 1.2e+07 | Same as above | ** |
| lognormal | MatrixKD_CHnzAm[m3/kg] | Matrix $K_d$ of Am for Calico Hills—nonwelded zeolitic [$m^3$/kg] (UZ) | 1.2e+01, 1.1e+07 | Same as above | ** |

| Distribution Type | Parameter Name | Description | Parameter Range | Remarks | Provided by |
|---|---|---|---|---|---|
| lognormal | MatrixKD_PPw_Am[m3/kg] | Matrix $K_d$ of Am for Prow Pass—welded [$m^3$/kg] (UZ) | 9.5e+00, 8.7e+06 | Same as above | ** |
| lognormal | MatrixKD_UCF_Am[m3/kg] | Matrix $K_d$ of Am for Upper Crater Flat [$m^3$/kg] (UZ) | 1.0e+01, 9.1e+06 | Same as above | ** |
| lognormal | MatrixKD_BFw_Am[m3/kg] | Matrix $K_d$ of Am for Bullfrog—welded [$m^3$/kg] (UZ) | 4.1e+00, 3.7e+06 | Same as above | ** |
| lognormal | MatrixKD_UFZ_Am[m3/kg] | Matrix $K_d$ of Am for Unsaturated Fracture Zone [$m^3$/kg] | 3.9e+00, 3.5e+06 | Same as above | ** |
| lognormal | MatrixKD_TSw_Np[m3/kg] | Matrix $K_d$ of Np Topopah Spring—welded [$m^3$/kg] (UZ) | 1.6e-06, 2.2e-01 | CNWRA best estimate. Calculated using surface complexation models and site specific geochemistry. | DRT 2/25/00 |
| lognormal | MatrixKD_CHnvNp[m3/kg] | Matrix $K_d$ of Np for Calico Hills—nonwelded vitric [$m^3$/kg] (UZ) | 4.8e-06, 6.6e-01 | Same as above | ** |
| lognormal | MatrixKD_CHnzNp[m3/kg] | Matrix $K_d$ of Np for Calico Hills—nonwelded zeolitic [$m^3$/kg] (UZ) | 4.4e-06, 6.0e-01 | Same as above | ** |
| lognormal | MatrixKD_PPw_Np[m3/kg] | Matrix $K_d$ of Np for Prow Pass—welded [$m^3$/kg] (UZ) | 3.6e-06, 5.0e-01 | Same as above | ** |

| Distribution Type | Parameter Name | Description | Parameter Range | Remarks | Provided by |
|---|---|---|---|---|---|
| lognormal | MatrixKD_UCF_Np[m3/kg] | Matrix $K_d$ of Np for Upper Crater Flat [$m^3$/kg] (UZ) | 3.8e-06, 5.2e-01 | Same as above | ** |
| lognormal | MatrixKD_BFw_Np[m3/kg] | Matrix $K_d$ of Np for Bullfrog—welded [$m^3$/kg] (UZ) | 1.5e-06, 2.1e-01 | Same as above | ** |
| lognormal | MatrixKD_UFZ_Np[m3/kg] | Matrix $K_d$ of Np for Unsaturated Fracture Zone [$m^3$/kg] (UZ) | 1.5e-06, 2.0e-01 | Same as above | ** |
| constant | MatrixKD_TSw_I[m3/kg] | Matrix $K_d$ of I for Topopah Spring—welded [$m^3$/kg] (UZ) | 0.0 | Triay et al. (1997) | ** |
| constant | MatrixKD_CHnvI[m3/kg] | Matrix $K_d$ of I for Calico Hills—nonwelded vitric [$m^3$/kg] (UZ) | 0.0 | Triay et al. (1997) | ** |
| constant | MatrixKD_CHnzI[m3/kg] | Matrix $K_d$ for I for Calico Hills—nonwelded zeolitic [$m^3$/kg] (UZ) | 0.0 | Triay et al. (1997) | ** |
| constant | MatrixKD_PPw_I[m3/kg] | Matrix $K_d$ of I for Prow Pass—welded [$m^3$/kg] (UZ) | 0.0 | Triay et al. (1997) | ** |
| constant | MatrixKD_UCF_I[m3/kg] | Matrix $K_d$ of I for Upper Crater Flat [$m^3$/kg] (UZ) | 0.0 | Triay et al. (1997) | ** |

| Distribution Type | Parameter Name | Description | Parameter Range | Remarks | Provided by |
|---|---|---|---|---|---|
| constant | MatrixKD_BFw_I[m3/kg] | Matrix $K_d$ of I for Bullfrog—welded [$m^3$/kg] (UZ) | 0.0 | Triay et al. (1997) | ** |
| constant | MatrixKD_UFZ_I[m3/kg] | Matrix $K_d$ of I for Unsaturated Fracture Zone [$m^3$/kg] (UZ) | 0.0 | Triay et al. (1997) | ** |
| constant | MatrixKD_TSw_Tc[m3/kg] | Matrix $K_d$ of Tc for Topopah Spring—welded [$m^3$/kg] (UZ) | 0.0 | Triay et al. (1997) | ** |
| constant | MatrixKD_CHnvTc[m3/kg] | Matrix $K_d$ of Tc for Calico Hills—nonwelded vitric [$m^3$/kg] (UZ) | 0.0 | Triay et al. (1997) | ** |
| constant | MatrixKD_CHnzTc[m3/kg] | Matrix $K_d$ of Tc for Calico Hills—nonwelded zeolitic [$m^3$/kg] (UZ) | 0.0 | Triay et al. (1997) | ** |
| constant | MatrixKD_PPw_Tc[m3/kg] | Matrix $K_d$ of Tc for Prow Pass—welded [$m^3$/kg] (UZ) | 0.0 | Triay et al. (1997) | ** |
| constant | MatrixKD_UCF_Tc[m3/kg] | Matrix $K_d$ of Tc for Upper Crater Flat [$m^3$/kg] (UZ) | 0.0 | Triay et al. (1997) | ** |
| constant | MatrixKD_BFw_Tc[m3/kg] | Matrix $K_d$ of Tc for Bullfrog—welded [$m^3$/kg] (UZ) | 0.0 | Triay et al. (1997) | ** |

| Distribution Type | Parameter Name | Description | Parameter Range | Remarks | Provided by |
|---|---|---|---|---|---|
| constant | MatrixKD_UFZ_Tc[m3/kg] | Matrix $K_d$ of Tc for Unsaturated Fracture Zone [$m^3$/kg] (UZ) | 0.0 | Triay et al. (1997) | ** |
| constant | MatrixKD_TSw_Cl[m3/kg] | Matrix $K_d$ of Cl for Topopah Spring—welded [$m^3$/kg] (UZ) | 0.0 | Triay et al. (1997) | ** |
| constant | MatrixKD_CHnvCl[m3/kg] | Matrix $K_d$ of Cl for Calico Hills—nonwelded vitric [$m^3$/kg] (UZ) | 0.0 | Triay et al. (1997) | ** |
| constant | MatrixKD_CHnzCl[m3/kg] | Matrix $K_d$ of Cl for Calico Hills—nonwelded zeolitic [$m^3$/kg] (UZ) | 0.0 | Triay et al. (1997) | ** |
| constant | MatrixKD_PPw_Cl[m3/kg] | Matrix $K_d$ of Cl for Prow Pass—welded [$m^3$/kg] (UZ) | 0.0 | Triay et al. (1997) | ** |
| constant | MatrixKD_UCF_Cl[m3/kg] | Matrix $K_d$ of Cl for Upper Crater Flat [$m^3$/kg] (UZ) | 0.0 | Triay et al. (1997) | ** |
| constant | MatrixKD_BFw_Cl[m3/kg] | Matrix $K_d$ of Cl for Bullfrog—welded [$m^3$/kg] (UZ) | 0.0 | Triay et al. (1997) | ** |
| constant | MatrixKD_UFZ_Cl[m3/kg] | Matrix $K_d$ of Cl for Unsaturated Fracture Zone [$m^3$/kg] (UZ) | 0.0 | Triay et al. (1997) | ** |

| Distribution Type | Parameter Name | Description | Parameter Range | Remarks | Provided by |
|---|---|---|---|---|---|
| constant | MatrixKD_TSw_Cm[m3/kg] | Matrix $K_d$ of Cm for Topopah Spring—welded [$m^3$/kg] (UZ) | 0.0 | No data, conservative assumption | DRT 2/25/00 |
| constant | MatrixKD_CHnvCm[m3/kg] | Matrix $K_d$ of Cm for Calico Hills—nonwelded vitric [$m^3$/kg] (UZ) | 0.0 | No data | ** |
| constant | MatrixKD_CHnzCm[m3/kg] | Matrix $K_d$ of Cm for Calico Hills—nonwelded zeolitic [$m^3$/kg] (UZ) | 0.0 | No data | ** |
| constant | MatrixKD_PPw_Cm[m3/kg] | Matrix $K_d$ of Cm for Prow Pass—welded [$m^3$/kg] (UZ) | 0.0 | No data | ** |
| constant | MatrixKD_UCF_Cm[m3/kg] | Matrix $K_d$ of Cm for Upper Crater Flat [$m^3$/kg] (UZ) | 0.0 | No data | ** |
| constant | MatrixKD_BFw_Cm[m3/kg] | Matrix $K_d$ of Cm for Bullfrog—welded [$m^3$/kg] (UZ) | 0.0 | No data | ** |
| constant | MatrixKD_UFZ_Cm[m3/kg] | Matrix $K_d$ of Cm for Unsaturated Fracture Zone [$m^3$/kg] (UZ) | 0.0 | No data | ** |
| lognormal | MatrixKD_TSw_U[m3/kg] | Matrix $K_d$ of U for Topopah Spring—welded [$m^3$/kg] | 4.2e-10, 1.1e+00 | CNWRA best estimate. Calculated using surface complexation models and site | DRT 2/25/00 |

| Distribution Type | Parameter Name | Description | Parameter Range | Remarks | Provided by |
|---|---|---|---|---|---|
| | | (UZ) | | specific geochemistry. | |
| lognormal | MatrixKD_CHnvU[m3/kg] | Matrix $K_d$ of U for Calico Hills—nonwelded vitric [$m^3$/kg] (UZ) | 1.3e-09, 3.3e+00 | CNWRA best estimate. | DRT 2/25/00 |
| lognormal | MatrixKD_CHnzU[m3/kg] | Matrix $K_d$ of U for Calico Hills—nonwelded zeolitic [$m^3$/kg] (UZ) | 1.2e-09, 3.0e+00 | Same as above | ** |
| lognormal | MatrixKD_PPw_U[m3/kg] | Matrix $K_d$ of U for Prow Pass—welded [$m^3$/kg] (UZ) | 9.6e-10, 2.5e+00 | Same as above | ** |
| lognormal | MatrixKD_UCF_U[m3/kg] | Matrix $K_d$ of U for Upper Crater Flat [$m^3$/kg] (UZ) | 1.0e-09, 2.6e+00 | Same as above | ** |
| lognormal | MatrixKD_BFw_U[m3/kg] | Matrix $K_d$ of U for Bullfrog—welded [$m^3$/kg] (UZ) | 4.1e-10, 1.0e+00 | Same as above | ** |
| lognormal | MatrixKD_UFZ_U[m3/kg] | Matrix $K_d$ of U for Unsaturated Fracture Zone [$m^3$/kg] (UZ) | 3.9e-10, 1.0e+00 | Same as above | ** |
| lognormal | MatrixKD_TSw_Pu[m3/kg] | Matrix $K_d$ of Pu for Topopah Spring—welded [$m^3$/kg] (UZ) | 2.3e-02, 2.2e+01 | CNWRA best estimate. Calculated using surface complexation models and site specific geochemistry. | DRT 2/25/00 |
| lognormal | MatrixKD_CHnvPu[m3/kg] | Matrix $K_d$ of Pu for Calico | 7.1e-02, 6.7e+01 | CNWRA best estimate. | DRT 2/25/00 |

| Distribution Type | Parameter Name | Description | Parameter Range | Remarks | Provided by |
|---|---|---|---|---|---|
| | | Hills—nonwelded vitric [$m^3$/kg] (UZ) | | | |
| lognormal | MatrixKD_CHnzPu[m3/kg] | Matrix $K_d$ of Pu for Calico Hills—nonwelded zeolitic [$m^3$/kg] (UZ) | 6.5e-02, 6.1e+01 | Same as above | ** |
| lognormal | MatrixKD_PPw_Pu[m3/kg] | Matrix $K_d$ of Pu for Prow Pass—welded [$m^3$/kg] (UZ) | 5.3e-02, 5.0e+01 | Same as above | ** |
| lognormal | MatrixKD_UCF_Pu[m3/kg] | Matrix $K_d$ of Pu for Upper Crater Flat [$m^3$/kg] (UZ) | 5.6e-02, 5.2e+01 | Same as above | ** |
| lognormal | MatrixKD_BFw_Pu[m3/kg] | Matrix $K_d$ of Pu for Bullfrog—welded [$m^3$/kg] (UZ) | 2.3e-02, 2.1e+01 | Same as above | ** |
| lognormal | MatrixKD_UFZ_Pu[m3/kg] | Matrix $K_d$ of Pu for Unsaturated Fracture Zone [$m^3$/kg] (UZ) | 2.2e-02, 2.1e+01 | Same as above | ** |
| lognormal | MatrixKD_TSw_Th[m3/kg] | Matrix $K_d$ of Th for Topopah Spring—welded [$m^3$/kg] (UZ) | 4.8e-05, 2.5e+03 | CNWRA best estimate. Calculated using surface complexation models and site specific geochemistry. | DRT 2/25/00 |
| lognormal | MatrixKD_CHnvTh[m3/kg] | Matrix $K_d$ of Th for Calico Hills—nonwelded vitric [$m^3$/kg] (UZ) | 1.5e-04, 7.6e+03 | CNWRA best estimate. | DRT 2/25/00 |

| Distribution Type | Parameter Name | Description | Parameter Range | Remarks | Provided by |
|---|---|---|---|---|---|
| lognormal | MatrixKD_CHnzTh[m3/kg] | Matrix $K_d$ of Th for Calico Hills—nonwelded zeolitic [$m^3$/kg] (UZ) | 1.3e-04, 6.9e+03 | Same as above | ** |
| lognormal | MatrixKD_PPw_Th[m3/kg] | Matrix $K_d$ of Th for Prow Pass—welded [$m^3$/kg] (UZ) | 1.1e-04, 5.7e+03 | Same as above | ** |
| lognormal | MatrixKD_UCF_Th[m3/kg] | Matrix $K_d$ of Th for Upper Crater Flat [$m^3$/kg] (UZ) | 1.1e-04, 5.9e+03 | Same as above | ** |
| lognormal | MatrixKD_BFw_Th[m3/kg] | Matrix $K_d$ of Th for Bullfrog—welded [$m^3$/kg] (UZ) | 4.7e-05, 2.4e+03 | Same as above | ** |
| lognormal | MatrixKD_UFZ_Th[m3/kg] | Matrix $K_d$ of Th for Unsaturated Fracture Zone [$m^3$/kg] (UZ) | 4.5e-05, 2.3e+03 | Same as above | ** |
| uniform | MatrixKD_TSw_Ra[m3/kg] | Matrix $K_d$ of Ra for Topopah Spring—welded [$m^3$/kg] (UZ) | 0.100, 0.500 | Triay et al. (1997) | ** |
| uniform | MatrixKD_CHnvRa[m3/kg] | Matrix $K_d$ of Ra for Calico Hills—nonwelded vitric [$m^3$/kg] (UZ) | 0.050, 0.100 | Triay et al. (1997) | ** |
| uniform | MatrixKD_CHnzRa[m3/kg] | Matrix $K_d$ of Ra for Calico | 1.0, 5.0 | Triay et al. (1997) | ** |

| Distribution Type | Parameter Name | Description | Parameter Range | Remarks | Provided by |
|---|---|---|---|---|---|
| | | Hills—nonwelded zeolitic [$m^3$/kg] (UZ) | | | |
| uniform | MatrixKD_PPw_Ra[m3/kg] | Matrix $K_d$ of Ra for Prow Pass—welded [$m^3$/kg] (UZ) | 0.1, 0.5 | Triay et al. (1997) | ** |
| uniform | MatrixKD_UCF_Ra[m3/kg] | Matrix $K_d$ of Ra for Upper Crater Flat [$m^3$/kg] (UZ) | 0.1, 0.5 | Triay et al. (1997) | ** |
| uniform | MatrixKD_BFw_Ra[m3/kg] | Matrix $K_d$ of Ra for Bullfrog—welded [$m^3$/kg] (UZ) | 0.1, 0.5 | Triay et al. (1997) | ** |
| uniform | MatrixKD_UFZ_Ra[m3/kg] | Matrix $K_d$ of Ra for Unsaturated Fracture Zone [$m^3$/kg] (UZ) | 0.1, 0.5 | Triay et al. (1997) | ** |
| uniform | MatrixKD_TSw_Pb[m3/kg] | Matrix $K_d$ of Pb for Topopah Spring—welded [$m^3$/kg] (UZ) | 0.100, 0.500 | Triay et al. (1997) | ** |
| uniform | MatrixKD_CHnvPb[m3/kg] | Matrix $K_d$ of Pb for Calico Hills—nonwelded vitric [$m^3$/kg] (UZ) | 0.100, 0.500 | Triay et al. (1997) | ** |

| Distribution Type | Parameter Name | Description | Parameter Range | Remarks | Provided by |
|---|---|---|---|---|---|
| uniform | MatrixKD_PPw_Pb[m3/kg] | Matrix $K_d$ of Pb for Prow Pass—welded [$m^3$/kg] (UZ) | 0.100, 0.500 | Triay et al. (1997) | ** |
| uniform | MatrixKD_UCF_Pb[m3/kg] | Matrix $K_d$ of Pb for Upper Crater Flat [$m^3$/kg] (UZ) | 0.100, 0.500 | Triay et al. (1997) | ** |
| uniform | MatrixKD_BFw_Pb[m3/kg] | Matrix $K_d$ of Pb for Bullfrog—welded [$m^3$/kg] (UZ) | 0.100, 0.500 | Triay et al. (1997) | ** |
| uniform | MatrixKD_UFZ_Pb[m3/kg] | Matrix $K_d$ of Pb for Unsaturated Fracture Zone [$m^3$/kg] (UZ) | 0.100, 0.500 | Triay et al. (1997) | ** |
| uniform | MatrixKD_TSw_Cs[m3/kg] | Matrix $K_d$ of Cs for Topopah Spring—welded [$m^3$/kg] (UZ) | 0.020, 1.000 | Triay et al. (1997) | ** |
| uniform | MatrixKD_CHnvCs[m3/kg] | Matrix $K_d$ of Cs for Calico Hills—nonwelded vitric [$m^3$/kg] (UZ) | 0.010, 0.100 | Triay et al. (1997) | ** |
| uniform | MatrixKD_CHnzCs[m3/kg] | Matrix $K_d$ of Cs for Calico Hills—nonwelded zeolitic [$m^3$/kg] (UZ) | 0.500, 5.000 | Triay et al. (1997) | ** |
| uniform | MatrixKD_PPw_Cs[m3/kg] | Matrix $K_d$ of Cs for Prow Pass—welded [$m^3$/kg] (UZ) | 0.020, 1.000 | Triay et al. (1997) | ** |

| Distribution Type | Parameter Name | Description | Parameter Range | Remarks | Provided by |
|---|---|---|---|---|---|
| uniform | MatrixKD_UCF_Cs[m3/kg] | Matrix $K_d$ of Cs for Upper Crater Flat [$m^3$/kg] (UZ) | 0.020, 1.000 | Triay et al. (1997) | ** |
| uniform | MatrixKD_BFw_Cs[m3/kg] | Matrix $K_d$ of Cs for Bullfrog—welded [$m^3$/kg] (UZ) | 0.020, 1.000 | Triay et al. (1997) | ** |
| uniform | MatrixKD_UFZ_Cs[m3/kg] | Matrix $K_d$ of Cs for Unsaturated Fracture Zone [$m^3$/kg] (UZ) | 0.020, 1.000 | Triay et al. (1997) | ** |
| uniform | MatrixKD_TSw_Ni[m3/kg] | Matrix $K_d$ of Ni for Topopah Spring—welded [$m^3$/kg] (UZ) | 5.0e-6, 0.500 | Triay et al. (1997). A value 5 orders of magnitude smaller than the maximum value was used as the lower bound. | ** |
| uniform | MatrixKD_CHnvNi[m3/kg] | Matrix $K_d$ of Ni for Calico Hills—nonwelded vitric [$m^3$/kg] (UZ) | 1.0e-6, 0.100 | Triay et al. (1997). A value 5 orders of magnitude smaller than the maximum value was used as the lower bound. | ** |
| uniform | MatrixKD_CHnzNi[m3/kg] | Matrix $K_d$ of Ni for Calico Hills—nonwelded zeolitic [$m^3$/kg] (UZ) | 5.0e-6, 0.500 | Triay et al. (1997). A value 5 orders of magnitude smaller than the maximum value was used as the lower bound. | ** |
| uniform | MatrixKD_PPw_Ni[m3/kg] | Matrix $K_d$ of Ni for Prow Pass—welded [$m^3$/kg] (UZ) | 5.0e-6, 0.500 | Triay et al. (1997). A value 5 orders of magnitude smaller than the maximum value was used as the lower bound. | ** |
| uniform | MatrixKD_UCF_Ni[m3/kg] | Matrix $K_d$ of Ni for Upper Crater Flat | 5.0e-6, 0.500 | Triay et al. (1997). A value 5 orders of magnitude smaller | ** |

| Distribution Type | Parameter Name | Description | Parameter Range | Remarks | Provided by |
|---|---|---|---|---|---|
| | | [$m^3$/kg] (UZ) | | than the maximum value was used as the lower bound. | |
| uniform | MatrixKD_BFw_Ni[m3/kg] | Matrix $K_d$ of Ni for Bullfrog—welded [$m^3$/kg] (UZ) | 5.0e-6, 0.500 | Triay et al. (1997). A value 5 orders of magnitude smaller than the maximum value was used as the lower bound. | ** |
| uniform | MatrixKD_UFZ_Ni[m3/kg] | Matrix $K_d$ of Ni for Unsaturated Fracture Zone [$m^3$/kg] (UZ) | 5.0e-6, 0.500 | Triay et al. (1997). A value 5 orders of magnitude smaller than the maximum value was used as the lower bound. | ** |
| constant | MatrixKD_TSw_C[m3/kg] | Matrix $K_d$ of C for Topopah Spring—welded [$m^3$/kg] (UZ) | 0.0 | Triay et al. (1997) | ** |
| constant | MatrixKD_CHnvC[m3/kg] | Matrix $K_d$ of C for Calico Hills—nonwelded vitric [$m^3$/kg] (UZ) | 0.0 | Triay et al. (1997) | ** |
| constant | MatrixKD_CHnzC[m3/kg] | Matrix $K_d$ of C for Calico Hills—nonwelded zeolitic [$m^3$/kg] (UZ) | 0.0 | Triay et al. (1997) | ** |
| constant | MatrixKD_PPw_C[m3/kg] | Matrix $K_d$ of C for Prow Pass—welded [$m^3$/kg] (UZ) | 0.0 | Triay et al. (1997) | ** |
| constant | MatrixKD_UCF_C[m3/kg] | Matrix $K_d$ of C for Upper Crater Flat | 0.0 | Triay et al. (1997) | ** |

| Distribution Type | Parameter Name | Description | Parameter Range | Remarks | Provided by |
|---|---|---|---|---|---|
| | | [$m^3$/kg] (UZ) | | | |
| constant | MatrixKD_BFw_C[m3/kg] | Matrix $K_d$ of C for Bullfrog—welded [$m^3$/kg] (UZ) | 0.0 | Triay et al. (1997) | ** |
| constant | MatrixKD_UFZ_C[m3/kg] | Matrix $K_d$ of C for Unsaturated Fracture Zone [$m^3$/kg] (UZ) | 0.0 | Triay et al. (1997) | ** |
| uniform | MatrixKD_TSw_Se[m3/kg] | Matrix $K_d$ of Se for Topopah Spring—welded [$m^3$/kg] (UZ) | 3.0e-7, 0.030 | Triay et al. (1997). A value 5 orders of magnitude smaller than the maximum value was used as the lower bound. | ** |
| uniform | MatrixKD_CHnvSe[m3/kg] | Matrix $K_d$ of Se for Calico Hills—nonwelded vitric [$m^3$/kg] (UZ) | 2.0e-7, 0.020 | Triay et al. (1997). A value 5 orders of magnitude smaller than the maximum value was used as the lower bound. | ** |
| uniform | MatrixKD_CHnzSe[m3/kg] | Matrix $K_d$ of Se for Calico Hills—nonwelded zeolitic [$m^3$/kg] (UZ) | 1.5e-7, 0.015 | Triay et al. (1997). A value 5 orders of magnitude smaller than the maximum value was used as the lower bound. | ** |
| uniform | MatrixKD_PPw_Se[m3/kg] | Matrix $K_d$ of Se for Prow Pass—welded [$m^3$/kg] (UZ) | 3.0e-7, 0.030 | Triay et al. (1997). A value 5 orders of magnitude smaller than the maximum value was used as the lower bound. | ** |
| uniform | MatrixKD_UCF_Se[m3/kg] | Matrix $K_d$ of Se for Upper Crater Flats [$m^3$/kg] (UZ) | 3.0e-7, 0.030 | Triay et al. (1997). A value 5 orders of magnitude smaller than the maximum value was used as the lower bound. | ** |

| Distribution Type | Parameter Name | Description | Parameter Range | Remarks | Provided by |
|---|---|---|---|---|---|
| uniform | MatrixKD_BFw_Se[m3/kg] | Matrix $K_d$ of Se for Bullfrog [$m^3$/kg] (UZ) | 3.0e-7, 0.030 | Triay et al. (1997). A value 5 orders of magnitude smaller than the maximum value was used as the lower bound. | ** |
| uniform | MatrixKD_UFZ_Se[m3/kg] | Matrix $K_d$ of Se for Unsaturated Fracture Zone [$m^3$/kg] (UZ) | 3.0e-7, 0.030 | Triay et al. (1997). A value 5 orders of magnitude smaller than the maximum value was used as the lower bound. | ** |
| constant | MatrixKD_TSw_Nb[m3/kg] | Matrix $K_d$ of Nb for Topopah Spring—welded [$m^3$/kg] (UZ) | 0.0 | Triay et al. (1997) | ** |
| constant | MatrixKD_CHnvNb[m3/kg] | Matrix $K_d$ of Nb for Calico Hills—nonwelded vitric [$m^3$/kg] (UZ) | 0.0 | Triay et al. (1997) | ** |
| constant | MatrixKD_CHnzNb[m3/kg] | Matrix $K_d$ of Nb for Calico Hills—nonwelded zeolitic [$m^3$/kg] (UZ) | 0.0 | Triay et al. (1997) | ** |
| constant | MatrixKD_PPw_Nb[m3/kg] | Matrix $K_d$ of Nb for Prow Pass—welded [$m^3$/kg] (UZ) | 0.0 | Triay et al. (1997) | ** |
| constant | MatrixKD_UCF_Nb[m3/kg] | Matrix $K_d$ of Nb for Upper Crater Flats [$m^3$/kg] (UZ) | 0.0 | Triay et al. (1997) | ** |

| Distribution Type | Parameter Name | Description | Parameter Range | Remarks | Provided by |
|---|---|---|---|---|---|
| constant | MatrixKD_UFZ_Nb[m3/kg] | Matrix $K_d$ of Nb for Unsaturated Fracture Zone [$m^3$/kg] (UZ) | 0.0 | Triay et al. (1997) | ** |
| constant | FractureRD_TSw_Am | Fracture retardation coefficient of Am for Topopah Spring—welded (UZ) | 1.0 | Conservative assumption of no retardation | ** |
| constant | FractureRD_CHnvAm | Fracture retardation coefficient of Am for Calico Hills—nonwelded vitric (UZ) | 1.0 | Conservative assumption of no retardation | ** |
| constant | FractureRD_CHnzAm | Fracture retardation coefficient of Am for Calico Hills—nonwelded zeolitic (UZ) | 1.0 | Conservative assumption of no retardation | ** |
| constant | FractureRD_PPw_Am | Fracture retardation coefficient of Am for Prow Pass—welded (UZ) | 1.0 | Conservative assumption of no retardation | ** |
| constant | FractureRD_UCF_Am | Fracture retardation coefficient of Am for Upper Crater Flat (UZ) | 1.0 | Conservative assumption of no retardation | ** |
| constant | FractureRD_BFw_Am | Fracture retardation coefficient of Am for Bullfrog—welded (UZ) | 1.0 | Conservative assumption of no retardation | ** |

| Distribution Type | Parameter Name | Description | Parameter Range | Remarks | Provided by |
|---|---|---|---|---|---|
| constant | FractureRD_UFZ_Am | Fracture retardation coefficient of Am for Unsaturated Fracture Zone (UZ) | 1.0 | Conservative assumption of no retardation | ** |
| constant | FractureRD_TSw_Np | Fracture retardation coefficient of Np for Topopah Spring—welded (UZ) | 1.0 | Conservative assumption of no retardation | ** |
| constant | FractureRD_CHnvNp | Fracture retardation coefficient of Np for Calico Hills—nonwelded vitric (UZ) | 1.0 | Conservative assumption of no retardation | ** |
| constant | FractureRD_CHnzNp | Fracture retardation coefficient of Np for Calico Hills—nonwelded zeolitic (UZ) | 1.0 | Conservative assumption of no retardation | ** |
| constant | FractureRD_PPw_Np | Fracture retardation coefficient of Np for Prow Pass—welded (UZ) | 1.0 | Conservative assumption of no retardation | ** |
| constant | FractureRD_UCF_Np | Fracture retardation coefficient of Np for Upper Crater Flat (UZ) | 1.0 | Conservative assumption of no retardation | ** |
| constant | FractureRD_BFw_Np | Fracture retardation coefficient of Np for Bullfrog—welded (UZ) | 1.0 | Conservative assumption of no retardation | ** |

| Distribution Type | Parameter Name | Description | Parameter Range | Remarks | Provided by |
|---|---|---|---|---|---|
| constant | FractureRD_UFZ_Np | Fracture retardation coefficient of Np for Unsaturated Fracture Zone (UZ) | 1.0 | Conservative assumption of no retardation | ** |
| constant | FractureRD_TSw_I | Fracture retardation coefficient of I for Topopah Spring—welded (UZ) | 1.0 | Conservative assumption of no retardation | ** |
| constant | FractureRD_CHnvI | Fracture retardation coefficient of I for Calico Hills—nonwelded vitric (UZ) | 1.0 | Conservative assumption of no retardation | ** |
| constant | FractureRD_CHnzI | Fracture retardation coefficient of I for Calico Hills—nonwelded zeolitic (UZ) | 1.0 | Conservative assumption of no retardation | ** |
| constant | FractureRD_PPw_I | Fracture retardation coefficient of I for Prow Pass—welded (UZ) | 1.0 | Conservative assumption of no retardation | ** |
| constant | FractureRD_UCF_I | Fracture retardation coefficient of I for Upper Crater Flat (UZ) | 1.0 | Conservative assumption of no retardation | ** |
| constant | FractureRD_BFw_I | Fracture retardation coefficient of I for Bullfrog—welded (UZ) | 1.0 | Conservative assumption of no retardation | ** |

| Distribution Type | Parameter Name | Description | Parameter Range | Remarks | Provided by |
|---|---|---|---|---|---|
| constant | FractureRD_UFZ_I | Fracture retardation coefficient of I for Unsaturated Fracture Zone (UZ) | 1.0 | Conservative assumption of no retardation | ** |
| constant | FractureRD_TSw_Tc | Fracture retardation coefficient of Tc for Topopah Spring—welded (UZ) | 1.0 | Conservative assumption of no retardation | ** |
| constant | FractureRD_CHnvTc | Fracture retardation coefficient of Tc for Calico Hills—nonwelded vitric (UZ) | 1.0 | Conservative assumption of no retardation | ** |
| constant | FractureRD_CHnzTc | Fracture retardation coefficient of Tc for Calico Hills—nonwelded zeolitic (UZ) | 1.0 | Conservative assumption of no retardation | ** |
| constant | FractureRD_PPw_Tc | Fracture retardation coefficient of Tc for Prow Pass—welded (UZ) | 1.0 | Conservative assumption of no retardation | ** |
| constant | FractureRD_UCF_Tc | Fracture retardation coefficient of Tc for Upper Crater Flat (UZ) | 1.0 | Conservative assumption of no retardation | ** |
| constant | FractureRD_BFw_Tc | Fracture retardation coefficient of Tc for Bullfrog—welded (UZ) | 1.0 | Conservative assumption of no retardation | ** |

| Distribution Type | Parameter Name | Description | Parameter Range | Remarks | Provided by |
|---|---|---|---|---|---|
| constant | FractureRD_UFZ_Tc | Fracture retardation coefficient of Tc for Unsaturated Fracture Zone (UZ) | 1.0 | Conservative assumption of no retardation | ** |
| constant | FractureRD_TSw_Cl | Fracture retardation coefficient of Cl for Topopah Spring—welded (UZ) | 1.0 | Conservative assumption of no retardation | ** |
| constant | FractureRD_CHnvCl | Fracture retardation coefficient of Cl for Calico Hills—nonwelded vitric (UZ) | 1.0 | Conservative assumption of no retardation | ** |
| constant | FractureRD_CHnzCl | Fracture retardation coefficient of Cl for Calico Hills—nonwelded zeolitic (UZ) | 1.0 | Conservative assumption of no retardation | ** |
| constant | FractureRD_PPw_Cl | Fracture retardation coefficient of Cl for Prow Pass—welded (UZ) | 1.0 | Conservative assumption of no retardation | ** |
| constant | FractureRD_UCF_Cl | Fracture retardation coefficient of Cl for Upper Crater Flat (UZ) | 1.0 | Conservative assumption of no retardation | ** |
| constant | FractureRD_BFw_Cl | Fracture retardation coefficient of Cl for Bullfrog—welded (UZ) | 1.0 | Conservative assumption of no retardation | ** |

| Distribution Type | Parameter Name | Description | Parameter Range | Remarks | Provided by |
|---|---|---|---|---|---|
| constant | FractureRD_UFZ_Cl | Fracture retardation coefficient of Unsaturated Fracture Zone (UZ) | 1.0 | Conservative assumption of no retardation | ** |
| constant | FractureRD_TSw_Cm | Fracture retardation coefficient of Cm for Topopah Spring—welded (UZ) | 1.0 | Conservative assumption of no retardation | ** |
| constant | FractureRD_CHnvCm | Fracture retardation coefficient of Cm for Calico Hills—nonwelded vitric (UZ) | 1.0 | Conservative assumption of no retardation | ** |
| constant | FractureRD_CHnzCm | Fracture retardation coefficient of Cm for Calico Hills—nonwelded zeolitic (UZ) | 1.0 | Conservative assumption of no retardation | ** |
| constant | FractureRD_PPw_Cm | Fracture retardation coefficient of Cm for Prow Pass—welded (UZ) | 1.0 | Conservative assumption of no retardation | ** |
| constant | FractureRD_UCF_Cm | Fracture retardation coefficient of Cm for Upper Crater Flat (UZ) | 1.0 | Conservative assumption of no retardation | ** |
| constant | FractureRD_BFw_Cm | Fracture retardation coefficient of Cm for Bullfrog—welded (UZ) | 1.0 | Conservative assumption of no retardation | ** |

| Distribution Type | Parameter Name | Description | Parameter Range | Remarks | Provided by |
|---|---|---|---|---|---|
| constant | FractureRD_UFZ_Cm | Fracture retardation coefficient of Unsaturated Fracture Zone (UZ) | 1.0 | Conservative assumption of no retardation | ** |
| constant | FractureRD_TSw_U | Fracture retardation coefficient of U for Topopah Spring—welded (UZ) | 1.0 | Conservative assumption of no retardation | ** |
| constant | FractureRD_CHnvU | Fracture retardation coefficient of U for Calico Hills—nonwelded vitric (UZ) | 1.0 | Conservative assumption of no retardation | ** |
| constant | FractureRD_CHnzU | Fracture retardation coefficient of U for Calico Hills—nonwelded zeolitic (UZ) | 1.0 | Conservative assumption of no retardation | ** |
| constant | FractureRD_PPw_U | Fracture retardation coefficient of U for Prow Pass—welded (UZ) | 1.0 | Conservative assumption of no retardation | ** |
| constant | FractureRD_UCF_U | Fracture retardation coefficient of U for Upper Crater Flat (UZ) | 1.0 | Conservative assumption of no retardation | ** |
| constant | FractureRD_BFw_U | Fracture retardation coefficient of U for Bullfrog—welded (UZ) | 1.0 | Conservative assumption of no retardation | ** |

| Distribution Type | Parameter Name | Description | Parameter Range | Remarks | Provided by |
|---|---|---|---|---|---|
| constant | FractureRD_UFZ_U | Fracture retardation coefficient of U for Unsaturated Fracture Zone (UZ) | 1.0 | Conservative assumption of no retardation | ** |
| constant | FractureRD_TSw_Pu | Fracture retardation coefficient of Pu for Topopah Spring—welded (UZ) | 1.0 | Conservative assumption of no retardation | ** |
| constant | FractureRD_CHnvPu | Fracture retardation coefficient of Pu for Calico Hills—nonwelded vitric (UZ) | 1.0 | Conservative assumption of no retardation | ** |
| constant | FractureRD_CHnzPu | Fracture retardation coefficient of Pu for Calico Hills—nonwelded zeolitic (UZ) | 1.0 | Conservative assumption of no retardation | ** |
| constant | FractureRD_PPw_Pu | Fracture retardation coefficient of Pu for Prow Pass—welded (UZ) | 1.0 | Conservative assumption of no retardation | ** |
| constant | FractureRD_UCF_Pu | Fracture retardation coefficient of Pu for Upper Crater Flat (UZ) | 1.0 | Conservative assumption of no retardation | ** |
| constant | FractureRD_BFw_Pu | Fracture retardation coefficient of Pu for Bullfrog—welded (UZ) | 1.0 | Conservative assumption of no retardation | ** |

| Distribution Type | Parameter Name | Description | Parameter Range | Remarks | Provided by |
|---|---|---|---|---|---|
| constant | FractureRD_UFZ_Pu | Fracture retardation coefficient of Pu for Unsaturated Fracture Zone (UZ) | 1.0 | Conservative assumption of no retardation | ** |
| constant | FractureRD_TSw_Th | Fracture retardation coefficient of Th for Topopah Spring—welded (UZ) | 1.0 | Conservative assumption of no retardation | ** |
| constant | FractureRD_CHnvTh | Fracture retardation coefficient of Th for Calico Hills—nonwelded vitric (UZ) | 1.0 | Conservative assumption of no retardation | ** |
| constant | FractureRD_CHnzTh | Fracture retardation coefficient of Th for Calico Hills—nonwelded zeolitic (UZ) | 1.0 | Conservative assumption of no retardation | ** |
| constant | FractureRD_PPw_Th | Fracture retardation coefficient of Th for Prow Pass—welded (UZ) | 1.0 | Conservative assumption of no retardation | ** |
| constant | FractureRD_UCF_Th | Fracture retardation coefficient of Th for Upper Crater Flat (UZ) | 1.0 | Conservative assumption of no retardation | ** |
| constant | FractureRD_BFw_Th | Fracture retardation coefficient of Th for Bullfrog—welded (UZ) | 1.0 | Conservative assumption of no retardation | ** |

| Distribution Type | Parameter Name | Description | Parameter Range | Remarks | Provided by |
|---|---|---|---|---|---|
| constant | FractureRD_UFZ_Th | Fracture retardation coefficient of Th for Unsaturated Fracture Zone (UZ) | 1.0 | Conservative assumption of no retardation | ** |
| constant | FractureRD_TSw_Ra | Fracture retardation coefficient of Ra for Topopah Spring—welded (UZ) | 1.0 | Conservative assumption of no retardation | ** |
| constant | FractureRD_CHnvRa | Fracture retardation coefficient of Ra for Calico Hills—nonwelded vitric (UZ) | 1.0 | Conservative assumption of no retardation | ** |
| constant | FractureRD_CHnzRa | Fracture retardation coefficient of Ra for Calico Hills—nonwelded zeolitic (UZ) | 1.0 | Conservative assumption of no retardation | ** |
| constant | FractureRD_PPw_Ra | Fracture retardation coefficient of Ra for Prow Pass—welded (UZ) | 1.0 | Conservative assumption of no retardation | ** |
| constant | FractureRD_UCF_Ra | Fracture retardation coefficient of Ra for Upper Crater Flat (UZ) | 1.0 | Conservative assumption of no retardation | ** |
| constant | FractureRD_BFw_Ra | Fracture retardation coefficient of Ra for Bullfrog—welded (UZ) | 1.0 | Conservative assumption of no retardation | ** |

| Distribution Type | Parameter Name | Description | Parameter Range | Remarks | Provided by |
|---|---|---|---|---|---|
| constant | FractureRD_UFZ_Ra | Fracture retardation coefficient of Ra for Unsaturated Fracture Zone (UZ) | 1.0 | Conservative assumption of no retardation | ** |
| constant | FractureRD_TSw_Pb | Fracture retardation coefficient of Pb for Topopah Spring—welded (UZ) | 1.0 | Conservative assumption of no retardation | ** |
| constant | FractureRD_CHnvPb | Fracture retardation coefficient of Pb for Calico Hills—nonwelded vitric (UZ) | 1.0 | Conservative assumption of no retardation | ** |
| constant | FractureRD_CHnzPb | Fracture retardation coefficient of Pb for Calico Hills—nonwelded zeolitic (UZ) | 1.0 | Conservative assumption of no retardation | ** |
| constant | FractureRD_PPw_Pb | Fracture retardation coefficient of Pb for Prow Pass—welded (UZ) | 1.0 | Conservative assumption of no retardation | ** |
| constant | FractureRD_UCF_Pb | Fracture retardation coefficient of Pb for Upper Crater Flat (UZ) | 1.0 | Conservative assumption of no retardation | ** |
| constant | FractureRD_BFw_Pb | Fracture retardation coefficient of Pb for Bullfrog—welded (UZ) | 1.0 | Conservative assumption of no retardation | ** |

| Distribution Type | Parameter Name | Description | Parameter Range | Remarks | Provided by |
|---|---|---|---|---|---|
| constant | FractureRD_UFZ_Pb | Fracture retardation coefficient of Pb for Unsaturated Fracture Zone (UZ) | 1.0 | Conservative assumption of no retardation | ** |
| constant | FractureRD_TSw_Cs | Fracture retardation coefficient of Cs for Topopah Spring—welded (UZ) | 1.0 | Conservative assumption of no retardation | ** |
| constant | FractureRD_CHnvCs | Fracture retardation coefficient of Cs for Calico Hills—nonwelded vitric (UZ) | 1.0 | Conservative assumption of no retardation | ** |
| constant | FractureRD_CHnzCs | Fracture retardation coefficient of Cs for Calico Hills—nonwelded zeolitic (UZ) | 1.0 | Conservative assumption of no retardation | ** |
| constant | FractureRD_PPw_Cs | Fracture retardation coefficient of Cs for Prow Pass—welded (UZ) | 1.0 | Conservative assumption of no retardation | ** |
| constant | FractureRD_UCF_Cs | Fracture retardation coefficient of Cs for Upper Crater Flat (UZ) | 1.0 | Conservative assumption of no retardation | ** |
| constant | FractureRD_BFw_Cs | Fracture retardation coefficient of Cs for Bullfrog—welded (UZ) | 1.0 | Conservative assumption of no retardation | ** |

| Distribution Type | Parameter Name | Description | Parameter Range | Remarks | Provided by |
|---|---|---|---|---|---|
| constant | FractureRD_UFZ_Cs | Fracture retardation coefficient of Cs for Unsaturated Fracture Zone (UZ) | 1.0 | Conservative assumption of no retardation | ** |
| constant | FractureRD_TSw_Ni | Fracture retardation coefficient of Ni for Topopah Spring—welded (UZ) | 1.0 | Conservative assumption of no retardation | ** |
| constant | FractureRD_CHnvNi | Fracture retardation coefficient of Ni for Calico Hills—nonwelded vitric (UZ) | 1.0 | Conservative assumption of no retardation | ** |
| constant | FractureRD_CHnzNi | Fracture retardation coefficient of Ni for Calico Hills—nonwelded zeolitic (UZ) | 1.0 | Conservative assumption of no retardation | ** |
| constant | FractureRD_PPw_Ni | Fracture retardation coefficient of Ni for Prow Pass—welded (UZ) | 1.0 | Conservative assumption of no retardation | ** |
| constant | FractureRD_UCF_Ni | Fracture retardation coefficient of Ni for Upper Crater Flat (UZ) | 1.0 | Conservative assumption of no retardation | ** |
| constant | FractureRD_BFw_Ni | Fracture retardation coefficient of Ni for Bullfrog—welded (UZ) | 1.0 | Conservative assumption of no retardation | ** |

| Distribution Type | Parameter Name | Description | Parameter Range | Remarks | Provided by |
|---|---|---|---|---|---|
| constant | FractureRD_UFZ_Ni | Fracture retardation coefficient of Ni for Unsaturated Fracture Zone (UZ) | 1.0 | Conservative assumption of no retardation | ** |
| constant | FractureRD_TSw_C | Fracture retardation coefficient of C for Topopah Spring—welded (UZ) | 1.0 | Conservative assumption of no retardation | ** |
| constant | FractureRD_CHnvC | Fracture retardation coefficient of C for Calico Hills—nonwelded vitric (UZ) | 1.0 | Conservative assumption of no retardation | ** |
| constant | FractureRD_CHnzC | Fracture retardation coefficient of C for Calico Hills—nonwelded zeolitic (UZ) | 1.0 | Conservative assumption of no retardation | ** |
| constant | FractureRD_PPw_C | Fracture retardation coefficient of C for Prow Pass—welded (UZ) | 1.0 | Conservative assumption of no retardation | ** |
| constant | FractureRD_UCF_C | Fracture retardation coefficient of C for Upper Crater Flat (UZ) | 1.0 | Conservative assumption of no retardation | ** |
| constant | FractureRD_BFw_C | Fracture retardation coefficient of C for Bullfrog—welded (UZ) | 1.0 | Conservative assumption of no retardation | ** |

| Distribution Type | Parameter Name | Description | Parameter Range | Remarks | Provided by |
|---|---|---|---|---|---|
| constant | FractureRD_UFZ_C | Fracture retardation coefficient of C for Unsaturated Fracture Zone (UZ) | 1.0 | Conservative assumption of no retardation | ** |
| constant | FractureRD_TSw_Se | Fracture retardation coefficient of Se for Topopah Spring—welded (UZ) | 1.0 | Conservative assumption of no retardation | ** |
| constant | FractureRD_CHnvSe | Fracture retardation coefficient of Se for Calico Hills—nonwelded vitric (UZ) | 1.0 | Conservative assumption of no retardation | ** |
| constant | FractureRD_CHnzSe | Fracture retardation coefficient of Se for Calico Hills—nonwelded zeolitic (UZ) | 1.0 | Conservative assumption of no retardation | ** |
| constant | FractureRD_PPw_Se | Fracture retardation coefficient of Se for Prow Pass—welded (UZ) | 1.0 | Conservative assumption of no retardation | ** |
| constant | FractureRD_UCF_Se | Fracture retardation coefficient of Se for Upper Crater Flat (UZ) | 1.0 | Conservative assumption of no retardation | ** |
| constant | FractureRD_BFw_Se | Fracture retardation coefficient of Se for Bullfrog—welded (UZ) | 1.0 | Conservative assumption of no retardation | ** |

| Distribution Type | Parameter Name | Description | Parameter Range | Remarks | Provided by |
|---|---|---|---|---|---|
| constant | FractureRD_UFZ_Se | Fracture retardation coefficient of Se for Unsaturated Fracture Zone (UZ) | 1.0 | Conservative assumption of no retardation | ** |
| constant | FractureRD_TSw_Nb | Fracture retardation coefficient of Nb for Topopah Spring—welded (UZ) | 1.0 | Conservative assumption of no retardation | ** |
| constant | FractureRD_CHnvNb | Fracture retardation coefficient of Nb for Calico Hills—nonwelded vitric (UZ) | 1.0 | Conservative assumption of no retardation | ** |
| constant | FractureRD_CHnzNb | Fracture retardation coefficient of Nb for Calico Hills—nonwelded zeolitic (UZ) | 1.0 | Conservative assumption of no retardation | ** |
| constant | FractureRD_PPw_Nb | Fracture retardation coefficient of Nb for Prow Pass—welded (UZ) | 1.0 | Conservative assumption of no retardation | ** |
| constant | FractureRD_UCF_Nb | Fracture retardation coefficient of Nb for Upper Crater Flat (UZ) | 1.0 | Conservative assumption of no retardation | ** |
| constant | FractureRD_BFw_Nb | Fracture retardation coefficient of Nb for Bullfrog—welded (UZ) | 1.0 | Conservative assumption of no retardation | ** |

| Distribution Type | Parameter Name | Description | Parameter Range | Remarks | Provided by |
|---|---|---|---|---|---|
| constant | FractureRD_UFZ_Nb | Fracture retardation coefficient of Nb for Unsaturated Fracture Zone (UZ) | 1.0 | Conservative assumption of no retardation | ** |
| lognormal | MatrixPermeability_TSw_[m 2] | Matrix permeability for Topopah Spring tuff—welded (UZ) ($m^2$) | 0.2e-19, 0.2e-17 | Numbers based on statistical average of subunits in report by Flint (1998). Distribution assumed as being typical for permeability values. | RWF 2/25/00 |
| lognormal | MatrixPermeability_CHnv[m 2] | Matrix permeability for Calico Hills—nonwelded vitric (UZ) ($m^2$) | 0.2e-14, 0.2e-12 | Numbers based on statistical average of subunits in report by Flint (1998). Distribution assumed as being typical for permeability values. | RWF 2/25/00 |
| lognormal | MatrixPermeability_CHnz[m 2] | Matrix permeability for Calico Hills—nonwelded zeolitic (UZ) ($m^2$) | 0.5e-18, 0.5e-16 | Numbers based on statistical average of subunits in report by Flint (1998). Distribution assumed as being typical for permeability values. | RWF 2/25/00 |
| lognormal | MatrixPermeability_PPw_[m 2] | Matrix permeability for Prow Pass—welded (UZ) ($m^2$) | 0.1e-17, 0.1e-15 | Numbers based on statistical average of subunits in report by Flint (1998). Distribution assumed as being typical for permeability values. | RWF 2/25/00 |
| lognormal | MatrixPermeability_UCF_[m 2] | Matrix permeability for Upper Crater Flat (UZ) ($m^2$) | 0.3e-18, 0.3e-16 | Numbers based on statistical average of subunits in report by Flint (1998). Distribution assumed as being typical for permeability values. | RWF 2/25/00 |

| Distribution Type | Parameter Name | Description | Parameter Range | Remarks | Provided by |
|---|---|---|---|---|---|
| lognormal | MatrixPermeability_BFw_[m 2] | Matrix permeability for Bullfrog—welded (UZ) ($m^2$) | 0.2e-19, 0.2e-17 | Numbers based on statistical average of subunits in report by Flint (1998). Distribution assumed as being typical for permeability values. | RWF 2/25/00 |
| lognormal | MatrixPermeability_UFZ_[m 2] | Matrix permeability for Unsaturated Fault Zone (UZ) ($m^2$) | 1.8e-18, 2.1e-16 | Flint (1998). Current best estimate, but this should be further evaluated in the IRSR update for USFIC. | RWF 2/25/00 |
| constant | MatrixPorosity_TSw_ | Matrix porosity for Topopah Spring—welded (UZ) ($m^2$) | 0.12 | Numbers based on statistical average of subunits in report by Flint (1998). Constant values assumed due to small variability in data set. | RWF 2/25/00 |
| constant | MatrixPorosity_CHnv | Matrix porosity for Calico Hills—nonwelded vitric (UZ) | 0.33 | Numbers based on statistical average of subunits in report by Flint (1998). Constant values assumed due to small variability in data set. | RWF 2/25/00 |
| constant | MatrixPorosity_CHnz | Matrix porosity for Calico Hills—nonwelded zeolitic (UZ) | 0.32 | Numbers based on statistical average of subunits in report by Flint (1998). Constant values assumed due to small variability in data set. | RWF 2/25/00 |
| constant | MatrixPorosity_PPw_ | Matrix porosity for Prow Pass—welded (UZ) | 0.28 | Numbers based on statistical average of subunits in report by Flint (1998). Constant values assumed due to small variability in data set. | RWF 2/25/00 |

| Distribution Type | Parameter Name | Description | Parameter Range | Remarks | Provided by |
|---|---|---|---|---|---|
| constant | MatrixPorosity_UCF_ | Matrix porosity for Upper Crater Flat (UZ) | 0.28 | Numbers based on statistical average of subunits in report by Flint (1998). Constant values assumed due to small variability in data set. | RWF 2/25/00 |
| constant | MatrixPorosity_BFw_ | Matrix porosity for Bullfrog—welded (UZ) | 0.12 | Numbers based on statistical average of subunits in report by Flint (1998). Constant values assumed due to small variability in data set. | RWF 2/25/00 |
| constant | MatrixPorosity_UFZ_ | Matrix porosity for Unsaturated Fault Zone (UZ) | 0.12 | Flint (1996). Current best estimate, but this should be further evaluated in the IRSR update for USFIC. | RWF 2/25/00 |
| constant | MatrixBeta_TSw_ | van Genuchten beta parameter for Topopah Spring—welded (matrix) (UZ) | 1.5 | Current best estimate by USFIC team. Also see Flint (1998). | RWF 2/25/00 |
| constant | MatrixBeta_CHnv | van Genuchten beta parameter for Calico Hills—nonwelded vitric (matrix) (UZ) | 1.3 | Current best estimate by USFIC team. Also see Flint (1998). | RWF 2/25/00 |
| constant | MatrixBeta_CHnz | van Genuchten beta parameter for Calico Hills—nonwelded zeolitic (matrix) (UZ) | 2.3 | Current best estimate by USFIC team. Also see Flint (1998). | RWF 2/25/00 |
| constant | MatrixBeta_PPw_ | van Genuchten beta parameter for Prow | 1.5 | Current best estimate by USFIC team. Also see Flint (1998). | RWF 2/25/00 |

| Distribution Type | Parameter Name | Description | Parameter Range | Remarks | Provided by |
|---|---|---|---|---|---|
| | | Pass—welded (matrix) (UZ) | | | |
| constant | MatrixBeta_UCF_ | van Genuchten beta parameter for Upper Crater Flat (matrix) (UZ) | 1.4 | Current best estimate by USFIC team. Also see Flint (1998). | RWF 2/25/00 |
| constant | MatrixBeta_BFw_ | van Genuchten beta parameter for Bullfrog—welded (matrix) (UZ) | 1.7 | Current best estimate by USFIC team. Also see Flint (1998) | RWF 2/25/00 |
| constant | MatrixBeta_UFZ_ | van Genuchten beta parameter for Unsaturated Fault Zone (matrix) (UZ) | 2.3 | Current best estimate by USFIC team. Also see Flint (1998) | RWF 2/25/00 |
| constant | MatrixGrainDensity_TSw_[kg/m3] | Matrix grain density for Topopah Spring—welded (UZ) ($kg/m^3$) | 2460.0 | Best estimate by the USFIC team. Based on averaging of subunit data reported by Flint (1998). Constant values assumed due to little variation in reported data. | RWF 2/25/00 |
| constant | MatrixGrainDensity_CHnv[kg/m3] | Matrix grain density for Calico Hills—nonwelded vitric (UZ) ($kg/m^3$) | 2260.0 | Best estimate by the USFIC team. Based on averaging of subunit data reported by Flint (1998). Constant values assumed due to little variation in reported data. | RWF 2/25/00 |

| Distribution Type | Parameter Name | Description | Parameter Range | Remarks | Provided by |
|---|---|---|---|---|---|
| constant | MatrixGrainDensity_CHnz[kg/m3] | Matrix grain density for Calico Hills—nonwelded zeolitic (UZ) ($kg/m^3$) | 2400.0 | Best estimate by the USFIC team. Based on averaging of subunit data reported by Flint (1998). Constant values assumed due to little variation in reported data. | RWF 2/25/00 |
| constant | MatrixGrainDensity_PPw_[kg/m3] | Matrix grain density for Prow Pass—welded (UZ) ($kg/m^3$) | 2540.0 | Best estimate by the USFIC team. Based on averaging of subunit data reported by Flint (1998). Constant values assumed due to little variation in reported data. | RWF 2/25/00 |
| constant | MatrixGrainDensity_UCF_[kg/m3] | Matrix grain density for Upper Crater Flat (UZ) ($kg/m^3$) | 2420.0 | Best estimate by the USFIC team. Based on averaging of subunit data reported by Flint (1998). Constant values assumed due to little variation in reported data. | 2/25/00 |
| constant | MatrixGrainDensity_BFw_[kg/m3] | Matrix grain density for Bullfrog—welded (UZ) ($kg/m^3$) | 2570.0 | Best estimate by the USFIC team. Based on averaging of subunit data reported by Flint (1998). Constant values assumed due to little variation in reported data. | RWF 2/25/00 |
| constant | MatrixGrainDensity_UFZ_[kg/m3] | Matrix grain density for Unsaturated Fault Zone (UZ) ($kg/m^3$) | 2630.0 | Best estimate by the USFIC team. Based on averaging of subunit data reported by Flint | RWF 2/25/00 |

| Distribution Type | Parameter Name | Description | Parameter Range | Remarks | Provided by |
|---|---|---|---|---|---|
| | | | | (1998). Constant values assumed due to little variation in reported data. | |
| lognormal | FracturePermeability_TSw_[m2] | Fracture permeability Topopah Spring—welded ($m^2$) (UZ) | 8.0e-15, 8.0e-11 | Current best estimate by the USFIC team based on Schenker et al. (1995) | RWF 2/25/00 |
| lognormal | FracturePermeability_CHnv[m2] | Calico Hills—nonwelded vitric fracture permeability ($m^2$) (UZ) | 8.0e-15, 8.0e-11 | Current best estimate by the USFIC team based on Schenker et al. (1995) | RWF 2/25/00 |
| lognormal | FracturePermeability_CHnz[m2] | Calico Hills—nonwelded zeolitic fracture permeability ($m^2$) (UZ) | 6.0e-15, 6.0e-11 | Current best estimate by the USFIC team based on Schenker et al. (1995) | RWF 2/25/00 |
| lognormal | FracturePermeability_PPw_[m2] | Prow Pass—welded fracture permeability ($m^2$) (UZ) | 6.0e-15, 6.0e-11 | Current best estimate by the USFIC based on Klavetter and Peters (1986) and Nuclear Regulatory Commission (1995) | RWF 2/25/00 |
| lognormal | FracturePermeability_UCF_[m2] | Upper Crater Flat fracture permeability ($m^2$) (UZ) | 6.0e-15, 6.0e-11 | Current best estimate by the USFIC based on Klavetter and Peters (1986) and Nuclear Regulatory Commission (1995) | RWF 2/25/00 |
| lognormal | FracturePermeability_BFw_[m2] | Bullfrog—welded fracture permeability ($m^2$) (UZ) | 3.0e-15, 3.0e-11 | Current best estimate by the USFIC team based on Klavetter and Peters (1986) and Nuclear Regulatory Commission (1995) | RWF 2/25/00 |

| Distribution Type | Parameter Name | Description | Parameter Range | Remarks | Provided by |
|---|---|---|---|---|---|
| lognormal | FracturePermeability_UFZ_[ m2] | Unsaturated Fracture Zone fracture permeability ($m^2$) (UZ) | 1.0e-13, 1.0e-11 | Current best estimate by the USFIC team based on Klavetter and Peters (1986) and Nuclear Regulatory Commission (1995) | RWF 2/25/00 |
| loguniform | FracturePorosity_TSw_ | Fracture porosity Topopah Spring—welded (UZ) | 1.0e-3, 1.0e-2 | Current best estimate based on CRWMS M&O (1999b). | RWF 2/25/00 |
| loguniform | FracturePorosity_CHnv | Calico Hills—nonwelded vitric fracture porosity (UZ) | 1.0e-4, 1.0e-3 | Current best estimate based on CRWMS M&O (1999b). | RWF 2/25/00 |
| loguniform | FracturePorosity_CHnz | Calico Hills—nonwelded zeolitic fracture porosity (UZ) | 1.0e-3, 1.0e-2 | Current best estimate based on CRWMS M&O (1999b). | RWF 2/25/00 |
| loguniform | FracturePorosity_PPw_ | Prow Pass—welded fracture porosity (UZ) | 1.0e-3, 1.0e-2 | Current best estimate based on CRWMS M&O (1999b). | RWF 2/25/00 |
| loguniform | FracturePorosity_UCF_ | Upper Crater Flat fracture porosity (UZ) | 1.0e-3, 1.0e-2 | Current best estimate based on CRWMS M&O (1999b). | RWF 2/25/00 |
| loguniform | FracturePorosity_BFw_ | Bullfrog—welded fracture porosity (UZ) | 1.0e-3, 1.0e-2 | Current best estimate based on CRWMS M&O (1999b). | RWF 2/25/00 |
| loguniform | FracturePorosity_UFZ_ | Unsaturated Fault Zone fracture porosity (UZ) | 1.0e-3, 1.0e-2 | Current best estimate based on CRWMS M&O (1999b). | RWF 2/25/00 |
| constant | FractureBeta_TSw_ | van Genuchten beta parameter for Topopah Spring—welded (UZ) | 2.0 | Best estimate based on calibrations reported in TRW Environmental Safety Systems, Inc. 1998 | RWF 2/25/00 |

| Distribution Type | Parameter Name | Description | Parameter Range | Remarks | Provided by |
|---|---|---|---|---|---|
| constant | FractureBeta_CHnv | van Genuchten beta parameter for Calico Hills—nonwelded vitric (UZ) | 2.0 | Best estimate based on calibrations reported in TRW Environmental Safety Systems, Inc. 1998 | RWF 2/25/00 |
| constant | FractureBeta_CHnz | van Genuchten beta parameter for Calico Hills—nonwelded zeolitic (UZ) | 2.0 | Best estimate based on calibrations reported in TRW Environmental Safety Systems, Inc. 1998 | RWF 2/25/00 |
| constant | FractureBeta_PPw_ | van Genuchten beta parameter for Prow Pass—welded (UZ) | 2.0 | Best estimate based on calibrations reported in TRW Environmental Safety Systems, Inc. 1998 | RWF 2/25/00 |
| constant | FractureBeta_UCF_ | van Genuchten beta parameter for Upper Crater Flat (UZ) | 2.0 | Best estimate based on calibrations reported in TRW Environmental Safety Systems, Inc. 1998 | RWF 2/25/00 |
| constant | FractureBeta_BFw_ | van Genuchten beta parameter for Bullfrog—welded (UZ) | 2.0 | Best estimate based on calibrations reported in TRW Environmental Safety Systems, Inc. 1998 | RWF 2/25/00 |
| constant | FractureBeta_UFZ_ | van Genuchten beta parameter for Unsaturated Fault Zone (UZ) | 1.6 | Best estimate based on calibrations reported in TRW Environmental Safety Systems, Inc. 1998. | RWF 2/25/00 |
| constant | InletArea__1SubArea[m2] | Inlet area ($m^2$) - subarea 1 (UZ) (not used) | 5.4e5 | Not used. CNWRA staff best estimate. | ** |

| Distribution Type | Parameter Name | Description | Parameter Range | Remarks | Provided by |
|---|---|---|---|---|---|
| constant | InletArea__2SubArea[m2] | Inlet area ($m^2$) - subarea 2 (UZ) (not used) | 5.4e5 | Not used. CNWRA staff best estimate. | ** |
| constant | InletArea__3SubArea[m2] | Inlet area ($m^2$) - subarea 3 (UZ) (not used) | 5.4e5 | Not used. CNWRA staff best estimate. | ** |
| constant | InletArea__4SubArea[m2] | Inlet area ($m^2$) - subarea 4 (UZ) (not used) | 5.4e5 | Not used. CNWRA staff best estimate. | ** |
| constant | InletArea__5SubArea[m2] | Inlet area ($m^2$) - subarea 5 (UZ) (not used) | 5.4e5 | Not used. CNWRA staff best estimate. | ** |
| constant | InletArea__6SubArea[m2] | Inlet area ($m^2$) - subarea 6 (UZ) (not used) | 5.4e5 | Not used. CNWRA staff best estimate. | ** |
| constant | InletArea__7SubArea[m2] | Inlet area ($m^2$) - subarea 7 (UZ) (not used) | 5.4e5 | Not used. CNWRA staff best estimate. | ** |
| constant | InletArea__8SubArea[m2] | Inlet area ($m^2$) - subarea 8 (UZ) (not used) | 5.4e5 | Not used. CNWRA staff best estimate. | ** |
| constant | TSw_Thickness_1SubArea[m] | Topopah Spring—welded thickness Subarea1 (m) (UZ) | 100 | Derived directly from the Geological Framework Model 3.1 (GFM 3.1) (CRWMS M&O, 1999c), EDA II design, and current best estimate of water table map | RWF 2/9/00 |
| constant | CHnvThickness_1SubArea[m] | Subarea1 Calico Hills—nonwelded vitric thickness (m) (UZ) | 19.00 | Current best estimate by Unsaturated and Saturated Flow under Isothermal Conditions (USFIC) team [see Winterle et al. (1999a, b) for methodology] | RWF 2/9/00 |

| Distribution Type | Parameter Name | Description | Parameter Range | Remarks | Provided by |
|---|---|---|---|---|---|
| constant | CHnzThickness_1SubArea[m] | Subarea1 Calico Hills—nonwelded zeolitic thickness (m) (UZ) | 72 | Current best estimate by USFIC team [see Winterle et al. (1999a,b) for methodology] | RWF 2/9/00 |
| constant | PPw_Thickness_1SubArea[m] | Subarea1 Prow Pass—welded thickness (m) (UZ) | 50 | Derived directly from the GFM 3.1 (CRWMS M&O, 1999c), EDA II design, and current best estimate of water table map | RWF 2/9/00 |
| constant | UCF_Thickness_1SubArea[m] | Subarea1 Upper Crater Flat thickness (m) (UZ) | 57 | Derived directly from the GFM 3.1 (CRWMS M&O, 1999c), EDA II design, and current best estimate of water table map | RWF 2/9/00 |
| constant | BFw_Thickness_1SubArea[m] | Subarea1 Bullfrog—welded thickness (m) (UZ) | 22.00 | Derived directly from the GFM 3.1 (CRWMS M&O, 1999c), EDA II design, and current best estimate of water table map | RWF 2/9/00 |
| constant | UFZ_Thickness_1SubArea[m] | Subarea1 Unsaturated Fracture Zone thickness (m) (UZ) | 0.00 | Derived directly from the GFM 3.1 (CRWMS M&O, 1999c), EDA II design, and current best estimate of water table map | RWF 2/9/00 |
| constant | TSw_Thickness_2SubArea[m] | Subarea2 Topopah Spring—welded thickness (m) (UZ) | 161 | Derived directly from the GFM 3.1 (CRWMS M&O, 1999c), EDA II design, and current best estimate of water table map | RWF 2/9/00 |
| constant | CHnvThickness_2SubArea[m] | Subarea2 Calico Hills—nonwelded vitric thickness (m) (UZ) | 0.00 | Current best estimate by USFIC team [see Winterle et al. (1999a,b) for methodology] | RWF TJM 10/30/00 |

| Distribution Type | Parameter Name | Description | Parameter Range | Remarks | Provided by |
|---|---|---|---|---|---|
| constant | CHnzThickness_2SubArea[m ] | Subarea2 Calico Hills—nonwelded zeolitic thickness (m) (UZ) | 108 | Current best estimate by USFIC team [see Winterle et al. (1999a,b) for methodology] | RWF 2/9/00 |
| constant | PPw_Thickness_2SubArea[m ] | Subarea2 Prow Pass—welded thickness (m) (UZ) | 50 | Derived directly from the GFM 3.1 (CRWMS M&O, 1999c), EDA II design, and current best estimate of water table map. | RWF 2/9/00 |
| constant | UCF_Thickness_2SubArea[m ] | Subarea2 Upper Crater Flat thickness (m) (UZ) | 18 | Derived directly from the GFM 3.1 (CRWMS M&O, 1999c), EDA II design, and current best estimate of water table map | RWF 2/9/00 |
| constant | BFw_Thickness_2SubArea[m ] | Subarea2 Bullfrog—welded thickness (m) (UZ) | 0.00 | Derived directly from the GFM 3.1 (CRWMS M&O, 1999c), EDA II design, and current best estimate of water table map | RWF 2/9/00 |
| constant | UFZ_Thickness_2SubArea[m ] | Subarea2 Unsaturated Fracture Zone thickness (m) (UZ) | 0.00 | Derived directly from the GFM 3.1 (CRWMS M&O, 1999c), EDA II design, and current best estimate of water table map | RWF 2/9/00 |
| constant | TSw_Thickness_3SubArea[m ] | Subarea3 Topopah Spring—welded thickness (m) (UZ) | 79 | Derived directly from the GFM 3.1 (CRWMS M&O, 1999c), EDA II design, and current best estimate of water table map | RWF 2/9/00 |
| constant | CHnvThickness_3SubArea[m ] | Subarea3 Calico Hills—nonwelded vitric thickness (m) (UZ) | 24.00 | Current best estimate by USFIC team [see Winterle et al. (1999a,b) for methodology] | RWF 2/9/00 |

| Distribution Type | Parameter Name | Description | Parameter Range | Remarks | Provided by |
|---|---|---|---|---|---|
| constant | CHnzThickness_3SubArea[m] | Subarea3 Calico Hills—nonwelded zeolitic thickness (m) (UZ) | 55 | Current best estimate by USFIC team [see Winterle et al. (1999a,b) for methodology] | RWF 2/9/00 |
| constant | UCF_Thickness_3SubArea[m] | Subarea3 Upper Crater Flat thickness (m) (UZ) | 68 | Derived directly from the GFM 3.1 (CRWMS M&O, 1999c), EDA II design, and current best estimate of water table map | RWF 2/9/00 |
| constant | BFw_Thickness_3SubArea[m] | Subarea3 Bullfrog—welded thickness (m) (UZ) | 81.00 | Derived directly from the GFM 3.1 (CRWMS M&O, 1999c), EDA II design, and current best estimate of water table map | RWF 2/9/00 |
| constant | UFZ_Thickness_3SubArea[m] | Subarea3 Unsaturated Fracture Zone thickness (m) (UZ) | 0.00 | Derived directly from the GFM 3.1 (CRWMS M&O, 1999c), EDA II design, and current best estimate of water table map | RWF 2/9/00 |
| constant | TSw_Thickness_4SubArea[m] | Subarea4 Topopah Spring—welded thickness (m) (UZ) | 144 | Derived directly from the GFM 3.1 (CRWMS M&O, 1999c), EDA II design, and current best estimate of water table map | RWF 2/9/00 |
| constant | CHnvThickness_4SubArea[m] | Subarea4 Calico Hills—nonwelded vitric thickness (m) (UZ) | 17.00 | Current best estimate by USFIC team [see Winterle et al. (1999a,b) for methodology] | RWF 2/9/00 |
| constant | CHnzThickness_4SubArea[m] | Subarea4 Calico Hills—nonwelded zeolitic thickness (m) (UZ) | 88 | Current best estimate by USFIC team [see Winterle et al. (1999a,b) for methodology] | RWF 2/9/00 |

| Distribution Type | Parameter Name | Description | Parameter Range | Remarks | Provided by |
|---|---|---|---|---|---|
| constant | PPw_Thickness_4SubArea[m] | Subarea4 Prow Pass—welded thickness (m) (UZ) | 56 | Derived directly from the GFM 3.1 (CRWMS M&O, 1999), EDA II design, and current best estimate of water table map | RWF 2/9/00 |
| constant | UCF_Thickness_4SubArea[m] | Subarea4 Upper Crater Flat thickness (m) (UZ) | 61 | Derived directly from the GFM 3.1 (CRWMS M&O, 1999c), EDA II design, and current best estimate of water table map | RWF 2/9/00 |
| constant | BFw_Thickness_4SubArea[m] | Subarea4 Bullfrog—welded thickness (m) (UZ) | 0.00 | Derived directly from the GFM 3.1 (CRWMS M&O, 1999c), EDA II design, and current best estimate of water table map | RWF 2/9/00 |
| constant | UFZ_Thickness_4SubArea[m] | Subarea4 Unsaturated Fracture Zone thickness (m) (UZ) | 0.00 | Derived directly from the GFM 3.1 (CRWMS M&O, 1999c), EDA II design, and current best estimate of water table map | RWF 2/9/00 |
| constant | TSw_Thickness_5SubArea[m] | Subarea5 Topopah Spring—welded thickness (m) (UZ) | 58 | Derived directly from the GFM 3.1 (CRWMS M&O, 1999c), EDA II design, and current best estimate of water table map | RWF 2/9/00 |
| constant | CHnvThickness_5SubArea[m] | Subarea5 Calico Hills—nonwelded vitric thickness (m) (UZ) | 31 | Current best estimate by USFIC team [see Winterle et al. (1999a,b) for methodology] | RWF 2/9/00 |
| constant | CHnzThickness_5SubArea[m] | Subarea5 Calico Hills—nonwelded zeolitic thickness (m) (UZ) | 49 | Current best estimate by USFIC team [see Winterle et al. (1999a,b) for methodology] | RWF 2/9/00 |

| Distribution Type | Parameter Name | Description | Parameter Range | Remarks | Provided by |
|---|---|---|---|---|---|
| constant | PPw_Thickness_5SubArea[m] | Subarea5 Prow Pass—welded thickness (m) (UZ) | 65 | Derived directly from the GFM 3.1 (CRWMS M&O, 1999c), EDA II design, and current best estimate of water table map | RWF 2/9/00 |
| constant | UCF_Thickness_5SubArea[m] | Subarea5 Upper Crater Flat thickness (m) (UZ) | 71 | Derived directly from the GFM 3.1 (CRWMS M&O, 1999c), EDA II design, and current best estimate of water table map | RWF 2/9/00 |
| constant | BFw_Thickness_5SubArea[m] | Subarea5 Bullfrog—welded thickness (m) (UZ) | 101 | Derived directly from the GFM 3.1 (CRWMS M&O, 1999c), EDA II design, and current best estimate of water table map | RWF 2/9/00 |
| constant | UFZ_Thickness_5SubArea[m] | Subarea5 Unsaturated Fracture Zone thickness (m) (UZ) | 0.00 | Derived directly from the GFM 3.1 (CRWMS M&O, 1999c), EDA II design, and current best estimate of water table map | RWF 2/9/00 |
| constant | TSw_Thickness_6SubArea[m] | Subarea6 Topopah Spring—welded thickness (m) (UZ) | 58 | Derived directly from the GFM 3.1 (CRWMS M&O, 1999c), EDA II design, and current best estimate of water table map | RWF 2/9/00 |
| constant | CHnvThickness_6SubArea[m] | Subarea6 Calico Hills—nonwelded vitric thickness (m) (UZ) | 37 | Current best estimate by USFIC team [see Winterle et al. (1999a,b) for methodology] | RWF 2/9/00 |
| constant | CHnzThickness_6SubArea[m] | Subarea6 Calico Hills—nonwelded zeolitic thickness (m) (UZ) | 58 | Current best estimate by USFIC team [see Winterle et al. (1999a,b) for methodology] | RWF 2/9/00 |

| Distribution Type | Parameter Name | Description | Parameter Range | Remarks | Provided by |
|---|---|---|---|---|---|
| constant | PPw_Thickness_6SubArea[m ] | Subarea6 Prow Pass—welded thickness (m) (UZ) | 66 | Derived directly from the GFM 3.1 (CRWMS M&O, 1999c), EDA II design, and current best estimate of water table map | RWF 2/9/00 |
| constant | UCF_Thickness_6SubArea[m ] | Subarea6 Upper Crater Flat thickness (m) (UZ) | 81 | Derived directly from the GFM 3.1 (CRWMS M&O, 1999c), EDA II design, and current best estimate of water table map | RWF 2/9/00 |
| constant | BFw_Thickness_6SubArea[m ] | Subarea6 Bullfrog—welded thickness (m) (UZ) | 51.00 | Derived directly from the GFM 3.1 (CRWMS M&O, 1999c), EDA II design, and current best estimate of water table map | RWF 2/9/00 |
| constant | UFZ_Thickness_6SubArea[m ] | Subarea6 Unsaturated Fracture Zone thickness (m) (UZ) | 0.00 | Derived directly from the GFM 3.1 (CRWMS M&O, 1999c), EDA II design, and current best estimate of water table map | RWF 2/9/00 |
| constant | TSw_Thickness_7SubArea[m ] | Subarea7 Topopah Spring—welded thickness (m) (UZ) | 138 | Derived directly from the GFM 3.1 (CRWMS M&O, 1999c), EDA II design, and current best estimate of water table map | RWF 2/9/00 |
| constant | CHnvThickness_7SubArea[m ] | Subarea7 Calico Hills—nonwelded vitric thickness (m) (UZ) | 44.00 | Current best estimate by USFIC team [see Winterle et al. (1999a,b) for methodology] | RWF 2/9/00 |
| constant | CHnzThickness_7SubArea[m ] | Subarea7 Calico Hills—nonwelded zeolitic thickness (m) (UZ) | 63 | Current best estimate by USFIC team [see Winterle et al. (1999a,b) for methodology] | RWF 2/9/00 |

| Distribution Type | Parameter Name | Description | Parameter Range | Remarks | Provided by |
|---|---|---|---|---|---|
| constant | PPw_Thickness_7SubArea[m] | Subarea7 Prow Pass—welded thickness (m) (UZ) | 66 | Derived directly from the GFM 3.1 (CRWMS M&O, 1999c), EDA II design, and current best estimate of water table map | RWF 2/9/00 |
| constant | UCF_Thickness_7SubArea[m] | Subarea7 Upper Crater Flat thickness (m) (UZ) | 67 | Derived directly from the GFM 3.1 (CRWMS M&O, 1999c), EDA II design, and current best estimate of water table map | RWF 2/9/00 |
| constant | BFw_Thickness_7SubArea[m] | Subarea7 Bullfrog—welded thickness (m) (UZ) | 0.00 | Derived directly from the GFM 3.1 (CRWMS M&O, 1999c), EDA II design, and current best estimate of water table map | RWF 2/9/00 |
| constant | UFZ_Thickness_7SubArea[m] | Subarea7 Unsaturated Fracture Zone thickness (m) (UZ) | 0.00 | Derived directly from the GFM 3.1 (CRWMS M&O, 1999c), EDA II design, and current best estimate of water table map | RWF 2/9/00 |
| constant | TSw_Thickness_8SubArea[m] | Subarea8 Topopah Spring—welded thickness (m) (UZ) | 163 | Derived directly from the GFM 3.1 (CRWMS M&O, 1999c), EDA II design, and current best estimate of water table map | RWF 2/9/00 |
| constant | CHnvThickness_8SubArea[m] | Subarea8 Calico Hills—nonwelded vitric thickness (m) (UZ) | 0 | Current best estimate by USFIC team [see Winterle et al. (1999a,b) for methodology] | RWF 2/9/00 |
| constant | CHnzThickness_8SubArea[m] | Subarea8 Calico Hills—nonwelded zeolitic thickness (m) (UZ) | 120 | Current best estimate by USFIC team [see Winterle et al. (1999a,b) for methodology] | RWF 2/9/00 |

| Distribution Type | Parameter Name | Description | Parameter Range | Remarks | Provided by |
|---|---|---|---|---|---|
| constant | PPw_Thickness_8SubArea[m] | Subarea8 Prow Pass—welded thickness (m) (UZ) | 25 | Derived directly from the GFM 3.1 (CRWMS M&O, 1999c), EDA II design, and current best estimate of water table map | RWF 2/9/00 |
| constant | UCF_Thickness_8SubArea[m] | Subarea8 Upper Crater Flat thickness (m) (UZ) | 0 | Derived directly from the GFM 3.1 (CRWMS M&O, 1999c), EDA II design, and current best estimate of water table map | RWF 2/9/00 |
| constant | BFw_Thickness_8SubArea[m] | Subarea8 Bullfrog—welded thickness (m) (UZ) | 0 | Derived directly from the GFM 3.1 (CRWMS M&O, 1999c), EDA II design, and current best estimate of water table map | RWF 2/9/00 |
| constant | UFZ_Thickness_8SubArea[m] | Subarea8 Unsaturated Fracture Zone thickness (m) (UZ) | 0 | Derived directly from the GFM 3.1 (CRWMS M&O, 1999c), EDA II design, and current best estimate of water table map | RWF 2/9/00 |
| ** **  ***>>> SZFT <<<*** **FileOpen (Filename: "D:\WPFIL\S.Mohanty\REPORTS\TPA 4.0 October 2000\appendix a.wpd") | | | | | |
| loguniform | ImmobilePorosityPenetration Fraction_STFF | Effective fraction of saturated rock matrix accessible to matrix diffusion during the time scale for transport from source to receptor, used to calculate effective | 0.01, 0.1 | CNWRA best estimate, considering uncertainty in pore velocity and effective diffusion rates<br>Basis described in chapter 10 | JRW TJM 2/25/00 |

| Distribution Type | Parameter Name | Description | Parameter Range | Remarks | Provided by |
|---|---|---|---|---|---|
| | | immobile porosity and the matrix diffusion mass-transfer rate coefficient in NEFTRAN | | | |
| constant | FracturesPerMeter_STFF[1/m] | Effective spacing between transmissive zones in the tuff aquifer, used to calculate the matrix diffusion mass-transfer rate coefficient in NEFTRAN II | 0.05 | CNWRA current best estimate, based on assumed transmissive interval spacing of 20 m (see Winterle et al., 2000) | JRW TJM 2/25/00 |
| constant | MixingZoneDispersionFraction | Dispersion fraction of the mixing zone (SZ) - longitudinal dispersion specified as a fraction of the path length | 0.01 | CNWRA best estimate. Assumed to be conservative. | ** |
| constant | DispersionFraction_STFF | Dispersion fraction of tuff (SZ) - longitudinal dispersion specified as a fraction of the path length | 0.01 | CNWRA best estimate. Assumed to be conservative. | ** |
| constant | DispersionFraction_SAV | Dispersion fraction of Amargosa Valley (SZ) - longitudinal dispersion specified as a fraction of the path length | 0.1 | de Marsily (1986) citing work of Lallemand-Barrés and Peaudcerf (1978) | ** |

| Distribution Type | Parameter Name | Description | Parameter Range | Remarks | Provided by |
|---|---|---|---|---|---|
| constant | MinimumResidenceTime_STFF[yr] | Minimum residence time in tuff (SZ) (yr) | 10.0 | Value selected for code efficiency reasons | ** |
| constant | MinimumResidenceTime_SAV[yr] | Minimum residence time in alluvium (SZ) (yr) | 10.0 | Value selected for code efficiency reasons | ** |
| constant | FractureRD_STFF_Am | Fracture retardation coefficient of tuff for Am (SZ) | 1.0 | Conservative assumption of no retardation | ** |
| lognormal | AlluviumMatrixRD_SAV_Am | Alluvium retardation coefficient for Am (SZ) | 7.5e4, 6.8e10 | CNWRA best estimate for $K_d$s. RD computed with porosity = 0.125 and grain density= 2470 kg/m$^3$. | ** |
| constant | FractureRD_STFF_Np | Fracture retardation coefficient of tuff for Np (SZ) | 1.0 | Conservative assumption of no retardation | ** |
| lognormal | AlluviumMatrixRD_SAV_Np | Alluvium retardation coefficient for Np (SZ) | 1.0, 3.9e3 | CNWRA best estimate for $K_d$s. RD computed with porosity = 0.125 and grain density= 2470 kg/m$^3$. | ** |
| constant | FractureRD_STFF_I | Fracture retardation coefficient of tuff for I (SZ) | 1.0 | Conservative assumption of no retardation | ** |
| loguniform | AlluviumMatrixRD_SAV_I | Alluvium retardation coefficient for I (SZ) | 1.0, 4.0 | Daniels, 1981 | ** |
| constant | FractureRD_STFF_Tc | Fracture retardation coefficient of tuff for Tc (SZ) | 1.0 | Conservative assumption of no retardation | ** |

| Distribution Type | Parameter Name | Description | Parameter Range | Remarks | Provided by |
|---|---|---|---|---|---|
| loguniform | AlluviumMatrixRD_SAV_Tc | Alluvium retardation coefficient for Tc (SZ) | 1.0, 30.0 | Meijer, 1990; crushed tuff analog | ** |
| constant | FractureRD_STFF_Cl | Fracture retardation coefficient of tuff for Cl (SZ) | 1.0 | Conservative assumption of no retardation | ** |
| constant | AlluviumMatrixRD_SAV_Cl | Alluvium retardation coefficient for Cl (SZ) | 1.0 | Conservative assumption of no retardation | ** |
| constant | FractureRD_STFF_Cm | Fracture retardation coefficient of tuff for Cm (SZ) | 1.0 | Conservative assumption of no retardation | ** |
| constant | AlluviumMatrixRD_SAV_Cm | Alluvium retardation coefficient for Cm (SZ) | 7.5e4 | Assumed equal to the lower bound for the Am alluvium $R_d$ | ** |
| constant | FractureRD_STFF_U | Fracture retardation coefficient of tuff for U (SZ) | 1.0 | Conservative assumption of no retardation | ** |
| lognormal | AlluviumMatrixRD_SAV_U | Alluvium retardation coefficient for U (SZ) | 1.0, 1.9e4 | CNWRA best estimate for $K_d$s. RD computed with porosity = 0.125 and grain density= 2470 kg/m$^3$ | ** |
| constant | FractureRD_STFF_Pu | Fracture retardation coefficient of tuff for Pu (SZ) | 1.0 | Conservative assumption of no retardation | ** |
| lognormal | AlluviumMatrixRD_SAV_Pu | Alluvium retardation coefficient for Pu (SZ) | 4.2e2, 3.9e5 | CNWRA best estimate for $K_d$s. RD computed with porosity = 0.125 and grain density= 2470 kg/m$^3$ | ** |

| Distribution Type | Parameter Name | Description | Parameter Range | Remarks | Provided by |
|---|---|---|---|---|---|
| constant | FractureRD_STFF_Th | Fracture retardation coefficient of tuff for Th (SZ) | 1.0 | Conservative assumption of no retardation | ** |
| lognormal | AlluviumMatrixRD_SAV_Th | Alluvium retardation coefficient for Th (SZ) | 1.9, 4.5e7 | CNWRA best estimate for $K_d$s. RD computed with porosity = 0.125 and grain density= 2470 kg/m$^3$ | ** |
| constant | FractureRD_STFF_Ra | Fracture retardation coefficient of tuff for Ra (SZ) | 1.0 | Conservative assumption of no retardation | ** |
| loguniform | AlluviumMatrixRD_SAV_Ra | Alluvium retardation coefficient for Ra (SZ) | 2.0e3, 8.0e3 | Triay et al., 1997; crushed tuff analog | ** |
| constant | FractureRD_STFF_Pb | Fracture retardation coefficient of tuff for Pb (SZ) | 1.0 | Conservative assumption of no retardation | ** |
| loguniform | AlluviumMatrixRD_SAV_Pb | Alluvium retardation coefficient for Pb (SZ) | 2.0e3, 8.0e3 | Triay et al., 1997; crushed tuff analog | ** |
| constant | FractureRD_STFF_Cs | Fracture retardation coefficient of tuff for Cs (SZ) | 1.0 | Conservative assumption of no retardation | ** |
| loguniform | AlluviumMatrixRD_SAV_Cs | Alluvium retardation coefficient for Cs (SZ) | 9.0e4, 1.0e5 | Wolfsberg, 1978 | ** |
| constant | FractureRD_STFF_Ni | Fracture retardation coefficient of tuff for Ni (SZ) | 1.0 | Conservative assumption of no retardation | ** |

| Distribution Type | Parameter Name | Description | Parameter Range | Remarks | Provided by |
|---|---|---|---|---|---|
| loguniform | AlluviumMatrixRD_SAV_Ni | Alluvium retardation coefficient for Ni (SZ) | 1.0, 8.0e3 | Triay et al., 1997; crushed tuff analog | ** |
| constant | FractureRD_STFF_C | Fracture retardation coefficient of tuff for C (SZ) | 1.0 | Conservative assumption of no retardation | ** |
| constant | AlluviumMatrixRD_SAV_C | Alluvium retardation coefficient for C (SZ) | 1.0 | Conservative assumption of no retardation | ** |
| constant | FractureRD_STFF_Se | Fracture retardation coefficient of tuff for Se (SZ) | 1.0 | Conservative assumption of no retardation | ** |
| loguniform | AlluviumMatrixRD_SAV_Se | Alluvium retardation coefficient for Se (SZ) | 1.0, 500.0 | Triay et al., 1997; crushed devitrified tuff analog | ** |
| constant | FractureRD_STFF_Nb | Fracture retardation coefficient of tuff for Nb (SZ) | 1.0 | Conservative assumption of no retardation | ** |
| loguniform | AlluviumMatrixRD_SAV_Nb | Alluvium retardation coefficient for Nb (SZ) | 2.0e3, 3.0e4 | Triay et al., 1997; crushed devitrified tuff analog | ** |
| loguniform | FracturePorosity_STFF | Effective fracture porosity of the saturated tuff (i.e. volume fraction through which the bulk of flow occurs) | 1.0e-3, 1.0e-2 | CNWRA current best estimate (CNWRA Letter Report—Porosity at YM, in prep.) | JW 2/25/00 |
| uniform | AlluviumMatrixPorosity_SAV | Alluvium effective porosity of Amargosa Valley alluvium | 1.0e-1, 1.5e-1 | Best estimate by USFIC team (Walker and Eakin, 1963; Fischer, 1992) | DAF 3/6/00 |

| Distribution Type | Parameter Name | Description | Parameter Range | Remarks | Provided by |
|---|---|---|---|---|---|
| constant | ImmobileRD_STFF_Am | Retardation factor for Am in matrix during matrix diffusion | 1.8e4 | Triay et al., 1997 | ** |
| constant | ImmobileRD_STFF_Np | Retardation factor for Np in matrix during matrix diffusion | 19.0 | Triay et al., 1997 | ** |
| constant | ImmobileRD_STFF_I | Retardation factor for I in matrix during matrix diffusion | 1.0 | Triay et al., 1997 | ** |
| constant | ImmobileRD_STFF_Tc | Retardation factor for Tc in matrix during matrix diffusion | 1.0 | Triay et al., 1997 | ** |
| constant | ImmobileRD_STFF_Cl | Retardation factor for Cl in matrix during matrix diffusion | 1.0 | Triay et al, 1997 | ** |
| constant | ImmobileRD_STFF_Cm | Retardation factor for Cm in matrix during matrix diffusion | 1.8e4 | Assumed equal to the Am immobile $R_d$ | ** |
| constant | ImmobileRD_STFF_U | Retardation factor for U in matrix during matrix diffusion | 37.0 | Triay et al., 1997 | ** |
| constant | ImmobileRD_STFF_Pu | Retardation factor for Pu in matrix during matrix diffusion | 1.8e3 | Triay et al., 1997 | ** |
| constant | ImmobileRD_STFF_Th | Retardation factor for Th in matrix during matrix diffusion | 1.8e4 | Triay et al., 1997 | ** |

| Distribution Type | Parameter Name | Description | Parameter Range | Remarks | Provided by |
|---|---|---|---|---|---|
| constant | ImmobileRD_STFF_Ra | Retardation factor for Ra in matrix during matrix diffusion | 5.4e3 | Triay et al., 1997 | ** |
| constant | ImmobileRD_STFF_Pb | Retardation factor for Pb in matrix during matrix diffusion | 5.4e3 | Triay et al., 1997 | ** |
| constant | ImmobileRD_STFF_Cs | Retardation factor for Cs in matrix during matrix diffusion | 9.0e3 | Triay et al., 1997 | ** |
| constant | ImmobileRD_STFF_Ni | Retardation factor for Ni in matrix during matrix diffusion | 1.8e3 | Triay et al., 1997 | ** |
| constant | ImmobileRD_STFF_C | Retardation factor for C in matrix during matrix diffusion | 1.0 | Triay et al., 1997 | ** |
| constant | ImmobileRD_STFF_Se | Retardation factor for Se in matrix during matrix diffusion | 55.0 | Triay et al., 1997 | ** |
| constant | ImmobileRD_STFF_Nb | Retardation factor for Nb in matrix during matrix diffusion | 1.8e4 | Triay et al., 1997 | ** |
| constant | ImmobilePorosity_STFF | Matrix porosity in saturated tuff | 0.2 | CNWRA current best estimate (CNWRA Letter Report—Porosity at YM, in prep.) | JW 2/29/00 |

| Distribution Type | Parameter Name | Description | Parameter Range | Remarks | Provided by |
|---|---|---|---|---|---|
| constant | DiffusionRate_STFF | Effective diffusion coefficient in saturated tuff ($m^2$/yr) | 1e-3 | Diffusion coefficient reported for $TCO_4$ anion by Triay et al. (1997) | JW 2/25/00 |
| uniform | DistanceToTuffAlluviumInterface[km] | Distance traveled in Tuff | 5.0, 20.0 | Currently based on estimates derived from CNWRA's geologic framework model [Sims et al., 1999] | DAF 2/25/00 |
| ** ** ** ***>>> DCAGW <<<*** ** | | | | | |
| constant | DistanceToReceptorGroup[km][should_be_10_or_20] | Distance to receptor group (km) | 20.0 | Farming is assumed to occur at a distance 20 km or greater at YM. | ** |
| uniform | WellPumpingRateAtReceptorGroup10km[gal/day] | Well pumping rate for residential receptor group located less than 20 km from YM (gal/day) | 1.5e4, 2.64e5 | Based on an assumed population of 100 to 880 (Fedors and Wittmeyer, 1998) and a range of per capita water use from 150 gpd for Tucson, AZ, to 300 gpd for Las Vegas, NV, water use (van der Leeden et al., 1990, table 5-16, p. 319) | ** |
| uniform | WellPumpingRateAtReceptorGroup20km[gal/day] | Well pumping rate for farming receptor group located greater than 20 km from YM (gal/day) | 4.5e6, 1.3e7 | Equivalent number of quarter-section center-pivot irrigation plots under cultivation with alfalfa. From 1989 LANDSAT image (Wittmeyer et al., 1996). Low value is based on actual | RWF 3/2/00 |

| Distribution Type | Parameter Name | Description | Parameter Range | Remarks | Provided by |
|---|---|---|---|---|---|
| | | | | irrigated area of 13 quarter-section plots. High value is based on evidence of as many as 27 quarter-section plots. 126 acres per quarter-section center-pivot irrigation plot. Low value is based on consumptive water use for alfalfa in semi-arid climates of 3.1 ft/yr near Los Angeles, CA (Linsley and Franzini, 1979, table 14-2, p. 377). High value is based on 4.38 ft/yr in Mesa, AZ (van der Leeden et al., 1990, table 2-50, p. 99). | |
| uniform | PlumeThickness5km[m] | Plume thickness at 5 km (m) | 10.0, 100.0 | — | DAF 3/2/00 |
| uniform | AquiferThickness5km[m] | Aquifer thickness at 5 km (m) | 300.0, 700.0 | Luckey et al. (1996), table 2, p. 19. Computed by subtracting the altitude of the base of the lower volcanic aquifer from the altitude of the water level in the well. | RWF 3/2/00 |
| uniform | MixingZoneThickness20km[m] | Mixing zone thickness at 20 km (m) | 50.0, 200.0 | Based on data on well screen depths obtained from the USGS GWSI database (Wittmeyer et al., 1995), the distance from the water table to the bottom of the first screened section for wells in the Amargosa Farms | RWF 3/2/00 |

| Distribution Type | Parameter Name | Description | Parameter Range | Remarks | Provided by |
|---|---|---|---|---|---|
| | | | | area ranges from approximately 40 to 245 m | |
| iflag | PlumeCaptureModel | Flag to allow the user to specify a value for the fraction of the plume captured, instead of performing calculations (0 = perform calculations, 1 = user-defined value) | 0 | — | ** |
| iflag | DilutionModel | Flag to allow the user to specify a value for the dilution volume, instead of performing calculations (0 = perform calculations, 1 = user-defined value) | 0 | — | ** |
| constant | UserDefinedPlumeCaptureFraction | Fraction of the plume mass captured by pumping when the PlumeCaptureModel flag = 1 | 1.0e0 | User-supplied value | ** |
| constant | UserDefinedDilutionVolume[gal/day] | Dilution volume used when the DilutionModel flag = 1 | 10901787.0 | User-supplied value | ** |
| iconstant | ReceptorAgeGroup(1=Nfnt,2=Tod,3=PTeen,4=Teen,5=Adlt,6=AdltFGR11) | Selection of receptor age group (1=infant, 2=toddler, 3=preteen, | 6 | ICRP72 refers to ICRP Publication 72 (International Council on Radiological | PAL 2/29/00 |

| Distribution Type | Parameter Name | Description | Parameter Range | Remarks | Provided by |
|---|---|---|---|---|---|
| | | 4=teen, 5=adult:ICRP72, and 6=adult:FGR11) | | Protection, 1996) and FGR11 refers to Federal Guidance Report 11 (Eckerman et al., 1988) | |
| triangular | InterceptionFraction/Irrigate | Irrigation interception fraction | 0.06, 0.4, 1.0 | Anspaugh (1987) | PAL 2/29/00 |
| constant | DepthOfSurfaceSoil[cm] | Depth of surface soil (cm) | 15 | Napier et al. (1988), p. 4.58 | PAL 2/29/00 |
| uniform | PluvialWellPumpingRate ReceptorGroup20km[gal/day] | Well pumping rate at 20 km location during pluvial period [gal/day] | 3.2e6, 9.23e6 | Rognon (1991); Tegen and Fung (1994); Anspaugh et al., (1975); Soldat (1973); Sehmel (1977); and Magill (1956). | PAL 2/29/00 |
| constant | PluvialSwitchTime[yr] | Time to switch from non pluvial to pluvial | 13000.0 | Based on the Milankovich cycle, the Pluvial period | |
| iconstant | YearsOfIrrigationPriorToIntakePeriod[yr] | Years of irrigation water deposition prior to the intake period (yr) | 15 | Assumption based on transient nature of farming in Amargosa Valley | PAL 2/29/00 |
| triangular | LeafyVegetableIrrigationRatePB[in/yr] | Leafy vegetable irrigation rate for pluvial biosphere (in/yr) | 23, 43, 43 | Ranges from pluvial analog state (Idaho) average irrigation for alfalfa (U.S. Department of Commerce, 1994) to pluvial rate for alfalfa derived from information and methods reported in LaPlante and Poor (1997) | PAL 2/29/00 |

| Distribution Type | Parameter Name | Description | Parameter Range | Remarks | Provided by |
|---|---|---|---|---|---|
| triangular | OtherVegetableIrrigationRatePB[in/yr] | Other vegetable irrigation rate for pluvial biosphere (in./yr) | 23, 43, 43 | Ranges from pluvial analog state (Idaho) average irrigation for alfalfa (U.S. Department of Commerce, 1994) to pluvial rate for alfalfa derived from information and methods reported in LaPlante and Poor (1997) | PAL 2/29/00 |
| triangular | FruitIrrigationRatePB[in/yr] | Fruit irrigation rate for pluvial biosphere (in./yr) | 23, 43, 43 | Ranges from pluvial analog state (Idaho) average irrigation for alfalfa (U.S. Department of Commerce, 1994) to pluvial rate for alfalfa derived from information and methods reported in LaPlante and Poor (1997) | PAL 2/29/00 |
| triangular | GrainIrrigationRatePB[in/yr] | Grain irrigation rate for pluvial biosphere (in./yr) | 23, 43, 43 | Ranges from pluvial analog state (Idaho) average irrigation for alfalfa (U.S. Department of Commerce, 1994) to pluvial rate for alfalfa derived from information and methods reported in LaPlante and Poor (1997) | PAL 2/29/00 |
| uniform | HomeIrrigationRatePB[in/yr] | Residential irrigation rate for pluvial biosphere (in./yr) | 18, 65 | Local range reported in LaPlante and Poor, 1997 adjusted for pluvial by 29% reduction derived from information and methods in | PAL 2/29/00 |

| Distribution Type | Parameter Name | Description | Parameter Range | Remarks | Provided by |
|---|---|---|---|---|---|
| | | | | LaPlante and Poor (1997) | |
| triangular | PoultryFeedIrrigationRatePB[in/yr] | Poultry feed irrigation rate for pluvial biosphere (in./yr) | 23, 43, 43 | Used value for grain [see GrainIrrigationRatePB] | PAL 2/29/00 |
| triangular | HenFeedIrrigationRatePB[in/yr] | Egg-laying hen feed irrigation rate for pluvial biosphere (in./yr) | 23, 43, 43 | Used value for grain [see GrainIrrigationRatePB] | PAL 2/29/00 |
| uniform | LeafyVegetableIrrigationTimePB[mo/yr] | Leafy vegetable irrigation time for pluvial biosphere (mo/yr) | 3, 10 | Derived from information in LaPlante and Poor (1997) | PAL 2/29/00 |
| uniform | OtherVegetableIrrigationTimePB[mo/yr] | Other vegetable irrigation time for pluvial biosphere (mo/yr) | 2, 10 | Derived from information in LaPlante and Poor (1997) | PAL 2/29/00 |
| uniform | FruitIrrigationTimePB[mo/yr] | Fruit irrigation time for pluvial biosphere (mo/yr) | 2, 6 | Derived from information in LaPlante and Poor (1997) | PAL 2/29/00 |
| uniform | GrainIrrigationTimePB[mo/yr] | Grain irrigation time for pluvial biosphere (mo/yr) | 6, 8 | Derived from information in LaPlante and Poor (1997) | PAL 2/29/00 |
| uniform | HomeIrrigationTimePB[mo/yr] | Residential irrigation time for pluvial biosphere (mo/yr) | 9, 12 | LaPlante and Poor (1997) | PAL 2/29/00 |

| Distribution Type | Parameter Name | Description | Parameter Range | Remarks | Provided by |
|---|---|---|---|---|---|
| uniform | PoultryFeedIrrigationTimePB [mo/yr] | Poultry feed irrigation time for pluvial biosphere (mo/yr) | 6, 8 | Derived from information in LaPlante and Poor (1997) | PAL 2/29/00 |
| uniform | HenFeedIrrigationTimePB[mo/yr] | Egg-laying hen feed irrigation time for pluvial biosphere (mo/yr) | 6, 8 | Derived from information in LaPlante and Poor (1997) | PAL 2/29/00 |
| uniform | LeafyVegetableIrrigationRateCB[in/yr] | Leafy vegetable irrigation rate for current biosphere (in./yr) | 37, 53 | Based on alfalfa irrigation rates for Los Angeles, CA (Linsley and Franzini, 1979) and Mesa, AZ (van der Leeden et al., 1990). | PAL 2/29/00 |
| uniform | OtherVegetableIrrigationRateCB[in/yr] | Other vegetable irrigation rate for current biosphere (in./yr) | 37, 53 | Based on alfalfa irrigation rates for Los Angeles, CA (Linsley and Franzini, 1979) and Mesa, AZ (van der Leeden et al., 1990). | PAL 2/29/00 |
| uniform | FruitIrrigationRateCB[in/yr] | Fruit irrigation rate for current biosphere (in./yr) | 37, 53 | Based on alfalfa irrigation rates for Los Angeles, CA (Linsley and Franzini, 1979) and Mesa, AZ (van der Leeden et al., 1990). | PAL 2/29/00 |
| uniform | GrainIrrigationRateCB[in/yr] | Grain irrigation rate for current biosphere (in./yr) | 37, 53 | Based on alfalfa irrigation rates for Los Angeles, CA (Linsley and Franzini, 1979) and Mesa, AZ (van der Leeden et al., 1990). | PAL 2/29/00 |

| Distribution Type | Parameter Name | Description | Parameter Range | Remarks | Provided by |
|---|---|---|---|---|---|
| uniform | HomeIrrigationRateCB[in/yr] | Residential irrigation rate for current biosphere (in./yr) | 26, 91 | LaPlante and Poor (1997) | PAL 2/29/00 |
| uniform | PoultryFeedIrrigationRateCB[ in/yr] | Poultry feed irrigation rate for current biosphere (in./yr) | 37, 53 | Based on alfalfa irrigation rates for Los Angeles, CA (Linsley and Franzini, 1979) and Mesa, AZ (van der Leeden et al., 1990). | PAL 2/29/00 |
| uniform | HenFeedIrrigationRateCB[in/ yr] | Egg-laying hen feed irrigation rate for current biosphere (in./yr) | 37, 53 | Based on alfalfa irrigation rates for Los Angeles, CA (Linsley and Franzini, 1979) and Mesa, AZ (van der Leeden et al., 1990). | PAL 2/29/00 |
| uniform | LeafyVegetableIrrigationTim eCB[mo/yr] | Leafy vegetable irrigation time for current biosphere (mo/yr) | 3, 8 | LaPlante and Poor (1997) | PAL 2/29/00 |
| uniform | OtherVegetableIrrigationTime CB[mo/yr] | Other vegetable irrigation time for current biosphere (mo/yr) | 2, 8 | LaPlante and Poor (1997) | PAL 2/29/00 |
| uniform | FruitIrrigationTimeCB[mo/yr ] | Fruit irrigation time for current biosphere (mo/yr) | 2, 3 | LaPlante and Poor (1997) | PAL 2/29/00 |
| uniform | GrainIrrigationTimeCB[mo/yr ] | Grain irrigation time for current biosphere (mo/yr) | 6, 8 | LaPlante and Poor (1997) | PAL 2/29/00 |

| Distribution Type | Parameter Name | Description | Parameter Range | Remarks | Provided by |
|---|---|---|---|---|---|
| uniform | HomeIrrigationTimeCB[mo/yr] | Residential irrigation time for current biosphere (mo/yr) | 6, 12 | LaPlante and Poor (1997) | PAL 2/29/00 |
| uniform | PoultryFeedIrrigationTimeCB[mo/yr] | Poultry feed irrigation time for current biosphere (mo/yr) | 6, 8 | Grain irrigation time from LaPlante and Poor (1997) | PAL 2/29/00 |
| uniform | HenFeedIrrigationTimeCB[mo/yr] | Egg-laying hen feed irrigation time for current biosphere (mo/yr) | 6, 8 | Grain irrigation time from LaPlante and Poor (1997) | PAL 2/29/00 |
| uniform | PoultryFeedGrowTime[day] | Poultry feed growing time (day) | 60, 90 | Grain growing time from LaPlante and Poor (1997) | PAL 2/29/00 |
| uniform | HenFeedGrowTime[day] | Egg-laying hen feed growing time (day) | 60, 90 | Grain growing time from LaPlante and Poor (1997) | PAL 2/29/00 |
| normal | BeefFreshForageDietFraction | Beef cattle fresh forage diet fraction | 0.12, 0.98 | Breshears et al. (1989) | PAL 2/29/00 |
| normal | MilkFreshForageDietFraction | Dairy cattle fresh forage diet fraction | 0.12, 0.98 | Breshears et al. (1989) | PAL 2/29/00 |
| uniform | BeefFreshForageGrowTime[day] | Beef cattle fresh forage growing time (day) | 30, 62 | LaPlante and Poor (1997) | PAL 2/29/00 |
| uniform | MilkFreshForageGrowTime[day] | Dairy cattle fresh forage growing time (day) | 30, 62 | LaPlante and Poor (1997) | PAL 2/29/00 |

| Distribution Type | Parameter Name | Description | Parameter Range | Remarks | Provided by |
|---|---|---|---|---|---|
| triangular | BeefFreshForageIrrigationRatePB[in/yr] | Beef cattle fresh forage irrigation rate for pluvial biosphere (in./yr) | 23, 43, 43 | Ranges from pluvial analog state (Idaho) average irrigation for alfalfa (U.S. Department of Commerce, 1994) to pluvial rate for alfalfa derived from information and methods reported in LaPlante and Poor (1997) | PAL 2/29/00 |
| triangular | MilkFreshForageIrrigationRatePB[in/yr] | Milk fresh forage irrigation rate for pluvial biosphere (in./yr) | 23, 43, 43 | Ranges from pluvial analog state (Idaho) average irrigation for alfalfa (U.S. Department of Commerce, 1994) to pluvial rate for alfalfa derived from information and methods reported in LaPlante and Poor (1997) | PAL 2/29/00 |
| uniform | BeefFreshForageIrrigationTimePB[mo/yr] | Beef cattle fresh forage irrigation time for pluvial biosphere (mo/yr) | 3, 10 | Derived from information in LaPlante and Poor (1997) | PAL 2/29/00 |
| uniform | MilkFreshForageIrrigationTimePB[mo/yr] | Dairy cattle fresh forage irrigation time for pluvial biosphere (mo/yr) | 3, 10 | Derived from information in LaPlante and Poor (1997) | PAL 2/29/00 |
| uniform | BeefFreshForageIrrigationRateCB[in/yr] | Beef cattle fresh forage irrigation rate for current biosphere (in/yr) | 37, 53 | Based on alfalfa irrigation rates for Los Angeles, CA (Linsley | PAL 2/29/00 |

| Distribution Type | Parameter Name | Description | Parameter Range | Remarks | Provided by |
|---|---|---|---|---|---|
| | | | | and Franzini, 1979) and Mesa, AZ (van der Leeden et al., 1990). | |
| uniform | MilkFreshForageIrrigationRateCB[in/yr] | Dairy cattle fresh forage irrigation rate for current biosphere (in./yr) | 37, 53 | Based on alfalfa irrigation rates for Los Angeles, CA (Linsley and Franzini, 1979) and Mesa, AZ (van der Leeden et al., 1990). | PAL 2/29/00 |
| uniform | BeefFreshForageIrrigationTimeCB[mo/yr] | Beef cattle fresh forage irrigation time for current biosphere (mo/yr) | 3, 8 | LaPlante and Poor (1997) | PAL 2/29/00 |
| uniform | MilkFreshForageIrrigationTimeCB[mo/yr] | Dairy cattle fresh forage irrigation time for current biosphere (mo/yr) | 3, 8 | LaPlante and Poor (1997) | PAL 2/29/00 |
| lognormal | DrinkingWaterConsumptionRate1[L/yr] | Drinking water consumption rate for infant (L/yr) | 12, 670 | Based on median and distribution statistics in table 3-30 in Environmental Protection Agency (1997) | PAL 2/29/00 |
| constant | LeafyVegetableConsumptionRate1[kg/yr] | Leafy vegetable consumption rate for infant (kg/yr) | 0 | Infant assumed to eat no solid food | PAL 2/29/00 |
| constant | OtherVegetableConsumptionRate1[kg/yr] | Other vegetable consumption rate for infant (kg/yr) | 0 | Infant assumed to eat no solid food | PAL 2/29/00 |

| Distribution Type | Parameter Name | Description | Parameter Range | Remarks | Provided by |
|---|---|---|---|---|---|
| constant | FruitConsumptionRate1[kg/yr] | Fruit consumption rate for infant (kg/yr) | 0 | Infant assumed to eat no solid food | PAL 2/29/00 |
| constant | GrainConsumptionRate1[kg/yr] | Grain consumption rate for infant (kg/yr) | 0 | Infant assumed to eat no solid food | PAL 2/29/00 |
| constant | BeefConsumptionRate1[kg/yr] | Beef consumption rate for infant (kg/yr) | 0 | Infant assumed to eat no solid food | PAL 2/29/00 |
| constant | PoultryConsumptionRate1[kg/yr] | Poultry consumption rate for infant (kg/yr) | 0 | Infant assumed to eat no solid food | PAL 2/29/00 |
| constant | MilkConsumptionRate1[kg/yr] | Milk consumption rate for infant (kg/yr) | 226 | Table 11-12 in U.S. Environmental Protection Agency (1997) | PAL 2/29/00 |
| constant | EggConsumptionRate1[kg/yr] | Egg consumption rate for infant (kg/yr) | 0 | Infant assumed to eat no solid food | PAL 2/29/00 |
| constant | InhalationExposureTime1[hr] | Inhalation exposure time for infant (hr/yr) | 4563 | Assumed 1 hr/day outdoors, 0.5 indoor exposure factor | PAL 2/29/00 |
| constant | InhalationRate1[cm3/s] | Inhalation rate for infant ($cm^3/s$) | 52 | Some reported values averaged to collapse age groupings (U.S. Environmental Protection Agency, 1997) | PAL 2/29/00 |
| constant | SoilContaminationExposureTime1[hr] | Soil contamination exposure time for infant (hr/yr) | 2770 | Assumed 1 hr/day outdoors, 0.33 indoor exposure factor | PAL 2/29/00 |

| Distribution Type | Parameter Name | Description | Parameter Range | Remarks | Provided by |
|---|---|---|---|---|---|
| lognormal | DrinkingWaterConsumptionRate2[L/yr] | Drinking water consumption rate for toddler (L/yr) | 50, 1240 | Based on median and distribution statistics in table 3-30 in U.S. Environmental Protection Agency (1997) | PAL 2/29/00 |
| constant | LeafyVegetableConsumptionRate2[kg/yr] | Leafy vegetable consumption rate for toddler (kg/yr) | 3.5 | Table 9-17 in U.S. Environmental Protection Agency (1997), 50% of mean all vegetable rate to account for local production assumption, scaled by ratio of leafy to total vegetable consumption rates as reported in table 2-4 in LaPlante and Poor (1997) | PAL 2/29/00 |
| constant | OtherVegetableConsumptionRate2[kg/yr] | Other vegetable consumption rate for toddler (kg/yr) | 16 | Table 9-17 in U.S.Environmental Protection Agency (1997), 50% of mean all vegetable value to account for local production assumption, scaled by ratio of other to total vegetable consumption rates as reported in table 2-4 in LaPlante and Poor (1997) | PAL 2/29/00 |
| constant | FruitConsumptionRate2[kg/yr] | Fruit consumption rate for toddler (kg/yr) | 48 | Table 9-15 in U.S. Environmental Protection Agency (1997), 50% of mean rate to account for local production assumption | PAL 2/29/00 |

| Distribution Type | Parameter Name | Description | Parameter Range | Remarks | Provided by |
|---|---|---|---|---|---|
| constant | GrainConsumptionRate2[kg/yr] | Grain consumption rate for toddler (kg/yr) | 30 | Table 12-14 in U.S Environmental Protection Agency (1997), 50% of mean rate to account for local production assumption | PAL 2/29/00 |
| constant | BeefConsumptionRate2[kg/yr] | Beef consumption rate for toddler (kg/yr) | 4 | Table 11-11 in U.S. Environmental Protection Agency (1997), 50% of mean rate to account for local production assumption | PAL 2/29/00 |
| constant | PoultryConsumptionRate2[kg/yr] | Poultry consumption rate for toddler (kg/yr) | 3 | Table 11-11 in U.S. Environmental Protection Agency (1997), 50% of mean rate to account for local production assumption | PAL 2/29/00 |
| constant | MilkConsumptionRate2[kg/yr] | Milk consumption rate for toddler (kg/yr) | 127 | Table 11-13 in U.S. Environmental Protection Agency (1997), 100% of mean rate to account for local production assumption | PAL 2/29/00 |
| constant | EggConsumptionRate2[kg/yr] | Egg consumption rate for toddler (kg/yr) | 1 | Table 11-13 in Environmental Protection Agency (1997), 30% of mean rate to account for local production assumption | PAL 2/29/00 |
| constant | InhalationExposureTime2[hr] | Inhalation exposure time for toddler (hr/yr) | 4790 | Table 15-132 in U.S. Environmental Protection Agency (1997), median outdoor | PAL 2/29/00 |

| Distribution Type | Parameter Name | Description | Parameter Range | Remarks | Provided by |
|---|---|---|---|---|---|
| | | | | time used, 0.5 indoor exposure factor, at residence all day | |
| constant | InhalationRate2[cm3/s] | Inhalation rate for toddler ($cm^3/s$) | 88 | Some reported values averaged to collapse age groupings (U.S. Environmental Protection Agency, 1997) | PAL 2/29/00 |
| constant | SoilContaminationExposureTime2[hr] | Soil contamination exposure time for toddler (hr/yr) | 2620 | Table 15-132 in U.S. Environmental Protection Agency (1997), median outdoor time used, 0.33 indoor exposure factor, at residence all day | PAL 2/29/00 |
| lognormal | DrinkingWaterConsumptionRate3[L/yr] | Drinking water consumption rate for preteen (L/yr) | 50, 1240 | Based on median and distribution statistics in table 3-30 in U.S. Environmental Protection Agency (1997) | PAL 2/29/00 |
| constant | LeafyVegetableConsumptionRate3[kg/yr] | Leafy vegetable consumption rate for preteen (kg/yr) | 4.8 | Table 9-17 in U.S. Environmental Protection Agency (1997), 50% of mean all vegetable rate to account for local production assumption, scaled by ratio of leafy to total vegetable consumption rates as reported in table 2-4 in LaPlante and Poor (1997) | PAL 2/29/00 |
| constant | OtherVegetableConsumptionRate3[kg/yr] | Other vegetable consumption rate for preteen (kg/yr) | 22 | Table 9-17 in U.S. Environmental Protection Agency (1997), 50% of mean all | PAL 2/29/00 |

| Distribution Type | Parameter Name | Description | Parameter Range | Remarks | Provided by |
|---|---|---|---|---|---|
| | | | | vegetable value to account for local production assumption, scaled by ratio of other to total vegetable consumption rates as reported in table 2-4 in LaPlante and Poor (1997) | |
| constant | FruitConsumptionRate3[kg/yr] | Fruit consumption rate for preteen (kg/yr) | 52 | Table 9-15 in U.S. Environmental Protection Agency (1997), 50% of mean rate to account for local production assumption | PAL 2/29/00 |
| constant | GrainConsumptionRate3[kg/yr] | Grain consumption rate for preteen (kg/yr) | 49 | Table 12-14 in U.S. Environmental Protection Agency (1997), 50% of mean rate to account for local production assumption | PAL 2/29/00 |
| constant | BeefConsumptionRate3[kg/yr] | Beef consumption rate for preteen (kg/yr) | 6 | Table 11-11 in U.S. Environmental Protection Agency (1997), 50% of mean rate to account for local production assumption | PAL 2/29/00 |
| constant | PoultryConsumptionRate3[kg/yr] | Poultry consumption rate for preteen (kg/yr) | 5 | Table 11-11 in U.S. Environmental Protection Agency (1997), 50% of mean rate to account for local production assumption | PAL 2/29/00 |

| Distribution Type | Parameter Name | Description | Parameter Range | Remarks | Provided by |
|---|---|---|---|---|---|
| constant | MilkConsumptionRate3[kg/yr] | Milk consumption rate for preteen (kg/yr) | 160 | Table 11-13 in U.S. Environmental Protection Agency (1997), 100% of mean rate to account for local production assumption | PAL 2/29/00 |
| constant | EggConsumptionRate3[kg/yr] | Egg consumption rate for preteen (kg/yr) | 2 | Table 11-13 in U.S. Environmental Protection Agency (1997), 30% of mean rate to account for local production assumption | PAL 2/29/00 |
| constant | InhalationExposureTime3[hr] | Inhalation exposure time for preteen (hr/yr) | 4840 | Table 15-132 in Environmental Protection Agency (1997), median outdoor time used, 0.5 indoor exposure factor, school time assumed in contaminated zone | PAL 2/29/00 |
| constant | InhalationRate3[cm3/s] | Inhalation rate for preteen ($cm^3/s$) | 139 | Some reported values averaged to collapse age groupings (U.S. Environmental Protection Agency, 1997) | PAL 2/29/00 |
| constant | SoilContaminationExposureTime3[hr] | Soil contamination exposure time for preteen (hr/yr) | 3500 | Table 15-132 in Environmental Protection Agency (1997), median outdoor time used, 0.33 indoor exposure factor, school time assumed in contaminated zone | PAL 2/29/00 |

| Distribution Type | Parameter Name | Description | Parameter Range | Remarks | Provided by |
|---|---|---|---|---|---|
| lognormal | DrinkingWaterConsumptionRate4[L/yr] | Drinking water consumption rate for teen (L/yr) | 55, 1850 | Based on median and distribution statistics in table 3-30 in U.S. Environmental Protection Agency (1997) | PAL 2/29/00 |
| constant | LeafyVegetableConsumptionRate4[kg/yr] | Leafy vegetable consumption rate for teen (kg/yr) | 6.6 | Table 9-17 in U.S. Environmental Protection Agency (1997), 50% of mean all vegetable rate to account for local production assumption, scaled by ratio of leafy to total vegetable consumption rates as reported in table 2-4 in LaPlante and Poor (1997) | PAL 2/29/00 |
| constant | OtherVegetableConsumptionRate4[kg/yr] | Other vegetable consumption rate for teen (kg/yr) | 30 | Table 9-17 in U.S. Environmental Protection Agency (1997), 50% of mean all vegetable value to account for local production assumption, scaled by ratio of other to total vegetable consumption rates as reported in table 2-4 in LaPlante and Poor (1997) | PAL 2/29/00 |
| constant | FruitConsumptionRate4[kg/yr] | Fruit consumption rate for teen (kg/yr) | 58 | Table 9-15 in U.S. Environmental Protection Agency (1997), 50% of mean rate to account for local production assumption | PAL 2/29/00 |

| Distribution Type | Parameter Name | Description | Parameter Range | Remarks | Provided by |
|---|---|---|---|---|---|
| constant | GrainConsumptionRate4[kg/yr] | Grain consumption rate for teen (kg/yr) | 56 | Table 12-14 in U.S. Environmental Protection Agency (1997), 50% of mean rate to account for local production assumption | PAL 2/29/00 |
| constant | BeefConsumptionRate4[kg/yr] | Beef consumption rate for teen (kg/yr) | 10 | Table 11-11 in U.S. Environmental Protection Agency (1997), 50% of mean rate to account for local production assumption | PAL 2/29/00 |
| constant | PoultryConsumptionRate4[kg/yr] | Poultry consumption rate for teen (kg/yr) | 5 | Table 11-11 in U.S. Environmental Protection Agency (1997), 50% of mean rate to account for local production assumption | PAL 2/29/00 |
| constant | MilkConsumptionRate4[kg/yr] | Milk consumption rate for teen (kg/yr) | 143 | Table 11-13 in U.S. Environmental Protection Agency (1997), 100% of mean rate to account for local production assumption | PAL 2/29/00 |
| constant | EggConsumptionRate4[kg/yr] | Egg consumption rate for teen (kg/yr) | 2 | Table 11-13 in U.S. Environmental Protection Agency (1997), 30% of mean rate to account for local production assumption | PAL 2/29/00 |
| constant | InhalationExposureTime4[hr] | Inhalation exposure time for teen (hr/yr) | 4690 | Table 15-132 in U.S. Environmental Protection | PAL 2/29/00 |

| Distribution Type | Parameter Name | Description | Parameter Range | Remarks | Provided by |
|---|---|---|---|---|---|
| | | | | Agency (1997), median outdoor time used, 0.5 indoor exposure factor, school time assumed in contaminated zone | |
| constant | InhalationRate4[cm3/s] | Inhalation rate for teen ($cm^3/s$) | 185 | Some reported values averaged to collapse age groupings (U.S. Environmental Protection Agency, 1997) | PAL 2/29/00 |
| constant | SoilContaminationExposureTime4[hr] | Soil contamination exposure time for teen (hr/yr) | 3310 | Table 15-132 in U.S. Environmental Protection Agency (1997), median outdoor time used, 0.33 indoor exposure factor, school time assumed in contaminated zone | PAL 2/29/00 |
| lognormal | DrinkingWaterConsumptionRate5[L/yr] | Drinking water consumption rate for adult:ICRP72 (L/yr) | 95, 2380 | Based on median and distribution statistics in table 3-30 in U.S. Environmental Protection Agency (1997) | PAL 2/29/00 |
| constant | LeafyVegetableConsumptionRate5[kg/yr] | Leafy vegetable consumption rate for adult:ICRP72 (kg/yr) | 8.9 | Table 9-17 in U.S. Environmental Protection Agency (1997), 50% of mean all vegetable rate to account for local production assumption, scaled by ratio of leafy to total vegetable consumption rates as reported in table 2-4 in LaPlante and Poor (1997) | PAL 2/29/00 |

| Distribution Type | Parameter Name | Description | Parameter Range | Remarks | Provided by |
|---|---|---|---|---|---|
| constant | OtherVegetableConsumption Rate5[kg/yr] | Other vegetable consumption rate for adult:ICRP72 (kg/yr) | 41 | Table 9-17 in U.S. Environmental Protection Agency (1997), 50% of mean all vegetable value to account for local production assumption, scaled by ratio of other to total vegetable consumption rates as reported in table 2-4 in LaPlante and Poor (1997) | PAL 2/29/00 |
| constant | FruitConsumptionRate5[kg/yr ] | Fruit consumption rate for adult:ICRP72 (kg/yr) | 52 | Table 9-15 in U.S. Environmental Protection Agency (1997), 50% of mean rate to account for local production assumption | PAL 2/29/00 |
| constant | GrainConsumptionRate5[kg/y r] | Grain consumption rate for adult:ICRP72 (kg/yr) | 50 | Table 12-14 in U.S. Environmental Protection Agency (1997), 50% of mean rate to account for local production assumption | PAL 2/29/00 |
| constant | BeefConsumptionRate5[kg/yr ] | Beef consumption rate for adult:ICRP72 (kg/yr) | 12 | Table 11-11 in U.S. Environmental Protection Agency (1997), 50% of mean rate to account for local production assumption | PAL 2/29/00 |
| constant | PoultryConsumptionRate5[kg /yr] | Poultry consumption rate for adult:ICRP72 (kg/yr) | 6 | Table 11-11 in U.S. Environmental Protection Agency (1997), 50% of mean | PAL 2/29/00 |

| Distribution Type | Parameter Name | Description | Parameter Range | Remarks | Provided by |
|---|---|---|---|---|---|
| | | | | rate to account for local production assumption | |
| constant | MilkConsumptionRate5[kg/yr] | Milk consumption rate for adult:ICRP72 (kg/yr) | 74 | Table 11-13 in U.S. Environmental Protection Agency (1997), 100% of mean rate to account for local production assumption | PAL 2/29/00 |
| constant | EggConsumptionRate5[kg/yr] | Egg consumption rate for adult:ICRP72 (kg/yr) | 2 | Table 11-13 in U.S. Environmental Protection Agency (1997), 30% of mean rate to account for local production assumption | PAL 2/29/00 |
| constant | InhalationExposureTime5[hr] | Inhalation exposure time for adult:ICRP72 (hr/yr) | 6910 | Table 15-112 in U.S. Environmental Protection Agency (1997), median outdoor time at farm used, 0.5 indoor exposure factor, all time spent in contaminated zone | PAL 2/29/00 |
| constant | InhalationRate5[cm3/s] | Inhalation rate for adult:ICRP72 ($cm^3/s$) | 176 | Some reported values averaged to collapse age groupings (U.S. Environmental Protection Agency, 1997) | PAL 2/29/00 |
| constant | SoilContaminationExposureTime5[hr] | Soil contamination exposure time adult:ICRP72 (hr/yr) | 3830 | Table 15-112 in U.S. Environmental Protection Agency (1997), median outdoor | PAL 2/29/00 |

| Distribution Type | Parameter Name | Description | Parameter Range | Remarks | Provided by |
|---|---|---|---|---|---|
| | | | | time at farm used, 0.33 indoor exposure factor, all time spent in contaminated zone | |
| constant | DrinkingWaterConsumptionRate6[L/yr] | Drinking water consumption rate for adult:FGR11 (L/yr) | 730 | NRC preferred value for dose assessments | PAL 9/15/00 |
| constant | LeafyVegetableConsumptionRate6[kg/yr] | Leafy vegetable consumption rate for adult:FGR11 (kg/yr) | 15 | CRWMS M&O (2000), mean consumption from survey of Amargosa Valley residents | PAL 9/15/00 |
| constant | OtherVegetableConsumptionRate6[kg/yr] | Other vegetable consumption rate for adult:FGR11 (kg/yr) | 7.8 | CRWMS M&O (2000), mean consumption from survey of Amargosa Valley residents | PAL 9/15/00 |
| constant | FruitConsumptionRate6[kg/yr] | Fruit consumption rate for adult:FGR11 (kg/yr) | 16 | CRWMS M&O (2000), mean consumption from survey of Amargosa Valley residents | PAL 9/15/00 |
| constant | GrainConsumptionRate6[kg/yr] | Grain consumption rate for adult:FGR11 (kg/yr) | .048 | CRWMS M&O (2000), mean consumption from survey of Amargosa Valley residents | PAL 9/15/00 |
| constant | BeefConsumptionRate6[kg/yr] | Beef consumption rate for adult:FGR11 (kg/yr) | 2.9 | CRWMS M&O (2000), mean consumption from survey of Amargosa Valley residents | PAL 9/15/00 |
| constant | PoultryConsumptionRate6[kg/yr] | Poultry consumption rate for adult:FGR11 (kg/yr) | 0.8 | CRWMS M&O (2000), mean consumption from survey of Amargosa Valley residents | PAL 9/15/00 |

| Distribution Type | Parameter Name | Description | Parameter Range | Remarks | Provided by |
|---|---|---|---|---|---|
| constant | MilkConsumptionRate6[kg/yr] | Milk consumption rate for adult:FGR11 (kg/yr) | 4.1 | CRWMS M&O (2000), mean consumption from survey of Amargosa Valley residents | PAL 9/15/00 |
| constant | EggConsumptionRate6[kg/yr] | Egg consumption rate for adult:FGR11 (kg/yr) | 6.7 | CRWMS M&O (2000), mean consumption from survey of Amargosa Valley residents | PAL 9/15/00 |
| constant | InhalationExposureTime6[hr] | Inhalation exposure time for adult:FGR11 (hr/yr) | 4,200 | LaPlante and Poor (1997) | PAL 2/29/00 |
| constant | InhalationRate6[cm3/s] | Inhalation rate for adult:FGR11 ($cm^3/s$) | 270 | LaPlante and Poor (1997) | PAL 2/29/00 |
| constant | SoilContaminationExposureTime6[hr] | Soil contamination exposure time adult:FGR11 (hr/yr) | 1,800 | LaPlante and Poor (1997) | PAL 2/29/00 |
| lognormal | PlantUptakeScaleFactor | Plant uptake scaling factor used to scale plant transfer factors in *gftrans.dat* | 0.10, 9.8 | LaPlante and Poor (1997) range recalculated 0.1 to 99.9% interval using distribution statistics from International Union of Radioecologists (1989) | PAL 2/29/00 |
| lognormal | AnimalUptakeScaleFactor | Animal uptake scaling factor used to scale animal transfer factors in *gftrans.dat* | 0.10, 9.8 | LaPlante and Poor (1997) range recalculated 0.1 to 99.9% interval using distribution statistics from International Union of Radioecologists (1989). Distribution statistics from plant factors applied to animal factors due to lack of information for animals. | PAL 2/29/00 |

| Distribution Type | Parameter Name | Description | Parameter Range | Remarks | Provided by |
|---|---|---|---|---|---|
| lognormal | KD_Soil_Cm[cm3/g] | Soil $K_d$ for Cm ($cm^3/g$) | 1.5, 1.1e+7 | Sandy soil values, geometric means, Sheppard and Thibault (1990) | PAL 2/29/00 |
| lognormal | KD_Soil_Pu[cm3/g] | Soil $K_d$ for Pu ($cm^3/g$) | 2.0, 1.5e+5 | Sandy soil values, geometric means, Sheppard and Thibault (1990) | PAL 2/29/00 |
| lognormal | KD_Soil_U[cm3/g] | Soil $K_d$ for U ($cm^3/g$) | 9.3e-4, 1.3e+6 | Sandy soil values, geometric means, Sheppard and Thibault (1990) | PAL 2/29/00 |
| lognormal | KD_Soil_Am[cm3/g] | Soil $K_d$ for Am ($cm^3/g$) | 3.7e-1, 9.9e+6 | Sandy soil values, geometric means, Sheppard and Thibault (1990) | PAL 2/29/00 |
| lognormal | KD_Soil_Np[cm3/g] | Soil $K_d$ for Np ($cm^3/g$) | 1.9e-2, 1.3e+3 | Sandy soil values, geometric means, Sheppard and Thibault (1990) | PAL 2/29/00 |
| lognormal | KD_Soil_Th[cm3/g] | Soil $K_d$ for Th ($cm^3/g$) | 3.2, 3.2e+6 | Sandy soil values, geometric means, Sheppard and Thibault (1990) | PAL 2/29/00 |
| lognormal | KD_Soil_Ra[cm3/g] | Soil $K_d$ for Ra ($cm^3/g$) | 1.3e-2, 1.9e+7 | Sandy soil values, geometric means, Sheppard and Thibault (1990) | PAL 2/29/00 |
| lognormal | KD_Soil_Pb[cm3/g] | Soil $K_d$ for Pb ($cm^3/g$) | 1.4e-1, 5.2e+05 | Sandy soil values, geometric means, Sheppard and Thibault (1990) | PAL 2/29/00 |

| Distribution Type | Parameter Name | Description | Parameter Range | Remarks | Provided by |
|---|---|---|---|---|---|
| lognormal | KD_Soil_Cs[cm3/g] | Soil $K_d$ for Cs ($cm^3/g$) | 7.5e-2, 1.0e+6 | Sandy soil values, geometric means, Sheppard and Thibault (1990) | PAL 2/29/00 |
| lognormal | KD_Soil_I[cm3/g] | Soil $K_d$ for I ($cm^3/g$) | 7.2e-4, 1.4e+3 | Sandy soil values, geometric means, Sheppard and Thibault (1990) | PAL 2/29/00 |
| lognormal | KD_Soil_Tc[cm3/g] | Soil $K_d$ for Tc ($cm^3/g$) | 2.7e-4, 3.7e+1 | Sandy soil values, geometric means, Sheppard and Thibault (1990) | PAL 2/29/00 |
| lognormal | KD_Soil_Ni[cm3/g] | Soil $K_d$ for Ni ($cm^3/g$) | 2.9, 5.6e+04 | Sandy soil values, geometric means, Sheppa and Thibault (1990) | PAL 2/29/00 |
| constant | KD_Soil_Cl[cm3/g] | Soil $K_d$ for Cl ($cm^3/g$) | 0.25 | Baes et al. (1984), no distribution information provided for Cl | PAL 2/29/00 |
| lognormal | KD_Soil_C[cm3/g] | Soil $K_d$ for C ($cm^3/g$) | 3.6e-1, 7.0e+1 | Sandy soil values, geometric means, Sheppard and Thibault (1990) | PAL 2/29/00 |
| lognormal | KD_Soil_Se[cm3/g] | Soil $K_d$ for Se ($cm^3/g$) | 1.5e+1, 2.1e+2 | Sandy soil values, geometric means, Sheppard and Thibault (1990) | PAL 2/29/00 |
| constant | KD_Soil_Nb[cm3/g] | Soil $K_d$ for Nb ($cm^3/g$) | 160 | Sandy soil value, no distribution stats, Sheppard and Thibault (1990) | PAL 2/29/00 |

| Distribution Type | Parameter Name | Description | Parameter Range | Remarks | Provided by |
|---|---|---|---|---|---|
| constant | AnnualPrecipitation[m/yr] | Annual precipitation rate (m/yr) | 0.085 | Wilson et al. (1994) | ** |
| constant | AnnualIrrigation[m/yr] | Annual irrigation rate (m/yr) | 1.52 | Nuclear Regulatory Commission (1995) p. 7-10 | ** |
| constant | SoilBulkDensity[g/cm3] | Soil bulk density ($g/cm^3$) | 1.5 | LaPlante and Poor (1997), based on Amargosa region soils | PAL 2/29/00 |
| constant | SoilVolumetricWaterContent | Soil volumetric water content ($ml/cm^3$) | 0.35 | Total porosity of gravelly sandy loam soil type from Tanner (1991). Soil type is similar to Amargosa Valley farming soils. | PAL 2/29/00 |
| constant | TotalAnnualEvapotranspiration[m]yr] | Total annual evapotranspiration (m/yr) | 0.80 | — | ** |
| ** ** ** ***>>> FAULTO <<<*** ** | | | | | |
| finiteexponential | TimeOfNextFaultingEventInRegionOfInterest[yr] | Time of next faulting event (years from present) | 100.0, 10000.0, 2.0e-5 | Based on PSHA data, U. S. Geological Survey (1996) | ** |
| userdistribution | ThresholdDisplacementforFaultDisruptionOfWP[m] | Threshold fault displacement for disruption (m); Data input order: number of fault displacement values to be provided followed by | 4, 0.1, 0.2, 0.3, 0.4 | Estimated values because no direct analyses of WP stability in fault zones exist. The 0.2-m value is the mean value of the original distribution and is consistent with the proposed fault zone displacement. | ** |

| Distribution Type | Parameter Name | Description | Parameter Range | Remarks | Provided by |
|---|---|---|---|---|---|
| | | equiprobable displacement values | | | |
| uniform | XLocationOfFaultingEventInRegionOfInterest[m] | X location of center of faulting event in region of interest (m) | 547400.0, 548600.0 | Within repository, based on use of 8 subareas | ** |
| uniform | YLocationOfFaultingEventInRegionOfInterest[m] | Y location of center of faulting event in region of interest (m) | 4076000.0, 4079600.0 | Within repository, based on use of 8 subareas | ** |
| constant | ProbabilityForNWOrientationOfFaults | Probability for NW orientation of faults | 0.05 | No longer used—All fault orientations now only in one distribution. Based on maps of Scott and Bonk (1984). | JAS 2/25/00 |
| uniform | RNtoDetermineFaultOrientation | A random number to determine fault orientation | 0.0, 1.0 | — | JAS 2/25/00 |
| constant | NWFaultStrikeOrientationMeasuredfromNorthClockwise[degrees] | NW strike orientation measured from N clockwise (degrees) | -32.5 | Not used. Based on map of Scott and Bonk (1984). | JAS 2/25/00 |
| constant | NEFaultStrikeOrientationMeasuredfromNorthClockwise[degrees] | NE strike orientation measured from N clockwise (degrees) | 10.0 | Based on map of Scott and Bonk (1984). Additional analyses to be published in IA IRSR Rev. 3.0. | JAS 2/25/00 |
| constant | NWFaultTraceLength[m] | NW fault trace length (m) | 4000.0 | Not used. Based on maps of Scott and Bonk (1984) and Simonds et al. (1995). | JAS 2/25/00 |

| Distribution Type | Parameter Name | Description | Parameter Range | Remarks | Provided by |
|---|---|---|---|---|---|
| constant | NEFaultTraceLength[m] | NE fault trace length (m) | 4000.0 | Based on maps of Scott and Bonk (1984) and Simonds et al. (1995) | JAS 2/25/00 |
| beta | NWFaultZoneWidth[m] | NW fault zone width (m) | 0.5, 275.0, 1.25, 15.0 | Not used. Based on observational data from ESF, Ghosh et al. (1997), p. 2-5; Stirewalt et al. (1995). | JAS 2/25/00 |
| beta | NEFaultZoneWidth[m] | NE fault zone width (m) | 0.5, 365.0, 1.25, 15.0 | Based on observational data from ESF, Ghosh et al. (1997), p. 2-5; Stirewalt et al. (1995). Additional analyses to be published in IA IRSR Rev. 3.0 | JAS 2/25/00 |
| lognormal | NWAmountOfLargestCredibleDisplacement[m] | NW largest credible displacement (m) | 5.41e-2, 3.3e-1 | Not used. CNWRA best estimate. | JAS 2/25/00 |
| lognormal | NEAmountOfLargestCredibleDisplacement[m] | NE largest credible displacement (m) | 5.41e-2, 3.3e-1 | CNWRA best estimate. Additional analyses to be published in IA IRSR Rev. 3.0. | JAS 2/25/00 |
| constant | NWCumulativeDisplacementRate[mm/yr] | NW cumulative displacement rate (m/yr) | 0.00005 | Not used. Based on Electric Power Research Institute (1993). | JAS 2/25/00 |
| constant | NECumulativeDisplacementRate[mm/yr] | NE cumulative displacement rate (m/yr) | 0.00005 | Not used. Based on Electric Power Research Institute (1993). | JAS 2/25/00 |
| ** | | | | | |
| ** | | | | | |
| ** ***>>> VOLCANO <<<*** | | | | | |
| ** | | | | | |

| Distribution Type | Parameter Name | Description | Parameter Range | Remarks | Provided by |
|---|---|---|---|---|---|
| iconstant | VolcanoModel(1=Geometric, 2-Distribution) | Use geometric constraints on WP disruption (1) or process-based constraints on WP disruption (2) | 1 | User selectable parameter to calculate number of WP failures using geometric constraints (same as in the TPA version 3.2 code) or process-based models (Nuclear Regulatory Commission, 1999). | BEH 2/28/00 |
| finiteexponential | TimeOfNextVolcanicEventinRegionOfInterest[yr] | Time of next volcanic event (yr) | 100.0, 10000.0, 1.0e-7 | Technical basis for probability of volcanic disruption of the proposed repository site is explained in the Connor et al. (1997) issue resolution status report on probability of igneous events. Additional methodologies are developed in Hill et al. (1996), p. 2-6 to 2-16, and Connor and Hill (1995). | BEH 2/28/00 |
| constant | XLocationInRegionOfInterest [m] | X-coordinate of the center of the dike (for VolcanoModel=1) | 548000.0 | Represents the x-coordinate of the center of the repository to ensure that the volcano will strike the repository when the volcanism scenario flag is turned on | BEH 2/28/00 |
| constant | YLocationInRegionOfInterest [m] | Y-coordinate of the center of the dike (for VolcanoModel=1) | 4078000.0 | Represents the y-coordinate of the center of the repository to ensure that the volcano will strike the repository when the volcanism scenario flag is turned on | BEH 2/28/00 |

| Distribution Type | Parameter Name | Description | Parameter Range | Remarks | Provided by |
|---|---|---|---|---|---|
| uniform | RNtoDetermineIfExtrusiveOrIntrusiveVolcanicEvent | Random number to determine volcanic event type | 0.0, 1.0 | This parameter has no effect on TPA calculations if the FractionOfTimeVolcanic-EventsIsEstrusive parameter is set at 1.0. In the current approach for computing probability-weight dose from igneous activity, there is no reason to assume that a random fraction of igneous events are not volcanic but instead are wholly intrusive. This parameter currently is maintained as a place holder for future versions of TPA that will evaluate effects associated with intrusive igneous activity. | BEH 2/28/00<br><br>SM 1/21/02 |
| constant | FractionOfTimeVolcanicEventIsExtrusive | Fraction of extrusive volcanic events | 1.0 | User-specified value to investigate effects of igneous events that are intrusive rather than extrusive. Results in failure of WPs based solely on area directly intersected by a dike that is constructed using subsequent uniform parameter distributions. A value of 1.0 is specified so that all events are extrusive. This parameter was developed for previous versions of TPA and currently is maintained as a placeholder for future versions of TPA that will | BEH 2/28/00<br><br>SM 1/21/02 |

| Distribution Type | Parameter Name | Description | Parameter Range | Remarks | Provided by |
|---|---|---|---|---|---|
| | | | | evaluate effects associated with intrusive igneous activity. | |
| uniform | AngleOfVolcanicDikeMeasuredFromNorthClockwise[degrees] | Dike angle (degree) (for VolcanoModel=1) | 0.0, 15.0 | The orientation of planar, vertical igneous intrusions (i.e., dikes) at shallow crustal levels is controlled by the 3-dimensional distribution of crustal stress (Anderson, 1938; Delaney et al., 1986). In addition, pre-existing crustal structures, such as faults, may serve as conduits for ascending magma at shallow crustal levels (Young et al., 1994; Jolly and Sanderson, 1997). Although the current direction of maximum horizontal compressive stress at YM is oriented 28° from north, faults at the proposed repository site are oriented between 0° and 15° from north (Morris et al., 1996, p. 277). This orientation serves as the most likely orientation direction for future igneous intrusions at the proposed repository site. | BEH 2/28/00 |

| Distribution Type | Parameter Name | Description | Parameter Range | Remarks | Provided by |
|---|---|---|---|---|---|
| uniform | WidthOfVolcanicDike[m] | Volcanic dike width (m) (for VolcanoModel=1) | 1.0, 10.0 | Few data are available on dike widths for the YMR. Staff have observed that dikes between 0.5 and 10 m currently are exposed at 3.8–12 Ma YMR basaltic volcanic and intrusive centers. A detailed geologic map by Gartner and Delaney (1988) of the San Rafael volcanic field, Utah, provides width information for more than 200 basaltic dikes that were originally emplaced 0.5–1.5 km from the surface (Delaney and Gartner, 1997, p. 1180-1185). The width range of 1–10 m accounts for the range observed by Gartner and Delaney (1988) and YMR dike widths. | BEH 2/28/00 |
| iconstant | SubareaOfVolcanicEvent[ ] | Subarea where igneous event originates | 2 | Localizes center of igneous event within selected subarea. Restricts total number of WP disrupted to those present in a subarea and uses subarea-specific groundwater pathway parameters. | BEH 2/28/00 |
| beta | NumberOfWPsEntrainedByEjecta[ ] | Number of WP that fail during a volcanic event and are erupted (for VolcanoModel=2) | 1.0, 150.0, 1, 2 | Abstracts a process in which ascending basaltic magma intersects a repository drift, fills drift with magma, and fractures drift roof to entrain waste in | BEH 2/28/00 |

| Distribution Type | Parameter Name | Description | Parameter Range | Remarks | Provided by |
|---|---|---|---|---|---|
| | | | | resulting volcanic conduit (Nuclear Regulatory Commission, 1999). Points of initial magma intersection with drift and breakout through roof can vary randomly (Nuclear Regulatory Commission, 1999), entraining 1–150 WP per drift using EDA-II loading strategy. Note that multiple drifts likely will be intersected, increasing the number of entrained WP per event. In addition, multiple vents also can form during a single volcanic event, each entraining some number of WP. Base file assumes only one drift disrupted with only 1 resulting volcanic vent. | |
| loguniform | NumberOfMagmaInducedMechanicalFailuresRemainingInDrift[ ] | Number of WP that fail during an intrusive event and remain in the disrupted drifts. (For VolcanoModel=2) | 1.0, 1402.0 | Abstracts a process in which ascending basaltic magma intersects a repository drift and fills drift with magma (Nuclear Regulatory Commission, 1999). Initial stages of volcanic eruptions commonly form 1-km-long fissures that are fed by shallow dikes (NRC, 1999). Model assumes 1–10 drifts are | BEH 2/28/00 |

| Distribution Type | Parameter Name | Description | Parameter Range | Remarks | Provided by |
|---|---|---|---|---|---|
| | | | | intersected by a shallow 1-km-long dike, with subsequent WP failure in each intersected drift. | |
| ** ** ** ***>>> ASHPLUMO <<<*** ** | | | | | |
| constant | DensityOfAirAtSTP[g/cm3] | Air density at standard temperature and pressure($g/cm^3$) | 0.00129 | Weast (1976), p. F-11 | ** |
| constant | ViscosityOfAirAtSTP[g/cm-s] | Air viscosity (g/cm/s) | 0.00018 | Weast (1976), p. F-13 to F-16 | ** |
| constant | ConstantRelatingFallTimeToEddyDiffusivity[cm2/s5/2] | Constant relating eddy diffusion to particle fall time ($cm^2/s^{5/2}$) | 400.0 | Suzuki (1983), p. 99 | ** |
| constant | MaximumParticleDiameterForParticleTransport[cm] | Maximum particle diameter for transport (cm) | 10.0 | Eruptions that are many orders of magnitude larger than the largest <10 Ma YMR basaltic eruption rarely transport particles >10 cm in diameter through convective dispersal (Pyle, 1989, p. 7-11). Grain-size analyses at YMR analog deposits have average maximum particle diameters of <4 cm at distance 1–10 km from the vent (Hill and Connor, 1995, p. 149), which decreases to <1 cm at distances > 10 km from the vent | ** |

| Distribution Type | Parameter Name | Description | Parameter Range | Remarks | Provided by |
|---|---|---|---|---|---|
| | | | | (e.g., Hill et al., 1997). Incompletely preserved YMR fall deposits exposed 0.5–3 km from the vent have maximum particle diameters <4 cm (Hill and Connor, 1995, p. 7-14 to 7-15) | |
| constant | MinimumFuelParticulateSize[cm] | Minimum fuel particle diameter (cm) | 0.0001 | SF has initial grain-size average diameters on the order of 100s of μm (e.g., U.S. Department of Energy, 1988). Crush-impact studies (Nuclear Regulatory Commission, 1988) indicate an average diameter of crushed HLW on the order of 100 μm. The thermal, mechanical, and chemical loads of a basaltic volcanic eruption clearly exceed those imposed by a falling ceiling panel. Basaltic eruption processes will thus fragment HLW further than crush-impact processes, supporting the basic assumption of a 10 μm median diameter for HLW transported by a basaltic volcanic eruption. Minimum diameter for a log-triangular distribution is assumed to be 1 log unit below the median diameter, based on grain-size distributions in U.S. Department of Energy (1988) | ** |

| Distribution Type | Parameter Name | Description | Parameter Range | Remarks | Provided by |
|---|---|---|---|---|---|
| | | | | and Nuclear Regulatory Commission (1988). | |
| constant | ModeFuelParticulateSize[cm] | Median fuel particle diameter (cm) | 0.001 | SF has initial grain-size average diameters on the order of 100s of μm (e.g., U.S. Department of Energy, 1988). Crush-impact studies (Nuclear Regulatory Commission, 1988) indicate an average diameter of crushed HLW on the order of 100 μm. The thermal, mechanical, and chemical loads of a basaltic volcanic eruption clearly exceed those imposed by a falling ceiling panel. Basaltic eruption processes will thus likely fragment HLW further than crush-impact processes, supporting the basic assumption of a 10 μm median diameter for HLW transported by a basaltic volcanic eruption. | ** |
| constant | MaximumFuelParticulateSize [cm] | Maximum fuel particle diameter (cm) | 0.01 | SF has initial grain-size average diameters on the order of 100s of μm (e.g., U.S. Department of Energy, 1988). Crush-impact studies (Nuclear Regulatory Commission, 1988) indicate an average diameter of crushed HLW on the order of 100 μm. The thermal, mechanical, and | ** |

| Distribution Type | Parameter Name | Description | Parameter Range | Remarks | Provided by |
|---|---|---|---|---|---|
| | | | | chemical loads of a basaltic volcanic eruption clearly exceed those imposed by a falling ceiling panel. Basaltic eruption processes will thus likely fragment HLW further than crush-impact processes, supporting the basic assumption of a 10-μm median diameter for HLW transported by a basaltic volcanic eruption. Maximum diameter for a log-triangular distribution is assumed to be 1 log unit above the median diameter, based on grain-size distributions in U.S. Department of Energy (1988) and Nuclear Regulatory Commission (1988). | |
| constant | MinimumAshDensityforVariationWithSize[g/cm3] | Minimum tephra density (g/cm3) | 0.8 | Basaltic tephra deposits 20 km from the vent have densities of 0.6 g/cm$^3$ (Hill et al., 1998), which represents the minimum deposit density. This deposit porosity also is around 20% (e.g., Walker et al., 1984). Clast densities thus average 1 g/cm$^3$ for deposits relatively far from the vent. | BEH 2/28/00 |
| constant | MaximumAshDensityforVariationWithSize[g/cm3] | Maximum tephra density (g/cm3) | 1.6 | Basaltic tephra deposits 1 km from the vent have densities of 1.2 g/cm$^3$ (Hill et al., 1998), | BEH 2/28/00 |

| Distribution Type | Parameter Name | Description | Parameter Range | Remarks | Provided by |
|---|---|---|---|---|---|
| | | | | which represents the maximum deposit density. This deposit porosity also is around 25% (e.g., Walker et al., 1984). Clast densities thus average 1.6 g/cm$^3$ for near-vent deposits. | |
| constant | MinimumAshLogdiameterForDensityVariation | Minimum value of logarithm of ash diameter in cm | -2.0 | The density of basaltic scoria is strongly controlled by average grain size. Basaltic scoria break along vesicle (i.e., bubble) walls during transport fragmentation, which results in a net loss of vesicle void-space and concomitant increase in bulk density. For example, Walker et al. (1984) measured a 40 percent increase in scoria density as average grain size decreased from about 1 cm to about 1 mm. Jarzemba and LaPlante (1996, p. 6–10) concluded that a range of 1 log unit in average grain size would effectively encompass the range in size-dependent density variations commonly observed in basaltic tephra-fall deposits (e.g., Hill et al., 1997, p. 10). | ** |
| constant | MaximumAshLogdiameterForDensityVariation | Maximum value of logarithm of ash diameter | -1.0 | The density of basaltic scoria is strongly controlled by average grain-size. Basaltic scoria break along vesicle (i.e., bubble) walls | ** |

| Distribution Type | Parameter Name | Description | Parameter Range | Remarks | Provided by |
|---|---|---|---|---|---|
| | | | | during transport fragmentation, which results in a net loss of vesicle void-space and concomitant increase in bulk density. For example, Walker et al. (1984) measured a 40 percent increase in scoria density as average grain-size decreased from about 1 cm to about 1 mm. Jarzemba and LaPlante (1996, p. 6–10) concluded that a range of 1 log unit in average grain-size would effectively encompass the range in size-dependent density variations commonly observed in basaltic tephra-fall deposits (e.g., Hill et al., 1997, p. 10). | |
| constant | ParticleShapeParameter | Ash particle shape parameter | 0.5 | The shape of irregular particles with axial lengths a, b, and c can be described as [b+c]/2a, where a is greater than b or c (Suzuki, 1983, p. 100). Hill et al. (1996, p. 2-23) concluded shape parameters between 0.5 and 0.25 describe irregularly shaped basaltic tephra and that variations within this range do not affect transport properties in the ASHPLUME module. | ** |

| Distribution Type | Parameter Name | Description | Parameter Range | Remarks | Provided by |
|---|---|---|---|---|---|
| constant | IncorporationRatio | SF incorporation ratio | 0.3 | Assumed value of 0.3 in Jarzemba and LaPlante (1996, p. 9–12). For critical group locations 20 km from the proposed repository site, Hill and Trapp (1997, p. 5–6) found that a uniform distribution of U[0.1, 1.0] for this parameter did not affect dose significantly for the default HLW grain-size characteristics. | ** |
| constant | WindDirection[degrees] | Wind direction relative to due east in the counter-clock-wise direction (degrees) | -90.0 | Setting wind direction to 90° clockwise from east (i.e., south) ensures that the wind blows to the receptor group during each run. This provides a conservative basis for evaluating the effects of volcanic eruptions on nuclear facilities (International Atomic Energy Agency, 1997, p. 19–20). In addition, Hill and Trapp (1997, p. 6) calculated that ground-surface dose is within one order-of-magnitude of peak dose when the wind blows within a 50° sector centered about a main dispersion axis of 90°. Surface topography strongly controls wind direction and speed measured at surface weather stations to altitudes of at least | ** |

| Distribution Type | Parameter Name | Description | Parameter Range | Remarks | Provided by |
|---|---|---|---|---|---|
| | | | | 100 m (U.S. Department of Energy, 1997, p. 3.63–3.71). Wind direction data are not available for altitudes of interest (2 km to about 6 km) above YM (U.S. Department of Energy 1997, inclusive). The nearest wind direction data to YM and the receptor group location are from Desert Rock airstrip, located about 50 km SE of YM. For altitudes of about 2 and 4 km (700 and 500 mbar pressure level), wind direction above Desert Rock is within the 50° sector centered on south 18, 15% of the time. | |
| exponential | WindSpeed[cm/s] | Wind speed (cm/s) | 0.00083 | Wind speed data are not available for altitudes of interest (2 km to about 6 km) above YM (U.S. Department of Energy, 1988; U.S. Department of Energy, 1997, inclusive). The nearest wind speed data to YM and the receptor group location are from Desert Rock airstrip, located about 50 km SE of YM. For altitudes of about 2 km (700 mbar pressure level), wind speed above Desert Rock within the NNW–NNE sector averages 6 m/s (U.S. Department of | ** |

| Distribution Type | Parameter Name | Description | Parameter Range | Remarks | Provided by |
|---|---|---|---|---|---|
| | | | | Energy, 1997, p. 3-63–3-71). For altitudes of about 4 km (500 mbar pressure level), wind speed above Desert Rock within the NNW–NNE sector averages 12 m/s (U.S. Department of Energy, 1997, p. 3-63–3-71). Basaltic eruption column associated with YMR-type eruptions likely reached aboveground altitudes of at least 6 km (e.g., Jarzemba, 1997). A mean wind speed for 4 km altitudes thus presents a reasonable mean value for 2–6 km high eruption columns. | |
| loguniform | VolcanicEventDuration[s] | Duration of the tephra-forming eruption (s) | 1.8e5, 1.3e6 | Current implementation of Suzuki (1983) in Jarzemba et al. (1997) samples eruption power and duration to calculate particle velocity and eruption volume. Duration ranges in Baca and Jarzemba (1997), although accurate for historical eruptions, result in exceptionally large volumes for YMR eruptions when power is sampled independent of duration. Using methods in Jarzemba et al. (1997), duration range is constrained for YMR eruptions having tephra volumes of | BEH 2/28/00 |

| Distribution Type | Parameter Name | Description | Parameter Range | Remarks | Provided by |
|---|---|---|---|---|---|
| | | | | $1\times10^6$ $m^3$ to $5\times10^7$ $m^3$ with columns 2–6 km high. | |
| loguniform | VolcanicEventPower[W] | Volcanic event power (W) | 3.5e9, 5.3e11 | Current implementation of Suzuki (1983) in Jarzemba et al. (1997) samples eruption power and duration to calculate particle velocity and eruption volume. Power ranges in Baca and Jarzemba (1997), although accurate for historical eruptions, result in exceptionally large volumes for YMR eruptions when power is sampled independent of duration. Using methods in Jarzemba et al. (1997), power range is constrained for YMR eruptions having tephra volumes of $1\times10^6$ $m^3$ to $5\times10^7$ $m^3$ with columns 2–6 km high. | BEH 2/28/00 |
| constant | VolcanicColumnConstantBeta | Shape parameter for the volcanic column | 10.0 | Hill and Trapp (1997, p. 10) concluded that this parameter was a relatively insensitive parameter and that setting this parameter to a constant value of 10 was sufficient for modeling YMR-type basaltic eruptions using ASHPLUME. This result was confirmed by sensitivity | ** |

| Distribution Type | Parameter Name | Description | Parameter Range | Remarks | Provided by |
|---|---|---|---|---|---|
| | | | | studies conducted by Hill et al. (1997) on the 1995 Cerro Negro eruption deposits. | |
| logtriangular | AshMeanParticleLogDiameter[d_in_cm] | Logarithm of the mean ash particle size in cm | 0.01, 0.1, 1.0 | Few data are available to characterize the mean particle diameter for an entire basaltic fall deposit. Hill et al. (1997, p. 4–5) calculated a mean diameter of 0.7 mm for the 1-mm and thicker fall deposits from the 1995 Cerro Negro eruption. Although this eruption was about an order of magnitude smaller than the smallest YMR eruptions, it is likely that overall grain-size characteristics remain fairly scale-independent for these types of basaltic eruptions (e.g., Walker and Croasdale, 1972). | ** |
| constant | AshParticleSizeDistributionStandardDeviation | Ash particle size distribution standard deviation | 1.0 | Hill et al. (1996, p. 2-21–2-23) showed that this parameter does not demonstrably affect tephra-deposit thicknesses modeled using the ASHPLUME code. Hill and Trapp (1997) recommended setting this parameter to a constant value of 1. | ** |

| Distribution Type | Parameter Name | Description | Parameter Range | Remarks | Provided by |
|---|---|---|---|---|---|
| ** ** ** ***>>> ASHRMOVO <<<*** ** | | | | | |
| constant | FractionOfPrecipitationLostToEvapotranspiration | Fraction of precipitation lost to evapotranspiration | 0.68 | Jarzemba and Manteufel (1997), p. 924. Based on the converse of the fraction of precipitation that can reach the deep soil | ** |
| constant | FractionOfIrrigationLostToEvapotranspiration | Fraction of irrigation water lost to evapotranspiration | 0.5 | Jarzemba and Manteufel (1997), p. 924 | ** |
| constant | FractionOfYearSoilIsSaturatedDueToPrecipitation | Fraction of year blanket saturated due to precipitation | 0.0054 | Jarzemba and Manteufel (1997), p. 924 | ** |
| constant | FractionOfYearSoilIsSaturatedDueToIrrigation | Fraction of year blanket saturated due to irrigation | 0.2 | LaPlante et al. (1995), table 2.1, p. 2-6, based on average growing time of crops from Chambers and May 5 (1994) | ** |
| constant | AshBulkDensity[g/cm3] | Bulk density for volcanic ash (g/cm3) | 1.4 | Based on data in Fisher and Schmincke (1984), table 5-6, p. 118 and fig. 5-28, p. 120 | ** |
| constant | AshVolumetricMoistureFractionAtSaturation | Volumetric fraction of moisture in volcanic ash at saturation | 0.4 | Calculated from bulk density of ash | ** |
| constant | DepthOfTheRootingZone[m] | Depth of rooting zone | 0.15 | Napier et al. (1988), p. 4.58 | ** |

| Distribution Type | Parameter Name | Description | Parameter Range | Remarks | Provided by |
|---|---|---|---|---|---|
| constant | KdOfUraniumInVolcanicAsh[cm3/g] | U distribution coefficient in volcanic ash ($cm^3/g$) | 35.0 | Sheppard and Thibault (1990), table 1, p. 472 | ** |
| constant | KdOfCuriumInVolcanicAsh[cm3/g] | Cm distribution coefficient in volcanic ash ($cm^3/g$) | 4000.0 | Sheppard and Thibault (1990), table 1, p. 472 | ** |
| constant | KdOfPlutoniumInVolcanicAsh[cm3/g] | Pu distribution coefficient in volcanic ash ($cm^3/g$) | 550.0 | Sheppard and Thibault (1990), table 1, p. 472 | ** |
| constant | KdOfAmericiumInVolcanicAsh[cm3/g] | Am distribution coefficient in volcanic ash ($cm^3/g$) | 1900.0 | Sheppard and Thibault (1990), table 1, p. 472 | ** |
| constant | KdOfThoriumInVolcanicAsh[cm3/g] | Th distribution coefficient in volcanic ash ($cm^3/g$) | 3200.0 | Sheppard and Thibault (1990), table 1, p. 472 | ** |
| constant | KdOfRadiumInVolcanicAsh[cm3/g] | Ra distribution coefficient in volcanic ash ($cm^3/g$) | 500.0 | Sheppard and Thibault (1990), table 1, p. 472 | ** |
| constant | KdOfLeadInVolcanicAsh[cm3/g] | Pb distribution coefficient in volcanic ash ($cm^3/g$) | 270.0 | Sheppard and Thibault (1990), table 1, p. 472 | ** |
| constant | KdOfProtactiniumInVolcanicAsh[cm3/g] | Pa distribution coefficient in volcanic ash ($cm^3/g$) | 550.0 | Sheppard and Thibault (1990), table 1, p. 472 | ** |
| constant | KdOfActiniumInVolcanicAsh[cm3/g] | Ac distribution coefficient in volcanic ash ($cm^3/g$) | 450.0 | Sheppard and Thibault (1990), table 1, p. 472 | ** |

| Distribution Type | Parameter Name | Description | Parameter Range | Remarks | Provided by |
|---|---|---|---|---|---|
| constant | KdOfNeptuniumInVolcanicAsh[cm3/g] | Np distribution coefficient in volcanic ash ($cm^3/g$) | 5.0 | Sheppard and Thibault (1990), table 1, p. 472 | ** |
| constant | KdOfSamariumInVolcanicAsh[cm3/g] | Sm distribution coefficient in volcanic ash ($cm^3/g$) | 245.0 | Sheppard and Thibault (1990), table 1, p. 472 | ** |
| constant | KdOfCesiumInVolcanicAsh[cm3/g] | Cs distribution coefficient in volcanic ash ($cm^3/g$) | 280.0 | Sheppard and Thibault (1990), table 1, p. 472 | ** |
| constant | KdOfIodineInVolcanicAsh[cm3/g] | I distribution coefficient in volcanic ash ($cm^3/g$) | 1.0 | Sheppard and Thibault (1990), table 1, p. 472 | ** |
| constant | KdOfTinInVolcanicAsh[cm3/g] | Sn distribution coefficient in volcanic ash ($cm^3/g$) | 130.0 | Sheppard and Thibault (1990), table 1, p. 472 | ** |
| constant | KdOfSilverInVolcanicAsh[cm3/g] | Ag distribution coefficient in volcanic ash ($cm^3/g$) | 55.0 | Sheppard and Thibault (1990), table 1, p. 472 | ** |
| constant | KdOfPaladiumInVolcanicAsh[cm3/g] | Pd distribution coefficient in volcanic ash ($cm^3/g$) | 55.0 | Sheppard and Thibault (1990), table 1, p. 472 | ** |
| constant | KdOfTechnetiumInVolcanicAsh[cm3/g] | Tc distribution coefficient in volcanic ash ($cm^3/g$) | 0.1 | Sheppard and Thibault (1990), table 1, p. 472 | ** |
| constant | KdOfMolybdenumInVolcanicAsh[cm3/g] | Mo distribution coefficient in volcanic ash ($cm^3/g$) | 10.0 | Sheppard and Thibault (1990), table 1, p. 472 | ** |

| Distribution Type | Parameter Name | Description | Parameter Range | Remarks | Provided by |
|---|---|---|---|---|---|
| constant | KdOfNiobiumInVolcanicAsh[cm3/g] | Nb distribution coefficient in volcanic ash ($cm^3/g$) | 160.0 | Sheppard and Thibault (1990), table 1, p. 472 | ** |
| constant | KdOfZirconiumInVolcanicAsh[cm3/g] | Zr distribution coefficient in volcanic ash ($cm^3/g$) | 600.0 | Sheppard and Thibault (1990), table 1, p. 472 | ** |
| constant | KdOfStrontiumInVolcanicAsh[cm3/g] | Sr distribution coefficient in volcanic ash ($cm^3/g$) | 15.0 | Sheppard and Thibault (1990), table 1, p. 472 | ** |
| constant | KdOfSeleniumInVolcanicAsh[cm3/g] | Se distribution coefficient in volcanic ash ($cm^3/g$) | 150.0 | Sheppard and Thibault (1990), table 1, p. 472 | ** |
| constant | KdOfNickelInVolcanicAsh[cm3/g] | Ni distribution coefficient in volcanic ash ($cm^3/g$) | 400.0 | Sheppard and Thibault (1990), table 1, p. 472 | ** |
| constant | KdOfChlorineInVolcanicAsh[cm3/g] | Cl distribution coefficient in volcanic ash ($cm^3/g$) | 0.25 | Triay et al. (1997) | JRW 2/25/00 |
| constant | KdOfCarbonInVolcanicAsh[cm3/g] | C distribution coefficient in volcanic ash ($cm^3/g$) | 5.0 | Sheppard and Thibault (1990), table 1, p. 472 | ** |
| constant | SolubilityOfUraniumInVolcanicAsh[moles/liter] | U solubility (mol/L) | 4.5e-5 | Wilson et al. (1994), table 9-2b, p. 9-7 | ** |
| constant | SolubilityOfCuriumInVolcanicAsh[moles/liter] | Cm solubility (mol/L) | 1.0e-6 | Kerrisk (1985), table 9, p. 14 | ** |

| Distribution Type | Parameter Name | Description | Parameter Range | Remarks | Provided by |
|---|---|---|---|---|---|
| constant | SolubilityOfPlutoniumInVolcanicAsh[moles/liter] | Pu solubility (mol/L) | 5.0e-6 | Wilson et al. (1994), table 9-2b, p. 9-7; Kerrisk (1985), table 9, p. 14 | ** |
| constant | SolubilityOfAmericiumInVolcanicAsh[moles/liter] | Am solubility (mol/L) | 1.0e-6 | Kerrisk (1985), table 9, p. 14 | ** |
| constant | SolubilityOfThoriumInVolcanicAsh[moles/liter] | Th solubility (mol/L) | 3.2e-9 | Wilson et al. (1994), table 9-2b, p. 9-7 | ** |
| constant | SolubilityOfRadiumInVolcanicAsh[moles/liter] | Ra solubility (mol/L) | 1.0e-7 | Wilson et al. (1994), table 9-2b, p. 9-7 | ** |
| constant | SolubilityOfLeadInVolcanicAsh[moles/liter] | Pb solubility (mol/L) | 3.2e-7 | Wilson et al. (1994), table 9-2b, p. 9-7 | ** |
| constant | SolubilityOfProtactiniumInVolcanicAsh[moles/liter] | Pa solubility (mol/L) | 3.2e-8 | Wilson et al. (1994), table 9-2b, p. 9-7 | ** |
| constant | SolubilityOfActiniumInVolcanicAsh[moles/liter] | Ac solubility (mol/L) | 1.0e-6 | Wilson et al. (1994), table 9-2b, p. 9-7 | ** |
| constant | SolubilityOfNeptuniumInVolcanicAsh[moles/liter] | Np solubility (mol/L) | 1.0e-4 | Wilson et al. (1994), table 9-2b, p. 9-7 | ** |
| constant | SolubilityOfSamariumInVolcanicAsh[moles/liter] | Sm solubility (mol/L) | 5.0e-6 | Kerrisk (1985), table 9, p. 14 | ** |
| constant | SolubilityOfCesiumInVolcanicAsh[moles/liter] | Cs solubility (mol/L) | 1.0 | Wilson et al. (1994), table 9-2b, p. 9-7; Kerrisk (1985), table 9, p. 14 | ** |
| constant | SolubilityOfIodineInVolcanicAsh[moles/liter] | I solubility (mol/L) | 1.0 | Wilson et al. (1994), p. 9-9; Kerrisk (1985), table 9, p. 14 | ** |

| Distribution Type | Parameter Name | Description | Parameter Range | Remarks | Provided by |
|---|---|---|---|---|---|
| constant | SolubilityOfTinInVolcanicAsh[moles/liter] | Sn solubility (mol/L) | 5.0e-8 | Wilson et al. (1994), table 9-2b, p. 9-7; Kerrisk (1985), table 9, p. 14 | ** |
| constant | SolubilityOfSilverInVolcanicAsh[moles/liter] | Ag solubility (mol/L) | 1.0 | Conservative estimation due to lack of data | ** |
| constant | SolubilityOfPaladiumInVolcanicAsh[moles/liter] | Pd solubility (mol/L) | 9.5e-4 | Wilson et al. (1994), table 9-2b, p. 9-7; Kerrisk (1985), table 9, p. 14 | ** |
| constant | SolubilityOfTechnetiumInVolcanicAsh[moles/liter] | Tc solubility (mol/L) | 1.0 | Wilson et al. (1994), p. 9-9; Kerrisk (1985), table 9, p. 14 | ** |
| constant | SolubilityOfMolybdenumInVolcanicAsh[moles/liter] | Mo solubility (mol/L) | 1.0 | Conservative estimation due to lack of data | ** |
| constant | SolubilityOfNiobiumInVolcanicAsh[moles/liter] | Nb solubility (mol/L) | 1.0e-8 | Wilson et al. (1994), table 9-2b, p. 9-7 | ** |
| constant | SolubilityOfZirconiumInVolcanicAsh[moles/liter] | Zr solubility (mol/L) | 3.2e-10 | Wilson et al. (1994), table 9-2b, p. 9-7 | ** |
| constant | SolubilityOfStrontiumInVolcanicAsh[moles/liter] | Sr solubility (mol/L) | 1.3e-4 | Wilson et al. (1994), table 9-2b, p. 9-7 | ** |
| constant | SolubilityOfSeleniumInVolcanicAsh[moles/liter] | Se solubility (mol/L) | 1.0 | Wilson et al. (1994), p. 9-9 | ** |
| constant | SolubilityOfNickelInVolcanicAsh[moles/liter] | Ni solubility (mol/L) | 2.0e-3 | Wilson et al. (1994), table 9-2b, p. 9-7 | ** |
| constant | SolubilityOfChlorineInVolcanicAsh[moles/liter] | Cl solubility (mol/L) | 1.0 | Wilson et al. (1994), p. 9-9 | ** |

| Distribution Type | Parameter Name | Description | Parameter Range | Remarks | Provided by |
|---|---|---|---|---|---|
| constant | SolubilityOfCarbonInVolcanicAsh[moles/liter] | C solubility (mol/L) | 1.0 | Wilson et al. (1994), p. 9-9; Kerrisk (1985), table 9, p. 14 | ** |
| ** ** ** ***>>> DCAGS <<<*** ** | | | | | |
| constant | DistanceCutoffForDoseConversionDualityInDCAGS[km] | Cutoff point between a farming and a residential group | 19.99 | Jarzemba and Weldy (1997), p. 8 | ** |
| loguniform | AirborneMassLoadAboveFreshAshBlanket[g/m3] | Mass of soil in the air above a fresh volcanic ash blanket | 2.5e-3, 3.3e-2 | Calculated average annual concentration based on an initial value of 0.1 – 1 $g/m^3$ immediately following eruption (National Council on Radiation Protection and Measurements, 1984) and 1 – 10 times the maximum that humans can barely tolerate (Stewart, 1964). Assumed to decrease with a half-life of 55 days during the first year based on data in Anspaugh (1975). Includes temporary increases due to plowing. | JRW 3/2/00 |
| constant | OccupancyFactorForVolcanismDoseCalculation[-] | Fraction of time that receptor is exposed to airborne volcanic ash | 0.605 | Kennedy and Strange (1992). Based on receptor spending 79% of time indoors, 20% outdoors, 1% gardening and raising alfalfa. Time spent indoors | PL 10/23/00 |

| Distribution Type | Parameter Name | Description | Parameter Range | Remarks | Provided by |
|---|---|---|---|---|---|
| | | | | reduces the airborne mass load by 50%. The 50% reduction is based on normal soil mass loading conditions and may be conservative for volcanic ash. | |
| constant | DepthOfResuspendableLayer[cm] | Thickness of the upper soil layer that is available for resuspension (cm) | 0.3 | — | ** |
| loguniform | AirborneMassLoadAboveSoil [g/m3] | Mass of soil in air above Amargosa Valley soil | 5e-5, 3e-4 | Based on data for particles < 100 µm from Tegen and Fung (1994), Sehmel (1977), Anspaugh et al. (1975), Soldat et al. (1973), and Rognon (1991) | JRW 3/2/00 |
| constant | RateOfReductionOfMassLoadingFactor[1/yr] | Rate at which mass load factor goes from value above ash to value above soil following the igneous event | 0.07 | Anspaugh et al. (1975) and Nuclear Regulatory Commission (1975) would support a half-life of approximately 1 yr. To account for the wide distribution of ash in the surrounding area potentially replenishing fine material in the blanket, increase half-life to 10 yr. | JRW 3/2/00 |
| ** | | | | | |
| ** | | | | | |
| ** ***>>> CORRELATED PARAMETERS <<<*** | | | | | |
| ** | | | | | |

| Distribution Type | Parameter Name | Description | Parameter Range | Remarks | Provided by |
|---|---|---|---|---|---|
| correlateinputs | SubAreaWetFraction and ArealAverageMeanAnnualInfiltrationAtStart[mm/yr] | Correlation between subarea wet fraction and areal average mean annual infiltration at start (mm/yr) | 0.631 | See appendix F | ** |
| correlateinputs | SubAreaWetFraction and MatrixPermeability_TSw_[m2] | Correlation between subarea wet fraction and matrix permeability of Topopah Spring | -0.623 | Same as above | ** |
| correlateinputs | AlluviumMatrixRD_SAV_Am and AlluviumMatrixRD_SAV_Pu | Correlation between alluvium matrix Rd for Am and alluvium matrix Rd for Pu | 0.964 | CNWRA best estimate | ** |
| correlateinputs | AlluviumMatrixRD_SAV_Am and AlluviumMatrixRD_SAV_U | Correlation between alluvium matrix Rd for Am and alluvium matrix Rd for U | 0.346 | Same as above | ** |
| correlateinputs | AlluviumMatrixRD_SAV_Am and AlluviumMatrixRD_SAV_Np | Correlation between alluvium matrix Rd for Am and alluvium matrix Rd for Np | 0.837 | Same as above | ** |
| correlateinputs | AlluviumMatrixRD_SAV_Am and AlluviumMatrixRD_SAV_Th | Correlation between alluvium matrix Rd for Am and alluvium matrix Rd for Th | 0.112 | Same as above | ** |
| correlateinputs | AlluviumMatrixRD_SAV_Pu and AlluviumMatrixRD_SAV_U | Correlation between alluvium matrix Rd for | 0.489 | Same as above | ** |

| Distribution Type | Parameter Name | Description | Parameter Range | Remarks | Provided by |
|---|---|---|---|---|---|
| | | Pu and alluvium matrix Rd for U | | | |
| correlateinputs | AlluviumMatrixRD_SAV_Pu and AlluviumMatrixRD_SAV_Np | Correlation between alluvium matrix Rd for Pu and alluvium matrix Rd for Np | 0.881 | Same as above | ** |
| correlateinputs | AlluviumMatrixRD_SAV_Pu and AlluviumMatrixRD_SAV_Th | Correlation between alluvium matrix Rd for Pu and alluvium matrix Rd for Th | 0.109 | Same as above | ** |
| correlateinputs | AlluviumMatrixRD_SAV_Np and AlluviumMatrixRD_SAV_Th | Correlation between alluvium matrix Rd for Np and alluvium matrix Rd for Th | 0.260 | Same as above | ** |
| correlateinputs | AlluviumMatrixRD_SAV_Np and AlluviumMatrixRD_SAV_U | Correlation between alluvium matrix Rd for Np and alluvium matrix Rd for U | 0.610 | Same as above | ** |
| correlateinputs | AlluviumMatrixRD_SAV_Th and AlluviumMatrixRD_SAV_U | Correlation between alluvium matrix Rd for Th and alluvium matrix Rd for U | 0.165 | Same as above | ** |
| ** endoffile | | | | | |

# APPENDIX A
# LIST OF INITIALS

| | |
|---|---|
| BEH | B.E. Hill |
| DAF | D.A. Farrell |
| DD | D. Dunn |
| DH | Debra Hughson |
| DRT | D.R. Turner |
| GC | G. Cragnolino |
| JAS | J.A. Stamatakos |
| JRW | J.R. Weldy |
| JW | J. Winterle |
| LY | L. Yang |
| OPR | O. Pensado-Rodgriguez |
| PAL | P.A. LaPlante |
| RWF | R.W. Fedors |
| SB | S. Brossia |
| SH | S. Hsiung |
| SM | S. Mohanty |
| TA | T. Ahn |
| TJM | T.J. McCartin |
| ** | Indicates that data from the TPA Version 3.2 code apply to the TPA Version 4.0 code. |

# APPENDIX A
# REFERENCES


Alvarez, M.G., and J.R. Galvele. The mechanism of pitting of high-purity iron in NaCl solutions. *Corrosion Science* 24: 27–8. 1984.

American Society for Testing and Materials. *Pressure Vessel Plates, Carbon Steel, for Moderate- and Lower-Temperature Service.* A516–90. West Conshohocken, PA: American Society for Testing and Materials. 1995.

American Society of Mechanical Engineers. *Boiler and Pressure Vessel Code.* Section II. New York: American Society of Mechanical Engineers. 1998.

Anderson, K. The dynamics of sheet intrusion. *Proceedings of the Royal Society of Edinburgh* 58: 242–251. 1938.

Andersson, K. *SKI Project-90: Chemical Data.* SKI TR 91:21. Stockholm, Sweden: Swedish Nuclear Power Inspectorate (SKI). 1988.

Anspaugh, L.R., J.H. Shinn, P.L. Phelps, and N.C. Kennedy. Resuspension and redistribution of plutonium in soils. *Health Physics* 29: 571–582, 1975.

Anspaugh, L.R. *Retention by Vegetation of Radionuclides Deposited in Rainfall—A Literature Summary.* UCRL–53810. Livermore, CA: Lawrence Livermore National Laboratory, 1987.

Baca, R.G., and M.S. Jarzemba., eds. *Detailed Review of Selected Aspects of Total System Performance Assessment—1995.* San Antonio, TX: Center for Nuclear Waste Regulatory Analyses. 1997.

Baes, C.F., III, R.D. Sharp, A.L. Sjoreen, and R.W. Shor. *A Review and Analysis of Parameters for Assessing Transport of Environmentally Released Radionuclides Through Agriculture.* ORNL-5786. Oak Ridge, TN: Oak Ridge National Laboratory. 1984.

Belle, J., ed. *Uranium Dioxide: Properties and Nuclear Applications.* Washington, DC: U.S. Atomic Energy Commission. 1961.

Bockris, J., and A. Reddy. *Modern Electrochemistry.* New York: Plenum Press: 2. 1970.

Bodvarsson, G.S., and T.M. Bandurraga. *Development and Calibration of the Three-Dimensional Site-Scale Unsaturated Zone Model of Yucca Mountain, Nevada.* LBNL–9315. Berkeley, CA: Berkeley National Laboratory. 1996.

Bradbury, M.H., and F.A. Sarott. *Sorption Databases for the Cementitious Near-Field of a L/ILW Repository for Performance Assessment.* PSI 95-06. Villigen, Switzerland: Paul Scherrer Institute. 1995.

Brandes, E.A. *Smithells Metals Reference Book.* 6th Edition. London, England: Butterworks: 14–31. 1983.

Brechtel, C.E., M. Lin, E. Martin, and D.S. Kessel. *Geotechnical Characterization of the North Ramp of the Exploratory Studies Facility.* Volume I: Data Summary. SAND95–0488/1 UC–814. Albuquerque, NM: Sandia National Laboratory. 1995.

Breshears, D.D., T.B. Kirchner, M.D. Otis, and F.W. Whicker. Uncertainty in predictions of fallout radionuclides in foods and of subsequent ingestion. *Health Physics* 57(6): 943–953, 1989.

Bruno, J., I. Casas, E. Cera, J. De Pablo, J. Giménez, and M. E. Torrero. Uranium (IV) dioxide and simfuel as chemical analogues of spent fuel matrix dissolution. A comparison of dissolution results in a standard NaCl/$NaHCO_3$ solution. *Materials Research Society Symposium Proceedings*. Pittsburgh, PA: Materials Research Society: Symposium Proceedings 353: 601–608. 1995.

Calvo, E.J. *Study of the electroreduction reaction of oxygen on passive metals in different aqueous media* (in Spanish). Ph.D. dissertation. Universidad Nacional de La Plata Argentina, Buenos Aires, Argentina. 1997.

Calvo, E.J., and D.J. Schriffrin. The electrochemical reduction of oxygen on passive iron in alkaline solutions. *Journal of Electroanalytical Chemistry* 243: 171–185. 1988.

Campbell, A.C., and K.M. Krupka. Application of geochemical data and modeling in performance assessments of low-level radioactive waste disposal facilities. *Symposium on Hydrogeologic and Geochemical Aspects of Waste Disposal. Waste Management '97 Proceedings, March 4, 1997.* Tucson, AZ: Waste Management Symposia, Inc. 1997.

Casas, I., J. Giménez, V. Marti, M. E. Torrero, and J. De Pablo. Kinetically controlled dissolution of $UO_2$(s) under oxidizing conditions. A combined dissolution-oxidation model. *Materials Research Society Symposium Proceedings*. Pittsburgh, PA: Materials Research Society: Symposium Proceedings 2,294: 61–67. 1993.

Chambers, D., and L. Mays. *The American Garden Guides: Vegetable Gardening*. New York: Pantheon Books. 1994.

Civilian Radioactive Waste Management System, Management and Operating Contractor. *Initial Summary Report for Repository/Waste Package Advance Conceptual Design.* B00000000–01717–57–5–00015. Revision 01. Las Vegas, NV: Civilian Radioactive Waste Management System, Management and Operating Contractor. 1994.

Civilian Radioactive Waste Management System, Management and Operating Contractor. *Mined Geologic Disposal System Advanced Conceptual Design Report.* B00000000–0717–5705–0027. Revision 00. Las Vegas, NV: Civilian Radioactive Waste Management System, Management and Operating Contractor. 1996.

Civilian Radioactive Waste Management System, Management and Operating Contractor. *License Application Design Selection Report.* B00000000–01717–4600–00123. Las Vegas, NV: Civilian Radioactive Waste Management System, Management and Operating Contractor. 1999a.

Civilian Radioactive Waste Management System, Management and Operating Contractor. *Development of Numerical Grids for UZ Flow and Transport Modeling.* ANL–NBS–HS–000015. Revision 00. Las Vegas, NV: Civilian Radioactive Waste Management System, Management and Operating Contractor. 1999b.

Civilian Radioactive Waste Management System, Management and Operating Contractor. *Integrated Site Model Progress Model Report.* TDR–NBS–GS–000002. Revision 00. Las Vegas, NV: Civilian Radioactive Waste Management System, Management and Operating Contractor. 1999c.

Clifton, J.R., L.I. Knab, E.J. Garboczi, and L.X. Xiong. 1991. *Chloride Ion Diffusion in Low Water-to-Solid Cement Pastes.* NUREG/CR-5727. Washington, DC: U.S. Nuclear Regulatory Commission.

Codell, R.B., N.A. Eisenberg, D.J. Fehringer, W.H. Ford, T.S. Margulies, T.J. McCartin, J.R. Park, and J.D. Randall. *Initial Demonstration of the NRC's Capability to Conduct a Performance Assessment for a High-Level Waste Repository.* NUREG–1327. Washington, DC: Nuclear Regulatory Commission. 1992.

Connor, C.B., and B.E. Hill. Three nonhomogeneous Poisson models for the probability of basaltic volcanism: Application to the Yucca Mountain region. *Journal of Geophysical Research* 100: 10,107–10,125. 1995.

Connor, C.B., S. Magsino, J. Stamatakos, R. Martin, P. LaFemina, B. Hill, and S. Lieber. Magnetic surveys help reassess volcanic hazards at Yucca Mountain. EOS, *Transactions, American Geophysical Union* 74(7): 73–78. 1997.

Connor, C.B., J.A. Stamatakos, D.A. Ferrill, B.E. Hill, G. Ofoegbu, F.M. Conway, B. Sagar, and J.S. Trapp. Geologic factors controlling patterns of small-volume basaltic volcanism: Application to a volcanic hazards assessment at Yucca Mountain, Nevada. *Journal of Geophysical Research* 105: 417–432. 2000.

Cragnolino, G.A., H.K. Manaktala, and Y-M. Pan. *Thermal Stability and Mechanical Properties of High-Level Radioactive Waste Container Materials: Assessment of Carbon and Low-Alloy Steels.* CNWRA 96-004. San Antonio, TX: Center for Nuclear Waste Regulatory Analyses. 1996.

Cragnolino, G.A., Dunn, D.S., P. Angell, Y-M. Pang, and N. Sridhar. Factors influencing the performance of carbon steel overpacks in the proposed high-level nuclear waste repository. *Proceedings of the CORROSION '98 Conference.* Paper No. 147. Houston, TX: NACE International. 1998.

Cragnolino, G.A., D.S. Dunn, C.S. Brossia, V. Jain, and K.S. Chan. *Assessment of Performance Issues Related to Alternate Engineered Barrier System Materials and Design Options.* CNWRA 99-003. San Antonio, TX: Center for Nuclear Waste Regulatory Analyses.1999.

Cunnane, J. *Commercial spent fuel tests at ANL. Presentation to Container Life and Source Term Appendix 7 Meeting.* July 7–8, 1999. Livermore, CA: Lawrence Livermore National Laboratory and Argonne, IL: Argonne National Laboratory. 1999.

Daniels, W.R. *Laboratory and Field Studies Related to Radionuclide Migration Project.* LA–9192–PR. Albuquerque, NM: Los Alamos National Laboratory. 1981.

Delaney, P.T., and A.E. Gartner. Physical processes of shallow mafic dike emplacement near the San Rafael Swell, Utah. *Geological Society of America Bulletin* 109: 1,177–1,192. 1997.

Delaney, P.T., D.D. Pollard, J.I. Ziony, and E.H. McKee. Field relations between dikes and joints: Emplacement processes and paleostress analysis. *Journal of Geophysical Research* 91(B5): 4,920–4,938. 1986.

Delgado-Granados, H., P. Cervantes-Laing, R. Molinero-Molinero, J. Nieto-Obregon, H.L. Macias-Gonzalex, C. Mendoza-Rosales, G. Silvia-Romo, and A. Pastrana. Geology of Xitle volcano (southern Mexico City): I. Stratigraphy and age. *Colima Volcano Sixth International Meeting*. Colima, Mexico: University of Colima: 114. 1998.

de Marsily, G. *Quantitative Hydrogeology*. Orlando, FL: Academic Press, Inc. 1986.

de Pablo, J., I. Casas, J. Giménez, M. Molera, and M. E. Torrero. Effect of temperature and bicarbonate concentration on the kinetics of $UO_2$(s) dissolution and under oxidizing condition. *Materials Research Society Symposium Proceedings*. Pittsburgh, PA: Materials Research Society: Symposium Proceedings 465: 535–542. 1997.

DeWispelare, A.R., L.T. Herren, M.P. Miklas, and R.T. Clemen. *Expert Elicitation of Future Climate in the Yucca Mountain Vicinity*. CNWRA 93–016. San Antonio, TX: Center for Nuclear Waste Regulatory Analyses. 1993.

Doering, T.W. *Dimensions of Waste Packages Barriers*. Las Vegas, NV: Civilian Radioactive Waste Management System, Management and Operating Contractor. 1995.

Doubik, P., and B.E. Hill. Magmatic and hydromagmatic conduit development during the 1975 Tolbachik eruption, Kamchatka, with implications for hazards assessment at Yucca Mountain, Nevada. *Journal of Volcanology and Geothermal Research* 91: 43–64. 1999.

Dunn, D.S., Y-M. Pan, and G.A. Cragnolino. *Effects of Environmental Factors on the Aqueous Corrosion of High-Level Radioactive Waste Containers—Experimental Results and Models*. CNWRA 99-004. San Antonio, TX: Center for Nuclear Waste Regulatory Analyses. 1999.

Dyer, J.R. *Radionuclide Solutbility Working Group (SolWOG) Meeting Report (SCP: N/A)*. Department of Energy Letter with Enclosure to Lawrence Livermore National Laboratory and Los Alamos National Laboratory. 1993.

Eckerman, K.F., A.B. Wolbarst, and A.C.B. Richardson. *Limiting Values of Radionuclide Intake and Air Concentration and Dose Conversion Factors for Inhalation, Submersion, and Ingestion*. Federal Guidance Report No. 11. Oak Ridge, TN: Oak Ridge National Laboratory. 1988.

Einziger, R.E., L.E. Thomas, H.C. Buchanan, and R.B. Stout. Oxidation of spent fuel in air at 175 to 195 °C. *Journal of Nuclear Materials* 190: 53–60. 1992.

Electrical Power Research Institute. *Earthquakes and Tectonics Expert Judgement Elicitation Project*. Geomatrix Project 3055-13, EPRI TR–102000. San Francisco, CA: Geomatrix Consultants, Inc. 1993.

Electrical Power Research Institute. *Alternative Approaches to Assessing the Performance and Suitability of Yucca Mountain for Spent Fuel*. Report TR–108732. Palo Alto, CA: EPRI: 5-49 through 5-50. 1998.

Electrical Power Research Institute. *Evaluation of Pipe Failure Potential Via Degradation Mechanism Assessment*. Report TR–110157. Palo Alto, CA: EPRI. 1998b.

Fedors, R.W., and G.W. Wittmeyer. *Initial Assessment of Dilution Effects Induced by Water Well Pumping in the Amargosa Farms Area*. San Antonio, TX: Center for Nuclear Waste Regulatory Analyses. 1998.

Finn, P.A., D.J. Wronkiewicz, R.J. Finch, J.C. Hoh, C. Mertz, J.W. Emery, E.C. Buck, J. Fortner, S.F. Wolf, L.A. Neimark, and J.K. Bates. *Yucca Mountain Project—Argonne National Laboratory, Annual Progress Report, FY 1997, for Activity WP 1221, Unsaturated Drip Condition Testing of Spent Fuel and Unsaturated Dissolution Tests of Glass*. ANL–98/12. Argonne, IL: Argonne National Laboratory. 1998.

Fischer, J.M. *Sediment Properties and Water Movement Through Shallow Unsaturated Alluvium at an Arid Site for Disposal of Low-Level Radioactive Waste Near Beatty, Nye County, Nevada.* Water Resources Investigations Report 92-4032. U.S. Geological Survey. 1992.

Fisher, R.V., and H-U. Schmincke. *Pyroclastic Rocks*. New York: Springer-Verlag. 1984.

Flint, L. *Characterization of Hydrologic Units Using Matrix Properties, Yucca Mountain, Nevada*. Report 97–4243. Denver, CO: U.S. Geological Survey. 1996.

Forsyth, R. *An Evaluation of Results from the Experimental Programme Performed in the Studsvik Hot Cell Laboratory*. SKB TR 97-25. Stockholm, Sweden: Swedish Nuclear Fuel and Waste Management Company.1997.

Forsyth, R.S., L.O. Wermer, and J. Bruno. The corrosion of spent $UO_2$ fuel in synthetic groundwater. *Journal of Nuclear Materials*. 138: 1–15. 1986.

Fuger, J. Thermodynamic properties of actinide aqueous species relevant to geochemical processes. *Radiochimica Acta* 58/59: 81–92. 1992.

Galvele, J.R. Present State of Understanding of the breakdown of passivity and repassivation. *Proceedings of the Fourth International Symposium on Passivity*. R.P. Frakenthal and J. Kruger, eds. Princeton, NJ: The Electrochemical Society, Inc. 1978.

García-Serrano, J., J. A. Serrano, P. P. Díaz-Arocas, J. Quiñones, and J. L. R. Almazan. Simfuel leaching studies in granite groundwater under oxidizing conditions. *Materials Research Society Symposium Proceedings*. Pittsburgh, PA: Materials Research Society: Symposium Proceedings 412: 83–90. 1996.

Gartner, A.E., and P.T. Delaney. *Geologic Map Showing a Late Cenozoic Basaltic Intrusive Complex, Emery, Sevier, and Wayne Counties, Utah.* U.S. Geological Survey. Miscellaneous Field Studies, Map MF–2052. Scale 1:48,000. 1988.

Gauthier, J. *Expert Elicitation of the Solubility Distributions to be Used in TSPA#2 Calculations*. Draft Report. Albuquerque, NM: Sandia National Laboratory. 1993.

Geldon, A.L., A.M.A. Umari, M.F. Fahy, J.D. Earle, J.M. Gemmel, and J. Darnell. *Results of Hydraulic and Conservative Tracer Tests in Miocene Tuffaceous Rocks at the C-Hole Complex, 1995 to 1997, Yucca Mountain, Nevada*. Milestone Report SP23PM3. Las Vegas, NV: U.S. Geological Survey. 1997.

Ghosh, A., R.D. Manteufel, and G.L. Stirewalt. *FAULTING Version 1.0—A Code for Simulation of Direct Fault Disruption: Technical Description and User's Guide.* CNWRA 97-002. San Antonio, TX: Center for Nuclear Waste Regulatory Analyses. 1997.

Gray, W.J., H.R. Leider, and S.A. Steward. Parametric study of LWR spent fuel dissolution kinetics. *Journal of Nuclear Materials* 190: 46–52. 1992.

Gray, W.J, and L.E. Thomas. Dissolution rates of as-received and partially oxidized spent fuel. *High Level Radioactive Waste Management: Proceedings of the Third International Conference.* LaGrange, IL: American Nuclear Society: 1,458–1,464. 1992.

Gray, W.J, L.E. Thomas, and R.E. Einziger. Effects of air oxidation on the dissolution rate of LWR spent fuel. *Materials Research Society Symposium Proceedings*. Pittsburgh, PA: Materials Research Society: Symposium Proceedings 294: 47–54. 1993.

Gray, W.J., S.A. Steward, J.C. Tait, and D.W. Shoesmith. *High Level Radioactive Waste Management: Proceedings of the Fifth Annual International Conference.* LaGrance, IL: American Nuclear Society: 2,597–2,601. 1994.

Gray, W.J. and C.N. Wilson. *Spent Fuel Dissolution Studies FY 1991 to 1994.* PNL–10540. Richland, WA: Pacific Northwest National Laboratory. 1995.

Green, R.T., F.T. Dodge, S.J. Svedeman, R.D. Manteufel, G. Rive, K.A. Meyer, and R.G. Baca. 1995. *Thermally Driven Moisture Redistribution in Partially Saturated Porous Media.* NUREG/CR–6348. Washington, DC: U.S. Nuclear Regulatory Commission.

Guenther, R.J., D.E. Blahnik, U.P. Jenquin, J.E. Mendel, L.E. Thomas, and C.K. Thornhill. *Characterization of Spent Fuel Approved Testing Material–ATM–104.* PNL–5109–104. Richland, WA: Pacific Northwest National Laboratory. 1991.

Heusler, K.E. Influence of temperature and pressure on the kinetics of electrode processes. *High Temperature, High Pressure Electrochemistry in Aqueous Systems*. D. deG. Jones and R.W. Staehle, eds. Houston, TX: National Association of Corrosion Engineers: 387–399. 1976.

Hill, B.E. *Constraints on the Potential Subsurface Area of Disruption Associated with Yucca Mountain Region Basaltic Volcanoes.* San Antonio, TX: Center for Nuclear Waste Regulatory Analyses. 1996.

Hill, B.E., and C.B. Connor. Field volcanism. *NRC High-Level Radioactive Waste Research at CNWRA, July–December 1994.* CNWRA 94-02S. San Antonio, TX: Center for Nuclear Waste Regulatory Analyses: 141–154. 1995.

Hill, B.E., and C.B. Connor. Volcanic systems of the basin and range. *NRC High-Level Radioactive Waste Research at CNWRA, July–December 1995.* CNWRA 95-02S. San Antonio, TX: Center for Nuclear Waste Regulatory Analyses: 5-1 to 5-21. 1996.

Hill, B.E., and J.S. Trapp. *Sensitivity Analysis for Key Parameters in the VOLCANO and ASHPLUME Modules of the TPA 3.1 Code.* San Antonio, TX: Center for Nuclear Waste Regulatory Analyses. 1997.

Hill, B.E., C.B. Connor, and J.S. Trapp. Igneous activity. *NRC High-Level Radioactive Waste Program Annual Progress Report, Fiscal Year 1996*. CNWRA 96-01A. San Antonio, TX: Center for Nuclear Waste Regulatory Analyses: 2-1 to 2-32. 1996.

Hill, B.E., C.B. Connor, M.S. Jarzemba, P.C. La Femina, M. Navarro, and W. Strauch. *1995 Eruptions of Cerro Negro Volcano, Nicaragua, and Risk Assessment for Future Eruptions*. San Antonio, TX: Center for Nuclear Waste Regulatory Analyses. 1997.

Hill, B.E., C.B. Connor, M.S. Jarzemba, P.C. La Femina, M. Navarro, and W. Strauch. 1995 eruptions of Cerro Negro volcano, Nicaragua, and risk assessment for future eruptions. *Geological Society of America Bulletin*. 10: 1,231–1,241. 1998.

Hoek, E., and E.T. Brown. *Underground Excavations in Rock*. London, England: Institution of Mining and Metallurgy. 1982.

Hoffman, F.O., R.H. Gardner, and K.F. Eckerman. *Variability in Dose Estimates Associated with the Food Chain Transport and Ingestion of Selected Radionuclides*. NUREG/CR–2612. Washington, DC: Nuclear Regulatory Commission. 1982.

Incropera, F.P., and D.P. DeWitt. *Fundamentals of Heat and Mass Transfer*. 3rd Edition. New York: John Wiley and Sons. 1995.

International Atomic Energy Agency. *Volcanoes and Associated Topics in Relation to Nuclear Power Plant Siting*. IAEA–TECDOC–VOLCANO8.WPW. Vienna, Austria: International Atomic Energy Agency. 1997.

International Commission on Radiological Protection. *Age-Dependent Doses to Members of the Public from Intake of Radionuclides. Part 5: Compilation of Ingestion and Inhalation Dose Coefficients*. ICRP 72. Annals of the International Commission on Radiological Protection. Tarrytown, NY: Elsevier Science Inc. 1996.

International Union of Radioecologists. *Sixth Report of the Working Group on Soil-to-Plant Transfer Factors*. Biltoven, The Netherlands: RIVM, 1989.

Jarzemba, M.S. Stochastic radionuclide distributions after a basaltic eruption for performance assessments of Yucca Mountain. *Nuclear Technology* 118(2): 132–141. 1997.

Jarzemba, M.S., and P.A. LaPlante. *Preliminary Calculations of Expected Dose from Extrusive Volcanic Events at Yucca Mountain*. San Antonio, TX: Center for Nuclear Waste Regulatory Analyses. 1996.

Jarzemba, M.S., and R.D. Manteufel. An analytically based model for the simultaneous leaching-chain decay of radionuclides from contaminated ground surface soil layers. *Health Physics* 73(6): 919–927. 1997.

Jarzemba, M.S., and J.R. Weldy. *A Summary of Information Relevant to Defining Critical Groups and Reference Biospheres*. San Antonio, TX: Center for Nuclear Waste Regulatory Analyses. 1997.

Jolly, R.J.H., and D.L. Sanderson. A Mohr circle construction for the opening of a fracture. *Journal of Structural Geology* 19: 887–892. 1997.

Johnson, L.H. and H.H. Joling. The dissolution of irradiated fuel under hydrothermal conditions. *Scientific Basis for Nuclear Waste Management*. Volume 6. S.V. Topp, ed. North-Holland: Physics Publishers. 1982.

Johnson, L.H., and J.C. Tait. *Release of Segregated Nuclides from Spent Fuel.* SKB 97-18. Stockholm, Sweden: Swedish Nuclear Fuel and Waste Management Company. 1997.

Kelly, E.J. *Modern Aspects of Electrochemistry*. No. 14. New York: Plenum Press: 319-424. 1982.

Kennedy, W.E., and D.L. Strenge. *Residual Radioactive Contamination from Decommissioning: Technical Basis for Translating Contamination Levels to Annual Total Effective Dose Equivalent.* NUREG/CR–5512. Volume 1. Washington, DC: Nuclear Regulatory Commission. 1992.

Kerrisk, J.F. *Solubility Limits on Radionuclide Dissolution at a Yucca Mountain Repository.* LA–9995–MS. NNA.870519.0049. Los Alamos, NM: Los Alamos National Laboratory. 1984.

Kerrisk, J.F. *An Assessment of the Important Radionuclides in Nuclear Waste.* LA–10414–MS. Los Alamos, NM: Los Alamos National Laboratory. 1985.

Klavetter, E.A., and R.R. Peters. *Estimation of Hydrologic Properties of an Unsaturated Fractured Rock Mass.* SAND84–2642. Albuquerque, NM: Sandia National Laboratories. 1986.

Kowaka, M. Selection of probability dissolution type. *Introduction to Life Prediction of Industrial Plant Materials*. Tokyo, Japan: Allerton Press. 1994.

Lallemand-Barreś , A., and P. Peaudcerf. Recherche des relations entre les valeurs mesurees de la dispersivite macroscopique d'un millieu aquifere, ses autres caracteristiques et les conditions de mesure. Etude bibliographique. *Bull. Bur. Rech.Geol. Min.* Ser. 2. Section III, 4-1978: 277–284. 1978.

LaPlante, P.A., S.J. Maheras, and M.S. Jarzemba. *Initial Analysis of Selected Site-Specific Dose Assessment Parameters and Exposure Pathways Applicable to a Groundwater Release Scenario at Yucca Mountain.* CNWRA 95-018. San Antonio, TX: Center for Nuclear Waste Regulatory Analyses. 1995.

LaPlante, P.A., and K. Poor. *Information and Analyses to Support Selection of Critical Groups and Reference Biospheres for Yucca Mountain Exposure Scenarios*. CNWRA 97-009. San Antonio, TX: Center for Nuclear Waste Regulatory Analyses. 1997.

Linsley, R.K., and J.R. Franzini. *Water-Resources Engineering*. New York: McGraw-Hill Book Company. 1979.

Lobnig, R.E., H.P. Schmidt, K. Hennesen, and H.J. Grabke. Diffusion of cations in Chromia layers grown on iron-base alloys. *Oxidation of Metals* 37: 81–93. 1992.

Luckey, R.R., P. Tucci, C.C. Faunt, E.M. Ervin, W.C. Steinkampf, F.A. D'Agnese, and G.L. Patterson. *Status of Understanding of the Saturated Zone Ground-Water Flow System at Yucca Mountain, Nevada, as of 1995.* U.S. Geological Survey Water Resources Investigations Report 96-4077. 1996.

Lyman, T., H.E. Boyer, P.M. Unterweiser, J.E. Foster, J.P. Hontas, and H. Lawton. *Metals Handbook. Volume 1: Properties and Selection of Metals*. American Society of Metals. 8th Edition: 423. 1960.

Magill, P.L., R.R. Holden, and C. Ackley, eds. *Air pollution handbook.* New York: McGraw Hill. 1956.

Manteufel, R.D. Effects on ventilation and backfill on a mined waste disposal facility. *Nuclear Engineering and Design* 172: 205–219. 1997.

Manteufel, R.D., and N.E. Todreas. Effective thermal conductivity and edge conductance model for a spent fuel assembly. *Nuclear Technology* 105(3): 421–440. 1994.

Marsh, G., and K. Taylor. An assessment of carbon steel containers for radioactive waste disposal. *Corrosion Science* 28: 289–320. 1988.

McCright, R.D. *Engineered Materials Characterization Report, Volume 3:Corrosion Data and Modeling.* UCRL–ID–119564. Revision 1.1. Livermore, CA: Lawrence Livermore National Laboratory. 1998.

Meijer, A. *Yucca Mountain Project Far-Field Sorption Studies and Data Needs.* LA–11671–MS. Los Alamos, NM: Los Alamos National Laboratory. 1990.

Mohanty S., G.A. Cragnolino, T. Ahn, D.S. Dunn, P.C. Lichtner, R.D. Manteufel, and N. Sridhar. *Engineered Barrier System Performance Assessment Code: EBSPAC Version 1.0 β, Technical Description and User's Manual.* CNWRA 96-001. San Antonio, TX: Center for Nuclear Waste Regulatory Analyses. 1996.

Mohanty, S., G.A. Cragnolino, T. Ahn, D.S. Dunn, P.C. Lichtner, R.D. Manteufel, and N. Sridhar. *Engineered Barrier System Performance Assessment Code: EBSPAC Version 1.1, Technical Description and User's Manual.* CNWRA 97-006. San Antonio, TX: Center for Nuclear Waste Regulatory Analyses. 1997.

Morris, A.P., D.A. Ferrill, and D.B. Henderson. Slip tendency analysis and fault reactivation. *Geology* 24: 275–278. 1996.

Murphy, W.M., E.C. Pearcy, and D.A. Pickett. Natural Analog Studies at Peña Blanca and Santorini. N. von Maravic and J. Smellie., eds. *Seventh EC Natural Analogue Working Group Meeting.* EUR 17851 EN European Commission: 105–112. 1997.

Napier, B.A., R.A. Peloquin, D.L. Strenge, and J.V. Ramsdell. *GENII: The Hanford Environmental Radiation Dosimetry Software System. Volumes 1, 2, and 3: Conceptual Representation, User's Manual, and Code Maintenance Manual.* PNL–6584. Richland, WA: Pacific Northwest National Laboratory. 1988.

National Council on Radiation Protection and Measurements. *Radiological Assessment: Predicting the Transport, Bioaccumulation, and Uptake by Man of Radionuclides Released to the Environment.* NCRP 76. Bethesda, MD: National Council on Radiation Protection and Measurements. 1984.

Nevada Division of Water Resources. *Preliminary Summary of Ground Water Pumpage Inventory for Amargosa Valley Basin No. 230 from 1989 through 1993.* Carson City, NV: Nevada Division of Water Resources. Unpublished report. 1995.

Nitsche, H., R.C. Gatti, E.M. Standifer, S.C. Lee, A. Muller, T. Prussin, R.S. Deinhammer, H. Maurer, K. Becraft, S. Leung, and S.A. Carpenter. *Measured Solubilities and Speciations of Neptunium, Plutonium, and Americium in a Typical Groundwater (J-13) from the Yucca Mountain Region.*

Milestone Report 3010–WBS 1.2.3.4.1.3.1. LA–12562–MS UC–802. Los Alamos, NM: Los Alamos National Laboratory. 1993.

Nuclear Regulatory Commission. *Manufacturing Defects in Boiling Water Reactor Control Rods*. RO Bulletin No. 73-5. Washington, DC: Nuclear Regulatory Commission. 1973.

Nuclear Regulatory Commission. *Reactor Safety Study, An Assessment of Accident Risks in U.S. Commercial Nuclear Power Plants*. WASH–1400. Washington, DC: Nuclear Regulatory Commission. 1975.

Nuclear Regulatory Commission. *Investigation and Evaluation of Stress-Corrosion Cracking in Piping of Light Water Reactor Plants*. NUREG–0531. Washington, DC: Nuclear Regulatory Commission. 1979.

Nuclear Regulatory Commission. *Report of the U.S. Nuclear Regulatroy Commission Piping Review Committee*. NUREG–1061. Washington, DC: Nuclear Regulatory Commission. Volume 1: August 1984. Volume 4: December. 1984.

Nuclear Regulatory Commission. *Nuclear Fuel Cycle Facility Accident Analysis Handbook*. NUREG–1320. Washington, DC: Nuclear Regulatory Commission. 1988a.

Nuclear Regulatory Commission. *Technical Report on Material Selection and Processing Guidelines for BWR Coolant Pressure Boundary Piping*. NUREG–0313. Washington, DC: Nuclear Regulatory Commission. Revision 2. January 1988b.

Nuclear Regulatory Commission. *NRC Iterative Performance Assessment Phase 2: Development of Capabilities for Review of a Performance Assessment for a High-Level Waste Repository*. NUREG–1464. Washington, DC: Nuclear Regulatory Commission. 1995.

Nuclear Regulatory Commission. *Issue Resolution Status Report on Methods to Evaluate Climatic Change and Associated Effects at Yucca Mountain*. Washington, DC: Nuclear Regulatory Commission. 1997.

Nuclear Regulatory Commission. *Issue Resolution Status Report. Key Technical Issue: Igneous Activity*. Revision 2. Washington, DC: Nuclear Regulatory Commission, Division of Waste Management. 1999.

Östhols, E., J. Bruno, and I. Grenthe. On the influence of carbonate on mineral dissolution III: The solubility of microcrystalline $ThO_2$ in $CO_2$-$H_2$) media. *Geochimica et Cosmochimica Acta* 58: 613–623. 1994.

Park, U. *Regulatory Overview and Recommendations on a Repository's Release of C-14*. San Diego, CA: Science Applications International Corporation. 1992.

Pei-Lin, T., M.D. Siegel, C.D. Updegraf, K.K. Wahi, and R.V. Guzowski. *Repository Site Data Report for Unsaturated Tuff, Yucca Mountain, Nevada*. NUREG/CR–4410. Washington, DC: Nuclear Regulatory Commission. 1985.

Popov, E.P. *Mechanics of Materials*. New York: Prentice-Hall. 1970.

Pyle, D.M. The thickness, volume and grain size of tephra fall deposits. *Bulletin of Volcanology* 51: 1–15. 1989.

Rai, D., A.R. Felmy, D.A. Moore, and M.J. Mason. The solubility of Th(IV) and U(IV) hydrous oxides in concentrated $NaHCO_3$ and $Na_2CO_3$ solutions. T. Murakami and R.C. Ewing, eds. *Scientific Basis for Nuclear Waste Management XVIII, Materials Research Society Symposium Proceedings Volume 353*. Pittsburgh, PA: Materials Research Society: 1,143–1,150. 1995.

Rognon, P. Field Measurement of dust near the ground, correlated with surrounding soils in the Sahara and Sahe. *Z. Geomorph.* NF.35(4): 491–501, 1991.

Schenker, A.R., D.C. Guerin, T.H. Robey, C.A. Rautman, and R.W. Bernard, *Stochastic Hydrogeologic Units and Hydrogeologic Properties Development for Total System Performance Assessments.* SAND94–0244. Albuquerque, NM: Sandia National Laboratories. 1995.

Scott, R.B., and J. Bonk. *Preliminary Geologic Map (1:12.000 scale) of Yucca Mountain, Nye County, Nevada, with Geologic Cross Sections*. U.S. Geological Survey Open-File Report 84-494. 1984.

Scully, J.R., and H.P. Hack. Galvanic corrosion prediction using long- and short-term polarization curves. *CORROSION '84*. Paper No. 34. Houston, TX: National Association of Corrosion Engineers. 1984.

Sehmel, G.A. *Radionuclide Particle Resuspension Research Experiments on the Hanford Reservation.* BNWL–2081. Richland, WA: Pacific Northwest National Laboratory. 1977.

Sheppard, M.I., and D.H. Thibault. Default soil solid/liquid partition coefficients, Kds, for four major soil types: A compendium. *Health Physics* 59: 471–482. 1990.

Shibata, T. and Y-C. Zhu. The effect of film formation conditions on the structure and composition of anodic oxide films on titanium. *Corrosion Science* 37: 253. 1995.

Shoesmith, D.W., S. Sunder, M.G. Bailey, and G.J. Wallace. The corrosion of nuclear fuel ($UO_2$) in oxygenated solutions. *Corrosion Science* 29: 1,115–1,128. 1989.

Shoesmith, D.W., S. Sunder, and J.C. Tait. Validation of an electrochemical model for the oxidative dissolution of used CANDU fuel. *Journal of Nuclear Materials* 257: 89–98. 1998.

Siegel, M.D., D.B. Ward, W.C. Cheng, C. Bryant, C.S. Chocas, and C.G. Reynolds. Preliminary characterization of materials for reactive transport model validation experiment. *Proceedings of the Fourth International Conference on High-Level Radioactive Waste Management.* La Grange Park, IL: American Nuclear Society: 348–358. 1993.

Simonds, W.F., J.W. Whitney, K. Fox, A. Ramelli, J.C. Yount, M.D. Carr, C.D. Menges, R. Dickerson, and R.B. Scott. *Map of Fault Activity of the Yucca Mountain Area, Nye County, Nevada.* U.S. Geological Survey Miscellaneous Investigations Series Map 1-2520. Scale 1: 24,000. 1995.

SKi, Swedish Nuclear Power Inspectorate. *Piping Failures in United States Nuclear Power Plants: 1961–1995*. SKi Report 96:20. Stockhold, Sweden: The Swedish Nuclear Power Inspectorate. 1996.

Smith, H., and Baldwin, D. An investigation of thermal release of C-14 from PWR spent fuel cladding. *FOCUS '89 Proceedings of the Topical Meeting on Nuclear Waste Isolation in the Unsaturated Zone, Las Vegas, Nevada, September 17–21, 1989*. LaGrange Park, IL: American Nuclear Society: 46–49. 1989.

Snell, R. Enhanced Design Alternative (EDA) II description and plans for refinement. *111th Meeting Advisory Committee on Nuclear Waste, Washington, DC, July 20, 1999*. Washington, DC: Nuclear Regulatory Commission. 1999.

Soldat, J.K., J.G. Droppo, Jr., W.H. Rickard, and L.G. Faust. *Assessment of the Environmental Impact of the Retrievable Surface Storage Factility.* BNWL–15–313. Richland, WA: Pacific Northwest National Laboratory. 1973.

Snell, R.D. 1997.*Transmittal of Subsurface Engineered Barrier (EB) Segment Design.* RP120M3E, WBS 1.2.4.7. Washington, DC: U.S. Department of Energy.

Sridhar, N., G.A. Cragnolino, and D.S. Dunn. *Experimental Investigations of Localized Corrosion of High-Level Waste Container Materials.* CNWRA 93-004. San Antonio, TX: Center for Nuclear Waste Regulatory Analyses. 1993.

Sridhar, N., G.A. Cragnolino, and D.S. Dunn. *Experimental Investigations of Failure Processes of High-Level Radioactive Waste Container Materials*. CNWRA 95-010. San Antonio, TX: Center for Nuclear Waste Regulatory Analyses. 1995.

Steward, S.A. and H.C. Weed. Model of $UO_2$ aqueous dissolution over a wide range of conditions. *Materials Research Society Symposium Proceedings.* Pittsburgh, PA: Materials Research Society: Symposium Proceedings 333: 409–416. 1994.

Stewart, K. The resuspension of particulate material from surfaces. *Proceedings of the Surface Contamination Symposium*. B.R. Fish, ed. New York: Pergamin Press. 1964.

Stirewalt, G.L., S.M. McDuffie, R.D. Manteufel, and R.W. Janetzke. *Technical Specifications for a Fault Displacement Module.* San Antonio, TX: Center for Nuclear Waste Regulatory Analyses. 1995.

Stockman, C. Discussion in the presentation of the near-field environment in the total system performance assessment: waste form degradation expert elicitation. *Workshop of Significant Issues and Available Data: Waste Form Degradation and Radionuclide Mobilization Expert Elicitation (WFEE) Project San Francisco, California*. Alburquerque, NM: Sandia National Laboratories. 1997.

Stothoff, S., H.M. Castellaw, and A.C. Bagtzoglou. 1997. *Simulating the Spatial Distribution of Infiltration at Yucca Mountain, Nevada*. San Antonio, TX: Center for Nuclear Waste Regulatory Analyses. 1997.

Streltsova, T.D. Well testing in heterogeneous formations. *Exxon Monograph*: 1-413. New York: John Wiley and Sons. 1988.

Stroes-Gascoyne, S., L. H. Johnson, P. A. Beeley and D. M. Sellinger. Dissolution of used CANDU fuel at various temperatures and redox conditions. *Materials Research Society Symposium Proceedings.* Pittsburgh, PA: Materials Research Society: 50: 317–326. 1985.

Stroes-Gascoyne, S., L.H. Johnson, J.C. Tait, J.L. McConnell, and R.J. Porth. Leach of used CANDU fuel: Results from a 19-year leach test under oxidizing conditions. *Materials Research Society Symposium Proceedings.* Pittsburgh, PA: Materials Research Society: 465: 511–518. 1997.

Summers, T.S.E., M.A.Wall, M. Kumar, S.J. Mathews, and R.B. Rebak. Phase stability and mechanical properties of C-22 alloy aged in the temperature range 590 to 760° for 16,000 hours. *Scientific Basis*

*for Nuclear Waste Management Symposium Proceedings*. Boston, MA: Materials Research Society: 556: 919–926. 1998.

Sunder, S., D. W. Shoesmith, N. H. Miller. Oxidation and dissolution of nuclear fuel ($UO_2$) by the products of alpha radiolysis of water. *Journal of Nuclear Materials* 244: 66–74. 1997.

Suzuki, T. *A Theoretical Model for Dispersion of Tephra. Arc Volcanism: Physics and Tectonics.* Tokyo, Japan: Terra Scientific Publishing: 95–113. 1983.

Tait, J. C. and J. M. Luht. *Dissolution Rates of Uranium from Unirradiated $UO_2$ and Uranium and Radionuclides from Used CANDU Fuel Using the Single-Pass Flow-through Apparatus.* 06819–REP–01200–0006–ROO. Toronto, Canada: Ontario Hydro. 1997.

Tanner, A.B. Methods of characterization of ground for assessment of indoor radon potential at a site. *Field Studies of Radon in Rock, Soils and Water, Part 1*. L.C.S. Gundersen and R.B. Wanty, eds. USGS Bulletin 1971. Reston, VA: U.S. Geological Survey. 1991.

Tegen, I. and I. Fung. Modeling of mineral dust in the atmosphere: sources, transport, and optical thickness. *Journal of Geophysical Research* 99(11): 22,897–22,914. 1994.

Thomas, G. F. and G. Till. The dissolution of unirradiated $UO_2$ fuel pellets under simulated disposal conditions. *Nuclear and Chemical Waste Management Symposium Proceedings* 5: 141–147. 1984.

Timmins, P.F. *Solution to Equipment Failures*. ISBN 0–87170–662–8. Materials Park, OH: ASM International. 1998.

Timoshenko, S.P. *Strength of Materials. Part II: Advanced Theory and Problems*. 3rd Edition. Princeton, NJ: D. Van Nostrand Company, Inc. 1956.

Triay, I.R., A. Meijer, J.L. Conca, S. Kung, R.S. Rundberg, and E.A. Strietelmeier. *Summary and Synthesis Report on Radionuclide Retardation for the Yucca Mountain Site Characterization Project.* Yucca Mountain Site Characterization Program Milestone 3784M. Draft. Los Alamos, NM: Los Alamos National Laboratory. 1997.

TRW Environmental Safety Systems, Inc. *Total System Performance Assessment—1995: An Evaluation of the Potential Yucca Mountain Repository*. B00000000–01717–2200–00136. Revision 01. Las Vegas, NV: TRW Environmental Safety Systems, Inc. 1995.

TRW Environmental Safety Systems, Inc. *Total System Performance Assessment—1998: Analyses Technical Basis Document. Chapter 2: Unsaturated Zone Hydrology Model*. B00000000–01717–4301–00002. Revision 01. Las Vegas, NV: TRW Environmental Safety Systems, Inc. 1998.

Tschoepe, E., F.F. Lyle, D.M. Dancer, C.G. Interrante, and P.K. Nair. *Field Engineering Experience With Structural Materials*. San Antonio, TX: Center for Nuclear Waste Regulatory Analyses. 1994.

Turnbull A., and M.K. Gardner. Electrochemical polarization studies of BS 4360 50D steel in 3.5% NaCl. *Corrosion Science* 22(7): 661–673. 1982.

Ugural A.C. and S.K. Fenster. *Advanced Strength and Applied Elasticity*. Englewood Cliffs, NJ: Prentice-Hall, Inc. 1995.

U.S. Department of Commerce. *Census of Agriculture: Farm and Ranch Irrigation Survey*. Washington, DC: U.S. Department of Commerce. 1994.

U.S. Department of Energy. *Characteristics of Spent Fuel, High Level Waste, and Other Radioactive Wastes Which May Require Long-Term Isolation.* DOE/RW–0184. Washington, DC: U.S. Department of Energy, Office of Civilian Radioactive Waste Management. 1987.

U.S. Department of Energy. *Site Characterization Plan: Yucca Mountain Site, Nevada Research and Development Area, Nevada.* DOE/RW–0199. Washington, DC: U.S. Department of Energy, Office of Civilian Radioactive Waste Management. 1988.

U.S. Department of Energy. *Yucca Mountain Project Reference Information Database.* YMP/CC–0002. Version 04.002. Las Vegas, NV: U.S. Department of Energy. 1990.

U.S. Department of Energy. *Yucca Mountain Site Characterization Project Reference Information Base.* YMP/93–02. Revision 3. Las Vegas, NV: U.S. Department of Energy. 1993.

U.S. Department of Energy. *Seismic Design Methodology for a Geologic Repository at Yucca Mountain Topical Report.* YMP–0030NP. Las Vegas, NV: U.S. Department of Energy. 1995.

U.S. Department of Energy. *Regional and Local Wind Patterns Near Yucca Mountain.* B00000000–01717–5705–00081. Washington, DC: U.S. Department of Energy, Office of Civilian Radioactive Waste Management. 1997.

U.S. Environmental Protection Agency. *Exposure Factors Handbook.* Volumes 1, 2, and 3. EPA/600/P–95/002Fa and b. Washington, DC: U.S. Environmental Protection Agency. 1997.

U.S. Geological Survey. *Seismotectonic Framework and Characterization of Faulting at Yucca Mountain, Nevada.* J.W. Whitney, coord. Denver, CO: U.S. Geological Survey. 1996.

van der Leeden, F., F.L. Troise, and D.K. Todd. *The Water Encyclopedia.* Chelsea, MI: Lewis Publishers. 1990.

Wanner, H., and I. Forest, eds. *Chemical Thermodynamics of Uranium*. New York: Elsevier Science Inc. 1992.

Walker, G.E., and T.E. Eakin. *Ground-Water Resources—Reconnaissance Series Report 14: Geology and Ground Water of Amargosa Desert, Nevada—California.* Carson City, NV: U.S. Geological Survey and U.S. Department of the Interior. 1963.

Walker, G.P.L., and R. Croasdale. Characteristics of some basaltic pyroclastics. *Bulletin of Volcanology* 35: 303–317. 1972.

Walker, G.P.L., S. Self, and L. Wilson. Tarawera 1886, New Zealand—A basaltic plinian fissure eruption. *Journal of Volcanology and Geothermal Research* 21: 61–78. 1984.

Weast, R.C. *CRC Handbook of Chemistry and Physics*. Cleveland, OH: CRC Press. 1976.

Weast, R.C., and M.J. Astle. *CRC Handbook of Chemistry and Physics.* Boca Raton, FL: CRC Press. 1984.

Wilson, C. *Results from NNWSI Series 3 Spent Fuel Dissolution Tests*. PNL–7170. Richland, WA: Pacific Northwest National Laboratory. 1990a.

Wilson, C.N. *Results from NNWSI Series 2 Bare Fuel Dissolution Tests*. PNL–7169. Richland, WA: Pacific Northwest National Laboratory. 1990b.

Wilson, M.L., J.H. Gauthier, R.W. Barnard, G.E. Barr, H.A. Dockery, E. Dunn, R.R. Eaton, D.C. Guerin, N. Lu, M.J. Martinez, R. Nilson, C.A. Rautman, T.H. Robey, B. Ross, E.E. Ryder, A.R. Scheneker, S.A. Shannon, L.H. Skinner, W.G. Halsey, J.D. Gansemer, L.C. Lewis, A.D. Lamont, I.R. Triay, A. Meijer, and D.E. Morris. *Total-System Performance Assessment for Yucca Mountain—SNL Second Iteration (TSPA–93)*. SAND93–2675. Volumes 1 and 2. Albuquerque, NM: Sandia National Laboratories. 1994.

Winterle, J.R., R.W. Fedors, D.L. Hughson, and S. Stothoff. *Review of the Unsaturated Zone Models Used to Support the Viability Assessment of a Repository at Yucca Mountain*. San Antonio, TX: Center for Nuclear Waste Regulatory Analyses. 1999a.

Winterle, J.R., R.W. Fedors, D.L. Hughson, and S.A. Stothoff. *Update of Hydrologic Parameters for the Total-system Performance Assessment Code*. San Antonio, TX: Center for Nuclear Waste Regulatory Analyses. 1999b.

Winterle, J.R., N.M. Coleman, W.A. Illman, and D. Hughson. *Review of Permeability Estimates Obtained from the Yucca Mountain Project*. San Antonio, TX: Center for Nuclear Waste Regulatory Analyses. 2000.

Wittmeyer, G.W., R. Klar, G. Rice, and W. Murphy. *The CNWRA Regional Hydrogeology Geographic Information System Database*. CNWRA 95-009. San Antonio, TX: Center for Nuclear Waste Regulatory Analyses. 1995.

Wittmeyer, G.W., M.P. Miklas, R.V. Klar, D. Williams, and D. Balin. *Use of Groundwater in the Arid and Semi-Arid Western United States: Implications for Yucca Mountain Area*. San Antonio, TX: Center for Nuclear Waste Regulatory Analyses. 1996.

Wolfsberg, K. *Sorption-desorption studies of Nevada Test Site Alluvium and Leaching Studies of Nuclear Test Debris*. LA–7216–MS. Society for Metals. Los Alamos, NM: Los Alamos National Laboratory. 1978.

Young, S.R., H.L. McKague, and R.W. Terhune. *Influence of Faults on Ascent of Mafic Magma by Dike Intrusion*. CNWRA 94-025. San Antonio, TX: Center for Nuclear Waste Regulatory Analyses. 1994.

# APPENDIX B

# APPENDIX B
# AUXILIARY INPUT DATA FILES

In addition to the primary *tpa.inp* input data file presented in appendix A, the Total-system Performance Assessment (TPA) Version 4.0 code requires auxiliary input data files presented in this appendix. The primary purpose of auxiliary input files is to provide data to the TPA code in large arrays, especially parameters that vary as functions of time. The user is not expected to change these data files frequently. Modules using these auxiliary files are identified in table B-1.

All auxiliary files are located in the subdirectory named *data*. In addition to auxiliary data files, the TPA code has other useful files in the subdirectory *data*. File *tefkti.inp* provides an option for using temperature and relative humidity data to the NFENV module computed external to the TPA code. This is not a file required by the TPA code. An exception to the files presented in table B-1 is the auxiliary data file *tpanames.dbs*. This file cannot be changed by the user. A brief description of the contents and use of each auxiliary data file follows. Also included below is either a complete or partial listing of each file.

**Table B-1. List of modules using auxiliary data files.**

| Module | Name of auxiliary data files |
|---|---|
| EXEC | *repdes.dat, tpanames.dbs* |
| INVENT | *burnup.dat, nuclides.dat* |
| EBSREL | *wpflow.def* |
| UZFLOW | *maidtbl.dat,climato1.dat, climato2.dat* |
| NFENV | *multiflo.dat, drythick.dat, tefkti.inp* |
| SZFT, DCAGW | *strmtube.dat* |
| DCAGS | *gs_cb_ad.dat, gs_cb_ci.dat, gs_pb_ad.dat, gs_pb_ci.dat* |
| DCAGW | *dilution.dat, FILENAME.DAT, gbioacl.dat, gdosinc2.dat, ggamen.dat, ggrdf.dat, gnewdf.dat, grmdlib.dat* |

**File name: *burnup.dat***

The file *burnup.dat* contains input data on the temporal evolution of thermal outputs from the pressurized water reactor (PWR) and boiling water reactor (BWR) wastes. The file also contains information on the mix of PWR and BWR wastes. Thermal outputs are presented in W/MTU. This input data file is read directly by *invent.f* instead of being read by *reader.f*. For thermal output as a function of time, the file is read until the *end-of-file* is encountered.

```
TITLE: New data introduced for TPA Version 4.0 (rwr 2/24/00)
0.35                                ! bwr blend
0.65                                ! pwr blend
```

| times (yr) | bwr (W/MTU) | pwr (W/MTU) |
|---|---|---|
| 1.0010005 | 4429.246 | 9036.769 |
| 1.010050167 | 4402.999 | 8982.422 |
| 1.105170918 | 4148.927 | 8456.606 |
| 2.718281828 | 2289.858 | 4626.182 |
| 7.389056099 | 1183.043 | 2366.689 |
| 20.08553692 | 611.2127 | 1210.764 |
| 54.59815003 | 315.7798 | 619.4099 |
| 148.4131591 | 163.1459 | 316.8813 |
| 403.4287935 | 84.28847 | 162.112 |
| 1096.633158 | 43.54719 | 82.93418 |
| 2980.957987 | 22.49842 | 42.42794 |
| 8103.083928 | 11.62369 | 21.70553 |
| 22026.46579 | 6.005316 | 11.10424 |
| 59874.14172 | 3.102614 | 5.680772 |
| 162754.7914 | 1.602949 | 2.906202 |
| 442413.3920 | 0.828155 | 1.486772 |
| 1202604.284 | 0.427862 | 0.760611 |

**File name:** ***climato1.dat***

The file *climato1.dat* contains data utilized by UZFLOW to determine the climatic conditions (i.e., distributions for temperature and precipitation). Specifically, the information in *climato1.dat* is the distributed perturbation data that are used to calculate the time-varying mean annual precipitation (MAP) and the mean annual temperature (MAT). The data from this file are utilized to add "noise" to MAP and MAT. The first 20 lines and last 5 lines of this file are listed below.

```
-5.7053335e-01
-1.0290445e+00
-1.1575096e+00
 9.8697251e-01
 1.2410360e+00
-3.0644614e-01
-1.9374674e-01
 1.1952564e+00
-1.1220900e+00
 6.9738339e-01
-5.2758746e-01
-8.1619222e-01
-2.0944012e-01
-1.7963021e+00
 8.7311825e-01
-1.4202760e-01
-1.4503307e-01
-5.1493563e-01
-3.9668029e-01
-7.5092842e-01

      .
      .
      .

-8.6848566e-01
-7.6236354e-01
-7.6825708e-01
-1.5438075e+00
```

```
-5.7736113e-01
```

**File name:** ***climato2.dat***

UZFLOW reads three columns of data from *climato2.dat*. The first column is time in 1,000-yr steps from 0 yr to 100,000 yr. The second and third columns are the fraction of full glacial *MAP* and *MAT*, respectively. These data represent the variance from present-day precipitation and temperature conditions (0 at 0 yr) to glacial conditions (1 at 50,000 yr) and back to the equivalent of present-day conditions at 100,000 yr. With these data, calculations performed in UZFLOW generate time-varying climatic conditions that provide distributions for *MAP* and *MAT*. The first 21 lines and last 5 lines of *climato2.dat* are presented below.

```
0 0 0
1000 0 0
2000 0.0253339 0.0253339
3000 0.0560985 0.0560985
4000 0.0906067 0.0906067
5000 0.128457 0.128457
6000 0.169215 0.169215
7000 0.21242 0.21242
8000 0.257593 0.257593
9000 0.304244 0.304244
10000 0.35188 0.35188
11000 0.40001 0.40001
12000 0.448158 0.448158
13000 0.495864 0.495864
14000 0.542693 0.542693
15000 0.588244 0.588244
16000 0.63215 0.63215
17000 0.674086 0.674086
18000 0.713773 0.713773
19000 0.750977 0.750977
20000 0.785517 0.785517
       .
      .
      .
96000 -0.0615372 -0.0615372
97000 -0.0541378 -0.0541378
98000 -0.0416805 -0.0416805
99000 -0.024316 -0.024316
100000 -0.00225362 -0.00225362
```

**File name:** ***dilution.dat***

For the residential receptor group, the calculation of the fraction of total plume mass captured from well pumping uses data in *dilution.dat*. The DCAGW module reads data from *dilution.dat* and performs linear interpolation to find capture width, capture thickness, and screen length. The *dilution.dat* file supplies data for well capture width and well capture thickness as functions of pumping rate and aquifer thickness. Additionally, data for the well screen length are provided as a function of pumping rate. The well pumping rate, aquifer thickness, and plume thickness are sampled parameters defined in *tpa.inp*. Using values for capture width, capture thickness, screen length, and plume thickness, along with the sum of all streamtube widths read from *strmtube.dat* file, the fraction of the total plume mass captured by pumping is calculated. A complete listing of *dilution.dat* is presented below.

```
TITLE: TPA4.0 Wellbore dilution data for the saturated zone.
TITLE: (data from R. Fedors 1/5/98 - prepared by rwr)
TITLE: (Updated 9/99)
** (data must be in the following sequence and format
**  with the same pump rates and aquifer thicknesses
**  for capture width and capture thicknesses - the screen
**  length pump rates can be different than those for
**  capture width and thickness)
**
**
** Number of Values for Pump Rate
  8
**
** Number of Values for Aquifer Thickness
  5
**
**
** Capture Width (meters)
**
**   Pump Rate              Aquifer Thickness
**    (m^3/d)                       (m)
                    300.    475.    650.    825.    1000.
**
         3.4         82.     82.     82.     82.      82.
        10.         142.    142.    142.    142.     142.
        50.         327.    323.    320.    319.     319.
       240.         850.    760.    730.    720.     712.
       430.        1292.   1084.   1010.    984.     966.
       620.        1728.   1378.   1260.   1204.    1178.
       810.        2180.   1662.   1490.   1412.    1370.
      1000.        2590.   1940.   1706.   1600.    1532.
**
**
** Capture Thickness (meters)
**
**   Pump Rate              Aquifer Thickness
**    (m^3/d)                       (m)
                    300.    475.    650.    825.    1000.
**
         3.4         41.     41.     41.     41.      41.
        10.          71.     71.     71.     71.      71.
        50.         150.    156.    158.    159.     159.
       240.         268.    314.    330.    338.     341.
       430.         300.    387.    423.    440.     449.
       620.         300.    427.    485.    513.     529.
       810.         300.    451.    530.    571.     593.
      1000.         300.    464.    564.    617.     646.
**
**
** Screen Length (meters)
**
** Number of Values for Screen Length Pump Rate
  8
**
**   Pump Rate      Screen Length
**    (m^3/d)            (m)
**
         3.4              3.
```

```
        10.                3.
        50.                8.
       240.               19.
       430.               27.
       620.               34.
       810.               40.
      1000.               45.
**
endoffile
```

**File name:** ***drythick.dat***

When the user selects the reflux3 model, calculations performed in the NFENV module utilize the data in *drythick.dat.* The dry-out zone modeled in the TPA code is the region above the drift and below the condensate zone where heat from the drift vaporizes water that resides in the rock pore volume. This vapor moves upward to the condensate zone where the temperature is below boiling. For water to flow onto the waste package from the reflux zone, the water must either penetrate the dry-out zone or the dry-out zone thickness must be zero. The data in *drythick.dat* provide the dry-out zone thickness in meters at 18 different time steps beginning at 1 yr through 900 yr. These values were derived from MULTIFLO simulations performed offline. A complete listing of *drythick.dat* is presented as follows.

```
17
  1     1.0     0.0
  2    10.0     0.1
  3    20.0     1.0
  4    30.0     1.5
  5    40.0     1.7
  6    50.0     1.5
  7    60.0     1.5
  8    70.0     1.8
  9    80.0     2.9
 10   100.0     4.6
 11   200.0     7.3
 12   300.0     7.4
 13   500.0     6.6
 14   600.0     5.6
 15   700.0     4.7
 16   800.0     3.8
 17   900.0     2.7
 18  1000.0     0.0
```

**File name:** ***FILENAME.DAT***

The file *FILENAME.DAT* contains the path and filenames of the input files used by the GENTPA Version 1.0 called in the DCAGW module. The file format matches that of *FILENAME.DAT* described in Napier et al. (1988). The first 20 lines and last 5 lines of this file are listed below.

```
 2          grmdlib.dat
 3          METADATA.DAT
 4          RMDBYELE.DAT
 5          ggenii.inp
 6          ggenii.out
 7          gwork.buf
 8          gftrans.inp
```

```
 9          gbioac1.dat
10          ggrdf.dat
11          genv.in
12          DOSSUM.DAT
13          genv.out
14          DOSE.OUT
15          INTDF.OUT
16          CDEINC.OUT
17          DITTY.OUT
18          INTDF.IN
19          DITTYQA.OUT
20          CDE.OUT
21          gmedia.out
      .
      .
      .

46          SEE2.DAT
47          SEE3.DAT
48
49          WORK2.BUF
50          WORK3.BUF
```

**File name:** ***gbioac1.dat***

The file *gbioac1.dat* contains bioaccumulation factors used by the GENTPA Version 1.0 code called in the DCAGW module. This file is not currently used, but this option is available. The bioaccumulation factors are used to relate the concentration of radionuclides in aquatic biota to the concentration of radionuclides in fresh and salt water. The file format matches that of *bioac1.dat* described in Napier et al. (1988). The first 20 lines and last 5 lines of this file are listed below.

```
Bioaccumulation Factor Library - (30-Aug-88) RAP
Salt: Fish   Crustacea Molluscs   Plants Fr:Fish   Crustacea Molluscs   Plants
Cleanup
AC     30.0    1000.0    1000.0    1000.0     330.0    1000.0    1000.0 10000. 0.7
AM   2500.0     360.0     290.0    2900.0     100.0     100.0     100.0  3000. 0.7
SB   1000.0     100.0    1200.0     100.0     200.0     100.0     100.0    1000.
0.8
BA     10.0       1.0      20.0     100.0     200.0     200.0     200.0     500.
0.4
BE   1000.0   10000.0   10000.0   10000.0      10.0      50.0      50.0     200.
0.2
BI     15.0    1000.0    1000.0   10000.0      15.0 100000.0 100000.0    1500. 0.9
BK     50.0     500.0   20000.0       1.0      50.0     500.0   20000.0       1.0
BR     10.0      10.0      10.0      10.0     420.0     330.0     330.0  50    .0
CD   2000.0    5000.0   10000.0    1000.0     200.0   10000.0   10000.0    500. 0.6
CA      2.0       5.0       1.0      50.0     200.0    2000.0    2000.0  1000.
0.2
CF     50.0     500.0    2000.0    5000.0      25.0    1000.0    1000.0  5000 .0
C    20000.0   20000.0   20000.0    1800.0    9000.0    9000.0    9000.0    4500.0
1.0
CE    100.0     500.0     500.0    5000.0     500.0    1000.0    1000.0  4000. 0.2
CS    100.0      30.0      30.0     700.0   15000.0     500.0     500.0  1000. 0.9
CL      1.0       1.0       1.0       1.0      50.0      50.0      50.0  50.0
1.0
 CR    600.0     500.0    1140.0    4000.0      20.0    2000.0    2000.0  4000 .0
```

```
CO     100.0    2000.0    3000.0     400.0     330.0    2000.0    2000.0    1000.
0.2

      .
      .
      .

ND     100.0    1000.0    1000.0    1000.0      25.0    1000.0    1000.0    5000.0.2
RN       1.0       1.0       1.0       1.0      57.0       1.0       1.0
1.0.0
SI   50000.0   50000.0   50000.0   50000.0    1000.0   10000.0   10000.0   50000.0 .7
GA    1000.0   10000.0   10000.0       1.0    1000.0   10000.0   10000.0       1.0
ER     100.0     500.0     500.0    5000.0     500.0    1000.0    1000.0    4000.0.2
```

**File name:** ***gdosinc2.dat***

The file *gdosinc2.dat* contains a single line header which describes the *gnewdf.dat* data file contents (for tracking file changes). The file format matches that of *dosinc2.dat* described in Napier et al. (1988). The entire file is listed below.

```
Worst-Case Solubilities, Yearly Dose Increments (25-Mar-96 PDR)
```

**File name:** ***ggamen.dat***

The file *ggamen.dat* contains gamma energies utilized by the GENTPA Version 1.0 code called in the DCAGW module. The file includes gamma energies (MeV/dis) for six energy groups for each radionuclide that are used in finite plume calculations. This file is not currently used, but is an available option. The GENTPA Version 1.0 code currently assumes an infinite plume size. The file format matches that of *gamen.dat* described in Napier et al. (1988). The first 20 lines and last 5 lines of this file are listed below.

```
EXTGAM - Gamma Energies by Group for Finite Plume (13-May-90 RAP)(1-26-00 MAS
Ag108m added)
 H 3          0.00000 0.00000 0.00000 0.00000 0.00000 0.00000
 BE7          0.00000 0.04976 0.00000 0.00000 0.00000 0.00000
 BE10         0.00000 0.00000 0.00000 0.00000 0.00000 0.00000
 C 14         0.00000 0.00000 0.00000 0.00000 0.00000 0.00000
 N 13         0.00000 0.00000 1.02001 0.00000 0.00000 0.00000
 F 18         0.00000 0.00000 0.98858 0.00000 0.00000 0.00000
 NA22         0.00000 0.00000 0.91878 1.27374 0.00000 0.00000
 NA24         0.00000 0.00000 0.00000 1.36849 0.00000 2.75275
 SI31         0.00000 0.00000 0.00000 0.00089 0.00000 0.00000
 P 32         0.00000 0.00000 0.00000 0.00000 0.00000 0.00000
 P 33         0.00000 0.00000 0.00000 0.00000 0.00000 0.00000
 S 35         0.00000 0.00000 0.00000 0.00000 0.00000 0.00000
 CL36         0.00000 0.00000 0.00000 0.00000 0.00000 0.00000
 K 40         0.00003 0.00000 0.00000 0.15587 0.00000 0.00000
 AR39         0.00000 0.00000 0.00000 0.00000 0.00000 0.00000
 AR41         0.00000 0.00000 0.00000 1.28273 0.00087 0.00000
 CA41         0.00041 0.00000 0.00000 0.00000 0.00000 0.00000
 CA45         0.00000 0.00000 0.00000 0.00000 0.00000 0.00000

      .
      .
      .
```

```
AM243       0.05833 0.00000 0.00000 0.00000 0.00000 0.00000
NP239       0.16029 0.01182 0.00000 0.00000 0.00000 0.00000
PU239       0.00065 0.00000 0.00000 0.00000 0.00000 0.00000
CM248       0.00105 0.00000 0.00000 0.00000 0.00000 0.00000
CF252       0.00111 0.00000 0.00000 0.00000 0.00000 0.00000
```

**File name:** ***ggrdf.dat***

The file *ggrdf.dat* contains external dose coefficients utilized by the GENTPA Version 1.0 code called in the DCAGW module. The file contains external dose coefficients for all radionuclides for air submersion, water surface, soil surface, deep soil, and buried waste. The file format matches that of *grdf.dat* described in Napier et al. (1988). The first 20 lines and last 5 lines of this file are listed below.

```
FGR 12 External DCFs(per-Sv/yr per Bq/n) (SJM/PAL) for 43 TSPA Nuclides, (MAS
1-26-00 Ag108m added, daughters updated), (MAS 1-28-00 FGR12 soil surface and
air submersion values added)
         FGR12 Air    Water   FGR12 Soil Buried     Buried     Buried
        Submersion   Surface   Surface    0.15 m     0.5 m      1.0 m
n           m^3          L         m^2         m^3        m^3         m^3

C 14     7.06E-12   2.02E-11   5.08E-13   8.89E-19   3.86E-24   3.56E-31
CL36     7.04E-10   1.05E-09   2.12E-11   5.16E-15   1.09E-17   4.80E-21
NI59     0.00E+00   1.08E-09   0.00E+00   0.00E+00   0.00E+00   0.00E+00
NI63     0.00E+00   9.47E-13   0.00E+00   6.96E-24   4.40E-34   0.00E+00
SE79     9.56E-12   1.50E-11   6.53E-13   5.17E-19   2.03E-24   1.33E-31
SR90     2.38E-10   4.90E-10   8.96E-12   1.28E-15   1.41E-18   3.85E-22
Y 90     6.00E-09   1.74E-08   1.68E-10   3.83E-13   3.52E-15   1.31E-17
MO93     7.95E-10   2.08E-09   1.69E-10   0.00E+00   0.00E+00   0.00E+00
ZR93     0.00E+00   7.06E-13   0.00E+00   1.35E-24   3.32E-35   0.00E+00
NB93M    1.40E-10   4.31E-10   2.96E-11   0.00E+00   0.00E+00   0.00E+00
NB94     2.43E-06   3.54E-06   4.83E-08   1.55E-10   1.39E-12   2.13E-15
TC99     5.11E-11   9.35E-11   2.46E-12   4.52E-17   2.44E-21   3.90E-26
PD107    0.00E+00   3.23E-14   0.00E+00   0.00E+00   0.00E+00   0.00E+00
AG108M   2.46E-06   6.60E-06   5.05E-08   3.54E-10   6.00E-12   3.29E-14
.
.
.

CM243    1.86E-07   2.62E-07   3.94E-09   2.07E-12   1.12E-15   3.55E-20
PU243    3.25E-08   3.36E-08   7.61E-10   1.92E-13   5.34E-16   1.69E-19
AM243    6.88E-08   6.55E-08   1.69E-09   1.82E-14   1.77E-19   1.11E-25
NP239    2.43E-07   3.58E-07   5.14E-09   3.17E-12   3.97E-15   9.31E-19
PU239    1.34E-10   2.58E-10   1.16E-11   3.30E-16   1.22E-20   7.75E-27
```

**File name:** ***gnewdf.dat***

The *gnewdf.dat* file contains internal dose coefficients utilized by the GENTPA Version 1.0 code called in the DCAGW module. The file contains age-dependent internal dose coefficients for infant, toddler, preteen, teen, and adult receptor groups based on ICRP Publication 72 (International Commission on Radiological Protection, 1996), with an alternative adult receptor group based on Federal Guidance Report 11 (U.S. Environmental Protection Agency, 1988). The first 20 lines and last 5 lines of this file are listed below.

Intake-to-Dose Conversion Factors for Inhalation and Ingestion from ICRP72 and Federal Guidance 11 (Sv/Bq) PAL 1/24/00, (MAS 1-26-00 Ag108m added), (MAS 1-27-00 new FGR11 values for Bi210, Pb212, Bi212), (PAL 1-27-00 Np238 added)

```
          Infant     Infant    Toddler    Toddler    Pre-teen   Pre-teen     Teen
    Teen     Adult72    Adult72  AdultFG11 AdultFG11
Nuclide --ing--^---inh---^---ing---^---inh---^---ing---^---inh---^---ing---^---
inh---^---ing---^---inh---^---ing---^---inh---
start_data
C 14     1.40E-09  1.90E-08  1.30E-09  1.40E-08  8.00E-10  7.40E-09  5.70E-10
6.40E-09  5.80E-10  5.80E-09  5.64E-10  5.64E-10
CL36     9.80E-09  3.10E-08  4.75E-09  2.05E-08  1.90E-09  1.00E-08  1.20E-09
8.80E-09  9.30E-10  7.30E-09  8.18E-10  5.93E-09
NI59     6.40E-10  1.70E-09  2.65E-10  1.23E-09  1.10E-10  5.90E-10  7.30E-11
4.60E-10  6.30E-11  4.40E-10  5.67E-11  7.31E-10
NI63     1.60E-09  4.80E-09  6.50E-10  3.50E-09  2.80E-10  1.70E-09  1.80E-10
1.30E-09  1.50E-10  1.30E-09  1.56E-10  1.70E-09
SE79     4.10E-08  2.30E-08  2.35E-08  1.65E-08  1.40E-08  8.70E-09  4.10E-09
7.60E-09  2.90E-09  6.80E-09  2.35E-09  2.66E-09
SR90     2.30E-07  4.20E-07  6.00E-08  3.35E-07  6.00E-08  1.80E-07  8.00E-08
1.60E-07  2.80E-08  1.60E-07  3.85E-08  3.51E-07
Y 90     3.10E-08  1.30E-08  1.50E-08  6.50E-09  5.90E-09  2.70E-09  3.30E-09
1.80E-09  2.70E-09  1.50E-09  2.91E-09  2.28E-09
MO93     7.90E-09  6.00E-09  5.95E-09  4.90E-09  4.00E-09  2.80E-09  3.40E-09
2.40E-09  3.10E-09  2.30E-09  3.64E-10  7.68E-09
ZR93     1.20E-09  7.00E-09  6.35E-10  5.45E-09  5.80E-10  3.30E-09  8.60E-10
3.30E-09  1.10E-09  3.30E-09  4.48E-10  8.67E-08
NB93M    1.50E-09  7.40E-09  6.85E-10  5.20E-09  2.70E-10  2.50E-09  1.50E-10
1.90E-09  1.20E-10  1.80E-09  1.41E-10  7.90E-09
NB94     1.50E-08  1.20E-07  7.50E-09  1.02E-07  3.40E-09  5.80E-08  2.10E-09
5.20E-08  1.70E-09  4.90E-08  1.93E-09  1.12E-07
TC99     1.00E-08  4.10E-08  3.55E-09  3.05E-08  1.30E-09  1.70E-08  8.20E-10
1.50E-08  6.40E-10  1.30E-08  3.95E-10  2.25E-09
PD107    4.40E-10  2.20E-09  2.10E-10  1.65E-09  8.10E-11  7.80E-10  4.60E-11
6.20E-10  3.70E-11  5.90E-10  4.04E-11  3.45E-09

      .
      .
      .

CM243    3.20E-06  1.60E-04  2.75E-07  1.23E-04  1.60E-07  7.30E-05  1.40E-07
6.50E-05  1.50E-07  6.90E-05  6.79E-07  8.30E-05
PU243    1.00E-09  6.00E-10  4.60E-10  3.00E-10  1.80E-10  1.40E-10  1.10E-10
9.20E-11  8.50E-11  8.60E-11  9.02E-11  4.44E-11
AM243    3.60E-06  1.80E-04  3.20E-07  1.45E-04  2.20E-07  1.00E-04  2.00E-07
9.10E-05  2.00E-07  9.60E-05  9.79E-07  1.19E-04
NP239    8.90E-09  5.60E-09  4.30E-09  3.10E-09  1.70E-09  1.60E-09  1.00E-09
1.30E-09  8.00E-10  1.00E-09  8.82E-10  6.78E-10
PU239    4.20E-06  2.10E-04  3.75E-07  1.75E-04  2.70E-07  1.20E-04  2.40E-07
1.10E-04  2.50E-07  1.20E-04  9.56E-07  1.16E-04
```

**File name: *grmdlib.dat***

The *grmdlib.dat* file is the radionuclide master library containing a list of all radionuclides and radiological decay data utilized by the GENTPA Version 1.0 code called in the DCAGW module. The file format matches that of *rmdlib.dat* described in Napier et al. (1988) and a summary is included in table B-2. For

more information about this file consult Napier et al. (1988). The first 20 lines and last 5 lines of this file are listed below.

```
Radionuclide Master Library    (11/28/90 RAP)(1-26-00 MAS Ag108m added)
H 3          4.49E+3 1 0 0.0000 0 0.0000    1       ND
BE7          5.33E+1 1 0 0.0000 0 0.0000    4       VY
BE10         5.84E+8 1 0 0.0000 0 0.0000    4       VY
C 14         2.09E+6 1 0 0.0000 0 0.0000    6       ND
N 13         6.92E-3 1 0 0.0000 0 0.0000    7       ND
F 18         7.62E-2 1 0 0.0000 0 0.0000    9       SD
NA22         9.50E+2 1 0 0.0000 0 0.0000   11       VD
NA24         6.25E-1 1 0 0.0000 0 0.0000   11       VD
SI31         1.09E-1 1 0 0.0000 0 0.0000   14       NW
P 32         1.43E+1 1 0 0.0000 0 0.0000   15       SD
P 33         2.54E+1 1 0 0.0000 0 0.0000   15       VD
S 35         8.74E+1 1 0 0.0000 0 0.0000   16       NW
CL36         1.10E+8 1 0 0.0000 0 0.0000   17       ND
K 40         4.67E11 1 0 0.0000 0 0.0000   19       ND
AR39         9.83E+4 1 0 0.0000 0 0.0000   18       ND
AR41         7.61E-2 1 0 0.0000 0 0.0000   18       ND
CA41         3.67E+7 1 0 0.0000 0 0.0000   20    1  VW
CA45         1.63E+2 1 0 0.0000 0 0.0000   20    1  VW
SC46         8.38E+1 1 0 0.0000 0 0.0000   21       VY

      .
      .
      .
NP239        2.36E+0 5 4 1.0000 0 0.0000   93       SW
PU239        8.81E+6 6 5 1.0000 2 0.9976   94 T     SY
CM248        1.24E+8 1 0 0.0000 0 0.0000   96       SW
CF252        9.63E+2 1 0 0.0000 0 0.0000   98       SW
                     0 0 0.0000 0 0.0000
```

**Table B-2. Summary of file format used in *grmdlib.dat*.**

| Column | Description |
|---|---|
| 1–2 | Element symbol and atomic weight |
| 3 | Radiological half-life (d) |
| 4 | Relative position in decay chain |
| 5 | Precursor in decay chain |
| 6 | Branching ratio of primary precursor |
| 7 | Alternate precursor in decay chain |
| 8 | Branching ratio of alternate precursor |
| 9 | Atomic number |
| 10 | Special-purpose research flag |
| 11 | Internal dosimetry model: 0=general model, 1=alkaline earth model, 2=iodine model |

**Table B-2. Summary of file format used in *grmdlib.dat*. (cont'd)**

| Column | Description |
|---|---|
| 12 | Descriptive flag: V=bone-volume seeker, S=bone-surface seeker, N=not applicable |
| 13 | Translocation classification |
| 14 | Number of implicit daughters |
| 15–38 | Implicit daughter information |

**Files With Dose Conversion Factors**

The dose conversion factors (DCFs) used to calculate doses from direct releases (ground surface pathway) are contained in four files: *gs_cb_ad.dat, gs_cb_ci.dat, gs_pb_ad.dat,* and *gs_pb_ci.dat*. The file names contain three two-letter abbreviations that identify the type of data in each file. All file names begin with "*gs*" to denote ground surface. These files are read by the DCAGS module and applied when there is an extrusive volcanic event. The second set of two-letter abbreviations, "*cb*" or "*pb*", specifies climate conditions for the current biosphere and the pluvial biosphere, respectively. The third abbreviation designates the receptor group distance that corresponds to the residential receptor group or close-in residential water user ("*ci*") (located within 20 km of the repository footprint) and the farming receptor group or Amargosa Desert farmer/rancher ("*ad*") (located at or beyond 20 km from the repository footprint). The distance to receptor group is a parameter set in *tpa.inp*.

The particular file utilized in a TPA run for the ground surface is determined based on the distance to the receptor group specified in *tpa.inp* and the current climate state. Specifically, the distance-to-receptor group determines whether the "*ci*" or "*ad*" set of DCF files are read and the UZFLOW climate conditions determine whether the "*cb*" or "*pb*" set of DCF files are read. The DCAGS module switches between using the current and pluvial biosphere DCFs based on a user specified time as described in chapter 11.

Headers in each file describe the exposure pathways and units for the DCFs. The files have 43 rows of data with each row representing one nuclide. The ordering of the 43 direct release nuclides is consistent with the sequence specified in the *invent.f* utility module (see section 3.3.2). The first 20 lines and last 5 lines of each file are listed below.

**File name:** ***gs_cb_ad.dat***

```
These dcf's are for the adfr CG in the current biosphere
and are in the order of; direct exposure, inhalation, ingestion
of animal products, and ingestion of crops.
All dcf's are in units of (rem/yr)/(Ci/m2)
except for inhalation which is (rem/yr)/(Ci/m2) per unit
resuspension factor (1/m) or (rem/yr)/(Ci/m3). They use the
standard TPA code ordering of nuclides.
LMD: 1/30/98 New dcf's were obtained from CNWRA 97-009
PAL: 6/3/98 New dcf's provided for all columns except dir exp.
New dcf's based on CNWRA 97-009 except internal dose factors were
changed to MAX class using 1996 GENII-S libraries.
Note: Ag110m DCFs were substituted for Ag108m. Pu-238 and Pu-241
dcf's were calculated using the Pu-239 dcf and ratio of dcf's
tabulated in Federal Guidance 11
```

start_data

| nuclide | dir exp | inh | ing ani prod | ing crop |
|---|---|---|---|---|
| U238 | 1.30E+01 | 1.24E+12 | 7.53E+01 | 9.02E+02 |
| Cm246 | 1.90E+01 | 4.73E+12 | 4.20E+01 | 1.00E+04 |
| Pu242 | 1.70E+01 | 4.31E+12 | 4.70E+00 | 9.00E+03 |
| Am242m | 7.30E+01 | 4.46E+12 | 1.41E+01 | 9.53E+03 |
| | | . | | |
| | | . | | |
| | | . | | |
| Se79 | 5.10E-01 | 1.03E+08 | 3.60E+01 | 6.20E+01 |
| Ni63 | 0.00E+00 | 6.60E+07 | 1.20E+01 | 5.20E+00 |
| Ni59 | 0.00E+00 | 2.83E+07 | 4.30E+00 | 1.90E+00 |
| Cl36 | 1.70E+01 | 2.30E+08 | 1.70E+04 | 3.90E+04 |
| C14 | 3.90E-01 | 2.19E+07 | 0.00E+00 | 1.70E-01 |

**File name:** ***gs_cb_ci.dat***

These dcf's are for the cirwu CG in the current biosphere
and are in the order of; direct exposure, and inhalation.
All dcf's are in units of (rem/yr)/(Ci/m2)
except for inhalation which is (rem/yr)/(Ci/m2) per unit
resuspension factor (1/m) or (rem/yr)/(Ci/m3). They use the
standard TPA code ordering of nuclides.
LMD: 1/30/98 New were obtained from CNWRA 97-009
Note: Ag110m DCFs were substituted for Ag108m. Pu-238 and Pu-241
dcf's were calculated using the Pu-239 dcf and ratio of dcf's
tabulated in the GENII PNL DCF library.
PAL: 6/4/98 Confirmed inhalation dcf's based on most conservative
FG11 lung class assumptions for internal dose factors consistent
with DCF revisions for other receptors. Breathing rate used in inh
calculation is 1.2m3/hr (source is ICRP "light activity" value
which is also used in NUREG CR-5512). start_data

| nuclide | dir exp | inh |
|---|---|---|
| U238 | 2.60E+00 | 1.24E+12 |
| Cm246 | 3.70E+00 | 4.73E+12 |
| Pu242 | 3.20E+00 | 4.31E+12 |
| | . | |
| | . | |
| | . | |
| Se79 | 9.90E-02 | 1.03E+08 |
| Ni63 | 0.00E+00 | 6.60E+07 |
| Ni59 | 0.00E+00 | 2.83E+07 |
| Cl36 | 3.20E+00 | 2.30E+08 |
| C14 | 7.70E-02 | 2.19E+07 |

**File name:** ***gs_pb_ad.dat***

These dcf's are for the adfr CG in a pluvial biosphere
and are in the order of; direct exposure, inhalation, ingestion
of animal products, and ingestion of crops.
All dcf's are in units of (rem/yr)/(Ci/m2)
except for inhalation which is (rem/yr)/(Ci/m2) per unit
resuspension factor (1/m) or (rem/yr)/(Ci/m3). They use the

```
standard TPA code ordering of nuclides.
LMD: 1/30/98 New dcf's were obtained from CNWRA 97-009
PAL: 6/3/98 New dcf's provided for all columns except dir exp.
New dcf's based on CNWRA 97-009 except internal dose factors were
changed to MAX class using 1996 GENII-S libraries.
Note: Ag110m DCFs were substituted for Ag108m. Pu-238 and Pu-241
dcf's were calculated using the Pu-239 dcf and ratio of dcf's
tabulated in Federal Guidance 11.
start_data

nuclide     dir exp     inh         ing ani prod          ing crop
U238        1.30E+01    1.24E+12    7.53E+01              9.02E+02
Cm246       1.90E+01    4.73E+12    4.20E+01              1.00E+04
Pu242       1.70E+01    4.31E+12    4.70E+00              9.00E+03
Am242m      7.30E+01    4.46E+12    1.41E+01              9.53E+03

                                .
                                .
                                .

Se79        5.10E-01    1.03E+08    3.60E+01              6.20E+01
Ni63        0.00E+00    6.60E+07    1.20E+01              5.20E+00
Ni59        0.00E+00    2.83E+07    4.30E+00              1.90E+00
Cl36        1.70E+01    2.30E+08    1.70E+04              3.90E+04
C14         3.90E-01    2.19E+07    0.00E+00              1.70E-01
```

**File name:** ***gs_pb_ci.dat***

```
These dcf's are for the cirwu CG in a pluvial biosphere
and are in the order of; direct exposure, and inhalation.
All dcf's are in units of (rem/yr)/(Ci/m2)
except for inhalation which is (rem/yr)/(Ci/m2) per unit
resuspension factor (1/m) or (rem/yr)/(Ci/m3). They use the
standard TPA code ordering of nuclides.
LMD: 1/30/98 New dcf's were obtained from CNWRA 97-009
Note: Ag110m DCF's were substituted for Ag108m. Pu-238 and Pu-239
were calculated using the Pu-239 dcf and ratio of dcf's
tabulated in the GENII PNL DCF library.
PAL: 6/4/98 Confirmed inhalation DCFs based on most conservative
FG11 lung class assumptions for internal dose factors consistent
with DCF revisions for other receptors. Breathing rate used in inh
calculation is 1.2m3/hr (source is  ICRP "light activity" value
which is also used in NUREG CR-5512).
start_data

nuclide    dir exp        inh
U238       2.60E+00     1.24E+12
Cm246      3.70E+00     4.73E+12
Pu242      3.20E+00     4.31E+12

               .
               .
               .

Se79       9.90E-02     1.03E+08
Ni63       0.00E+00     6.60E+07
Ni59       0.00E+00     2.83E+07
Cl36       3.20E+00     2.30E+08
```

```
C14          7.70E-02        2.19E+07
```

**File name:** ***maidtbl.dat***

The module UZFLOW obtains mean annual infiltration (mm/yr) from the data file *maidtbl.dat* for a range of precipitation and temperature values. The six header lines describe the number of columns and rows of data, the southwest corner map position in Universal Transverse Mercator (UTM) NAD27 (m) easting and northing coordinates, the cell size in m, and a flag for no data value. The cell size is variable and is limited in the infiltration tabulator for Yucca Mountain (ITYM) preprocessor (appendix H) to values that are multiples of 30. The remainder of the file is a series of digital elevation models (DEMs) stacked one on another. For each DEM, the relevant precipitation (mm/yr) and temperature (degrees Celcius) are listed as VAR1 and VAR2 followed by the infiltration values (mm/yr) corresponding to cell blocks beginning at the upper left-hand corner of the grid and continuing to the right (east) for each cell block. The second row of cell blocks from the top (to the north of the first row) of the grid moving left to right comprise the next set of soil depths, and so forth for all of the rows of the infiltration map. The last record in the file is an end of file flag. The first 20 lines (excluding the header lines) and last 7 lines of the file *maidtbl.dat* are provided below.

```
# DEM table of expected MAI [mm/yr] for each pixel
# Table is a function of MAP [mm/yr] and MAT [C]
# Coordinate system is UTM NAD27 [m]
# File generated on Thu Mar 23 06:47:17 2000
NCOLS        49
NROWS        75
XLLCORNER    545010.000000
YLLCORNER   4074000.000000
CELLSIZE        120.000000
NODATA_VALUE     -9999.000000
VAR1   1.0000000E+02
VAR2   0.0000000E+00
 7.23192569E+00
 8.11515613E+00
 8.57002278E+00
 8.79862242E+00
 8.60854144E+00
 7.50135501E+00
 9.37095935E+00
 9.73997409E+00
 .
 .
 .
 1.23902228E+02
 1.10734377E+02
 1.06025492E+02
 1.06066394E+02
 1.03847387E+02
 1.04049763E+02
NCOLS 0
```

**File name:** ***multiflo.dat***

The file *multiflo.dat* consists of output from a MULTIFLO simulation organized into 14 columns with each line representing one time step. The TPA code uses time and chloride concentration from this file. NFENV reads time from the first column and chloride concentration from the twelfth column.

The chloride concentrations are mapped onto TPA time steps, stored in an array, and passed to the EXEC in the NFENV argument list. This array is then passed to the EBSFAIL consequence module and the values written in the file *chloridemf.dat*. The stand-alone code *failt.f* reads the chloride concentration from *chloridemf.dat* and uses this information to calculate the waste package (WP) failure time. The first 20 lines and last 5 lines of *multiflo.dat* are provided below.

```
!date: 3/16/2000 file:copied multiflo output for {time,chloride} onto standard
tpa input format
! property: pH, logO2aq, ...
! Time (years)              delt          pH    72        logO2a   72  ca+2      72
      mg+2      72  na+       72  k+        72        h+        72        hco3-     72
      sio2(a   72  Cl (molal)  so4-2    72  o2(aq)   72
1.00E-08    0.00E+00    0.00E+00    0.00E+00    0.00E+00    0.00E+00    0.00E+00
      0.00E+00    0.00E+00    0.00E+00    0.00E+00    0.000200    0.00E+00
      0.00E+00
5.42E-06    0.00E+00    0.00E+00    0.00E+00    0.00E+00    0.00E+00    0.00E+00
      0.00E+00    0.00E+00    0.00E+00    0.00E+00    0.000200    0.00E+00
      0.00E+00
0.001609    0.00E+00    0.00E+00    0.00E+00    0.00E+00    0.00E+00    0.00E+00
      0.00E+00    0.00E+00    0.00E+00    0.00E+00    0.000200    0.00E+00
      0.00E+00
0.004543    0.00E+00    0.00E+00    0.00E+00    0.00E+00    0.00E+00    0.00E+00
      0.00E+00    0.00E+00    0.00E+00    0.00E+00    0.000200    0.00E+00
      0.00E+00
0.008452    0.00E+00    0.00E+00    0.00E+00    0.00E+00    0.00E+00    0.00E+00
      0.00E+00    0.00E+00    0.00E+00    0.00E+00    0.000200    0.00E+00
      0.00E+00
0.029853    0.00E+00    0.00E+00    0.00E+00    0.00E+00    0.00E+00    0.00E+00
      0.00E+00    0.00E+00    0.00E+00    0.00E+00    0.000200    0.00E+00
      0.00E+00
0.070545    0.00E+00    0.00E+00    0.00E+00    0.00E+00    0.00E+00    0.00E+00
      0.00E+00    0.00E+00    0.00E+00    0.00E+00    0.000200    0.00E+00
      0.00E+00
0.116320    0.00E+00    0.00E+00    0.00E+00    0.00E+00    0.00E+00    0.00E+00
      0.00E+00    0.00E+00    0.00E+00    0.00E+00    0.000200    0.00E+00
      0.00E+00
0.152290    0.00E+00    0.00E+00    0.00E+00    0.00E+00    0.00E+00    0.00E+00
      0.00E+00    0.00E+00    0.00E+00    0.00E+00    0.000200    0.00E+00
      0.00E+00
0.200000    0.00E+00    0.00E+00    0.00E+00    0.00E+00    0.00E+00    0.00E+00
      0.00E+00    0.00E+00    0.00E+00    0.00E+00    0.000200    0.00E+00
      0.00E+00
0.244820    0.00E+00    0.00E+00    0.00E+00    0.00E+00    0.00E+00    0.00E+00
      0.00E+00    0.00E+00    0.00E+00    0.00E+00    0.000200    0.00E+00
      0.00E+00
0.285640    0.00E+00    0.00E+00    0.00E+00    0.00E+00    0.00E+00    0.00E+00
      0.00E+00    0.00E+00    0.00E+00    0.00E+00    0.000200    0.00E+00
      0.00E+00
```

```
0.331770    0.00E+00    0.00E+00    0.00E+00    0.00E+00    0.00E+00    0.00E+00
      0.00E+00    0.00E+00    0.00E+00    0.00E+00    0.000201    0.00E+00
      0.00E+00
0.373280    0.00E+00    0.00E+00    0.00E+00    0.00E+00    0.00E+00    0.00E+00
      0.00E+00    0.00E+00    0.00E+00    0.00E+00    0.000201    0.00E+00
      0.00E+00
0.383790    0.00E+00    0.00E+00    0.00E+00    0.00E+00    0.00E+00    0.00E+00
      0.00E+00    0.00E+00    0.00E+00    0.00E+00    0.000201    0.00E+00
      0.00E+00
0.388800    0.00E+00    0.00E+00    0.00E+00    0.00E+00    0.00E+00    0.00E+00
      0.00E+00    0.00E+00    0.00E+00    0.00E+00    0.000202    0.00E+00
      0.00E+00
0.399690    0.00E+00    0.00E+00    0.00E+00    0.00E+00    0.00E+00    0.00E+00
      0.00E+00    0.00E+00    0.00E+00    0.00E+00    0.000203    0.00E+00
      0.00E+00
.
.
.
9956.300000       0.00E+00    0.00E+00    0.00E+00    0.00E+00    0.00E+00
      0.00E+00    0.00E+00    0.00E+00    0.00E+00    0.00E+00    0.000231
      0.00E+00    0.00E+00
9980.100000       0.00E+00    0.00E+00    0.00E+00    0.00E+00    0.00E+00
      0.00E+00    0.00E+00    0.00E+00    0.00E+00    0.00E+00    0.000231
      0.00E+00    0.00E+00
1.00E+04    0.00E+00    0.00E+00    0.00E+00    0.00E+00    0.00E+00    0.00E+00
      0.00E+00    0.00E+00    0.00E+00    0.00E+00    0.000231    0.00E+00
      0.00E+00
1.00E+05    0.00E+00    0.00E+00    0.00E+00    0.00E+00    0.00E+00    0.00E+00
      0.00E+00    0.00E+00    0.00E+00    0.00E+00    0.000200    0.00E+00
      0.00E+00
1.00E+06    0.00E+00    0.00E+00    0.00E+00    0.00E+00    0.00E+00    0.00E+00
      0.00E+00    0.00E+00    0.00E+00    0.00E+00    0.000200    0.00E+00
      0.00E+00
```

**File name:** ***nuclides.dat***

The file *nuclides.dat* contains radionuclide-specific information and is read by the *invent.f* module. The file provides indices identifying nuclides, names of radionuclides and radioelements, molecular weights (isotopic weights) in g/mol, half-lives in years, EPA limits (unitless), and inventories in Ci/MTU. This file contains information for 43 radioniclides and serves as the radionuclide database for the TPA code. The contents of the *nuclides.dat* file is presented here in its entirety.

```
TITLE: TPA4.0 nuclide data used for the invent.f module.
TITLE: (data extracted from invent.f - prepared by jmm)
**       idx = Nuclide index
**       NIS = namesisotopesave
**       NES = nameselemsave
** CPMTU@10 = cipermtuat10yr
**       --- = unitless
** Number of nuclides to be read follows:
43
**idx,      NIS,     NIS2,     NIS3, NES,     wmole, halflife,    epalim, CPMTU@10
**---         ---,       ---,       ---, ---,   [g/mol],       [yr], [Ci/MTU],
[Ci/MTU]
    01       U238    U238       U238        U    238.0d0    4.468d9        0.10
3.15d-01
```

```
    02     Cm246    Cm246     CM246     Cm    246.0d0    4.731d3        0.10 1.76d-01
    03     Pu242    Pu242     PU242     Pu    242.0d0    3.869d5        0.10 2.37d+00
    04    Am242m   Am242m    AM242M     Am    242.0d0    1.520d2        0.10
1.19d+01
    05     Pu238    Pu238     PU238     Pu    238.0d0    8.774d1        0.10 3.67d+03
    06      U234     U234      U234      U    234.0d0    2.445d5        0.10
1.25d+00
    07     Th230    Th230     TH230     Th    230.0d0    7.700d4        0.01 1.48d-04
    08     Ra226    Ra226     RA226     Ra    226.0d0    1.600d3        0.10 4.50d-07
    09     Pb210    Pb210     PB210     Pb    210.0d0    2.230d1        1.00 6.49d-08
    10     Cm243    Cm243     CM243     Cm    243.0d0    2.850d1        0.10 3.00d+01
    11     Am243    Am243     AM243     Am    243.0d0    7.380d3        0.10 2.89d+01
    12     Pu239    Pu239     PU239     Pu    239.0d0    2.406d4        0.10 3.36d+02
    13      U235     U235      U235      U    235.0d0    7.038d8        0.10
1.78d-02
    14     Pa231    Pa231     PA231     Pa    231.0d0    3.277d4        0.10 2.83d-05
    15     Ac227    Ac227     AC227     Ac    227.0d0    2.177d1        0.10 7.97d-06
    16     Cm245    Cm245     CM245     Cm    245.0d0    8.499d3        0.10 4.71d-01
    17     Pu241    Pu241     PU241     Pu    241.0d0    1.440d1     1000.00
9.26d+04
    18     Am241    Am241     AM241     Am    241.0d0    4.322d2        0.10 2.09d+03
    19     Np237    Np237     NP237     Np    237.0d0    2.140d6        0.10 3.99d-01
    20      U233     U233      U233      U    233.0d0    1.585d5        0.10
3.23d-05
    21     Th229    Th229     TH229     Th    229.0d0    7.339d3        0.10 3.95d-07
    22     Cm244    Cm244     CM244     Cm    244.0d0    1.811d1     1000.00
3.19d+03
    23     Pu240    Pu240     PU240     Pu    240.0d0    6.537d3        0.10 5.38d+02
    24      U236     U236      U236      U    236.0d0    2.341d7        0.10
2.96d-01
    25      U232     U232      U232      U    232.0d0    7.200d1        0.10
4.63d-02
    26     Sm151    Sm151     SM151     Sm    151.0d0    8.999d1        1.00 3.86d+02
    27     Cs137    Cs137     CS137     Cs    137.0d0    3.000d1        1.00 9.62d+04
    28     Cs135    Cs135     CS135     Cs    135.0d0    2.300d6        1.00 5.02d-01
    29      I129     I129      I129      I    129.0d0    1.570d7        0.10
3.73d-02
    30     Sn126    Sn126     SN126     Sn    126.0d0    1.000d5        1.00 9.16d-01
    31    Sn121m   Sn121m    SN121M     Sn    121.0d0    4.997d1        1.00
1.05d+00
    32    Ag108m   Ag108m    AG108M     Ag    108.0d0    4.180d2        1.00
1.36d-02
    33     Pd107    Pd107     PD107     Pd    107.0d0    6.496d6        1.00 1.40d-01
    34      Tc99     Tc99      TC99      Tc     99.0d0    2.130d5       10.00
1.51d+01
    35      Mo93     Mo93      MO93      Mo     93.0d0    3.498d3        1.00
2.10d-02
    36      Nb94     Nb94      NB94      Nb     94.0d0    2.030d4        1.00
1.06d+00
    37      Zr93     Zr93      ZR93      Zr     93.0d0    1.530d6        1.00
2.35d+00
    38      Sr90     Sr90      SR90      Sr     90.0d0    2.912d1        1.00
6.55d+04
    39      Se79     Se79      SE79      Se     79.0d0    1.100d6        1.00
4.82d-01
    40      Ni63     Ni63      NI63      Ni     63.0d0    9.200d1        1.00
5.07d+02
```

```
    41       Ni59     Ni59       NI59       Ni      59.0d0     8.000d4          1.00
3.46d+00
    42       Cl36     Cl36       CL36       Cl      36.0d0     3.010d5          1.00
1.27d-02
    43         C14      C14         C14         C        14.0d0      5.729d3
0.101.71d+00
```

**File name:** ***repdes.dat***

The data file *repdes.dat* contains the coordinates defining the repository outline. The *reader.f* module uses the data in this file to compute the coordinates for the drift endpoints that are written to the *drifts.dat* file. The coordinate pairs in *repdes.dat* represent UTM easting and UTM northing in meters for the repository outline. The last point of the outline must be the same as the first to fully close the polygon. This discretization is illustrated in figure 5-1. Information provided in the *tpa.inp* file to define the subarea coordinates must coincide with the repository outline coordinates presented in this file. If the subareas are larger than the repository outline, then the subareas will be partially filled since the drifts are restricted to the repository outline. It the subareas are smaller then the repository, then not all of the emplaced waste will be accounted for in the full set of subareas.

This file also provides the angle (in radians) of inclination of the drifts with respect to the east-west direction. The succeeding section identifies the number of points defining the repository outline followed by the coordinates. The repository is divided into two large blocks, referred to as emplacement blocks. Each emplacement block is defined by two points, referred to as starting and stopping points. The first point identifies the point on the western boundary of the repository at which drift placement begins; that is, the northwest corner of subarea 1. The first drift is offset from the northern boundary of subarea 1 by one-half of the drift spacing specified in the *tpa.inp* file in order to avoid any difficulties in computing the geometry of the drifts. The second point identifies the point of furthest y-value (UTM northing) excursion from the starting point for the emplacement block, that is the southern most point of the repository. A similar scheme is used for the second emplacement block starting again with the northwest corner of subarea 1 and stopping at the northern most point of subarea 8. The direction that drift placement takes place depends on the coordinates of the stopping point relative to the starting point.

The drift placement starts in the first emplacement block. If the number of drifts exceeds the capacity [defined in *tpa.inp* through drift spacing, WP spacing, and amount of waste in the repository (MTUs)] of the first emplacement block, then the second block is used for drift placement. A complete list of the *repdes.dat* file is presented below.

```
TITLE: TPA 4.0 repository design and emplacement data.
**
** angle - radians
**
-.304d0
**
** rep outline vertices.
**
13
547645.27,4079656.06
548588.98,4079377.55
548569.32,4078981.
548504.06,4077664.24
548479.71,4077173.06
548455,4076674.51
```

```
548155.7,4075962.63
547897.79,4076045.46
547655.97,4076123.07
547474.7,4077282.6
547370.95,4077922.04
547514.88,4079310.61
547645.27,4079656.06
**
** emplacement blocks
**
2
547504.18,    4079310.6, 548155.70,    4075962.6
547504.18,    4079310.6, 547732.82,    4081208.1
```

**File name:** ***strmtube.dat***

The data for streamtube widths and lengths as a function of distance to the tuff/alluvium interface are provided in *strmtube.dat*. Additionally, saturated zone streamtube flow rates are provided in this file. The information in *strmtube.dat* defines three saturated zone streamtubes. The file is divided into sections for the residential receptor group (referred to as near field) and the farming receptor group (referred to as far field). A distance of 20 km is specified in the *strmtube.dat* file to represent the far field or the farming receptor group. For convenience, the midpoint between the repository footprint and the far field (i.e., 10 km) is specified as the distance to represent the near field or the residential receptor group. In the TPA input file *tpa.inp*, the distance is set at 10 km to select the residential receptor group and 20 km to select the farming receptor group.

The SZFT module utilizes streamtube locations to assign the closest of the three streamtubes to the subarea being analyzed. The distance from the subarea centroid to each of the three streamtubes is calculated in SZFT. The assignment of a streamtube to a subarea is based on the smallest of these three distances, and data from the selected streamtube are written to the saturated zone NEFTRAN input file *nefii.inp*.

When the calculations are conducted for the residential receptor group, only values for the near field are written to *nefii.inp*. While, when the calculations are conducted for the farming receptor group, the near-field and far-field values are both written to *nefii.inp*. Additional parameters written to *nefii.inp* for the saturated zone hydrogeologic properties, such as porosities and retardation factors, are specified in *tpa.inp*.

The DCAGW and DCAGS consequence modules also read *strmtube.dat*. Both DCAGW and DCAGS read the near-field and far-field receptor group distances from *strmtube.dat* as part of an error check to evaluate whether the cutoff distance specified in the DCAGS section of *tpa.inp* is set outside the near-field and far-field receptor group distances. This check is useful in ensuring that the correct set of DCFs, either for the "*ci*" or "*ad*" receptor group, is utilized in DCAGW and DCAGS to compute dose. DCAGW also reads the streamtube widths from *strmtube.dat*, determines the sum of the width of all streamtubes, and uses the result to calculate the fraction of the plume mass captured by the residential receptor group and the dilution volume for the farming receptor group. A complete list of the *strmtube.dat* file is presented below.

```
TITLE: TPA4.0 StreamTube data for the saturated zone.
TITLE: (data from J. Winterle 1/10/00)
TITLE: (based on flow net analysis using water table contours)
TITLE: (reduced number of streamtubes to 3)
**
  3       Number of streamtubes.
```

```
**
** Flow Rates (m^3/yr/m)
**
  3
600.
730.
470.
**
** Distance to Receptor Well
** ( set 2 values: near field and far field distance in [m]
**   and match this distance with the value specified for
**   "DistanceToReceptorGroup..." in tpa.inp and with the
**   well pumping and mixing zone data for DCAGW in tpa.inp )
**
10.0, 20.0
**
**
** In TPA 4 mass flux from each repository subarea is input to
** the streamtube with centerline closest to the centroid of
** the subarea.
**
** The following defines points on StreamTube Center Lines
** between western and eastern edges of repository footprint.
1
  3         Points defining centerline of tube 1 beneath repository.
UTM-x[m]    UTM-y[m]
547590.,   4076500.
547900.,   4076300.
548150.,   4076000.
**
2
  3         Points defining centerline of tube 2 beneath repository.
UTM-x[m]    UTM-y[m]
547500.,   4078940.
547950.,   4078570.
548540.,   4078520.
**
3
  3         Points defining centerline of tube 3 beneath repository.
UTM-x[m]    UTM-y[m]
547700.,   4081000.
548145.,   4080630.
548632.,   4080300.
**
**
** In the following, "I/F_Dist" indicates where streamtubes centerlines
** cross an imaginary boundary where straight line distance from the
** edge of the repository is 0.0 km, 1.0 km, 2.0 km...etc;
** "width[m]" is streamtube width normal to centerline at each
** these boundaries, used by TPA 4.0 to scale transport velocities
** in proportion to changes in streamtube width; "tube_length[m] is
** the cumulative arc length of the streamtube at each of the
** I/F_Dist boundaries. (jrw 3/14/00)
**
**   Streamtube 1
  20        Number of points for tube 1.
I/F_Dist    width[m]   tube_length[m]
0.0   900.,        0.
```

```
2.0   2000.,       2100.
3.0   2350.,       3100.
4.0   2250.,       4100.
5.0   1650.,       5140.
6.0   1650.,       6150.
7.0   1550.,       7160.
8.0   1050.,       8200.
9.0   800.,        9300.
10.0  700.,        10440.
11.0  550.,        11560.
12.0  500.,        12690.
13.0  430.,        13820.
14.0  430.,        15000.
15.0  430.,        16100.
16.0  430.,        17240.
17.0  430.,        18340.
18.0  430.,        19430.
19.0  430.,        20500.
20.0  430.,        21563.
**
** Streamtube 2
  20       Number of points for tube 2.
I/F_Dist    width[m]   tube_length[m]
0.0   3600.,       0.
2.0   3370.,       2567.
3.0   3350.,       3573.
4.0   3320.,       4795.
5.0   2980.,       5952.
6.0   3600.,       7260.
7.0   2780.,       9062.
8.0   1620.,       10865.
9.0   850.,        12458.
10.0  650.,        13880.
11.0  520.,        15240.
12.0  390.,        16430.
13.0  390.,        17640.
14.0  390.,        18830.
15.0  390.,        19980.
16.0  390.,        21110.
17.0  390.,        22190.
18.0  390.,        23320.
19.0  390.,        24410.
20.0  390.,        25490.
**
** Streamtube 3
  20       Number of points for tube 3.
I/F_Dist    width[m]   tube_length[m]
0.0   1000.,       0.
2.0   1600.,       2045.
3.0   2070.,       3040.
4.0   1920.,       4135.
5.0   1830.,       5410.
6.0   1590.,       7030.
7.0   790.,        10430.
8.0   720.,        13100.
9.0   620.,        15150.
10.0  540.,        16760.
11.0  475.,        18230.
```

```
12.0  430.,       19550.
13.0  410.,       20750.
14.0  410.,       22010.
15.0  410.,       23200.
16.0  410.,       24350.
17.0  410.,       25460.
18.0  410.,       26560.
19.0  410.,       27710.
20.0  410.,       28800.
**
endoffile
```

**File name:** ***tefkti.inp***

The TPA code user has the option of supplying data for time-varying WP temperature and relative humidity (RH) in *tefkti.inp*, instead of calculating these values. This option may be selected in *tpa.inp* by changing the NFENV parameter "TabularTemperatureRHFlag" flag from the default value of 0 to 1. The user must also specify in *tpa.inp* the parameter "nsetUsedToPickTempRHDataSet," which can range from one to four. This value identifies the data set for WP temperature and RH values in *tefkti.inp*, which will be utilized in TPA computations.

The file *tefkti.inp* contains 16 columns that are composed of 4 data sets. Each data set has four columns. These data were generated outside of the TPA code. The user can replace the data sets with different values or provide another data file. However, as currently implemented, the TPA code will read data only from any of the first four sets.

NFENV requires a specific file structure for *tefkti.inp*. The first line of *tefkti.inp* provides column headers. The remaining lines are organized in groups of four columns. For the second line, the first number in each group of four columns specifies the number of time steps in the data set and the next three values are read, but not currently used. From the third line to the end of the file, each data set provides time, WP temperature, a value that is read but not used, and RH. The first 20 lines and last 5 lines of Data Set 1 in *tefkti.inp* are presented below.

```
Time        Twpnv60     Twnv80yb    RHnv60yb
829         999999999   999999999   999999999
1.00E-07    2.37E+01    2.37E+01    9.98E-01
3.00E-07    2.37E+01    2.37E+01    9.98E-01
7.00E-07    2.37E+01    2.37E+01    9.98E-01
1.50E-06    2.37E+01    2.37E+01    9.98E-01
3.10E-06    2.37E+01    2.37E+01    9.98E-01
6.30E-06    2.37E+01    2.37E+01    9.98E-01
1.27E-05    2.37E+01    2.37E+01    9.98E-01
2.55E-05    2.38E+01    2.37E+01    9.98E-01
5.11E-05    2.38E+01    2.37E+01    9.98E-01
1.02E-04    2.39E+01    2.37E+01    9.98E-01
2.05E-04    2.41E+01    2.37E+01    9.98E-01
4.10E-04    2.45E+01    2.37E+01    9.98E-01
8.19E-04    2.52E+01    2.37E+01    9.98E-01
1.64E-03    2.63E+01    2.37E+01    9.98E-01
3.13E-03    2.79E+01    2.38E+01    9.98E-01
5.29E-03    2.96E+01    2.39E+01    9.98E-01
8.31E-03    3.13E+01    2.41E+01    9.98E-01
1.24E-02    3.31E+01    2.44E+01    9.98E-01
```

```
3.37E+04    2.42E+01    2.42E+01    9.97E-01
3.50E+04    2.41E+01    2.40E+01    9.97E-01
3.76E+04    2.39E+01    2.39E+01    9.97E-01
4.00E+04    2.38E+01    2.38E+01    9.97E-01
4.50E+04    2.37E+01    2.37E+01    9.97E-01
```

**File name:** ***tpanames.dbs***

The *tpanames.dbs* file provides a list of all parameter names that can be sampled (i.e., non-constant) in *tpa.inp* with an accompanying eight-character abbreviation for each name. The parameters that are specified as constants in *tpa.inp* are listed in the file *cp.tpa* described in table 20-6.

The EXEC opens and reads information in the *tpanames.dbs* file and then writes the abbreviations for the sampled parameters to *samplpar.abb* and the parameter names and abbreviations to *samplpar.hdr*. Furthermore, the EXEC automatically updates the *tpanames.dbs* file when new input parameters are added to the *tpa.inp* and creates an abbreviation for the new parameter name. The user has the option of accepting or modifying this abbreviation. The order of the abbreviations and parameter names in *samplpar.abb* and *samplpar.hdr* matches the order of the sampled parameters in *tpa.inp*. The first 20 lines and last 5 lines of the file *tpanames.dbs* are presented below.

```
SeedForRandomNumber                                                    Rnd#Seed
NumberOfRealizations                                                   #OfRlztn
StartAtRealization                                                     BegRlztn
StopAtRealization                                                      EndRlztn
StartAtSubarea                                                          BegSuba
StopAtSubarea                                                           EndSuba
MaximumTime[yr]                                                         MaxTime
NumberOfTimeSteps                                                      #TimeStp
RatioOfLastToFirstTimeStep                                             LTStoFTS
OutputMode(0=None,1=All,2=UserDefined)                                  OutMode
UserDefinedLowerRealizationAppended                                     UsrDLRA
UserDefinedUpperRealizationAppended                                     UsrDURA
ArealAverageMeanAnnualInfiltrationAtStart[mm/yr]                        AAMAI@S
MeanAveragePrecipitationMultiplierAtGlacialMaximum                      MAPM@GM
MeanAverageTemperatureIncreaseAtGlacialMaximum[degC]                    MATI@GM
TimeStepForClimate[yr]                                                  Clmt-TS
StandardDeviationOfMAPAboutMeanInOneTimePeriod[mm/yr]                  SDMAP/TP
StandardDeviationOfMATAboutMeanInOneTimePeriod[degC]                   SDMAT/TP
CorrelationBetweenMAPAndMAT                                            cMAP&MAT
ClimatePerturbationSet                                                 ClmtPrtS
      .
      .
      .
NumberOfWeightsForGaussLegendreIntegration[]                           GLIntWts
TotalAnnualEvapotranspiration[m/yr]                                     gen_tae
ReceptorAgeGroup(1=Nfnt,2Tod,3PTeen,4Teen,5Adlt,6AdltFGR11)             gen_RAG
InterceptionFraction/Irrigate                                           gen_ifi
DepthOfSurfaceSoil[cm]                                                  gen_dss
```

**File name:** ***wpflow.def***

The file *wpflow.def* provides time evolution of flow diversion factors ($F_{mult}$ and $F_{ow}$) used in EBSREL module. The three columns present time, $F_{mult}$, and $F_{ow}$, respectively. These time-dependent factors replace

the sampled factors used in the previous version of the TPA code. These factors are read by the EBSREL module and are passed on to the stand-alone code *releaset.f* in the *ebsflow.dat* file.

Time history of the factors for flow diversion (Fmult) and flow contacting waste packages (Fow) used in releaset (rwr 1/17/00)

| time (yr) | Fmult | Fow |
|---|---|---|
| 0.0000 | 0.044721 | 0.173205 |
| 250.0000 | 0.044721 | 0.173205 |
| 500.0000 | 0.044721 | 0.173205 |
| 750.0000 | 0.044721 | 0.173205 |
| 1000.0000 | 0.044721 | 0.173205 |
| 1250.0000 | 0.044721 | 0.173205 |
| 1500.0000 | 0.044721 | 0.173205 |
| 1750.0000 | 0.044721 | 0.173205 |
| 2000.0000 | 0.044721 | 0.173205 |
| 2250.0000 | 0.044721 | 0.173205 |
| 2500.0000 | 0.044721 | 0.173205 |
| 2750.0000 | 0.044721 | 0.173205 |
| 3000.0000 | 0.044721 | 0.173205 |
| 3250.0000 | 0.044721 | 0.173205 |
| 3500.0000 | 0.044721 | 0.173205 |
| 3750.0000 | 0.044721 | 0.173205 |
| 4000.0000 | 0.044721 | 0.173205 |
| 4250.0000 | 0.044721 | 0.173205 |
| 4500.0000 | 0.044721 | 0.173205 |
| 4750.0000 | 0.044721 | 0.173205 |
| 5000.0000 | 0.044721 | 0.173205 |
| | | . |
| | | . |
| | | . |
| 99000.0000 | 0.044721 | 0.173205 |
| 99250.0000 | 0.044721 | 0.173205 |
| 99500.0000 | 0.044721 | 0.173205 |
| 99750.0000 | 0.044721 | 0.173205 |
| 100000.0000 | 0.044721 | 0.173205 |

# APPENDIX B REFERENCES


International Commission on Radiological Protection. *Age-Dependent Doses to Members of the Public from Intake of Radionuclides. Part 5: Compilation of Ingestion and Inhalation Dose Coefficients.* ICRP Publication 72. Tarrytown, NY: Elsevier Science Inc. 1996.

Napier, B.A., R.A. Peloquin, D.L. Strenge, and J.V. Ramsdell. *GENII: The Hanford Environmental Radiation Dosimetry Software System.* Volumes 1: Conceptual Representation. Volume 2: User's Manual.. Volume 3: Code Maintenance. PNL–6584. Richland, WA: Pacific Northwest National Laboratory. 1988.

U.S. Environmental Protection Agency. *Federal Guidance Report No. 11: Limiting Values of Radionuclides Intake and Air Concentration and Dose Conversion Factors for Inhalation, Submersion, and Ingestion.* EPA–520/1–88–020. Washington, DC: U.S. Environmental Protection Agency. 1988.

# APPENDIX C

# APPENDIX C
# UTILITY MODULE DESCRIPTION

As described in section 3.3, the total-system performance assessment (TPA) Version 4.0 code uses utility modules to perform various initializations, input and output processing, and intermediate calculations. Out of the seven primary utility modules, INVENT, SAMPLER, and SNLLHS were described in chapter 3, and the utility modules described in this appendix include READER, MODULE VARIABLE, SUBAREA, and ARRAY. Secondary utility modules are also briefly described in this appendix. Each of these utility modules is composed of a variety of subroutines and function routines that provide centralized support to the algorithms in the consequence modules.

**SUBAREA**

SUBAREA is a utility module that performs storage and retrieval of repository subarea information. The data are read in the READER utility module and stored for use by all modules. The consequence modules can acquire information about the subarea discretization but are not allowed to change (i.e., inadvertently corrupt) the information.

The subareas are defined in the *tpa.inp* file by providing Universal Transverse Mercator (UTM) location coordinates for the vertices of quadrilateral elements. The SUBAREA utility module has subroutines to query (or determine):

- Footprint area of subarea
- Metric ton of uranium (MTU) of waste in subarea
- Number of waste packages (WPs) in subarea
- Subarea coordinates
- Total number of subareas
- Coordinates of a subarea midpoint
- If a point is located within a specified subarea
- If a circle is located within a specified subarea
- If a line is located within a specified subarea

For example, figure C-1 shows four line segments that may represent faults or volcanic dikes that may intersect a given subarea. Subroutines in SUBAREA are currently being called in the FAULTO, SZFT, READER, and VOLCANO modules for just such calculations. SUBAREA takes as input the coordinates of the end points of a given line segment and the vertices of a quadrilateral emplacement region. The routine then uses each segment of the boundary of the emplacement area, checks if there is a real intersection, and calculates the intersection point. SUBAREA then checks to determine if both ends of the line fall within the given region. If both ends of the line are within the given region, then the intersection length is the length of the line. If one end or both ends fall outside the given region, then SUBAREA determines the intersection point(s) of the line with the sides of the quadrilateral region. There will be one or two real intersection points, depending on whether one or two end points fall outside the region. The intersection length for the first case is the distance between the real intersection point and the end point of the line that falls within the region. The intersected length for the second case is the distance between the two intersection points. In figure C-1,

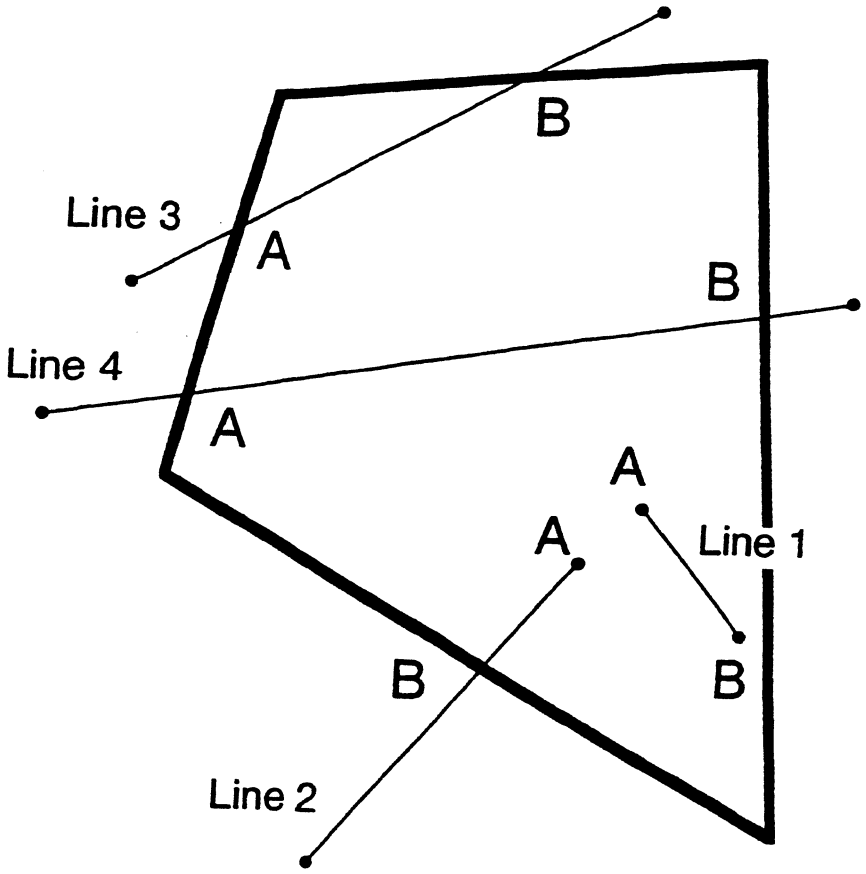


**Figure C-1. Subarea intersection example**

for example, the intersection length of line 1 would be the full length, line 2 intersection length would be AB (need to find B only), and for lines 3 and 4, the intersection lengths would be AB (need to find both A and B). SUBAREA calculates the intersection lengths of the lines in this example.

**MODULE VARIABLE**

The MODULE VARIABLE utility module consists of subroutines for storing values computed by consequence modules. MODULE VARIABLE provides a database for storing consequence module results (i.e., subsystem and system performance measures) and provides a special index to identify each parameter value. This procedure provides data security, such that only the subroutine that introduced the data knows the index for a given parameter and may change its value within the database. Other modules within the TPA Version 4.0 code are allowed to query the value; however, they are unable to change the value in the database.

MODULE VARIABLE provides the analyst using the TPA Version 4.0 code with a tool for storing parameter values for later correlation with the output. For example, the analyst may decide to save the time for each faulting event to assess the sensitivity of the resulting dose to the event time. Examples of the types of variable information generally saved to the MODULE VARIABLE utility module include:

- WP Failure Time (yr)
- Fractional Release Rate (1/yr)
- Time of Peak Annual Dose (yr)
- Magnitude of Peak Annual Dose (rem/yr)
- Cumulative Normalized Release

**READER**

READER is a utility module that preprocesses the data from the *tpa.inp* file and is the only subroutine that reads the *tpa.inp* file. The *tpa.inp* file contains data specific for the TPA code execution as well as all probability density function (PDF) definitions for parameters that will be provided to the consequence modules. Additional discussion on the specific input parameters and format requirements are provided in chapter 19.

One significant feature of READER is that it has a large number of error traps that detect problems with the input data and provide specific error messages directing the analyst to the problem. This is a feature that did not exist in the TPA Version 2.0 code. Based on experience exercising the earlier version of the code, it was considered highly desirable to have a READER with numerous built-in error traps. READER also calls other modules such as SAMPLER which have additional embedded error traps. Additionally, the EXEC program contains error traps to ensure consistent format and content of input data. Most error traps also identify the line number of the *tpa.inp* file where the error was detected. Error traps contained within READER are listed in table C-1.

Below are a few examples of errors and associated error messages generated by READER.

READER will enter an error trap if the user has only one title line in the *tpa.inp* file. Below is an example of a title being defined ("title" is the keyword), but the second title line is missing:

```
**
title
First line of title - Only one title line supplied
**
```

The asterisks (**) are comment lines that help the user visually block the input data into groups. The error generated by READER is as follows:

```
***>>> Error in Reader <<<***
  Second line of title is blank or comment line
  title line is:
 **
  Look on Line Number =  4
```

The error message prints the second line of the title (which is read as a comment line, **) and the line number of the *tpa.inp* file where the error was detected.

Another example of a READER error trap is when the user specifies that zero time steps are to be used:

```
**
iconstant
NumberOfTimeStepsInCompliancePeriod
```

**Table C-1. Requirements to prevent error traps in READER utility module**

| |
|---|
| First non-comment line of *tpa.inp* is keyword "title" |
| First line of title is not empty |
| Second line of title is not empty |
| All keywords lower case |
| Keyword "endoffile" is last line of *tpa.inp* |
| PDF distributions are physically consistent, e.g., min < max, no duplicate values in user defined distributions |
| Radionuclides specified are correctly defined for aqueous releases |
| Subarea definitions have consistent coordinates |
| PDF type keywords are correct |
| Random number seed is a constant between $10^8$ and $10^9$ |
| Waste package payload (MTU) is a constant |
| Repository area and areal mass loading are consistent |
| Number of realizations is constant |
| Maxtime is greater than 10 yr |
| Number of time steps is defined, constant, greater than 1, and less than maxtime |
| Ratio of last to first timestep is defined, (if ratio is between 0 and 1, equal timesteps are assigned) |
| All defined variable names present |
| All named variables defined correctly |
| Checks the decay chains specified in *tpa.inp* |

```
      0
      **
```

then the following error message is provided by READER:

```
      ***>>> Error in Reader <<<***
        NumberOfTimeStepsInCompliancePeriod .le. 1
        needs to be >= 2
```

The last example of a READER error trap is when the user specifies a uniform distribution but the lower limit is greater than the upper limit:

```
      **
```

```
uniform
ArealAverageMeanAnnualInfiltrationAtStartmm/yr]
2.5, 2.0
**
```

READER generates the following error message:

```
***>>> Error in Reader <<<***
  for uniform distribution
  name = ArealAverageMeanAnnualInfiltrationAtStartmm/yr]
  xmax .le. xmin
  xmax =      2.0000000000000
  xmin =      2.5000000000000
  Look on Line Number =   176
```

An error trap performed with SAMPLER when called by READER is when a flag value is set to a value other than zero or one:

```
**
iflag
SeismicDisruptiveScenarioFag(yes=1,no=0)
5
**
```

The resulting error message is:

```
***>>> Error in Reader <<<***
  (iflag .ne. 0) .and. (iflag .ne. 1)
  iflag =   5
  Look on Line Number =   16
```

Descriptions of keywords recognized by READER are contained in chapter 19. The above examples only highlight that READER has many error traps to assist the analyst in developing an acceptable input file for the TPA Version 4.0 code.

Another feature of the READER module is that it contains a drift calculator. The calculator is contained in the subroutine called DRIFTS and is designed to create an output file called *drifts.dat* that contains the endpoint coordinates of each drift in the repository. This file is read by subroutines FILLSUBAREAS to calculate the number of WPs in a subarea based on the WP spacing parameter in the *tpa.inp* file. The drift calculator reads the repository design data file called *repdes.dat* that contains the coordinates defining the repository outline. The coordinate pairs represent UTM easting and UTM northing in meters. This discretization is illustrated in figure 5-1. Information provided in the *tpa.inp* file to define the subarea coordinates must coincide with the repository outline coordinates presented in this file. This file also provides the angle (in radians) of inclination of the drift with respect to the east-west direction. The data file identifies the number of points defining the repository outline followed by the coordinates. The repository is divided into two large blocks, referred to as emplacement blocks. Each emplacement block is defined by two corner points, referred to as starting and stopping points. The drift emplacement starts in the first emplacement block. If the number of drifts exceeds the capacity [defined in *tpa.inp* through drift spacing, WP spacing, and amount of waste in the repository (MTUs)] of the first emplacement block, then the second block is used for drift emplacement. The direction in which drifts are advanced during drift emplacement depends on the coordinates of the stopping point relative to the starting point.

### ARRAY

The ARRAY utility module contains 20 subroutines for the manipulation of various data types (i.e., floating point, integer, and character). These subroutines can be called by other modules to perform routine functions. The functionality of those subroutines ranges from ARRAY initialization, vector operations, variance calculations, index mapping, and sorting. The subroutines called by the ARRAY utility module are identified and described in table C-2.

### SECONDARY UTILITY MODULES

Secondary utility modules include FILEUNIT, FINDELEV, NUMRECIP, PEAKFINDER, and RAN. These modules provide support primarily to the utility modules previously described in this chapter, but may also be called by other TPA Version 4.0 modules. Table C-3 lists the function of these secondary modules.

# APPENDIX C
# REFERENCES

Press, W.H., B.P. Flannery, S.A. Tekolsky, and W.T. Vetterling. *Numerical Recipes in FORTRAN.* Cambridge, UK: Cambridge University Press. 1986.

**Table C-2. Standard subroutines located in the ARRAY utility module**

| Subroutine | Operational Description |
|---|---|
| zero | zeros out a vector |
| zeroi | zeros out integer vector |
| clearchar | clears character string |
| initr | sets all elements of a double precision array to a given value |
| initi | sets all elements of an integer array to a given value |
| initchar | sets all characters of a string to a given character |
| transpose | transposes the contents of a matrix |
| scale | scales a vector |
| scopy | scales and copies a vector |
| acopy | copies vector and adds a constant to each entry |
| ascopy | add, scale, and copy vector |
| addto | adds one vector to another |
| isoneofset | determines if an integer is part of an integer set |
| ainterl | linearly interpolates in list of {time, value} data to find value at time of interest |
| avar | calculates variance of an array of values |
| amean | calculates mean of an array of values |
| checkinorder | determines if array of values are in order, either ascending or descending |
| sortqr | sorts based on pointers to array of values – sorts from smallest to largest value |
| maplist | maps data in first list into second list given the first set of {x,y} and the second set of {x}, and finds the second set of {y} |
| maptimeofevent | fills each element of an array with one of two input values depending on the time of the event |
| checkforduplicates | determines if a double precision array of sorted values has any duplicates |
| icheckforduplicates | determines if an integer array of sorted values has any duplicates |

**Table C-3. Description of secondary utility modules**

| Module | Function |
|---|---|
| FILEUNIT | assigns unit numbers for all modules and ensures different modules have unique unit numbers |
| FINDELEV | finds elevation of ground surface for a given set of UTM coordinates |
| NUMRECIP | contains multiple subroutines for solving equations as modified from Press et al. (1986) |
| PEAKFINDER | finds and reports time and magnitude of peak doses for each nuclide and summed dose for all nuclides |
| RAN | generates random vectors for Monte Carlo sampling and random values for the seismic hazard curve |

# APPENDIX D

# APPENDIX D
# PROBABILITY DISTRIBUTION FUNCTIONS

The mathematical representation of distribution functions available in the Latin Hypercube Sampling (LHS) sampler (i.e., *snllhs.f* ) are described below. Any distribution function that is not available in the LHS sampler of the total-system performance assessment (TPA) code can be approximated by either the beta distribution or user distribution options in the LHS code. While the information presented in this appendix provides mathematical representations of the distribution functions, the user should refer to the description presented in chapter 19 and table 3-2 to help prepare the input data set in the *tpa.inp* file. Whereas individual distribution functions are presented in this section, description on correlated inputs is presented in chapter 3.

**Constant Distribution**

A parameter may be specified as a constant such that it remains at a fixed value for the simulation. The constant can be described as a probability density function (PDF) consisting of a Dirac delta function located at the value of the constant [see Boyce and DiPrima (1977) for a discussion of the Dirac delta function]. However, this level of mathematical complexity is not needed for this discussion.

**Uniform Distribution**

The PDF for the uniform distribution is:

$$f(x) = \frac{1}{(B-A)}, \qquad A\langle x\langle B \tag{D-1}$$

The mean of the uniform distribution is:

$$\mu = \frac{(A+B)}{2} \tag{D-2}$$

and the variance of the uniform distribution is:

$$\sigma^2 = \frac{(B-A)^2}{12} \tag{D-3}$$

To assign the uniform distribution to an input parameter, the user must specify the endpoints $A$ and $B$. An example is shown in figure 3-5 (along with examples of other distributions described in this appendix) where the end points are $A$ = 1.2 and $B$ = 2.45.

**Integer-Uniform Distribution**

The integer uniform distribution is calculated from the uniform distribution by the following changes:

(i) The lower limit is specified to be $A$-1
(ii) The outputs are rounded up to the next whole number.

These changes assume that both the lower and upper limits, $A$ and $B$, are included in the output distribution.

**Log-Uniform Distribution**

The log-uniform distribution is a variation of the uniform distribution and is built upon calling the uniform distribution. The actual end points of the log-uniform distribution are ($a$, $b$). The endpoints passed to the uniform distribution are the log-transformation of the actual end points [e.g., $A$ = log ($a$), $B$ = log ($b$)][1]. The exponential of the sampled value from the uniform distribution is then returned as the value for the log-uniform distribution. An example is shown in figure 3-5.

**Normal Distribution**

The PDF of the normal distribution is:

$$f(x) = \frac{1}{\sigma\sqrt{2\pi}} \exp\left[-\frac{(x-\mu)^2}{2\sigma^2}\right], \quad -\infty < x < \infty \tag{D-4}$$

where $\mu$ and $\sigma$ are the mean and standard deviation of the distribution, respectively. SAMPLER generates samples having standard normal distribution (mean of 0.0 and standard deviation of 1.0) with lower and upper cut-off $A$ and $B$. Sampling from the normal PDF is based on the algorithm described by Press et al. (1986) when Monte Carlo Sampling (MCS) is selected, and when LHS is specified, the algorithm in the code by Iman and Shortencarier (1984) is used. SAMPLER requires specification of $A$ and $B$ at the 0.001 and 0.999 quantiles of the normal distribution:

$$P(x < A) = 0.001 \tag{D-5}$$

and

$$P(x < B) = 0.999 \tag{D-6}$$

The mean of the normal distribution is:

$$\mu = \frac{A+B}{2} \tag{D-7}$$

and the variance of the normal distribution is:

[1]A value of 0.0 as a lower endpoint is undefined for the log-uniform distribution.

$$\sigma^2 \approx \left(\frac{B-A}{6.180465}\right)^2 \tag{D-8}$$

An example of a normal distribution with a mean of 2.0 and standard deviation of 3.5 is shown in figure 3-5. With this mean and standard deviation, the 0.001 and 0.999 quantiles are $A = -8.816$ and $B = 12.816$, respectively.

**Lognormal Distribution**

The log-normal distribution is built upon using the normal distribution. Here, the logarithm of the 0.001 and 0.999 quantiles [e.g., $A = \log(a)$, $B = \log(b)$] are used as inputs to sample from the normal distribution. An example is shown in figure 3-5.

**Triangular Distribution**

The triangular distribution is described by a minimum value ($A$), maximum value ($C$), and a mode or peak value ($B$). The PDF of the triangular distribution is:

$$f(x) = \begin{cases} \dfrac{2(x-A)}{(C-A)(B-A)}, & A\langle x\langle B \\ \dfrac{2(C-x)}{(C-A)(C-B)}, & B\langle x\langle C \end{cases} \tag{D-9}$$

The mean of the triangular distribution is:

$$\mu = \left(\frac{A+B+C}{3}\right) \tag{D-10}$$

and the variance of the triangular distribution is:

$$\sigma^2 = \frac{A(A-B)+B(B-C)+C(C-A)}{18} \tag{D-11}$$

An example of triangular distribution is shown in figure 3-5. Here the lower limit, the peak, and the upper limit are $A = -2$, $B = 4$, and $C = 14$, respectively.

**Log-Triangular Distribution**

The log-triangular distribution is based on the triangular distribution. The minimum, peak, and maximum locations ($a$,$b$,$c$) are logarithmically transformed [e.g., $A = \log(a)$, $B = \log(b)$, and $C = \log(c)$]. The samples are then drawn from the triangular distribution. The exponential of this sample is then returned for the log-triangular distribution. An example is shown in figure 3-5.

**Beta Distribution**

The PDF of the beta distribution within 0 and 1 (standard beta distribution) is defined as:

$$f(y) = \frac{\Gamma(\alpha+\beta)}{\Gamma(\alpha)\Gamma(\beta)} y^{\alpha-1}(1-y)^{\beta-1}, \quad 0 < y < 1 \tag{D-12}$$

where $\alpha$ and $\beta$ are positive shape parameters of the distribution and $\Gamma(\eta)$ is the Gamma function which is defined as:

$$\Gamma(\eta) = \int_0^\infty z^{\eta-1} e^{-z}\, dz \tag{D-13}$$

The mean and variance of the standard beta distribution are:

$$\mu = \frac{\alpha}{\alpha+\beta} \tag{D-14}$$

and

$$\sigma^2 = \frac{\alpha\beta}{(\alpha+\beta)^2(\alpha+\beta+1)} \tag{D-15}$$

When MCS is selected, the algorithm by Ang and Tang (1984) is employed. The algorithm uses at least two random numbers, $u_1$ and $u_2$. If the two random numbers satisfy

$$u_1^{1/\alpha} + u_2^{1/\beta} \leq 1 \tag{D-16}$$

then the algorithm proceeds, otherwise new pairs of random numbers are drawn until the above criterion is satisfied. The sample from the standard beta distribution is then:

$$y = \frac{u_1^{1/\alpha}}{u_1^{1/\alpha} + u_2^{1/\beta}} \tag{D-17}$$

The general beta distribution with lower and upper bounds $A$ and $B$ (i.e., $A< x < B$) may be obtained from mapping the standard beta distribution:

$$x = A + y\left(B - A\right) \tag{D-18}$$

where $y$ corresponds to the sample from the standard beta distribution. Figure 3-6 gives one example of beta distributions. Beta distributions are further discussed later with regard to LHS.

**Log-Beta Distribution**

The log-beta distribution uses the beta distribution. The upper and lower bounds are transformed by taking the logarithm [e.g., $A = \log(a)$, $B = \log(b)$]. The sample is then drawn from the beta, and the exponential of the sample is returned from the log-beta.

**Exponential Distribution**

The PDF of an exponential distribution is:

$$f(x) = \lambda e^{-\lambda x}, \qquad 0\langle x \tag{D-19}$$

where $\lambda$ is the recurrence probability. The exponential distribution is frequently used to describe the time of the next event such as faulting, volcanism, or seismic activity. In these cases, $\lambda$ is the annual recurrence probability that is the reciprocal of the return period. The mean of the exponential distribution is:

$$\mu = \frac{1}{\lambda} \tag{D-20}$$

and the variance is:

$$\sigma^2 = \left(\frac{1}{\lambda}\right)^2 \tag{D-21}$$

A random sample is drawn from the exponential distribution by

$$x = \frac{-1\mathrm{n}\left(1-u\right)}{\lambda} \tag{D-22}$$

An example of an exponential distribution is shown in figure 3-6. Here, the recurrence probability is equal to 0.4. The figure also illustrates that $x$ is strictly positive.

**Finite-Exponential Distribution**

The PDF for the finite exponential distribution is:

$$f(x) = \left( \frac{\lambda}{e^{-\lambda A} - e^{-\lambda B}} \right) e^{-\lambda x} \qquad 0 \leq A \langle x \langle B \tag{D-23}$$

The PDF is equal to zero outside the range from $A$ to $B$. When the return period, $1/\lambda$ is long compared to $(B - A)$, the finite exponential is approximately a uniform distribution.

A random sample from the finite exponential is drawn by

$$x = \frac{-\ln \left[ e^{-\lambda A} - \left( e^{-\lambda A} - e^{-\lambda B} \right) u \right]}{\lambda} \tag{D-24}$$

An example of a finite-exponential distribution is shown in figure 3-6. Here the recurrence probability is 0.4, and the lower and upper limits are $A = 2$ and $B = 5$, respectively.

# APPENDIX D REFERENCES


Ang, A.H-S., and W.H. Tang. *Probability Concepts in Engineering Planning and Design. Volume II: Decision, Risk, and Reliability.* New York: John Wiley and Sons. 1984.

Boyce, W.E., and R.C. DiPrima. *Elementary Differential Equations and Boundary Value Problems.* New York: John Wiley and Sons. 1977.

Iman, R.L., and M.J. Shortencarier. *A FORTRAN 77 Program and User's Guide for the Generation of Latin Hypercube and Random Samples for Use With Computer Models.* NUREG/CR–3624. Washington, DC: Nuclear Regulatory Commission. 1984.

Press, W.H., B.P. Flannery, S.A. Teukolsky, and W.T. Vetterling. *Numerical Recipes in FORTRAN.* Cambridge, UK: Cambridge University Press. 1986.

# APPENDIX E

# APPENDIX E
# INTERMEDIATE DATA TRANSFER FILES

The total-systems performance assessments (TPA) Version 4.0 code uses seven stand-alone codes *ashplume.f, ebsfiltlf, failt.f, nefmks.f, releaset.f,* GENTPA, and *snllhs.f.* Each stand-alone code has input and output files that may or may not be used directly in the TPA code. Data transfer from the TPA code to the stand-alone codes takes place through the input files of the stand-alone codes. Not all features of the stand-alone codes are used in the TPA code. Consequently, some of the files created by these stand-alone codes are not relevant to the TPA calculations. However, the files are listed and briefly described in table E-1 for the sake of completeness. These files are overwritten when a new realization is computed and contain information only of the last subarea of the last realization in the TPA calculations.

**Table E-1. Description of input and output files of the stand-alone codes**

| File | Description |
|---|---|
| *ashplume.out* | The *ashplume.out* file is output from the *ashplume.f* stand-alone code. This file provides an echo of the input data specified in the ASHPLUMO section of *tpa.inp* and the *ashplume.f* results for the ash and spent fuel areal densities ($Ci/m^2$). The *ashplume.out* file is overwritten every time ASHPLUMO executes *ashplume.f.* Consequently, values in *ashplume.out* are from the final realization. The information in *ashplume.out* for all realizations is available in *ashout.res* and *ashplumo.rlt.* Values in *ashplume.out* are also included in the *junk.out* file. |
| *chlrdmf.dat* | The EBSFAIL module uses the time history of chloride concentration (mol/L) read from *multiflo.dat* in the NFENV module and then writes the information to *chlrdmf.dat.* The chloride concentration data are used by *failt.f* to determine the waste package (WP) failure time. The *chlrdmf.dat* file is overwritten every time EBSFAIL is executed. Consequently, values in *chlrdmf.dat* are from the final subarea and realization. |
| *corrode.out* | The *corrode.out* file is output from *failt.f.* The time history of WP corrosion depth (m) and corrosion potential (Vshe) is provided in this file. The *corrode.out* file is overwritten every time EBSFAIL executes *failt.f.* Consequently, values in *corrode.out* are from the final subarea and realization. This information is also available in the *failt.out* file. |
| *cumrelse.out* | This file is an output file from the execution of *releaset.f.* It contains the amount (Ci) of a radionuclide outside the WP as a function of time for a given subarea. These values are interpolated from the internal time scale as given in the *treleasel.out* file onto the TPA system time scale. This file is not used by the TPA system. This file is overwritten when a new subarea is processed. |
| *diagnose.out* | The *diagnose.out* file contains output from the *releaset.f* stand-alone code. This information is for diagnostic purposes only. To examine the *releaset.f* output for the groundwater nuclide release rates, the user should access *ebsnef.dat.* |

**Table E-1. Description of input and output files of the stand-alone codes (cont'd)**

| File | Description |
|---|---|
| *ebsfail.def* | The EBSFAIL module uses *ebsfail.def* as a template file for *ebsfail.inp*. EBSFAIL copies the contents of *ebsfail.def*, replaces a part of this information with the parameters set in the EBSFAIL section of *tpa.inp*, and writes the *failt.f* input file *ebsfail.inp*. |
| *ebsfail.inp* | The *ebsfail.inp* file is a *failt.f* input file. EBSFAIL utilizes a template file (*ebsfail.def*) and the corrosion related parameters specified in the EBSFAIL section of *tpa.inp* to write *ebsfail.inp*. Portions of the *ebsfail.def* template (e.g., numerical control parameters) that do not have values defined in *tpa.inp* are transferred directly from the *ebsfail.def* template file to *ebsfail.inp*. The *ebsfail.inp* file is overwritten every time EBSFAIL executes *failt.f*. Consequently, values in *ebsfail.inp* are from the final subarea and realization. |
| *ebsfilt.def* | The EBSREL module uses *ebsfilt.def* as a template file for *ebsfilt.inp*. EBSREL updates the contents of *ebsfilt.def* with invert parameters set in the EBSREL section of *tpa.inp*, and writes the *ebsfilt.inp* input file for *ebsfilt.f*. |
| *ebsfilt.inp* | The *ebsfilt.inp* file is an *ebsfilt.f* input file. EBSREL utilizes a template file (*ebsfilt.def*) and invert related parameters specified in the EBSREL section of *tpa.inp* to write *ebsfilt.inp*. The *ebsfilt.inp* file is overwritten every time EBSREL executes *ebsfilt.f*. Consequently, values in *ebsfilt.inp* are from the final subarea and realization. |
| *ebsfilt.out* | This file is the standard output file from *ebsfilt.f*. This file is not used by the TPA system. This file is overwritten when a new subarea is processed. |
| *ebsflo.dat* | The time-varying flow rates of groundwater hitting the WP ($m^3$/yr) from NFENV modified by the WPFlowMultiplicationFactor in *tpa.inp* and the factors that account for flow contacting the WP ($F_{mult}$ and $F_{ow}$) are written by EBSREL to *ebsflo.dat*. This file is input to the *releaset.f* stand-alone code. The *ebsflo.dat* file is overwritten every time EBSREL executes *releaset.f*. Consequently, values in *ebsflo.dat* are from the final subarea and realization. |
| *ebsnef.dat* | Results of the engineered barrier system (EBS) release rates for all groundwater nuclides computed in the stand-alone code *releaset.f* are provided in *ebsnef.dat*. EBSREL accesses the release rates in *ebsnef.dat*, and the information is then used as input to the *ebsfilt.f* stand-alone code. The *ebsnef.dat* file is overwritten every time EBSREL executes *releaset.f*. Consequently, values in *ebsnef.dat* are from the final subarea and realization. |
| *ebsnef2.dat* | Results of the EBS release rates for all groundwater nuclides computed in the stand-alone code *ebsfilt.f* are provided in *ebsnef2.dat*. EBSREL accesses the release rates in *ebsnef2.dat*, and the information is then used as input to UZFT. The *ebsnef2.dat* file is overwritten every time EBSREL executes *ebsfilt.f*. Consequently, values in *ebsnef2.dat* are from the final subarea and realization. |

**Table E-1. Description of input and output files of the stand-alone codes (cont'd)**

| File | Description |
|---|---|
| *ebspac.nuc* | The *ebspac.nuc* file is a *releaset.f* input file. EBSREL utilizes a template file (*ebsnuc.dat*), solubilities, retardation factors, and gap fractions specified in the EBSREL section of *tpa.inp*, and nuclide-specific information for initial inventories and half-lives from the INVENT module to write *ebspac.nuc*. The *ebspac.nuc* file is overwritten every time EBSREL executes *releaset.f*. Consequently, values in *ebspac.nuc* are from the final subarea and realization. |
| *ebsrel.def* | The EBSREL module uses *ebsrel.def* as a template file for *ebsrel.inp*. EBSREL copies the contents of *ebsrel.def*, replaces a part of this information with the parameters set in the EBSREL section of *tpa.inp*, and writes the *releaset.f* input file *ebsrel.inp*. |
| *ebsrel.inp* | The *ebsrel.inp* file is a *releaset.f* input file. EBSREL utilizes a template file (*ebsrel.def*) and the release and flow related parameters specified in the EBSREL section of *tpa.inp* to write *ebsrel.inp*. Portions of the *ebsrel.def* template (e.g., values setting numerical control, rock parameters, and diffusion rates) that do not have values defined in *tpa.inp* are transferred directly from the *ebsrel.def* template file to *ebsrel.inp*. The *ebsrel.inp* file is overwritten every time EBSREL executes *releaset.f*. Consequently, values in *ebsrel.inp* are from the final subarea and realization. |
| *ebstrh.dat* | The time history of WP and repository temperatures (°C) and relative humidity from NFENV and the corrosion failure time (yr) computed in *failt.f* are available in *ebstrh.dat*. The *failt.f* stand-alone code writes *ebstrh.dat* and EBSFAIL accesses the corrosion failure time from this file. The *ebstrh.dat* file is overwritten every time EBSFAIL executes *failt.f*. Consequently, values in *ebstrh.dat* are from the final subarea and realization. For the subarea averaged WP temperature and the corrosion failure time from all realizations, the *nearfld.res* and *wpsfail.res* files can be examined. The temperature and relative humidity information in *ebstrh.dat* is also available in *ebstrhc.inp*. |
| *ebstrhc.inp* | The time history of WP and repository temperatures (°C) and the relative humidity from NFENV is available in *ebstrhc.inp*. The EBSFAIL module writes *ebstrhc.inp*, and the stand-alone code *failt.f* accesses this information to compute the corrosion failure time. The *ebstrhc.inp* file is overwritten every time EBSFAIL executes. Consequently, values in *ebstrhc.inp* are from the final subarea and realization. To view the subarea averaged WP temperature from all realizations, the *nearfld.res* file can be examined. The temperature and relative humidity information in *ebstrhc.inp* is also available in *ebstrh.dat*. |
| *echofail.dat* | The *echofail.dat* file provides an echo of the *ebsfail.inp* data that is utilized by the *failt.f* stand-alone code to determine the corrosion failure time. The *echofail.dat* file is overwritten every time EBSFAIL executes *failt.f*. Consequently, values in *echofail.dat* are from the final subarea and realization. |

**Table E-1. Description of input and output files of the stand-alone codes (cont'd)**

| File | Description |
|---|---|
| *echofilt.dat* | The *echofilt.dat* file provides an echo of the *ebsfilt.inp* and *ebsnef.dat* data that are utilized by the *ebsfilt.f* stand-alone code to determine the EBS release rates from the invert. The *echofilt.dat* file is overwritten every time EBSREL executes *ebsfilt.f*. Consequently, values in *echofilt.dat* are from the final subarea and realization. |
| *failt.out* | The *failt.out* file is output from *failt.f*. The time history of WP corrosion depth (m) and corrosion potential (Vshe) is provided in this file. The *failt.out* file is overwritten every time EBSFAIL executes *failt.f*. Consequently, values in *failt.out* are from the final subarea and realization. This information is also available in the *corrode.out* file. |
| *frac_rel.out* | The *frac_rel.out* file is written by the *releaset.f* stand-alone code and contains the same information as *ebsnef.dat*. However, none of the TPA code modules utilize the information in *frac_rel.out*. The *frac_rel.out* file is overwritten every time EBSREL executes *releaset.f*. Consequently, values in *frac_rel.out* are from the final subarea and realization. |
| *ggenii.def* | The DCAGW module uses *ggenii.def* as a template for *ggenii.inp*. DCAGW copies the contents of *ggenii.def*, replaces part of this information and prepare the *ggenii.inp* input file. |
| *ggenii.out* | The input parameters are echoed for each GENTPA execution in *ggenii.out*. The *ggenii.out* is overwritten each realization. |
| *genv.in* | Input file for ENV program of GENTPA . The *genv.in* file contains the output of ENVIN program written into a structured input file for the ENV program. Use of file is transparent to the user. |
| *genv.out* | Output file for the ENV program of GENTPA. The *genv.out* file contains the yearly exposure rates by pathway and radionuclide. These exposure rates are then converted to dose by DCAGW. This file is overwritten each realization. |
| *gdefault.def* | The DCAGW module uses *gdefault.def* as a template for *gdefault.inp*. DCAGW copies the contents of *gdefault.def*, replaces part of this information with the parameters set in the DCAGW section of *tpa.inp*, and writes the GENTPA input file *gdefault.inp*. |
| *gdefault.inp* | Miscellaneous default input parameters. The *gdefault.def* is copied to create *gdefault.inp*, the file read by GENTPA which also contains sampled values of selected parameters from *tpa.inp*. |
| *gftrans.def* | The DCAGW module uses *gftrans.def* as a template for *gftrans.inp*. DCAGW copies the contents of *gftrans.def*, replaces part of this information with parameters in the DCAGW section of *tpa.inp*, and writes the GENTPA input file *gftrans.inp*. |

**Table E-1. Description of input and output files of the stand-alone codes (cont'd)**

| File | Description |
|---|---|
| *gftrans.inp* | The *gftrans.inp* file is an input file for GENTPA and contains food transfer coefficients for all elements by pathway including leafy vegetable, other vegetable, fruit, grain, beef, poultry, milk, and egg. The file also contains leaching factors for loss of radionuclides from surface to deep soil and deposition velocities. Each realization, the product of each transfer coefficient read from *gftrans.def* and the appropriate sampled scale factor from *tpa.inp*, is written to *gftrans.inp*. |
| *ggenii.inp* | Primary input parameter file that contains fixed parameter values. *Ggenii.def* is copied to create *ggenii.inp*, the file read by GENTPA v1.0 which also contains sampled values of parameters from *tpa.inp*. |
| *gmedia.out* | Output of media concentrations (e.g., air, surface soil, deep soil, groundwater) by radionuclide and year. This file is overwritten each realization. |
| *gwork.buf* | Workspace used by various programs in GENTPA v1.0. |
| *infile.ash* | The *infile.ash* file is an *ashplume.f* input file. ASHPLUMO utilizes the parameters specified in the ASHPLUMO section of *tpa.inp* to write *infile.ash*. The *infile.ash* file is overwritten every time ASHPLUMO executes *ashplume.f*. Consequently, values in *infile.ash* are from the final realization. |
| *inv1000.out* | The *inv1000.out* file is output from *releaset.f* and contains the inventory (Ci) of the groundwater nuclides at 1,000 yr and the initial inventory (Ci/WP) from *ebspac.nuc*. The *inv1000.out* file is overwritten every time EBSREL executes *releaset.f*. Consequently, values in *inv1000.out* are from the final subarea and realization. |
| *junk.out* | The *junk.out* file is output from *ashplume.f*. The *junk.out* file is overwritten every time ASHPLUMO executes *ashplume.f*. Consequently, values in *junk.out* are from the final realization. The information in *junk.out* for all realizations is available in *ashout.res* and *ashplumo.rlt*. Values in *junk.out* are also included in the *ashplume.out* file. |
| *maxrel.dat* | The *maxrel.dat* file is written by the *releaset.f* stand-alone code. However, none of the TPA code modules utilize the information in *maxrel.dat*. This file contains the maximum fractional release of C14 followed by the maximum fractional release of the selected aqueous nuclides. The *maxrel.dat* file is overwritten every time EBSREL executes *releaset.f*. Consequently, values in *maxrel.dat* are from the final subarea and realization. |

**Table E-1. Description of input and output files of the stand-alone codes (cont'd)**

| File | Description |
|---|---|
| *nefii.inp* | This is the standard input file for *nefmks.f*. It contains the input parameters required by *nefmks.f* for a given run. The format of this file is complex and is described in the User's Manual for the NEFTRAN II Computer Code. A new file is generated automatically for each subarea by the UZFT and SZFT modules for their respective *nefmks.f* runs. |
| *nefii.out* | This is the standard output from *nefmks.f*. It contains an echo of the input parameters and the discharge rates (Ci/yr) as a function of time for all the radionuclides used for a single run of the *nefmks.f* code. It is not used by any other modules in the TPA system. These discharge rates are also provided in the *nefii.dis* output file.<br><br>*Nefmks.f* may be run from zero to two times per subarea, since it may be invoked by UZFT and SZFT. This file contains the output from the last *nefmks.f* call issued by the TPA system. It is copied to either *nefiiuz.out* or *nefiisz.out* upon completion, depending on which module invoked the *nefmks.f* task. |
| *nefii.rel* | This file contains the output from *nefmks.f*. It contains the total release (Ci) for each nuclide. It is not used by any other module in the TPA system. It is the output of an *nefmks.f* run spawned by either UZFT or SZFT. This file is overwritten when a new subarea is processed. |
| *NEFIL.VEL* | The UZFT module creates *NEFIL.VEL* as an input file for *nefmks.f*. Time-dependent velocities (ft/yr) computed from the UZFLOW deep percolation rate for each leg that meets the minimum velocity change factor criteria specified in the UZFT section of *tpa.inp* are included in this file. The *NEFIL.VEL* file is overwritten every time UZFT executes *nefmks.f*. Consequently, values in *NEFIL.VEL* are from the final subarea and realization. Additionally, after executing *nefmks.f*, UZFT copies the *NEFIL.VEL* file to *nefiiuz.vel*. |
| *nefiisz.inp* | This file is a copy of the *nefii.inp* file that was used for the most recent SZFT run. It is copied by the executive upon completion of the *nefmks.f* code. This file is overwritten when a new subarea is processed. |
| *nefiisz.src* | This file is a copy of the *nefii.src* file that was used for the most recent SZFT *nefmks.f* run. It is copied by the executive upon completion of the *nefmks.f* code. It contains a time history of release rates (Ci/yr) for each radionuclide, and is created by the SZFT module. This file is overwritten when a new subarea is processed. |
| *nefiisz.out* | This file is a copy of the *nefii.out* file that was generated during the most recent SZFT *nefmks.f* run. It is copied by the executive upon completion of the *nefmks.f* code. This file is overwritten when a new subarea is processed. |

**Table E-1. Description of input and output files of the stand-alone codes (cont'd)**

| File | Description |
|---|---|
| *nefiiuz.inp* | This file is a copy of the *nefii.inp* file that was used for the most recent UZFT *nefmks.f* run. It is copied by the executive upon completion of the *nefmks.f* code. |
| *nefiiuz.out* | This file is a copy of the *nefii.out* file that was generated during the most recent UZFT *nefmks.f* run. It is copied by the executive upon completion of the *nefmks.f* code. This file is overwritten when a new subarea is processed. |
| *nefiiuz.src* | This file is a copy of the *nefii.src* file that was used for the most recent UZFT *nefmks.f* run. It is copied by the executive upon completion of the *nefmks.f* code. It contains a time history of release rates (Ci/yr) for each radionuclide, and is created by the UZFT module. This file is overwritten when a new subarea is processed. |
| *nefiiuz.vel* | This file is a copy of the *nefii.vel* file that was used for the most recent UZFT *nefmks.f* run. It is copied by the executive upon completion of the *nefmks.f* code. It contains a time history of groundwater velocities, and is created by the UZFT module. This file is overwritten when a new subarea is processed. |
| *relcum.out* | This file is an output file from the execution of *releaset*. It contains the total release (Ci) of a radionuclide remaining outside the WP and the remaining fraction inside the WP of each radionuclide for a given subarea at the end time of the simulation. This file is not used by the TPA system. This file is overwritten when a new subarea is processed. |
| *releaset.out* | This file is the standard output file from *releaset*. The contents track internal variables of the code that monitor the mass balance equation. This file is not used by the TPA system. This file is overwritten when a new subarea is processed. |
| *relfrac.out* | This file is an output file from the execution of *releaset*. It contains the time (yr) of maximum fractional release rate as well as the maximum fractional release rate for each radionuclide for a given subarea. This information is used by *ebsrel*. This file is overwritten when a new subarea is processed. |
| *sotnef.dat* | This file is generated by UZFT and SZFT for their respective *nefmks.f* runs. It is an input file for *nefmks.f*. In the case of UZFT, it contains the reformatted release rates supplied by *releaset* in the file *ebsnef.dat*. In the case of SZFT, it contains the reformatted release rates supplied by the UZFT *nefmks.f* run in the file *nefii.dis*. |
| *trelease.out* | This file is generated by *releaset*. It contains the amount (Ci) of a radionuclide outside the WP as a function of the internal *releaset* time steps (yr). This file is not used by the TPA system. This file is overwritten when a new subarea is processed. |

# APPENDIX F

# APPENDIX F
# DERIVATION OF FLOW FACTORS

Within the TPA code, three main factors ($F_{ow}$, $F_{mult}$, and $F_{wet}$) have been defined that contribute to modification of the amount of water that reaches the waste package (WP) from the mean deep percolation rate. Technical support for the flow factors is sparse, but is an area of active research. The following is a description of the process used to develop the abstracted water contact parameters implemented in the TPA Version 4.0 code. It is expected that future implementations will improve on the initial attempt that follows. The water contact parameters can be described as:

- $F_{ow}$ is a convergence/divergence factor to account for large-scale (greater than the drift) features that create focusing/divergence of deep percolation toward or away from the drift.

- $F_{wet}$ is the fraction of WPs that are dripped on by flowing fractures. This factor is used to account for the potential that not all of the fractures may be flowing. Fracture density information suggests that many fractures will intersect the drift surface above a given WP. However, observations on fracture flow in geologic systems under unsaturated conditions suggests that a few fractures may transmit most of the percolation.

- $F_{mult}$ is a factor to represent the fraction of dripping water that will enter the WP. It is comprised of four main components:
  - — Diversion by a capillary barrier process in the drift wall
  - — Diversion down the surface of the drift wall
  - — Intersection of a falling drip with a hole in the WP
  - — Presence of corrosion products in the hole in the WP

This appendix is structured into two parts: (i) a derivation of the flow factors for the case of no-temporal variation (static) and (ii) a discussion of potential sources of temporal variation in the flow factors. Most of the implementation of temporal variation in the flow factors is deferred to sensitivity studies due to a lack of supporting technical bases.

## DERIVATION OF STATIC FLOW FACTORS

The factors $F_{mult}$ and $F_{ow}$ could have been combined into a single factor for use in the TPA code; however, these factors were kept separate because $F_{ow}$ is strongly correlated with the initial infiltration rate at Yucca Mountain (YM), $\langle I \rangle$, and the matrix saturated hydraulic conductivity for the Topopah Spring-welded layer at YM, $\langle K_{sat} \rangle$, while $F_{mult}$ is considered to be an independent random variable. The angular bracket represents spatial averaging over the repository area. $F_{ow}$ is also correlated to $F_{wet}$. The specified $\langle I \rangle$ and $\langle K_{sat} \rangle$ are used in the derivation of these static flow factor values as described below.

### Derivation of Estimates for $F_{wet}$ and $F_{ow}$

$F_{wet}$ is the fraction of WPs dripped on by flowing fractures. This entails the assumption that the number of wetted WPs is time invariant, and does not consider changing dripping locations. Some data (Wilder, 1996) indicate that drip locations in tunnels move with time. Therefore, dripping eventually can be considered to spread over all WPs, producing a lower average flow rate for each WP.

Wilder (1996) proposed that the net infiltration to the repository level flows in either the rock matrix or fractures depending on the local values of infiltration and matrix hydraulic conductivity. Variabilities of the local values for $I$ and $K_{sat}$ within a realization are characterized by their coefficients of variation $C_{vi}$ and $C_{vk}$. Both $I$ and $K_{sat}$ are assumed to be lognormally distributed within the subarea and correlated with each other.

The dripping model requires that the spatial scale of variability in $K_{sat}$ and $I$ be greater than the size of an individual WP. If not (for example, the flowing fractures are closely spaced), then variability from point to point would, in the limit, cause every WP to always be wetted. This is similar in some respects to the "weeps" model of TSPA93 (Wilson et al., 1994) that assumes that in the limit of many small seeps, all WPs would be wetted. However, the condition of high fracture frequency is not sufficient to support the assumption of $F_{wet}$ approaching 1.0 because many fractures may remain dry.

If the scale of the dripping phenomenon is larger than the WP scale, then only the interaction of the variability of $I$ and $K_{sat}$ needs to be considered. Correlation between $I$ and $K_{sat}$ may be important if there are definite paths with high conductivity, so infiltration at the drift would be determined by the high conductivity of these paths. While the present model allows correlation between $K_{sat}$ and $I$, only the uncorrelated case is considered here.

## Assumption about the Distribution of Model Parameters

For the derivation of $F_{ow}$ and $F_{wet}$, the mean infiltration $\langle I \rangle$ is uniformly distributed from 1 to 20 mm/yr with a coefficient of variation ($C_{vi}$) range from 0 to 2, and $\langle K_{sat} \rangle$ is uniformly distributed from 0.1 to 20 mm/yr with a $C_{vk}$ range from 0 to 2. The local parameters $K_{sat}$ and $I$ are described by the mean and standard deviation in most reported data on YM. However, this conceptualization assumes that these local parameters are lognormally distributed; it is, therefore, necessary to convert between the two distributions. As an example using $K_{sat}$, given the arithmetic mean and coefficients of variation, the standard deviation in the log-transformed space can be described (Benjamin and Cornell, 1970) as follows.

$$\sigma = \sqrt{\ln\left(C_{VK}^2 + 1\right)} \tag{F-1}$$

$$\mu = \ln\left(\langle K_{sat} \rangle e^{-\sigma^2/2}\right) \tag{F-2}$$

The $F_{ow}$ and $F_{wet}$ factors are generated from Monte Carlo runs, which sample the parameters $\langle I \rangle$, $\langle K_{sat} \rangle$, $C_{vi}$ and $C_{vk}$. Referring to figure F-1, consider the repository subarea to be broken into $n$ equal parts (subsubareas). For each Monte Carlo sample of $\langle I \rangle$, $\langle K_{sat} \rangle$, $C_{vi}$ and $C_{vk}$, a lognormal distribution is generated for the local values $I$ and $K_{sat}$ for each of the sub-subareas. If ($I$ - $K_{sat}$) is greater than zero, the number of wet areas $N_{wet}$ is incremented, and the sum of the positive values of ($I$ - $K_{sat}$) is collected into $q_{wet}$, which represents the potential dripping water. For the current Monte Carlo sample of $\langle I \rangle$, $\langle K_{sat} \rangle$, $C_{vi}$ and $C_{vk}$, the factor $F_{wet}$ is the ratio $N_{wet}/N$, where $N$ is the total number of WPs. The ratio of $q_{wet}/I/N_{wet}$ averaged over the entire area is $F_{ow}$. The fraction of wetted cells represents the potential fraction of wetted WPs.

The histograms of $F_{wet}$ and $F_{ow}$, based on 6,000 samples with 1,000 sub-subareas per sample, are plotted in figures F-2 and F-3. The covariances among $I$, $K_{sat}$, $F_{wet}$, and $F_{ow}$ are presented in table F-1.

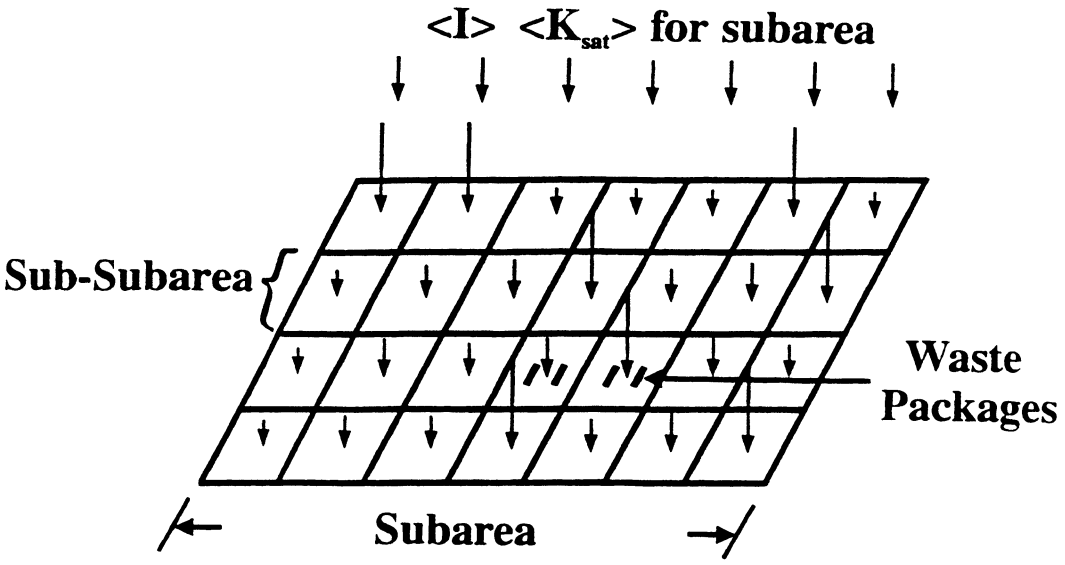


**Figure F-1. Conceptual dripping model**

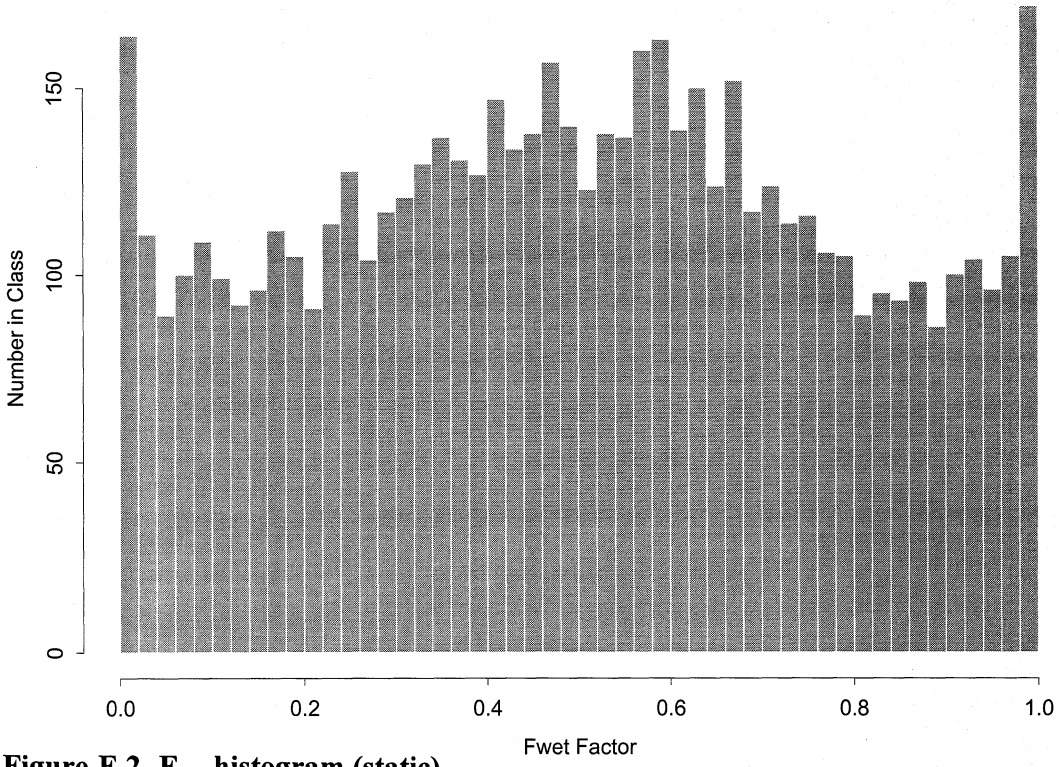


**Figure F-2. $F_{wet}$ histogram (static)**

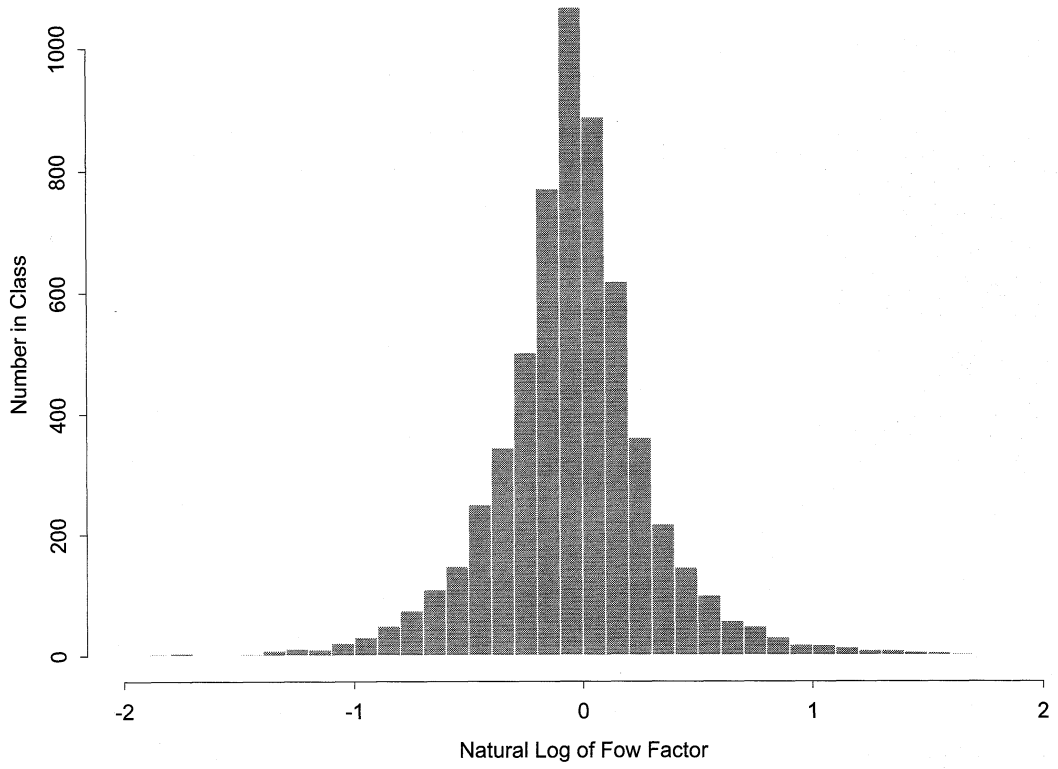


**Figure F-3. $F_{ow}$ histogram (static)**

## Determination of the Flow Diversion Factor $F_{mult}$

The flow diversion factor $F_{mult}$ is defined as the fraction of potentially dripping water that will enter the WP and contribute to the release and transport of radionuclides. Only a fraction of the water intercepting the drifts is expected to come into direct contact with the WPs. Only a portion of the water dripping onto the WPs is expected to get inside where it can interact with the waste form. Factors considered in estimating $F_{mult}$ include

- Flow to WPs is reduced due to diversion of water around the drift by the capillary barrier. This is estimated as a uniform distribution between 0.8 and 1.0. Water flow into the drift will face a capillary barrier if the fractures are small enough. Water can easily move across the capillary break, and can be diverted in the fracture around the drift opening. If the drift were in a homogenous, unsaturated porous medium, there would be a precise relationship between infiltration rate and flow, with a clear diversion around the opening, and perching of water at the crest of the opening [e.g, Phillip and Waechter (1989), Ross (1990)]. However, most of the flow is expected to occur in fractures, and may be largely episodic in nature. Under these conditions, the flow may appear to be more saturated than unsaturated (Birkholzer et al., 1997). Flow in large fractures may occur as unstable fingers

**Table F-1. Dripping parameter correlation matrix**

| Parameter | <*MAI*> | <$K_{sat}$> | $F_{wet}$ | $F_{ow}$ |
|---|---|---|---|---|
| <*MAI*> | 1 | 0 | 0.631 | -0.224 |
| <$K_{sat}$> | — | 1 | -0.623 | 0.13 |
| $F_{wet}$ | — | — | 1 | -0.366 |
| $F_{ow}$ | — | — | — | 1 |

or rivulets on one face or the other (Glass, 1993), which for all intents and purposes is not tractable by mathematical models. The relatively minor importance attached to this factor (0.8 to 1.0 range) reflects the large uncertainties in the phenomena.

- Water may be diverted by flowing down the drift wall. The fraction not diverted down the drift wall is estimated to be uniformly distributed from 0.5 to 0.8. Water flow managing to break the capillary barrier into the drift can drip from the ceiling or from protuberances along the drift. Much of the water, however, is likely to flow as a sheet along the drift walls rather than drip from the ceiling onto the containers. The closer to the crest of the tunnel, the greater the propensity to drip. Away from the crest, the slope of the tunnel walls divert water to sheet flow along the walls. The placement of the canisters affect this factor. Some designs have the canisters aligned with the tunnel centerline, while other designs have the canisters offset from the centerline. The current design has the canister along the center of the placement drifts.

- Some fraction of dripping water will fall directly onto an open WP hole. This factor is assumed to be uniformly distributed with a range of 0.1 to 0.5. Water dripping from the ceiling would have to fall onto the WP in such a way that it could enter an open hole. If the drop were directly in the path of an open hole (e.g., the hole was caused by the corrosion from dripping water), then this condition would be fulfilled. However, the current corrosion model does not require dripping water, and, in fact, such a condition might actually diminish corrosion by lowering the chloride concentration. In the present model, drip impingement has no direct bearing on the location of the corrosion holes, therefore not all drips falling onto the container surface would fall directly into a hole. As more corrosion holes occur, this condition increases the likelihood of a drop falling into a corrosion hole. Otherwise, a large fraction of the water will run off the WP and not enter a hole. As time goes on, more pits form on a WP and the likelihood that water drips on a hole increases (temporal variability for this component of $F_{mult}$).

- Some fraction of drops may be poised to enter a corrosion hole, but may be unable to do so because of the presence of corrosion products. This factor is estimated as a uniformly distributed variable from 0.2 to 0.5. Products from the corrosion of the steel overpack and inner barrier may be flaky, porous, or gel-like. The density of the corrosion products will be considerably less than the steel itself, and, without a high rate of water flux, there will be no mechanism to dislodge them. If this is the case, then water dripping into the corrosion hole will have difficulty entering the canister and will simply flow off. Holes at

the crest will have a higher probability that water will enter because there is a reduced propensity for water to flow off. Holes on the side will have higher probability that the water would flow off rather than enter.

### Combining Factors into $F_{mult}$

The factor, $F_{mult}$, was formulated by sampling each of the above factors and forming their product. The histogram of the resulting factor is shown in figure F-4. The fraction of WPs getting wetted and the average flow per WP are determined from the above procedure for fixed values of infiltration. Water infiltration at the repository horizon is determined by the NFENV module and is time-varying because of changes in climate and thermal reflux. Under conditions of increased infiltration or reflux, it is expected both the wetting fraction and average flow to the WPs will increase. Potential temporal variation in the flow factors is addressed in the next section.

## POTENTIAL TEMPORAL VARIATION IN THE FLOW FACTORS

Each of the three main factors ($F_{ow}$, $F_{mult}$, and $F_{wet}$) that contribute to modification of the amount of water that reaches the WP from the mean deep percolation rate may change over time. Technical support for the flow factors is sparse, with support for the temporal variation in the flow factors non-existent. Therefore, the following discussion is intended to present the possible features that may contribute to temporal variation with implementation deferred (except for one component) from the basecase to sensitivity studies.

### $F_{ow}$ Factor Temporal Variability

The $F_{ow}$ factor is used to account for divergence/convergence away from the surface of the drift. The TPA Version 3.2 code assumed a lognormal distribution from 0.01 to 3.0, developed from Monte Carlo simulations of infiltration. Thermo-mechanical alteration or Thermo-hydrological-chemical (THC) alteration of the host geology would be the most likely factors to cause temporal variability in $F_{ow}$. Changes to the fracture permeability and frequency distributions could result in modification to the amount of convergence/divergence. Because there is a large degree of uncertainty to the assumed endpoints of a distribution and the shape of a distribution, there is no justification to add temporal variability to the $F_{ow}$ factor for the basecase. However, temporal variability to $F_{ow}$ can be tested with sensitivity studies or alternative conceptual models.

### $F_{wet}$ Factor Temporal Variability

$F_{wet}$ is a factor used to represent the fraction of WPs that are dripped on by flowing fractures. It is used to account for the fact that not all fractures (or locations in a fracture) may be flowing. Four main components can potentially influence $F_{wet}$:

- Spatial and temporal variability of deep percolation
- Thermal effects on flow (thermohydrology)
- THC alteration of fractures
- Thermomechanical alteration of fractures

Deep percolation is variable in space and in time. The current NRC model applies a deep percolation rate that is variable in time caused by global climate change. The temporal variability in deep percolation caused

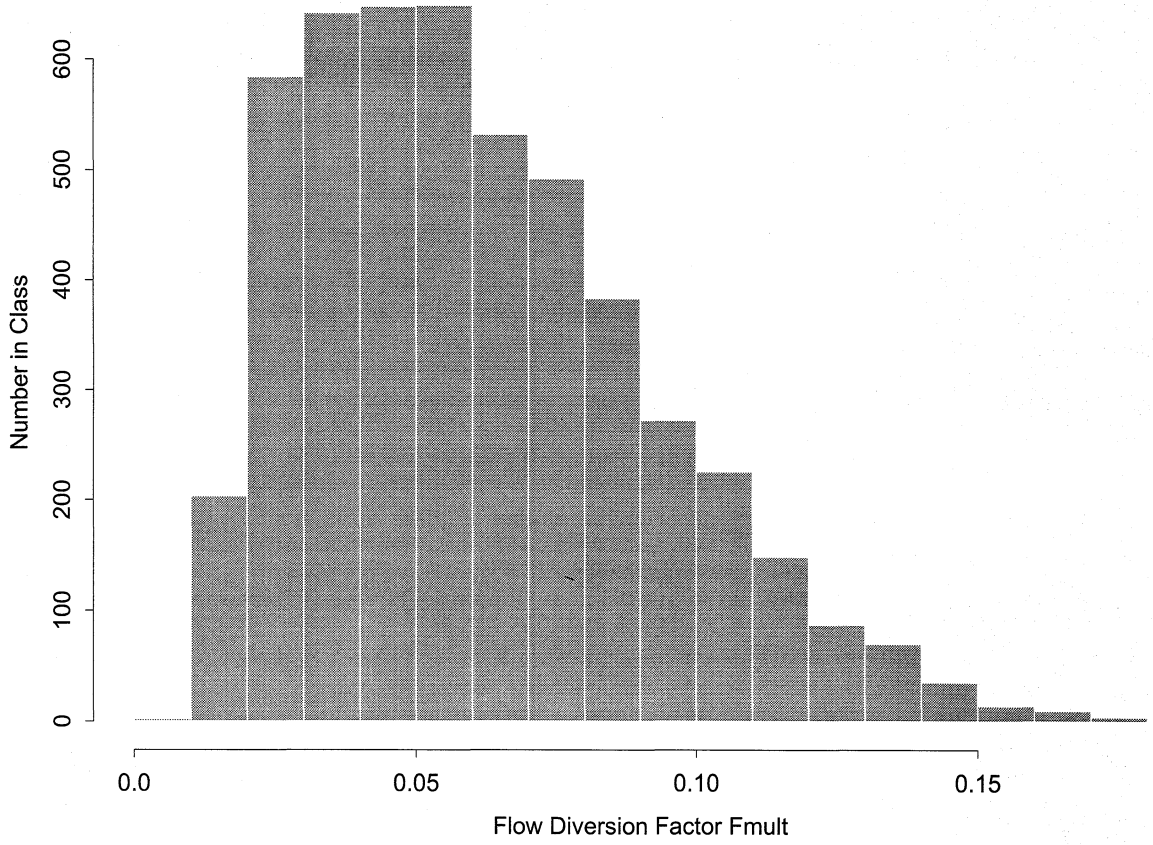


**Figure F-4. $F_{mult}$ histogram (static)**

by the temporal variability in precipitation/infiltration is assumed to be attenuated by the time the moisture reaches the repository horizon. A conservative assumption is to conclude that $F_{wet}$ should increase as the magnitude of deep percolation increases. More water results in more flowing fractures which means a larger fraction of WPs will be dripped on.

Thermohydrology can result in a drastic modification of flow from ambient deep percolation rates in the vicinity of the WPs. During periods of intense thermal reflux following repository dry-out, it is proposed that $F_{wet}$ would increase compared to the ambient values. In some instances, the quantity of reflux may exceed the permeability of the available fracture system which would result in all fractures flowing. A return to ambient hydrology would probably result in a return of $F_{wet}$ to its pre-thermally modified value.

Both THC alteration of fractures and thermomechanical alteration of fractures could influence $F_{wet}$. Because $F_{wet}$ is ultimately tied to the fracture frequency and permeability distributions, modification of these distributions could result in an increase or decrease to $F_{wet}$. The addition or subtraction of fractures due to the aforementioned processes does not necessarily change the number of flowing fractures. The fractures

are, in general, permeable enough to handle much more infiltration than the deep percolation rate. The number of flowing fractures is probably determined by the physics of the UZ flow processes.

Currently, there is no justification to add temporal variability to the $F_{wet}$ factor for the basecase. However, temporal variability to $F_{wet}$ can be tested with sensitivity studies.

## $F_{mult}$ Factor Temporal Variability

$F_{mult}$ is a factor used to represent the fraction of dripping water that will enter a WP. As mentioned earlier, it is composed of four main factors. Each of these factors may experience temporal variability. The expected changes are:

- Capillary diversion: The capillary diversion component could be expected to increase or decrease depending on the amount and distribution of infiltration, thermomechanical alteration of fractures, and THC alteration of fractures.

- Film flow: The magnitude of film flow would be expected to increase as the amount and distribution of infiltration increases. Also, the fraction of water that is diverted due to film flow as infiltration increases would be expected to decrease as a result of increasing gravitational effects (more dripping).

- WP corrosion: The WP corrosion component of $F_{mult}$ would be expected to increase as the WP corrodes. More corrosion should result in more holes and also potentially bigger holes as the package degrades.

- Corrosion products: Corrosion product formation in the holes of a degraded WP would vary over time depending primarily on the near-field geochemical conditions.

For the potential temporal variability in the $F_{mult}$ components, only the increase in the WP corrosion factor with time has a moderate level of confidence. Currently, the TPA code does not internally utilize information from infiltration, near-field geochemistry, or WP corrosion in flow factor derivation. However, the basecase parameter distribution will include the temporal variation in the WP corrosion component of $F_{mult}$. Because the WP failure time is currently independent of the quantity of dripping water, the WP failure time distribution can be simulated for the basecase and then utilized to add temporal variation to the WP corrosion component of $F_{mult}$. The approach taken is to evaluate the fraction of packages failed by corrosion at a given time, then increase the "WP hole" component accordingly. For example, the "WP hole" factor has a range of [0.1, 0.5] and is uniformly distributed in the basecase. If the value of "WP hole" for a given realization is 0.3, at a time when 50 percent of the WPs have failed the "WP hole" component of $F_{mult}$ will have increased to: (Fraction failed) $\times$ (1.0-$F_{mult}$ initial)+$F_{mult}$ initial = (0.5) $\times$ (1.0–0.3)+0.3 = 0.65.

Granted, the packages that have recently failed will have $F_{mult}$ values that are close to 0.3, so it is overly conservative to apply the aforementioned model. The overly conservative model will be relaxed upon development of adequate technical bases. The impact of different conceptual models used to link WP corrosion with $F_{mult}$ will be evaluated in sensitivity studies.

# APPENDIX F REFERENCES


Benjamin, J.R., and C.A. Cornell. *Probability, Statistics, and Decision for Civil Engineers.* New York: McGraw-Hill. 1970.

Birkholzer, J., G. Li, C. Tsang, and T. Tsang. Drifts in unsaturated rock at Yucca Mountain. *FTAM Workshop.* December 15–16. Berkeley, CA: Lawrence Berkeley Laboratories. 1997.

Glass, R.J. Modeling gravity-driven fingering in rough-walled fractures using modified percolation theory. *Proceedings of the 4th Annual International Conference on High-Level Radioactive Waste Management, Las Vegas, Nevada.* La Grange Park, IL: American Nuclear Society: 2,042–2,053. 1993.

Phillip, J.R., and R.T. Waechter. Unsaturated seepage and subterranean holes: Conspectus and the exclusion problem for circular cylindrical cavities. *Water Resources Research* 25: 16–18. 1989.

Ross, B. Quasi-linear analysis of water flow in the unsaturated zone at Yucca Mountain, Nevada USA. *Memories of the 22nd Congress IAH, Vol XXII.* Lausanne, Switzerland: 166–173. 1990.

Wilder, D.G. *Near-Field and Altered Zone Environmental Report.* Volume 2. UCRL 124998. Berkeley, CA: Lawrence Livermore National Laboratory. 1996.

Wilson, M.L., J.H. Gauthier, R.W. Barnard, G.E. Barr, H.A. Dockery, E. Dunn, R.R. Eaton, D.C. Guerin, N. Lu, M.J. Martinez, R. Nilson, C.A. Rautman, T.H. Robey, B. Ross, E.E. Ryder, A.R. Scheneker, S.A. Shannon, L.H. Skinner, W.G. Halsey, J.D. Gansemer, L.C. Lewis, A.D. Lamont, I.R. Triay, A. Meijer, and D.E. Morris. *Total-System Performance Assessment for Yucca Mountain-SNL Second Iteration (TSPA-1993).* SAND93–2675. Volume 1 and 2. Albuquerque, NM: Sandia National Laboratories. 1994.

# APPENDIX G

# APPENDIX G
# AUXILIARY BIOSPHERE INPUT DATA FILES

As described in chapters 11 and 12, the Total-System Performance Assessment (TPA) Version 4.0 code uses GENTPA Version 1.0 to calculate radionuclide exposure rates. GENTPA Version 1.0 uses the following two input files that the user may wish to modify: *ggenii.def* and *gdefault.def*. Although many of the values for parameters included in these files are written directly from *tpa.inp*, the occasion may arise when other parameter values will need to be modified by the user. The *ggenii.def* and *gdefault.def* files are included below in their entirety. For a more detailed description of these files consult Napier et al. (1988).

**File name: *ggenii.def***

```
########################## Program GENII Input File ############  8 Jul 88 ####
Title: tpa4.0 input using genii w/ 93 update and CNWRA 97-009 data files

       \GENII\tpa.in                              Created on 02-10-2000 at 17:35
OPTIONS======================== Default ====================================
T    Near-field scenario?      (Far-field)    NEAR-FIELD: narrowly-focused
F    Population dose?         (Individual)                release, single site
F    Acute release?             (Chronic)     FAR-FIELD:  wide-scale release,
     Maximum Individual data set used                     multiple sites
                                 Complete                                 Complete
TRANSPORT OPTIONS============ Section   EXPOSURE PATHWAY OPTIONS===== Section
F  Air Transport                   1     F  Finite plume, external       5
F  Surface Water Transport         2     T  Infinite plume, external     5
F  Biotic Transport (near-field)  3,4    T  Ground, external              5
F  Waste Form Degradation (near)  3,4    F  Recreation, external          5
                                         T  Inhalation uptake            5,6
REPORT OPTIONS======================     T  Drinking water ingestion     7,8
T  Report AEDE only                      F  Aquatic foods ingestion      7,8
T  Report by radionuclide                T  Terrestrial foods ingestion  7,9
T  Report by exposure pathway            T  Animal product ingestion     7,10
F  Debug report on screen                T  Inadvertent soil ingestion

INVENTORY ##########################################################################

 3   Inventory input activity units: (1-pCi  2-uCi  3-mCi  4-Ci  5-Bq)
 0   Surface soil source units (1- m2  2- m3  3- kg)
     Equilibrium question goes here

     --------|----Release Terms------|----------Basic Concentrations---------|
     Use when|  transport selected    |  near-field scenario, optionally      |
     --------|------------------------|---------------------------------------|
     Release |         Surface Buried |         Surface Deep    Ground  Surface|
     Radio-  |Air      Water   Waste  |Air      Soil    Soil    Water   Water  |
     nuclide |/yr      /yr     /m3    |/m3      /unit   /m3     /L      /L     |
     --------|------- ------- -------|------- ------- ------- ------- -------|
     C 14                                                    1.0E+00
     CL36                                                    1.0E+00
     NI59                                                    1.0E+00
     NI63                                                    1.0E+00
     SE79                                                    1.0E+00
     SR90                                                    1.0E+00
     ZR93                                                    1.0E+00
```

| | |
|---|---|
| NB94 | 1.0E+00 |
| MO93 | 1.0E+00 |
| TC99 | 1.0E+00 |
| PD107 | 1.0E+00 |
| AG108M | 1.0E+00 |
| SN121M | 1.0E+00 |
| SN126 | 1.0E+00 |
| I 129 | 1.0E+00 |
| CS135 | 1.0E+00 |
| CS137 | 1.0E+00 |
| SM151 | 1.0E+00 |
| PB210 | 1.0E+00 |
| RA226 | 1.0E+00 |
| AC227 | 1.0E+00 |
| TH229 | 1.0E+00 |
| TH230 | 1.0E+00 |
| PA231 | 1.0E+00 |
| U 232 | 1.0E+00 |
| U 233 | 1.0E+00 |
| U 234 | 1.0E+00 |
| U 235 | 1.0E+00 |
| U 236 | 1.0E+00 |
| U 238 | 1.0E+00 |
| NP237 | 1.0E+00 |
| PU238 | 1.0E+00 |
| PU239 | 1.0E+00 |
| PU240 | 1.0E+00 |
| PU241 | 1.0E+00 |
| PU242 | 1.0E+00 |
| AM241 | 1.0E+00 |
| AM242M | 1.0E+00 |
| AM243 | 1.0E+00 |
| CM243 | 1.0E+00 |
| CM244 | 1.0E+00 |
| CM245 | 1.0E+00 |
| CM246 | 1.0E+00 |

| Use when | ----Derived Concentrations----- measured values are known | | | |
|---|---|---|---|---|
| Release Radio-nuclide | Terres. Plant /kg | Animal Product /kg | Drink Water /L | Aquatic Food /kg |

TIME ##########################################################################

1 Intake ends after (yr)
50 Dose calc. ends after (yr)
0 Release ends after (yr)
0 No. of years of air deposition prior to the intake period
0 No. of years of irrigation water deposition prior to the intake period

FAR-FIELD SCENARIOS (IF POPULATION DOSE) ####################################

0 Definition option: 1-Use population grid in file POP.IN
0 2-Use total entered on this line

```
NEAR-FIELD SCENARIOS ###########################################################

            Prior to the beginning of the intake period: (yr)
0             When was the inventory disposed?  (Package degradation starts)
0             When was LOIC?  (Biotic transport starts)
1.0         Fraction of roots in upper soil (top 15 cm)
0           Fraction of roots in deep soil
0.0         Manual redistribution: deep soil/surface soil dilution factor
0           Source area for external dose modification factor (m2)
TRANSPORT ######################################################################
            ====AIR TRANSPORT=====================================SECTION 1=====
                    0-Calculate PM              |0        Release type (0-3)
 1          Option: 1-Use chi/Q or PM value     |F        Stack release (T/F)
                    2-Select MI dist & dir      |0        Stack height (m)
                    3-Specify MI dist & dir     |0        Stack flow (m3/sec)
0           Chi/Q or PM value                   |0        Stack radius (m)
0           MI sector index (1=S)               |0        Effluent temp. (C)
0           MI distance from release point (m)  |0        Building x-section (m2)
T           Use jf data, (T/F) else chi/Q grid  |0        Building height (m)

            ====SURFACE WATER TRANSPORT==========================SECTION 2=====
0           Mixing ratio model: 0-use value, 1-river, 2-lake
0           Mixing ratio, dimensionless
0           Average river flow rate for: MIXFLG=0 (m3/s), MIXFLG=1,2 (m/s),
0           Transit time to irrigation withdrawal location (hr)
            If mixing ratio model > 0:
0             Rate of effluent discharge to receiving water body (m3/s)
0             Longshore distance from release point to usage location (m)
0             Offshore distance to the water intake (m)
0             Average water depth in surface water body (m)
0             Average river width (m), MIXFLG=1 only
0             Depth of effluent discharge point to surface water (m), lake only

            ====WASTE FORM AVAILABILITY==========================SECTION 3=====
0           Waste form/package half life, (yr)
0           Waste thickness, (m)
0           Depth of soil overburden, m

            ====BIOTIC TRANSPORT OF BURIED SOURCE================SECTION 4=====
T           Consider during inventory decay/buildup period (T/F)?
T           Consider during intake period (T/F)?    | 1-Arid non agricultural
0          Pre-Intake site condition.............| 2-Humid non agricultural
                                                  | 3-Agricultural

EXPOSURE #######################################################################

            ====EXTERNAL EXPOSURE================================SECTION 5=====
            Exposure time:                |   Residential irrigation:
3384.0        Plume (hr)                  | T       Consider: (T/F)
1800.0        Soil contamination (hr)     | 1       Source: 1-ground water
0             Swimming (hr)               |                 2-surface water
0             Boating (hr)                | 58.0    Application rate (in/yr)
0             Shoreline activities (hr)   | 9.0     Duration (mo/yr)
0           Shoreline type: (1-river, 2-lake, 3-ocean, 4-tidal basin)
0           Transit time for release to reach aquatic recreation (hr)
0           Average fraction of time submersed in acute cloud (hr/person hr)

            ====INHALATION=======================================SECTION 6=====
```

```
4200.0      Hours of exposure to contamination per year
1           0-No resus-  1-Use Mass Loading          2-Use Anspaugh model
.0001         pension      Mass loading factor (g/m3)   Top soil available (cm)

            ====INGESTION POPULATION============================SECTION 7=====
0           Atmospheric production definition (select option):
2             0-Use food-weighted chi/Q, (food-sec/m3), enter value on this line
              1-Use population-weighted chi/Q
              2-Use uniform production
              3-Use chi/Q and production grids (PRODUCTION will be overridden)
0           Population ingesting aquatic foods, 0 defaults to total (person)
0           Population ingesting drinking water, 0 defaults to total (person)
F           Consider dose from food exported out of region (default=F)

            Note below: S* or Source: 0-none, 1-ground water, 2-surface water
                                      3-Derived concentration entered above
            ==== AQUATIC FOODS / DRINKING WATER INGESTION=========SECTION 8====

F           Salt water? (default is fresh)
```

| USE ? T/F | FOOD TYPE | TRANSIT hr | PRODUCTION kg/yr | CONSUMPTION HOLDUP da | CONSUMPTION RATE kg/yr | DRINKING WATER |
|---|---|---|---|---|---|---|
| F | FISH | 0.00 | 0.0E+00 | 0.00 | 0.0 | 1 Source (see above) |
| F | MOLLUS | 0.00 | 0.0E+00 | 0.00 | 0.0 | F Treatment? T/F |
| F | CRUSTA | 0.00 | 0.0E+00 | 0.00 | 0.0 | 0.0 Holdup/transit(da) |
| F | PLANTS | 0.00 | 0.0E+00 | 0.00 | 0.0 | 730.0 Consumption (L/yr) |

```
            ====TERRESTRIAL FOOD INGESTION=======================SECTION 9=====
```

| USE ? T/F | FOOD TYPE | GROW TIME da | S * | IRRIGATION RATE in/yr | IRRIGATION TIME mo/yr | YIELD kg/m2 | PRODUCTION kg/yr | CONSUMPTION HOLDUP da | CONSUMPTION RATE kg/yr |
|---|---|---|---|---|---|---|---|---|---|
| T | LEAF V | 80.00 | 1 | 60.0 | 3.0 | 2.0 | 0.0E+00 | 1.0 | 6.0 |
| T | ROOT V | 85.00 | 1 | 60.0 | 5.0 | 4.0 | 0.0E+00 | 14.0 | 26.0 |
| T | FRUIT | 80.00 | 1 | 60.0 | 2.5 | 3.0 | 0.0E+00 | 14.0 | 23.0 |
| T | GRAIN | 75.00 | 1 | 60.0 | 5.0 | 0.54 | 0.0E+00 | 14.0 | 34.0 |

```
            ====ANIMAL PRODUCTION CONSUMPTION===================SECTION 10====
```

| USE ? T/F | FOOD TYPE | HUMAN CONSUMPTION RATE kg/yr | HUMAN HOLDUP da | TOTAL PRODUCTION kg/yr | DRINK WATER CONTAM FRACT. | STORED FEED DIET FRACTION | STORED FEED GROW TIME da | STORED FEED IRRIGATION S * | STORED FEED IRRIGATION RATE in/yr | STORED FEED IRRIGATION TIME mo/yr | STORED FEED YIELD kg/m3 | STORED FEED STORAGE da |
|---|---|---|---|---|---|---|---|---|---|---|---|---|
| T | BEEF | 29.5 | 20.0 | 29.50 | 1.00 | 0.00 | 30.0 | 1 | 60.0 | 5.50 | 1.23 | 20.0 |
| T | POULTR | 0.0 | 20.0 | 0.00 | 1.00 | 1.00 | 75.0 | 1 | 60.0 | 5.00 | 0.54 | 14.0 |
| T | MILK | 100.0 | 1.0 | 100.00 | 1.00 | 0.00 | 30.0 | 1 | 60.0 | 5.50 | 1.23 | 20.0 |
| T | EGG | 3.0 | 1.0 | 3.00 | 1.00 | 1.00 | 75.0 | 1 | 60.0 | 5.00 | 0.54 | 14.0 |
| | | | | | | FRESH FORAGE | | | | | | |
| | BEEF | | | | | 0.56 | 46.0 | 1 | 60.0 | 5.50 | 1.23 | 1.0 |
| | MILK | | | | | 0.56 | 46.0 | 1 | 60.0 | 5.50 | 1.23 | 1.0 |

```
##########################################################################
```

**File name:** ***gdefault.def***

```
GENII Default Parameter Values for Current YM Biosphere (16-Jul-97 PAL)

INVENTORY PARAMETERS-----------------------------------------------------------
0.037, 3.7E4, 3.7E7, 3.7E10, 1.0          NVU     Source input conversion
1.0, 0.15, 224.0                          SVU     Soil source conversion
ENVIRONMENTAL PARAMETERS-------------------------------------------------------
0.008                                     ABSHUM  Absolute humidity (kg/m3)
2                                         PRCNTI  Air dispersion conserv. flag
0.001                                     DPVRES  Deposition vel./resuspension
4.4E-10                                   LEAFRS  Leaf resuspension factor
2.0,2.0,3.0,0.8,0.8,0.8,1.0,0.8,1.0,1.5   BIOMAS  BIOMA2 Biomass (kg/m2)
0.4                                       DEPFR2  Interception frac./irrigate
15.0                                      SURCM   Depth of surface soil (cm)
225.0                                     SLDN    Surface soil density (kg/m2)
1.5E3                                     SSLDN   Soil density (kg/m3)
True                                      HARVST  Harvest removal considered?
50.0                                      SOLING  Soil ingested (mg/da)
14.0                                      WTIM    Weathering time (da)
1.0, 0.1, 0.1, 0.1                        TRANS   Translocation, plants
0.1, 0.1, 0.1, 0.1, 1.0, 1.0              TRANSA  Translocation, animal food
33.0, 0.08, 73.0, 0.11, 33.0, 73.0        CONSUM  Animal Consumption (kg/da)
60.0, 0.3, 100., 0.3                      DWATER  Animal drinking water (L/da)
0.0, 0.8, 1.0, 0.8                        FRACUT  Acute fresh forage by season
0.2, 0.3, 0.5, 1.0                        SHORWI  Shore width factors
0.02                                      INGWAT  Swim water ingested (L/hr)
25295.0                                   TCWS    H2O/sed. transfer (L/m2/yr)
0.4,  5.0, 4.0                            YELDBT  BIOT: Veg. prod. (kg/m2/yr)
9.41E-4, 2*7.48E-4                        TOTEXC  BIOT: Excavation (m2/m3-yr)
1.0, 0.81, 0.19, 0.02, 0.008, 0.002,      EXCAV   BIOT: Frac. soil brought to
1.0, 0.9, 0.096, 0.006, 0.0005, 0.0005,           surface from within the
1.0, 0.9, 0.096, 0.006, 0.0005, 0.0005            waste by animal excavation
270.0                                     RINH    Chronic breathing (cm3/sec)
330.0                                     RINHA   Acute breathing (cm3/sec)
10                                        NDIST   Number of distances
805.0, 2414.0, 4023.0, 5632.0, 7241.0,
12068.0, 24135.0, 40255.0, 56315.0,
72405.0                                   X       JF/chi/Q/pop grid dist. (m)
0.2,0.25,0.18,0.91,3*0.22,0.91,2*0.22     DRYFAC, DRYFA2 dry/wet ratio

METABOLIC PARAMETERS-----------------------------------------------------------
0.5, 50.0, 500.0                                  XDIV
0.5,  0.5,  0.95, 0.05,  0.8, 0.0, 0.0,   0.2, 0.0,     ADJ
0.1,  0.9,  0.5,  0.5,  0.15, 0.4, 0.4,  0.05, 0.0,
0.01, 0.99, 0.01, 0.99, 0.05, 0.4, 0.4, 0.135, 0.015

DOSE PARAMETERS----------------------------------------------------------------
0.25, 0.15, 0.12, 0.12, 0.03, 0.03, 5*0.06        WT   Weighting factors
2.0                                               SI2I Semi-infinite/inf
================================================================================
```

# APPENDIX G
# REFERENCES

Napier, B.A., R.A. Peloquin, D.L. Strenge, and J.V. Ramsdell. *GENII: The Hanford Environmental Radiation Dosimetry Software System. Volumes 1, 2, and 3: Conceptual Representation, User's Manual, Code Maintenance Manual.* PNL–6584. Richland, WA: Pacific Northwest Laboratory. 1988.

# APPENDIX H

# APPENDIX H
# INFILTRATION TABULATOR FOR YUCCA MOUNTAIN PREPROCESSOR DESCRIPTION

The Infiltration Tabulator for Yucca Mountain (ITYM) preprocessor calculates the net amount of water infiltrating from the ground surface into the unsaturated zone (UZ) above the repository. Water that has infiltrated the subsurface affects the repository near-field environment and is available for waste package (WP) corrosion, dissolution of material in the WP, and transport of material released from WPs. Specifically, ITYM determines the spatial variation of percolation water flux below the rooting zone for a set of climatic states. The resulting information is used by the UZFLOW module in the total-system performance assessment (TPA) Version 4.0 code to estimate the temporal and spatial variation of deep percolation at the repository horizon in the absence of thermal effects. Additional information on modeling of climate change and its effect on percolation flux can be found in Stothoff et al. (1997) and Stothoff (1999).

## INFORMATION FLOW WITHIN INFILTRATION TABULATOR FOR YUCCA MOUNTAIN

### Information Supplied to Infiltration Tabulator for Yucca Mountain

Input provided to the ITYM module consists of detailed information on ground surface elevation, soil thickness, and soil and bedrock classification (provided via external files), and parameters that specify the uncertainty and variability of hydraulic and climatic properties (provided in *itym.dat*). Ground surface elevation is supplied as a digital elevation model (DEM) in the static file entitled *elevdem.dat*. A DEM with the same discretization, *soildem.dat*, provides soil thicknesses. Similarly, soil, bedrock, and wind speed classifications are provided in DEMs called *sunitdem.dat*, *bunitdem.dat*, and *winddem.dat*, respectively. A table is also provided of mean annual shortwave radiation as a function ground orientation called *maswtab.dat*. All other input parameters to ITYM are in *itym.dat*.

### Information Provided by Infiltration Tabulator for Yucca Mountain

ITYM creates a table of DEMs describing expected mean annual infiltration (*MAI*) for various climatic states. This table is used by the UZFLOW module to estimate a time history of *MAI* given a time history of mean annual precipitation (*MAP*) and mean annual temperature (*MAT*). Although the standard deviation may readily be calculated along with the expected mean of *MAI*, this version of ITYM does not pass the standard deviation along to the UZFLOW module. Future versions can incorporate the standard deviation within the UZFLOW module to be used as part of the TPA stochastic sampling scheme as a means of directly assessing uncertainty of changes to hydraulic properties resulting from climate change.

## CONCEPTUAL MODEL

Figure 4-1 illustrates the shallow infiltration conceptual model, including water and energy balances for a system of shallow surficial soil above a fractured impermeable bedrock. Water and heat enter and exit the soil at the ground surface. A portion of the water that infiltrates during and after precipitation, which does not evaporate, moves into the deep subsurface (below the root zone) via fracture flow. Thus, water escaping evaporation becomes deep percolation. Offline simulations of shallow infiltration using this conceptual

model were performed for a simulated time period of at least a decade using hourly time steps (Stothoff et al., 1997; Stothoff, 1999). The simulations were performed using the BREATH code (Stothoff, 1995), a one-dimensional (1D) finite-volume simulator that considers liquid, vapor, and energy transport in unsaturated media. Using the results from approximately 500 bare-soil simulations, the resulting time-varying infiltration is abstracted into relationships between *MAI*, decade-average climate (i.e., *MAP* and *MAT*), and soil and bedrock hydraulic properties (Stothoff, 1999). Thus, *MAI* can be estimated at a local scale given the hydraulic and climatic inputs. Note, however, that the abstractions do not account for lateral flow or transpiration.

The surface above the repository is rugged, with variable bedrock properties and soil cover. To estimate the spatial distribution of *MAI* the footprint is divided into numerous small grid blocks, each with potentially different elevation, slope, soil cover, climatic inputs, soil properties, and bedrock composition. With all of the information required for the abstracted 1D relationships available for each grid block, the relationships may be used to estimate *MAI* for each of the grid blocks.

Unfortunately, none of the input values are certain for any grid block, and the climatic parameters vary in time as well. To make matters worse, *MAI* responds exponentially to changes in input parameters, so that the expected value of *MAI* is underestimated using the expected value for each parameter. In order to estimate the expected value of *MAI* for each grid block, it is necessary to account for the variability in each input parameter (e.g., through Monte-Carlo analysis).

Monte Carlo analysis requires that the statistical properties of the input parameters are known. None of the input-parameter statistical properties are known with certainty at the Yucca Mountain (YM) site; however, the uncertainty in the properties can be estimated and formally accounted for in the Monte-Carlo analysis in a three-step process. In the first step, the statistical properties describing variability are sampled. In the second step, the sampled statistical properties are used to generate realizations of the input properties for each grid block, which are in turn used to estimate *MAI* for the grid block. In the third step, the set of *MAI* realizations is used to estimate expected *MAI* for each grid block.

**Bare-Soil Infiltration Abstractions**

Several abstraction equations have been developed describing the response of *MAI* to climatic and hydraulic input parameters. All of these equations are based on 1D simulation results using a 10-yr record of hourly meteorological observations at Desert Rock, Nevada. Each of the simulations repeated the record until predicted *MAI* for the decade reached a cyclic steady state. The different simulations resulted from different combinations of hydraulic properties and modifications to the climatic record.

The abstraction used in TPA3 is based on simulations describing shallow soil above an unfilled fracture. It is assumed that the bedrock and any fractures with fillings can be neglected. The TPA Version 3.2 code abstraction is extremely sensitive to soil thickness.

For the TPA Version 4.0 code two additional abstractions have been developed (Stothoff, 1999), describing *MAI* for shallow soil above a capillary barrier or attractor, respectively. A capillary barrier results when the overlying soil is finer than the underlying medium, resulting in a resistance for water to enter the underlying medium until a threshold pressure is achieved. An unfilled fracture presents a capillary barrier to an overlying soil. A capillary attractor is the opposite case, where the finer material underlies the soil and preferentially draws water from the soil. The underlying medium in the capillary attractor typically has a smaller saturated hydraulic conductivity than the overlying medium, but may be more conductive for

unsaturated conditions. Bedrock and carbonate-filled fractures represent capillary attractors to overlying soil.

Several options are available for estimating bare-soil *MAI* using the abstractions. One option is to use exclusively the abstraction which neglect the contributions of filled fractures and bedrock to *MAI*. The remaining options all independently evaluate contributions to *MAI* via several pathways (bedrock as well as unfilled, soil-filled, and carbonate-filled fractures) within each grid cell. Two options are given in the ITYM preprocessor input file. One option is to add contributions from all pathways to estimate *MAI*; in another, only the pathway with the largest contribution is used. Due to capillary effects, the various pathways compete to some extent and the actual values of *MAI* may be intermediate between the two extremes.

**Modifications to Infiltration Due to Vegetation**

All of the abstractions developed using simulations are based on bare-soil conditions (no vegetation). Transpiration is known to play a significant role in the hydrologic balance, although bare-soil evaporation alone is quite effective at limiting *MAI* under present-day semiarid climatic conditions. Neglect of transpiration is likely to result in increasingly significant overestimation of *MAI* as the climate becomes cooler and wetter.

A simple heuristic model is available to account for the effect of vegetation in limiting bare-soil *MAI*. The model recognizes that vegetation is extremely efficient at limiting *MAI* in the alluvial valleys, scavenging essentially all of the moisture that would otherwise percolate below the root zone. However, bedrock provides a significant barrier to the scavenging process when the soils are shallow, as is typical above the repository footprint. The heuristic model assumes that bedrock completely blocks plant uptake with no soil present, while vegetation becomes increasingly effective at scavenging as the soil thicknesses increase. With soil thicknesses greater than a threshold value, the maximal scavenge efficiency is reached. The threshold value and the scavenge efficiency are both considered functions of climate, with a deeper threshold and smaller scavenge efficiency under wetter and cooler conditions.

Noting that the root-mass distribution of a plant in deep soil tends to be approximately exponentially decreasing with depth, the simple model used for plant scavenging of water is

$$f_{scav} = E_0 + [1 - \exp(-\alpha B)](E_1 - E_0) \tag{H-1}$$

where $f_{scav}$ is the fraction of *MAI* scavenged, $B$ is the soil moisture capacity, $\alpha$ is an uptake decay factor with soil moisture capacity, and $E_0$ and $E_1$ are the efficiencies with zero and infinite soil capacity. The efficiencies and uptake decay factors are dependent on the vegetation type and density, which in turn is dependent on the climate. The three parameters are assumed to be of the form

$$\begin{aligned} E_0(MAI) &= E_{00} + G_0 \log_{10}(MAI) \\ E_1(MAI) &= E_{10} + G_1 \log_{10}(MAI) \\ \alpha(MAI) &= \alpha_{10} + G_\alpha \log_{10}(MAI) \end{aligned} \tag{H-2}$$

For calculation of present-day infiltration, the parameters could be set so that simulated *MAI* matches current estimates based on other approaches. The parameters are consider uncertain in ITYM, thus are sampled.

**Accounting for Uncertainty**

All of the inputs required to estimate *MAI* are uncertain and are usually spatially or temporally variable. Often an input parameter is correlated to one or more other inputs. In order to account for variability in correlated parameters, the following expression is used

$$u = C\,\varepsilon \tag{H-3}$$

where $u$ is the vector of normalized variates [$u_i=(x_i-\mu/\sigma]$, $x_i$ is a normally distributed variable with mean $\mu$ and standard deviation $\sigma$, $C$ is the correlation matrix, and $\varepsilon$ is normally distributed [$N(0,1)$] noise. This matrix form is the lag-0 simplification of a lag-0/lag-1 expression by Matalas (1967). The actual realization of $x_i$ is directly calculated from $\mu_i$ for normally distributed variables. For lognormally distributed variables, $x_i$ is transformed after sampling. Only normally and lognormally distributed variables are considered in ITYM.

The statistical parameters describing the individual distributions (i.e., $\mu$, $\sigma$, $C$) are themselves uncertain. Assuming that the uncertainty in each parameter is uncorrelated to the uncertainty in all other parameters, the uncertainty in each statistical parameter is expressed as a normal distribution in ITYM.

Some of the sampled parameters are bounded due to physical or mathematical considerations. Limits are provided for all parameters, although the limits can be arbitrarily unlikely for unbounded parameters. If a realization of a sampled parameter falls out of the allowed range, it is discarded and resampled.

## ASSUMPTIONS AND CONSERVATISM OF THE INFILTRATION TABULATOR FOR YUCCA MOUNTAIN APPROACH

The ITYM preprocessor is an abstraction of the processes controlling mean annual infiltration and redistribution of infiltrating waters above the repository horizon. The main processes that control infiltration are (i) climatic conditions and (ii) near-surface processes such as evapotranspiration and runoff that are affected by soil and bedrock properties.

Estimates of infiltration are sensitive to a number of processes affecting near-surface conditions, such as temperature, precipitation, soil depth, evaporation, incident solar radiation, plant transpiration, and surface water runoff. Results of detailed 1D simulations of mass and energy fluxes under a range of conditions representative of the surface of YM were used to develop abstracted, predictive equations for *MAI* as a function of climate, soil depth, and hydraulic properties. The detailed model simulations do not account for plant transpiration or lateral redistribution. Plant transpiration is heuristically accommodated by modifying the abstracted values of *MAI*. Lateral redistribution is not considered. Lateral redistribution would tend to reduce estimates of *MAI* along ridgetops and increase estimates of *MAI* at the base of slopes and in channels. Under present-day conditions, total channel infiltration is expected to be small relative to areal-average distributed infiltration (Woolhiser et al., 1999) at the scale of a repository subarea. Although

redistribution of water downslope will change the spatial distribution of *MAI*, it is uncertain whether this would result in a net increase or net decrease in *MAI* across the repository footprint.

Over glacial cycles, climatic change induces changes in soil thickness and composition as weathering, dust deposition, and erosion responds to the climatic influences. The fillings in the bedrock fractures may also respond to climatic influences. Such changes are not considered in ITYM, nor are any changes in the near-surface conditions induced by the thermal pulse due to repository heating.

There are specific assumptions related to the ITYM preprocessor:

- Infiltration is assumed to be directly related to climatic influences, increasing as precipitation increases and temperature decreases. The linkage between climate and infiltration is calculated assuming that infiltration occurs under bare-soil conditions. The values of infiltration can then be adjusted by a heuristic formula that accounts for the scavenging of soil moisture by vegetation.

- For the computation of shallow infiltration, it is assumed that hydrologic properties and soil thickness will not change during the simulation.

- It is assumed that *MAT* decreases linearly with increasing elevation, while both *MAP* and atmospheric vapor density vary exponentially with elevation and the gradients remain the same over time.

## INPUT FILES FOR INFILTRATION TABULATOR YUCCA MOUNTAIN PREPROCESSOR

### Infiltration Tabulator Yucca Mountain Input

Input into the ITYM code is conceptually broken into several sections: (i) control, (ii) sampling, (iii) merging porous media into composite continua, (iv) input of distributed parameters [Digital Elevation Models (DEMs)], and (v) input of tabulated parameters. The input structure for ITYM is described by these sections.

### Input Conventions

Input is driven by keywords, which may stand alone or may have additional parameters associated with them. Associated parameters can be located on the same line or the next line(s). Keywords that control the size of the *maidtbl.dat* file as listed in table H-1 are found at the top of the *itym.dat* input file. Typically, no other records in *itym.dat* should be changed by routine users.

Comment lines are denoted by a number sign ("#"). Anything on a line after this symbol is ignored. Blank lines in the input file are also ignored. Multiple entries on a record are separated by a tab. Up to 120 characters can be on an input-file line; numbers or characters beyond that point are ignored.

**Table H-1. Control parameters used to define an infiltration tabulator Yucca Mountain run**

| Keyword | Type | Restrictions | Description |
|---|---|---|---|
| Table Size | | | |
| num_*MAP*_table | integer | >0 | Number of table entries for *MAP* |
| num_*MAT*_table | integer | >0 | Number of table entries for *MAT* |
| num_pixel_merge | integer | >0 | Number of DEM pixels on a side to merge for table output; for example, if 1, the table is output using the raw pixels, while, if 2, the output pixels have four times the area |
| num_realize_per_table | integer | >0 | Number of realizations to use when calculating a table entry |
| Reference Values | | | |
| *MAP*_min[mm/yr] | mm/yr | >0 | Minimum value of *MAP* to use in table output |
| *MAP*_max[mm/yr] | mm/yr | >0 | Maximum value of *MAP* to use in table output |
| *MAT*_min[degreeC] | C | real | Minimum value of *MAT* to use in table output |
| *MAT*_max[degreeC] | C | real | Maximum value of *MAT* to use in table output |
| base_elev[km] | km | >0 | Minimum value of *MAP* to use in table output |
| zDTBLout | char | name of file | Output file for DEM table |
| Options | | | |
| RegrForm | char | TPA3 | Use regression equations developed for TPA3 (one bare-soil/unfilled bedrock fracture pathway with specified soil/bedrock/climate inputs) |
| PathwaySum | | TPA4 | Use regression equations developed for TPA4 (multiple bedrock pathways with site-specific properties) |
| | char | MaxOnly | Use bedrock scenario with maximum infiltration |
| | | All | Use composite of four bedrock pathways/scenarios |

**Control Parameters**

Control parameters are used to specify characteristics of the output table, the names of associated data files, and reference values. Each keyword is *itym.inp* has one associated parameter. The keyword/parameter descriptions are shown in table H-1.

**Differences Between the TPA Code Versions 3.2 and 4.0**

In the TPA Version 3.2 code, the values of all hydrologic and most climatic variables are assumed known and are hard-coded into the simulator. In the TPA Version 4.0 code approach, each hydrologic and climatic variable is uncertain and variable, thus is sampled numerous times. Obviously the data requirements are far greater in the latter case. The keyword for choosing the TPA code Version 3.2 or Version 4.0 option is *Regrform* (table H-1).

When reproducing the values used in the TPA Version 3.2 code case, only a restricted input file and a few of the external files are used. Commands and external files used to reproduce the Version 3.2 results are indicated in the tables below. Note that all commands and external files specified in the *itym.inp* input file are read, but values not necessary for generating the Version 3.2 results are ignored.

When working with the expanded Version 4.0 case, the entire command and file structure is used. Note that the default is to use the Version 3.2 case.

**External Files**

Several parameters are inherently variable across the site and cannot be easily specified through linear relationships. These parameters are typically entered as DEM files, all registered to the same grid. Other information is most conveniently defined as tabular inputs. Keywords defining the file names containing these DEM coverages and tabular inputs are presented in table H-2.

The DEM describing the ground surface elevation is typically the starting point for analysis. This not only provides the grid for analysis, but is used to directly or indirectly specify the spatial distribution of all climatic inputs. External routines can also use the surface elevation to estimate soil thickness and the distribution of mean annual windspeed (MAW).

The distribution of soil thickness at YM is not easily specified, as there is no measurement technique that readily measures soil thickness for the rugged YM conditions. The soil thickness distribution used by the U.S. Department of Energy (DOE) is estimated according to position on the terrain. An alternative approach is to use a mass-balance calculation on the landscape defined by the DEM, accounting for processes such as dust deposition, weathering, erosion, and creep. The soil-thickness file provided with the code was estimated in this way.

The wind speed distribution is also not easily measured, although information is available from a series of meteorological stations. The wind speed file provided with the code was estimated by using the meteorological-station data and an indicator variable specifying how strongly a particular pixel is considered a wash or an open area. The washes are protected from the wind observed on Yucca Crest and alluvial basins, thus reducing MAW in the washes. The indicator variable accounts for local ground surface curvature and orientation. The washes are oriented predominantly east-west, thus steep north-south slopes are indicators that the pixel is in a wash.

**Table H-2. Commands defining external files used to define spatially distributed parameters and tabular information. Commands used to specify files used in the TPA Version 3.2 code runs are denoted with an asterisk.**

| Keyword | File Name | Data Type | Description |
|---|---|---|---|
| zElevDEM* | elevdem.dat | real | Ground surface elevation [m] DEM |
| zWindDEM | winddem.dat | real | Wind speed [m/s] DEM |
| zSoilDEM* | soildem.dat | real | Soil thickness [m] DEM |
| zBUnitDEM | bunitdem.dat | integer | Bedrock unit classification DEM |
| zSUnitDEM | sunitdem.dat | integer | Soil unit classification DEM |
| zMASWtbl | maswtab.dat | real | Table of mean-annual clear-sky shortwave radiation [$W/m^2$] as a function of ground rotation |

Bedrock and soil units have been mapped by the DOE (Day et al., 1998). The coverages of these units are available; external routines map each coverage to the individual grid blocks in the DEM.

The table of mean annual clear-sky shortwave radiation is used to estimate actual shortwave radiation incident on the ground surface. An external routine calculates the clear-sky shortwave radiation for each 15 minutes of the year to average over the year. As this calculation is extensive, it is performed for various ground orientations and tabulated rather than performed for each pixel.

The tabulated fraction of exposed sky as a function of ground rotation is used to estimate incoming longwave radiation. Longwave radiation originates primarily from cloud cover and from adjacent ground surfaces. Incident longwave radiation on horizontal surfaces is assumed to originate from the sky; on sloping surfaces it is assumed that there is a symmetric slope nearby that provides a component of longwave radiation independent of cloud cover. Wash topography is not considered in any greater detail.

**External DEM Files**

Each file representing a DEM has the same format. First is a set of header commands to define the grid, then a string of values that specify the entries in the DEM. The DEM values must be provided row by row in the order that a picture would be drawn on a screen. In other words, the values must start in the top left (NW) corner and proceed to the top right (NE) corner, move to the next row lower and proceed from west to east, and so forth, ending in the bottom right (SE) corner. Typically the values are provided as one long column of numbers, although this is not necessary. Each grid cell is a square, with all grid cells having identical sizes. All DEM files must use the same DEM grid.

**External Table Files**

External table files provide a table defining a function in terms of two variables. External table files are similar in concept to the DEM files, although the commands are somewhat different. Each row has a uniform grid, as does each column. As the variables defining the rows and columns are different, different increments are defined for the row and column variables. As with the DEM files, the values are entered

row-wise starting in the top left corner. There must be NROW times NCOL values following the header commands, and comments and blank lines are handled just like in the command file.

The table file describing a function of ground surface rotation uses east-west rotation (degrees from horizontal) as the row-wise interpolating variable. Similarly, north-south rotation (degrees from horizontal) is the column-wise interpolating variable.

**Sampling Control**

Sampling of uncertain and variable parameters is controlled using uncertainty tables. An uncertainty table collects related (i.e., possibly correlated) variables, and samples these variables simultaneously to account for the correlation between the parameters. For example, the hydraulic properties of a porous medium are correlated; thus, each porous medium is described with an uncertainty table. Table H-3 contains an example where the mean standard deviation and correlation tale is listed for the four hydraulic properties of a particular soil type. There may be numerous uncertainty tables required to describe all of the climatic, porous media, and vegetation parameters within a site-scale problem.

The sampling procedure accounts for both variability and uncertainty. Variability describes either the spatial or temporal variability that parameters may have across the site and over time. However, there may be uncertainty regarding the actual parameters describing the variability, due to limited sample sizes or short record lengths. An uncertainty table is described by a number of control parameters, responsible for specifying the table size, type, parameters in the table, and a unique identifier for the table. Variability and uncertainty are specified with separate commands. An example from *itym.dat* for one of the soil types is presented in table H-3.

Variability is accounted for within an uncertainty table using the command **UncertaintyTableMean**, which provides the expected mean, standard deviation, and correlation matrix for the parameters in the table. Some parameters may also be functions of a separate variable, such as the elevation-dependence of climatic parameters; coefficients describing such functional dependence are also incorporated into the uncertainty table.

**UncertaintyTableSet**

The form of the parameters following a keyword of **UncertaintyTableMean** is

$$T = [m\ s\ a\ c] \tag{H-4}$$

where $\boldsymbol{T}$ is the entire uncertainty table, $m$ is a column vector of mean values, $s$ is a column vector of standard-deviation values, $a$ is an array of coefficient values for separate variables (and has zero width if not needed), and $\boldsymbol{c}$ is a square array for the correlation matrix.

The number of parameters in the uncertainty table is specified by the last previous **UncertaintyTableNumPar** keyword/parameter pair. The number of columns in the uncertainty table is specified by the last previous **UncertaintyTableNumCol** keyword/parameter pair. The width of $a$ is implied by the difference between the two (noting that 2 columns are needed for $m$ and $s$). Thus, if there are 4 parameters and 7 columns, the width of $a$ is 7 - 4 - 2 = 1.

**Table H-3. Sample from *itym.dat* file illustrating format of sampling control**

```
###### Start of Soil Property Tables ######


UncertaintyTableNumPar  4
UncertaintyTableNumCol  6
UncertaintyTableType          Porous
UncertaintyTablePars
      log10(IntrinsicPermeability[cm2])
      log10(Pcap0[kPa])
      vanGenuchten_m
      log10(Porosity)

UncertaintyTableID      TypicArgidurids

# mean      sdev        corr1:numpar
UncertaintyTableMean
-8.243      0.1         1     -0.6  0     0.7
0.284       0.5         -0.6  1     0     -0.5
0.1935      0.05        0     0     1     0
-0.4365     0.05        0.7   -0.5  0     1

# mean      sdev        corr1:numpar
UncertaintyTableSdev
  0.1             0.05        0     0.2   0.2   0.2
  0.5             0.05        0.2   0     0.2   0.2
 0.05             0.01        0.2   0.2   0     0.2
 0.05             0.01        0.2   0.2   0.2   0

# mean      sdev        corr1:numpar
UncertaintyTableUbnd
1e+032      1e+032      1     1     1     1
1e+032      1e+032      1     1     1     1
 0.99            1e+032      1     1     1     1
    0            1e+032      1     1     1     1

# mean      sdev        corr1:numpar
UncertaintyTableLbnd
-1e+032     0           -1    -1    -1    -1
-1e+032     0           -1    -1    -1    -1
 0.01            0           -1    -1    -1    -1
   -2            0           -1    -1    -1    -1
```

Uncertainty is accounted for within an uncertainty table using the command **UncertaintyTableSdev**, which provides the standard deviation due to uncertainty of each of the values specified by the matching **UncertaintyTableMean** command. If the parameter describing variability is considered known, the corresponding parameter describing uncertainty is set to zero. Each of the parameters following the **UncertaintyTableMean** keyword are uncertain, thus the parameters following the **UncertaintyTableSdev** keyword correspond exactly to the parameters following the **UncertaintyTableMean** keyword.

Sampling may result in nonphysical values for individual realizations. Allowable upper and lower bounds for the sampled variables are specified using the commands **UncertaintyTableUbnd** and **UncertaintyTableLbnd**, respectively. If the parameter does not have a bound, the corresponding value should be a number far outside the likely range (e.g., $10^{32}$, $-10^{32}$). Again, the parameters following the

keywords for upper and lower bounds correspond exactly to the parameters following the **UncertaintyTableMean** keyword.

**Merge Control**

Both the overlying soil and underlying bedrock are considered composites of separate porous media in ITYM. For example, soil typically consists of a matrix of fine material with embedded rock fragments. Bedrock consists of the actual rock matrix and fractures, providing several pathways for water to leave the soil. The spatial distribution of each composite media is specified in an externally supplied soil-unit or bedrock-unit DEM, with the properties controlled by uncertainty tables and merge control.

Each composite medium is defined by specifying: (i) the individual porous media, using uncertainty tables; (ii) all volume fractions for each media in each composite, using uncertainty tables; and (iii) the porous medium properties and volume fraction information associated with each DEM soil or bedrock unit, using merge control.

Association of indexes in a DEM with a composite porous medium is accomplished using the **MergeDEMType** and **MergeIDList** commands (table H-4). The name IDs defined with the **MergeIDList** command are associated with a volume fraction uncertainty table and a corresponding list of porous-medium-property uncertainty tables using the **MergeDEMNameID**, **MergeVolCase**, and **MergePorList** commands. Each association is processed using a **MergeSet** command.

**Auxiliary Files Supplied to Infiltration Tabulator Yucca Mountain**

All auxiliary files are located in the data subdirectory. In addition to auxiliary data files, the ITYM preprocessor code has other useful files in the itym subdirectory. A brief description of the contents and use of each auxiliary data file follows. Also included below is either a complete or partial listing of each file.

**File name:** ***elevdem.dat***

The ITYM preprocessor software obtains ground surface elevations (m) from the data file *elevdem.dat*. A DEM is used to assign a ground surface elevation to each pixel in the repository discretization. The same discretization is utilized to generate all of the DEM files listed in table H-2. The discretization consists of 199 columns and 300 rows with the lower left (SW) grid coordinate (545010, 4074000) expressed in Universal Transverse Mercator (UTM) NAD27 easting and northing (m). The grid size is 30 m × 30 m. Ground surface elevation data correspond to pixels beginning at the upper left-hand (NW) corner of the grid and continuing to the right every 30 m. The second row of pixels from the top of the grid moving left to right comprise the next set of ground surface elevations, and so forth for all 300 rows. The first 20 lines and last 5 lines of the file *elevdem.dat* are provided below.

```
# DEM of ground surface elevation [m] for each pixel; used in ITYM
preprocessor software.
NCOLS 199
NROWS 300
XLLCORNER 545010
YLLCORNER 4074000
CELLSIZE 30
NODATA_VALUE -9999
```

**Table H-4. Sample from *itym.dat* file illustrating format of sampling control**

```
###### Start of Lithology Merge Information ######

MergeDEMType      Bedrock
MergeIDList
1     Qtac
2     Qtc
3     cnw
4     tul
5     tmn
6     tll
7     tcw
8     tc
9     cuc
10    cul
11    bt2
12    bt3
13    bt4
14    tpp
15    tr
/


MergeDEMNameID    Qtac
MergeVolCase      Qtac
MergePorList      Qtac  carbfill    soilfill    unfilled
MergeSet


1464
1465
1465
1468
1476
1484
1490
1494
1498
1504
1510
1516
1521
   .
   .
   .
1135
1129
1121
1116
1112
```

**File name:** ***winddem.dat***

The ITYM preprocessor software obtains wind speed (m/s) from the data file *winddem.dat*. This DEM is used to assign a wind speed to each pixel in the repository discretization. The same discretization is utilized

to generate all of the DEM listed in table H-2. The discretization consists of 199 columns and 300 rows with the lower left (SW) grid coordinate (545010, 4074000) expressed in UTM NAD27 easting and northing (m). The grid size is 30 m x 30 m. Ground surface elevation data correspond to pixels beginning at the upper left-hand (NW) corner of the grid and continuing to the right every 30 m. The second row of pixels from the top of the grid moving left to right comprise the next set of ground surface elevations, and so forth for all 300 rows. The first 20 lines and last 5 lines of the file *winddem.dat* are provided below.

```
# DEM of wind speed [m/s] for each pixel; used in ITYM preprocessor software.
NROWS 300
NCOLS 199
XLLCORNER    545010
YLLCORNER   4074000
CELLSIZE 30
NODATA_VALUE -9999
3.90536
3.92542
3.981
3.92809
3.78322
3.59776
3.4067
3.31308
3.30678
3.38482
3.3542
3.29629
3.22809
     .
     .
     .
3.23755
3.22683
3.24639
3.24542
3.24828
```

**File name:** ***soildem.dat***

The ITYM preprocessor software obtains soil depths (m) from the data file *soildem.dat*. This DEM assigns a soil depth to each pixel in the repository discretization. The same discretization is used for the soil depth data and the ground surface elevation data in *elevdem.dat*, and all other DEM listed in table H-2. The discretization consists of 199 columns and 300 rows with the lower left (SW) grid coordinate (545010, 4074000) expressed in UTM easting and northing (m). The grid size is 30 m x 30 m. Soil depth data correspond to pixels beginning at the upper left-hand (NW) corner of the grid and continuing to the right every 30 m. The second row of pixels from the top of the grid moving left to right comprise the next set of soil depths, and so forth for all 300 rows of soil depths. The first 20 lines and last 5 lines of the file *soildem.dat* are provided below.

```
# DEM of soil depth [m] for each pixel; used in ITYM preprocessor software.
NROWS 300
NCOLS 199
XLLCORNER    545010
YLLCORNER   4074000
CELLSIZE 30
```

```
NODATA_VALUE -9999
0.13615
0.13615
0.435741
0.624657
0.147408
0.258274
0.159285
0.129658
0.170063
0.129678
0.308515
0.125574
0.130158
     .
     .
     .
0.14188
0.137268
0.142815
0.368732
0.233834
```

**File name:** ***bunitdem.dat***

The ITYM preprocessor software obtains bedrock type from the data file *bunitdem.dat*. This DEM assigns a bedrock unit to each pixel in the repository discretization according to the geologic map of Day et al. (1998). The same discretization is used for all other DEM listed in table H-2. The discretization consists of 199 columns and 300 rows with the lower left (SW) grid coordinate (545010, 4074000) expressed in UTM NAD27 easting and northing (m). The grid size is 30 m × 30 m. Bedrock unit data correspond to pixels beginning at the upper left-hand (NW) corner of the grid and continuing to the right every 30 m. The second row of pixels from the top of the grid moving left to right comprise the next set of bedrock unit, and so forth for all 300 rows of bedrock type. The first 15 lines and last 5 lines of the file *bunitdem.dat* are provided below.

```
# DEM of bedrock unit for each pixel; used in ITYM preprocessor software.
NROWS 300
NCOLS 199
XLLCORNER    545010
YLLCORNER   4074000
CELLSIZE 30
NODATA_VALUE -9999
1
1
1
1
1
1
1
1
     .
     .
     .
1
1
```

```
1
1
1
```

**File name:** ***sunitdem.dat***

The ITYM preprocessor software obtains soil type from the data file *sunitdem.dat*. This DEM assigns a soil type to each pixel in the repository discretization based on TRW Environmental Safety Systems, Inc. (1997). The same discretization is used for all other DEM listed in table H-2. The discretization consists of 199 columns and 300 rows with the lower left grid coordinate (545010, 4074000) expressed in UTM NAD27 easting and northing (m). The grid size is 30 x 30 m. Soil type data correspond to pixels beginning at the upper left-hand (NW) corner of the grid and continuing to the right every 30 m. The second row of pixels from the top of the grid moving left to right comprise the next set of soil types, and so forth for all 300 rows of soil types. The first 15 lines and last 5 lines of the file *sunitdem.dat* are provided below.

```
# DEM of soil type for each pixel; used in ITYM preprocessor software.
NROWS 300
NCOLS 199
XLLCORNER    545010
YLLCORNER   4074000
CELLSIZE 30
NODATA_VALUE -9999
1
1
3
1
5
5
5
5
.
.
.
5
5
5
5
5
```

**File name:** ***maswtab.dat***

Table mean annual clear-sky shortwave radiation [W/m$^2$] calculates for different ground orientations used to estimate actual incoming shortwave radiation incident on the ground surface. Increments in north-south and east-west (YVLLCORNER, XVINCREMENT) are in degrees. The table describes a function of ground surface rotation using east-west rotation (degrees from horizontal) as the row-wise interpolating variable. Similarly, north-south rotation (degrees from horizontal) is the column-wise interpolating variable. The parameters XVLLCORNER and YVLLCORNER span the entire 180 range. The first 35 lines and last 5 lines of the file *maswtab.dat* are provided below.

```
# Mean annual clear-sky shortwave radiation [W/m²] as a function of ground
orientation; used in ITYM.
NROWS 37
NCOLS 37
```

```
XVLLCORNER         90
YVLLCORNER        -90
XVINCREMENT         -5
YVINCREMENT         -5
172.013
155.679
138.16
119.845
102.119
84.1245
66.7618
50.0491
34.5612
20.5591
9.07223
1.93457
0.0141618
0
0
0
0
0
0
0
0
0
0
0.0141618
1.93457
9.07223
20.5591
    .
    .
    .
236.36
221.43
206.316
189.887
172.013
```

**Input Control File for Infiltration Tabulator Yucca Mountain**

The input control file for running the ITYM preprocessor software contains many records that should not generally be modified. The parameters listed in table H-2 control the size and the range of precipitation and temperature used to generate the *maidtbl.dat* file, and are generally the only parameters that should be changed. The first 24 lines and the last 5 lines of the input control file *itym.dat* described in section H-4.1 are provided below.

```
# Input control file itym.dat for ITYM preprocessor software version 1.0,
TPA 4.0
###### Size of Tables ######

num_MAP_table     3
num_MAT_table     5
num_pixel_merge   4
```

```
num_realize_per_table   500

###### Options ######

PathwaySum  MaxOnly
Sampling    Allow
RegrForm    TPA4
zElevDEM    elevdem.dat
zWindDEM    winddem.dat
zSoilDEM    soildem.dat
zBUnitDEM   bunitdem.dat
zSUnitDEM   sunitdem.dat
zMASWtbl    maswtbl.dat
zDTBLout    maidtbl.dat

###### Minimum, Maximum, and Typical Values ######

MAP_min[mm/yr]     50
MAP_max[mm/yr]     800
MAT_min[degreeC]   0
MAT_max[degreeC]   22
base_elev[km]      1.4

#Do not change any record below this line

     .
     .
     .
MergeSet
MergeDEMNameID    tr
MergeVolCase      tr       carfill       soilfill       unfilled
MergeSet
```

# REFERENCES


Day, W., C. Potter, D. Sweetkind, and C. San Juan. *Bedrock Geologic Map of the Central Block Area, Yucca Mountain, Nye County, Nevada.* USGS Miscellaneous Investigations Series, Map I–2601. Scale 1: 6000. 1998.

Matalas, N.C. Mathematical assessment of synthetic hydrology. *Water Resources Research* 3(4): 937–945. 1967.

Stothoff. S. *BREATH Version 1.1—Coupled Flow and Energy Transport in Porous Media.* NUREG/CR–6333. Washington, DC: Nuclear Regulatory Commission. 1995.

Stothoff, S., H.M. Castellaw, and A.C. Bagtzoglou. *Simulating the Spatial Distribution of Infiltration at Yucca Mountain.* San Antonio, TX: Center for Nuclear Waste Regulatory Analyses. 1997.

Stothoff, S. *Infiltration Abstractions for Shallow Soil Over Fractured Bedrock in a Semiarid Climate.* San Antonio, TX: Center for Nuclear Waste Regulatory Analyses. 1999.

TRW Environmental Safety Systems. *Site Atlas 1997. Part 1: Yucca Mountain, Nye County, Nevada.* Yucca Mountain Site Characterization Project. Las Vegas, NV: TRW Environmental Safety Systems, Inc. Technical Data Management. 1997.

Woolhiser, D., S. Stothoff, and G. Wittmeyer. *Estimating Channel Infiltration from Surface Runoff in the Solitario Canyon Watershed, Yucca Mountain, Nevada.* San Antonio, TX: Center for Nuclear Waste Regulatory Analyses. 1999.